



# SENSORY ADAPTATION

EDITED BY: Mehdi Adibi, Davide Zoccolan and Colin W. G. Clifford

PUBLISHED IN: Frontiers in Systems Neuroscience, Frontiers in Neural Circuits,  
Frontiers in Neuroscience and Frontiers in Psychology



# frontiers

## Frontiers eBook Copyright Statement

The copyright in the text of individual articles in this eBook is the property of their respective authors or their respective institutions or funders. The copyright in graphics and images within each article may be subject to copyright of other parties. In both cases this is subject to a license granted to Frontiers.

The compilation of articles constituting this eBook is the property of Frontiers.

Each article within this eBook, and the eBook itself, are published under the most recent version of the Creative Commons CC-BY licence.

The version current at the date of publication of this eBook is CC-BY 4.0. If the CC-BY licence is updated, the licence granted by Frontiers is automatically updated to the new version.

When exercising any right under the CC-BY licence, Frontiers must be attributed as the original publisher of the article or eBook, as applicable.

Authors have the responsibility of ensuring that any graphics or other materials which are the property of others may be included in the CC-BY licence, but this should be checked before relying on the CC-BY licence to reproduce those materials. Any copyright notices relating to those materials must be complied with.

Copyright and source acknowledgement notices may not be removed and must be displayed in any copy, derivative work or partial copy which includes the elements in question.

All copyright, and all rights therein, are protected by national and international copyright laws. The above represents a summary only. For further information please read Frontiers' Conditions for Website Use and Copyright Statement, and the applicable CC-BY licence.

ISSN 1664-8714

ISBN 978-2-88974-179-3

DOI 10.3389/9978-2-88974-179-3

## About Frontiers

Frontiers is more than just an open-access publisher of scholarly articles: it is a pioneering approach to the world of academia, radically improving the way scholarly research is managed. The grand vision of Frontiers is a world where all people have an equal opportunity to seek, share and generate knowledge. Frontiers provides immediate and permanent online open access to all its publications, but this alone is not enough to realize our grand goals.

## Frontiers Journal Series

The Frontiers Journal Series is a multi-tier and interdisciplinary set of open-access, online journals, promising a paradigm shift from the current review, selection and dissemination processes in academic publishing. All Frontiers journals are driven by researchers for researchers; therefore, they constitute a service to the scholarly community. At the same time, the Frontiers Journal Series operates on a revolutionary invention, the tiered publishing system, initially addressing specific communities of scholars, and gradually climbing up to broader public understanding, thus serving the interests of the lay society, too.

## Dedication to Quality

Each Frontiers article is a landmark of the highest quality, thanks to genuinely collaborative interactions between authors and review editors, who include some of the world's best academicians. Research must be certified by peers before entering a stream of knowledge that may eventually reach the public - and shape society; therefore, Frontiers only applies the most rigorous and unbiased reviews.

Frontiers revolutionizes research publishing by freely delivering the most outstanding research, evaluated with no bias from both the academic and social point of view. By applying the most advanced information technologies, Frontiers is catapulting scholarly publishing into a new generation.

## What are Frontiers Research Topics?

Frontiers Research Topics are very popular trademarks of the Frontiers Journals Series: they are collections of at least ten articles, all centered on a particular subject. With their unique mix of varied contributions from Original Research to Review Articles, Frontiers Research Topics unify the most influential researchers, the latest key findings and historical advances in a hot research area! Find out more on how to host your own Frontiers Research Topic or contribute to one as an author by contacting the Frontiers Editorial Office: [frontiersin.org/about/contact](https://frontiersin.org/about/contact)

# SENSORY ADAPTATION

Topic Editors:

**Mehdi Adibi**, Monash University, Australia

**Davide Zoccolan**, International School for Advanced Studies (SISSA), Italy

**Colin W. G. Clifford**, University of New South Wales, Australia

**Citation:** Adibi, M., Zoccolan, D., Clifford, C. W. G., eds. (2022). Sensory Adaptation. Lausanne: Frontiers Media SA. doi: 10.3389/978-2-88974-179-3

# Table of Contents

05	<b><i>Editorial: Sensory Adaptation</i></b>	Mehdi Adibi, Davide Zoccolan and Colin W. G. Clifford
08	<b><i>Intrinsic and Synaptic Dynamics Contribute to Adaptation in the Core of the Avian Central Nucleus of the Inferior Colliculus</i></b>	Sebastian T. Malinowski, Jana Wolf and Thomas Kuenzel
27	<b><i>Global Jitter Motion of the Retinal Image Dynamically Alters the Receptive Field Properties of Retinal Ganglion Cells</i></b>	Akihiro Matsumoto and Masao Tachibana
39	<b><i>Supraspinal Shaping of Adaptive Transitions in the State of Functional Connectivity Between Segmentally Distributed Dorsal Horn Neuronal Populations in Response to Nociception and Antinociception</i></b>	Mario Martín, Javier Béjar, Diógenes Chávez, Adrian Ramírez-Morales, Edson Hernández, Leonardo Moreno, Enrique Contreras-Hernández, Silvio Glusman, Ulises Cortés and Pablo Rudomin
61	<b><i>Short-Term Attractive Tilt Aftereffects Predicted by a Recurrent Network Model of Primary Visual Cortex</i></b>	Maria del Mar Quiroga, Adam P. Morris and Bart Krekelberg
75	<b><i>Similar Expectation Effects for Immediate and Delayed Stimulus Repetitions</i></b>	Catarina Amado, Sophie-Marie Rostalski, Mareike Grotheer, Nadine Wanke and Gyula Kovács
87	<b><i>Face Adaptation and Face Priming as Tools for Getting Insights Into the Quality of Face Space</i></b>	Ronja Mueller, Sandra Utz, Claus-Christian Carbon and Tilo Strobach
104	<b><i>Cortical Microcircuit Mechanisms of Mismatch Negativity and Its Underlying Subcomponents</i></b>	Jordan M. Ross and Jordan P. Hamm
119	<b><i>The Role of Temporal and Spatial Attention in Size Adaptation</i></b>	Alessia Tonelli, Arezoo Pooresmaeili and Roberto Arrighi
128	<b><i>Adaptation Modulates Spike-Phase Coupling Tuning Curve in the Rat Primary Auditory Cortex</i></b>	Mohammad Zarei, Mohsen Parto Dezfouli, Mehran Jahed and Mohammad Reza Daliri
139	<b><i>Capturing Multiple Timescales of Adaptation to Second-Order Statistics With Generalized Linear Models: Gain Scaling and Fractional Differentiation</i></b>	Kenneth W. Latimer and Adrienne L. Fairhall
152	<b><i>Cross-Whisker Adaptation of Neurons in Layer 2/3 of the Rat Barrel Cortex</i></b>	Yonatan Katz and Ilan Lampl
162	<b><i>Disentangling of Local and Wide-Field Motion Adaptation</i></b>	Jinglin Li, Miriam Niemeier, Roland Kern and Martin Egelhaaf

**175 Sensory Adaptation in the Whisker-Mediated Tactile System: Physiology, Theory, and Function**

Mehdi Adibi and Ilan Lampl

**198 Contrast Adaptation in Face Perception Revealed Through EEG and Behavior**

O. Scott Gwinn, Talia L. Retter, Sean F. O'Neil and Michael A. Webster



# Editorial: Sensory Adaptation

Mehdi Adibi<sup>1\*</sup>, Davide Zoccolan<sup>2</sup> and Colin W. G. Clifford<sup>3</sup>

<sup>1</sup> Neurodigit Lab, Department of Physiology, Biomedicine Discovery Institute, Monash University, Clayton, VIC, Australia,

<sup>2</sup> Visual Neuroscience Lab, International School for Advanced Studies (SISSA), Trieste, Italy, <sup>3</sup> School of Psychology, University of New South Wales, Sydney, NSW, Australia

**Keywords:** context, neuronal adaptation, neural network, salience detection, aftereffect, perceptual adaptation, sensory system, face adaptation

## Editorial on the Research Topic

### Sensory Adaptation

In the natural world, organisms are constantly exposed to continuous streams of sensory input. These inputs are dynamic and can undergo major changes in level, at times involving over 100-fold variations in the range of the physical parameters describing the sensory *context* surrounding us. In other instances, the overall strength of the sensory signal (e.g., the luminance or contrast of a visual pattern) may remain roughly constant but the quality of the perceptual features contained in the signal may vary dramatically (e.g., a face changing its expression). In both cases, sensory neurons can adjust their sensitivity based on recent stimulus history, a process known as *sensory adaptation* or *neuronal adaptation*. Neuronal adaptation is a universal phenomenon across sensory modalities and occurs at multiple stages of processing (Solomon and Kohn, 2014; Whitmire and Stanley, 2016). Despite the wealth of research on sensory adaptation in psychophysics and physiology, its possible functions and underlying neuronal mechanisms remain debated. The present Research Topic provides a multidisciplinary survey of recent research aimed at better understanding how the brain functions adaptively to make sense of its surrounding environment. The experimental approaches covered by this Research Topic range from human electrophysiology, functional brain imaging and psychophysics to *in vivo* and *in vitro* whole-cell and extracellular electrophysiology, histology and pharmacological manipulations in a broad range of model systems (from insects to birds, rodents and cats), attesting to the breadth of current research on this topic.

What modulatory effects of adaptation arise from the intrinsic properties of individual neurons as opposed to their connectivity within a neuronal network? This question underpins the theme of two research articles in this Research Topic. Using *in vitro* whole-cell electrophysiology from neurons in the auditory midbrain of embryonic birds, Malinowski et al. identified a link between the rapid adaptation behaviour of neurons and their intrinsic physiological properties but not their morphological classification. Physically spiking neurons exhibiting strong adaptation with faster recovery were found to have higher thresholds, lower membrane resistance and lower membrane time-constants compared to tonically spiking neurons. These two populations exhibited few dendritic morphological differences. Conversely, neurons with different dendritic morphological structures (stellate vs. elongated neurons) showed no significant difference in their intrinsic properties and spiking patterns. Quiroga et al., taking a computational approach, predicted that recurrent connections in a population of orientation selective neurons can give rise, over short time scales of a few hundred ms, to attractive perceptual aftereffects instead of commonly reported repulsive aftereffects. They further employed a psychophysical paradigm, appositely designed to capture aftereffects over short time scales, in order to verify this prediction. Their results indicate how recurrent network dynamics can contribute to shape perceptual adaptation.

## OPEN ACCESS

### Edited and reviewed by:

Stefano Panzeri,  
University of Trento, Italy

### \*Correspondence:

Mehdi Adibi  
mehdi.adibi@monash.edu

**Received:** 04 November 2021

**Accepted:** 22 November 2021

**Published:** 08 December 2021

### Citation:

Adibi M, Zoccolan D and Clifford CWG  
(2021) Editorial: Sensory Adaptation.  
*Front. Syst. Neurosci.* 15:809000.  
doi: 10.3389/fnsys.2021.809000

How does adaptation affect network dynamics and patterns of functional connectivity? Martin et al. addressed this question in a well-understood and relatively simple spinal network. Using a combination of graph theoretic and Markov analyses of cord dorsum potentials recorded from cat lumbar segments, they characterised how pharmacologically-delivered nociceptive stimulation alters functional connectivity. These alterations represent transitions between different states of synchrony in the network activity shaped by supra-spinal inputs. Adibi and Lampl identified different profiles of stimulus-dependent synchrony in sensory thalamus versus cortex over various levels of adaptation, with sensory cortex maintaining its pattern of synchrony in spiking activity across spontaneous and adapted cortical states. Zarei et al. quantified the temporal coupling of spike times to phasic field potentials as a function of stimulus (frequency of auditory signal) in rat auditory cortex in adapted and non-adapted conditions. They observed that phase coupling is tuned to stimulus frequency and reduces with adaptation. Collectively, the findings in these studies illustrate the diversity of the effects adaptation generates at the network level.

What neuronal computations underlie sensory adaptation? Latimer and Fairhall investigated this question using a simple statistical model of spiking neurons based on an inhomogeneous Poisson process with a rate that is a linear combination of the stimulus and recent spiking history. This model explains how adaptation can change the gain of neuronal responses based on the variance of the stimulus as well as capturing observations of adaptation across multiple time scales.

Over the last two decades, accumulated evidence has revealed adaptation to high-level features and complex elements of perception including facial signals such as emotion and eye gaze. Gwinn et al. show electro-physiological and perceptual effects of adaptation to the variance of different facial configurations, suggesting that adaptation shapes face perception not only based on the average characteristics of the faces we observe, but also based on the range of faces. Whereas, adaptation typically tends to bias perception away from the adaptor (in the form of negative or repulsive after-effects), the phenomenon of priming indicates that the processing of a repeated stimulus can be facilitated. In a review of the literature on face adaptation and face priming, Mueller et al. draw upon these two phenomena to gain insight into the nature of the perceptual “space” within which faces are represented for recognition. As we ascend the visual hierarchy the ability of attention to modulate processing tends to increase (Reynolds and Chelazzi, 2004). Thus, the extent to which adaptation to a particular stimulus attribute depends on the amount of attention to the adaptor can be used to infer the level(s) of processing involved. Tonelli et al. show that the amount of attention a subject pays to an adapting stimulus does not affect adaptation to the size of a visual stimulus, consistent with previous findings suggesting that local gain control in primary visual cortex mediates size adaptation (Murray et al., 2006; Fang et al., 2008; Sperandio et al., 2012; Pooresmaeili et al., 2013).

Motion is a fundamental quality of vision that can create strong adaptation effects at various stages of processing (Barlow and Hill, 1963; Hammond et al., 1985; Petersen et al., 1985;

Huk et al., 2001) for review see (Anstis et al., 1998; Mather et al., 1998). Despite diverse evolutionary constraints across different species, from insects and cephalopods to vertebrates, visual systems have converged to provide motion detection by conceptually similar mechanisms to detect local and global (whole retinal image) motion crucial to maintaining accurate vision during eye and/or body movement (Clifford and Ibbotson, 2002). Matsumoto and Tachibana studied how motion simulating the jitter of the retinal image during fixation affects the receptive field (RF) of retinal ganglion cells. Their study revealed that global motion leads to elongated RFs and temporal sharpening of evoked responses in a group of ganglion cells with phasic response profile. Pharmacological manipulations identified two plausible mechanisms underlying these RF alterations: electrical coupling between bipolar cell dendrites, and presynaptic inhibition by amacrine cells. Li et al. developed an innovative stimulus paradigm to disentangle local motion adaptation at the level of elementary motion detectors in blowflies from global motion adaptation affecting wide-field neurons that pool the output of elementary detectors. They found that global motion adaptation is strongly direction dependent, while local motion adaptation is largely direction independent, potentially leading to a robust representation of the direction of local motion independent of global motion direction.

Adaptation is a hallmark not only of vision but also of tactile perception and has considerable behavioural relevance to animals such as rats and mice whose primary sensory modality is their whisker-mediated tactile system (Adibi, 2019). Adibi and Lampl provide a thorough review of the physiology of neuronal adaptation along the somatosensory pathways from receptors to brainstem, sensory thalamus and cortex, outlining distinctive features of sensory adaptation in the rodent whisker-mediated tactile system. They further comment on the underlying mechanisms of adaptation and its functional roles, suggesting a diverse range of functions including shifting the operating mode of cortical computation along the continuum of coincidence detection and temporal integration, optimising receptive fields, performing noise reduction, enhancing salience detection, and frequency-domain filtering properties, depending on the dynamics of stimulation in the environment. Using intracellular recording of neurons in rat barrel cortex, Katz and Lampl showed that in most layer 2/3 neurons, similar to layer 4 neurons, adaptation is whisker-specific, despite their multi-whisker receptive fields. This finding indicates that multi-whisker receptive fields in layer 2/3 mainly emerge from intracortical horizontal connections with neighboring barrels rather than being inherited from layer 4 neurons. This allows high responsiveness in complex environments.

A consequence of statistical regularities in the environment is increased *predictability* of specific stimuli. Adibi and Lampl suggest that reduced responsiveness of sensory neurons to repetitive stimuli over time may represent a reduction in *prediction error* (also a hallmark of predictive coding theory) and provides a mechanism for enhanced detection of deviant stimuli from the background (for further review refer to Pazo-Alvarez et al., 2003; Winkler and Czigler, 2012; Grimm et al., 2016; Carbajal and Malmierca, 2018).

Ross and Hamm summarised recent evidence on the potential neuronal mechanisms underlying adaptation and deviance detection, particularly in the context of “mismatch negativity” (MMN), a negative event-related scalp potential recorded at about 150 ms post-stimulus onset in response to deviant stimuli compared to redundant stimuli in an oddball paradigm. To dissociate stimulus repetition suppression (adaptation) and expectation suppression (prediction) of fMRI responses in the human brain, Amado et al. used pairs of face stimuli presented with inter-stimulus intervals (ISIs) between 0.5 and 3.75 s, where the gender of the first stimulus indicated either repetition of the same face or predicted a novel face. They found repetition and expectation suppression effects in face-sensitive

visual cortex that were both independent of the length of the ISI.

Our hope is these brief introductory remarks will spark the interest of readers to delve deeper into a field of research that, despite a long history and a well-established body of literature, still continues to flourish and yield new insights into the mechanisms and functions of a key aspect of sensory processing and perception.

## AUTHOR CONTRIBUTIONS

MA: original draft. All authors edited and approved the final version.

## REFERENCES

- Adibi, M. (2019). Whisker-mediated touch system in rodents: from neuron to behavior. *Front. Syst. Neurosci.* 13:40. doi: 10.3389/fnsys.2019.00040
- Anstis, S., Verstraten, F. A., and Mather, G. (1998). The motion aftereffect. *Trends Cogn. Sci.* 2, 111–117. doi: 10.1016/S1364-6613(98)01142-5
- Barlow, H. B., and Hill, R. M. (1963). Evidence for a physiological explanation of the waterfall phenomenon and figural after-effects. *Nature* 200, 1345–1347. doi: 10.1038/2001345a0
- Carbajal, G. V., and Malmierca, M. S. (2018). The neuronal basis of predictive coding along the auditory pathway: from the subcortical roots to cortical deviance detection. *Trends Hear.* 22:2331216518784822. doi: 10.1177/2331216518784822
- Clifford, C. W., and Ibbotson, M. (2002). Fundamental mechanisms of visual motion detection: models, cells and functions. *Progr. Neurobiol.* 68, 409–437. doi: 10.1016/S0304-0082(02)00154-5
- Fang, F., Boyaci, H., Kersten, D., and Murray, S. O. (2008). Attention-dependent representation of a size illusion in human v1. *Curr. Biol.* 18, 1707–1712. doi: 10.1016/j.cub.2008.09.025
- Grimm, S., Escera, C., and Nelken, I. (2016). Early indices of deviance detection in humans and animal models. *Biol. Psychol.* 116, 23–27. doi: 10.1016/j.biopsycho.2015.11.017
- Hammond, P., Mouat, G., and Smith, A. (1985). Motion after-effects in cat striate cortex elicited by moving gratings. *Exp. Brain Res.* 60, 411–416. doi: 10.1007/BF00235938
- Huk, A. C., Ress, D., and Heeger, D. J. (2001). Neuronal basis of the motion aftereffect reconsidered. *Neuron* 32, 161–172. doi: 10.1016/S0896-6273(01)00452-4
- Mather, G. E., Verstraten, F. E., and Anstis, S. E. (1998). *The Motion Aftereffect: A Modern Perspective*. Cambridge, MA: The MIT Press.
- Murray, S. O., Boyaci, H., and Kersten, D. (2006). The representation of perceived angular size in human primary visual cortex. *Nat. Neurosci.* 9, 429–434. doi: 10.1038/nn1641
- Pazo-Alvarez, P., Cadaveira, F., and Amenedo, E. (2003). Mmn in the visual modality: a review. *Biol. Psychol.* 63, 199–236. doi: 10.1016/S0304-0511(03)00049-8
- Petersen, S. E., Baker, J. F., and Allman, J. M. (1985). Direction-specific adaptation in area mt of the owl monkey. *Brain Res.* 346, 146–150. doi: 10.1016/0006-8993(85)91105-9
- Pooresmaeli, A., Arrighi, R., Biagi, L., and Morrone, M. C. (2013). Blood oxygen level-dependent activation of the primary visual cortex predicts size adaptation illusion. *J. Neurosci.* 33, 15999–16008. doi: 10.1523/JNEUROSCI.1770-13.2013
- Reynolds, J. H., and Chelazzi, L. (2004). Attentional modulation of visual processing. *Annu. Rev. Neurosci.* 27, 611–647. doi: 10.1146/annurev.neuro.26.041002.131039
- Solomon, S. G., and Kohn, A. (2014). Moving sensory adaptation beyond suppressive effects in single neurons. *Curr. Biol.* 24, R1012–R1022. doi: 10.1016/j.cub.2014.09.001
- Sperandio, I., Chouinard, P. A., and Goodale, M. A. (2012). Retinotopic activity in v1 reflects the perceived and not the retinal size of an afterimage. *Nat. Neurosci.* 15, 540–542. doi: 10.1038/nn.3069
- Whitmire, C. J., and Stanley, G. B. (2016). Rapid sensory adaptation redux: a circuit perspective. *Neuron* 92, 298–315. doi: 10.1016/j.neuron.2016.09.046
- Winkler, I., and Czigler, I. (2012). Evidence from auditory and visual event-related potential (erp) studies of deviance detection (mmn and vmmn) linking predictive coding theories and perceptual object representations. *Int. J. Psychophysiol.* 83, 132–143. doi: 10.1016/j.ijpsycho.2011.10.001

**Conflict of Interest:** The authors declare that the research was conducted in the absence of any commercial or financial relationships that could be construed as a potential conflict of interest.

**Publisher's Note:** All claims expressed in this article are solely those of the authors and do not necessarily represent those of their affiliated organizations, or those of the publisher, the editors and the reviewers. Any product that may be evaluated in this article, or claim that may be made by its manufacturer, is not guaranteed or endorsed by the publisher.

Copyright © 2021 Adibi, Zoccolan and Clifford. This is an open-access article distributed under the terms of the Creative Commons Attribution License (CC BY). The use, distribution or reproduction in other forums is permitted, provided the original author(s) and the copyright owner(s) are credited and that the original publication in this journal is cited, in accordance with accepted academic practice. No use, distribution or reproduction is permitted which does not comply with these terms.



# Intrinsic and Synaptic Dynamics Contribute to Adaptation in the Core of the Avian Central Nucleus of the Inferior Colliculus

Sebastian T. Malinowski<sup>1,2</sup>, Jana Wolf<sup>1</sup> and Thomas Kuenzel<sup>1\*</sup>

<sup>1</sup> Auditory Neurophysiology Group, Department of Chemosensation, RWTH Aachen University, Aachen, Germany,

<sup>2</sup> Department of Chemosensation, RWTH Aachen University, Aachen, Germany

## OPEN ACCESS

### Edited by:

Mehdi Adibi,  
University of New South Wales,  
Australia

### Reviewed by:

Attila Szűcs,  
University of California, San Diego,  
United States

Stephen M. Johnson,  
University of Wisconsin-Madison,  
United States

### \*Correspondence:

Thomas Kuenzel  
kuenzel@bio2.rwth-aachen.de

**Received:** 03 May 2019

**Accepted:** 01 July 2019

**Published:** 16 July 2019

### Citation:

Malinowski ST, Wolf J and Kuenzel T  
(2019) Intrinsic and Synaptic  
Dynamics Contribute to Adaptation in  
the Core of the Avian Central Nucleus  
of the Inferior Colliculus.  
*Front. Neural Circuits* 13:46.  
doi: 10.3389/fncir.2019.00046

The reduction of neuronal responses to repeated stimulus presentation occurs in many sensory neurons, also in the inferior colliculus of birds. The cellular mechanisms that cause response adaptation are not well described. Adaptation must be explicable by changes in the activity of input neurons, short-term synaptic plasticity of the incoming connections, excitability changes of the neuron under consideration or influences of inhibitory or modulatory network connections. Using whole-cell recordings in acute brain slices of the embryonic chicken brain we wanted to understand the intrinsic and synaptic contributions to adaptation in the core of the central nucleus of the inferior colliculus (ICCc). We described two neuron types in the chicken ICCc based on their action potential firing patterns: Phasic/onset neurons showed strong intrinsic adaptation but recovered more rapidly. Tonic/sustained firing neurons had weaker adaptation but often had additional slow components of recovery from adaptation. Morphological analysis suggested two neuron classes, but no physiological parameter aligned with this classification. Chicken ICCc neurons received mostly mixed AMPA- and NMDA-type glutamatergic synaptic inputs. In the majority of ICCc neurons the input synapses underwent short-term depression. With a simulation of the putative population output activity of the chicken ICCc we showed that the different adaptation profiles of the neuron classes could shift the emphasize of stimulus encoding from transients at long intervals to ongoing parts at short intervals. Thus, we report here that description of biophysical and synaptic properties can help to explain adaptive phenomena in central auditory neurons.

**Keywords:** auditory midbrain, inferior colliculus, avian, response adaptation, *Gallus gallus*, acute brain slice, fiber stimulation

## 1. INTRODUCTION

Adaptation, the reduction of neuronal responses to repetitive stimuli, is a common phenomenon throughout several sensory modalities (Hille, 2001), including the auditory system. The reduction of the overall strength of the response of a given neuron to repeated presentation of the same stimulus is called response adaptation (Singheiser et al., 2012b; Pérez-González and Malmierca, 2014). Response adaptation depends on the interval of presentation (Gutfreund and Knudsen, 2006; Singheiser et al., 2012a), persists even in the absence of the stimulus for a certain recovery

time and is thus implicated in diverse perceptual phenomena like forward masking (Nelson et al., 2009) or the precedence effect (Litovsky and Yin, 1998; Spitzer et al., 2004). Response adaptation occurs in several auditory brain areas (Ulanovsky et al., 2003; Ingham and McAlpine, 2004; Dean et al., 2005; Wang and Peña, 2013; Ferger et al., 2018) and time-constants of release from adaptation in the hundreds of milliseconds were measured (Ingham and McAlpine, 2004; Gutfreund and Knudsen, 2006; Singheiser et al., 2012a; Wang and Peña, 2013; Ferger et al., 2018). In higher stations of the auditory pathway a related type of adaptation was described: neurons adapt their response to repeated presentation of a certain stimulus but respond normally to a qualitatively different, uncommon stimulus. This phenomenon was termed stimulus-specific adaptation (Ulanovsky et al., 2003; Pérez-González and Malmierca, 2014) and it was described in the mammalian auditory cortex, auditory thalamus and the inferior colliculus (IC) (Malmierca et al., 2009, 2015; Ayala and Malmierca, 2012) and also in the external nucleus of the IC (Reches and Gutfreund, 2008) and forebrain areas (Reches et al., 2010) of birds.

Adaptation is commonly regarded as a type of short-term memory function emerging from properties of the neuronal network (Pérez-González et al., 2012; Ayala et al., 2016). Due to its stimulus-driven properties and the relative conceptual simplicity, a complete understanding of its mechanisms seems possible. This makes adaptation an appealing target for experimental analysis of higher brain function, both on cellular and network levels. Few attempts are however usually made to mechanistically describe adaptive phenomena on the level of the synaptic physiology and the biophysics of the neurons. We want to argue here that any adaptation of the response of a given neuron must be explicable by either upstream changes in input rate, short-term synaptic plasticity of the ascending connections (Friauf et al., 2015), intrinsic biophysical excitability changes of the neuron under consideration (Debanne et al., 2019) or, indeed, influence of the network in the form of lateral or descending inhibitory or modulatory synaptic connections (Ayala et al., 2016). In order to fully understand an adaptive phenomenon it is crucial to take the biophysical and synaptic factors that dynamically shape information processing at a given neuron into account. In order to attempt such a dissection of factors underlying adaptation we recorded with *in-vitro* whole-cell techniques from neurons in the avian core of the central nucleus of the IC (ICCc), which exhibit response adaptation (Singheiser et al., 2012a) *in vivo*. We will describe here the intrinsic dynamics of excitability and the dynamics of ascending lemniscal axonal connections and how these two factors differ for two physiologically defined neurons classes in the avian IC. Since the neurons we analyzed are the starting points of the input stream for space-specific neurons in the external nucleus of the IC, we will also provide *in-silico* experiments to assess the impact of the response dynamics of ICCc neurons on sound processing further along in the auditory pathway. Thus, our study contributes to mechanistic understanding of a higher brain function, adaptation, on the level of cellular physiology and biophysics.

## 2. MATERIALS AND METHODS

### 2.1. Animal Handling and Brain Slice Preparation

A total of 76 chicken embryos between embryonic day 19 and 21 (HH stages 45/46) were sacrificed for this study. All experimental procedures performed on animals in this study were approved by the local animal welfare officer and state authorities (Landespräsidium für Natur, Umwelt und Verbraucherschutz Nordrhein-Westfalen, Recklinghausen, Germany).

Fertilized chicken eggs (*Gallus gallus domesticus*) were obtained from a local poultry farm (Moonen & Waagemans Kuikenbroeders B.V., Nederweert, The Netherlands) and incubated at 37 °C. and 50% relative humidity in a rolling incubator until use. Eggs were then opened and chicken embryos were rapidly decapitated *in ovo* before any further manipulations. Embryos were staged according to Hamburger and Hamilton (1951).

Standard methods (Weigel and Luksch, 2012) were used to prepare and maintain acute brain slices of embryonic chicken as previously reported (Goyer et al., 2015). Briefly, chicken heads were immediately immersed in ice-cold cutting buffer (im mM: 240 sucrose, 3 KCL, 5 MgCl<sub>2</sub>, 0.5 CaCl<sub>2</sub>, 1.2 NaH<sub>2</sub>PO<sub>4</sub>, 23 NaHCO<sub>3</sub>, 11 D-glucose; oxygenated with 95%O<sub>2</sub>/5%CO<sub>2</sub>). Brains were removed from the skull and midbrain hemispheres dissected. Midbrain hemispheres were embedded in agarose gel (2% low melting point agarose, 290 mM saccharose, 2 mM KCL, 3 mM MgCl<sub>2</sub>, 5 mM HEPES). After curing, agarose blocks were trimmed and midbrains cut into 250 μm slices on a vibratome (Leica VT1200S; Leica Biosystems) while immersed in cutting buffer. Coronal brain slices were cut except for recordings of ascending synaptic connections, which were cut in a parasagittal plane. Slices were transferred for holding into artificial cerebrospinal fluid (ACSF; in mM: 120 NaCl, 3 KCL, 1 MgCl<sub>2</sub>, 2 CaCl<sub>2</sub>, 1.2 NaH<sub>2</sub>PO<sub>4</sub>, 23 NaHCO<sub>3</sub>, 11 D-glucose; oxygenated with 95%O<sub>2</sub>/5%CO<sub>2</sub>) and equilibrated at room temperature for 1 h. Immediately prior to transfer into the recording chamber (see next section) the optic tectum overlaying the inferior colliculus were routinely dissected to improve handling of the slices.

### 2.2. Whole-Cell Patch-Clamp Recordings

#### 2.2.1. Recording Setup

Whole-cell patch recordings (Hamill et al., 1981) of neurons in the central nucleus of the inferior colliculus (ICCc) of E19 to E21 embryonic chicken were performed in a custom-built recording setup. The slices were prepared from animals of  $19.4 \pm 0.6$  embryonic days ( $N = 76$ ). Slices containing the IC were transferred into a recording chamber on the stage of a fixed-stage microscope (Nikon Eclipse FN-1) and observed with IR-DIC optics under infrared illumination. The recording chamber was perfused with oxygenated ACSF at room temperature (25 °C) at a rate of 100 ml/h (chamber volume was 1.5ml). Neurons in the ICCc were targeted using a 40x immersion objective (Nikon NIR APO 40x/0.80w). ICCc location in frontal and sagittal sections was routinely identified using a histological atlas of the chicken brain (Puelles et al., 2007) and histological experiments

prior to this study (data not shown). Patch electrodes were manufactured from borosilicate glass capillaries (GB150F-8P; Science Products, Hofheim, Germany) with a horizontal pipet puller (DMZ Universalpuller; Zeitz Instruments, Martinsried, Germany). For all recordings in this study, pipets were filled with potassium-gluconate based internal solution (in mM: 100 K-gluconate, 40 KCL, 0.1 CaCl<sub>2</sub>, 10 HEPES, 1.1 EGTA, 2 Mg-ATP, 0.4 GTP, 0.1 Alexa Fluor 488 hydrazide, 3mg/ml biocytin; pH adjusted to 7.2 with KOH, osmolarity 280 mOsm; Alexa dye and biocytin obtained from Thermo Fisher Scientific). Liquid junction potential was estimated to be -11 mV and remained uncorrected. Whole-cell recordings were performed with a SEC05LX dSEVC amplifier (npi, Tamm, Germany) in bridge mode or in voltage clamp mode (25 kHz switching frequency). In bridge mode, series resistance compensation was routinely set to twice the electrode resistance measured in the bath solution. This procedure in some cases resulted in residual uncompensated series resistance. Signals were low-pass filtered (5 kHz cutoff frequency) and sampled at 50 kHz (NI-DAQ PCI-6281; National Instruments, Austin TX, USA). Stimulus generation and data collection was performed with custom software written in MATLAB (MATLAB data acquisition toolbox).

### 2.2.2. Biophysical Characterization

Initial resting membrane potential of all neurons was noted immediately after obtaining whole-cell access. Membrane resistance was measured from sets of small current injections (21 steps from -150 to +300pA) by constructing the current-voltage curves and fitting a linear function to the hyperpolarizing conditions. Exponential functions were fitted to the onset of the voltage responses to estimate the membrane time constant. Membrane time-constant was determined for at least three hyperpolarizing current steps and the values were averaged. Membrane capacitance was then estimated from the measured  $R_m$  and averaged  $\tau_m$  readings. Next, action-potential (AP) threshold was determined with repeated single current injections. Then, a current-AP rate relation (F/I) was measured with 10 repetitions of 15 depolarizing current steps between 50 and 300% threshold current. From these F/I curves, AP firing behavior was determined to be either phasic or tonic: phasic neurons fired only one or two AP per stimulus over a wide range of currents while tonic neurons showed an increase of AP numbers with increasing current.

### 2.2.3. Measurement of Intrinsic Adaptation

Intrinsic adaptation was measured by applying pairs of rectangular stimulus currents (100 ms duration each, amplitude was 300% AP threshold current) with increasing inter-stimulus intervals (1–500 ms in logarithmical steps). For every interval 10 repetitions were recorded, 3 s intervals between repetitions were included to allow recovery of neurons. With the help of custom software AP were automatically detected and analyzed in these recordings. A number of parameters was derived from these data: number of AP per stimulus, latency of the first AP peak re the onset of the stimulus, amplitude of the first AP peak, maximum upward and downward slope of the first AP and finally the width of the first AP measured as the time between the points of steepest

up- and downward slope. From these data we constructed adaptation curves by plotting the average “parameter” (from 10 repetitions each) derived from the second stimulus as a function of the inter-stimulus interval, normalized by the average “parameter” derived from the first stimulus. Adaptation curves were then fitted by one of two double exponential functions, depending on the effect of adaptation: if the intrinsic adaptation caused a reduction of the normalized “parameter” (AP count, AP amplitude, AP maximal slopes), we fitted:

$$P(\text{ISI}) = 1 - [(A_{\text{fast}} \cdot e^{\frac{-\text{ISI}}{\tau_{\text{fast}}}}) + (A_{\text{slow}} \cdot e^{\frac{-\text{ISI}}{\tau_{\text{slow}}}})] \quad (1)$$

with  $P(\text{ISI})$  describing the change of the “parameter” as a function of ISI. If intrinsic adaptation caused an increase of the normalized “parameter” (AP latency, AP width), we fitted:

$$P(\text{ISI}) = 1 + [(A_{\text{fast}} \cdot e^{\frac{-\text{ISI}}{\tau_{\text{fast}}}}) + (A_{\text{slow}} \cdot e^{\frac{-\text{ISI}}{\tau_{\text{slow}}}})] \quad (2)$$

From this double-exponential fits we derived a weighted exponential time-constant:

$$\tau_w = \frac{(A_{\text{fast}} \cdot \tau_{\text{fast}} + A_{\text{slow}} \cdot \tau_{\text{slow}})}{A_{\text{fast}} + A_{\text{slow}}} \quad (3)$$

The weighted time-constants of all cells (grouped according to either AP firing behavior (see above) or dendrite morphology (see below) were averaged and compared. We also averaged the adaptation functions (i.e., the parameter vs. ISI functions per cell) of all cells and fitted Equations 1 or 2 to these average adaptation functions as appropriate.

### 2.2.4. Measurement of Synaptic Events and Pharmacology

Synaptic events in ICCc neurons were evoked by electrically activating axons ascending into to ICCc. For this we placed a bipolar tungsten electrode (2 MΩ impedance) in the hilus of the lateral lemniscus fibers entering the IC. This structure is labeled “HilT” in the atlas by Puelles et al. (2007). Indeed, parallel ascending fibers were clearly visible in IR-DIC optics in parasagittal slices in the region depicted in the atlas. Stimulation pulses (200 μs duration, monopolar, up to 90 V; mean 42 ± 15V,  $n = 20$ ) were generated with a Grass S44 stimulator and delivered through an AMPI-Flex optical stimulus isolator (A.M.P.I., Jerusalem, Israel). We either recorded post-synaptic potentials in bridge-mode or post-synaptic currents in voltage-clamp mode. For voltage clamp, the cells were held at -60 mV holding potential. We first determined the apparent stimulation threshold by gradually increasing stimulus voltage. All further experiments were then performed at 200% threshold voltage, which may be considered a form of maximum stimulation, although this was not rigorously confirmed for all cells. Blockers for AMPA (6,7-dinitroquinoxaline-2,3-dione, DNQX, 100 μM, Tocris/Biotechne) and NMDA (D-2-amino-5-phosphonovalerate, D-AP5, 50 μM, Tocris/Biotechne) type glutamatergic receptors were used for pharmacological dissection. Stimulus protocols for paired-pulse stimulation at

various intervals (5–500 ms) were generated by the recording software and repeated 10 times per interval with delays of at least 3s between repetitions to allow the synapses to fully return to steady state. Postsynaptic currents were analyzed with custom software as previously reported (Goyer et al., 2015). Stationary parameters (EPSC amplitude, 10% to 90% risetime, decay time-constant) were measured from the first EPSC of every repetition per cell. Recovery from short-term plasticity was measured by constructing recovery functions from the paired-pulse recordings. Here, the second EPSC amplitude was normalized to the average first EPSC amplitude. Recovery functions were visually categorized into facilitating, depressing or unclear/mixed. Recovery functions of all cells or the respective groups were averaged and fitted with exponential functions. We used a double-exponential function for the average recovery functions of depressing-only or facilitating-only cells:

$$EPSC_2(ISI) = offset + [(A_{fast} \cdot e^{\frac{-ISI}{\tau_{fast}}} + (A_{slow} \cdot e^{\frac{-ISI}{\tau_{slow}}})] \quad (4)$$

For the average recovery function of all measured cells we used a triple-exponential function to fit a double-exponential depression and an exponential facilitation:

$$EPSC_2(ISI) = offset + \left[ (A_{fast-depr} \cdot e^{\frac{-ISI}{\tau_{fast-depr}}} + (A_{slow-depr} \cdot e^{\frac{-ISI}{\tau_{slow-depr}}} + (A_{facil} \cdot e^{\frac{-ISI}{\tau_{facil}}}) \right] \quad (5)$$

Weighted time-constants of the double exponential fits were calculated as in Equation 3 and degree-of-freedom adjusted coefficient of determination ( $r^2$ ) is given as calculated by the MATLAB function *fit.m*.

## 2.3. Morphological Analysis of Recorded Neurons

Cells were recovered after recording for *post-hoc* anatomical analysis as previously described (Goyer et al., 2016). Briefly, slices were fixed in 4% PFA in phosphate buffer overnight, washed with phosphate buffered saline and 0.3% Triton X-100 multiple times and incubated with streptavidin solution (0.1% Triton X-100, 1% bovine serum albumin in phosphate buffer, 1:800 Alexa-fluor-streptavidin conjugate # S11223 from Thermo Fisher Scientific) for 3h at RT. After multiple washing steps (0.3% Triton X-100 in TRIS-buffered saline solution) a counterstaining with DAPI was performed. Finally, stained slices were mounted in Fluoprep (bioMerieux) between 24 × 60 mm coverslips between frames of 240 μm adhesive sheets (Grace Bio-Labs). Cells were scanned at high magnification with a laser-scanning confocal microscope (Leica TCS SP2, Leica Microsystems) at high z-resolution ( $\leq 0.5\mu\text{m}$  per image in confocal stacks). Single images at low magnification were scanned to confirm the location of the cell in the ICCc. 23 cells for which ICCc location could not be confirmed were not included in the adaptation study. For a subset of neurons a full morphological analysis was performed. Soma, axon and dendrites were visually identified and 3D reconstructed using the “Simple Neurite Tracer” plugin (Longair et al., 2011) in

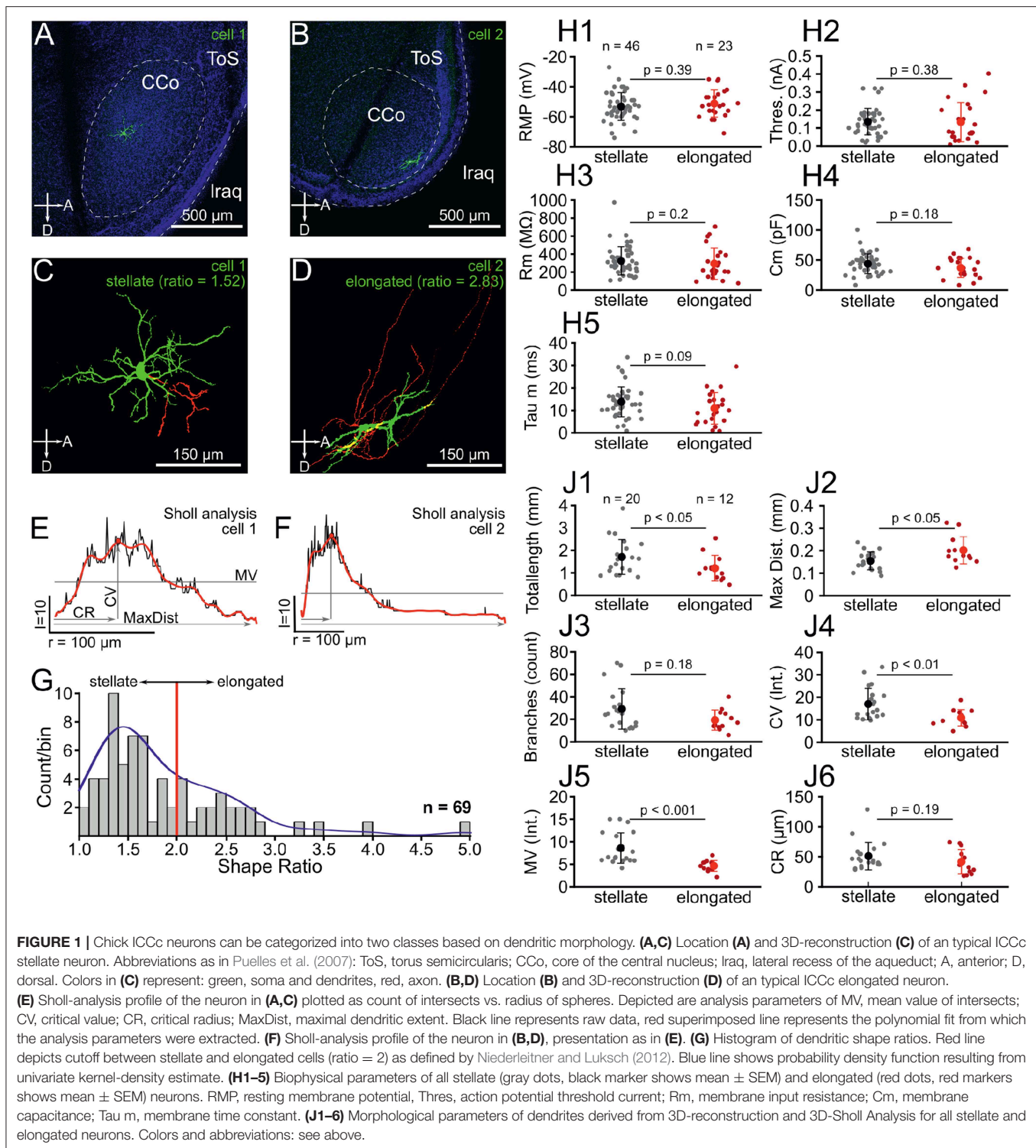
Fiji/ImageJ (Schindelin et al., 2012). Reconstructed morphology for soma and dendrites only (omitting the axonal structure, which was only used for visualization of neurons) were analyzed: first, we fitted the minimum volume ellipsoid that enclosed all dendritic points in 3D-space using established algorithms (Aelst and Rousseeuw, 2009) for every cell. We calculated the ratio of the longest and second-longest axis of the resulting ellipsoid to quantify the shape of the dendritic tree. As proposed by Niederleitner and Luksch (2012) neurons with a shape ratio between 1 and 2 were classified as “stellate” and those with a ratio  $\geq 2$  were classified as “elongated.” Minimum volume ellipsoids were also fitted to z-projected confocal stacks of non-reconstructed cells in 2D-space. In these cases, the ratio of long to short axis was calculated. Furthermore, we performed a Sholl analysis (Sholl, 1953) in 3D space by counting the number of intersects of dendritic structures with spheres of varying radii centered on the soma for every cell. Number of intersects per sphere was plotted against sphere-radius, data was smoothed by fitting a high order polynomial function. From the Sholl analysis a number of parameters that describe the complexity of the dendritic tree were derived for every cell: the mean value (MV) is the average number of intersects over all radii, the critical value (CV) is the maximum number of intersects, the critical radius (CR) is the radius at which the CV occurs. The maximum distance (MaxDist) is the radius at which no more intersects occur. In addition to these parameters we also extracted the number of branchpoints and the total dendritic pathlength from our 3D reconstruction data. All software for morphological analysis was custom written in Python 2.7.

## 2.4. Data Analysis and Statistics

If not noted otherwise, non-parametric tests for statistical significance were used throughout this study. Physiological and morphological parameters were compared pairwise between groups of neurons with the Mann-Whitney *U*-Test (Figures 1–4). A Kruskal-Wallis test was used to analyze pharmacological data (Figure 5). In all cases a criterion of  $p < 0.05$  for significance was used. Modality of parameter distribution (Figure 1G) was estimated by calculating the bimodality index for finite samples as follows:

$$b = \frac{g^2 + 1}{k + \frac{3(n-1)^2}{(n-2)(n-3)}} \quad (6)$$

with  $n$  being the number of observations,  $g$  the sample skewness and  $k$  the excess kurtosis of the sample. Here, values of  $b > \frac{5}{9}$  are usually considered as indicative of bimodality. In addition we estimated the probability density of the sample distribution with an univariate kernel-density estimate (from the python module *statsmodels* 0.8.0) and determined the kernel bandwidth with Silverman’s rule of thumb estimator. The statistical independence of shape and firing pattern classification was tested by constructing a contingency-table and performing Pearson’s chi-squared test with the Python 2.7 function *scipy.stats.chi2-contingency*. For exponential fits throughout the study we report the goodness-of-fit as the coefficient of determination ( $r^2$ )

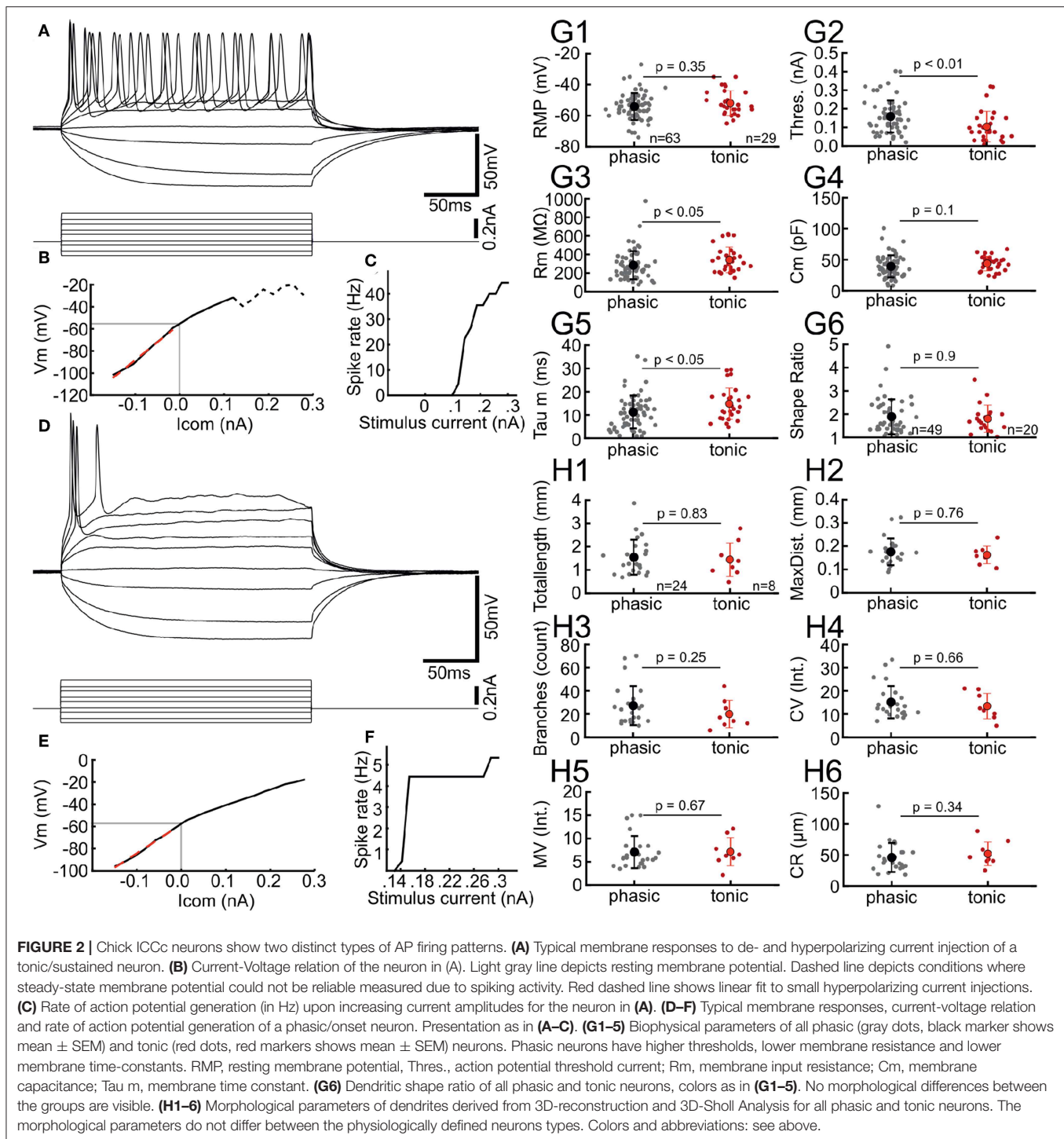


adjusted for degrees of freedom (as returned by the MATLAB function *fit.m*).

## 2.5. Numerical Simulations

For a simple numerical model of ICCc population output we simulated the post-stimulus time histogram (PSTH) of a

hypothetical unit receiving inputs from both phasic (70%) and tonic (30%) ICCc units. For this, random spiketimes were generated following either a very flat, shifted and cut-off gaussian distribution (to model tonic neurons) or a steep shifted gaussian distribution (to model phasic neurons). In both cases, the distributions were shifted to simulate an average



IC onset latency of 10 ms. Both shifting-value (“latency”) and probability of occurrence of a spikes per stimulus (“spike probability”) were dependent on an ISI-parameter according to the average adaptation functions per unit-type we determined experimentally. For this we directly employed the double-exponential fits of AP count and AP latency (**Figure 4**) per unit type as ISI-dependent modifier functions to the starting

target value of spike per stimulus ( $n = 1$  for phasic,  $n = 4$  for tonic) and onset-latency (10 ms). Please note: only spiketimes were randomly generated, no neuronal or synaptic physiology was simulated. The phasic and tonic simulated PSTH were then summed and normalized for number of repetitions and number of inputs to give instantaneous firing rate of the theoretical target cell in Hz, again without taking any neuronal or synaptic

physiology into account. Further, we also normalized to the maximum value to better compare the shape of the resulting PSTH. The maximum rate and the average rate of the last 50 ms were used to calculate onset/sustained-ratio (here, values of 1 would mean a completely flat PSTH and high values indicate a strong emphasize of the phasic onset component). These simulations were performed in MATLAB.

### 3. RESULTS

#### 3.1. Morphological Categorization of Chicken ICCc Neurons

In this study we recorded from a total of  $N = 93$  neurons in acute slices of the chicken IC. The majority of these neurons ( $N = 69$ ) were confirmed to be located in the ICCc based on *post-hoc* histological analysis (Figures 1A,B). Morphological 3D-reconstruction of dendritic structure was performed in a subset of these identified neurons ( $N = 32$ ), which allowed detailed analysis of dendritic shapes (Figures 1C,D). First, we fitted a minimum volume ellipsoid to both the 3D-data ( $N = 32$ ) and to z-projections of confocal stacks of non-reconstructed ICCc neurons ( $N = 37$ ) and expressed the dendritic shape as either stellate (ratio  $< 2$ ) or elongated (ratio  $> 2$ ) based on the long to short axis ratio, following Niederleitner and Luksch (2012). The mean shape ratio of ICCc neurons was  $1.8 \pm 0.7$  ( $N = 69$ ). Overall, we found 67% of ICCc neurons to be of stellate morphology (46/69 neurons) and 33% (23/69 neurons) to be of elongated morphology. In the subset of neurons in which we performed detailed morphological analysis, 63% (20/32 neurons) were of stellate morphology. ICCc dendritic trees had on average a total pathlength of  $1520 \pm 745 \mu\text{m}$  ( $N = 32$ ), with a mean of  $25.5 \pm 16.0$  branchpoints ( $N = 32$ ). ICCc dendrites reached on average a maximal distance of  $172 \pm 53 \mu\text{m}$  ( $N = 32$ ) from the soma. Sholl-analysis (Figures 1E,F) of dendritic complexity revealed a critical range (CR) of  $47.5 \pm 22.5 \mu\text{m}$  ( $N = 32$ ) at which a critical value (CV) of  $14.7 \pm 6.7$  intersects ( $N = 32$ ) was reached. ICCc dendrites had on average a mean value (MV) of  $7.1 \pm 3.3$  intersects ( $N = 32$ ).

We also analyzed biophysical properties of ICCc neurons by performing current-clamp recordings in whole-cell configuration. Our ICCc neurons had an average resting membrane potential of  $-53.4 \pm 8.5$  mV ( $N = 69$ ), average membrane resistance of  $302 \pm 150 \text{M}\Omega$  ( $N = 69$ ) and average membrane capacitance of  $40.5 \pm 16.4$  pF ( $N = 69$ ). The membrane biophysics resulted in an average membrane time-constant of  $12.3 \pm 7.2$  ms ( $N = 69$ ). Action potential threshold current was on average  $0.14 \pm 0.08$  nA ( $N = 69$ ).

We next asked whether the neurons categorized as stellate and elongated represented actual populations of distinct neuronal classes. The distribution of shape ratios (Figure 1G) did not show two completely separate maxima. However, the bimodality index (see Equation 6) of this sample was  $b = 0.564$ . Since values of  $b > \frac{5}{9}$  (0.555...) are usually considered as indicative of a bimodal distribution we conclude that the distribution of shape ratios agreed better with a mixture of two morphological populations. Additional support for this came from performing a kernel density estimate using a rule-of-thumb bandwidth estimator

(resulting bandwidth  $h = 0.246$ ), which resulted in a kernel-density estimate for the sample of shape ratios more in line with an underlying mixture of gaussians than a single skewed gaussian. Thus, we interpreted the sample of shape ratios found by our morphological analysis to be caused by two distinct populations of neurons as opposed to a wide continuum of shapes resulting from a single diverse neuron class. Accordingly, we divided our biophysical and morphological data into two groups (stellate vs. elongated) and asked, whether the two putative classes of neurons would have an influence on the analyzed parameters. Surprisingly, there were no statistically significant differences in either of the biophysical parameters we analyzed (Figure 1H). Neither resting membrane potential ( $-53.2 \pm 9.3$  mV vs.  $-51.2 \pm 9$  mV,  $p = 0.39$ , Figure 1H1), action potential threshold ( $0.14 \pm 0.07$  nA vs.  $0.13 \pm 0.11$  nA,  $p = 0.38$ , Figure 1H2), membrane resistance ( $325 \pm 157 \text{M}\Omega$  vs.  $294 \pm 174 \text{M}\Omega$ ,  $p = 0.2$ , Figure 1H3), membrane capacitance ( $44.8 \pm 16.5$  pF vs.  $37 \pm 16.8$  pF,  $p = 0.18$ , Figure 1H4) nor membrane time-constant ( $13.8 \pm 6.6$  ms vs.  $10.9 \pm 7$  ms,  $p = 0.09$ , Figure 1H5) were significantly different for stellate vs. elongated cells.

However, when we compared the morphological parameters between stellate and elongated neurons, statistically significant differences resulted (Figure 1J). We would like to emphasize that the morphological parameters analyzed here and the grouping criterion (i.e., the shape ratio) were derived from independent analyses. Stellate neurons had on average a significantly greater total dendritic path length ( $1707 \pm 774 \mu\text{m}$  vs.  $1209 \pm 571 \mu\text{m}$ ,  $p < 0.05$ , Figure 1J1) but reached to a shorter average maximal distance from the soma ( $154 \pm 39 \mu\text{m}$  vs.  $202 \pm 60 \mu\text{m}$ ,  $p < 0.05$ , Figure 1J2). Although the difference in the average number of branch points failed to reach statistical significance ( $29 \pm 18$  vs.  $19 \pm 9$ ,  $p = 0.18$ , Figure 1J3), the Sholl analysis parameters critical value ( $17.0 \pm 7.0$  vs.  $10.9 \pm 3.6$ ,  $p < 0.01$ , Figure 1J4) and mean value ( $8.6 \pm 3.4$  vs.  $4.5 \pm 1.2$ ,  $p < 0.001$ , Figure 1J5) were on average significantly different between stellate and elongated neurons. The critical range, on average, was not statistically different ( $51 \pm 23 \mu\text{m}$  vs.  $42 \pm 20 \mu\text{m}$ ,  $p = 0.19$ , Figure 1J6). Taken together, stellate ICCc neurons had significantly more complex dendritic trees that densely covered an area closer to the soma of the neuron. The dendritic trees of elongated neurons on the other hand reached further from the soma of the neuron. Morphological differences likely translate into a different function in information processing in the ICCc for these neurons given the highly laminated organization of this brain area.

#### 3.2. Two Physiological Classes of Neurons in the Chicken ICCc *in vitro*

Neuron classes defined by dendritic morphology did not differ in their basic biophysical parameters. In order to investigate whether physiological parameters beyond basic biophysics could be used to characterize these classes of neurons in the chicken ICCc, we analyzed the action potential firing patterns. Indeed, we found that AP firing patterns represented a neuron classification orthogonal to the morphological grouping (Figure 2). AP firing pattern was classified in all  $N = 93$  IC neurons. A number of neurons (32%, 29/93) showed tonic firing behavior characterized by ongoing generation of AP during stimulation

with suprathreshold depolarizing currents (**Figure 2A**). From these families of stimulus currents we generated current-voltage curves as shown in **Figure 2B**. AP frequency in response to various stimulus currents was analyzed by constructing current-frequency curves (**Figure 2C**). For tonic neurons these were characterized by higher AP frequencies (i.e., multiple AP per stimulus) and monotonically increasing frequencies with increasing current. Phasic neurons (**Figures 2D–F**), on the other hand, occurred more frequently (68%, 63/93). These neurons were characterized by a single (or two) AP generated only at the onset of the stimulus, almost regardless of stimulus amplitude. This was clearly visible in the saturating shape of the current-frequency plot (**Figure 2F**).

When we compared biophysical features of ICCc neurons based on their AP firing behavior (**Figure 2G**), statistically significant differences became evident. While the resting membrane potential was very similar ( $-54.1 \pm 8.7$  mV vs.  $-51.9 \pm 8.0$  mV,  $p = 0.35$ , **Figure 2G1**), AP threshold ( $0.16 \pm 0.09$  nA vs.  $0.1 \pm 0.08$  nA,  $p < 0.01$ , **Figure 2G2**) and membrane resistance ( $284 \pm 151 M\Omega$  vs.  $342 \pm 137 M\Omega$ ,  $p < 0.05$ , **Figure 2G3**) differed significantly between phasic and tonic groups. Membrane capacitance did not appear to be different ( $39 \pm 18$  pF vs.  $44 \pm 11$  pF,  $p = 0.1$ , **Figure 2G4**), which was in line with the morphological analysis presented in the next paragraph. The membrane time-constant, on the other hand, was significantly different ( $11.2 \pm 7.1$  ms vs.  $14.8 \pm 6.8$  ms,  $p < 0.05$ , **Figure 2G5**) between phasic and tonic neurons. We thus found that phasic neurons were harder to excite but had more rapid membrane time-constants, while tonic neurons were easier to excite but showed slower membrane time-constants.

Next we asked whether the AP firing behaviors corresponded to the morphological classification. When we compared the average dendritic shape ratio ( $1.9 \pm 0.75$  vs.  $1.8 \pm 0.58$ ,  $p = 0.9$ , **Figure 2G6**) between phasic and tonic neurons, no statistical differences were evident. In fact, when we performed Pearson's chi-square test we found that the parameters of shape and of AP firing pattern were statistically independent from each other ( $\chi^2 = 0.364$ , degrees-of-freedom = 1,  $p = 0.546$ ). Further, none of the simple or derived morphological parameters (**Figures 2H1–6**) from the 3D reconstruction of neurons appeared statistically different between phasic and tonic neurons.

We concluded therefore, that the AP firing behavior of the neurons did not predict the dendritic shape or complexity. In other words, both physiological AP firing modes appeared in comparable statistical frequencies in the groups of morphologically defined stellate and elongated chicken ICCc neurons.

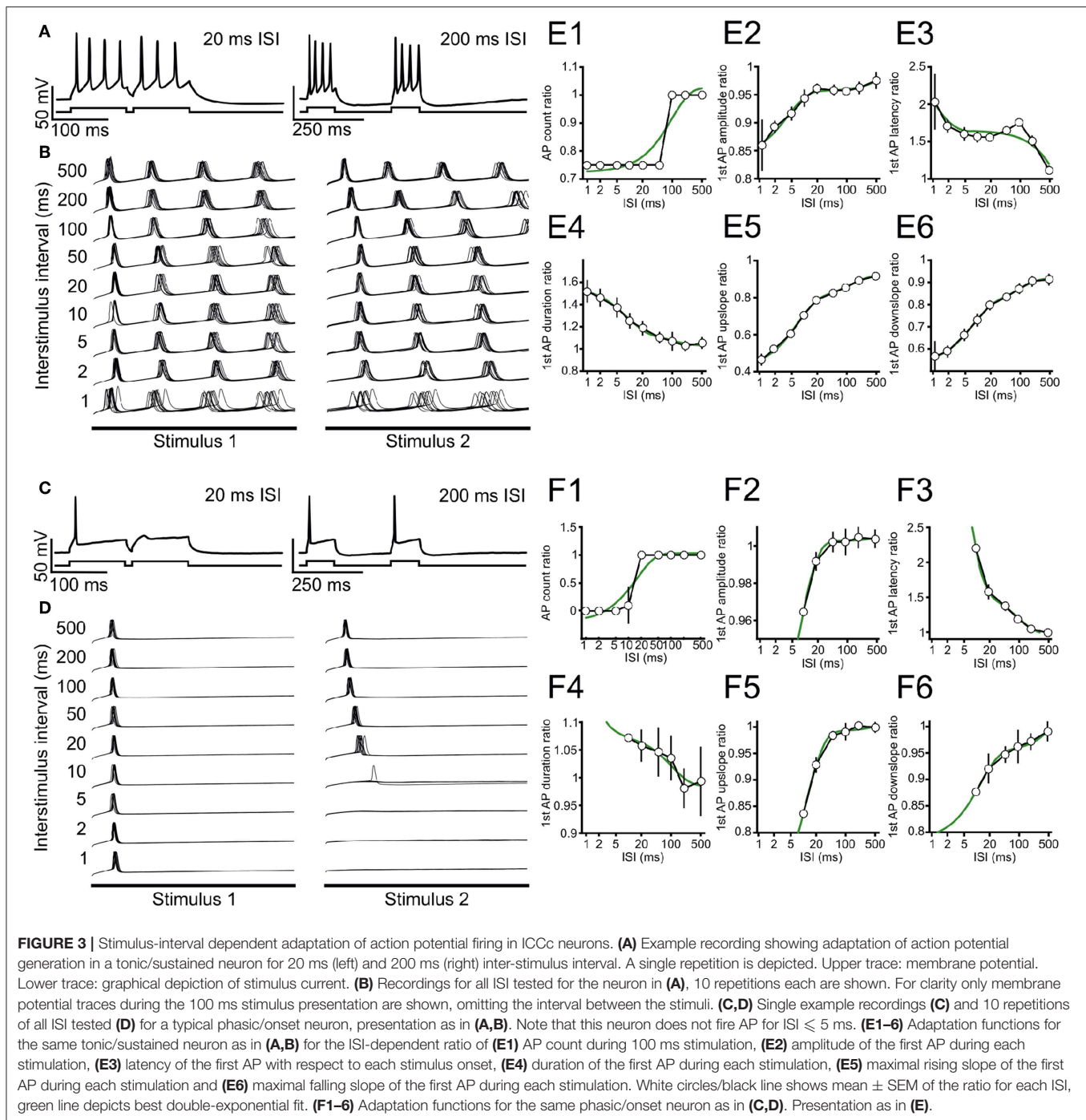
### 3.3. Interval-Dependent Dynamics of Intrinsic Neuronal Excitability in the Chicken ICCc *in vitro*

With our biophysical characterization we established that phasic and tonic neurons differed in their excitability. However, we

believed that intermittent, repeated activity (possibly at intervals in the range of milliseconds) was the more physiologically relevant stimulus regime for an auditory brainstem neuron. We therefore analyzed the interval-dependency of intrinsic neuronal excitability with double-stimulation in current-clamp mode (**Figure 3**).

We show here two typical example neurons from our measurement of intrinsic adaptation of excitability for tonic (**Figures 3A,B,E**) and phasic (**Figures 3C,D,F**) ICCc neurons in acute slices. In the following we will refer to the AP in response to the first or second stimulus as AP<sub>1</sub> or AP<sub>2</sub>, respectively, regardless of AP firing behavior. When we stimulated ICCc neurons with pairs of depolarizing currents at short intervals below 20 ms, phasic neurons often failed to generate AP<sub>2</sub> (**Figure 3C**). Tonic neurons always generated AP<sub>2</sub>, regardless of the inter-stimulus interval, but the number of generated AP<sub>2</sub> per stimulus was reduced (**Figure 3A**). AP<sub>2</sub> numbers returned to normal at long stimulus intervals (**Figures 3A,C**). However, the latency and shape of the AP<sub>2</sub> often still differed for very long ISI (**Figures 3B,D**). We quantified adaptation for a range of stimulus intervals and repetitions. We not only analyzed AP probability/count but also the latency of the generated AP and kinetic parameters (amplitude, maximum up- and downslopes, AP duration) for every AP. The reason for analyzing AP kinetic parameters was to observe subthreshold adaptive phenomena. By this we mean subtle effects on ion channels directly or indirectly involved in AP generation, which do not overtly change the total number of AP generated but nevertheless might substantially affect the temporal precision and/or time-course of the AP and thus information processing in the ICCc. We expressed the parameters as the ratio of parameters for AP<sub>2</sub> divided by AP<sub>1</sub>, to highlight the change caused by adaptation. We plotted the obtained ratio as the average of 10 repetitions vs. inter-stimulus interval (ISI) for the tonic (**Figures 3E1–6**) and phasic (**Figures 3F1–6**) neurons to obtain adaptation functions for the various parameters. Here the maximal/minimal value is a measure for the severity of adaptive processes. By fitting a double-exponential function to the adaptation functions (green lines in **Figures 3E,F**) we calculated a weighted time-constant of adaptation for these parameters (as in Equation 3) to also quantify the dynamics of adaptation.

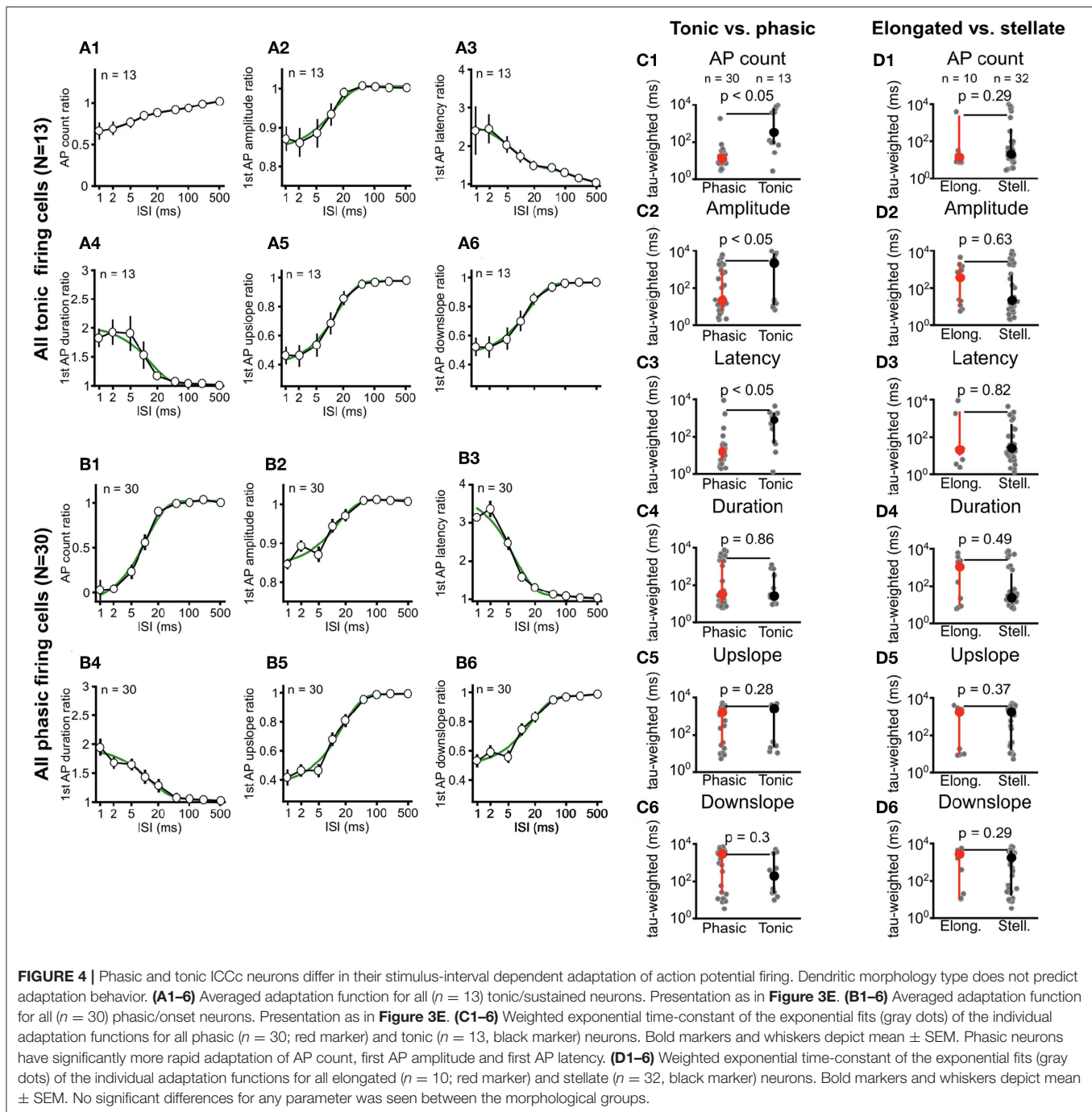
Adaptation of AP number was more severe for the phasic example neuron (**Figure 3F1**) compared to the tonic example neuron (**Figure 3E1**), but recovered with a faster weighted time-constant (17.3 ms,  $r^2 = 0.89$  vs. 98.1 ms,  $r^2 = 0.85$ ). The amplitude of AP<sub>2</sub> shows almost no adaptation with a ratio of 0.96 for the phasic neuron (**Figure 3F2**), while the AP<sub>2</sub> amplitude of the tonic example neurons was marginally more adapted (ratio 0.86). In both cases the unrestrained double-exponential fit described the adaptation function of AP amplitude well ( $r^2 = 0.99$  vs.  $r^2 = 0.98$ ), but resulted in very long weighted time-constants of recovery (2.1s vs. 6.2s). Adaptation of AP<sub>2</sub> latency showed comparable severity for the phasic (**Figure 3F3**) and tonic (**Figure 3E3**) neuron, but again recovered faster for the phasic neuron (15.7 ms,  $r^2 = 0.99$  vs. 98.9 ms,  $r^2 = 0.83$ ). In line with the lack of adaptation of AP amplitude, the phasic example neuron also showed relatively little change of AP<sub>2</sub> duration



(1.07), up- (0.84) or downslope (0.87; **Figures 3F4–6**). These mild adaptive effects recovered with very slow weighted time-constants for the phasic cell (0.2s, 3.2s and 4.6s). The tonic cells showed robust adaptation of AP<sub>2</sub> duration (1.54,  $\tau_w = 31$  ms, **Figure 3E4**), maximal upslope (0.47,  $\tau_w = 40$  ms, **Figure 3E5**) and maximal downslope (0.58,  $\tau_w = 38$  ms, **Figure 3E6**).

Adaptation differed between phasic and tonic neurons with regard to severity and dynamics of recovery. In order to analyze this, we averaged all adaptation functions from tonic

neurons (**Figure 4A**) and phasic neurons (**Figure 4B**) and, again, fitted double-exponential functions to the resulting group-adaptation functions. For the adaptation of the number of AP<sub>2</sub> (**Figures 4A1,B1**), group data confirms that phasic neurons adapt more severely but recover faster from adaptation ( $\tau_w = 10.8$  ms,  $r^2 = 0.99$ ). AP<sub>2</sub> numbers of tonic neurons adapt less severely but recover markedly slower from adaptation ( $\tau_w = 62.7$  ms,  $r^2 = 0.99$ ). The individual weighted time-constants of adaptation of AP count (**Figure 4C1**) were on average significantly smaller



for phasic neurons vs. tonic neurons (14 ms vs. 3.7s;  $U$ -test  $p < 0.05$ ). Group recovery functions of AP<sub>2</sub> amplitude (**Figures 4A2,B2**) were very similar for phasic vs. tonic neurons (13.3 ms,  $r^2 = 0.95$  vs. 12.1 ms,  $r^2 = 0.98$ ), while the individual weighted time-constants of the recovery functions (**Figure 4C2**) were significantly different (21 ms vs. 2.1s;  $U$ -test  $p < 0.05$ ). For the AP<sub>2</sub> latency (**Figures 4A3,B3**) the group adaptation functions (17.9 ms,  $r^2 = 0.97$  vs. 62.5 ms,  $r^2 = 0.99$ ) as well as the individual weighted time-constants (16.5 ms vs.

0.81s;  $U$ -test  $p < 0.05$ ; **Figure 4C3**) were different. For the kinetic parameters of AP<sub>2</sub> no differences between phasic and tonic neurons were evident from neither the group adaptation functions (**Figures 4A4–6,B4–6**), nor the average individual weighted time-constants (**Figures 4C4–6**).

Neither the group adaptation functions (data not shown), nor the averaged individual weighted time-constants of recovery from adaptation (**Figures 4D1–6**) showed any significant differences for stellate vs. elongated ICCc neurons. This further

corroborated our finding (see section 3.1) that the morphological classification did not predict physiological characteristics in chicken ICCc neurons but rather represented an orthogonal categorization of neurons.

Taken together we concluded that the interval-dependent adaptation of the number and latency of AP<sub>2</sub> was significantly different between phasic and tonic firing ICCc neurons. A much more pronounced slow-exponential component (which was evident from the group adaptation functions and the consecutively slower weighted time-constant of recovery) contributed to adaptation in tonic neurons. This slow component appeared, on average, to be mostly absent in phasic firing neurons.

### 3.4. Properties of Ascending Synaptic Connections to Neurons in the Chicken ICCc *in vitro*

Next we wanted to study the properties of ascending connections into the chicken ICCc for two reasons. First, in order to understand the underlying cellular mechanisms that govern adaptive behavior in avian ICCc that was observed *in vivo*, it is vital to understand the properties and dynamics of the synaptic input to the cells under consideration. Synaptic dynamics might in fact be a major contributor to adaptation. The avian ICCc neurons are an ideal testbed for this idea, as these neurons should receive rather uniform, narrow-bandwidth ascending inputs from the auditory brainstem via lateral lemniscus fibers (Puelles et al., 1994; Wang and Karten, 2010). In addition to this, very little quantitative data on synaptic properties in the avian IC has been published before.

Upon brief electrical shocks delivered to the ascending lateral lemniscus fibers (Figure 5A), excitatory postsynaptic potentials (EPSP) could be recorded in ICCc neurons (Figure 5B) that gradually increased in amplitude with increasing stimulation voltage due to recruiting of fibers and eventually elicited AP in the postsynaptic cells (Figure 5B). EPSP in ICCc neurons could be reliably evoked at  $34.5 \pm 23.3$  V ( $N = 11$ ) stimulation strength. However, this apparent threshold was likely mostly determined by electrode placement and slice condition and thus does not really carry much biological meaning. We nevertheless determined the threshold for every cell and performed pharmacological experiments at 200% threshold level. The just suprathreshold EPSP had an average amplitude of  $5.9 \pm 2.4$  mV ( $N = 8$ ). Notably, we never observed evoked hyperpolarizing synaptic responses one would expect for inhibitory postsynaptic responses (IPSP) at any stimulation level, although spontaneous IPSP were occasionally observed (not shown). To confirm the pure excitatory nature of the ascending lemniscal inputs we applied blockers of glutamatergic synaptic transmission to the bath solution in a first set of experiments. Upon wash-in of 100  $\mu$ M DNQX a noticeable reduction of EPSP amplitudes compared to control conditions at identical stimulation voltage occurred (Figure 5C). The DNQX-sensitive part of the synaptic events accounted on average for  $39 \pm 12\%$  ( $N = 7$ ; median: 46.1%) of the EPSP amplitude. Wash-in of 100  $\mu$ M DNQX + 50  $\mu$ M AP5 further reduced the

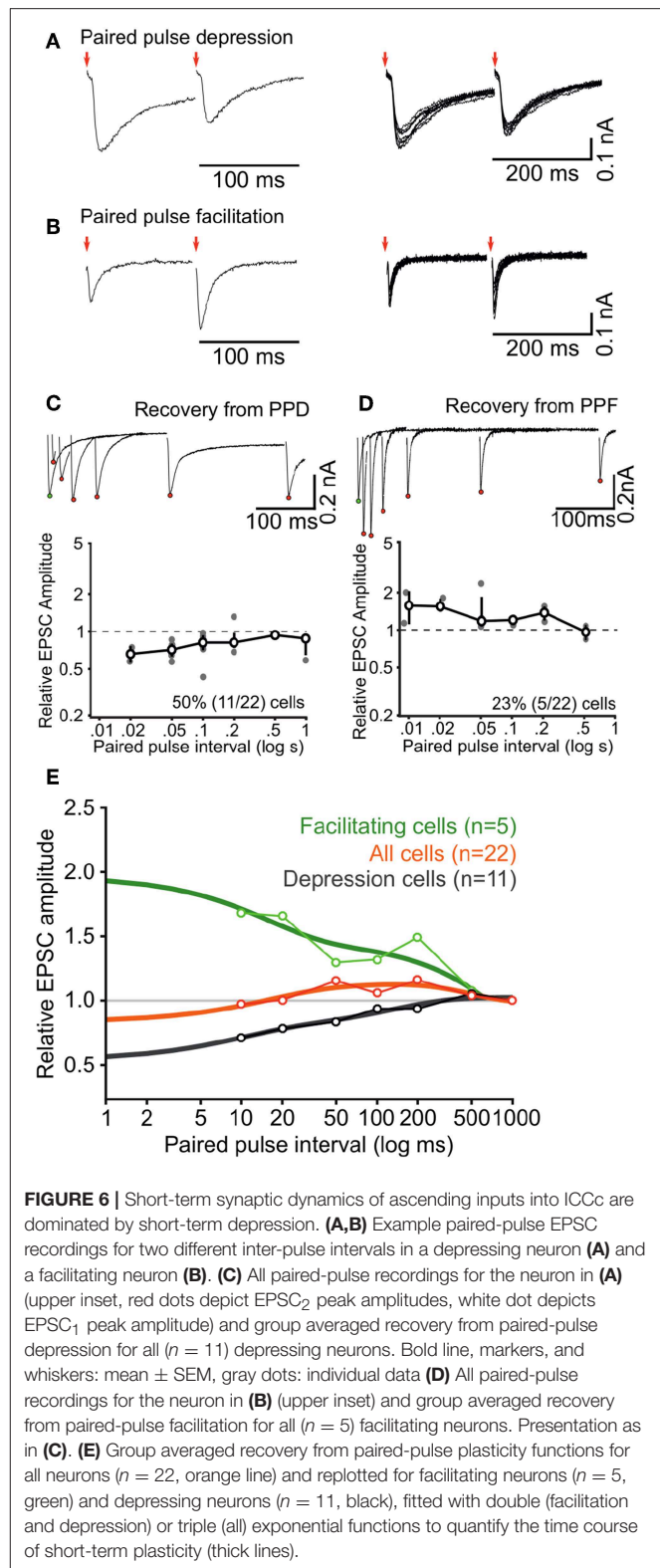
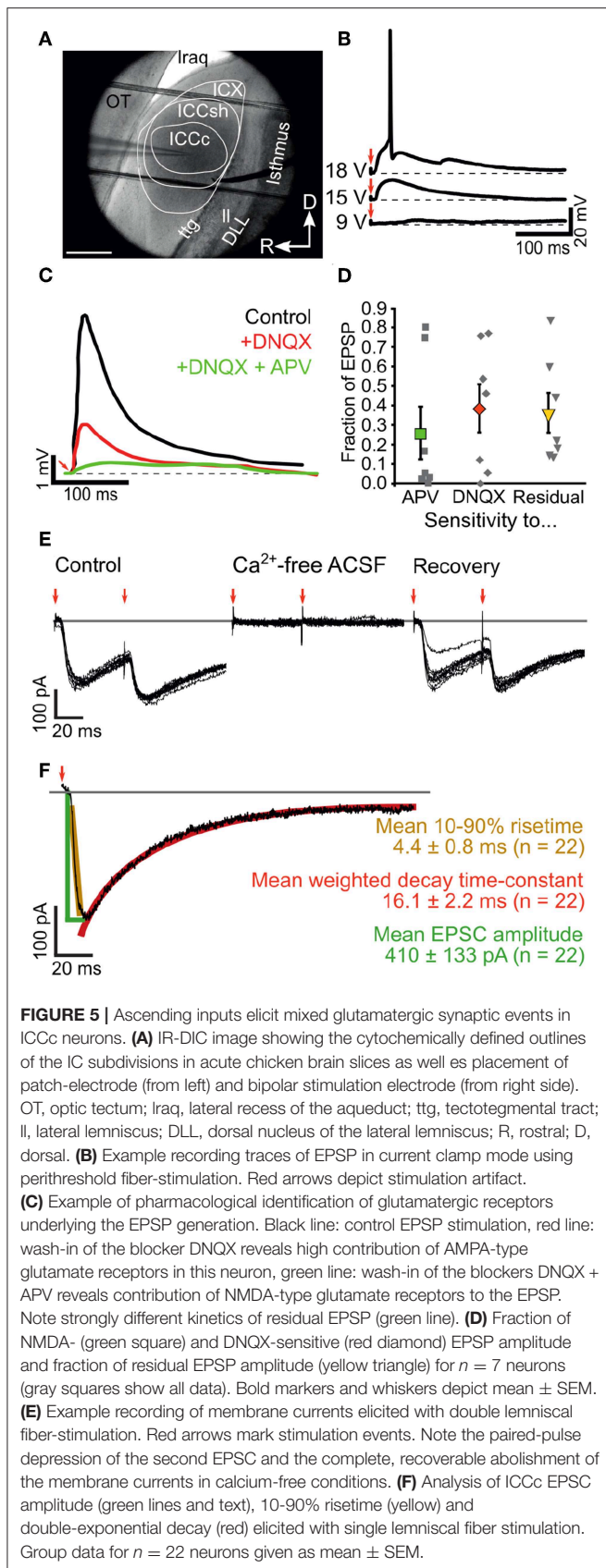
EPSP amplitude (Figure 5C). Thus, the AP5-sensitive part of the synaptic events accounted on average for another  $26\% \pm 13\%$  ( $N = 7$ ; median: 5.1%) of the EPSP amplitude. In most cells a substantial residual EPSP remained that could not be blocked by both DNQX and AP5. This residual component accounted on average for  $36\% \pm 10\%$  ( $N = 7$ ; median: 21.8%) of the EPSP amplitude. A statistical comparison of these data (Kruskal-Wallis test,  $\chi^2 = 1.68$ ,  $df = 20$ ,  $p = 0.43$ ) did not reveal any significant differences between the pharmacological groups. The identity of the residual EPSP could not be confirmed in our experiments. Neither a cholinergic blocker (50  $\mu$ M d-tubocurarin,  $N = 3$ ) nor a mix of glycinergic and gabaergic blockers (1  $\mu$ M strychnine + 10  $\mu$ M gabazine + 2  $\mu$ M CGP-55845,  $N = 2$ ) reduced the amplitudes of lemniscally evoked EPSP in ICCc neurons (data from these experiments not shown). We nevertheless concluded that overall a substantial proportion of the synaptic event elicited by ascending lemniscal fibers in chicken ICCc neurons was mediated by DNQX-sensitive, and thus AMPA- or Kainate-type, glutamatergic receptors.

In a different set of experiments we recorded postsynaptic inward currents from ICCc neurons in voltage-clamp mode ( $V_H = 60$  mV) upon electrical stimulation of ascending lemniscal fibers (Figures 5E,F). To rule out direct stimulation we showed that the occurrence of these inward currents depended on the presence of calcium ions in the bath solution (Figure 5E). Further indication for synaptic vs. direct origin of these inward currents was provided by the common occurrence of short-term plasticity: note the reduction of the inward current amplitude in Figure 5E upon the second pulse (red arrows). We will return to short-term plasticity in section 3.5. We initially analyzed the static properties of lemniscally evoked synaptic inward currents in  $N = 22$  ICCc neurons (Figure 5F) at room temperature and 200% threshold level. The inward currents were rapidly-rising (mean 10%-90% risetime of  $4.4 \pm 0.8$  ms,  $N = 22$ ) and quite strong (mean amplitude  $410 \pm 133$  pA,  $N = 22$ ). They showed a rapid decay best described by a double-exponential function (mean weighted decay time-constant of  $16.1 \pm 2.2$  ms,  $N = 22$ ).

Taken together we report here for the first time on ascending lemniscal synaptic connections in the chicken ICCc. These lemniscal axons elicited fast and strong inward currents via mostly AMPA-glutamatergic receptors. The kinetics and amplitude of these lemniscal synaptic events were in line with the function of the ICCc in temporal coding and sound-localization.

### 3.5. Synaptic Dynamics in the Chicken ICCc *in vitro* Are Dominated by Short-Term Depression

After having established the static or resting properties of the ascending excitatory connections to ICCc neurons we wanted to explore their dynamics upon repeated stimulation at short intervals. As detailed above synaptic short-term plasticity may be considered a major contributor to adaptive processes in many neuronal system. To our knowledge, nothing is known yet about short-term synaptic plasticity in the chicken ICCc. In order to get a first estimate of short-term synaptic dynamics we recorded in whole-cell voltage clamp mode from  $N = 22$  ICCc neurons



and employed a paired-pulse stimulus paradigm (Figure 6). We found that the majority of ICCc neurons (50%, 11/22) showed interval-dependent short-term depression (Figure 6A).

Surprisingly, other ICCc neurons (23%, 5/22) showed interval-dependent short-term facilitation (**Figure 6B**) and a number of ICCc neurons (27%, 6/22) showed some a mixture of both depression and facilitation and/or could not be clearly classified as either (not shown). By plotting the normalized average EPSC amplitudes vs. the paired-pulse interval we obtained functions of recovery from short-term plasticity for ICCc neurons. This was illustrated for a neuron with short-term depression in **Figure 6C**, upper plot. We average all paired-pulse recovery functions for depressing cells (**Figure 6C**, lower plot). The same analysis was performed for facilitating ICCc neurons (**Figure 6D**), the unclear/unclassified neurons (not shown) and all neurons (not shown). We then fitted double-exponential functions to the averaged recovery functions of depressing or facilitating ICCc (**Figure 6E**) and obtained a weighted time-constant of recovery. The depressing ICCc neurons on average recovered from short-term plasticity with  $\tau_w = 76\text{ms}$  ( $r^2 = 0.87$ ). Facilitating ICCc neurons recovered slower ( $\tau_w = 338\text{ms}$ ,  $r^2 = 0.71$ ). For the average of all ICCc neurons a tri-exponential fit (double-exponential depression + single-exponential facilitation) was sufficient to fit the data ( $r^2 = 0.75$ ,  $\tau_{\text{fast-depr.}} = 14.8\text{ ms}$ ,  $\tau_{\text{slow-depr.}} = 170\text{ ms}$ ,  $\tau_{\text{facil.}} = 194\text{ ms}$ ).

Did the categories of short-term plasticity correspond with the physiological groups determined before? We have data on AP firing pattern for all  $N = 22$  neurons analyzed in this section. When depressing synaptic inputs were observed, 63% (7/11) of neurons showed tonic AP firing behavior. When one of the other short-term plasticity categories (facilitating and unclear) were observed, only 37% (4/11) of the neurons showed tonic firing behavior. Whether this indicates a predominance of short-term depression in tonic firing neurons is unclear however, because the frequency of tonic neurons is unusually high (50%, 11/22) in the subset of neurons used for analysis of short-term plasticity.

Keeping the quantitative limitations of our dataset in mind we took the observed numbers of the categories and the severity of short-term plasticity into account and concluded for the population of ICCc neurons that the ascending lemniscal fibers on average showed moderate short-term depression at short intervals below 20 ms and weak facilitation for medium intervals (20 ms to 200 ms), before returning to baseline state at intervals of around 500 ms.

### 3.6. Adaptation Changes the Representation of Stimulus Onset in Chicken ICCc Neurons

We described firing pattern specific intrinsic adaptation for ICCc neurons in acute chicken brain slices (see section 3.3). We next wanted to estimate the impact this finding would have on information processing in ICCc neurons *in vivo*. For this, we established a simple first-order numerical simulation that uses the following assumptions based on our *in-vitro* findings:

(1) A hypothetical target neuron of ICCc output (most likely in the shell of the central nucleus of the inferior colliculus) was contacted by a high number of ICCc neurons, with the phasic and tonic neurons distributed according to the frequency of occurrence in our dataset (we chose: 70% phasic, 30% tonic).

(2) At rest (no adaptation) each theoretical ICCc output neuron produced a similar maximal number of AP as the *in-vitro* neurons during 100 ms current stimulation, which we chose to be one AP for phasic and four AP for tonic neurons (cf. **Figure 2**). In the adapted state the spike probability was reduced according to the adaptation functions of AP count (**Figures 4A1,B1**).

(3) Onset latency of responses to a given ongoing sound stimulus at rest were identical for the classes of neurons we found *in-vitro* (we chose 10 ms). In the adapted state, onset latency was prolonged according to the adaptation functions of the AP latency for each neuron class (**Figures 4A3,B3**).

(4) The *in-vitro* firing patterns were translated into a specific probability distribution of spike occurrence relative to stimulus onset, so that phasic neurons had a steep gaussian distribution of spiketimes around the onset of the stimulus (plus latency) and the tonic neurons had a very shallow (almost uniform) gaussian distribution aligned with the total duration of the stimulus that was cut off both at the onset (plus latency) and offset of the stimulus. No neuronal or synaptic physiology was simulated, only the numbers and times of AP occurrence was generated according to the premises outlined above. We admit that this represents a substantial simplification and that the resulting distribution of spiketimes represented only a very rough first-order approximation of onset and sustained response patterns described *in vivo*.

In addition to these simplified assumptions, the first order numerical model also ignored synaptic dynamics.

An schematic overview of the numerical simulation is shown in **Figure 7A** for the unadapted and in **Figure 7B** for an adapted state. Note that the AP probability is smaller in the adapted state and the latency of the generated AP is increased. The reduction of the AP probability for phasic or tonic neurons and the amount of latency increase was looked-up in the population adaptation curves in **Figures 4A1,A3,B1,B3**.

We randomly generated 100,000 ICCc responses to a sound stimulus presented 500 ms after the (unsimulated) first stimulus presentation and plotted a histogram of spiketimes relative to the simulated stimulus onset (ICCc output PSTH; **Figure 7C**, dark red line). The number of generated responses could be readily interpreted as resulting from 1000 repetitions of 100 ms stimulus presentation and the observation of a target neuron that received a total of 100 ICCc inputs, 70 phasic firing and 30 tonic firing. The resulting PSTH at 500 ms ISI showed a very pronounced peak of spike rate at 10 ms re the stimulus onset, because at very long ISI the temporally much more confined activity of the phasic neurons strongly dominated the simulated ICCc output. Indeed, simulated instantaneous spike rate at the onset peak was about 25x larger than the average sustained rate during the last half of the stimulus. With reduction of ISI the following trends were observed: the instantaneous rate of the onset peak was gradually reduced from 77.9 APs<sup>-1</sup> at 500 ms ISI to 7.4 APs<sup>-1</sup> at 1 ms ISI, the maximum response was shifted to longer latencies from 10 ms at 500 ms ISI to 18.5 ms at 1 ms ISI and the onset peak became increasingly broader. At very short intervals below 10 ms the onset-like characteristic of the PSTH was changed to a phasic-tonic or, at maximal adaptation, almost sustained-like response (see **Figure 7C**). By normalizing

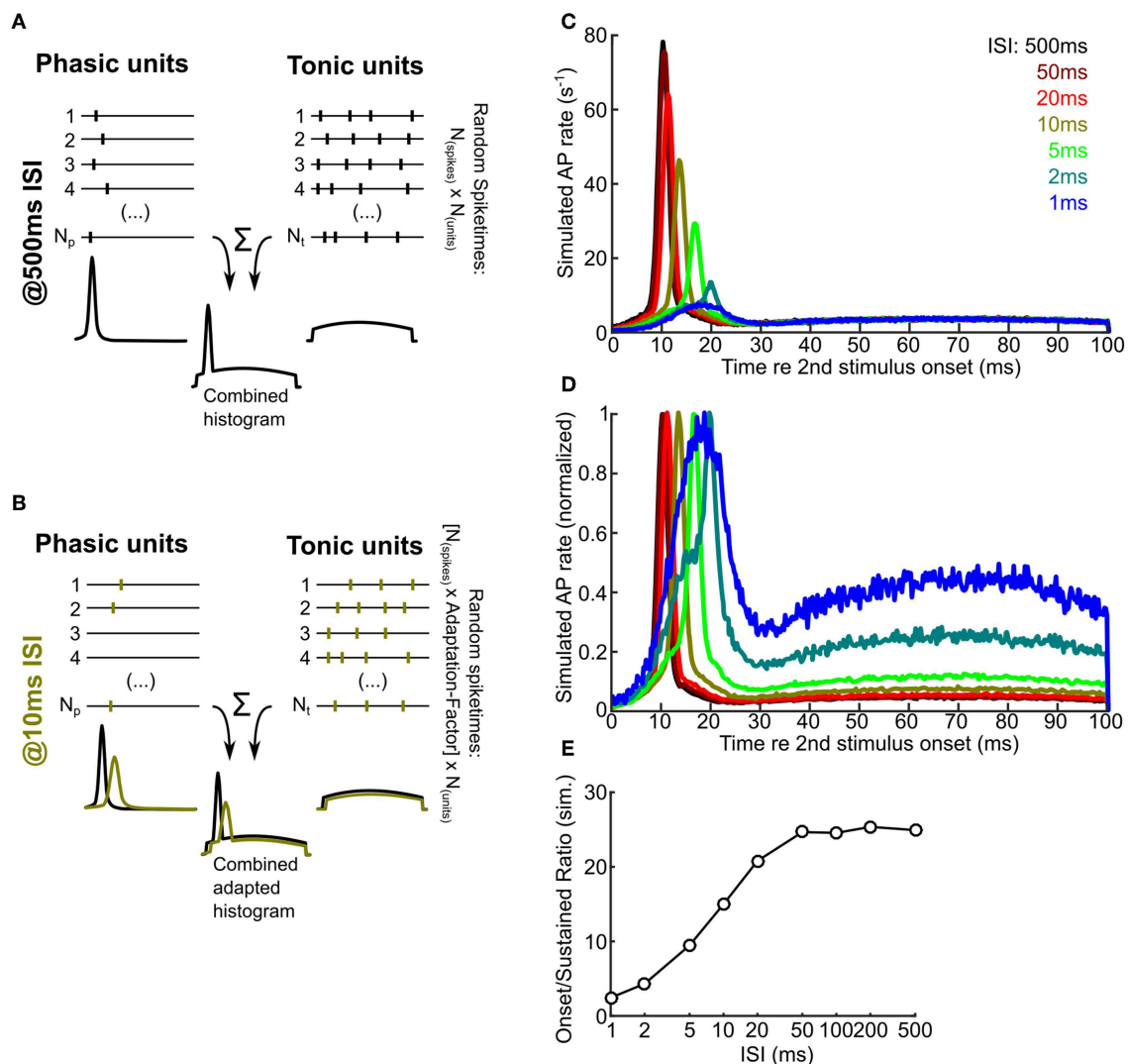


**FIGURE 7 |** A numerical model predicts that intrinsic adaptation alters the temporal characteristics of ICCc output. **(A,B)** A schematic drawing illustrating the principle of the numerical simulation. Random spiketimes are generated for a large number ( $N_p$ ,  $N_t$ ) of phasic **(A, left)** and tonic **(A, right)** neurons, shown as black traces (vertical bars depict occurrence of simulated action potentials). The peristimulus time histogram of the unit types is shown below the example traces and illustrate the random distributions from which the spiketimes are drawn. All spiketimes of all units ( $N_p + N_t$ ) are combined to generate a peristimulus time histogram. In the adapted state **(B)**, the spike probability is lower and the onset latency is larger (cf. **Figure 4**). Green bars / histograms depict the simulated adapted response, black histograms as in **A** for comparison. Please note that neither cellular nor synaptic mechanisms are simulated. **(C)** Simulated ICCc output as received by a hypothetical ICCsh neuron. Averaged PSTH of the second response for different ISI (from black, 500 ms to blue, 1 ms). Note the strong reduction of the onset peak and the shift of the latency of maximal response. **(D)** Simulated ICCc output as in **(C)** shown as averaged PSTH of the second response for different ISI. Note the drastic increase of the relative amount of AP generated during the ongoing part of the stimulus. Presentation as in **(C)**. **(E)** Quantification of the ratio between maximal AP rate in the onset-peak and the average ongoing AP rate for different ISI.

the PSTH for every ISI condition we tried to better visualize (**Figure 7D**) the temporal shift and broadening of the onset peak. In this figure the shape of PSTH at the minimal ISI of 1 ms (light blue) appeared peculiar. However, the shape may be explained by the residual activity of almost fully adapted phasic neurons at the onset and the broad, shallow distribution of spikes resulting from the minority of tonic neurons. We also quantified the ratio of sustained rate of the PSTH to the maximal rate at the onset of the PSTH and plotted this against ISI (**Figure 7E**). The ratio

changed from 24.9 at 500 ms ISI to 2.4 at 1 ms ISI. We interpret this plot as the spike rate adaptation of the hypothetical ICCsh neuron that was caused by the intrinsic adaptation “upstream” in the ICCc neurons. It showed that with shorter ISI the onset feature of a stimulus segment was less represented and the representation of the ongoing features of the sound stimulus was relatively much more dominant in the ICCc output. We therefore conclude from our numerical simulation that intrinsic adaptation has the potential to change and shape the relative representation

of different features of a perceived sound stimulus in the avian ICCc.

## 4. DISCUSSION

In this study we showed intrinsic biophysical and synaptic dynamics of neurons in the chicken ICCc that shape adaptation to repeated stimulus presentation at this level of the auditory pathway. We found with whole-cell recordings in acute brain slices that two classes of neurons could be distinguished in the chicken ICCc based on action potential firing pattern: phasic/onset and tonic/sustained firing neurons. We measured intrinsic adaptation of excitability by analyzing the number and kinetics of action potentials upon repeated stimulation and found tonic neurons to have weaker but more prolonged adaptation whereas phasic neurons showed stronger adaptation but also faster recovery from adaptation. We also characterized ascending glutamatergic synaptic inputs into the chicken ICCc for the first time and demonstrated that a majority of synaptic connections showed a form of short term synaptic depression. Together, intrinsic and synaptic dynamics thus must shape the action potential output of chicken ICCc neurons in a celltype specific manner. In a phenomenological model of ICCc population activity we found that the temporal characteristics of ICCc population output were shifted from strongly responding to the onset of stimulations at long inter-stimulation intervals to emphasizing the encoding of ongoing sections of the stimulus in situations of low inter-stimulation intervals or for sustained inputs. These results show that adaptive processes in the IC can be understood by study of the underlying physiological processes that contribute to the dynamics of excitation on the level of individual neurons.

The connectivity and functional physiology of the avian IC was best described in the barn owl, an auditory specialist for hunting in low light conditions using sound localization (Singheiser et al., 2012b). Accordingly, the brain areas used for sound localization circuitry are enlarged in the barn owl brain (Gutiérrez-Ibáñez et al., 2011) and tuning of the neurons to binaural parameters is very distinct and almost stereotypically precise. This is not necessarily the case in the chicken, an auditory generalist. Histologically, the overall structure and subdivisions of the IC are nevertheless also present in the chicken (Puelles et al., 1994; Niederleitner and Luksch, 2012). Thus, we presume that the pathway described in the owl (Singheiser et al., 2012b) from the brainstem to the ICCc, on to the shell of the ICC and subsequently to space-specific neurons in the external nucleus of the IC is also present in the chicken. However, tracing studies showed that ascending binaural inputs from the ITD-coding nucleus laminaris neurons only formed a small subset of inputs in to the chicken IC (Wang and Karten, 2010), a substantial part of the histochemically defined ICCc received inputs from other parts of the cochlear nucleus complex. In accordance with this, a recent physiological study in anesthetized chicken found the same physiological response types known from the barn owl IC, albeit embedded in a greater variety of response types and unit classes (Aralla et al., 2018). The same study

suggested that in principle the grid-like organization of tuning to physical parameters (i.e., ITD and frequency) as described in the barn owl (Wagner et al., 2002; Bremen et al., 2007) can be found in the chicken, in a somewhat more diffuse form. Thus, we cannot rule out that some of the diversity of intrinsic and especially synaptic dynamics we observed between unit types in our data can be explained by neurons belonging to completely different ascending streams of information, i.e., the narrow-band ITD coding pathway vs. the frequency and intensity encoding portion of the auditory pathway (Wang and Karten, 2010). It was reported from the mammalian IC that neurons belonging to the non-lemniscal pathway usually show a greater diversity of adaptive phenomena (Nelken, 2014). Based on our reconstructions we located all neurons included in this study in the ICCc, which we defined immunocytochemically following the work of Puelles et al. (1994) and Niederleitner and Luksch (2012). Lacking conclusive histological evidence we cannot say whether this immunocytochemically defined ICC-subdivision is identical to the area of the ICC receiving ITD-sensitive inputs, as shown by Wang and Karten (2010). We conclude that it appears likely that in the chicken a greater variety of physiological and functional properties can be explained by a greater proportion of the non-ITD coding components of the ascending auditory connections, even in the area identified as the core of the ICC.

In our current study we described physiologically defined groups of neurons in the ICCc of the chicken with regards to action potential firing pattern, biophysical properties of the membrane as well as strength and dynamics of the intrinsic and synaptic adaptation. From our data and other studies it becomes apparent that neurons in the IC do indeed form distinct functional categories best described by a combination of parameters (Ito and Oliver, 2012). For example, we describe phasic firing neurons that not only showed biophysical properties tuned toward temporal precision but also recovered faster from adaptation than other ICCc neurons. One is tempted to speculate that the phasic/onset neurons play a functional role in the ITD-coding narrow-band part of the IC circuitry and are specialized to encode differences in onsets or transients of sounds with high precision. However, our results showed no clear correlation between morphology and physiology or function of the IC neurons. By analyzing the 3D structure of the dendritic trees in detail we could indeed confirm earlier reports from the chicken IC that stellate and elongated neurons represent distinct morphological groups (Niederleitner and Luksch, 2012), possibly related to the laminar functional organization of the ICC (Schreiner and Langner, 1997; Wagner et al., 2002; Malmierca et al., 2008). Interestingly, there is not a single physiological parameter that on average differed between these morphologically defined groups. This is in line with reports from the mammalian IC (Peruzzi et al., 2000). Although a greater diversity of physiologically defined neuron groups were found in the mammalian IC (Peruzzi et al., 2000), possibly due to the postnatal development stage usually used in these experiments, no correlations between form and physiology were apparent in the mammalian IC either. In fact, the understanding of IC circuitry is hampered by the lack of functionally defined neuron types. Only very recently have studies, employing genetic

and optogenetic approaches, begun to identify and characterize molecularly defined classes of IC neurons in mice (Goyer et al., 2019). We hope that these studies will finally be able to bridge the gap between *in-vitro* studies and *in-vivo* physiology in the IC and contribute much to resolving the functional circuitry of the IC in both mammals and other vertebrates.

To our knowledge we are the first to characterize ascending synaptic connections into the ICCc of birds. Similar to ascending inputs into the mammalian ICC (Ma et al., 2002; Wu et al., 2002, 2004; Sivaramakrishnan and Oliver, 2006) we describe glutamatergic connections that are mediated to a large degree by both AMPA- and NMDA-type glutamate receptors. This is also in line with the few studies that analyzed synaptic connections between the shell of the ICC and the external nucleus in birds (Penzo and Peña, 2009, 2011). These studies also suggested a combined AMPA- and NMDA-mediated glutamatergic transmission. The postsynaptic currents elicited by lemniscal fiber-stimulation have a much smaller amplitude and much slower kinetics than postsynaptic currents measured in the brainstem nuclei of the auditory pathway (Brenowitz and Trussell, 2001; Goyer et al., 2015), in line with the lesser degree of physiological and morphological specialization. However, compared to reports from the mammalian IC, the ICCc EPSC have similar rise and decay kinetics (Ma et al., 2002; Wu et al., 2002, 2004; Sivaramakrishnan and Oliver, 2006). Furthermore, the EPSC in the ICCc are larger than EPSC recorded in the external nucleus of the IC in the chicken (Penzo and Peña, 2009). We also analyzed short-term plasticity for ascending synaptic connections in the ICCc. The majority of synapses in our dataset showed a form of short-term depression. Compared to synapses in the lower auditory pathway (Cook et al., 2003; Oline and Burger, 2014; Goyer et al., 2015) the short-term depression is not very severe which is surprising given the embryonic recording age of our dataset. We conclude that ascending synaptic connections in the ICCc show a certain resistance against short-term depression. Unfortunately, there is little data on short-term plasticity in the IC to compare our results with. Similar to our findings one study reports the occurrence of both short-term depression (caused mostly by the AMPA component) and facilitation (due to the NMDA component) in glutamatergic synapses in the rat IC (Wu et al., 2004). The relative differences in the abundance of AMPA vs. NMDA channels in ICCc neurons would thus provide an elegant explanation of the diversity of short-term dynamics we found. For technical reasons we however did not systematically check the AMPA vs. NMDA ratio in the neurons for which we quantified short-term plasticity. At the ICCsh to ICX synapse at least two types of long term plasticity have been described (Penzo and Peña, 2009, 2011), but short-term plasticity was not analyzed. Overall we conclude that our dataset is a valuable first approach to describing the synaptic dynamics in the IC, but more studies need to be performed before a definitive answer about the role of synaptic dynamics in sound encoding in the IC can be given.

We sought to better understand adaptive phenomena described in studies performed in anesthetized animals by analyzing intrinsic and synaptic dynamics of the ICCc neurons. But do our results agree with the *in-vivo* studies? First, one has

to keep in mind that by studying the processes that contribute to adaptation in isolation, a considerable amount of complexity might be missed. This complexity might arise from dynamic interactions between various processes, which is not possible in the *in-vitro* system employing simple current stimuli. Second, *in vivo* neurons receive a high number of synaptic contacts as inputs, which might fundamentally follow different physiological rules than we observe with current stimuli *in vitro*. Nevertheless, we think that we can compare the adaptation of action potential count and first AP latency to physiological data *in vivo*, albeit with some caution. Furthermore, our recordings were performed at room temperature. Usually a factor of 3 can be assumed for every 10°C difference (Hille, 2001). This means that the single-exponential or fast double-exponential time-constants of the intrinsic parameters we documented ( $\leq 20$  ms) could almost match the very fast components of adaptation (1.5 ms) that were sometimes reported *in vivo* (Singheiser et al., 2012a). Due to the rapid time-constant this type of adaptation of excitability is most likely related to the relative refractory period (Kuenzel et al., 2011; Yang and Xu-Friedman, 2015) and thus mediated by sodium channel inactivation and lingering potassium channel activation. The shape of the responses, especially for the phasic firing neurons, and the responses at the shortest ISIs could also be shaped by low-voltage activated potassium channels of the Kv1 family, which are expressed in the auditory pathway (Trussell, 1997). This could also explain the more severe adaptation at short intervals present in phasic firing ICCc neurons in our study. The majority of *in-vivo* studies in the IC report time-constants of adaptation in the range of tens of milliseconds or longer (Gutfreund and Knudsen, 2006; Singheiser et al., 2012a; Ferger et al., 2018). We conclude that only the synaptic short-term depression we demonstrated and the slower double-exponential changes of excitability can thus fully explain *in-vivo* adaptation phenomena. In the bouton-like glutamatergic synapses of the IC short-term depression is most likely mediated by vesicle pool depletion (Friauf et al., 2015). The slow changes of intrinsic excitability on the other hand could be mediated by calcium-activated potassium channels such as the BK or SK channels that cause repolarization and slow afterhyperpolarization. Indeed, calcium-activated potassium currents ( $K_{Ca}$ ) have been reported to occur differentially in physiologically defined neuron types in the mouse IC (Sivaramakrishnan and Oliver, 2001). These authors find that onset type neurons lack  $K_{Ca}$  while many sustained firing neurons show various types of  $K_{Ca}$  currents. This would provide an explanation for smaller contribution of slow adaptation components in the chicken ICCc phasic neurons, but  $K_{Ca}$  was not investigated specifically in our study.

In this study embryonic brains were examined. Although the structures projecting to the ICCc in the auditory brainstem are quite mature already before hatching (Gao and Lu, 2008), further maturation of ICCc physiology and circuitry is likely to be expected. Chickens can indeed hear airborne sounds as early as P17 (Jones et al., 2006) and show sensory functionality immediately after hatching (only one or two days after the time period examined in our study). In mammals, the inferior colliculus is known to develop toward mature-like functions for several days after the onset of hearing (Shnerson and Willott,

1979). Also, the physiology of ascending synaptic inputs still changes in the first one or 2 weeks after hearing onset (Kitagawa and Sakaba, 2019). Very little information is unfortunately available about maturation of IC physiology in the chicken. We conclude that the chicken ICCc is functional but not yet fully matured at the embryonic ages we examined. We thus caution the reader that the absolute values of time-constants of adaptation we describe probably will differ between the late embryonic and the mature state.

With the help of a phenomenological model we predicted drastic changes of the shape of the response to sound stimuli in subsequent neurons of the IC (i.e., the shell of the ICC), caused by the differential adaptation in ICCc neurons. We supposed that subsequent neurons receive an bouquet of input types simply based on the distribution of neurons types we found. The number of ICCc axons converging on ICCsh neurons and their physiological identity has not been documented. Also, no neuronal or synaptic physiology whatsoever was included in the model. Thus, some assumptions of our model are highly speculative. However, the fact that the shape of the PSTH is altered by adaptive processes has been described before in other animals or brain areas (Epping, 1990; Pérez-González and Malmierca, 2012). This challenges the classical view that the shape of the PSTH conveys the fixed coding or information processing function of the neuron. Our model rather suggests that due to the adaptation of their inputs alone ICCsh neurons respond maximally to different aspects of the sound stimulus, dependent on the auditory context. In long intervals (or silence) onsets and transients cause strong activation of the majority of (phasic) ICCc neurons. This would facilitate detection and localization of sudden stimuli in quiet surroundings (cf. Dean et al., 2005). During ongoing stimulation the onset neurons strongly adapt and the information is then mainly processed by sustained neurons, which would possibly emphasize identification and analysis of sounds by spectral and intensity cues. We hypothesize that due to differential adaptation of their inputs the neurons in the IC circuitry could thus participate in several quite different physiological roles depending on stimulus context. Adaptive processes are indeed often thought to underlie even more advanced auditory processing functions like

novelty detection (Ulanovsky et al., 2003), contrast enhancement (Willmore et al., 2016; Cooke et al., 2018), auditory attention (Fritz et al., 2007) or segregation of auditory streams (Scholes et al., 2015). Whether the dynamic change of stimulus preference of ICCsh neurons through adaptation can be demonstrated in anesthetized animals must be subject to further studies.

## DATA AVAILABILITY

The datasets generated for this study are available on request to the corresponding author.

## ETHICS STATEMENT

All experimental procedures performed on animals in this study were approved by the local animal welfare officer and state authorities (Landespräsidium für Natur, Umwelt und Verbraucherschutz Nordrhein-Westfalen, Recklinghausen, Germany).

## AUTHOR CONTRIBUTIONS

TK conceived and designed the study. SM, JW, and TK performed experiments and analyzed data. SM and TK wrote the manuscript. All authors discussed results and commented on the manuscript.

## FUNDING

Part of this work was supported by the DFG Priority Program 1608 Ultrafast and temporally precise information processing: Normal and dysfunctional hearing [KU2529/2-1, KU2529/2-2].

## ACKNOWLEDGMENTS

We thank Stefanie Kurth and Andrzej Steckiewicz (Institute for Biology II, RWTH Aachen University) for their excellent technical assistance with the 3D-reconstruction of neurons. We thank Hermann Wagner for discussions and critical comments on the manuscript.

## REFERENCES

- Aelst, S. V., and Rousseeuw, P. (2009). Minimum volume ellipsoid. *Wiley Int. Rev. Comput. Stat.* 1, 71–82. doi: 10.1002/wics.19
- Aralla, R., Ashida, G., and Köppl, C. (2018). Binaural responses in the auditory midbrain of chicken (*Gallus gallus*). *Eur J Neurosci.* doi: 10.1111/ejn.13891
- Ayala, Y. A., and Malmierca, M. S. (2012). Stimulus-specific adaptation and deviance detection in the inferior colliculus. *Front. Neural Circ.* 6:89. doi: 10.3389/fncir.2012.00089
- Ayala, Y. A., Pérez-González, D., and Malmierca, M. S. (2016). Stimulus-specific adaptation in the inferior colliculus: the role of excitatory, inhibitory and modulatory inputs. *Biol. Psychol.* 116, 10–22. doi: 10.1016/j.biopsycho.2015.06.016
- Bremen, P., Poganiatz, I., von Campenhausen, M., and Wagner, H. (2007). Sensitivity to interaural time difference and representation of azimuth in central nucleus of inferior colliculus in the barn owl. *J. Compar. Physiol. A* 193, 99–112. doi: 10.1007/s00359-006-0172-z
- Brenowitz, S., and Trussell, L. O. (2001). Maturation of synaptic transmission at end-bulb synapses of the cochlear nucleus. *J. Neurosci.* 21, 9487–9498. doi: 10.1523/JNEUROSCI.21-23-09487.2001
- Cook, D. L., Schwandt, P. C., Grande, L. A., and Spain, W. J. (2003). Synaptic depression in the localization of sound. *Nature* 421, 66–70. doi: 10.1038/nature01248
- Cooke, J. E., King, A. J., Willmore, B. D. B., and Schnupp, J. W. H. (2018). Contrast gain control in mouse auditory cortex. *J. Neurophysiol.* 120, 1872–1884. doi: 10.1152/jn.00847.2017
- Dean, I., Harper, N. S., and McAlpine, D. (2005). Neural population coding of sound level adapts to stimulus statistics. *Nat. Neurosci.* 8, 1684–1689. doi: 10.1038/nn1541
- Debanne, D., Inglebert, Y., and Russier, M. (2019). Plasticity of intrinsic neuronal excitability. *Curr. Opin. Neurobiol.* 54, 73–82. doi: 10.1016/j.conb.2018.09.001
- Epping, W. J. (1990). Influence of adaptation on neural sensitivity to temporal characteristics of sound in the dorsal medullary nucleus

- and torus semicircularis of the grassfrog. *Hear. Res.* 45, 1–13. doi: 10.1016/0378-5955(90)90178-R
- Ferger, R., Pawlowsky, K., Singheiser, M., and Wagner, H. (2018). Response adaptation in the barn owl's auditory space map. *J. Neurophysiol.* 119, 1235–1247. doi: 10.1152/jn.00769.2017
- Friauf, E., Fischer, A. U., and Fuhr, M. F. (2015). Synaptic plasticity in the auditory system: a review. *Cell Tissue Res.* 361, 177–213. doi: 10.1007/s00441-015-2176-x
- Fritz, J. B., Elhilali, M., David, S. V., and Shamma, S. A. (2007). Auditory attention-focusing the searchlight on sound. *Curr. Opin. Neurobiol.* 17, 437–455. doi: 10.1016/j.conb.2007.07.011
- Gao, H., and Lu, Y. (2008). Early development of intrinsic and synaptic properties of chicken nucleus laminaris neurons. *Neuroscience* 153, 131–143. doi: 10.1016/j.neuroscience.2008.01.059
- Goyer, D., Fensky, L., Hilverling, A. M., Kurth, S., and Kuenzel, T. (2015). Expression of the postsynaptic scaffold PSD-95 and development of synaptic physiology during giant terminal formation in the auditory brainstem of the chicken. *Eur. J. Neurosci.* 41, 1416–1429. doi: 10.1111/ejn.12902
- Goyer, D., Kurth, S., Gillet, C., Keine, C., Rübsamen, R., and Kuenzel, T. (2016). Slow cholinergic modulation of spike probability in ultra-fast time-coding sensory neurons. *eNeuro* 3:ENEURO.0186-16.2016. doi: 10.1523/ENEURO.0186-16.2016
- Goyer, D., Silveira, M. A., George, A. P., Beebe, N. L., Schofield, B. R., and Roberts, M. T. (2019). A feedforward inhibitory circuit that limits epsp duration in the inferior colliculus of mice. *Assoc. Res. Otolaryngol. Abs.* 42:223.
- Gutfreund, Y., and Knudsen, E. I. (2006). Adaptation in the auditory space map of the barn owl. *J. Neurophysiol.* 96, 813–825. doi: 10.1152/jn.01144.2005
- Gutiérrez-Ibáñez, C., Iwaniuk, A. N., and Wylie, D. R. (2011). Relative size of auditory pathways in symmetrically and asymmetrically eared owls. *Brain Behav. Evol.* 78, 286–301. doi: 10.1159/000330359
- Hamburger, V., and Hamilton, H. L. (1951). A series of normal stages in the development of the chick embryo. *J. Morphol.* 88, 49–92.
- Hamill, O. P., Marty, A., Neher, E., Sakmann, B., and Sigworth, F. J. (1981). Improved patch-clamp techniques for high-resolution current recording from cells and cell-free membrane patches. *Pflügers Archiv. Eur. J. Physiol.* 391, 85–100.
- Hille, B. (2001). *Ion Channels of Excitable Membranes*. Sunderland, MA: Sinauer Associates.
- Ingham, N. J., and McAlpine, D. (2004). Spike-frequency adaptation in the inferior colliculus. *J. Neurophysiol.* 91, 632–645. doi: 10.1152/jn.00779.2003
- Ito, T., and Oliver, D. L. (2012). The basic circuit of the ic: tectothalamic neurons with different patterns of synaptic organization send different messages to the thalamus. *Front. Neural Circ.* 6:48. doi: 10.3389/fncir.2012.00048
- Jones, T. A., Jones, S. M., and Paggett, K. C. (2006). Emergence of hearing in the chicken embryo. *J. Neurophysiol.* 96, 128–141. doi: 10.1152/jn.00599.2005
- Kitagawa, M., and Sakaba, T. (2019). Developmental changes in the excitatory short-term plasticity at input synapses in the rat inferior colliculus. *Eur. J. Neurosci.* doi: 10.1111/ejn.14422. [Epub ahead of print].
- Kuenzel, T., Borst, J. G. G., and van der Heijden, M. (2011). Factors controlling the input-output relationship of spherical bushy cells in the gerbil cochlear nucleus. *J. Neurosci.* 31, 4260–4273. doi: 10.1523/JNEUROSCI.5433-10.2011
- Litovsky, R. Y., and Yin, T. C. (1998). Physiological studies of the precedence effect in the inferior colliculus of the cat. ii. neural mechanisms. *J. Neurophysiol.* 80, 1302–1316.
- Longair, M. H., Baker, D. A., and Armstrong, J. D. (2011). Simple neurite tracer: open source software for reconstruction, visualization and analysis of neuronal processes. *Bioinformatics* 27, 2453–2454. doi: 10.1093/bioinformatics/btr390
- Ma, C. L., Kelly, J. B., and Wu, S. H. (2002). Ampa and nmda receptors mediate synaptic excitation in the rat's inferior colliculus. *Hear. Res.* 168, 25–34. doi: 10.1016/S0378-5955(02)00370-2
- Malmierca, M. S., Anderson, L. A., and Antunes, F. M. (2015). The cortical modulation of stimulus-specific adaptation in the auditory midbrain and thalamus: a potential neuronal correlate for predictive coding. *Front. Syst. Neurosci.* 9:19. doi: 10.3389/fnsys.2015.00019
- Malmierca, M. S., Cristaudo, S., Pérez-González, D., and Covey, E. (2009). Stimulus-specific adaptation in the inferior colliculus of the anesthetized rat. *J. Neurosci.* 29, 5483–5493. doi: 10.1523/JNEUROSCI.4153-08.2009
- Malmierca, M. S., Izquierdo, M. A., Cristaudo, S., Hernández, O., Pérez-González, D., Covey, E., et al. (2008). A discontinuous tonotopic organization in the inferior colliculus of the rat. *J. Neurosci.* 28, 4767–4776. doi: 10.1523/JNEUROSCI.0238-08.2008
- Nelken, I. (2014). Stimulus-specific adaptation and deviance detection in the auditory system: experiments and models. *Biol. Cybernet.* 108, 655–663. doi: 10.1007/s00422-014-0585-7
- Nelson, P. C., Smith, Z. M., and Young, E. D. (2009). Wide-dynamic-range forward suppression in marmoset inferior colliculus neurons is generated centrally and accounts for perceptual masking. *J. Neurosci.* 29, 2553–2562. doi: 10.1523/JNEUROSCI.5359-08.2009
- Niederleithner, B., and Luksch, H. (2012). Neuronal morphology in subdivisions of the inferior colliculus of chicken (*Gallus gallus*). *J. Chem. Neuroanat.* 44, 24–33. doi: 10.1016/j.jchemneu.2012.03.004
- Oline, S. N., and Burger, R. M. (2014). Short-term synaptic depression is topographically distributed in the cochlear nucleus of the chicken. *J. Neurosci.* 34, 1314–1324. doi: 10.1523/JNEUROSCI.3073-13.2014
- Penzo, M. A., and Peña, J. L. (2009). Endocannabinoid-mediated long-term depression in the avian midbrain expressed presynaptically and postsynaptically. *J. Neurosci.* 29, 4131–4139. doi: 10.1523/JNEUROSCI.5466-08.2009
- Penzo, M. A., and Peña, J. L. (2011). Depolarization-induced suppression of spontaneous release in the avian midbrain. *J. Neurosci.* 31, 3602–3609. doi: 10.1523/JNEUROSCI.6388-10.2011
- Pérez-González, D., Hernández, O., Covey, E., and Malmierca, M. S. (2012). Gaba(a)-mediated inhibition modulates stimulus-specific adaptation in the inferior colliculus. *PLoS ONE* 7:e34297. doi: 10.1371/journal.pone.0034297
- Pérez-González, D., and Malmierca, M. S. (2012). Variability of the time course of stimulus-specific adaptation in the inferior colliculus. *Front. Neural Circ.* 6:107. doi: 10.3389/fncir.2012.00107
- Pérez-González, D., and Malmierca, M. S. (2014). Adaptation in the auditory system: an overview. *Front. Integr. Neurosci.* 8:19. doi: 10.3389/fnint.2014.00019
- Peruzzi, D., Sivaramakrishnan, S., and Oliver, D. L. (2000). Identification of cell types in brain slices of the inferior colliculus. *Neuroscience* 101, 403–416. doi: 10.1016/S0306-4522(00)00382-1
- Puelles, L., de-la Torre, M. M., Paxinos, G., Watson, C., and Martinez, S. (2007). *The Chick Brain in Stereotaxic Coordinates: An Atlas featuring Neuromeric Subdivisions and Mammalian Homologies, 1st Edn*. New York, NY: Academic Press.
- Puelles, L., Robles, C., Martínez-de-la Torre, M., and Martínez, S. (1994). New subdivision schema for the avian torus semicircularis: neurochemical maps in the chick. *J. Compar. Neurol.* 340, 98–125.
- Reches, A., and Gutfreund, Y. (2008). Stimulus-specific adaptations in the gaze control system of the barn owl. *J. Neurosci.* 28, 1523–1533. doi: 10.1523/JNEUROSCI.3785-07.2008
- Reches, A., Netser, S., and Gutfreund, Y. (2010). Interactions between stimulus-specific adaptation and visual auditory integration in the forebrain of the barn owl. *J. Neurosci.* 30, 6991–6998. doi: 10.1523/JNEUROSCI.5723-09.2010
- Schindelin, J., Arganda-Carreras, I., Frise, E., Kaynig, V., Longair, M., Pietzsch, T., et al. (2012). Fiji: an open-source platform for biological-image analysis. *Nat. Methods* 9, 676–682. doi: 10.1038/nmeth.2019
- Scholes, C., Palmer, A. R., and Sumner, C. J. (2015). Stream segregation in the anesthetized auditory cortex. *Hear. Res.* 328, 48–58. doi: 10.1016/j.heares.2015.07.004
- Schreiner, C. E., and Langner, G. (1997). Laminar fine structure of frequency organization in auditory midbrain. *Nature* 388, 383–386.
- Shnerson, A., and Willott, J. F. (1979). Development of inferior colliculus response properties in c57bl/6j mouse pups. *Exp. Brain Res.* 37, 373–385.
- Sholl, D. A. (1953). Dendritic organization in the neurons of the visual and motor cortices of the cat. *J. Anatomy* 87, 387–406.
- Singheiser, M., Ferger, R., von Campenhausen, M., and Wagner, H. (2012a). Adaptation in the auditory midbrain of the barn owl (*Tyto alba*) induced by tonal double stimulation. *Eur. J. Neurosci.* 35, 445–456. doi: 10.1111/j.1460-9568.2011.07967.x
- Singheiser, M., Gutfreund, Y., and Wagner, H. (2012b). The representation of sound localization cues in the barn owl's inferior colliculus. *Front. Neural Circ.* 6:45. doi: 10.3389/fncir.2012.00045

- Sivaramakrishnan, S., and Oliver, D. L. (2001). Distinct k currents result in physiologically distinct cell types in the inferior colliculus of the rat. *J. Neurosci.* 21, 2861–2877. doi: 10.1523/JNEUROSCI.21-08-02861.2001
- Sivaramakrishnan, S., and Oliver, D. L. (2006). Neuronal responses to lemniscal stimulation in laminar brain slices of the inferior colliculus. *J. Assoc. Res. Otolaryngol.* 7, 1–14. doi: 10.1007/s10162-005-0017-4
- Spitzer, M. W., Bala, A. D. S., and Takahashi, T. T. (2004). A neuronal correlate of the precedence effect is associated with spatial selectivity in the barn owl's auditory midbrain. *J. Neurophysiol.* 92, 2051–2070. doi: 10.1152/jn.01235.2003
- Trussell, L. O. (1997). Cellular mechanisms for preservation of timing in central auditory pathways. *Curr. Opin. Neurobiol.* 7, 487–92. doi: 10.1016/S0959-4388(97)80027-X
- Ulanovsky, N., Las, L., and Nelken, I. (2003). Processing of low-probability sounds by cortical neurons. *Nat. Neurosci.* 6, 391–398. doi: 10.1038/nn1032
- Wagner, H., Mazer, J. A., and von Campenhausen, M. (2002). Response properties of neurons in the core of the central nucleus of the inferior colliculus of the barn owl. *Eur. J. Neurosci.* 15, 1343–1352. doi: 10.1046/j.1460-9568.2002.01970.x
- Wang, Y., and Karten, H. J. (2010). Three subdivisions of the auditory midbrain in chicks (*Gallus gallus*) identified by their afferent and commissural projections. *J. Compar. Neurol.* 518, 1199–219. doi: 10.1002/cne.22269
- Wang, Y., and Peña, J. L. (2013). Direction selectivity mediated by adaptation in the owl's inferior colliculus. *J. Neurosci.* 33, 19167–19175. doi: 10.1523/JNEUROSCI.2920-13.2013
- Weigel, S., and Luksch, H. (2012). Spatiotemporal analysis of electrically evoked activity in the chicken optic tectum: a VSDI study. *J. Neurophysiol.* 107, 640–648. doi: 10.1152/jn.00541.2011
- Willmore, B. D. B., Schoppe, O., King, A. J., Schnupp, J. W. H., and Harper, N. S. (2016). Incorporating midbrain adaptation to mean sound level improves models of auditory cortical processing. *J. Neurosci.* 36, 280–289. doi: 10.1523/JNEUROSCI.2441-15.2016
- Wu, S. H., Ma, C. L., and Kelly, J. B. (2004). Contribution of ampa, nmda, and gaba(a) receptors to temporal pattern of postsynaptic responses in the inferior colliculus of the rat. *J. Neurosci.* 24, 4625–4634. doi: 10.1523/JNEUROSCI.0318-04.2004
- Wu, S. H., Ma, C. L., Sivaramakrishnan, S., and Oliver, D. L. (2002). Synaptic modification in neurons of the central nucleus of the inferior colliculus. *Hear. Res.* 168, 43–54. doi: 10.1016/S0378-5955(02)00375-1
- Yang, H., and Xu-Friedman, M. A. (2015). Skipped-stimulus approach reveals that short-term plasticity dominates synaptic strength during ongoing activity. *J. Neurosci.* 35, 8297–307. doi: 10.1523/JNEUROSCI.4299-14.2015

**Conflict of Interest Statement:** The authors declare that the research was conducted in the absence of any commercial or financial relationships that could be construed as a potential conflict of interest.

Copyright © 2019 Malinowski, Wolf and Kuenzel. This is an open-access article distributed under the terms of the Creative Commons Attribution License (CC BY). The use, distribution or reproduction in other forums is permitted, provided the original author(s) and the copyright owner(s) are credited and that the original publication in this journal is cited, in accordance with accepted academic practice. No use, distribution or reproduction is permitted which does not comply with these terms.



# Global Jitter Motion of the Retinal Image Dynamically Alters the Receptive Field Properties of Retinal Ganglion Cells

Akihiro Matsumoto<sup>1,2,3</sup> and Masao Tachibana<sup>1,4\*</sup>

<sup>1</sup> Department of Psychology, Graduate School of Humanities and Sociology, The University of Tokyo, Tokyo, Japan,

<sup>2</sup> Ritsumeikan Global Innovation Research Organization (R-GIRO), Ritsumeikan University, Kusatsu, Japan, <sup>3</sup> Danish Research Institute of Translational Neuroscience (DANDRITE), Department of Biomedicine, Aarhus University, Aarhus, Denmark,

<sup>4</sup> Research Organization of Science and Technology, Ritsumeikan University, Kusatsu, Japan

## OPEN ACCESS

### Edited by:

Mehdi Adibi,  
University of New South Wales,  
Australia

### Reviewed by:

Masoud Ghodrati,  
Monash University, Australia  
William Martin Connelly,  
University of Tasmania, Australia

### \*Correspondence:

Masao Tachibana  
mstchbn@fc.ritsumei.ac.jp

### Specialty section:

This article was submitted to  
Perception Science,  
a section of the journal  
Frontiers in Neuroscience

**Received:** 01 July 2019

**Accepted:** 30 August 2019

**Published:** 13 September 2019

### Citation:

Matsumoto A and Tachibana M  
(2019) Global Jitter Motion of the  
Retinal Image Dynamically Alters  
the Receptive Field Properties  
of Retinal Ganglion Cells.  
*Front. Neurosci.* 13:979.  
doi: 10.3389/fnins.2019.00979

Fixational eye movements induce aperiodic motion of the retinal image. However, it is not yet fully understood how fixational eye movements affect retinal information processing. Here we show that global jitter motion, simulating the image motion during fixation, alters the spatiotemporal receptive field properties of retinal ganglion cells. Using multi-electrode and whole-cell recording techniques, we investigated light-evoked responses from ganglion cells in the isolated goldfish retina. Ganglion cells were classified into six groups based on the filtering property of light stimulus, the membrane properties, and the cell morphology. The spatiotemporal receptive field profiles of retinal ganglion cells were estimated by the reverse correlation method, where the dense noise stimulus was applied on the dark or random-dot background. We found that the jitter motion of the random-dot background elongated the receptive field along the rostral-caudal axis and temporally sensitized in a specific group of ganglion cells: Fast-transient ganglion cells. At the newly emerged regions of the receptive field local light stimulation evoked excitatory postsynaptic currents with large amplitude and fast kinetics without changing the properties of inhibitory postsynaptic currents. Pharmacological experiments suggested two presynaptic mechanisms underlying the receptive field alteration: (i) electrical coupling between bipolar cells, which expands the receptive field in all directions; (ii) GABAergic presynaptic inhibition from amacrine cells, which reduces the dorsal and ventral regions of the expanded receptive field, resulting in elongation along the rostral-caudal axis. Our study demonstrates that the receptive field of Fast-transient ganglion cells is not static but dynamically altered depending on the visual inputs. The receptive field elongation during fixational eye movements may contribute to prompt firing to a target in the succeeding saccade.

**Keywords:** retina, retinal ganglion cells, receptive field, eye movements, gap junctions

## INTRODUCTION

In living animals, the retina receives unstable visual inputs induced by movements of body, head, and eyes (Land, 2009). Even when an animal is fixating an object, the whole image on the retina is shifted by the presence of incessant microscopic eye movements (“fixational eye movements”) (Martinez-Conde et al., 2004; Rucci and Poletti, 2015). Once fixational eye movements are

stabilized, visual perception fades rapidly (Yarbus, 1967; Murakami, 2006). It has been shown that fixational eye movements affect visual performance such as visual acuity (Keesey, 1960), contrast sensitivity (Tulunay-Keesey and Jones, 1976), and detection of visual features (Rucci et al., 2007). Physiological evidence indicates that the image motion induced by fixational eye movements prevents the adaptation of neural activity (Martinez-Conde et al., 2004; Rucci and Poletti, 2015). Involuntary small eye movements during fixation, called microsaccades, increase firing activity of primate visual cortical neurons (V1, Martinez-Conde et al., 2000; area MT, Bair and O'Keefe, 1998). Retinal ganglion cells (GCs) respond with higher firing rate to the jittering image than the static image, together with synchronization (Greschner et al., 2002) or with decorrelation (Segal et al., 2015).

In natural vision, animals repeat fixations and brief gaze shifts (saccades) (Wurtz, 2008; Land, 2009). It has been shown that firing of GCs is increased (Noda and Adey, 1974) or suppressed (Roska and Werblin, 2003; Tien et al., 2015) by saccade-like image shift depending on cell types. A burst firing is evoked by image recurrence across eye-movement-like image transitions in mouse specific GCs (Krishnamoorthy et al., 2017). Glycinergic and GABAergic inhibitory inputs from amacrine cells seem to contribute to the firing modulation during the rapid image shift (Roska and Werblin, 2003; Tien et al., 2015; Krishnamoorthy et al., 2017).

In our previous study, applying a multi-electrode array to GCs in the goldfish isolated retina, we showed that firing properties of specific GC groups were modulated by a rapid shift of a target following a period of jitter motion of a global random-dot background (Matsumoto and Tachibana, 2017). In particular, the response latency to a rapidly moving target was shortened in Fast-transient (Ft) GCs only when rapid motion was preceded by global jitter motion. Intriguingly, the response modulation was specific to rapid motion along the rostral-caudal axis. These results suggest that the receptive field (RF) properties of Ft GCs may have been altered during a period of global jitter motion prior to rapid motion. However, global jitter motion *per se* did not evoke firing in Ft GCs, and thus, it remains to be solved how global jitter motion alters the RF properties of Ft GCs and what mechanisms underlie the alteration.

Here, applying the whole-cell clamp technique as well as the multi-electrode technique to goldfish retinal GCs, we analyzed the effects of global jitter motion on the spatiotemporal RF profiles. We found that the RF of Ft GCs was spatially elongated along the rostral-caudal axis and temporally sensitized by jitter motion. At the newly emerged regions, local light stimulation frequently evoked excitatory postsynaptic currents with large amplitude and fast kinetics. Pharmacological experiments suggested that the RF alterations were mediated by activation of electrical coupling between bipolar cells and GABAergic inhibition from amacrine cells to bipolar cell terminals. Elongation of the RF of Ft GCs during jitter motion may contribute to prompt response to a rapidly moving target in the succeeding saccade.

## MATERIALS AND METHODS

### Experimental Model and Subject Details

Goldfish (*Carassius auratus*; 8–12 cm;  $n = 62$ ) was used for the experiments. Animals were kept in a room maintained at 23°C on a 12 h light/dark cycle. All protocols complied with “A Manual for the Conduct of Animal Experiments in The University of Tokyo” and “Guiding Principles for the Care and Use of Animals in the Field of Physiological Sciences, The Physiological Society of Japan.”

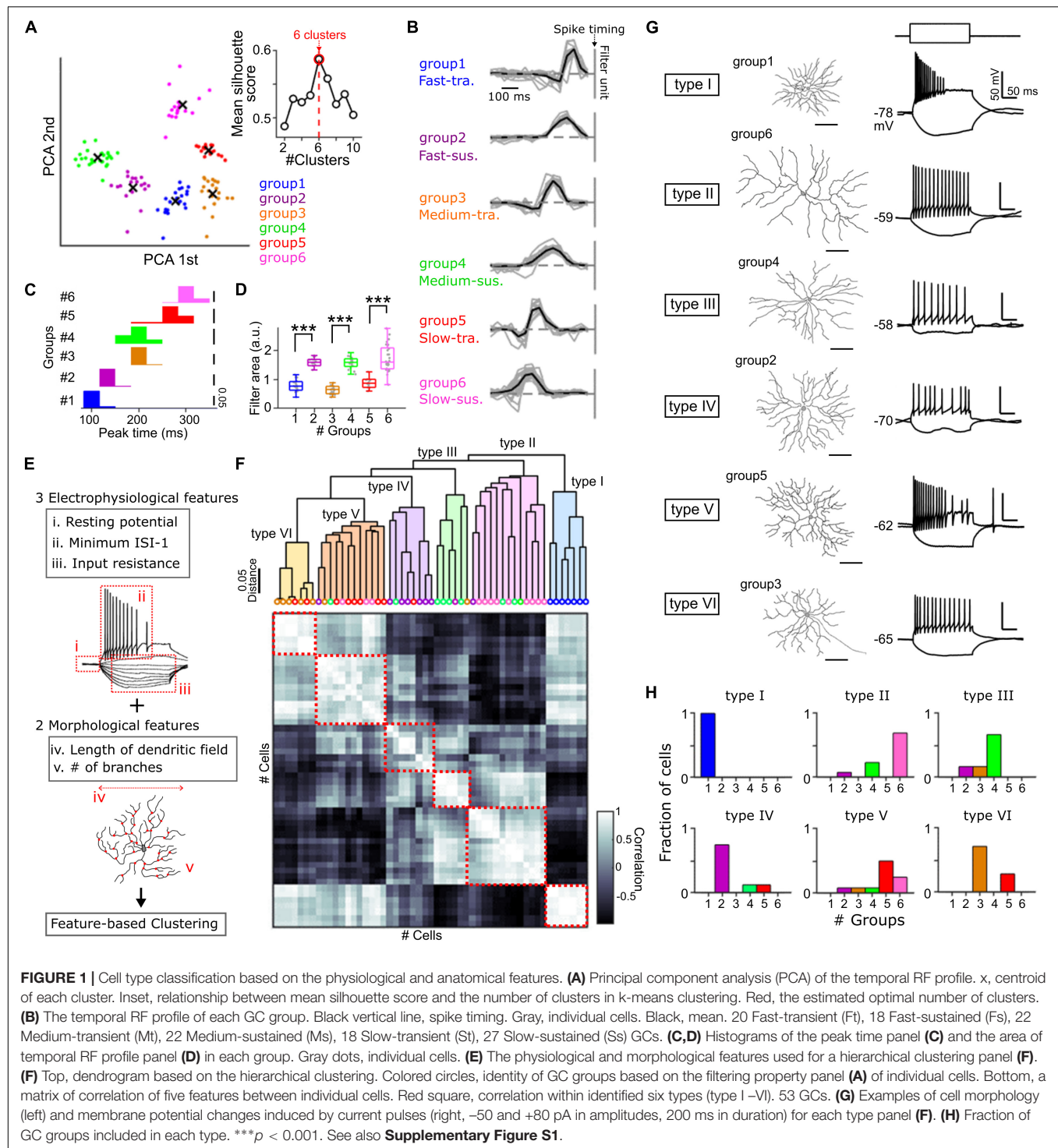
### Method Details

#### Retinal Preparation

Goldfish were dark-adapted for more than 1 h before experiments. Under a dim red light, a goldfish was double-pithed, and eyes were enucleated. The following procedure was performed under a stereomicroscope equipped with infrared (IR) image converter (C5100, Hamamatsu photonics) and IR illuminator (HVL-IRM, Sony). After the cornea and lens were ablated, the eye cup was treated with a mixture of hyaluronidase and collagenase (4 mg/mL each, Sigma-Aldrich Corp.) for a few min. A small cut was made at the dorsal part of the eye cup as a landmark and thus the ventral retina isolated from the pigment epithelium was properly oriented and positioned on the multi-electrode array or in the recording chamber for whole-cell recordings.

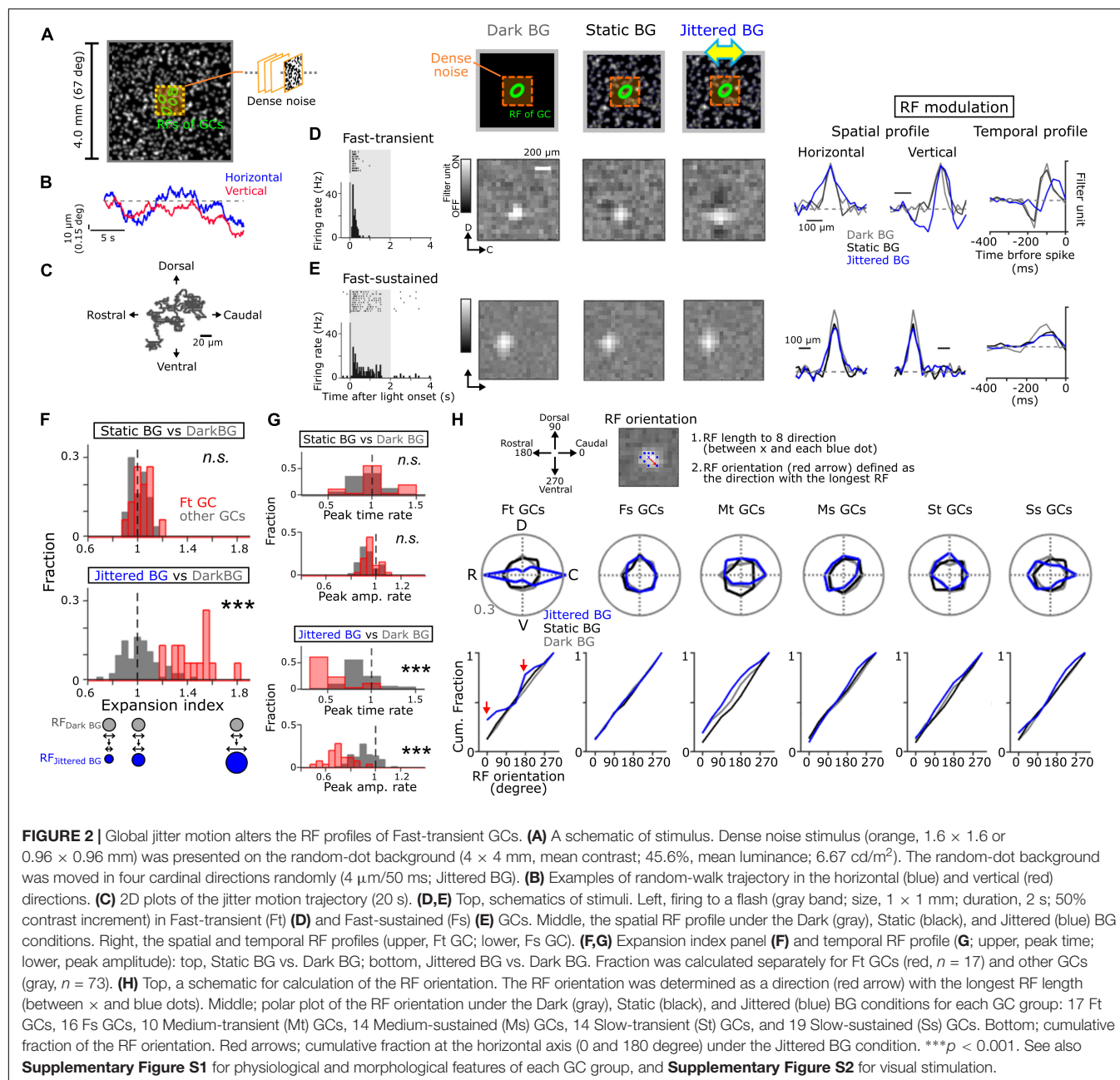
#### Recordings

For multi-electrode recordings (Figures 1, 2), the isolated retina was placed on the electrode array (60 electrodes, electrode diameter 30  $\mu\text{m}$ , electrode spacing 200  $\mu\text{m}$ ; 60pMEA200/30iR-Ti, Multichannel Systems) with the GC layer facing down, and light stimulation was applied from the photoreceptor side. The recorded signals were stored at 16 kHz through AD converter with 16 channels (PowerLab 16/35; AD Instruments). The retina was continuously superfused with an extracellular solution bubbled with 95% O<sub>2</sub>/5% CO<sub>2</sub> at the rate of 1 mL/min. The solution consisted of (in mM) 106 NaCl, 2.6 KCl, 28 NaHCO<sub>3</sub>, 2.5 CaCl<sub>2</sub>, 1 MgCl<sub>2</sub>, 1 Na-pyruvate, 10 D-glucose, 4 mg/L phenol red. For pharmacological experiments, drugs were added to the extracellular solution. Drugs were obtained from Sigma-Aldrich. Recorded spike discharges were band-pass filtered between 100 and 3,000 Hz and sorted into single unit activities by principal component analysis (PCA) and the template-matching method with custom programs using MATLAB (Lewicki, 1998; Zhang et al., 2004; Matsumoto and Tachibana, 2017). For further analysis, we selected up to 3 single units/electrode, showing robust light-evoked responses based on two criteria: responsibility and reliability. Responsibility was evaluated by comparing mean firing probability before and during light stimulus using two-tailed *t*-test. Reliability was evaluated by trial-to-trial variability in spike counts during light stimulus based on Pearson's correlation. To verify the accuracy of sorting, we calculated the auto-correlation of the sorted spike train for each unit, and confirmed a lack of events corresponding to the refractory period of spikes (Supplementary Figure S1A) (Lewicki, 1998; Rey et al., 2015).



For whole-cell recordings (Figures 1, 3, 4), the isolated retina was placed on the recording chamber with the GC layer facing up, and light stimulation was applied from the photoreceptor side. The retina was continuously superfused with the bubbled extracellular solution. The pipette was filled with intracellular solution (in mM): 128 K gluconate, 10 KCl, 10 HEPES, 0.5 EGTA,

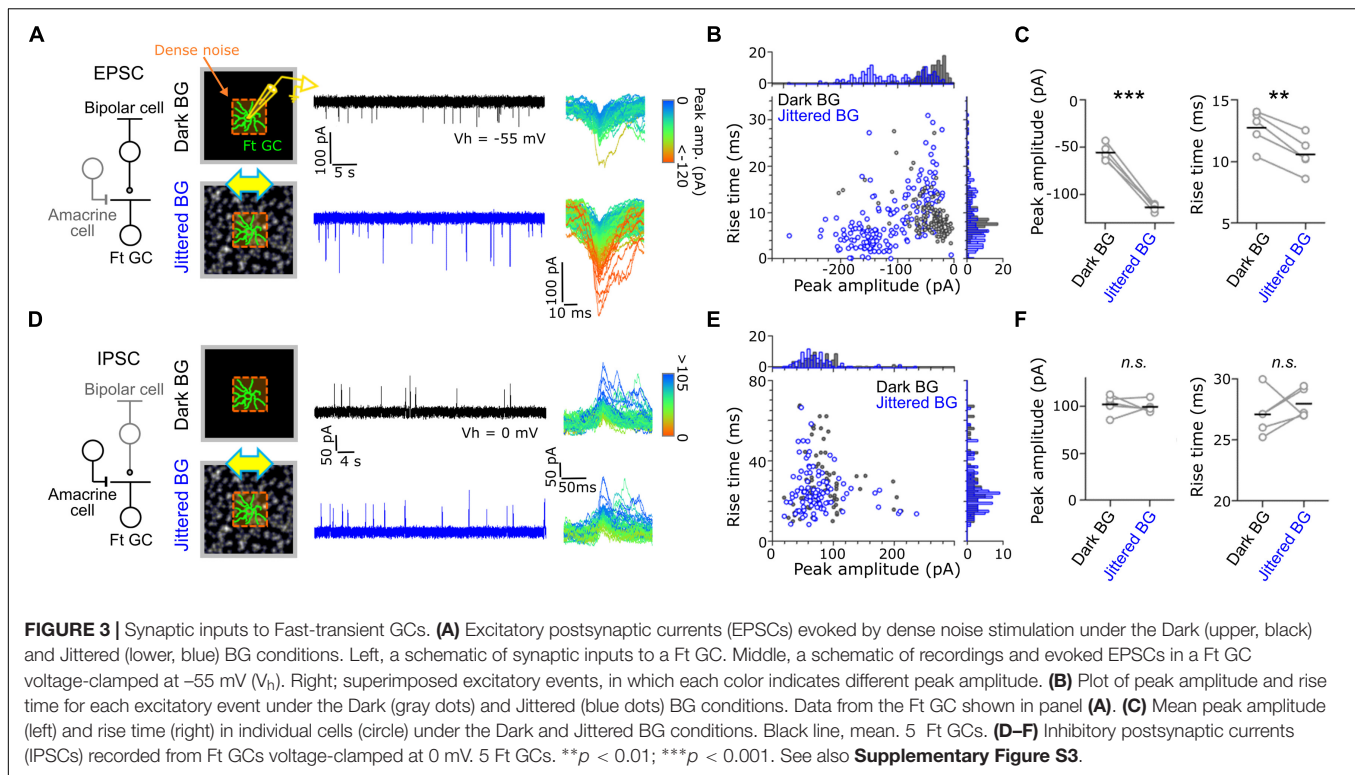
0.05  $\text{CaCl}_2$ , 2  $\text{MgCl}_2$ , 5 ATP- $\text{Na}_2$ , 0.5 GTP- $\text{Na}_3$ , and 0.08% Lucifer yellow-2K (pH 7.4 with KOH) for current-clamp recordings, and 118  $\text{CsMeSO}_3$ , 10 TEA-Cl, 10 HEPES, 0.5 EGTA, 0.05  $\text{CaCl}_2$ , 2  $\text{MgCl}_2$ , 5 ATP- $\text{Na}_2$ , 0.5 GTP- $\text{Na}_3$ , 5 QX314-Br, and 0.08% Lucifer yellow-2K (pH 7.4 with CsOH) for voltage-clamp recordings.  $E_{\text{Cl}}$  was calculated as  $-55$  mV. The membrane potential was



corrected for liquid junction potential which was measured before experiments. For pharmacological experiments (**Figure 5**), we added picrotoxin (GABA receptor blocker;  $100 \mu\text{M}$ , Sigma) or mefloquine (gap junction blocker;  $10 \mu\text{M}$ , Sigma) to the extracellular solution. Recordings were performed using EPC 10 (HEKA Elektronik) controlled by Patchmaster (version 2.73.5). Current and voltage records were sampled at 16 kHz and low-pass filtered at 2.9 KHz. We used a borosilicate glass electrode (CNC 1.5; Ken Enterprise), which was pulled by a puller (P97; Sutter Instrument). The resistance of recording pipettes was 6–11 M $\Omega$ . For cell group identification, light-evoked spikes were recorded in the cell-attached mode before whole-cell recording.

## Light Stimulation

Light patterns were generated by Psychtoolbox3 on MATLAB (Mathworks) (Brainard, 1997; Pelli, 1997). For multi-electrode recordings, a multi-electrode array was placed on the stage of an inverted microscope (IX70; Olympus). The light stimulus was projected from a cathode-ray tube display (S501J, refresh rate 60 Hz,  $1,280 \times 1,024$  pixels, Iiyama) to the photoreceptor layer of the retina through optics. For whole-cell recordings, a patch pipette was approached from the ganglion cell side. The light stimulus was projected from a DLP projector (L51W, refresh rate 60 Hz,  $1,280 \times 1,024$  pixels, NEC) to the photoreceptor layer through an objective



lens ( $4 \times /0.10$ , Nikon), with which a condenser lens of an upright microscope (Eclipse E600-FN; Nikon) was replaced. In either recording condition, the stimulus image was not distorted because the electrode was positioned on the opposite side of the incident light.

We used a background frame ( $4.0 \times 4.0$  mm) which was either uniformly dark or a Gaussian-filtered ( $\sigma$ ,  $40 \mu\text{m}$ ) random-dot pattern ( $51,325$  dots/ $1,000^2$  pixels,  $4 \mu\text{m}/\text{pixel}$ , **Figure 1A**, see details in Matsumoto and Tachibana, 2017). Background Contrast ( $C_{BK}$ ) was calculated by

$$C_{BK} = (\text{luminance}_{BK} - \text{luminance}_{\text{dark}}) / \text{luminance}_{\text{max}}$$

where  $\text{luminance}_{BK}$ ,  $\text{luminance}_{\text{dark}}$ , and  $\text{luminance}_{\text{max}}$  were the mean intensity of the random-dot pattern, 0.11 and  $14.4 \text{ cd/m}^2$ , respectively. We introduced global jitter motion to simulate the *in vivo* fixational eye movements of goldfish (**Figures 2A–C**) (Easter et al., 1974; Mensh et al., 2004). Global jitter motion was a horizontally biased random walk, in which a shift ( $4 \mu\text{m}/50 \text{ ms}$ ) to one of the four cardinal direction occurred in each stimulus frame, and the probability of horizontal shift was two times higher than that of vertical shift.

## Receptive Field Estimation

The spatiotemporal receptive field (RF) was estimated by the reverse correlation method (Meister et al., 1994; Matsumoto and Tachibana, 2017). The retina was stimulated with dense noise consisted of pseudorandom (M-sequence) checkerboard patterns. Each frame ( $32 \times 32$  pixels with

black or white; pixel size,  $50 \times 50 \mu\text{m}$  or  $30 \times 30 \mu\text{m}$ ) was updated at  $30 \text{ Hz}$ . The dense noise was placed on the center region ( $1.6 \times 1.6$  or  $0.96 \times 0.96 \text{ mm}$ ; **Figure 2A**, orange) of the background ( $4.0 \times 4.0 \text{ mm}$ ). The checkerboard frames that preceded each spike discharge were averaged (STA, spike-triggered average).

To define the orientation and size of the RF, we determined an “edge” (a position of a pixel with the intensity six times higher than the SD of the intensity in uncorrelated image) along 8 directions ( $0$ – $315^\circ$ ,  $\Delta 45^\circ$ ) from the RF “center” (a pixel with maximal intensity). Eight edges were fitted by an ellipse based on the method of least squares. RF size was calculated by a length of major axis in the fitted ellipse. RF orientation (**Figure 2H**) was defined by the direction with the longest length among eight directions. The temporal RF profile was obtained by calculating the mean intensity of  $3 \times 3$  pixels in the RF center region for a series of the averaged frames.

The temporal RF profile was used for classification of GC groups (Matsumoto and Tachibana, 2017; **Figures 1A–D** and **Supplementary Figure S1B**). In brief, we first created an input matrix from the temporal RF profile of each GC, in which the temporal RF profiles were upsampled using *interp* function with a rate of 3 in MATLAB, and smoothed by a moving average filter. After the smoothing, the temporal filters were downsampled to the original rate using *downsample* function in MATLAB. Next, principal component analysis (PCA) was applied to visualize the features of temporal RFs (**Figure 1A**). Then, clustering was performed by k-means clustering using *kmeans* function in MATLAB. The number of

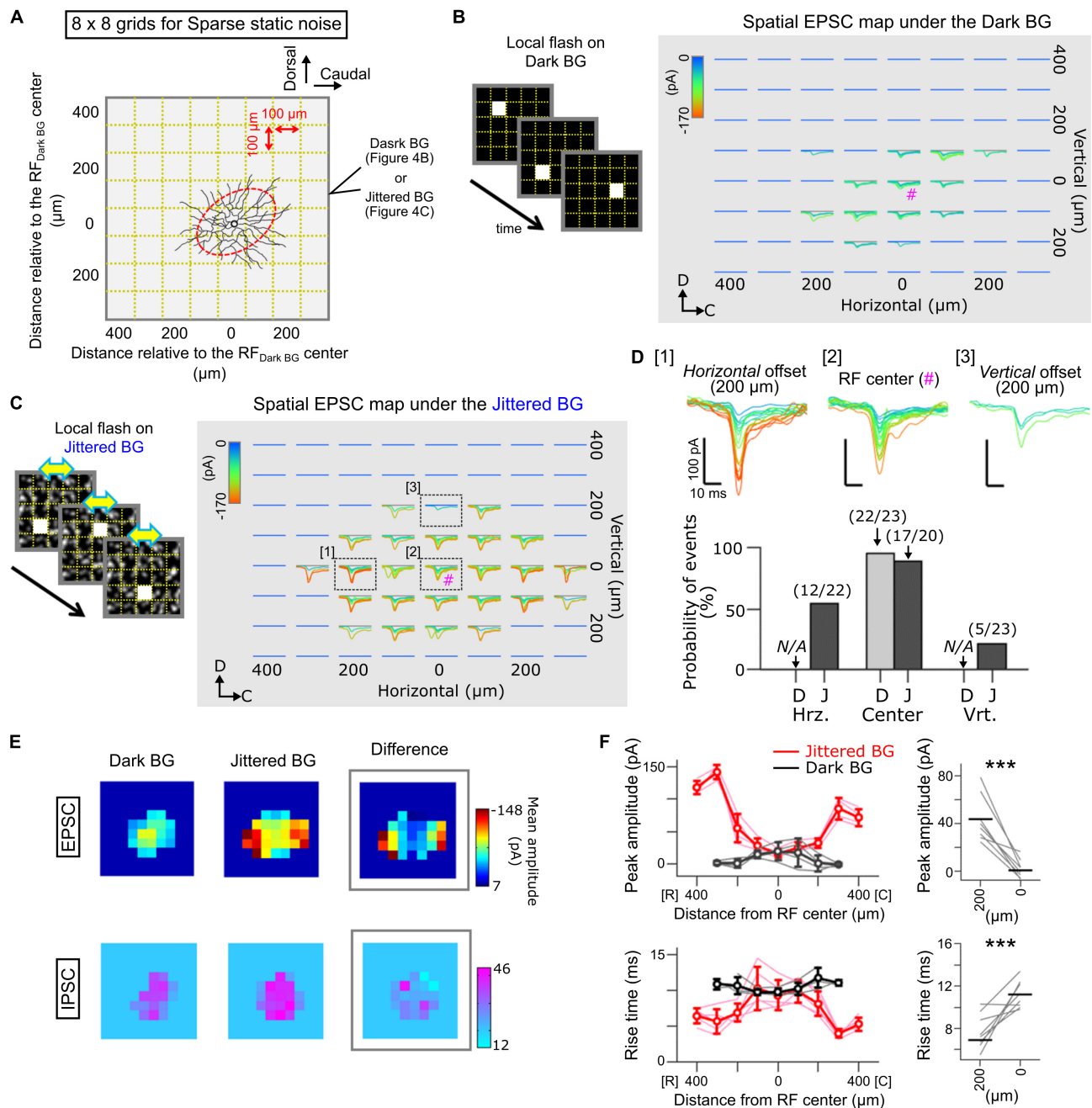
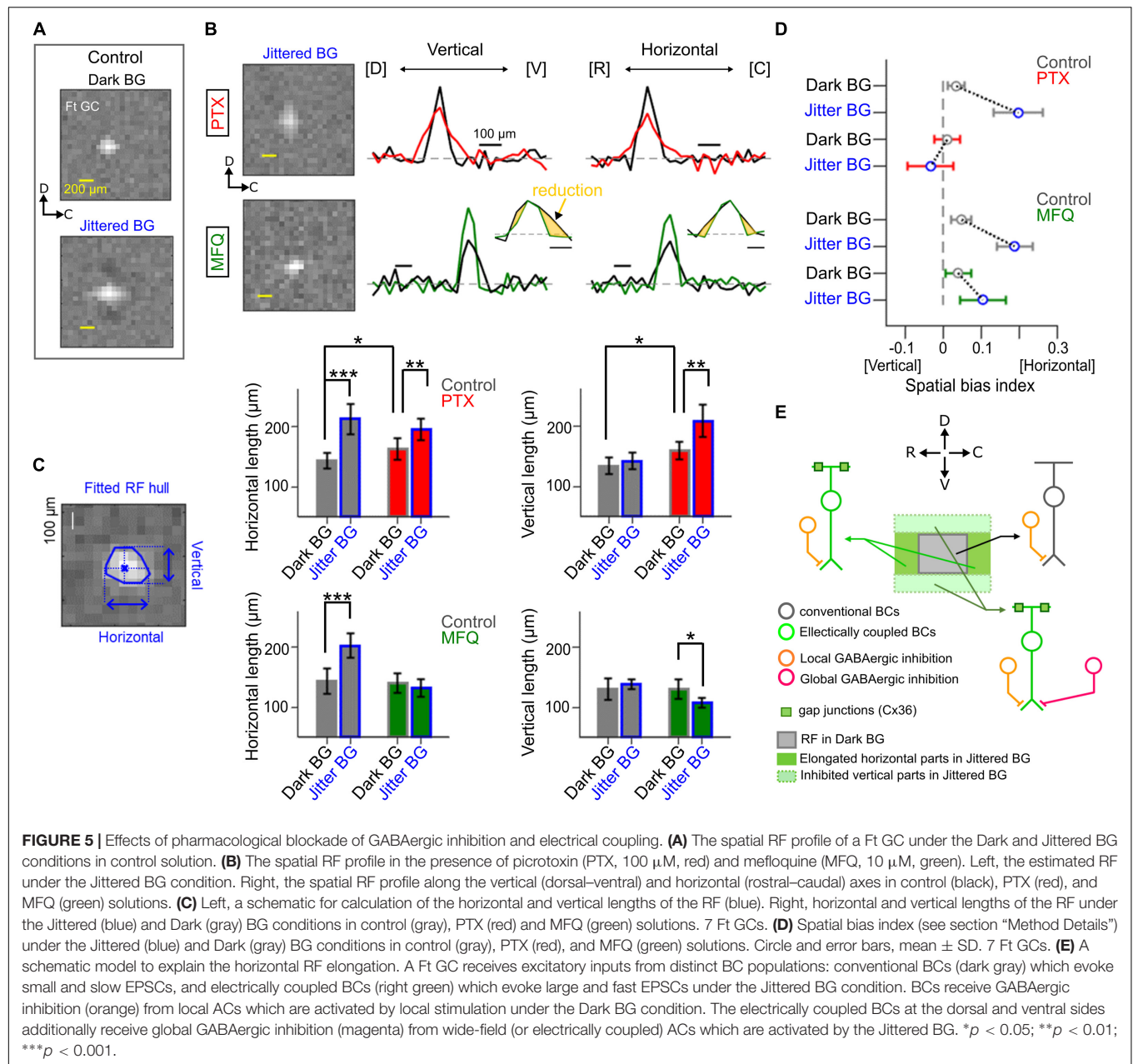


**FIGURE 4 |** Spatial map of EPSCs evoked by local flash stimulation in Ft GCs. **(A)** A schematic of sparse noise stimulation on the Dark **(B)** and Jittered BG **(C)**. The sparse noise was a sequence of a static flash (size, 100 × 100 μm; duration, 50 ms) randomly applied at one of the 8 × 8 grids (gold dotted lines). Stimulus location was described from the RF center estimated under the Dark BG condition (red). **(B,C)** Superimposed EPSCs evoked by local flash stimulation presented on the Dark **(B)** and Jittered **(C)** BGs. EPSCs are colored based on the peak amplitude. #: the RF center. **(D)** Top, EPSCs evoked at three locations: [1] horizontally 200 μm away from the RF center, [2] the RF center, and [3] vertically 200 μm away from the RF center. Bottom, probability of EPSC events evoked by local flash stimulation. Numbers, EPSC events/stimulation. N/A, no evoked EPSCs. D, Dark BG. J, Jittered BG. **(E)** Heatmaps showing the peak amplitude of EPSCs (top) and IPSCs (bottom) evoked by local flash stimulation on the Dark (left) and Jittered (center) BGs. Right, a heatmap showing differences of amplitude between the Dark and Jittered BGs. Data from the Ft GC **(C)**. **(F)** Left, peak amplitude (upper) and rise time (lower) of the evoked EPSCs are plotted against the position relative to the RF center (5 Ft GCs) under the Dark (black) and Jittered (red) BG conditions. Thin lines, data from individual cells. Right, mean peak amplitude (upper) and rise time (lower) of EPSCs evoked by flash stimulation 200 μm away from the RF center and at the RF center (0 μm). \*\*\*p < 0.001.



clusters was determined based on the mean silhouette scores  $[s(i)]$  (Figure 1A),

$$s(i) = b(i) - a(i) / \max\{a(i), b(i)\},$$

where  $i$  is each cell,  $a(i)$  is average distance between  $i$  and all other points included in the same cluster, and  $b(i)$  is the smallest average distance of  $i$  to all other points (Rousseeuw, 1987; Yuan and Yang, 2019). We adopted the cluster numbers with the highest mean silhouette score for k-means clustering (Martínez et al., 2017).

To quantify the horizontal and vertical lengths of RF, we first fitted a hull to the RF (Figure 5C) using *convex*

*hull* function in MATLAB. A centroid where the horizontal and vertical axes crossed was calculated in the fitted hull, and then, we measured the horizontal and vertical lengths through the centroid. To quantify the spatial bias of the RF profile, the spatial bias index (SBI) was defined by,

$$SBI = (\text{length}_{\text{Horizontal}} - \text{length}_{\text{Vertical}}) / (\text{length}_{\text{Horizontal}} + \text{length}_{\text{Vertical}})$$

where  $\text{length}_{\text{Horizontal}}$  and  $\text{length}_{\text{Vertical}}$  are the measured RF length along the horizontal and vertical axes, respectively

(Figure 5D). The positive and negative values indicate the horizontal and vertical bias of the RF, respectively.

### Waveform Analysis

For whole-cell voltage-clamp recordings (Figures 3, 4), wave event was detected as the postsynaptic current when the current amplitude crossed a threshold defined by

$$\text{Threshold} = |\text{Mean}_c| + \text{SD}_c * 3,$$

where C indicates the currents recorded during dense noise stimulation. To quantify the postsynaptic currents, we calculated the amplitude and rise time of each detected wave event. The rise time was defined as the time required for the response to reach from 63% to 100% of the peak.

### Analysis of Membrane Properties

To characterize the membrane properties of GCs, we recorded the membrane potential changes induced by current pulses (duration, 200 ms; amplitude, from  $-50$  to  $100$  pA; increment,  $10$  pA). For hierarchical clustering (Figure 1F), we used three features (Supplementary Figure S1D): the resting membrane potential, the maximum instantaneous firing rate, and the input resistance. The resting membrane potential was calculated as an average potential  $100$  ms before application of current pulses. The maximum firing rate was calculated as an inverse of minimum inter-spike intervals during current pulses [Supplementary Figure S1D, (i)]. The input resistance was calculated as a slope of the current-voltage function below subthreshold membrane potentials [Supplementary Figure S1D, (ii)]. We performed a hierarchical clustering based on the correlation distance in the standardized feature space using *linkage* and *dendrogram* functions in MATLAB (Baden et al., 2016).

### Morphological Analysis

Lucifer yellow was introduced through a recording patch pipette to visualize the cell morphology. Using ImageJ (NIH) and customized program in MATLAB, we quantified the dendritic field, shape, and dendritic branches of each GC (Figure 1 and Supplementary Figure S1E). The dendritic tips of a stained GC were fitted to a polygon, and then its major axis and the aspect ratio of major to minor axis were used as the measure of the length and the shape, respectively. The number of branches normalized by an area of the polygon was used as the measure of the dendritic branches.

### Quantification and Statistical Analysis

In Figures 2F–H, Kolmogorov-Smirnov test (KS test) was used. In Figure 2H, Hodges-Ajne test was used to evaluate the bias in distribution of the RF orientation. In Figures 3C,F, 4F, paired *t*-test was used. In Figure 5C, Mann-Whitney *U* test (MWU test) with Tukey's *post hoc* test was used. All measures for population data were described as mean  $\pm$  SD. Error bar indicates SD. \*\*\* $p < 0.001$ ; \*\* $p < 0.01$ ; \* $p < 0.05$ .

## RESULTS

### Classification of Retinal Ganglion Cells Based on the Physiological and Anatomical Features

Applying a multi-electrode array to the goldfish isolated retina, we estimated the spatiotemporal receptive field (RF) profiles of retinal ganglion cells (GCs) by the reverse correlation method (Meister et al., 1994). The shape of the temporal RF is one of the criteria to define ganglion cell types functionally (DeVries and Baylor, 1997; Hilgen et al., 2017; Matsumoto and Tachibana, 2017). To dissect GC types, we performed feature detection using principal component analysis for the temporal RF (Matsumoto and Tachibana, 2017), and the resulting features were clustered into six GC groups based on k-means clustering (Figures 1A,B and Supplementary Figure S1B; Rousseeuw, 1987; Yuan and Yang, 2019). The differences among the GC groups were summarized by two temporal features: peak time (Fast/Medium/Slow; Figure 1C) and kinetics (transient/sustained; Figure 1D). Thus, individual GC groups were defined as Fast-transient (Ft, group 1), Fast-sustained (Fs, group 2), Medium-transient (Mt, group 3), Medium-sustained (Ms, group 4), Slow-transient (St, group 5), and Slow-sustained (Ss, group 6) GCs (Figure 1B and Supplementary Figure S1C).

We then assessed whether each GC group could share common physiological and anatomical features. We performed whole-cell recordings from randomly selected GCs and dye loading through the recording pipette to visualize the cell morphology (Supplementary Figures S1D–F). Based on three physiological features which represent the membrane properties (Figure 1E, i–iii) and two morphological features (Figure 1E, iv, v), a hierarchical clustering (Martínez et al., 2017; Gouwens et al., 2019) revealed that GCs were branched into six types (Figure 1F, type I to VI). Intriguingly, each type defined by physiological and anatomical features was populated dominantly by a GC group defined by the filtering property (Figures 1G,H). These results highlight the correlation between the filtering property and the physiological and anatomical features to characterize GCs.

### Global Jitter Motion Changes Spatiotemporal Receptive Field Profiles of a Specific Group of Retinal Ganglion Cells

To explore how the RF properties of GCs are affected by fixational eye movements, dense noise stimulus was presented on a large background (BG;  $4 \times 4$  mm on the retina, visual angle  $> \sim 67^\circ$ ; Figure 2A; Macy and Easter, 1981). We used three kinds of BG patterns: a uniformly dark pattern ("Dark BG"), a static random-dot pattern ("Static BG," a Gaussian-filtered random-dot pattern; mean luminance,  $6.67 \text{ cd/m}^2$ ), and a jittered random-dot pattern ("Jittered BG," the Gaussian-filtered random-dot pattern jittered randomly) (Matsumoto and Tachibana, 2017). The jitter motion was a horizontally biased random walk (probability of horizontal shift/vertical shift = 2; each shift,  $4 \mu\text{m}/50 \text{ ms}$ ; Figures 2B,C and Supplementary Figure S2C) that simulated the goldfish

fixational eye movements (Easter et al., 1974; Mensh et al., 2004). Both the Static and Jittered BGs covered the area far away from the RFs of recorded GCs (**Supplementary Figure S2A**). Based on the responses to dense noise stimulus, we estimated the spatiotemporal RF of GCs under different BG conditions: RF<sub>DarkBG</sub> (gray), RF<sub>StaticBG</sub> (black), and RF<sub>JitteredBG</sub> (blue).

We found that the Jittered BG altered the spatiotemporal RF profile of Ft GCs (**Figure 2D**). The size of RF<sub>JitteredBG</sub> (major axis of the RF;  $161.9 \pm 13.2 \mu\text{m}$ , 21 Ft GCs) was larger than that of either RF<sub>DarkBG</sub> ( $112.5 \pm 13.7 \mu\text{m}$ ,  $p = 0.001$ ; paired *t*-test) or RF<sub>StaticBG</sub> ( $115.6 \pm 22.9 \mu\text{m}$ ,  $p = 0.002$ ). Expansion index, the ratio of the RF size under different BG conditions, was large only under the Jittered BG condition (Jittered BG vs. Dark BG,  $p = 8.91 \times 10^{-9}$ ; Static BG vs. Dark BG,  $p = 0.38$ ; KS test, 21 Ft GCs; **Figure 2F**, red). Other GC groups did not show prominent changes (**Figures 2E,F**, gray).

The temporal profile of RF<sub>JitteredBG</sub> in Ft GCs showed faster peak time and smaller peak amplitude than those of RF<sub>DarkBG</sub> and RF<sub>StaticBG</sub> (**Figures 2D,G**), indicating that the Jittered BG sensitized firing and input integration kinetics. These alterations of the temporal RF profile were specific to Ft GCs (peak time, Jittered BG vs. Dark BG,  $p = 2.35 \times 10^{-9}$ , Static BG vs. Dark BG,  $p = 0.097$ ; peak amplitude, Jittered BG vs. Dark BG,  $p = 9.03 \times 10^{-9}$ , Static BG vs. Dark BG,  $p = 0.084$ ; KS test, 21 Ft GCs; **Figure 2G**, red). The Jittered BG did not affect the temporal RF profile of other GC groups (**Figures 2E,G**, gray), indicating that the RF alterations are not ascribed to light adaptation to the random-dot background.

Intriguingly, RF<sub>JitteredBG</sub> of Ft GCs was oriented along the retinal rostral-caudal (horizontal) axis ( $p = 0.019$ , Hodges-Ajne test, 21 Ft GCs; **Figure 2H**, blue), indicating that the RF expansion is biased along the retinal horizontal axis but not along the dorsal-ventral (vertical) axis (**Figure 2H**, bottom, red arrows). Since RF<sub>DarkBG</sub> and RF<sub>StaticBG</sub> did not show orientation bias (RF<sub>DarkBG</sub>,  $p = 0.7763$ ; RF<sub>StaticBG</sub>,  $p = 0.7763$ ; Hodges-Ajne test, 21 Ft GCs), the horizontal bias is not intrinsic to Ft GCs. Other GC groups showed no significant orientation bias under three BG conditions. It should be noted that the non-coherent (flickering) random noise BG did not alter the spatial RF profile of Ft GCs (RF size, Dark BG,  $125.6 \pm 21.1 \mu\text{m}$ ; Flickering random noise BG,  $121.9 \pm 17.6 \mu\text{m}$ ,  $p = 0.31$ ; paired *t*-test, 17 Ft GCs; **Supplementary Figure S2B**). Therefore, global jitter motion is essential for the RF alterations in Ft GCs.

## Synaptic Currents Evoked by the Dense Noise Stimulus Under the Jittered BG Condition in Ft GCs

Effects of the global jitter motion on the spatiotemporal RF profiles were prominent in Ft GCs. To elucidate the underlying mechanisms, we recorded postsynaptic currents from Ft GCs in the whole-cell voltage-clamp configuration (**Figure 3**). Ft GCs were identified based on the temporal RF profile estimated by firing to dense noise stimulus in the cell-attached configuration. We found that excitatory postsynaptic currents (EPSCs) under the Jittered BG condition were larger in amplitude (Jittered BG,  $-110.2 \pm 56.8 \text{ pA}$ ; Dark BG,  $-42.8 \pm 33.9 \text{ pA}$ ;  $p = 0.001$ , paired

*t*-test, 5 Ft GCs), and faster in kinetics (Jittered BG,  $-110.2 \pm 56.8 \text{ pA}$ ; Dark BG,  $-42.8 \pm 33.9 \text{ pA}$ ;  $p = 3.85 \times 10^{-5}$ , paired *t*-test, 5 Ft GCs) than those under the Dark BG condition (**Figures 3B,C**). EPSCs under the Static BG condition were not significantly different in both amplitude and kinetics from those under the Dark BG condition (Static BG,  $-45.7 \pm 20.9 \text{ pA}$ ,  $10.6 \pm 2.5 \text{ ms}$ ,  $p > 0.3$ ; paired *t*-test, 5 Ft GCs; **Supplementary Figure S3**), indicating that emergence of large and fast EPSCs is not ascribed to adaptation to mean contrast increment (Dark BG vs. Static BG) but to alteration induced by the global jitter motion (Static BG vs. Jittered BG).

In contrast, inhibitory postsynaptic currents (IPSCs; **Figure 3D**) were not affected by the Jittered BG (amplitude, Jittered BG,  $99.1 \pm 64.5 \text{ pA}$ ; Dark BG,  $102.6 \pm 66.9 \text{ pA}$ ; kinetics, Jittered BG,  $28.1 \pm 15.5 \text{ ms}$ , Dark BG  $27.2 \pm 16.7 \text{ ms}$ ,  $p > 0.3$ ; paired *t*-test, 5 Ft GCs; **Figures 3E,F**). Therefore, it is likely that the RF alterations under the Jittered BG condition were induced not by feedforward inhibitory synaptic inputs from amacrine cells (ACs) to Ft GCs but by excitatory synaptic inputs from bipolar cells (BCs) to Ft GCs.

## Alterations of the Spatial Distribution of Excitatory Inputs to Ft GCs by the Jittered BG

To examine the spatial RF profile under the Jittered BG condition in detail, we mapped the distribution of EPSCs evoked by local light stimulation (Spatial EPSC map; **Figure 4**). A whole-cell voltage-clamped Ft GC was stimulated by a small flash (**Figure 4A**; size,  $100 \times 100 \mu\text{m}$ ; duration, 50 ms; inter-flash interval, 1 s), which was presented randomly at various locations on the Dark BG (**Figure 4B**) or on the Jittered BG (**Figure 4C**). We found that the EPSC map under the Jittered BG condition was spatially expanded along the retinal horizontal axis (**Figures 4C–E**), corresponding to the horizontally elongated RF<sub>JitteredBG</sub> (**Figure 2D**).

Interestingly, we found that the properties of evoked EPSCs were not homogeneous across the RF under the Jittered BG condition: small and slow inputs at the center region (**Figure 4D** [2] and **Figure 4F**;  $17.8 \pm 9.87 \text{ pA}$ ,  $9.54 \pm 1.54 \text{ ms}$ ); large and fast inputs at the horizontally-expanded region (**Figure 4D** [1] and **Figure 4F**;  $43.7 \pm 19.39 \text{ pA}$ ,  $7.54 \pm 1.53 \text{ ms}$ ). It is likely that the emergence of large and fast EPSCs mediates the horizontally elongated RF of Ft GCs under the Jittered BG condition.

## Contribution of GABAergic and Electrical Pathways to RF Elongation in Ft GCs

In the goldfish retina both GABAergic inhibition from AC to Mb1 (ON) BC terminal (Tachibana and Kaneko, 1988) and electrical coupling through connexin 36 (Cx36) between Mb1 BC dendrites contribute to global information processing (Arai et al., 2010; Tanaka and Tachibana, 2013; Matsumoto and Tachibana, 2017). It is possible that the horizontal RF elongation in Ft GCs may be attributable to deactivation of lateral inhibition mediated by ACs and/or activation of electrically coupled excitatory network (Bloomfield and Völgyi, 2009; Werblin, 2011).

Using a multi-electrode array, we examined the effects of pharmacological blockers on the properties of RF<sub>JitteredBG</sub> (**Figure 5**). Application of a GABA receptor blocker picrotoxin (PTX, 100  $\mu$ M) increased the RF<sub>DarkBG</sub> size (horizontal length,  $142.7 \pm 12.4 \mu\text{m}$  in Control,  $162.3 \pm 18.1 \mu\text{m}$  in PTX,  $p = 0.03$ ; vertical length,  $133.5 \pm 13.9 \mu\text{m}$  in Control,  $158.6 \pm 14.8 \mu\text{m}$  in PTX,  $p = 0.01$ ; Mann-Whitney  $U$  (MWU) test, 7 Ft GCs; **Figures 5B,C**). Even in the presence of PTX, the Jittered BG increased further the RF size (RF<sub>JitteredBG</sub>, horizontal length  $194.5 \pm 17.9 \mu\text{m}$ ,  $p = 0.007$ ; vertical length  $208.2 \pm 27.3 \mu\text{m}$ ,  $p = 0.0012$ ; MWU test, 7 Ft GCs, **Figure 5C**), although the spatial bias disappeared (**Figure 5D**). These results suggest that two different GABAergic mechanisms may mediate the surround inhibition (Werblin, 2011): the local inhibition which works under the dark BG condition, and the global inhibition which contributes to emphasizing the horizontal bias of the RF under the Jittered BG condition.

In the presence of gap junction blocker mefloquine (MFQ, 10  $\mu$ M; Cruikshank et al., 2004), the Jittered BG did not increase the horizontal length of the RF<sub>JitteredBG</sub> (horizontal length, Dark BG,  $140.7 \pm 16.1 \mu\text{m}$ ; Jittered BG,  $132.7 \pm 14.8 \mu\text{m}$ ,  $p = 0.32$ ; MWU test, 7 Ft GCs; **Figures 5B,C**), but decreased the vertical length of the RF<sub>JitteredBG</sub> significantly (vertical length,  $130.3 \pm 15.9 \mu\text{m}$  under the Dark BG,  $107.3 \pm 8.3 \mu\text{m}$  under the Jittered BG,  $p = 0.0175$ ; MWU test, 7 Ft GCs; **Figure 5C**). These results suggest that electrical coupling may mediate the spatial expansion of the RF<sub>JitteredBG</sub>. Indeed, spatial bias index (see section “Method Details”) indicates that the horizontal bias of the RF<sub>JitteredBG</sub> was still maintained in the presence of MFQ (**Figure 5D**, green), whereas the horizontal bias was not observed in the presence of PTX (**Figure 5D**, red).

Therefore, the potential mechanism for the RF alterations may be the following: the Jittered BG expands the RF in all directions by electrical coupling, perhaps between Mb1 BCs (Arai et al., 2010); and the dorsal and ventral sides of the expanded RF are suppressed by activated GABAergic lateral inhibition (Tanaka and Tachibana, 2013), resulting in the horizontally elongated RF (**Figure 5E**). Lateral inhibition may be ascribed not to the feedforward input from AC to Ft GC but to the feedback input from AC to Mb1 BC terminal (Tanaka and Tachibana, 2013) because IPSCs in Ft GCs were not altered by the Jittered BG (**Figures 3E,F**).

## DISCUSSION

In our previous study, we showed that firing properties of specific GCs in the goldfish retina were modulated by a rapid shift of a target following a period of jitter motion of a global random-dot background (Matsumoto and Tachibana, 2017). Here, we examined how global jitter motion alters the RF properties of Ft GCs and what mechanisms underlies the RF alteration. We found that global jitter motion induced the RF elongation along the retinal horizontal (caudal-rostral) axis (**Figure 2**) in Ft GCs (**Figure 1**). At the elongated region, EPSCs with large amplitude and fast kinetics were dominated (**Figures 3, 4**). Pharmacological experiments revealed that both GABAergic

lateral inhibition and electrical coupling contributed to the horizontal RF elongation (**Figure 5**).

## Synaptic Modulation Mediated by Electrical and GABAergic Pathways

Our results indicate that the RF alteration in Ft GCs is mediated by lateral interaction pathways: electrical and GABAergic pathways (**Figure 5**). In the goldfish retina, excitation of an Mb1 BC spreads to neighboring Mb1 BCs through gap junction between their dendrites (Arai et al., 2010). Such lateral spread of excitation could expand the RF. It is possible that the synchronous transient glutamate release from electrically coupled BCs may evoke EPSCs with large amplitude and fast kinetics. It is conceivable that Ft GCs may receive excitatory inputs from a population of BCs under the Dark BG (“conventional BCs” in **Figure 5E**), and large and fast excitatory inputs from another population of electrically coupled BCs which are additionally activated by the Jittered BG (“Electrically coupled BCs” in **Figure 5E**).

In the goldfish retina, global stimulation activates the electrically coupled Mb1 BC network, which in turn activates wide-field ACs and/or electrically coupled ACs (Tanaka and Tachibana, 2013). Blockade of GABA receptors under the Dark BG condition increased the size of RF in all directions (**Figure 5C**), indicating that the local GABAergic inhibition was not biased spatially (**Figure 5E**). However, blockade of GABA receptors under the Jittered BG condition impaired the horizontal bias (**Figure 5D**). These observations indicate that the global inhibitory mechanism could affect the electrically coupled BCs at the dorsal and vertical side of the expanded RF (“Global GABAergic inhibition,” **Figure 5E**).

On the other hand, the horizontal bias remained even after blockade of electrical coupling (**Figure 5D**). This result indicates that the inputs from electrically coupled BCs may not be the unique resource to drive the global inhibitory mechanism. It is possible that the continuous jitter motion may prevent the BCs from adaptation, resulting in augmentation of the synaptic inputs to the wide-field ACs. Another possible resource may be the ACs electrically coupled through non-Cx36 (Mark et al., 1988; Völgyi et al., 2013), which are also activated by the Jittered BG. This mechanism could explain the observed horizontal bias in the presence of a gap junction blocker. Since AC circuits in the goldfish retina are not yet fully understood, further studies are needed to clarify the circuit mechanism.

## Diverse Features of Fixational Eye Movements

In this study we used randomly jittering motion to mimic the retinal image during fixation, which was similar to the random walk used in the previous studies (Ölveczky et al., 2003; Baccus et al., 2008; Segal et al., 2015). The stimulus was summarized by oscillatory image motion with small amplitude, which approximates to an animal’s tremor (e.g., archer fish, 12  $\mu\text{m}$  in mean amplitude, 5 Hz in frequency, Segev et al., 2007). Nevertheless, the features of fixational eye movements are more complicated in amplitude, speed, and frequency: drift, slow motion occurring together with tremor; microsaccades,

small but rapid and involuntary shifts of eyes (Martinez-Conde et al., 2004; Rucci and Poletti, 2015). Global jitter motion used in this study may be similar to tremor and drift in periodicity and slow frequency components (0.5–8 Hz; **Supplementary Figure S2C**). On the other hand, our stimulus did not include the small and rapid displacements corresponding to microsaccades. Furthermore, it is not yet clear how three components of fixational eye movements interact with one another and affect the retinal circuit. It is likely that the RF alterations shown in this study may be a part of the effects induced by fixational eye movements. Further studies are required to dissect the relationship between the diverse features of fixational eye movements and the retinal information processing.

## Functional Relevance of RF Elongation

Goldfish makes horizontally biased saccades spontaneously (Salas et al., 1997). Thus, the horizontal elongation of RF in Ft GCs during global jitter motion seems to be advantageous to responding quickly to a target in a succeeding rapid gaze shift (saccade). Indeed, we have shown that horizontal, but not vertical, rapid shift of a target following jitter motion evoked firing in Ft GCs before arrival of the target to the RF estimated under the Dark BG condition (Matsumoto and Tachibana, 2017). In some visual neurons in the brain, their RFs spatially shift or expand toward the future position of eyes before saccade initiation (frontal eye field; Umeno and Goldberg, 1997; prefrontal cortex; Zirnsak et al., 2014). These dynamic RF changes in visual neurons may contribute to fast and efficient processing of visual information during repetitive sequence of eye movements (Hosoya et al., 2005; Gollisch and Meister, 2008; Wurtz, 2008; Zirnsak et al., 2014). It is possible that, in natural environment, the RF profiles of specific GCs are tuned to global image motion induced by eye movements to facilitate processing in the visual system.

## REFERENCES

- Arai, I., Tanaka, M., and Tachibana, M. (2010). Active role of electrical coupled bipolar cell network in the adult retina. *J. Neurosci.* 30, 9260–9270. doi: 10.1523/JNEUROSCI.1590-10.2010
- Baccus, S. A., Ölveczky, B. P., Manu, M., and Meister, M. (2008). A retinal circuit that computes object motion. *J. Neurosci.* 28, 6807–6817. doi: 10.1523/JNEUROSCI.4206-07.2008
- Baden, T., Berens, P., Franke, K., Román Rosón, M., Bethge, M., and Euler, T. (2016). The functional diversity of retinal ganglion cells in the mouse. *Nature* 529, 345–350. doi: 10.1038/nature16468
- Bair, W., and O'Keefe, L. P. (1998). The influence of fixational eye movements on the response of neurons in area MT of the macaque. *Vis. Neurosci.* 5, 779–786. doi: 10.1017/S0952523898154160
- Bloomfield, S., and Völgyi, B. (2009). The diverse functional roles and regulation of neuronal gap junctions in the retina. *Nat. Rev. Neurosci.* 10, 495–506. doi: 10.1038/nrn2636
- Brainard, D. (1997). The psychophysics tool box. *Spat. Vis.* 10, 443–446.
- Cruikshank, S., Hopperstad, M., Younger, M., Connors, B., Spray, D., and Srinivas, M. (2004). Potent block of Cx36 and Cx50 gap junction channels by mefloquine. *Proc. Natl. Acad. Sci. U.S.A.* 101, 12364–12369. doi: 10.1073/pnas.0402044101
- DeVries, S. H., and Baylor, D. A. (1997). Mosaic arrangement of ganglion cell receptive fields in rabbit retina. *J. Neurophysiol.* 78, 2048–2060. doi: 10.1152/jn.1997.78.4.2048

## DATA AVAILABILITY

The data and codes that used in this research are available at the corresponding author, MT (mstchbn@fc.ritsumei.ac.jp) upon reasonable requests.

## ETHICS STATEMENT

The animal study was reviewed and approved by Committee of Animal Experiments in The University of Tokyo.

## AUTHOR CONTRIBUTIONS

Both authors designed the study, performed all experiments, and wrote the manuscript. AM performed the data analysis.

## FUNDING

This work was supported by Core Research for Evolutional Science and Technology, Japan Science and Technology Agency (CREST, JST) and JST KAKENHI Grant Number JP19K06915 to MT and by Grants-in-Aid for Scientific Research, Japan Society for the Promotion of Science (JSPS) Fellows to AM.

## SUPPLEMENTARY MATERIAL

The Supplementary Material for this article can be found online at: <https://www.frontiersin.org/articles/10.3389/fnins.2019.00979/full#supplementary-material>

- Easter, S., Pamela, R., and Heckenlively, D. (1974). Horizontal compensatory eye movements in goldfish (*Carassius auratus*). *J. Comp. Physiol.* 92, 23–35. doi: 10.1007/bf00696524
- Gollisch, T., and Meister, M. (2008). Rapid neural coding in the retina with relative spike latencies. *Science* 319, 1108–1111. doi: 10.1126/science.1149639
- Gouwens, N. W., Sorensen, S. A., Berg, J., Lee, C., Jarsky, T., Ting, J., et al. (2019). Classification of electrophysiological and morphological neuron types in the mouse visual cortex. *Nat. Neurosci.* 22, 1182–1195. doi: 10.1038/s41593-019-0417-0
- Greschner, M., Bongard, M., Rujan, P., and Ammermüller, J. (2002). Retinal ganglion cell synchronization by fixational eye movements improves feature estimation. *Nat. Neurosci.* 5, 341–347. doi: 10.1038/nn821
- Hilgen, G., Pirmoradian, S., Pamplona, D., Komprobst, P., Cessac, B., Hennig, M. H., et al. (2017). Pan-retinal characterization of light responses from ganglion cells in the developing mouse retina. *Sci. Rep.* 7:42330.
- Hosoya, T., Baccus, S. A., and Meister, M. (2005). Dynamic predictive coding by the retina. *Nature* 436, 71–77. doi: 10.1038/nature03689
- Keesey, U. T. (1960). Effects of involuntary eye movements on visual acuity. *J. Opt. Soc. Am.* 50:769. doi: 10.1364/josa.50.000769
- Krishnamoorthy, V., Weick, M., and Gollisch, T. (2017). Sensitivity to image recurrence across eye-movement-like image transitions through local serial inhibition in the retina. *eLife* 6:e22431. doi: 10.7554/eLife.22431
- Land, M. F. (2009). Vision, eye movements, and natural behavior. *Vis. Neurosci.* 26, 51–62. doi: 10.1017/S0952523808080899

- Lewicki, M. S. (1998). A review of methods for spike sorting: the detection and classification of neural action potentials. *Network* 9, R53–R78.
- Macy, A., and Easter, S. (1981). Growth-related changes in the size of receptive field centers of retinal ganglion cells in goldfish. *Vis. Res.* 21, 1497–1504. doi: 10.1016/0042-6989(81)90221-2
- Mark, R. E., Liu, W. L., and Muller, J. E. (1988). Gap junctions in the inner plexiform layer of the goldfish retina. *Vis. Res.* 28, 9–24. doi: 10.1016/0042-6989(88)90003-x
- Martínez, J. J., Rahsepar, B., and White, J. A. (2017). Anatomical and electrophysiological clustering of superficial medial entorhinal cortex interneurons. *eNeuro* 4:ENEURO.0263-16.2017. doi: 10.1523/ENEURO.0263-16.2017
- Martinez-Conde, S., Macknik, S., and Hubel, D. (2004). The role of fixational eye movements in visual perception. *Nat. Rev. Neurosci.* 5, 229–240. doi: 10.1038/nrn1348
- Martinez-Conde, S., Macknik, S. L., and Hubel, D. H. (2000). Microsaccadic eye movements and firing of single cells in the striate cortex of macaque monkeys. *Nat. Neurosci.* 3, 251–258. doi: 10.1038/72961
- Matsumoto, A., and Tachibana, M. (2017). Rapid and coordinated processing of global motion images by local clusters of retinal ganglion cells. *Proc. JPN. Acad. Ser. B Phys. Biol. Sci.* 93, 234–249. doi: 10.2183/pjab.93.015
- Meister, M., Pine, J., and Baylor, D. A. (1994). Multi-neuronal signals from the retina: acquisition and analysis. *J. Neurosci. Methods* 51, 95–106. doi: 10.1016/0165-0270(94)90030-2
- Mensh, B., Aksay, E., Lee, D., Seung, H., and Tank, D. (2004). Spontaneous eye movements in goldfish: oculomotor integrator performance, plasticity, and dependence on visual feedback. *Vis. Res.* 44, 711–726. doi: 10.1016/j.visres.2003.10.015
- Murakami, I. (2006). Fixational eye movements and motion perception. *Prog. Brain Res.* 154, 193–209. doi: 10.1016/S0079-6123(06)54010-5
- Noda, H., and Adey, W. R. (1974). Retinal ganglion cells of the cat transfer information on saccadic eye movement and quick target motion. *Brain Res.* 70, 340–345. doi: 10.1016/0006-8993(74)90323-0
- Ölveczky, B. P., Baccus, S. A., and Meister, M. (2003). Segregation of object and background motion in the retina. *Nature* 423, 401–408. doi: 10.1038/nature01652
- Pelli, D. (1997). The videotoolbox software for visual psychophysics: transforming numbers into movies. *Spat. Vis.* 10, 437–442. doi: 10.1163/156856897x00366
- Rey, H. G., Pedreira, C., and Quiroga, R. (2015). Past, present and future of spike sorting techniques. *Brain Res. Bull.* 119, 106–117. doi: 10.1016/j.brainresbull.2015.04.007
- Roska, B., and Werblin, F. (2003). Rapid global shifts in natural scenes block spiking in specific ganglion cells types. *Nat. Neurosci.* 6, 600–608. doi: 10.1038/nn1061
- Rousseuw, P. J. (1987). Silhouettes: a graphical aid to the interpretation and validation of cluster analysis. *J. Comput. Appl. Math.* 20, 53–65. doi: 10.1016/0377-0427(87)90125-7
- Rucci, M., Iovin, R., Poletti, M., and Santini, F. (2007). Miniature eye movements enhance fine spatial detail. *Nature* 447, 852–855. doi: 10.1038/nature05866
- Rucci, M., and Poletti, M. (2015). Control and functions of fixational eye movements. *Annu. Rev. Vis. Sci.* 1, 499–518. doi: 10.1146/annurev-vision-082114-035742
- Salas, C., Herrero, L., Rodriguez, F., and Torres, B. (1997). Tectal codification of eye movements in goldfish studied by electrical microstimulation. *Neuroscience* 78, 271–288. doi: 10.1016/S0306-4522(97)83048-5
- Segal, I. Y., Giladi, C., Gedalin, M., Rucci, M., Ben-Tov, M., Kushinsky, Y., et al. (2015). Decorrelation of retinal response to natural scenes by fixational eye movements. *Proc. Natl. Acad. Sci. U.S.A.* 112, 3110–3115. doi: 10.1073/pnas.1412059112
- Segev, R., Schneidman, E., Goodhouse, J., and Berry, M. J. (2007). Role of eye movements in the retinal code for a size discrimination task. *J. Neurophysiol.* 98, 1380–1391. doi: 10.1152/jn.00395.2007
- Tachibana, M., and Kaneko, A. (1988). Retinal bipolar cells receive negative feedback input from GABAergic amacrine cells. *Vis. Neurosci.* 1, 297–305. doi: 10.1017/s0952523800001954
- Tanaka, M., and Tachibana, M. (2013). Independent control of reciprocal and lateral inhibition at the axon terminal of retinal bipolar cells. *J. Physiol.* 591, 3833–3851. doi: 10.1113/jphysiol.2013.253179
- Tien, N. W., Pearson, J. T., Heller, C. R., Demas, J., and Kerschensteiner, D. (2015). Genetically identified suppressed-by-contrast retinal ganglion cells reliably signal self-generated visual stimuli. *J. Neurosci.* 35, 10815–10820. doi: 10.1523/JNEUROSCI.1521-15.2015
- Tulunay-Keesey, U., and Jones, R. M. (1976). The effects of micromovements of the eye and exposure duration on contrast sensitivity. *Vis. Res.* 16, 481–488. doi: 10.1016/0042-6989(76)90026-2
- Umeno, M. M., and Goldberg, M. E. (1997). Spatial processing in the monkey frontal eye field. I. predictive visual responses. *J. Neurophysiol.* 78, 1373–1383. doi: 10.1152/jn.1997.78.3.1373
- Völgyi, B., Kovács-Oller, T., Atlasz, T., Wilhelm, M., and Gábel, R. (2013). Gap junctional coupling in the vertebrate retina: variations on the theme? *Prog. Retin. Eye Res.* 34, 1–18. doi: 10.1016/j.preteyeres.2012.12.002
- Werblin, F. (2011). The retinal hypercircuit: a repeating synaptic interactive motif underlying visual function. *J. Physiol.* 589, 3691–3702. doi: 10.1113/jphysiol.2011.210617
- Wurtz, R. (2008). Neuronal mechanisms of visual stability. *Vis. Res.* 48, 2070–2089. doi: 10.1016/j.visres.2008.03.021
- Yarbus, A. L. (1967). *Eye Movements and Vision*. New York, NY: Plenum.
- Yuan, C., and Yang, H. (2019). Research on K-value selection method of K-means clustering algorithm. *J. Multidiscip. Sci.* 2, 226–235. doi: 10.3390/j2020016
- Zhang, P. M., Wu, J. Y., Zhou, Y., Liang, P. J., and Yuan, J. Q. (2004). Spike sorting based on automatic template reconstruction with a partial solution to the overlapping problem. *J. Neurosci. Methods* 135, 55–65. doi: 10.1016/j.jneumeth.2003.12.001
- Zirnsak, M., Steinmetz, N. A., Noudoost, B., Xu, K. Z., and Moore, T. (2014). Visual space is compressed in prefrontal cortex before eye movements. *Nature* 507, 504–507. doi: 10.1038/nature13149

**Conflict of Interest Statement:** The authors declare that the research was conducted in the absence of any commercial or financial relationships that could be construed as a potential conflict of interest.

Copyright © 2019 Matsumoto and Tachibana. This is an open-access article distributed under the terms of the Creative Commons Attribution License (CC BY). The use, distribution or reproduction in other forums is permitted, provided the original author(s) and the copyright owner(s) are credited and that the original publication in this journal is cited, in accordance with accepted academic practice. No use, distribution or reproduction is permitted which does not comply with these terms.



# Supraspinal Shaping of Adaptive Transitions in the State of Functional Connectivity Between Segmentally Distributed Dorsal Horn Neuronal Populations in Response to Nociception and Antinociception

Mario Martín<sup>1,2\*</sup>, Javier Béjar<sup>1,2</sup>, Diógenes Chávez<sup>3</sup>, Adrian Ramírez-Morales<sup>3</sup>, Edson Hernández<sup>3</sup>, Leonardo Moreno<sup>3</sup>, Enrique Contreras-Hernández<sup>3</sup>, Silvio Glusman<sup>3,4</sup>, Ulises Cortés<sup>1,2</sup> and Pablo Rudomin<sup>3,5\*</sup>

<sup>1</sup> BarcelonaTech, Universitat Politècnica de Catalunya, Catalonia, Spain, <sup>2</sup> Barcelona Supercomputing Center, Catalonia, Spain, <sup>3</sup> Department of Physiology, Biophysics and Neurosciences, Center for Research and Advanced Studies, National Polytechnic Institute, Mexico City, Mexico, <sup>4</sup> Stroger Cook County Hospital, Chicago, IL, United States, <sup>5</sup> El Colegio Nacional, Mexico City, Mexico

## OPEN ACCESS

### Edited by:

Mehdi Adibi,  
University of New South Wales,  
Australia

### Reviewed by:

Kyle Baumbauer,  
University of Kansas Medical Center,  
United States  
Michelle Hook,  
Texas A&M University, United States

### \*Correspondence:

Mario Martín  
mmartin@cs.upc.edu  
Pablo Rudomin  
rudomin@fisio.cinvestav.mx;  
pablo.rudomin@gmail.com

**Received:** 26 April 2019

**Accepted:** 26 August 2019

**Published:** 26 September 2019

### Citation:

Martín M, Béjar J, Chávez D, Ramírez-Morales A, Hernández E, Moreno L, Contreras-Hernández E, Glusman S, Cortés U and Rudomin P (2019) Supraspinal Shaping of Adaptive Transitions in the State of Functional Connectivity Between Segmentally Distributed Dorsal Horn Neuronal Populations in Response to Nociception and Antinociception. *Front. Syst. Neurosci.* 13:47. doi: 10.3389/fnsys.2019.00047

In the anesthetized cat the correlation between the ongoing cord dorsum potentials (CDPs) recorded from different lumbar spinal segments has a non-random structure, suggesting relatively stable patterns of functional connectivity between the dorsal horn neuronal ensembles involved in the generation of these potentials. During the nociception induced by the intradermic injection of capsaicin, the patterns of segmental correlation between the spontaneous CDPs acquire other non-random configurations that are temporarily reversed to their pre-capsaicin state by the systemic injection of lidocaine, a procedure known to decrease the manifestation of neuropathic pain in both animals and humans. We have now extended these studies and utilized machine learning for the automatic extraction and selection of particular classes of CDPs according to their shapes and amplitudes. By using a Markovian analysis, we disclosed the transitions between the different kinds of CDPs induced by capsaicin and lidocaine and constructed a global model based on the changes in the behavior of the CDPs generated along the whole set of lumbar segments. This allowed the identification of the different states of functional connectivity within the whole ensemble of dorsal horn neurones attained during nociception and their transitory reversal by systemic administration of lidocaine in preparations with the intact neuroaxis and after spinalization. The present observations provide additional information on the state of self-organized criticality that leads to the adaptive behavior of the dorsal horn neuronal networks during nociception and antinociception both shaped by supraspinal descending influences.

**Keywords:** cord dorsum potentials, dorsal horn neurons, functional connectivity, machine learning, Markov process, state transitions, nociception, antinociception

## INTRODUCTION

Previous work has shown that in the anesthetized cat the spontaneous cord dorsum potentials (CDPs) recorded in a given lumbar segment have different shapes and amplitudes and may appear synchronized with potentials generated in other spinal segments (Contreras-Hernández et al., 2018). The correlation matrix between the CDPs recorded from different segments had a non-random structure, suggesting relatively stable patterns of functional connectivity between the dorsal horn neuronal ensembles involved in the generation of these potentials. During the chemical nociception induced by the intradermic injection of capsaicin, the patterns of segmental correlation between the spontaneous CDPs were reorganized and acquired other non-random configurations that were temporarily reversed to their pre-capsaicin state by the systemic injection of a small dose of lidocaine, a procedure known to reduce neuropathic pain in humans.

At present, we have limited information on the identity of the neuronal populations underlying the changes in the correlation between the spontaneous CDPs induced by nociceptive stimulation and their reversal by lidocaine. While searching for intermediate nucleus interneurons mediating presynaptic inhibition (Rudomin et al., 1987), we found one set of neurones (Type I) whose activity was preceded by negative CDPs (nCDPs) and another set (Type II) that was instead preceded by negative-positive CDPs (npCDPs). The activation of type I neurones led to the generation of short-lasting glycinergic inhibitory potentials in motoneurones, while the activation of Type II neurones was instead associated with the generation of inhibitory GABAergic potentials in motoneurones and with primary afferent depolarization (PAD) and presynaptic inhibition.

We initially assumed that separate populations of dorsal horn neurones generated the nCDPs and npCDPs (Rudomin et al., 1987). However, subsequent work has indicated that depending on the magnitude of the ongoing neuronal synchronization, nCDPs and npCDPs could be generated by the same population of dorsal horn neurones (Contreras-Hernández et al., 2015). During low levels of synchronization, activation of the dorsal horn neuronal ensemble would mainly generate nCDPs, and there would be a concurrent activation of the pathways mediating non-reciprocal glycinergic post-synaptic inhibition. In contrast, during higher states of neuronal synchronization, the activation of the same set of dorsal horn neurones would lead to the generation of npCDPs and to a preferential activation of the pathways mediating a GABA<sub>A</sub> PAD and presynaptic inhibition.

These observations indicated that the intrinsic patterns of functional connectivity between the populations of dorsal horn neurones determines their interaction with other neuronal networks. Yet, several questions remained to be addressed, among them, (a) how the functional connectivity of the neuronal populations generating the different classes of spontaneous CDPs changes after nociception and antinociception, (b) how the concurrent changes in neuronal connectivity affect information transmission and organization in sensory and motor pathways, and (c) which neurones are involved in the generation of

the different classes of spontaneous CDPs, in addition to the nCDPs and npCDPs.

To approach the first two questions we utilized Machine Learning procedures that use similarity criteria for the automatic selection and classification of the ongoing CDPs according to their shape and amplitude (see Béjar et al., 2015; Martin et al., 2015). We used this procedure to build dictionaries with CDPs selected under basal (control) conditions to estimate the changes produced during nociception and antinociception on the probabilities of occurrence of the different classes of CDPs, a task that would be otherwise difficult to achieve using predetermined template selection methods such as those employed in previous studies (see Chávez et al., 2012; Contreras-Hernández et al., 2015).

The present study shows that in preparations with intact neuroaxis, the intradermic injection of capsaicin reduced the fractional probabilities of occurrence of most of the classes comprising the small amplitude CDPs and increased the probabilities of the largest CDPs. Following the systemic injection of a small dose of lidocaine, the different classes of CDPs temporarily displayed, rather closely, their fractional probabilities of occurrence attained before the nociceptive stimulation.

The changes displayed by the different classes of CDPs during the action of capsaicin and lidocaine were largely attenuated in previously spinalized preparations, a finding suggesting that supraspinal influences shape the activation and adaptability of spinal networks in response to nociception.

By using a Markovian analysis, we further estimated the transitions between the different kinds of CDPs induced by capsaicin and lidocaine and constructed a global model based on the changes in the behavior of the CDPs generated along the whole set of lumbar segments. This allowed the identification of the different states of functional connectivity within the whole ensemble of dorsal horn neurones attained during nociception and after the systemic administration of lidocaine in preparations with the intact neuroaxis as well as in previously spinalized preparations. These observations provide additional evidence pertaining the role of supraspinal influences in the shaping of the functional connectivity between dorsal horn neurones, a process of significance for information transmission and processing in the spinal cord. A previous account of these findings has been presented in Rudomin et al. (2016).

## MATERIALS AND METHODS

### General Procedures

The data analyzed in this report were obtained from experiments included in a previous study (Contreras-Hernández et al., 2018) performed in adult cats of both sexes weighting between 2.4 and 4.5 Kg, initially anaesthetized with pentobarbitone sodium (40 mg/kg i.p.). During the dissection additional doses of pentobarbitone sodium (5 mg/kg/h) were given intravenously to maintain an adequate level of anesthesia, tested by assessing that withdrawal reflexes were absent, that the pupils were constricted

and that systolic arterial blood pressure was between 100 and 120 mm Hg.

The lumbosacral and low thoracic spinal segments were exposed by laminectomy and opening of the dura mater. After the primary surgical procedures, the animals were transferred to a stereotaxic metal frame allowing immobilization of the head and spinal cord and pools were made with the skin flaps that were filled with paraffin oil to prevent desiccation of the exposed tissues. The temperature was maintained between 36 and 37°C using radiant heat.

Subsequently, the animals were paralyzed with pancuronium bromide (0.1 mg/kg) and artificially ventilated. The tidal volume was adjusted to maintain 4% of CO<sub>2</sub> concentration in the expired air. During paralysis, adequacy of anesthesia was ensured with supplementary doses of anesthetic (2 mg/kg in an hour) and by repeatedly assessing that the pupils remained constricted and that heart rate and blood pressure were not changed following a noxious stimulus (paw pinch).

Cord dorsum potentials were simultaneously recorded by means of 8–12 silver ball electrodes placed on the surface of the L4–L7 segments on both sides of the spinal cord using separate preamplifiers (bandpass filters 0.3 Hz to 1 kHz), visualized on-line and digitally stored for further analysis with software written in MatLab (MathWorks) and LabView version 14 (National Instruments).

As described by Rudomin and Hernández (2008), 30 µl of 1% solution of capsaicin diluted in 10% Tween 80 and 90% saline (around 7.5 µg/kg) were injected in the plantar cushion of the left hindlimb. To avoid desensitization, capsaicin was injected only once (Sakurada et al., 1992). The effects of capsaicin started around 10–20 min after injection, attained maximum values between 100 and 180 min and persisted up to 4 h. The injection of capsaicin produced a clear inflammatory response around the injection site (see Rudomin and Hernández, 2008).

In this series of experiments, a solution of Lidocaine (5 mg/kg diluted in 6 cc of isotonic saline) was slowly injected (20–30 min) through a separate catheter inserted in the right femoral vein. We used systemic application of lidocaine because this is the procedure that has been successfully used both clinically and experimentally to reduce neuropathic pain and preemptive analgesia (see Woolf and Chong, 1993; Kissin, 2000).

The usual procedure was to make control recordings of the spontaneous CDPs during 30–60 min that were followed by recordings made after the intradermic injection of capsaicin into the footpad of the left hindlimb and also after the systemic administration of lidocaine. Spinalization was performed by bathing the exposed T4 segment with chilled Ringer solution for about 10 min, spraying it with liquid nitrogen until it was completely frozen and sectioned thereafter. At the end of the experiment, the animal was euthanized with a pentobarbital overdose and perfused with 10 p.c. formalin. The spinal cord was removed for fixation and dehydration to examine the completeness of the spinal sections.

## Data Processing

### Extraction of Spontaneous CDPs With Specific Shapes and Amplitudes

To extract the CDP sequences we used the Machine Learning method described in a previous study (Martin et al., 2015). To this end, the whole procedure was divided into several steps that included: (a) the extraction of the CDPs from the raw recordings, (b) the classification and discretization of the selected CDPs, and (c) the analysis of their behavior at different levels of granularity in the spatial and temporal domain. This included the construction of histograms to display the fractional probability of occurrence of each class of the selected CDPs relative to the total number of CDPs extracted from a fixed time window (5–10 min). See **Appendix** for further details.

### Sequential Behavior of the CDPs Recorded in Lumbar Segments

We have previously shown (Martin et al., 2015) that the dictionaries made with the CDPs extracted from control recordings made in different experiments were relatively stable during prolonged time periods (30–60 min). We also found that in a given segment, each time set had a specific dynamical behavior that was changed by the intradermic injection of capsaicin as well as by spinalization.

In order to capture these differences and to obtain a high-level description of the changes in the CDPs occurring during the experiment in different spinal segments, we considered that the firing of one set of neurones (and so, the generation of a given class of CDP) depended on the last activated ensemble of neurones. That is, on the preceding CDP. In other words, we assumed that the generation of a given CDP could be described as a Markovian process of degree 1 (see Martin et al., 2017).

This means that the organization of the networks involved in the generation of the CDPs is not a simple probabilistic independent activation of the different ensembles of neurones, but rather a consequence of the structured connectivity between them. Hence, we assumed that the set of transition probabilities between the different classes of CDPs could provide relevant information on the state of functional connectivity between the different neuronal ensembles involved in the generation of the examined CDPs, both at rest and during the different experimental procedures. See **Appendix** for further details.

### Likelihood Computation and Similarity Index Definition

To compare sequences of CDPs generated in the same segment during different experimental procedures, we defined a new similarity measure. First, each segment and time step was represented by a model consisting of the probability matrix of conditional dependence limited to the last CDP. This model was built from the sequence of CDPs recorded in segment  $l$ , at time step  $s$  under the assumption of a Markovian behavior of the sequence of order 1 (see Martin et al., 2017). We then computed the likelihood of this model to generate data recorded in another time step  $s'$ . This likelihood was used to estimate if different time steps obtained from the same lumbar segment under a specific experimental condition (e.g., control recordings)

had or not a similar behavior. To build a similarity index for the different steps, instead of working with probability values, we worked (for numerical stability reasons) with the logarithm of the probabilities.

Finally, given that maximum likelihood for a given sequence obtained from the experimental data resembled the sequence from which the model was created, we normalized the log likelihood values to allow an easy comparison between steps. Values were within the range [0.1], with 0 when the probability of the model to generate a given sequence was 0, and 1 when the probability of generating the sequence was the same as that generated by the source data from which the model was built. Notice that this is not a symmetric measure. However, we still used it as an index of similarity to build neighborhood graphs, where non-symmetric relations are common.

### Similarity Graph Generation

This approach was used to obtain a high-level interpretation of the behavior of the CDPs recorded in different spinal segments induced by several experimental procedures. To this end, for a given spinal segment, we computed the similarity index between CDPs recorded during successive time steps with a comparable Markovian structure. This information was visualized by constructing a neighborhood graph where each node represented a time step of the experiment and the edges connected steps that were considered similar using the criteria described in the previous section. In these graphs, nodes were connected only to the most similar nodes that also exceeded a threshold of similarity index. This procedure allowed display of only the highly significant connections. As detailed in the **Appendix**, the WalkTrap method (Pons and Latapy, 2005) was followed to identify clusters of nodes that share significant similarities.

### Consensus Graph Generation

To obtain a general vision of the behavior of the whole lumbar ensemble of dorsal horn neurones generating the selected classes of CDPs, we generated a single consensus graph that included the information obtained from all segments. To this end, we applied ensemble methods used in machine learning that consider the expert's predictions to obtain a single consensus graph. In order to increase the reliability of the obtained graphs we implemented a majority voting procedure to obtain a single representation of the whole behavior of the CDPs.

This procedure included the following: (a) given a lumbar segment, for each step in that segment we made a list with the most similar steps above a threshold. This list was considered as votes for the similar steps in that segment, (b) we collected the votes produced in all lumbar segments, (c) a consensus graph was built with a node for each step with lines joining the  $k$  most voted steps, and (d) the graph was segmented into clusters of nodes using the WalkTrap method. The consensus graph not only describes the overall behavior of the neuronal networks but also describes it with a degree or reliability higher than that obtained by observing the selected set of CDPs in each segment (see **Appendix** for more details).

### Similitude Between Pairs of Histograms of CDPs

In order to assess the similarity in the probability distribution of the CDPs generated in a given segment during different maneuvers, we used a similarity measure to compare the histograms of the clusters of CDPs. This measure is based on the test developed in Bityukov et al. (2016). Let us consider a simple model with two histograms where the random variable in each bin obeys the normal distribution

$$p(x|n_{ik}) = \frac{1}{\sqrt{2\pi}\sigma_{ik}} e^{-\frac{(x-n_{ik})^2}{2\sigma_{ik}^2}} \quad (1)$$

where the expected value in the bin  $i$  is equal to  $n_{ik}$  and the variance  $\sigma_{ik}^2 = n_{ik}$  and  $k$  is the histogram number ( $k = 1, 2$ ). We define the significance as

$$\hat{S}_i = \frac{\hat{n}_{i1} - \hat{n}_{i2}}{\sqrt{\hat{\sigma}_{i1}^2 + \hat{\sigma}_{i2}^2}} \quad (2)$$

where  $\hat{n}_{ik}$  is an observed value in the bin  $i$  of the histogram  $k$  and  $\hat{\sigma}_{ik}^2 = \hat{n}_{ik}$ . This model can be considered as the approximation of the Poisson distribution by the Normal distribution. The values  $n_{ik}$  ( $i = 1, 2, \dots, M$ ,  $k = 1, 2$ ) are the numbers of events appeared in the bin  $i$  for the histogram  $k$ . We consider the *RMS* (the root mean square) of the distribution of the significances

$$RMS = \sqrt{\frac{\sum_{i=1}^M (\hat{S}_i - \bar{S})^2}{M}} \quad (3)$$

Here,  $\bar{S}$  is the mean value of  $\hat{S}_i$ . The *RMS* measures the distance between two histograms. If total number of events  $N_1$  in the histogram 1 and total number of events  $N_2$  in the histogram 2 are different, then the normalized significance  $\hat{S}_i(K)$  is calculated as follows

$$\hat{S}_i(K) = \frac{\hat{n}_{i1} - K\hat{n}_{i2}}{\sqrt{\hat{\sigma}_{i1}^2 + K^2\hat{\sigma}_{i2}^2}} \quad (4)$$

where  $K = N_1/N_2$ . The relation  $RMS^2 = \chi^2/M - \bar{S}^2$  exists for the distribution of significances where  $\chi^2 = \sum_{i=1}^M \hat{S}_i^2$ . One can show that the distribution of observed significances is close to normal distribution with the  $RMS \sim 1$ . This distance measure between two histograms has a clear interpretation:  $RMS \sim 0$  histograms are identical,  $RMS \sim 1$  both histograms are obtained from the same parent distribution,  $RMS \gg 1$  histograms are obtained from different parent distributions.

## RESULTS

### Effects of Capsaicin and Lidocaine on Different Classes of CDPs Recorded in Preparations With Intact Neuroaxis

As in previous studies (Manjarrez et al., 2000, 2003; Chávez et al., 2012; Contreras-Hernández et al., 2015; Martin et al., 2017), we found that the ongoing potentials recorded in the dorsum of the lumbar spinal segments included a series of brief potentials

(CDPs), some of which appeared synchronously in different segments (**Figure 1A**). By 1 h after the nociceptive stimulation produced by the intradermal injection of capsaicin, the ongoing CDPs showed, in addition to the brief potentials, a series of slow synchronized oscillations (**Figure 1B**) that were transiently suppressed after the systemic injection of lidocaine, leaving sequences of brief potentials that resembled those recorded before the injection of capsaicin (**Figure 1C**). As the effect of lidocaine faded, the slow oscillations reappeared and were, in fact, more apparent than those recorded just before the administration of lidocaine (**Figure 1D**). Following acute spinalization, the slow synchronized oscillations were no longer observed and brief synchronized potentials were again generated (**Figure 1E**). These potentials appeared to be marginally affected by the second injection of lidocaine (**Figure 1F**).

One of the questions that were left unanswered in our previous study (Contreras-Hernández et al., 2018) pertained the mode of action of capsaicin and lidocaine on the patterns of functional connectivity between the dorsal horn neuronal ensembles involved in the generation of specific sets of CDPs. We assumed that some clues could be obtained by examining the changes on the probabilities of occurrence of the different classes of ongoing CDPs induced by nociception as well as during the antinociception produced by systemic lidocaine. To this end, we used machine learning (see section “Materials and Methods” and specially Martin et al., 2015) to identify and select the ongoing CDPs recorded in each segment according to their shape and amplitude and examine how capsaicin, lidocaine, and spinalization affected the fractional probabilities of occurrence of each class of CDPs.

**Figures 1G,H** show the means of the 12 different classes of CDPs selected from recordings made in segments *L5rL* (left rostral L5 lumbar segment) and *L6rL* (left rostral L6 lumbar segment). These CDPs were ordered according to their *control* probabilities of occurrence during each of the 10 min steps and displayed as vertical black bars in the corresponding histograms.

It may be seen that some of the selected CDPs started from a flat baseline and were purely negative, resembling the nCDPs reported in previous studies (e.g., classes 2 and 9 in *L5rL* and classes 1 and 6 in *L6rL*), while others were negative-positive (classes 8 and 12 in *L5rL* and classes 5, 9, and 12 in *L6rL*) resembling the npCDPs. There were in addition other classes of CDPs in which the main negative potential was preceded either by a slow negative component (classes 6, 7, and 10 in *L5rL* and classes 4, 7, and 8 in *L6rL*), or by a positive component (classes 1, 4, and 11 in *L5rL* and classes 3 and 11 in *L6rL*).

As shown by the black bars in the histograms, in both segments the fractional probabilities of occurrence of each class of the selected CDPs were relatively constant during the control periods (three consecutive 10 min bins in this case). Quite interestingly, the classes comprising the smallest CDPs recorded during the control periods had higher fractional probabilities of occurrence than the classes including the largest CDPs (see also Martin et al., 2015).

The red bars in the histograms show that the intradermal injection of capsaicin had mixed effects on the fractional probabilities of occurrence of the CDPs: they were gradually

reduced in some of the classes comprising the smallest CDPs (classes 1–5 in segment *L5rL* and classes 1–3 in segment *L6rL*), increased in other classes of CDPs (classes 7, 8, and 10 in segment *L5rL* and classes 7, 8, 10–12 in segment *L6rL*), or else remained unaffected.

After the systemic injection of lidocaine (blue bars), the effects of capsaicin were reversed in a differential manner for a short time period (20–40 min). That is, lidocaine increased the probabilities of those CDPs showing low probabilities of occurrence after capsaicin and reduced the probabilities of the CDPs with higher probabilities. The reversal by lidocaine of the effects of capsaicin was over by 60–80 min after its systemic administration. After spinalization, the probabilities of occurrence of the different classes of CDPs (white bars) were also changed but to a smaller extent by a second injection of lidocaine.

We have performed a Student's *t*-test to assess the changes in the fractional probabilities of occurrence in each of the different classes of CDPs displayed in the histograms of **Figures 1G,H** induced by capsaicin, lidocaine, and spinalization. To this end we used as reference the average of the three control probabilities that were compared with those obtained during the different procedures at the times indicated with the brackets on the histograms. Statistical significance between the different sets is indicated in the figure by the asterisks ( $***p < 0.001$ ,  $**p < 0.01$ , and  $*p < 0.05$ ).

The finding that the shapes of the different classes of the CDPs selected in segment *L5rL* resembled rather closely those extracted from recordings made in segment *L6rL* (and in other lumbar segments as well) further supports our previous proposal that the different classes of CDPs are generated by the activation of a segmentally distributed ensemble of interconnected dorsal horn neurones (Manjarrez et al., 2000, 2003; Chávez et al., 2012; Contreras-Hernández et al., 2015; Martin et al., 2017).

## State Transitions

To have some information on the global state of the neuronal networks involved in the generation of the different classes of CDPs, we used similarity procedures to compare the probabilities of occurrence of all the classes of CDPs generated in a given segment during a particular moment with the probabilities of the potentials generated at another time in the same segment. For example, on the extent to which the set of CDPs recorded during the Control 1 period resembled the potentials recorded during the Control 2 period and so on.

In order to assess the differences between the probabilities of occurrence of the whole set of the selected classes of CDPs during the different maneuvers we used a test based on the significance of differences between histograms (see section “Similitude Between Pairs of Histograms of CDPs”). The obtained RMS values were displayed in a matrix relating the similarity of the histograms. **Figures 2A,B** shows the evolution of the changes in the probabilities of occurrence of the CDPs recorded in two neighboring spinal segments (*L5rL* and *L6rL*), measured by the RMS of the distribution of significances.

This figure displays the RMS values between pairs of histograms. The lower the RMS values, the more similar the histograms (see color scale on the right). A zero RMS would

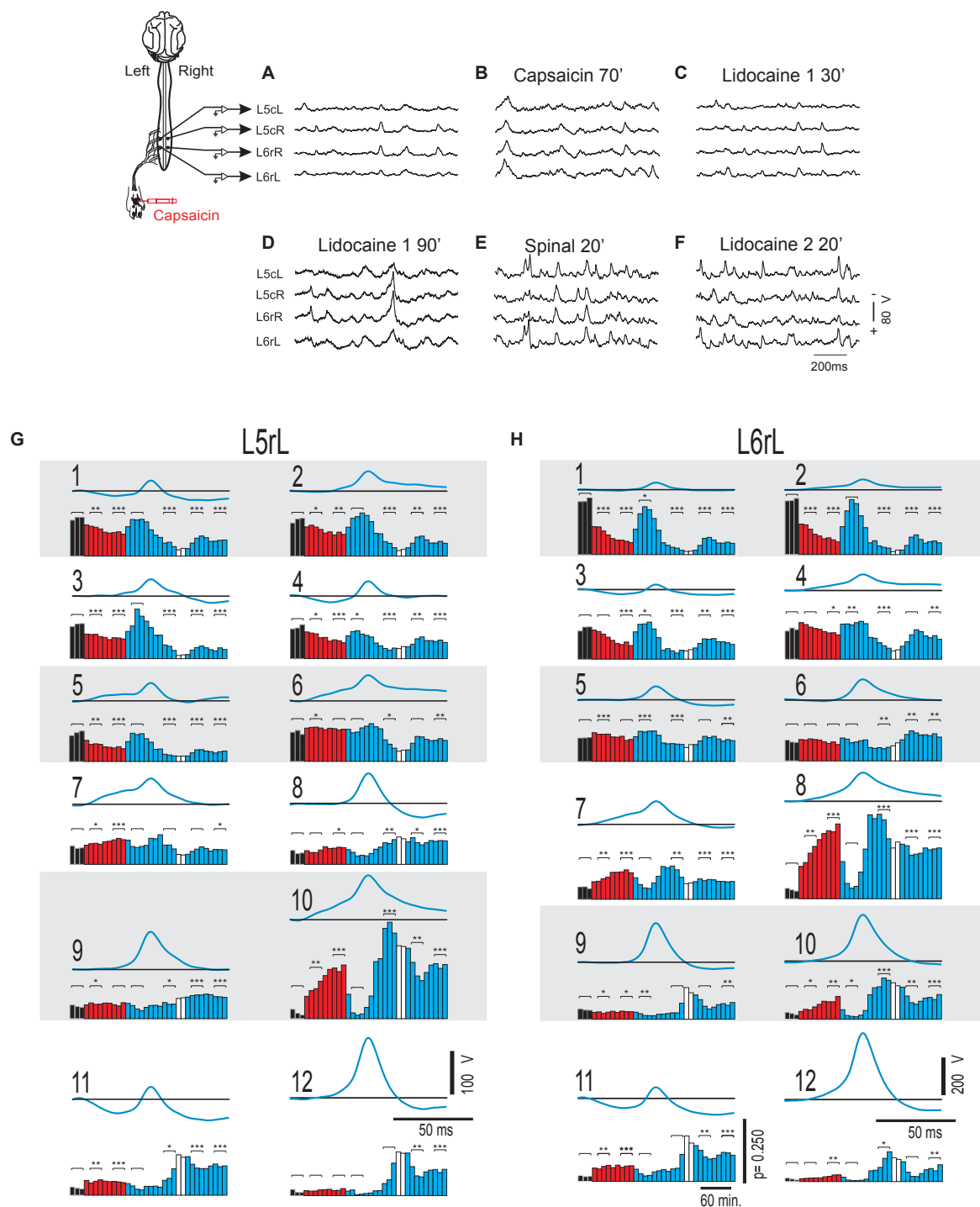


**FIGURE 1 |** Changes in the shape dictionaries of the CDPs recorded in two spinal segments during the action of capsaicin and lidocaine and after spinalization. **(A–F)** Samples of raw recordings of the ongoing CDPs made in the left and right sides of the caudal region of the L5 segment (L5cL and L5cR) and rostral region of the L6 segment (L6rL and L6rR), as indicated. **(A)** Control. **(B)** 70 min after the intradermic injection of capsaicin in the left hindpaw. **(C,D)** 30 and 90 min after the first injection of lidocaine. **(E)** 20 min after a complete spinal transection at T4 and **(F)** 20 min after a second injection of lidocaine. **(G,H)** Shape dictionaries of the CDPs recorded in the L5rL and L6rL lumbar segments and histograms of the fractional probabilities of occurrence of each shape during successive time steps, as indicated. Black bars, control steps; Red bars, capsaicin steps; Blue bars, spinalization steps followed by a second administration of lidocaine. White bars, spinalization steps followed by a second administration of lidocaine. The brackets and asterisks over each set of columns indicate the statistical significance of the fractional probabilities of occurrence of each class of CDPs and the corresponding control probabilities (\*\*\* $p < 0.001$ , \*\* $p < 0.01$ , and \* $p < 0.05$ ). See text for further explanations.

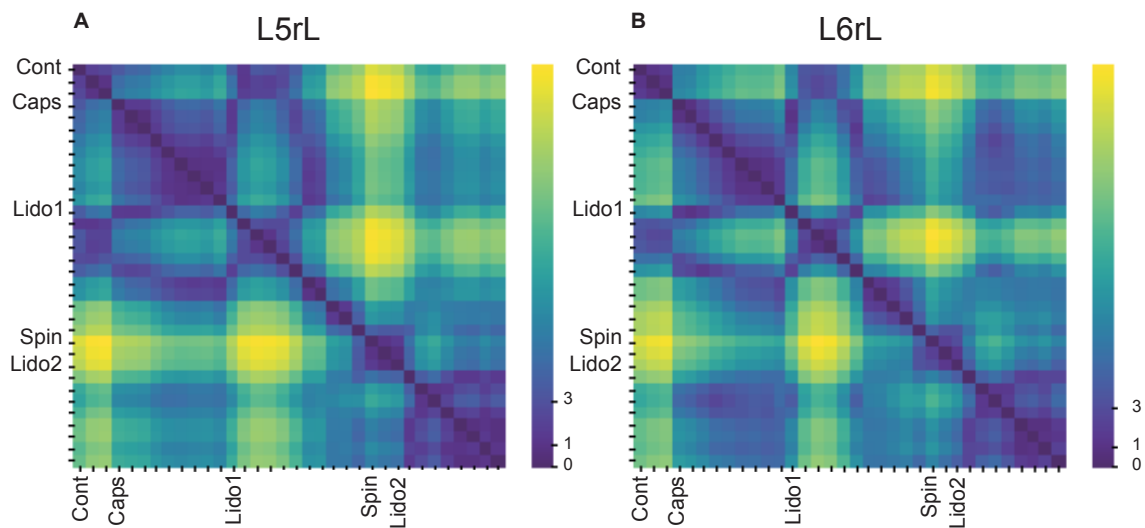


**FIGURE 2 | (A,B)** Comparison of the histograms of probabilities of the CDPs recorded in two spinal segments (*L5rL*, *L6rL*) during the action of capsaicin and lidocaine and after spinalization using the RMS of the distribution of significances. Each change in maneuver induces an important change in the distribution of the probabilities of occurrence of the CDPs with different shapes. Each matrix value shows RMS statistic for a given pair of steps of the experiment. Values closer to approximately 0–2 (darkest colors) mean that histograms of probabilities of CDPs in both steps are significantly similar according to RMS significance test. The higher the value of RMS, the higher the differences in the histogram of probability of the CDPs. See section “Similitude Between Pairs of Histograms of CDPs” for further details.

indicate that both histograms were identical. Higher RMS values would mean increasing dissimilarities. It may be seen that both matrices were remarkably similar in general with minor differences in detail (see color patterns). For example, the first three vertical columns in the left side of the figure (control histograms) were rather similar to each other in both segments (low RMS values, dark blue). They became gradually dissimilar during the action of capsaicin, slightly more in the L6 than in the L5 segment (light blue, steps 1–3 to green, steps 4–9). The histograms obtained after the first injection of lidocaine became temporarily similar to the control histograms in both segments (shift to dark blue, steps 1–6) and dissimilar later on (shift to light green, steps 7–11), thus resembling the effects of capsaicin. Spinalization reduced similarity with control histograms rather abruptly (shift to yellow) that was again slightly increased after the second injection of lidocaine. Notice that the effects produced by lidocaine before and after spinalization were quite dissimilar.

**Figures 3A,B** illustrates the transitions produced by capsaicin, lidocaine, and spinalization on the different classes of CDPs extracted from the rostral regions of the *L5* and *L6* segments in the left side obtained from the same set of data as those used to generate **Figure 1**. Each graph shows the similarity of the whole set of CDPs obtained at a given moment with the CDPs recorded at other times. The structure of the CDPs recorded during each procedure can be identified by the internal similarities among each one of the steps as show in **Figure 2**. For example, in **Figures 3A,B**, control steps 1, 2, and 3 appear close together, both in segment *L5rL* and in segment *L6rL*, suggesting that the control distributions of the different classes of CDPs in each segment were rather similar and behaved alike in these segments. These

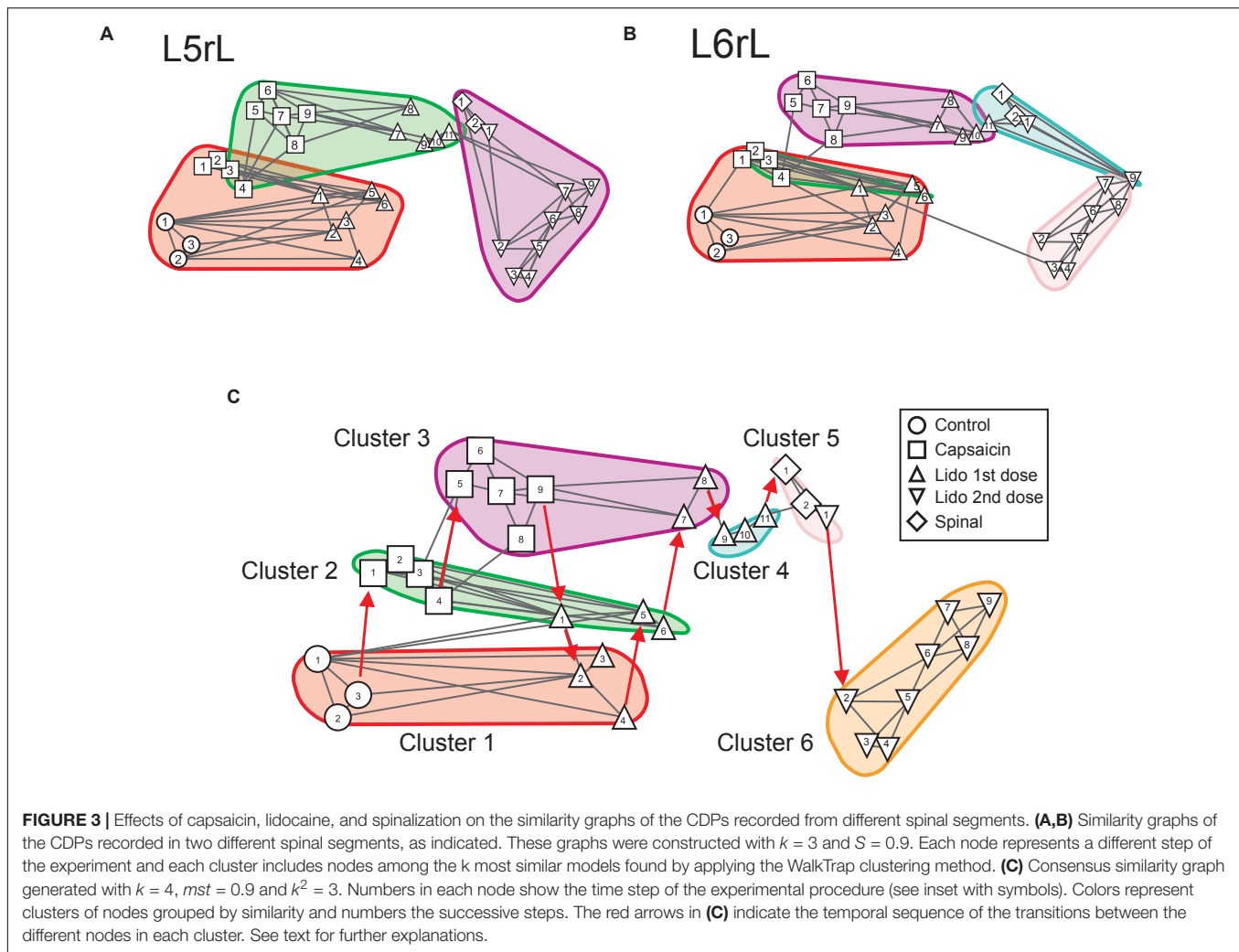
control groups became clearly differentiated from the capsaicin steps 5–9 in segments *L5rL* and *L6rL*.

After lidocaine, the node distributions transiently resembled the control distributions (e.g., lidocaine steps 1–6 in *L5rL* and in *L6rL*). Later on (steps 7–11), the distributions attained in segments *L5rL* and *L6rL* resembled those seen during capsaicin steps 5–9. They became separated after spinalization (spinal steps 1 and 2). Quite interestingly, after the second injection of lidocaine applied in the already spinalized preparation, the distributions remained within the same cluster in segment *L5rL* but not in segment *L6rL*. The transitions between the different classes of CDPs produced by capsaicin and lidocaine illustrated in **Figures 3A,B** were not limited to the *L5* and *L6* segments, but were also seen in all the other spinal segments (not illustrated). Although each one of them displayed its own particular features, the transitions between the different classes of CDPs followed similar patterns, in the sense that in all segments each experimental procedure shifted the state of functional connectivity in a similar direction.

In other words, every group of steps from the individual graphs remained clustered nearly in the same way in all lumbar segments. So, if these structures were similar at the local level, it is possible that they would also do it in a global level.

## Consensus Graphs

We have used the consensus graphs to examine the effects of nociception and antinociception on the global behavior of the CDPs recorded in both sides in the *L4* to *L7* spinal segments. The data depicted in **Figures 3A,B** show state transitions of the CDPs generated in two spinal segments following the



intradermal injection of capsaicin, how the systemic injection of lidocaine temporarily reversed these state transitions and how they were affected by a subsequent spinalization. It thus seemed of interest to examine the state transitions of the whole segmental ensemble of CDPs induced by the different experimental procedures. That is, of the global state transitions. This was achieved by building a unique consensus graph using a majority voting procedure (see section “Materials and Methods” and **Appendix**).

**Figure 3C** shows the consensus graph obtained from the data recorded in segments L4–L7 in both sides, in the same experiment as that of **Figure 1**. In this case, similar nodes were grouped in the same cluster. The red arrows indicate the temporal sequence of the transitions between the different nodes in each cluster induced by capsaicin, lidocaine, and spinalization.

Cluster 1 includes the control nodes (control steps 1–3, circles). The injection of capsaicin produced an initial transition of the nodes to cluster 2 (capsaicin steps 1–4, squares), and later on to cluster 3 (capsaicin steps 5–9, squares). The injection of lidocaine again shifted the nodes, initially to cluster 2 (lidocaine

step 1, upward triangle) and later on to cluster 1 (lidocaine steps 2–4, upward triangles) resembling the control nodes.

As the effect of lidocaine faded, the nodes appeared in cluster 2 (lidocaine steps 5–6, upward triangles), later on in cluster 3 (lidocaine steps 7–8, upward triangles) and then in cluster 4 (lidocaine steps 9–11, upward triangles). Clusters 5 and 6 include the nodes obtained after spinalization (diamonds) and the second injection of lidocaine (downward triangles), respectively. It is quite clear that the configuration of the CDPs in these clusters had no resemblance with the configuration seen before spinalization.

In Contreras-Hernández et al. (2018), we examined the functional relations between the dorsal horn neuronal networks involved in the generation of the synchronized activity in different spinal segments by calculating the coefficients of correlation between the different sets of segmental potentials recorded during 10 min periods. These data were used to construct the correlogram illustrated in **Figure 4A**. The first column in this correlogram (Control 0) displays the coefficients of correlation between the different paired sets of L4–L7 CDPs recorded with the ensemble of 12 electrodes. These coefficients were arranged in decreasing order and displayed vertically (see

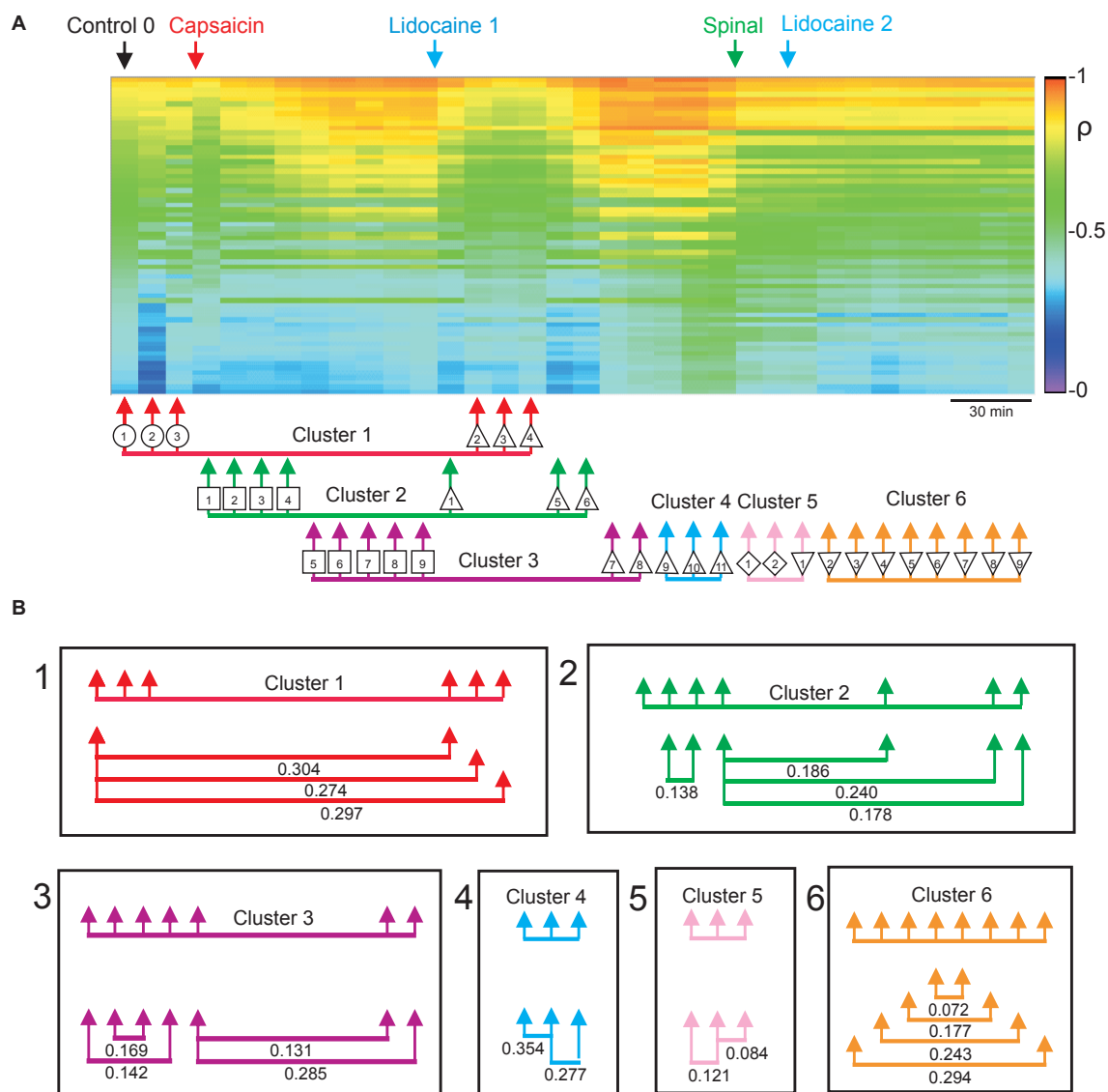


**FIGURE 4 |** Changes in correlation and similarity between paired sets of CDPs produced by capsaicin, lidocaine, and spinalization. **(A)** Coefficients of correlation between paired sets of CDPs generated during successive 10 min recording periods. The coefficients of correlation obtained during the Control 0 period are shown in descending order as a vertical column. The coefficients of correlation of recordings made at subsequent times are displayed keeping the same order as the Control 0 coefficients. Colors show the magnitude of the correlation (see scale). Arrows show time of capsaicin and lidocaine injections and of spinalization. The arrows joined with a horizontal line below the correlogram comprise the nodes with similar classes of CDPs shown in the consensus graph of **Figure 3C**. **(B)** Similarity indices between the sets of coefficients of correlation included in each of the clusters shown in the consensus graph. Note that the arrangement of the clusters and nodes obtained from the consensus graphs after the different experimental procedures resembles rather closely the concurrent changes in the correlation between paired sets of CDPs, as indicated by the similarity indices. Further explanations in the text. The graph displayed in A was taken from Contreras-Hernández et al. (2018) and is reproduced with permission of *Journal of Physiology*.

colored scale). The other columns show the coefficients obtained during successive 10 min non-overlapping recording periods made continuously along the whole experiment. They were displayed keeping the same order as that of the coefficients obtained during the control 0 recording period.

It may be seen that capsaicin gradually increased the correlation between the CDPs recorded from different segments and that this effect was transiently reduced after the systemic

injection of lidocaine. The patterns in correlation observed after the effects of lidocaine faded were drastically changed after a high acute spinalization and were barely affected by the second injection of lidocaine (for more details see Contreras-Hernández et al., 2018).

This graph was introduced to compare the changes in the coefficients of correlation between the CDPs induced by capsaicin, lidocaine, and spinalization with the state transitions

inferred from the consensus graph displayed in **Figure 3C**. The arrows and symbols together with the horizontal lines at the bottom of the correlogram in **Figure 4A** show the distribution of the six clusters and their nodes obtained from the consensus graph illustrated in **Figure 3C**. The nodes belonging to the same cluster are joined with a horizontal line.

As shown in **Figure 4B**, there was a clear correspondence between the grouping of the nodes in particular clusters and the patterns of correlation between the CDPs displayed during the different periods. This correspondence was assessed by comparing the similarity indices between the sets of coefficients of correlation indicated by the nodes obtained from the consensus graphs illustrated in **Figure 3C**. A similarity index of 0 would indicate identity between the two sets of coefficients of correlation, while an index of 1.0 would indicate that the two sets were completely different (see section “Materials and Methods”).

It then follows that the data sets included within cluster 1 had similarity indices between 0.274 and 0.304, suggesting a reasonable similarity between them. This was also the case for the data included in clusters 2 and 3, as well as for clusters 4–6. It should be noted that after spinalization, the similarity indices of the data included in clusters 5 and 6 were pretty low, suggesting that in the absence of descending influences, the correlation between the CDPs recorded from different segments was relatively steady, even after the second injection of lidocaine (see Contreras-Hernández et al., 2018, for further details).

**Figure 5** shows the consensus graph obtained in another experiment where we followed the same protocol. In this case, the nodes were grouped in three clusters. Cluster 1 comprised six similar control nodes (steps 1–6, circles). By 10 min after the injection of capsaicin, the nodes shifted to cluster 2 where they remained during 3 h (steps 1–18, squares). Immediately after the injection of lidocaine (step 1, upward triangles) the node shifted again to cluster 1 and so were the nine following steps (steps 2–10, upward triangles). Later on, lidocaine steps 11 and 12 shifted back to capsaicin cluster 2. After spinalization, the nodes were again shifted, this time to a separate cluster and remained there for at least 1 h (spinal steps 1–6).

In summary, the consensus graphs depicted in **Figures 3C**, **5** indicate that capsaicin changes the state of functional connectivity between the neurones involved in the generation of the different classes of CDPs and that the acquired state is temporarily reverted to the control configuration by lidocaine. They also show that the transition between clusters produced by capsaicin and lidocaine is shaped by supraspinal influences that are suppressed after spinalization.

## Which Are the Effects of Capsaicin and Lidocaine Applied in Previously Spinalized Preparations?

In Contreras-Hernández et al. (2018), we showed that after spinalization the effects of capsaicin and lidocaine on the correlation between different sets of CDPs were significantly

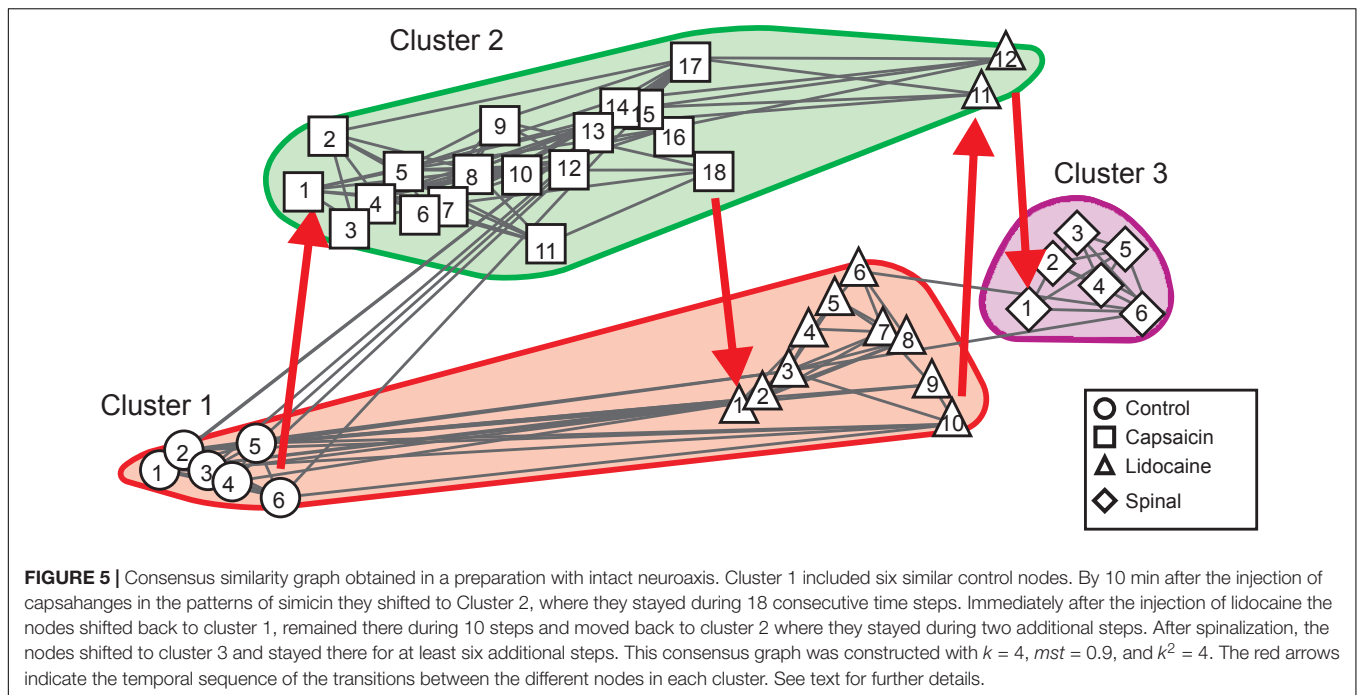
attenuated. Yet, the question remained if capsaicin and lidocaine had some action when applied in previously spinalized preparations. Clearly these two situations are not necessarily equivalent, because capsaicin applied in a preparation with intact neuroaxis will activate ascending pathways reaching supraspinal structures which in turn promote descending influences that modulate the functional connectivity between the dorsal horn neuronal ensembles distributed along the lumbar segments (Ramírez-Morales et al., 2019). These descending control mechanisms include activation of 5-HT and dopaminergic fibers that may produce long lasting changes of synaptic transmission along a diversity of spinal pathways, including activation of silent synapses (Suzuki et al., 2004). Application of capsaicin in a previously spinalized preparation would certainly eliminate the descending control activated by the nociceptive stimulus.

**Figures 6A–E** shows the ongoing CDPs recorded in the *L5* and *L6* segments in both sides of the spinal cord and how this activity was changed by spinalization and by the subsequent injection of capsaicin and lidocaine. It may be seen that spinalization increased the frequency of the ongoing CDPs, some of which remained synchronized (**Figures 6A,B**). The records displayed in **Figure 6C** were taken 65 min after the intradermal injection of capsaicin and resembled those displayed in **Figure 6B**, suggesting that capsaicin had a relatively weak effect on the functional relations between the neuronal sets involved in the generation of the different classes of CDPs. Nevertheless, the low frequency activity recorded after the injection of capsaicin was temporarily reduced following the systemic injection of lidocaine (**Figures 6D,E**).

**Figures 6F,G** shows the 12 classes of CDPs that were selected with the machine learning procedures from recordings made in the *L5rL* and *L6rL* segments, respectively. These classes were obtained from recordings made before spinalization and were used as a reference for the selection of the different classes of CDPs generated after spinalization as well as after the administration of capsaicin and lidocaine. In general, the selected CDPs resembled those observed in the preparation with intact neuroaxis displayed in **Figures 1G,H**. That is, some classes of CDPs started from a flat baseline and were negative or negative positive, while slow negative or positive potentials preceded other classes of CDPs.

The histograms displayed below the CDPs show that spinalization slightly increased the probability of occurrence of some of these potentials (e.g., classes 3, 9, 10, and 12 in segment *L5rL* and classes 6, 7, 8, and 11 in segment *L6rL*, while at the same time the probabilities of other classes were reduced (classes 1, 2, 4, 5, and 6, in *L5rL* and classes 3, 4, and 5 in *L6rL*), or else remained unchanged.

In contrast with what has been observed in the preparation with intact neuroaxis (**Figures 1G,H**), capsaicin injected after spinalization had rather small effects on the fractional probabilities of occurrence of the CDPs. Some were weakly and transiently increased (classes 5 and 10 in *L5rL* and classes 6, 7, and 11 in *L6rL*) while others were slightly reduced (classes 1 and 3 in *L5rL* and classes 8, 9, and 10 in *L6rL*). The statistical significance of the changes produced by capsaicin and lidocaine on the



fractional probabilities of occurrence of the different classes of CDPs relative to the probabilities of the potentials recorded after spinalization (white columns) is indicated by the brackets and asterisks above the corresponding columns.

Another difference with the changes of the CDPs observed in the preparation with intact neuroaxis was that in the spinalized preparation the capsaicin-induced changes had a slower time course. Lidocaine applied after capsaicin also increased the probabilities of occurrence of some classes of CDPs and reduced the probabilities of other classes, but the effects were relatively small.

**Figures 7A,B** show the changes in the patterns of similarity between the different sets of CDP histograms. It may be seen that after spinalization the histograms representing the global behavior of the CDPs recorded in the *L5rL* and *L6rL* segments showed no similarity with the histograms obtained before the spinal section. Yet, capsaicin and lidocaine changed the similarity patterns, apparently in the same direction as in the preparation with intact neuroaxis. These changes lead to the grouping of the histograms in separate clusters (**Figures 8A,B**).

**Figure 8C** shows the consensus graph of the effects produced by capsaicin and lidocaine applied after spinalization. These graphs were obtained from the data recorded in all segments in the same experiment as that of **Figure 6**. In the consensus graph, similar nodes were grouped in five clusters. The red arrows indicate the temporal sequence of the transitions between the different clusters induced by spinalization, capsaicin, and lidocaine. It may be seen that spinalization first shifted the control nodes (control steps 1–3, circles) from cluster 1 to cluster 2 (spinal steps 1–2, diamonds) and later on to cluster

3 (spinal steps 3–4, diamonds). The injection of capsaicin shifted the nodes to cluster 4 (capsaicin steps 1–4, squares) and later on to cluster 5 (capsaicin steps 5–8, squares) that also included the CDPs recorded during the first 20 min after the injection of lidocaine (lidocaine steps 1–2, upward triangles). After that, the nodes first shifted to cluster 2 (lidocaine steps 3–6, upward triangles) and later on to cluster 3 where they remained until the end of the recording period (lidocaine steps 7–11, upward triangles). The correlogram depicted in **Figure 9A** allows comparison of the changes in the patterns of correlation between the CDPs induced by capsaicin and lidocaine in the already spinalized preparation with the distribution of the nodes and clusters obtained from the consensus graphs displayed in **Figure 8C**. It may be seen that in the absence of a supraspinal control, capsaicin and lidocaine still affected the functional connectivity between the dorsal horn neurones, even though the changes in correlation between the CDPs recorded from different segments were not as marked as those seen in preparations with intact neuroaxis (see Contreras-Hernández et al., 2018, for further details).

**Figure 10** displays the consensus graph constructed with data obtained in another experiment. It may be seen that the nodes of the segmental CDPs recorded before spinalization (steps 1–4, circles) were rather similar and were grouped in cluster 1. Those obtained soon after spinalization (steps 1–4, diamonds) were transiently shifted to cluster 2, then to cluster 3 (steps 5–8, diamonds) and back to cluster 2 (steps 9–10, diamonds), that also comprised the nodes obtained during the first 40 min after the injection of capsaicin (steps 1–4, squares). Subsequently, the nodes shifted to cluster 4 (steps 5–10, squares) that also included the

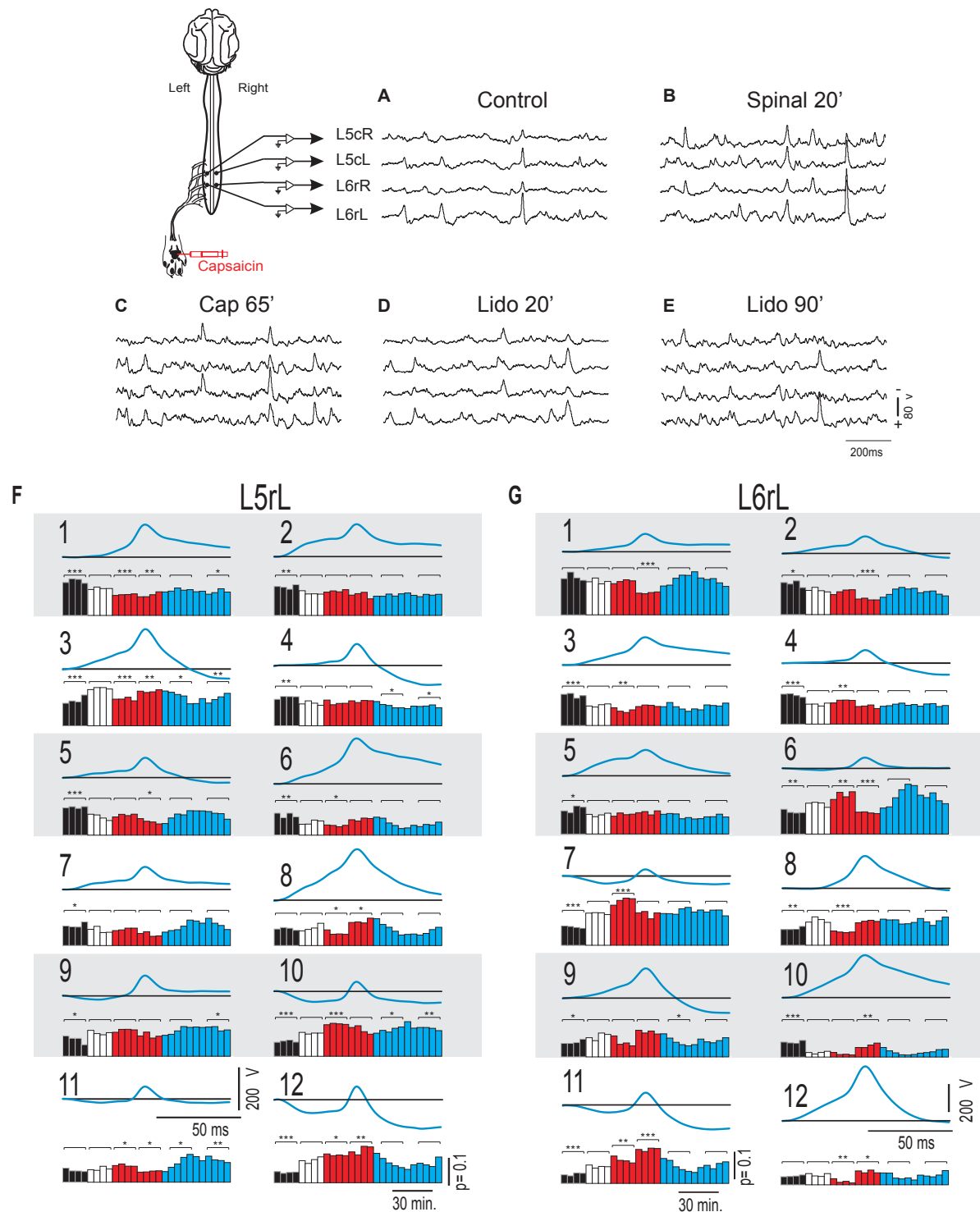


**FIGURE 6 |** Changes in the shape dictionaries of the CDPs during the action of capsaicin and lidocaine injected in a previously spinalized preparation. **(A–E)** Spontaneous CDPs recorded in the left and right sides of the caudal region of the L5 segment and rostral region of the L6 segments, as indicated. **(A)** Control. **(B)** 20 min after spinalization. **(C)** 65 min after the intradermic injection of capsaicin in the left hindpaw. **(D,E)** 20 and 90 min after the systemic injection of lidocaine. **(F,G)** Shape dictionaries of the CDPs recorded in the L5rL and L6rL segments and histograms of fractional probabilities of occurrence for each shape at different time steps as indicated. The brackets and asterisks over the columns indicate the statistical significance of the fractional probabilities of occurrence of each class of CDPs relative to the fractional probabilities attained just after spinalization (\*\*\*)  $p < 0.001$ , \*\*  $p < 0.01$ , and \*  $p < 0.05$ ). See text for further explanations.

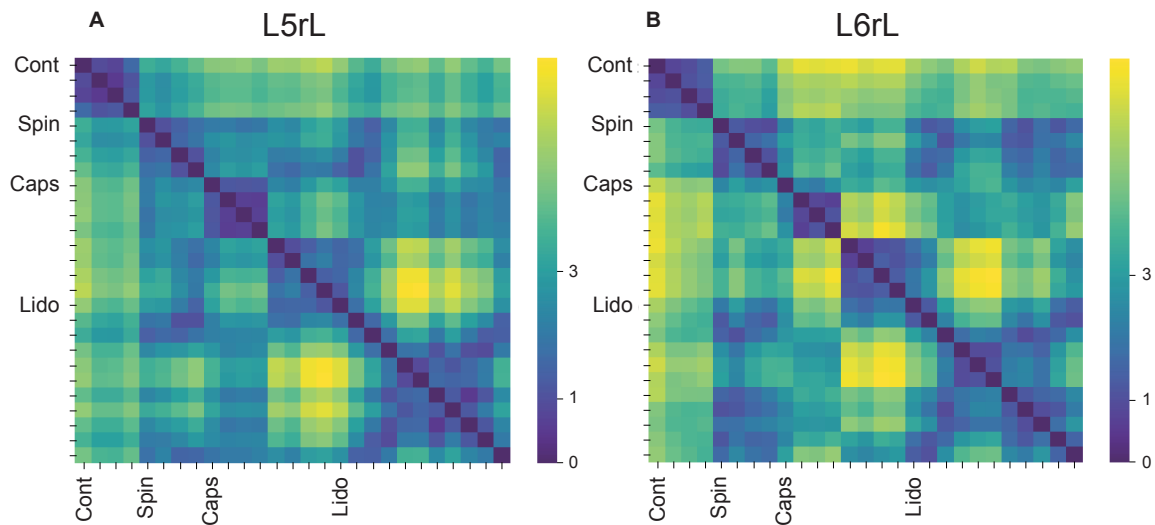


**FIGURE 7 | (A,B)** Comparison of the histograms of probabilities of the CDPs recorded in two spinal segments (L5rL, L6rL) during the action of capsaicin and lidocaine in a previously spinalized preparation. Same format as that of **Figure 2**. Note that immediately after spinalization the patterns of the ongoing CDPs were drastically changed and were quite different from the control patterns (shift from deep blue to green). Yet, they were still modified following the administration of capsaicin and lidocaine suggesting persistence of dynamic processes. See text for further explanations.

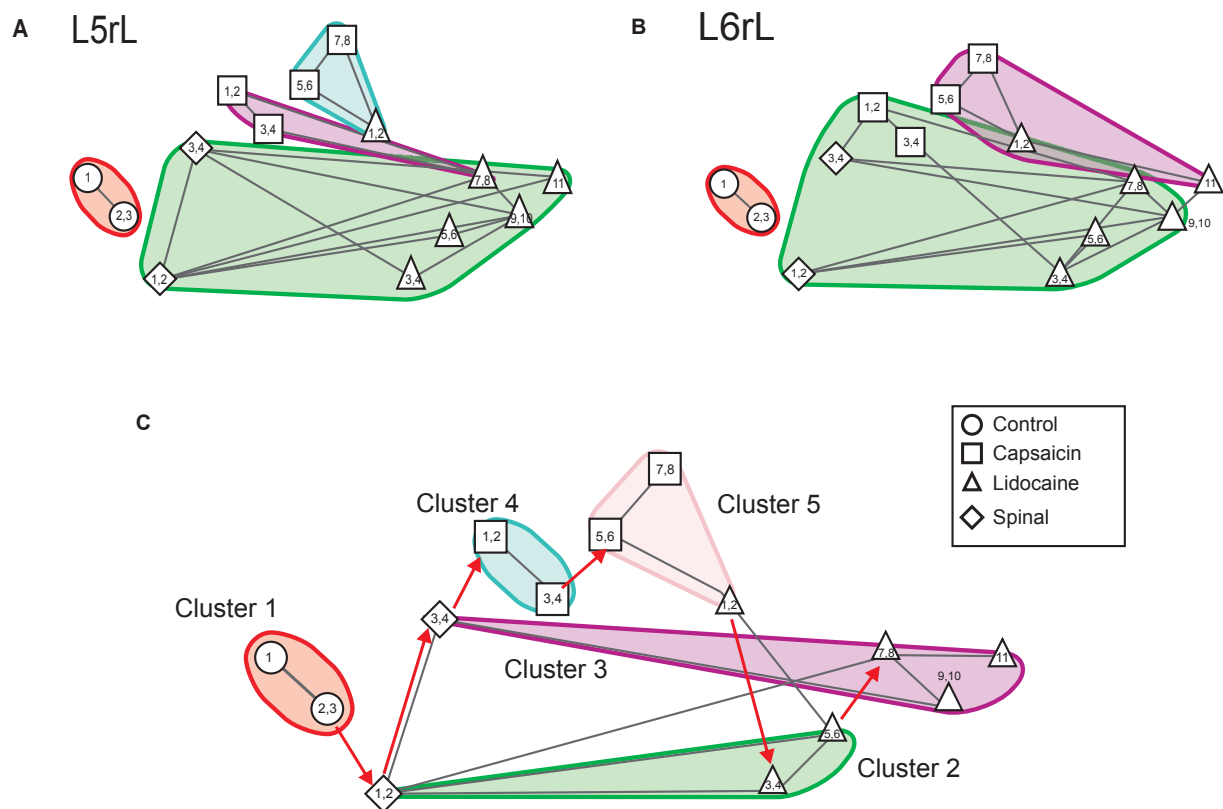


**FIGURE 8 |** Effects of capsaicin and lidocaine applied after spinalization on the similarity and consensus graphs of the CDPs recorded from different spinal segments. **(A,B)** Similarity graphs of CDPs recorded in two different spinal segments, as indicated. These graphs were constructed with  $k = 3$  and  $S = 0.9$ . As in **Figures 3A,B**, each node represents a different step of the experiment and each cluster includes nodes among the  $k$  most similar models found by applying the WalkTrap clustering method. **(C)** Consensus similarity graph ( $k = 4$ ,  $mst = 0.9$ ,  $k^2 = 3$ ). See text for further explanations.

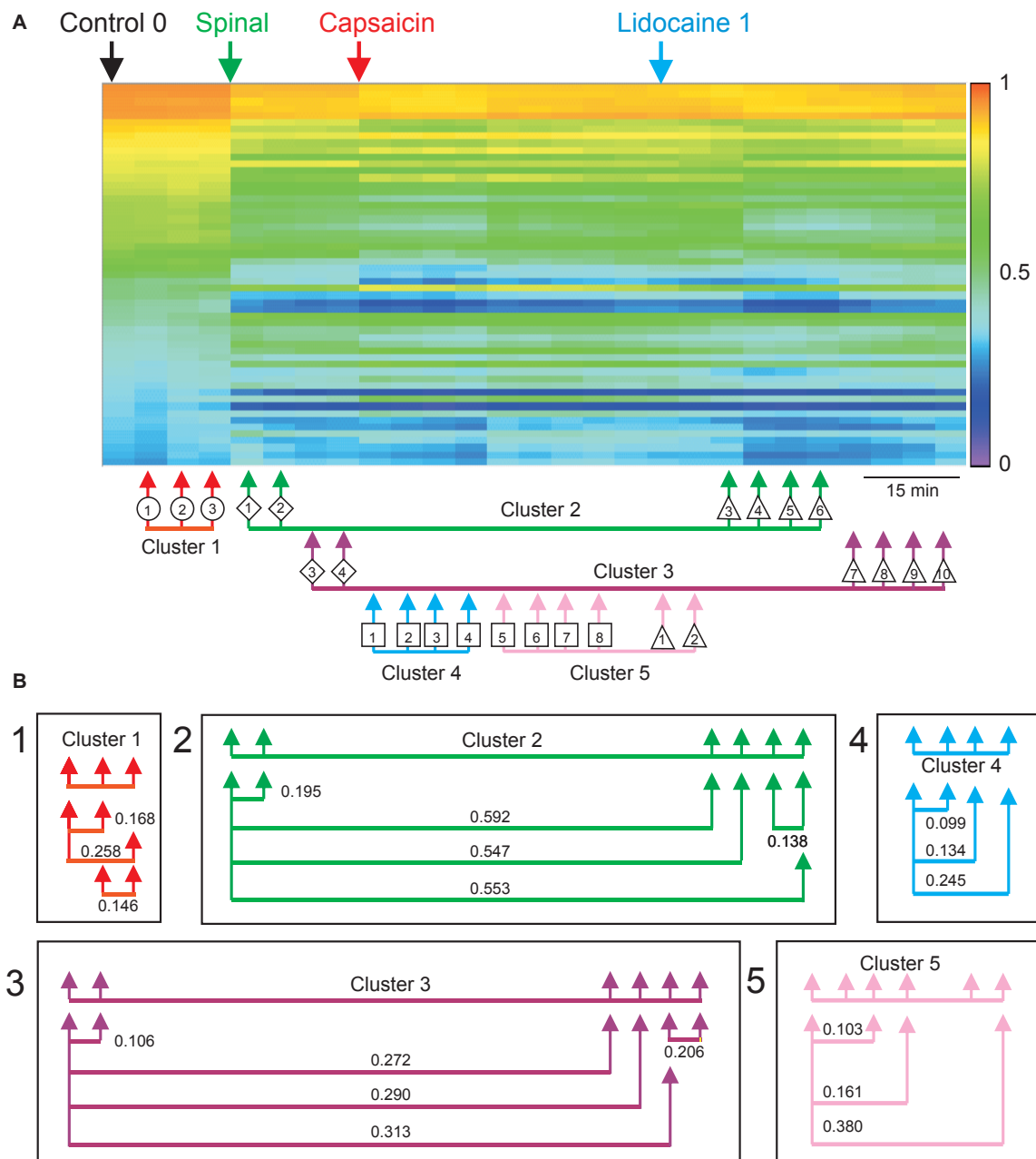


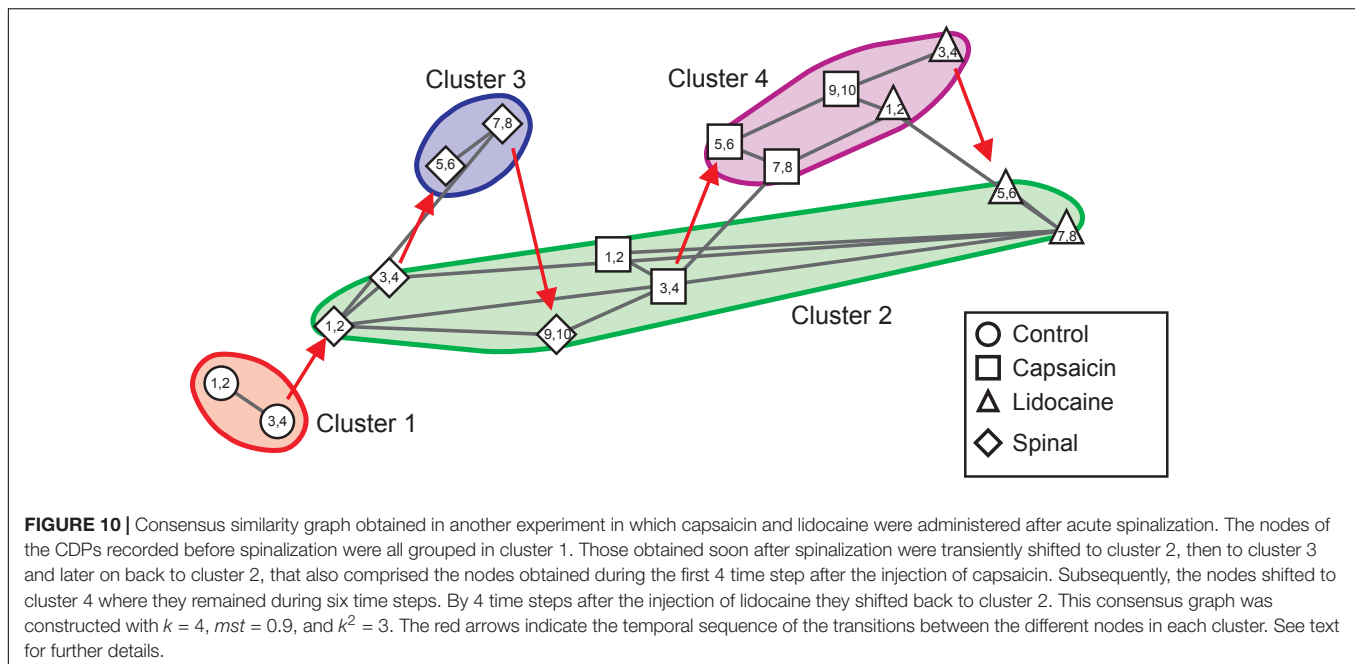
**FIGURE 9 |** Effects of capsaicin and lidocaine applied after spinalization on the correlation between the paired sets of CDPs. Same format as that of **Figure 4**.

**(A)** Changes in correlation between the different paired sets of CDPs produced by spinalization, capsaicin, and lidocaine. The arrows joined with an horizontal line displayed below the correlogram comprise nodes with similar classes of CDPs taken from the consensus graph shown in **Figure 8C**. **(B)** Similarity indices between the sets of coefficients of correlation during some of the steps obtained from the consensus graph, as indicated. Further explanations in text. The graph displayed in A was taken from Contreras-Hernández et al. (2018) and is reproduced with permission of *Journal of Physiology*.

nodes generated during the first 40 min after lidocaine (steps 1–4, upward triangles) and finally to cluster 2 (steps 5–8, upward triangles).

In summary, the consensus graphs depicted in **Figures 8C, 10** indicate that in the previously spinalized preparation, capsaicin, and lidocaine also change the state of functional connectivity between the neurones involved in the generation of the

different classes of CDPs. Yet, as shown in **Figure 9A** (see also Contreras-Hernández et al., 2018), in the spinal preparation the effects on the overall correlation between the CDPs produced by capsaicin and lidocaine were relatively weak, suggesting that in the preparation with intact neuroaxis the transitions between clusters during nociception and antinociception is dominated by supraspinal influences. At



this point, we have no information on whether in the spinal preparation the same or different dorsal horn neurones are activated by capsaicin before or after spinalization and on the kind of interaction that these neurones have with other spinal pathways.

## DISCUSSION

### Capsaicin and Lidocaine Change in a Structured Manner the CDPs Selected With Machine Learning Procedures

We have now used machine learning similarity procedures to build dictionaries of spontaneous CDPs selected according to their shape and amplitude to disclose the changes produced in each of them by the experimental procedures associated with nociception (see Martin et al., 2015). We found that under control conditions (i.e., before capsaicin, lidocaine, or spinalization) most of the classes comprising the smallest CDPs were produced during a state of low neuronal synchronization. They occurred more often than classes comprising the largest CDPs that were instead generated during states of higher synchronization. We also found that capsaicin had opposite effects on the fractional probabilities of occurrence of some classes comprising the smallest and largest CDPs.

The differential action of capsaicin on the different classes of CDPs could be explained assuming that these population potentials were generated by a segmentally distributed ensemble of interconnected dorsal horn neurones, and that the changes in the probabilities of occurrence of each class resulted from dynamic modifications in the interaction

between neurones within the same ensemble, as it has been proposed for the generation of the nCDPs and npCDPs (Contreras-Hernández et al., 2015).

An alternate explanation to the differential action of capsaicin in preparations with intact neuroaxis would be that each class of CDPs was generated by a specific set of strongly interconnected neurones (modules?) distributed along the different spinal segments. Capsaicin would inhibit, either directly, or via descending pathways, the neurones in some of the modules and at the same time activate the neurones in other modules, perhaps via the on and off brain-stem neurones (Basbaum and Fields, 1978; Urban and Gebhart, 1999; Vanegas and Schaible, 2004; Brooks and Tracey, 2005; Smith et al., 2006; Ossipov et al., 2010; Brink et al., 2012).

It should be noted that a fair number of the selected CDPs were preceded by slow negative or positive potentials and few started from a flat baseline (see Figures 1G,H, 6F,G). At present we don't know if these potentials were produced by the same neuronal ensemble that generates the selected CDPs or if they were generated by the activation of separate neuronal ensembles that affected the probabilities of occurrence of the ensembles involved in the generation of the CDPs, as suggested by Markovian analysis (see below).

The finding of some classes of CDPs whose probabilities of occurrence were not changed by capsaicin and lidocaine suggests in addition that the neurones involved in the generation of these potentials were not directly related to nociception but could still control information transmission in other pathways as suggested by recent observations of Ramírez-Morales et al. (2019), who found that the dorsal horn field potentials produced by activation of low threshold afferents signaling joint position, were basically unaffected after the intradermic injection of capsaicin, in

contrast with the facilitation of the responses produced by stimulation of high threshold myelinated fibers conveying nociceptive information.

Future research should be addressed to relate the activity of individual, functionally characterized dorsal horn neurones with the different classes of CDPs and to examine how this relation is affected during nociception and antinociception.

## The Assemblage of CDPs in a Specific Cluster Defines the State of Functional Connectivity Between Specific Sets of Dorsal Horn Neurones

By using a Markovian approach, we were able to compare the similarities between the whole set of CDPs recorded in a given segment with the CDPs generated in the same segment under different experimental conditions (**Figures 3A,B**). We assumed that grouping in the same cluster the different classes of CDPs according to similarity criteria defines the functional state of connectivity of the dorsal horn neuronal network in that particular segment at a given moment. In contrast, the uniquely generated consensus graphs (see **Figure 3C**) provide a general vision of the behavior of the whole ensemble of dorsal horn neurones by including information obtained from all segments with a degree of reliability higher than that obtained by observing the selected sets of CDPs in each segment. The clusters displayed in the consensus graphs would then illustrate the transition between the different functional states induced by nociception and antinociception.

Our observations suggest further that the system does not operate as a causally deterministic relay but instead as a probability system able to process and/or modulate the output behavior (increased/decreased/total blockade) through the operation of specific sets of intraspinal neurones. It is tempting to suggest that the spontaneous synchronous and coordinated neuronal activity recorded in the dorsal horn of the spinal cord represents pieces of complex dynamic adaptive behaviors associated to particular functional states of the spinal neuronal networks that may behave as functional units that control the balance between excitation and inhibition, as part of the homeostatic processes involved in health and disease. It thus seems possible, as suggested in our previous study (see Contreras-Hernández et al., 2018), that the changes in spinal circuitry produced by acute nociceptive stimulation are part of the response of the system in conditions of self-organized criticality in which descending control can shift the spinal neuronal networks to a different functional state.

In this context, we would like to point out that even though the term “adaptation” has been traditionally used to describe the reduction of the responses recorded in afferent fibers following sustained activation of peripheral receptors (Adrian and Zotterman, 1926), as well as the modifications of the reflex responses produced by repeated sensory stimulation (Grau et al., 2014), a more general definition of adaptation comprises the frequently used term “adaptive” that characterizes dynamic changes in neuronal connectivity under a variety of physiological

and pharmacological conditions used to induce contextual modulations in neuronal functional connectivity lasting for minutes that shape transmission of sensory information in a structured manner (Holland, 2006).

The exact nature and mechanisms of criticality, and its functional role are still an open question. Criticality is a fundamental concept to understand the operation of complex adaptive systems and is defined as a specific type of behavior observed when a system undergoes a transition between different phases (Strogatz, 2000). Criticality maximizes the dynamic range of the responses to different inputs (Kinouchi and Copelli, 2006; Shew et al., 2009, 2011; Yang et al., 2012; Meisel et al., 2013), and it has been proposed that complex dynamical adaptive systems such as large neuronal networks in the central nervous system operate in a critical state through an active decentralized process known as self-organized criticality (Bak et al., 1988; Bornholdt and Rohlf, 2000; Levina et al., 2009; Meisel and Gross, 2009; Droste et al., 2013). One possible explanation to the differential action of capsaicin on the functional connectivity (correlation) between the dorsal horn neuronal networks involved in the generation of the different classes of CDPs, as well as on their different probabilities of occurrence, might be related to different states of criticality induced by nociception simultaneously on different neuronal ensembles.

## Some Functional Implications of the Capsaicin-Induced Changes on the Probabilities of Occurrence of the Different Classes of CDPs

We have shown previously that the spontaneous nCDPs recorded in the lumbar cord were associated with states of low neuronal synchronization and that in these conditions there was a concurrent activation of the pathways mediating non-reciprocal Ib post-synaptic inhibition. In contrast, during states of increased neuronal synchronization, as well as after the acute section of the superficial peroneal (SP) and sural (SU) nerves, npCDPs were preferentially generated, suggesting increased activation of the pathways leading to primary afferent depolarization and presynaptic inhibition (Chávez et al., 2012; Contreras-Hernández et al., 2015).

These findings led us to examine the extent to which the nociceptive stimulation produced by the intradermal injection of capsaicin in preparations with intact neuroaxis affected the probabilities of occurrence of the CDPs selected with the machine learning procedures, even though so far the nCDPs and npCDPs are the only classes of CDPs that we have been able to associate with the activation of specific inhibitory pathways.

The data displayed in **Figures 1G,H** show that capsaicin had a differential action on the fractional probabilities of occurrence on the different classes of CDPs. We have assumed that these changes contribute to the development of the capsaicin-induced hyperalgesia. Although the individual and global contribution of each class to the development of hyperalgesia remains as an open question, it is tempting to suggest that the decreased probabilities of occurrence of the smallest CDPs (most of them

nCDPs) led to a reduced activation of glycinergic neurones and this effect had some role in the development of hyperalgesia and allodynia, as suggested by the observations of Foster et al. (2015) who showed that the targeted ablation or silencing of glycinergic dorsal horn neurones induces localized mechanical, heat and cold hyperalgesia. It should be noted that there were other negative CDPs whose fractional probabilities of occurrence were instead increased by capsaicin (e.g., classes 7 and 10 in L5rL and classes 7, 8, and 10 in L6rL; **Figures 1G,H**) whose role in the activation of inhibitory pathways is still unknown.

In the experiment of **Figure 1**, the capsaicin-induced changes on the npCDPs were rather small, suggesting that activation of the pathways mediating PAD and presynaptic inhibition was not as strong as expected. However, in other experiments (see Martin et al., 2015), in addition to the capsaicin-induced reduction of the probabilities of occurrence of the classes comprising the smallest nCDPs, the probabilities of occurrence of some npCDPs were clearly increased, just as it was observed following the acute section of a cutaneous nerve (see Chávez et al., 2012), although it should be considered that these two procedures (capsaicin and nerve section) are not necessarily equivalent.

It thus seems possible that the scarce effects of capsaicin on the probabilities of generation of npCDPs in the experiment illustrated in **Figures 1G,H** were determined by the state of functional neuronal connectivity exhibited by the ensemble at the time of the intradermic injection of capsaicin (see Contreras-Hernández et al., 2018) which may to some extent depend on anesthesia depth as well as on the magnitude of the descending inhibitory control incremented by nociceptive stimulation (see Ramírez-Morales et al., 2019).

## CONCLUSION

The present set of observations was performed to further disclose the changes in functional connectivity between the segmental populations of dorsal horn neurones under conditions of nociception-antinociception and to evaluate the extent to which these changes were shaped by supraspinal influences.

The method presently employed goes beyond the measurement of global changes in correlation between the activity recorded from different spinal segments (Contreras-Hernández et al., 2018). It focuses on the changes in the fractional probabilities of occurrence of specific classes of CDPs selected by machine learning according to their shape and amplitude.

Our observations provide evidence of an intrinsic organization of the neuronal ensembles generating the different classes of CDPs as well as of the participation of descending influences in this organization during nociception and antinociception. It is tempting to speculate that the interaction between subpopulations of neurones through changes in the frequency of the CDPs (probabilities) observed under different experimental conditions represents the activation of specific sets of strongly interconnected sets of neurones acting as biological switches that address nociceptive information flow to particular pathways in the spinal cord and also to supraspinal structures.

Our present findings should not be taken as an assertion that spinal neuronal circuitry devoid of supraspinal control is unable to change its patterns of functional connectivity and their interaction with other spinal pathways in response to nociception and antinociception. In fact, as shown in **Figures 7–10**, in the previously spinalized preparation, the transition and consensus graphs representing population neuronal activity, do change after the administration of capsaicin and lidocaine. This situation could well-underlie the plasticity and learning of the spinal circuitry in response of nociceptive stimulation demonstrated by Grau et al. (2014) in chronically spinalized rats. It will be interesting to investigate if this form of plasticity can be also demonstrated in the acute preparation using the methodology presently described.

The effect of systemic lidocaine is remarkable in the sense that this local anesthetic counteracts the plastic neuronal changes induced by capsaicin. One possibility would be that lidocaine temporarily *erases* the state of central sensitization developed in a variety of supraspinal structures (i.e., brainstem, hippocampal and thalamocortical networks; see Drdla-Schutting et al., 2012; Bonin and De Koninck, 2014). Another possibility, suggested by recent observations (Plamenov et al., 2018) would be that lidocaine decorrelates and/or decouples the information flowing from the brainstem nuclei to the spinal circuitry, without significantly affecting the process of central sensitization that persists at higher levels.

We wondered on the extent to which the changes produced by capsaicin and lidocaine disclosed by the consensus graphs had a functional meaning, in the sense that they indeed represented different states of functional connectivity between the different ensembles of dorsal horn neurones at rest and after nociceptive stimulation and antinociception, or if they were computational constructions made without considering the context in which each of the specific classes of CDPs were generated. That is, of the state of functional connectivity displayed by the neuronal ensembles in the lumbar segments at that moment. In our view, the close resemblance between the arrangements of the clusters and nodes obtained from the consensus graphs and the concurrent changes in the patterns of global correlation induced after the administration of capsaicin and lidocaine illustrated in **Figures 4, 9** validates the use of the consensus graphs as indicators of global changes in functional state observed during nociception and antinociception. It provides a tool to examine the changes in the functional role of the different populations of dorsal horn neurones that generate the spontaneous CDPs during different physiological and pathological conditions.

## SIGNIFICANCE

We used Machine Learning and Markovian methods to examine the effects of nociception and antinociception analgesia on specific classes of the ongoing cord dorsum potentials (CDPs) generated in the lumbar segments of the anesthetized cat.

We found that in preparations with intact neuroaxis, the machine learning selected classes of CDPs displayed structured (non-random) configurations that were changed by the intradermic injection of capsaicin to other, also non-random configurations. The systemic injection of lidocaine, a procedure known to decrease the manifestations of neuropathic pain, transiently reversed these configurations to their pre-capsaicin structure. It is suggested that the dorsal horn neuronal networks involved in the generation of the different classes of CDPs operate in a state of self-organized criticality as part of the homeostatic processes shaped by supraspinal descending influences in response to nociception.

## DATA AVAILABILITY

The datasets generated for this study are available on request to the corresponding author.

## ETHICS STATEMENT

Cats were bred and housed under veterinary supervision at the Centro de Investigación y de Estudios Avanzados of the Instituto Politécnico Nacional Animal Care unit (SAGARPA permission AUT-B-C-0114-007). All experiments were approved by the Institutional Ethics Committee for Animal Research (protocol no. 126-03) and of the National Institutes of Health (Bethesda, MD, United States; Animal Welfare Assurance No. A5036-01). The Guide for the Care and Use of Laboratory Animals (National Research Council, 2010) was followed in all cases.

## REFERENCES

- Adrian, E., and Zotterman, Y. (1926). The impulses produced by sensory nerve-endings. *part 3* impulses set up by touch and pressure. *J. Physiol.* 61, 465–483. doi: 10.1113/jphysiol.1926.sp002308
- Bak, P., Tang, C., and Wiesenfeld, K. (1988). Self-organized criticality. *Phys. Rev. A* 38, 364–374. doi: 10.1103/PhysRevA.38.364
- Basbaum, A. I., and Fields, H. L. (1978). Endogenous pain control mechanisms: review and hypothesis. *Ann. Neurol.* 4, 451–462. doi: 10.1002/ana.410040511
- Béjar, J., Martín, M., Esposito, G., Contreras, E., Chávez, D., Cortés, U., et al. (2015). A data mining methodology for event analysis in neurophysiological signals. in *Proceedings of the 18th International Conference of the Catalan Association for Artificial Intelligence*, Valencia, doi: 10.3233/978-1-61499-578-4-80
- Bitukov, S., Maksimushkina, A., and Smirnova, V. (2016). Comparison of histograms in physical research. *Nucl. Energy Technol.* 2, 108–113. doi: 10.1016/j.nucet.2016.05.007
- Bonin, R. P., and De Koninck, Y. (2014). A spinal analog of memory reconsolidation enables reversal of hyperalgesia. *Nat. Neurosci.* 17, 1043–1045. doi: 10.1038/nn.3758
- Bornholdt, S., and Rohlf, T. (2000). Topological evolution of dynamical networks: global criticality from local dynamics. *Phys. Rev. Lett.* 84, 6114–6117. doi: 10.1103/PhysRevLett.84.6114
- Brandes, U., Delling, D., Gaertler, M., Gorke, R., Hofer, M., Nikoloski, Z., et al. (2008). On modularity clustering. *IEEE Trans. Knowl. Data Eng.* 20, 172–188. doi: 10.1109/TKDE.2007.190689

## AUTHOR CONTRIBUTIONS

PR, SG, DC, and EC-H conceived and designed the experiments. DC, EH, EC-H, SG, and PR conducted the experiments. DC, EC-H, SG, and PR collected and interpreted the data. MM, JB, UC, AR-M, and LM programmed and analyzed the data. PR, SG, MM, BJ, and UC drafted the manuscript and reviewed it critically for important intellectual content. MM, JB, and UC performed the machine learning and the Markovian analysis of the experimental data. All authors have approved the final version of the manuscript and agreed to be accountable for all the aspects of the work.

## FUNDING

This work was partially supported by the CONACyT grant 255548, by the Joint Study Agreement No. W156463 under the IBM/BSC Deep Learning Center agreement, and by the BarcelonaTech, Universitat Politècnica de Catalunya, Catalonia, Spain.

## ACKNOWLEDGMENTS

We would like to thank Dr. E. Hernández Lemus for his critical comments in an earlier version of this manuscript, C. León for the technical assistance, B. Alatríste for his help with editing, and E. Rosales for her excellent secretarial support. Experiments and data analysis were performed at the Department of Physiology, Biophysics and Neurosciences of the Centre of Research and Advanced Studies from the Instituto Politécnico Nacional, Mexico.

- Brink, T. S., Pacharinsak, C., Khasabov, S. G., Beitz, A. J., and Simone, D. A. (2012). Differential modulation of neurons in the rostral ventromedial medulla by neurokinin-1 receptors. *J. Neurophysiol.* 107, 1210–1221. doi: 10.1152/jn.00678.2011
- Brooks, J., and Tracey, I. (2005). Review: from nociception to pain perception: imaging the spinal and supraspinal pathways. *J. Anat.* 207, 19–33. doi: 10.1111/j.1469-7580.2005.00428.x
- Chávez, D., Rodríguez, E., Jiménez, I., and Rudomin, P. (2012). Changes in correlation between spontaneous activity of dorsal horn neurons lead to differential recruitment of inhibitory pathways in the cat spinal cord. *J. Physiol.* 590, 1563–1584. doi: 10.1113/jphysiol.2011.223271
- Contreras-Hernández, E., Chávez, D., Hernández, E., Velázquez, E., Reyes, P., Béjar, J., et al. (2018). Supraspinal modulation of neuronal synchronization by nociceptive stimulation induces an enduring reorganization of dorsal horn neuronal connectivity. *J. Physiol.* 596, 1747–1776. doi: 10.1113/JP275228
- Contreras-Hernández, E., Chávez, D., and Rudomin, P. (2015). Dynamic synchronization of ongoing neuronal activity across spinal segments regulates sensory information flow. *J. Physiol.* 593, 2343–2363. doi: 10.1113/jphysiol.2014.288134
- Drdla-Schutting, R., Benrath, J., Wunderbaldinger, G., and Sandkuhler, J. (2012). Erasure of a spinal memory trace of pain by a brief, high-dose opioid administration. *Science* 335, 235–238. doi: 10.1126/science.1211726
- Droste, F., Do, A. L., and Gross, T. (2013). Analytical investigation of self-organized criticality in neural networks. *J. R. Soc. Interface* 10:20120558. doi: 10.1098/rsif.2012.0558

- Fortunato, S. (2010). Community detection in graphs. *Phys. Rep.* 486, 75–174. doi: 10.1016/j.physrep.2009.11.002
- Foster, E., Wildner, H., Tudeau, L., Haueter, S., Ralvenius, W. T., Jegen, M., et al. (2015). Targeted ablation, silencing, and activation establish glycinergic dorsal horn neurons as key components of a spinal gate for pain and itch. *Neuron* 85, 1289–1304. doi: 10.1016/j.neuron.2015.02.028
- Grau, J. W., Huie, J. R., Lee, K. H., Hoy, K. C., Huang, Y.-J., Turtle, J. D., et al. (2014). Metaplasticity and behavior: how training and inflammation affect plastic potential within the spinal cord and recovery after injury. *Front. Neural Circ.* 8:100. doi: 10.3389/fncir.2014.00100
- Holland, J. (2006). Studying complex adaptive systems. *J. Syst. Sci. Compl.* 19, 1–8. doi: 10.1007/s11424-006-0001-z
- Kinouchi, O., and Copelli, M. (2006). Optimal dynamical range of excitable networks at criticality. *Nat. Phys.* 2, 348–351. doi: 10.1038/nphys289
- Kissin, I. (2000). Preemptive analgesia. *Anesthesiology* 93, 1138–1143.
- Levina, A., Herrmann, J. M., and Geisel, T. (2009). Phase transitions towards criticality in a neural system with adaptive interactions. *Phys. Rev. Lett.* 102:118110. doi: 10.1103/PhysRevLett.102.118110
- Manjarrez, E., Jiménez, I., and Rudomin, P. (2003). Intersegmental synchronization of spontaneous activity of dorsal horn neurons in the cat spinal cord. *Exp. Brain Res.* 148, 401–413. doi: 10.1007/s00221-002-1303-6
- Manjarrez, E., Piloni, J. R., Jiménez, I., and Rudomin, P. (2000). Modulation of synaptic transmission from segmental afferents by spontaneous activity of dorsal horn spinal neurons in the cat. *J. Physiol.* 529, 445–460. doi: 10.1111/j.1469-7793.2000.00445.x
- Martin, M., Béjar, J., Esposito, G., Chávez, D., Contreras-Hernández, E., Glusman, S., et al. (2017). Markovian analysis of the sequential behavior of the spontaneous spinal cord dorsum potentials induced by acute nociceptive stimulation in the anesthetized cat. *Front. Comput. Neurosci.* 11:32. doi: 10.3389/fncom.2017.00032
- Martin, M., Contreras-Hernández, E., Béjar, J., Esposito, G., Chávez, D., Glusman, S., et al. (2015). A machine learning methodology for the selection and classification of spontaneous spinal cord dorsum potentials allows disclosure of structured (non-random) changes in neuronal connectivity induced by nociceptive stimulation. *Front. Neuroinformatics* 9:21. doi: 10.3389/fninf.2015.00021
- Meisel, C., and Gross, T. (2009). Adaptive self-organization in a realistic neural network model. *Phys. Rev. E* 80:061917. doi: 10.1103/PhysRevE.80.061917
- Meisel, C., Olbrich, E., Shriki, O., and Achermann, P. (2013). Fading signatures of critical brain dynamics during sustained wakefulness in humans. *J. Neurosci.* 33, 17363–17372. doi: 10.1523/JNEUROSCI.1516-13.2013
- National Research Council (2010). *Guide for the Care and Use of Laboratory Animals*, 8th Edn. Washington, DC: National Academies Press.
- Ossipov, M. H., Dussor, G. O., and Porreca, F. (2010). Central modulation of pain. *J. Clin. Invest.* 120, 3779–3787. doi: 10.1172/JCI43766
- Plamenov, N., Moreno, L., Álvarez, B., Ramírez, A., Chávez, D., Hernández, E., et al. (2018). Nociceptive stimulation produces non-random (structured) changes in the timing and direction of the information flowing between the dorsal horn neurons and the brainstem nuclei. *ABS Soc. Neurosci.* 389:18.
- Pons, P., and Latapy, M. (2005). “Chap. Computing Communities in Large Networks Using Random Walks,” in *Proceedings of the 20th International Symposium Computer and Information Sciences*, (Berlin: Springer-Verlag), 284–293. doi: 10.1007/11569596\_31
- Ramírez-Morales, A., Hernández, E., and Rudomin, P. (2019). Descending inhibition selectively counteracts the capsaicin-induced facilitation of dorsal horn neurons activated by joint nociceptive afferents. *Exp. Brain Res.* 237, 1629–1641. doi: 10.1007/s00221-019-05535-w
- Rokach, L. (2010). Ensemble-based classifiers. *Artif. Intell. Rev.* 33, 1–39. doi: 10.1007/s10462-009-9124-7
- Rudomin, P., and Hernández, E. (2008). Changes in synaptic effectiveness of myelinated joint afferents during capsaicin-induced inflammation of the footpad in the anesthetized cat. *Exp. Brain Res.* 187, 71–84. doi: 10.1007/s00221-008-1281-4
- Rudomin, P., Martin, M., Contreras-Hernández, E., Béjar, J., Esposito, G., Chávez, D., et al. (2016). Markovian analysis of spontaneous spinal cord dorsum potentials reveals non random dynamic adaptive changes in the configuration of the functional connectivity between segmental populations of dorsal horn neurons in response to acute nociceptive stimulation. *ABS Soc. Neurosci.* 239:19.
- Rudomin, P., Solodkin, M., and Jiménez, I. (1987). Synaptic potentials of primary afferent fibers and motoneurons evoked by single intermediate nucleus interneurons in the cat spinal cord. *J. Neurophysiol.* 57, 1288–1313. doi: 10.1152/jn.1987.57.5.1288
- Sakurada, T., Katsumata, K., Tan-No, K., Sakurada, S., and Kisara, K. (1992). The capsaicin test in mice for evaluating tachykinin antagonists in the spinal cord. *Neuropharmacology* 31, 1279–1285. doi: 10.1016/0028-3908(92)90057-v
- Schaeffer, S. E. (2007). Survey: graph clustering. *Comput. Sci. Rev.* 1, 27–64. doi: 10.1016/j.cosrev.2007.05.001
- Shew, W. L., Yang, H., Petermann, T., Roy, R., and Plenz, D. (2009). Neuronal avalanches imply maximum dynamic range in cortical networks at criticality. *J. Neurosci.* 29, 15595–15600. doi: 10.1523/JNEUROSCI.3864-09.2009
- Shew, W. L., Yang, H., Yu, S., Roy, R., and Plenz, D. (2011). Information capacity and transmission are maximized in balanced cortical networks with neuronal avalanches. *J. Neurosci.* 31, 55–63. doi: 10.1523/JNEUROSCI.4637-10.2011
- Smith, V. A., Beyer, C. E., and Brandt, M. R. (2006). Neurochemical changes in the rvm associated with peripheral inflammatory pain stimuli. *Brain Res.* 1095, 65–72. doi: 10.1016/j.brainres.2006.04.018
- Strogatz, S. H. (2000). *Nonlinear Dynamics and Chaos*. Boulder, CO: Westview Press.
- Suzuki, R., Rygh, L. J., and Dickenson, A. H. (2004). Bad news from the brain: descending 5-HT pathways that control spinal pain processing. *Trends Pharmacol. Sci.* 25, 613–617. doi: 10.1016/j.tips.2004.10.002
- Urban, M. O., and Gebhart, G. F. (1999). Supraspinal contributions to hyperalgesia. *Proc. Natl. Acad. Sci. U.S.A.* 96, 7687–7692. doi: 10.1073/pnas.96.14.7687
- Vanegas, H., and Schaible, H.-G. (2004). Descending control of persistent pain: inhibitory or facilitatory? *Brain Res. Rev.* 46, 295–309. doi: 10.1016/j.brainresrev.2004.07.004
- Woolf, C. J., and Chong, M. S. (1993). Preemptive analgesia—treating postoperative pain by preventing the establishment of central sensitization. *Anesth. Analg.* 77, 362–379. doi: 10.1213/00000539-199308000-00026
- Yang, H., Shew, W. L., Roy, R., and Plenz, D. (2012). Maximal variability of phase synchrony in cortical networks with neuronal avalanches. *J. Neurosci.* 32, 1061–1072. doi: 10.1523/JNEUROSCI.2771-11.2012
- Zhou, Z.-H. (2012). *Ensemble Methods: Foundations and Algorithms*, 1st Edn. London: Chapman & Hall.

**Conflict of Interest Statement:** The authors declare that the research was conducted in the absence of any commercial or financial relationships that could be construed as a potential conflict of interest.

Copyright © 2019 Martín, Béjar, Chávez, Ramírez-Morales, Hernández, Moreno, Contreras-Hernández, Glusman, Cortés and Rudomin. This is an open-access article distributed under the terms of the Creative Commons Attribution License (CC BY). The use, distribution or reproduction in other forums is permitted, provided the original author(s) and the copyright owner(s) are credited and that the original publication in this journal is cited, in accordance with accepted academic practice. No use, distribution or reproduction is permitted which does not comply with these terms.

## APPENDIX

### Extraction of CDPs

The first step aimed to build dictionaries of events that were relevant for the analysis. In our domain, these events were the CDPs. As the initial step, an automated and unsupervised CDP detection method was applied. This method assumes smoothness in the definition of the CDP candidates and considers that they appear as peaks in the signal. We have assumed that the noise in the background of the recordings is stationary and Gaussian, and also independent of the neuronal signal. Given these assumptions, the signal was subjected to an automatic event extraction algorithm that detects peaks. This algorithm uses a sliding window with a length large enough to contain the relevant events (between 100 and 150 ms). The signal contained inside the window was smoothed using a bandpass filter that eliminated all frequencies higher than 70 Hz. This smoothing also reduced the possibility of detecting spurious events by maximizing the noise-signal ratio. The window was selected only if a peak was present at its center and some shape constraints held. These constraints were related to the distribution of the integral of the signal inside the window.

After the CDP candidates were identified, and before generating the basic dictionary of events, we proceeded as follows:

The time-stamp of a detected CDP corresponds to the time of its maximum value in the considered event window. Experts' knowledge was used to define a suitable time window ( $T_w$ ) around the identified event maximum. In our case, this window had a duration of 100 ms. The signal inside this window was extracted and preprocessed to prepare it for clustering. To this end, we first resampled the signal from 10 to 1.6 kHz for data reduction. In addition, we removed the potential baseline offset by subtracting the average of a subset of the initial points of the signal. This simplified the comparison of different CDPs. Given that the signal must also be sufficiently smooth, the CDPs were processed using PCA as a feature extraction method to compute the most relevant dimensions that describe the whole set of identified CDPs. Finally, only the dimensions that accounted for 98% of the variance were used to reconstruct each CDP. This eliminated all the high-frequency variations in the signal.

To build the dictionary for each signal we used the  $k$ -means algorithm. The main reason for choosing this algorithm was that resulting cluster prototypes were interpretable and meaningful for the experts. A combination of methods was used for the estimation of the number of clusters required to build the dictionaries to assure the consistency of the result (see Martin et al., 2015). **Figures 1G,H** shows shape dictionaries obtained from the peaks of signals extracted from the left  $L5$  and  $L6$  rostral segments. The symbols from these dictionaries were used in the next step to discretize the signals recorded from each segment and time step in the experiment. Each event was associated with the closest cluster in their corresponding dictionary and labeled accordingly. Because there were periods in the signal where no event was detected, a *pause symbol* (\$ symbol) was introduced representing this situation. This pause symbol corresponds to parts of the signal not selected and was discarded from the analysis. They do not correspond to a lack of activity but to random fluctuations or events without enough quality to be considered. The duration of this pause symbol was experimentally estimated from the distribution of the time distance among consecutive peaks. The mean of this distribution was used as its duration. If the distance between consecutive events was a multiple of this duration, multiple pause symbols were introduced among them.

### Markovian Behavior of CDPs

In Martin et al. (2015), we showed that the firing of one ensemble of neurons (and so, the appearance of one CDP) depended on the last activated ensemble of neurons (the last appeared CDP). Mathematically, the firing dependence of groups of neurons can be modeled as a Markovian process. With these results, we assumed that the best representation of the dynamical behavior of the recorded sequences are the transition probabilities matrices that describe the behavior as Markov processes of order one. Therefore, we modeled the behavior of lumbar segment  $l$  in step  $s$  of the experiment with a matrix  $m_{l,s}$  consisting in the complete set of transition probabilities between each pair of CDPs:

$$m_{l,s} = \{P(c_i^{t+1} = c_j | c_{l,s}^{t+1} = c_j) | \forall c_i, c_j \in CDPs\} \quad (5)$$

where probabilities of transitions  $P(c_i | c_j)$  were estimated from sequence  $C_{l,s}$  of CDPs recorded in lumbar segment  $l$  and step  $s$ . An example of such matrices for two different steps of the experiment in the same lumbar segment is shown in **Figures 1G,H**.

Finally, we modeled the complete experiment by setting  $M$ :

$$M = \{m_{l,s} | \forall l \in \mathcal{L}, s \in S\} \quad (6)$$

where  $\mathcal{L}$  is the set of studied lumbar segments, and  $S$  is the set of recorded temporal steps. Remember that a temporal step consists of data recorded during the experiment that spans for several minutes, usually 10. **Table 1A** contains a description of the notation and a description for each entry.

### Likelihood Computation and Similarity Index Definition

Here, we aimed to obtain a high-level interpretation of the behavior of the potentials recorded in the spinal cord dorsum. We computed for a given lumbar segment  $l$  the similarity index described above between all pairs of step  $s \in S$ . So, for any given step  $s$  recorded in lumbar segment  $l$ , we had an index on *how similar* were the data recorded to all other steps, from the Markovian point of view. We

decided to visualize that information by depicting a neighborhood graph for the given lumbar segment  $l$ . In the graph, each node represents a time step of the experiment and edges connect steps of the experiment that are considered *similar*. Following standard procedures to build neighborhood graphs to represent only significant similarities, we allowed connections between nodes only when the following two constraints were fulfilled:

- *k-closest neighbors constraint*: Nodes can only be connected to the  $k$  most similar nodes. Parameter  $k$  was set in our experiments in the range [2,10]. Two was the minimum to ensure connections to other nodes. Larger values imply a much more connected network. This constraint avoided graphs overpopulated with too many connections. To set this parameter, we used the method described for the experiment in the previous section. We started from 2 and increased the value of  $k$  until we found that among the  $k$  steps with the highest likelihood we recovered the original step in 80% of the cases. According to results shown in **Table 1B**, it would be  $k = 4$ .
- *Minimum similarity constraint*: Only nodes with similarity higher than a threshold  $mst$  were connected. Usually, this parameter was set from 0.9 to 0.99, allowing only connections between highly similar nodes. This parameter was used to avoid connections between nodes where a minimum similarity was not achieved. If set to a too high value, all steps were disconnected. To fix this parameter, we started from value 0.99 (from which all nodes are disconnected) and repeatedly reduced the value in 0.01 until each node was connected to at least another one or when we reached the limit of 0.9.

An inspection of the resulting graphs (displayed in **Figures 3A,B**) shows groups of nodes highly connected among themselves and with few connections with other nodes. However, the structure of the graphs was not evident without a careful examination. In order help to the visualization of the graph's structure, we applied the methods described in the literature for graph partitioning or clustering (Schaeffer, 2007; Brandes et al., 2008; Fortunato, 2010). Clustering allows a more straightforward interpretation of the graph by separating steps of the experiment with different Markovian behavior. In the graphs depicted in this paper (see **Figures 3, 5, 8, 10**) we represented clusters of steps of the experiment with the same color. We have experimented with different algorithms obtaining very similar results. However, we decided to use the Walking trap method (Pons and Latapy, 2005), that is based on random walks, because it worked well for relatively small graphs as in this case, and because it allowed building a dendrogram of the obtained clusters for a finely grained study of the results.

## Consensus Graph Generation

For a given experiment, we could examine the graphs obtained for each segment of the spinal cord  $l$ . However, to obtain a *general vision* of the dynamical behavior of the spinal neuronal network during the experiment, we generated a unique *consensus graph* considering information from all segments. In order to build this consensus graph, we applied ensemble methods, widely used in machine learning

**TABLE 1A** | Description of major symbols used in the text.

Notation	Description
$L$	Set of lumbar segments
$S$	Set of time steps
$C_{l,s}$	Sequence of CDPs from lumbar segment $l$ and time step $s$
$C_{l,s}^{100}$	Subsequence of the last 100 CDPs from sequence $C_{l,s}$
$C_{l,s}^{n-100}$	Subsequence CDPs from sequence $C_{l,s}$ without the last 100 CDPs
$C_{l,s}^t$	CDP from a sequence $C_{l,s}$ at time instant $t$
$m_{l,s}$	Probability model for lumbar segment $l$ and time step $s$ estimated from a sequence $C_{l,s}$ of CDPs
$\hat{m}_{l,s}$	Probability model for lumbar segment $l$ and time step $s$ estimated from sequence $C_{l,s}^{n-100}$
$P(C_{l,s} m_{l,s})$	Likelihood of sequence $C_{l,s}$ for lumbar segment $l$ and time step $s$ given model $M_{l,s}$
$P(C_{l,s}^{t+1} C_{l,s}^t;m_{l,s})$	Probability of CDP $C_{l,s}^{t+1}$ given CDP $C_{l,s}^t$ and model $m_{l,s}$
$S(s_i,s_j)$	Similarity index between time step $s_i$ and $s_j$

**TABLE 1B** | Percentage of success using consensus procedure described in section "Consensus Graph Generation" compared with average and random classifier.

	$k$					
Lumbar segment	1	2	3	4	5	6
Random classifier	6	11	17	23	28	32
Average	35	55	71	81	87	90
Consensus	55	82	88	91	91	97

(Rokach, 2010). Ensemble methods consider several different predictions of different machine learning models to consensuate one, like in real life one would consider diagnoses of different experts to obtain a reliable outcome. A straightforward way to combine predictions of different models (and very successful in ML) is the simple majority voting (Zhou, 2012). Mathematically, it has been proved that, under general conditions, accuracy in predictions using this technique outperforms prediction and reliability of even the best expert model in the ensemble. So, benefits of following this procedure are not only that we obtain a single representation of the whole behavior of the system but also that we increase the reliability and accuracy of the graph represented.

In our case, we consider each  $m_{l,s}$  a ML model built from data for a particular lumbar segment  $l$  and step of experiment  $s$ . Each model predicts (using recorded data) which are the “more similar” steps from the point of view data recorded in that segment (by considering the likelihood of the model  $m_{l,s}$  to generate the data of that step  $s_t$ ). The expression of the majority vote for these models is what we call “consensus graph.” To build this consensus graph we used the following procedure:

As we stated above, we implemented *majority voting* procedure (see Zhou, 2012). We built the consensus graphs by using the *majority voting* scheme as follows:

1. Given a lumbar segment  $l$ , for each step  $s$  of that lumbar segment, we made a list with the  $k$  most similar steps above threshold  $mst$  as described in section “Likelihood Computation and Similarity Index Definition.” This list was considered as votes for similar steps of  $s$  in the lumbar segment  $l$ .
2. Given a step  $s_i$ , we collected the votes produced in all lumbar segments  $l$ . The result was a list of pairs  $(s_j, n_{i,j})$  where  $n_{i,j}$  is the number of votes, that is, the number of lumbar segments for which  $s_j$  is among the  $k$  most similar steps to  $s_i$ .
3. For each step  $s_i$ , we kept the  $k2$  more voted steps ( $k2$  is a new parameter to implement the consensus procedure). In case of ties in votes, we also kept all tied steps. Parameter  $k2$  avoids graphs overcrowded with edges and was set to values in the range  $[2,10]$ . It plays a role similar to parameter  $k$  in the building of particular graphs described in the previous section, so it is usually set to  $k$  or  $k - 1$  value used for specific graphs in point one of this procedure, depending on the number of edges of the final graph.
4. We built a *consensus graph*, with a node for each step of the experiment and edges between steps  $s_i$  and  $s_j$  if  $s_j$  is among the  $k2$  most voted steps of  $s_i$ . As in the case of particular similarity graphs, we did not consider the direction in edges.
5. Finally, the graph was segmented into clusters of nodes using the WalkTrap method as described in the previous section. Nodes belonging to the same cluster were represented with the same color in the figures of the paper.

The consensus graph not only describes the overall behavior of the system, but it also describes it with a degree of reliability higher than each of the individual graphs. One property of the majority vote procedure is that aggregate prediction is more accurate than the average forecast of the events occurring in all the selected segments.



# Short-Term Attractive Tilt Aftereffects Predicted by a Recurrent Network Model of Primary Visual Cortex

Maria del Mar Quiroga<sup>1,2</sup>, Adam P. Morris<sup>1,3</sup> and Bart Krekelberg<sup>1\*</sup>

<sup>1</sup> Center for Molecular and Behavioral Neuroscience, Rutgers University, Newark, NJ, United States, <sup>2</sup> Behavioral and Neural Sciences Graduate Program, Rutgers University, Newark, NJ, United States, <sup>3</sup> Neuroscience Program, Department of Physiology, Biomedicine Discovery Institute, Monash University, Clayton, VIC, Australia

Adaptation is a multi-faceted phenomenon that is of interest in terms of both its function and its potential to reveal underlying neural processing. Many behavioral studies have shown that after exposure to an oriented adapter the perceived orientation of a subsequent test is repulsed away from the orientation of the adapter. This is the well-known Tilt Aftereffect (TAE). Recently, we showed that the dynamics of recurrently connected networks may contribute substantially to the neural changes induced by adaptation, especially on short time scales. Here we extended the network model and made the novel behavioral prediction that the TAE should be attractive, not repulsive, on a time scale of a few 100 ms. Our experiments, using a novel adaptation protocol that specifically targeted adaptation on a short time scale, confirmed this prediction. These results support our hypothesis that recurrent network dynamics may contribute to short-term adaptation. More broadly, they show that understanding the neural processing of visual inputs that change on the time scale of a typical fixation requires a detailed analysis of not only the intrinsic properties of neurons, but also the slow and complex dynamics that emerge from their recurrent connectivity. We argue that this is but one example of how even simple recurrent networks can underlie surprisingly complex information processing, and are involved in rudimentary forms of memory, spatio-temporal integration, and signal amplification.

**Keywords: V1, orientation, tilt aftereffect, adaptation, perception, recurrent connections, model**

## INTRODUCTION

In a broad sense, sensory adaptation is the phenomenon that perception depends not only on the current stimulus, but also what was presented before. Adaptation is found across a wide range of time scales, from contrast adaptation occurring within a few hundreds of milliseconds (Shapley and Victor, 1978; Heinrich and Bach, 2001) to slow serial dependence spanning beyond seconds (Chopin and Mamassian, 2012; Fischer and Whitney, 2014). These behavioral phenomena are of interest in terms of their function, but also as a tool to gain insight into the underlying neural mechanisms. Here, we focus on visual adaptation on the timescale of a few 100 ms. This has high ecological relevance as it corresponds to the typical duration of a single fixation in the primate.

It is well-known that exposure to an oriented stimulus (the “adapter”) affects the perceived orientation of a subsequent stimulus (the “test”). In behavioral experiments with such an adaptation protocol, subjects typically report that the test orientation is more different from the adapter than

## OPEN ACCESS

### Edited by:

Colin W. G. Clifford,  
University of New South  
Wales, Australia

### Reviewed by:

J. Patrick Mayo,  
Duke University, United States  
James Edwin Dickinson,  
University of Western  
Australia, Australia

### \*Correspondence:

Bart Krekelberg  
bart@vision.rutgers.edu

**Received:** 20 June 2019

**Accepted:** 22 October 2019

**Published:** 08 November 2019

### Citation:

Quiroga M, Morris AP and  
Krekelberg B (2019) Short-Term  
Attractive Tilt Aftereffects Predicted by  
a Recurrent Network Model of Primary  
Visual Cortex.  
*Front. Syst. Neurosci.* 13:67.  
doi: 10.3389/fnsys.2019.00067

it really is. This is called the tilt aftereffect (TAE); the test is repulsed away from the adapter (Gibson, 1933). Functionally, this phenomenon is thought to reflect the visual system's constant adjustment and recalibration to improve its ability to discriminate visual inputs (Clifford et al., 2000; Krekelberg et al., 2006a; Kohn, 2007; Schwartz et al., 2007; Kristjansson, 2011).

In primary visual cortex, similar adaptation protocols result in two well-documented changes (Gilbert and Wiesel, 1990; Müller et al., 1999; Dragoi et al., 2000; Felsen et al., 2002; Wissig and Kohn, 2012; Patterson et al., 2013, 2014). First, neurons shift their preferred orientation. The dependence of these shifts on the properties of the adapter are complex, but repulsive shifts (away from the adapter) dominate at short time scales (Wissig and Kohn, 2012; Patterson et al., 2013, 2014). Second, neurons change their peak response to the test stimulus. Here too the neural changes are complex, but rate suppression is found when the adapter is small compared to the receptive field (Wissig and Kohn, 2012; Patterson et al., 2013, 2014).

Although tuning shifts and rate suppression are sometimes both described as being the consequence of plasticity (Yao and Dan, 2001; Felsen et al., 2002), we recently showed that tuning shifts could arise from the attractor dynamics imposed by a network's recurrent connections. We studied the dynamics of orientation-tuned units in a recurrently connected network model without any form of plasticity (i.e., no changes in the biophysical, intrinsic properties of neurons or their synaptic connections) and showed that this model quantitatively captured the tuning shifts observed in monkey and cat V1 (Quiroga et al., 2016). This model, however, could not account for rate suppression, which does appear to require a mechanism involving some form of plasticity (Sanchez-Vives et al., 2000a,b).

Several modeling studies have linked the neural to the behavioral phenomena. As has been noted previously (Gilbert and Wiesel, 1990; Yao and Dan, 2001; Teich and Qian, 2003; Jin et al., 2005), tuning curve repulsion predicts (perhaps counterintuitively) an *attraction* of the percept, contrary to the typical TAE. However, rate suppression predicts a *repulsion* of the percept. Hence, to account for the fact that the behavioral TAE is typically repulsive, we have to assume that, in a typical TAE experiment, rate suppression is more potent than tuning shifts (Jin et al., 2005; Ursino et al., 2008). In the current contribution, we use this link between neural and behavioral findings to generate behavioral predictions based on our model, and test them in healthy human subjects.

Specifically, we reasoned that a hypothetical V1 with recurrent connections but without plasticity (i.e., with tuning shifts, but without rate suppression) should lead to an attractive TAE, while a V1 with plasticity but without recurrent connections should lead to a repulsive TAE. Given that no experimental methods can block all plasticity or remove all recurrent connectivity, testing this prediction will necessarily be somewhat indirect. Our experimental test relies on two observations. First, our previous modeling results show that the influence of attractor dynamics plays a significant role for adaptation on a time scale of at most a few 100 ms. Second, experimental data in macaque V1 show that rate-suppression is a comparatively slow process; its magnitude is small when adaptation is brief, and it increases substantially on

a time scale of several hundreds of milliseconds (Patterson et al., 2013). This leads to the prediction that the attractive TAE (caused by the recurrent connectivity) should dominate at short time scales. To test this prediction, we designed a novel variant of the TAE adaptation protocol that minimizes long-term adaptation. Our experiments show that the TAE in human subjects is indeed attractive on a time scale of <200 ms. In the discussion we return to the question of how this informs our view of early visual processing, and the role of recurrent connections in particular.

## METHODS

All experimental procedures were approved by the local Institutional Review Board, followed the Declaration of Helsinki, and the National Institutes of Health's guidelines for the ethical treatment of human subjects. All subjects provided written informed consent.

### Apparatus

Stimuli were presented on a Sony FD Trinitron (GDM-C520) CRT monitor using custom software (Neurostim, <http://neurostim.sourceforge.net>). The display measured 40° (width) × 30° (height) at a viewing distance of 57 cm. Eye-position was monitored using a 500 Hz video-based eye tracker (Eyelink II; SR Research, Mississauga, Canada) and the subject's head was stabilized using a bite bar.

### Short-Term Adaptation Paradigm

Subjects were required to maintain fixation within a 3° × 3° square at the center of the display (around the fixation point) for the duration of each trial (excluding the response epochs). Each trial started when the subject fixated; trials in which subjects failed to fixate appropriately were terminated immediately, discarded, and repeated at a random later time within the block.

The trial started 250 ms after fixation with the presentation of the adapter (an oriented Gabor) on the left or right (selected randomly) and a null adapter (See section Visual Stimuli) on the other side. The null adapter was included to match spatial frequency and contrast adaptation on both sides of fixation and to maintain relative symmetry in the display (to prevent shifts of attention to one side). Immediately after, two oriented Gabors were presented for a variable duration, one on either side of the fixation point. Subjects were instructed to report which of these Gabors was tilted more clockwise. The Gabor that appeared in the same location as the adapter is referred to as the "test" (right Gabor in the example trial shown in **Figure 2A**), and the Gabor that appeared in the location of the null-adapter is the "reference" (left Gabor in the example trial shown in **Figure 2A**). After the presentation of the test and reference stimuli, two masks were presented in the same spatial locations on either side of the screen for 500 ms. These masks were identical to the null-adapters; they served to minimize afterimages and limit the amount of temporal integration of the target stimuli. Subjects indicated which Gabor (left/right) appeared more clockwise by pressing one of two designated keys on the keyboard.

In a traditional adaptation paradigm, the same (or similar) adapter orientation is repeated on every trial. In such a paradigm, effects can accumulate across trials and therefore mix the influence of mechanisms that operate on a short and long time scale (Discussion). Here, we minimized the contribution of long-term effects by choosing a new random adapter orientation on each trial (orientation drawn from a flat distribution between 0 and 180°), thereby spreading long-term orientation-specific effects equally across orientation space over the session. Under these circumstances, orientation-specific behavioral consequences of adaptation can only be ascribed to a mechanism that operates on the timescales of single trials.

Subjectively, this paradigm is substantially more difficult to perform than a standard orientation discrimination paradigm. The reasons for this include the variation of the reference across trials (which requires subjects to compare the two test stimuli on each trial), the brief duration of the test, and the potent masking stimuli. For this reason, all subjects practiced the task (without adapters) for at least two and up to 5 h prior to completing experimental trials. Auditory feedback was provided during these practice runs and the data were only used to assess whether the subject consistently performed the task.

### Invisible Adapter TAE Experiment

Eight naïve subjects (three males, five female) participated. All participants had normal or corrected-to-normal vision, were aged between 17 and 36, and right-handed.

In this experiment, we used adapters that were high enough in spatial frequency that their orientations could not be resolved by the subjects ("invisible" adapters; see "Isolating Short-term Attractive Aftereffects" in Results for the rationale). The spatial frequency of the adapter Gabors was fixed for the duration of the experiment but varied per subject, according to their individual ability to perceive orientation at high spatial frequencies (based on the screening experiment, below). To avoid the necessity of using spatial frequencies beyond the limits of our monitor (resolution: 1,280 × 960 at a refresh rate of 90 Hz), the stimuli were placed at relatively high eccentricity (centers at 12 degrees of visual angle (dva) to either side of the fixation dot).

Both experimental data (Felsen et al., 2002) and our model (Quiroga et al., 2016) show that the largest tuning curve shifts occur when the difference between the adapter and the test is ~20°. Hence, to maximize the expected attractive TAE, we jittered the offset between the reference and the adapter using a uniform probability distribution between 17° and 23° or between -17° and -23°, all in randomly interleaved trials. In the main analysis, we ignored the small variation around the ±20° mean and grouped the trials based only the sign of the offset between the reference and the adapter (clockwise condition: +20° or counterclockwise condition: -20°).

We used an adaptive procedure (Kontsevich and Tyler, 1999) to choose the orientation offset between the test and reference Gabors in each trial and estimate the point of subjective equality. The adapting stimulus was presented for 200 ms.

To test subjects' ability to perceive the orientation of the adapter, we randomly interleaved (10%) catch trials. In these

trials, the test Gabor was replaced by a null-adapter, leaving the adapter as the only oriented element on that side of the screen.

Trials were presented in blocks of 64 trials for each test duration: [50, 100, 200] ms. Each 15-min run consisted of four blocks, and subjects typically completed two to three runs in a 1-h session. Subjects completed between 6000 and 9000 trials (mean 7000) across multiple days.

### Screening Experiment

We mapped each participant's ability to discriminate the orientation of two Gabors at 12 dva eccentricity as a function of spatial frequency. The task was identical to the TAE experiment except that there were no adapters and no masks (i.e., only the reference and test were shown). The spatial frequencies for the reference and test were chosen from [3, 4, 5, 6, 7, 8] cycles per degree of visual angle (cpd) across trials (though always matched on each trial). Because our goal was to measure the discriminability of the orientation of the adapter and the reference in the main experiment, the orientation offset between the test and the reference in the screening experiment was ±20° plus a random jitter of ±3° (following the same procedure as the TAE experiment). As for the other experiments, the subjects' task was to identify the most clockwise stimulus (left or right). The test was presented for 200 ms, matching the longest test in the TAE experiment, and thus provided an upper bound to visibility for all test durations.

From their responses, we determined two spatial frequencies per subject. The first was the highest spatial frequency for which they performed the task at least 80% correct; this was used for the test stimulus in the invisible adapter TAE experiment. The second was the lowest spatial frequency that was higher than that of the test and for which the subject was at or close to chance performance. This was used as the spatial frequency of the adapter in the invisible adapter TAE experiment. This ensured that the subject was unable to judge the orientation of the adapter stimulus accurately, while keeping the spatial frequencies of the adapter and test as similar as possible (see section Results for rationale).

### Visible Adapter TAE Experiment

In this control experiment, the centers of the stimuli were positioned 3 dva to either side of the fixation dot. The spatial frequency of the sinusoidal modulations underlying both Gabors and null-adapters was 2 cpd. The orientation of the test was offset from that of the reference by -12, -8, -4, 0, 4, 8, or 12°, which allowed us to compute a psychometric curve. The adapting stimulus was presented for 100 ms. All other procedures matched those in the invisible adapter TAE experiment. Three subjects participated in this experiment. One subject could not reliably perform this task at the shortest test duration (50 ms), even for the largest differences between test and reference. Hence, we excluded this condition from the analysis for this subject.

### Visual Stimuli

The adapter, test, and reference stimuli were oriented Gabors (sinusoidal luminance gratings modulated by a Gaussian contrast envelope to fade smoothly into the background). The standard

deviation of the Gaussian envelope was 0.8 dva, the contrast was 75%, and the phase of each was randomized independently on each trial. We constructed the null-adapters by adding together eight Gabors whose orientations spanned  $180^\circ$  evenly with a random phase offset. These null-adapters were matched in spatial frequency to the adapting and testing Gabors, but contained little orientation specific energy (Figure 2). The contrast of the component gratings in the null-adapters was adjusted to produce an approximate perceptual match to the contrast of the single Gabor stimuli. The fixation stimulus was a small red square located in the center of the screen, which remained visible for the duration of the trial. The mean luminance of the equal energy white screen was set to  $30 \text{ cd/m}^2$ .

## Data Analysis

The adapter orientation was randomized between  $0^\circ$  and  $180^\circ$  across trials (to avoid accumulation of adaptation across the session; see above), but the reference and test orientation were defined relative to the adapter on each trial. This allowed us to analyze the data in the standard way, by calculating psychometric functions for adapters that were either clockwise or counterclockwise (relative to the reference). To estimate the lapse rate, we fitted a logistic psychometric function to the data [using the *psignifit* toolbox (Wichmann and Hill, 2001b)] while pooling across clockwise and counterclockwise adapters, separately for each subject. Then, we fitted the responses in the trials with clockwise and counterclockwise adapters separately, fixing the lapse rates to the previously estimated values. We defined the shift in perceived orientation (i.e., the TAE) as the difference between the points of subjective equivalence (PSE) in these two curves. A positive difference signals an attractive shift; that is, the perceived orientation of the test was biased toward that of the adapter. Statistical comparison of the PSE differences in individual subjects was performed using Monte Carlo simulations based on the response data, as implemented in the *pfcmp* function for Matlab (Wichmann and Hill, 2001a).

At the group level, we used the increased power of parametric tests (Student *T*-test, and repeated measures analysis of variance) after confirming that the dependent measures (the TAE) did not deviate significantly from normality using the Lilliefors test.

## Model

### Recurrent Network and Dynamics

We implemented an artificial network consisting of a bank of orientation-tuned V1 units, each receiving weakly tuned feedforward input (representing V1 neurons' judicious selection of LGN inputs), and recurrent excitatory and inhibitory input from its neighbors (Carandini and Ringach, 1997; Teich and Qian, 2003). All model parameters were rooted in empirically observed measurements and the units exhibited typical V1-like tuning curves and response dynamics to isolated oriented stimuli. We list the essential model specifications here, but for full details see Quiroga et al. (2016).

Each of the 256 model neurons was modeled as a single passive voltage compartment, whose membrane potential  $V^\theta$  obeyed the differential equation:

$$\tau \frac{dV^\theta}{dt} + V^\theta = V_{\text{lgn}}^\theta + V_{\text{cortex}}^\theta, \quad (1)$$

with  $\tau$  the membrane time constant,  $V_{\text{lgn}}^\theta$  the synaptic potential generated by the thalamic inputs to the model neuron and  $V_{\text{cortex}}^\theta$  is the net synaptic input to the neuron from its cortical neighbors (Carandini and Ringach, 1997; Teich and Qian, 2003). For each neuron, the input from LGN was a function of stimulus orientation  $\omega$  and contrast  $c$ :

$$V_{\text{lgn}}^\theta(\omega, c) = c J_{\text{lgn}} f(\omega|\theta, \kappa_{\text{lgn}}), \quad (2)$$

where  $J_{\text{lgn}}$  represents the strength of the input and  $f(\omega|\theta, \kappa_{\text{lgn}})$  is a von Mises function with period  $\pi$ , mean  $\theta$ , and concentration  $\kappa_{\text{lgn}}$

$$f(x|\mu, \kappa) = e^{\kappa \cos(2(x-\mu))} / 2\pi I_0(\kappa), \quad (3)$$

and  $I_0(\kappa)$  is the modified Bessel function of order zero. The recurrent connection profiles were modeled as the difference of an excitatory and inhibitory von Mises distribution:

$$F^\theta(\phi) = J_{\text{cortex}} (f(\phi|\theta, \kappa_E) - r_{IE} f(\phi|\theta, \kappa_I)). \quad (4)$$

In this recurrent connection profile  $J_{\text{cortex}}$  represents the strength of the cortical connections, and  $r_{IE}$  the ratio of the strength of inhibition to the strength of excitation. With this connection profile we can define the recurrent input as:

$$V_{\text{cortex}}^\theta(t) = \sum_{\phi} F^\theta(\phi) R^\phi(t) \quad (5)$$

The instantaneous firing rate was calculated as a piecewise linear function of the membrane potential:

$$R^\theta(t) = \alpha \max(V^\theta(t), 0), \quad (6)$$

with  $\alpha$  a gain factor (i.e., increase in firing rate in spikes per second for a 1 mV increase in the membrane potential above zero). The model and all simulations were implemented in MATLAB and solved numerically using *ode45*, an adaptive time step Runge-Kutta method. Model parameters were determined in a non-linear optimization procedure that resulted in a quantitative match with the tuning curve shifts observed for brief duration adaptation in anesthetized macaque V1 (i.e., Figure 5 in Patterson et al., 2013). For details of this procedure see Quiroga et al. (2016). The parameters were:  $\tau = 8 \text{ ms}$ ;  $\alpha = 3.88 \text{ Hz/mV}$ ;  $J_{\text{lgn}} = 11.04 \text{ mV/Hz}$ ;  $\kappa_{\text{lgn}} = 0.47$ ;  $J_{\text{cortex}} = 2.84 \text{ mV/Hz}$ ;  $r_{IE} = 1.24$ ;  $\kappa_E = 1.12$ ;  $\kappa_I = 0.56$ .

## Rate Suppression

The recurrent network model reported previously (Quiroga et al., 2016) was developed specifically to isolate the role of recurrent connections and show that they are sufficient to explain dynamic tuning curve shifts even in the absence of all plasticity. Here we extended the model to investigate the potential interaction of recurrent dynamics with the changes in intrinsic properties that are also known to occur in the brain. In visual cortex, exposure to a stimulus is known to result in the reduction of the response to subsequent stimuli (Patterson et al., 2013). We modeled this as a reduction in rate that is proportional (with gain  $\beta$ ) to the neuron's mean firing rate in the adaptation period ( $R^\theta$ ) and recovers on an exponential time course with time constant  $\rho$  after the offset of the adapter at  $t = t_0$ . Formally:

$$R_{\text{adapt}}^\theta(t) = R^\theta(t) - \beta \langle R^\theta \rangle e^{-\frac{t-t_0}{\rho}} \quad (7)$$

## RESULTS

We first present model simulations based on macaque V1 responses that lead to the prediction of a short-term attractive TAE, and then the results of a set of psychophysical experiments that test and confirm the prediction in human observers.

### Model Simulations

We used a network model of orientation processing in V1 in which the neurons' weak orientation selectivity that arises from the afferent input is sharpened by strong, Mexican-hat type, recurrent intracortical connectivity (see section Methods). **Figure 1A** shows the population activity dynamics in the model for a simulated experiment in which an adapter with orientation  $20^\circ$  is first presented for 200 ms and then followed immediately by a  $0^\circ$  test stimulus. At the start of the adaptation phase (yellow;  $t = 5$  ms), the hill of activity is broad, reflecting the tuning that arises from the combination of LGN input. While the adapter is on the screen ( $t < 200$  ms) the hill of activity grows and narrows under the influence of the recurrent connections.

When the  $0^\circ$  test stimulus is shown ( $t = 200$  ms), the LGN input is switched immediately (afferent delays to the LGN are ignored in this simulation) to provide maximal input to the unit that prefers  $0^\circ$ ; and yet, the hill of activity in V1 moves only gradually toward the neuron that prefers  $0^\circ$ . Quiroga et al. (2016) showed that these population dynamics can be surprisingly slow, even though all neurons in the network have short membrane time constants (here 8 ms; see section Methods). The traveling speed of the hill of population activity is a complex function of the network connectivity, but using parameters estimated from macaque V1 (Patterson et al., 2013), it takes several hundreds of milliseconds after test stimulus onset before the hill reaches its stable state (**Figure 1B**). For a full discussion of the model, and how it captures the magnitude and dynamics of tuning curve shifts observed in cat and monkey V1, we refer to Quiroga et al. (2016). Here we focused on behavioral predictions of the model.

We used a labeled line readout to translate population activity into a (predicted) perceived orientation. Specifically, the decoded orientation was defined as the sum of the preferred orientations

of the neurons, weighted by their instantaneous firing rate. To match the experimental protocol (see below), we did this separately for a  $20^\circ$  adapter and a  $-20^\circ$  adapter and defined the TAE as the difference in the model's perceptual readout for these two conditions (**Figure 1C**; blue curve).

By design, the model of Quiroga et al. (2016) captured only the influence of network dynamics and not the changes in intrinsic neuron properties that can lead to a suppression of firing after adaptation. Hence, in a model without plasticity (blue curve in **Figure 1C**), one would predict an attractive TAE with a magnitude  $< 15$  degrees (the value early after test stimulus onset), and because the curve almost reaches zero in 300 ms, the duration of the attractive TAE should be  $< 300$  ms.

However, rate suppression clearly does occur during adaptation; we extended the model to quantify the contribution of rate suppression. We made no specific assumptions about the underlying cellular mechanisms, but assumed that each neuron's firing rate suppression was proportional ( $\beta$ ) to its average response to the adapter (i.e., we assumed that suppression was tuned) and that this response suppression recovered with an exponential ( $\rho$ ) time course (Methods). We estimated these parameters based on Figures 2, 5 in Patterson et al. (2013). For adaptation periods on the order of seconds, the Patterson et al. data show that rate suppression is substantial ( $\beta = 50\%$ ) and recovery slow ( $\sigma = 500$  ms). Entering these parameter estimates into the model leads to the prediction of a repulsive TAE ("strong suppression;" **Figure 1C**; red dashed line). This is consistent with behavioral findings and conceptually similar to the explanation of the repulsive TAE by Jin et al. (2005) and Teich and Qian (2003). For adapters that are presented for at most a few 100 ms, however, rate suppression in V1 is small ( $\beta = 20\%$ ) and recovers rapidly ( $\rho = 100$  ms). Therefore, the model predicts an attractive TAE ("weak suppression;" **Figure 1C**; red solid line), for adaptation protocols that isolate short-term adaptation.

### Isolating Short-Term Attractive Aftereffects

To measure a short-term attractive TAE, we need to address two important issues. First, to emphasize short-term effects, the design should minimize the accumulation of adaptation both within a trial but also across trials. We addressed this by using brief adapters, and, unlike common TAE protocols, a random adapter orientation on each trial.

More specifically, subjects were instructed to respond which of two oriented Gabors (presented on each side of the fixation stimulus) was tilted more clockwise. One of these Gabors (the "test") was preceded by an oriented adapter at the same spatial location, whereas the other ("reference") was preceded by a non-oriented stimulus (null-adapter; see section Methods). Importantly, the orientation of the adapter was chosen randomly on each trial (i.e., any angle between  $0$  and  $180^\circ$ ). The reference was on average oriented either  $20^\circ$  clockwise or  $20^\circ$  counterclockwise to the adapter orientation; this offset generates the largest tuning curve shifts in V1 and in the model (see section Methods). Randomization of the adapter orientation minimized the build-up of plasticity effects (i.e., rate suppression) across trials. This paradigm therefore allowed our measurements to isolate perceptual effects that are induced on the time scale of

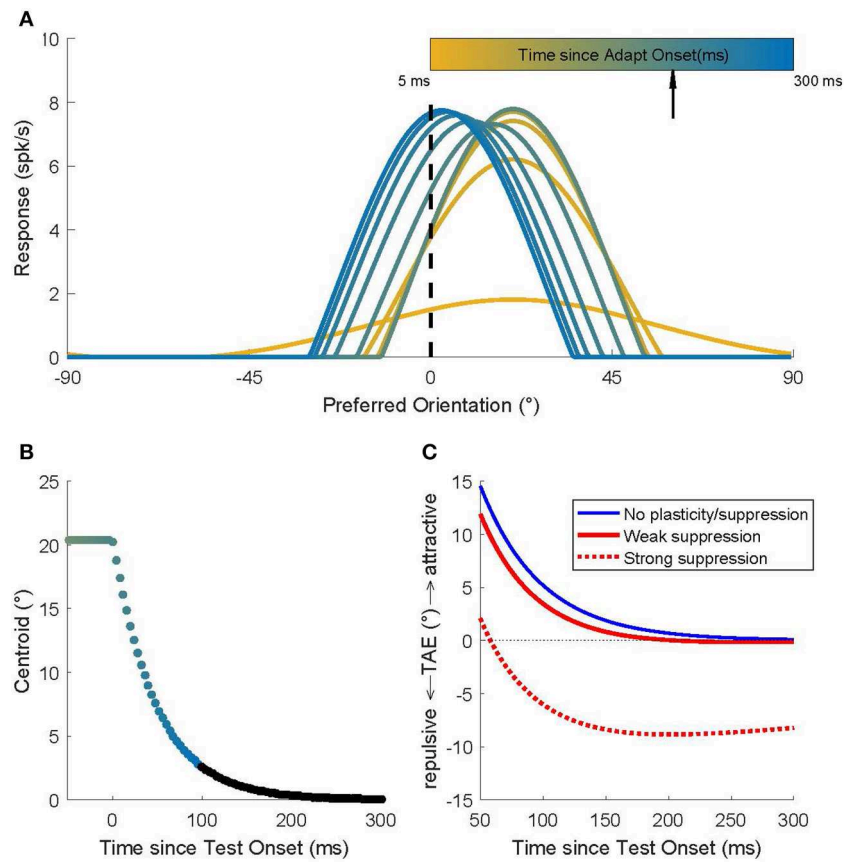


**FIGURE 1 |** Recurrent network model simulations of an adaptation protocol in which a 20° adapter was followed by a 0° test. **(A)** Population activity dynamics in a model without plasticity. Color indicates progression over time. The earliest pattern (orange) represents the activity at the start ( $t = 5$  ms) of the adaptation phase; the hill of activity is broad but, due to the recurrent connections, it gradually narrows around the neurons that prefer 20°. After 200 ms (black arrow) the 0° test stimulus is presented and the hill of activity gradually moves to position itself around the neurons that prefer 0°. **(B)** The dynamics of the location of the hill of population activity (here represented by its centroid). In the adaptation phase ( $t < 0$  ms), the hill is centered on 20°. Once the 0° test is presented, the hill moves toward 0°, but this takes a surprisingly long time (Quiroga et al., 2016). Colors match those used to represent time in **(A)**. Time points omitted for clarity from **(A)** are shown here in black. **(C)** Predicted TAE in three models. One model (blue curve) has no plasticity and its tuning curve shifts are the consequence of the recurrent network dynamics alone. The other two models include the effect of spike rate suppression that occurs for prolonged (seconds) adapter presentations (red dashed curve; strong suppression) or for brief adapter presentations (red solid curve; weak suppression). These modeling results predict that the common long-term adaptation protocols should evoke the well-documented repulsive TAE, while an adaptation protocol that isolates (or emphasizes) the contribution of short-term effects should result in an attractive TAE.

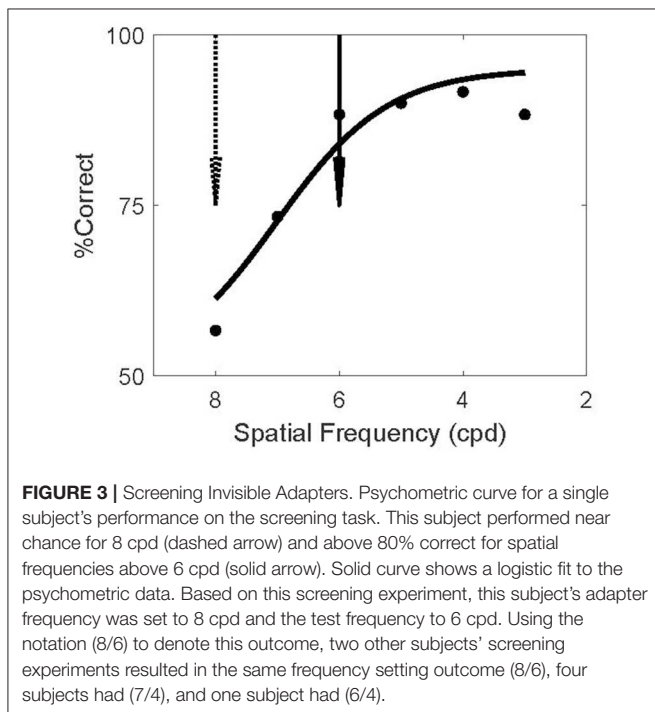
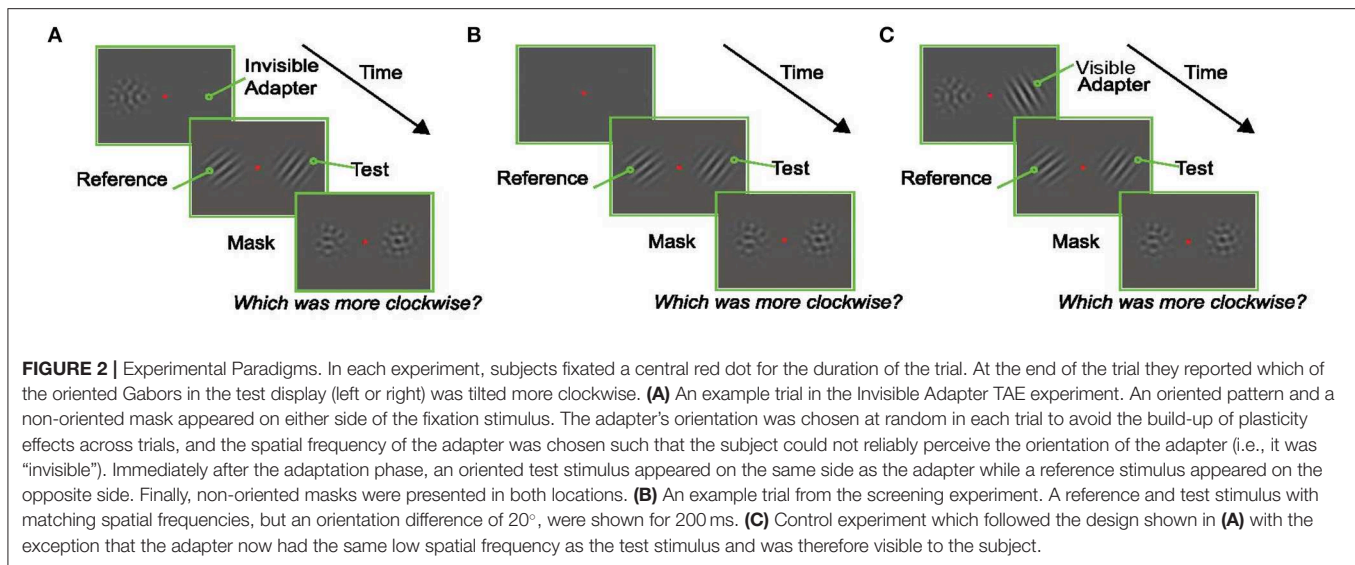
adapter presentation (200 ms in this experiment, matching the simulations in **Figure 1**). We measured the recovery time scale of these effects by presenting the “test” stimulus for one of three durations: 50, 100, and 200 ms, which the model predicts to be associated with progressively weaker attractive aftereffects (**Figure 1B**).

The second issue addressed by our design was a potential substitution confound. Given the brief test stimulus presentations, it is conceivable that on some trials subjects could compare the adapter (rather than the test) to the reference orientation. From this, we would infer the presence of an attractive aftereffect, independent of any true influence of adaptation. To address this, we exploited the invisible adapter paradigm of He and MacLeod (2001). They used laser interferometry to create a grating stimulus directly on the fovea with a spatial frequency so high that its orientation was invisible to the participants. Such invisible patterns nevertheless

evoked a TAE in test stimuli with a lower spatial frequency (and therefore visible orientation) (He and MacLeod, 2001; Rajimehr, 2004). This offers an opportunity to study the TAE without the presence of the substitution confound. Our experiment was analogous to He and MacLeod, except that, lacking an interferometer, we presented the gratings at high eccentricity where even the orientation of gratings with more modest spatial frequencies cannot be resolved. Although strictly speaking only the orientation of these patterns was invisible, we refer to these patterns as invisible adapters.

## Screening Experiment

The screening experiment was designed to find such invisible patterns, separately for each subject. For each subject we assessed the ability to discriminate orientation as a function of spatial frequency. This experiment matched the test phase of the main experiments but no adapters or masks were present (because the



adapters in the main study were not forward masked; **Figure 2B**). The example subject in **Figure 3** could not reliably discriminate the orientation of 8 cpd patterns (dashed arrow). In the TAE experiment of this subject, the spatial frequency of the adapter was therefore set to 8 cpd; thus minimizing the possibility that the subject could report the orientation of the adapter.

In the model, the TAE results from the recurrent connections between neurons representing the adapter and the test. In V1 such connections are likely stronger between neurons with similar spatial frequency preference (Ts'o et al., 1986; Malach

et al., 1993). Hence the model predicts a larger TAE if the test stimulus has a high spatial frequency similar to the adapter, while the logic of the experiment requires that the test stimulus spatial frequency is low enough to make it visible. We compromised between these conflicting demands by setting the test frequency to the highest spatial frequency at which the subject could reliably perform the task in the screening experiment ( $>80\%$  correct). For the example subject this was 6 cpd (solid arrow).

### Invisible Adapter TAE Experiment

**Figure 4A** shows a stacked histogram of TAE sizes for all subjects. The overall mean TAE was  $1.5^\circ$ , which was significantly larger than zero ( $p < 0.05$ ; one-sided *T*-test), and confirms our prediction that the TAE for brief (200 ms) adapters is attractive for a short time after ( $\leq 200$  ms). This overall measure, however, averages over an underlying decay time-course that is seen more clearly in the average across subjects in **Figure 4B**. Statistical analysis confirmed a significant effect of duration on the TAE [ $F_{(2)} = 38$ ,  $p < 0.001$ ; one-way repeated measures ANOVA], reflecting the rapid recovery of the TAE on a 200 ms time scale. *Post-hoc* tests showed that only the shortest duration test (50 ms) led to a significant positive TAE ( $p < 0.01$ ; one-sided *T*-test). For this shortest test duration, the effect was  $3.9^\circ$  in magnitude. TAE at test durations of 100 and 200 ms were not significantly larger than zero ( $p > 0.5$ ), nor were they significantly different from each other ( $p > 0.7$ ). At the single subject level, the TAE at the shortest duration was attractive for all but one subject, and significantly larger than zero in 4 out of 8 subjects ( $p < 0.05$ ; Monte Carlo comparison of PSEs; see section Methods). No subjects had a significantly repulsive TAE.

The experiment was designed to make the adapter's orientation invisible and thereby remove the potential confound that the subjects reported based on the orientation of the adapter instead of the test. However, due to drifts in subject thresholds, it is possible that subjects performed near chance for a high spatial frequency in the screening experiment, but were still

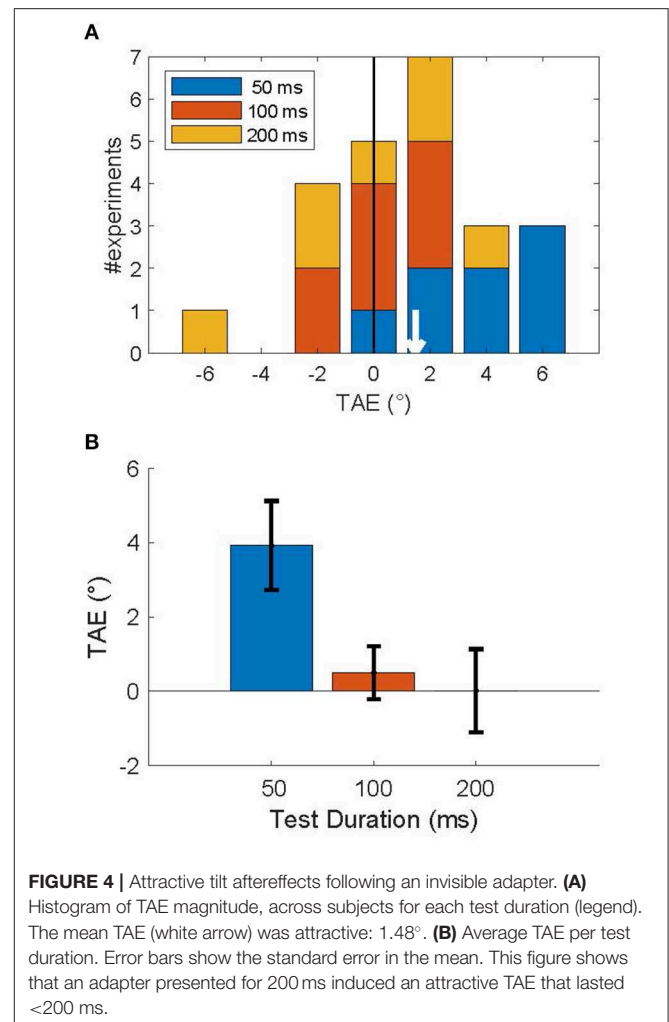
able to detect the pattern's orientation in the TAE experiment. To assess whether this could account for the attractive TAE, we used interleaved catch trials in which the test grating was replaced by a null-adaptor. In these trials the adaptor was the only oriented element on the test side of the display. If the subjects could see the adaptor, they would likely respond clockwise if the adaptor was clockwise to the reference. We used this to estimate adaptor visibility by calculating the proportion of trials in which the subject's report (CW vs. CCW) was consistent with the relation between the adaptor and the reference. The extent to which these proportions differed from 50% provides a measure of adaptor visibility. **Figure 5** shows the relationship between the TAE and adaptor visibility. On average, adaptor visibility was  $5.7 \pm 4.2\%$  (mean  $\pm$  standard deviation), suggesting little awareness of adaptor orientation, as intended by our design. For five of the data points (data points surrounded by black squares in **Figure 5**), we could not reject the null hypothesis that the adaptor was invisible ( $p < 0.05$ , binomial test). These data points, however, did not drive the main results illustrated in **Figure 4**. Notably, even after excluding these data points, the mean TAE was significantly larger than zero ( $p < 0.05$ ; one-sided  $T$ -test) and the TAE depended significantly on adaptor duration [ $F_{(2)} = 23$ ;  $p < 0.001$ ]. Furthermore, if inadvertent adaptor visibility caused the attractive TAE, it should be larger in conditions with high adaptor visibility. **Figure 5**, however, shows that the magnitude of the TAE did not depend on the visibility of the adaptor (Pearson correlation  $r = -0.084$ ,  $p > 0.69$ ).

### Visible Adapter TAE Experiment

As explained above, we used an invisible adaptor to avoid the possibility that the subjects reported the orientation of the adaptor, instead of the test. For completeness, and to demonstrate that the attractive TAE is not restricted to the use of an invisible adaptor, we performed a control experiment using a standard, visible, adaptor. In this experiment all Gabor stimuli (adaptor, test, null) had a spatial frequency of 2 cpd, and were presented at  $3^\circ$  eccentricity. Subjects performed the same orientation discrimination task (**Figure 2C**), but we used the method of constant stimuli to obtain better estimates of the full psychometric functions. In this experiment, the adaptor was presented for only 100 ms (compared to the 200 ms used in the invisible adaptor experiment). The example subject whose results are shown in **Figure 6** had a significant, attractive TAE for a 50 ms test duration ( $p < 0.05$ ; Monte Carlo simulations; see section Methods), but not for the longer test stimuli.

**Figure 7** shows the average size of the TAE across the three subjects that performed this experiment, as a function of test duration. Each subject had a significant, attractive TAE at the shortest test duration for which they could perform the task ( $p < 0.05$ , Monte Carlo simulations; see section Methods). This result is consistent with the findings for invisible adaptors (**Figure 4**); brief adaptation results in an attractive TAE that decays on a time scale faster than 200 ms.

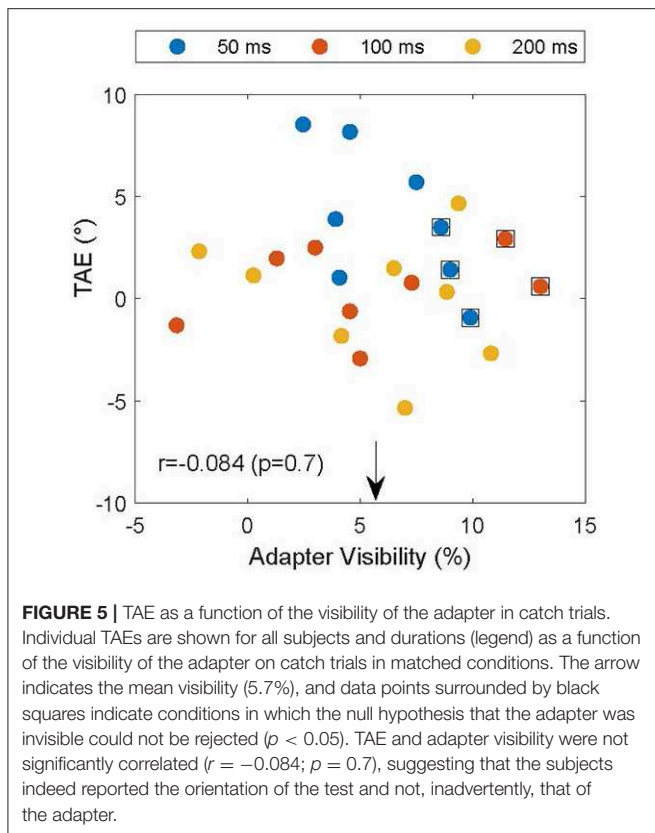
As explained above, in this experiment, we cannot exclude the possibility that subjects inadvertently reported the orientation of the adaptor. We note, however, that the full psychometric curves (e.g., **Figure 6**) suggest that subjects primarily reported



the orientation of the test (as instructed) and not the adaptor. Notably, if the subject always reported the adaptor orientation, the psychometric curves would have been independent of the test orientation (i.e., the figure would have shown two flat lines with the green line (a clockwise adaptor) above the blue line (counterclockwise adaptor)). The sigmoidal shape of the subjects' psychometric functions showed that they responded primarily to the test stimulus, not to the adaptor. Given, however, that this potential confound limits the forcefulness with which these data can be interpreted, we did not pursue this experimental design with a larger number of subjects.

## DISCUSSION

Our experiments show that briefly presented oriented stimuli are perceived to be more similar to immediately preceding stimuli than they really are. This effect is opposite to the well-known (repulsive) tilt aftereffect. Under the conditions of these experiments, it is induced on a time-scale of 100–200 ms and recovers on a similar time scale: it is a short-term attractive tilt aftereffect. The attractive nature of the aftereffect and its fast

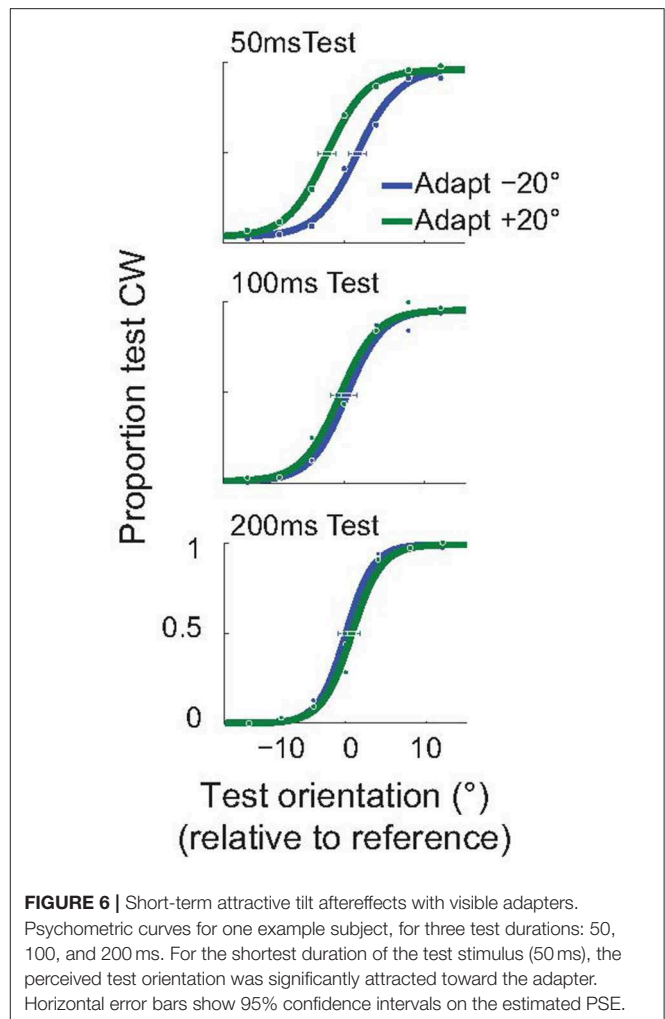


recovery were predicted by our recurrent network model and therefore supports the view that orientation tuning curve shifts in V1 on the order of hundreds of milliseconds may be generated by the attractor dynamics of recurrent networks.

## Attractive and Repulsive Tilt Aftereffects

Gibson and Radner (1937) showed that 1 min of exposure to an adapter leads to a sizable tilt aftereffect. Even in that first paper, both repulsive and attractive aftereffects were reported. Repulsion was found when the orientation difference between the adapter and the test was between  $10^\circ$  and  $30^\circ$  (the so-called direct TAE), while attraction was observed in trials with large orientation differences ( $50^\circ$ – $90^\circ$ ; the indirect TAE). Our model predicted an attractive TAE even for small orientation differences, hence we focused on the direct TAE where the prediction appeared to conflict with well-established findings of a repulsive TAE even for brief test stimuli (Sekuler and Littlejohn, 1974; Wolfe, 1984). The apparent conflict is resolved by distinguishing two, logically distinct time scales involved in adaptation.

The first is the time scale of recovery from adaptation. This time scale can be probed, for instance, by leaving a gap between adapter and test or by varying the duration of the test stimulus. Previous studies have probed this recovery timescale extensively and concluded that shorter test stimuli generate larger TAEs (Wolfe, 1984; Magnussen and Johnsen, 1986; Harris and Calvert, 1989; Wenderoth and van der Zwan, 1989). The horizontal axes



in **Figures 4B, 7** represent this recovery time scale, and these figures show that our findings are consistent with those previous reports; short test flashes produce larger aftereffects.

The second is the time scale of the induction of adaptation. The duration of the adapter partially determines this time scale and previous work has shown that TAE magnitude increases with longer induction (Magnussen and Johnsen, 1986). Importantly, the duration of the adapter on a single trial is not the only determinant of the time scale of induction. In fact, Magnussen and Johnsen (1986) showed that multiple short presentations of the same adapter generate more adaptation than a single long presentation with the same total duration. This demonstrates that—as long as the adapter stays the same—adaptation accumulates over multiple trials (This is likely part of the reason why the commonly used top-up paradigm generates large adaptation effects even with brief top-up adapters). In previous work, the same adapter (or a small set of adapters) was presented repeatedly. This allowed such paradigms to tap into induction mechanisms operating on slow time scales, even when individual adapters were presented only briefly (Sekuler and Littlejohn, 1974).

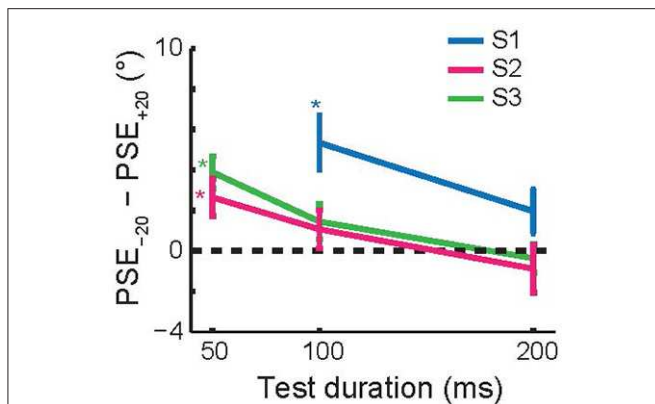


**FIGURE 7 |** Recovery time course of short-term tilt aftereffects. The figure shows the change in PSE as a function of the test duration. For each of the subjects, the aftereffect was attractive at the shortest test duration at which they reliably performed the task (50 or 100 ms). Error bars show 95% confidence intervals based on Monte Carlo simulations (see section Methods).

In our experimental paradigm, adapter orientation was randomized across trials. Therefore, adaptation could not accumulate across trials in an orientation specific manner, and this isolated the TAE that is generated on a short induction time scale. There is therefore no contradiction between our finding of an attractive (direct) TAE and previous reports of a repulsive (direct) TAE; the separate induction time scales account for the difference.

## Time Scales

Although the time scale of the attractive TAE may seem short in terms of traditional behavioral adaptation experiments, it is actually well-matched to natural behavior. During normal exploratory behavior, primates make eye movements two to three times per second, hence new inputs arrive in the visual system on a time scale of hundreds of milliseconds (Ibbotson and Krekelberg, 2011). Our findings suggest that the V1 recurrent network is well-suited for the need to integrate and amplify information available within a typical fixation period.

Of course, recurrent network dynamics are unlikely to be responsible for neural and behavioral response changes on very long time scales. For instance, training on an orientation discrimination task results in tuning changes in early visual cortex (Schoups et al., 2001; Ghose et al., 2002). The link between these neural changes and behavioral improvements [i.e., perceptual learning (Watanabe and Sasaki, 2015)] is only partially understood (Ghose et al., 2002; Teich and Qian, 2003) and models that incorporate plastic changes (Teich and Qian, 2003; Chelaru and Dragoi, 2008; Ursino et al., 2008) are needed to understand this link. In a recurrent network, however, changes in connectivity can cause substantial changes in network dynamics (e.g., Figures 3, 4 in Quiroga et al., 2016). This shows that changes taking place on the slow time scale of learning can influence dynamics at the rapid sub-second time scale. Considering this aspect may help to generate testable predictions

for changes in neural response properties and how these affect behavioral performance.

## Motion

Kanai and Verstraten (2005) reported repulsive motion aftereffects for long induction time scales, and attractive motion aftereffects for induction time scales below 200 ms. This phenomenological similarity of the short-term aftereffects in the motion and orientation domain is intriguing and suggests that similar recurrent network mechanisms could underlie these phenomena. This view is supported by theoretical and empirical work demonstrating that recurrent network dynamics could play a fundamental role in motion tuning (Mineiro and Zipser, 1998; Joukes et al., 2014; Pachitariu and Sahani, 2017).

Because there is substantial interaction between orientation and motion processing (Krekelberg et al., 2003; Kourtzi et al., 2008), one can also ask whether motion signals may lead to the short-term attractive TAE. In any adaptation paradigm, the successive presentation of the adapter and test has the potential to generate apparent motion signals, and theoretically, these could affect the perception of orientation. This would be analogous to the many ways in which translational motion can induce a misperception of position (Krekelberg, 2001; Krekelberg and Lappe, 2001; Müsseler et al., 2002). In our view, however, it is unlikely that the apparent motion signal played an important role in the perception of orientation in our experiments. First, the phase of the adapter and test were randomized independently, this should limit the strength of apparent motion. Second, in the invisible adapter experiment the spatial frequency of the adapter was higher than that of the test. This further reduces the strength of apparent motion and yet, the attractive TAE was of a similar magnitude. Of course, these arguments do not preclude the possibility that stronger motion signals could affect orientation adaptation. In fact, our recent findings show that one link between the neural mechanisms of complex form and motion processing is their reliance on recurrent connectivity (Joukes et al., 2017). This predicts that some of the adaptation effects resulting from recurrent connectivity could affect both form and motion perception.

## Neural Mechanisms

Previously, we showed that our model can account quantitatively for the repulsive tuning curve shifts observed in V1 (Quiroga et al., 2016). Here, we show that these repulsive tuning curve shifts predict an attractive TAE. Although counterintuitive, this apparent contradiction follows directly from the labeled line code (Gilbert and Wiesel, 1990; Yao and Dan, 2001; Teich and Qian, 2003; Jin et al., 2005). Consider a neuron that normally prefers  $0^\circ$ —in any labeled line decoder, spikes from this neuron are always interpreted as evidence in favor of  $0^\circ$ . Across a population of labeled line neurons, the percept is given by the location of the peak or center of the population activity. The statement that “adaptation causes a repulsive tuning curve shift” means, for example, that after adaptation at  $-10^\circ$ , the  $0^\circ$  neuron responds most strongly to a  $2^\circ$  stimulus. That implies, however, that for a  $2^\circ$  stimulus, the population activity is centered on  $0^\circ$ . And this, in turn, means that the  $2^\circ$  stimulus is decoded as  $0^\circ$ . In

other words, the  $2^\circ$  stimulus is attracted to the  $-10^\circ$  adapter. The inversion from repulsion to attraction occurs because the former describes tuning curves (the response of a single neuron to different stimuli; a theoretical construct that exists only across trials), while the latter describes population activity (the response of many neurons to a single stimulus; this construct exists in each trial and underlies perception). For a more extensive discussion of these issues in the context of speed perception see Krekelberg et al. (2006b).

In our model, repulsive tuning curve shifts (and therefore the attractive TAE) results from the persistence of neural activity evoked by the adapter. This persistence is determined by the strength of the recurrent connections (as discussed in detail by Quiroga et al., 2016) and results in a predicted recovery time scale of the aftereffect on the order of a few 100 ms (Figure 1). Given that the model parameters were determined solely from the macaque V1 responses, the match between the model prediction and the behavioral results is surprisingly good and supports our claim that recurrent connections could underlie this behavioral effect.

Quantitatively, the model (Figure 1) predicts a larger TAE than we observed in our subjects. Part of this could be explained by well-known, but uncontrolled experimental factors. For instance, occasional reductions in attentional focus would reduce adaptation (Rezec et al., 2004) and fixational instability during the brief presentation of the adapter could also reduce adaptation. Our data provide support for the latter hypothesis; the interquartile range of fixational eye positions during the presentation of the adapter was negatively correlated with the TAE (Pearson  $r = -0.7$ ;  $p = 0.03$ ).

At the same time, because the model parameters were constrained only by data obtained in the anesthetized macaque, a mismatch between the model and human behavior should not be too surprising. The magnitude of tuning curve shifts increases when excitatory lateral connections are narrowly tuned, when inhibitory connections are broadly tuned, or when the overall strength of lateral connections is large compared to the afferent thalamic input (Quiroga et al., 2016). Most likely, these parameters are not the same across species, or even across individuals, or across retinal location within an individual. This implies that a range of TAE magnitudes is to be expected, just as the magnitude of tuning curve shifts also varies considerably across studies (Dragoi et al., 2000; Felsen et al., 2002; Patterson et al., 2013).

It would be interesting to find better methods to constrain model parameters. In principle, it should be possible to use behavioral responses to sequences of oriented gratings to infer the underlying functional connectivity in a network model. However, this problem is ill-constrained and adaptation is a poor replacement for an electrode (Krekelberg et al., 2006a; Sawamura et al., 2006; Hegdé, 2009; Solomon and Kohn, 2014; Kar and Krekelberg, 2016). Nevertheless, we believe that progress could be made by using carefully tailored paradigms, and models that are constrained not only by behavioral data, but also by the properties of rapid adaptation at the single neuron level (Benucci et al., 2009).

## Function

In our model, the short-term attractive TAE can be attributed to repulsive tuning curve shifts, which are caused by the pushing and pulling of population activity in a network with Mexican hat shaped recurrent connectivity (Quiroga et al., 2016). This connectivity pattern has many potential benefits. For instance, it sharpens orientation tuning and amplifies weak signals (Carandini and Ringach, 1997; Hahnloser et al., 2002; Teich and Qian, 2003), or it can implement a statistical prior assumption that changes in the sensory input are typically small (Deneve et al., 2001; Schwartz et al., 2007). The attractive TAE could therefore be interpreted as a side effect of such mechanisms that optimize orientation processing. The fact that these side-effects are not immediately obvious from the model, but require detailed simulations and exploration, attests to the fact that even simple recurrent networks can generate surprisingly complex responses. Phrased more positively, recurrent networks can underlie highly complex functionality. For instance, recurrent networks are able to implement rudimentary forms of memory that are needed in motion detection (Joukes et al., 2014), generate sensitivity for higher-order statistics (Joukes et al., 2017), or amplify weak stimuli in a state-dependent manner (Rutishauser and Douglas, 2009). These are elementary computations that are useful in perception and cognition and may be a reason why recurrent connections are ubiquitous across cortex.

## Alternative Models

The attractive TAE can be seen as an example of temporal integration; the response to the test is integrated with the response to the adapter and therefore the test looks like the adapter. This is an appealing, simple phenomenological description, but our goal is to understand the underlying neural mechanisms. In other words, one can postulate that a hill of persisting activity represents the adapter in a set of orientation-tuned neurons, and the interaction of this persisting activity with activity generated by the test could result in an attractive aftereffect. This description, however, does not answer the question of how such persistence is generated. Our model provides one answer to this question: we propose that recurrent connections lead to persistence and underlie temporal integration. In the model, the recurrent connections are necessary to explain an attractive TAE that lasts 50–100 ms (Figures 4, 7) because without them persistence is short, as activity dissipates on the time scale of the membrane time constant (8 ms).

There may well be other answers to the question of what generates (or contributes to) the persistence and temporal integration. For instance, prolonged exposure to visual input could affect the state or dynamics of slow channels and thereby result in persisting activity, or at least subthreshold depolarization, on a time scale of several 100 ms in individual neurons. Experimental data from cat visual cortex, however, show that prolonged exposure to visual input hyperpolarizes neurons by opening K-channels, and reduces their spiking activity (Sanchez-Vives et al., 2000a,b). The model shows that such effects shorten the recovery time course, and, when spike

rate suppression is large enough, result in a repulsive, not an attractive TAE (**Figure 1C**).

Another possibility is that exposure to the adapter strengthens lateral connections between V1 neurons. This can generate repulsive tuning curve shifts (Felsen et al., 2002) and would therefore also lead to attractive aftereffects. To explain our findings, however, one would have to assume that a single 200 ms presentation of an adapter is sufficient to change the effective synaptic connectivity between neurons. We are not aware of experimental data that support the existence of such rapid plasticity in V1. Instead, plasticity is typically observed after the repeated exposure to the same (pairs of) stimuli (Yao and Dan, 2001). Just like the traditional TAE paradigm, this potentially taps into slow mechanisms that accumulate over seconds, even if the individual stimulus presentations are brief.

Of course, the neural mechanisms underlying the TAE need not be restricted to V1. The orientation-specificity of the TAE, however, demonstrates that the integrators must be orientation-tuned, which argues for at least a cortical locus. In addition, the finding that the TAE occurs even without conscious awareness of the adapter orientation (as in our invisible adapter experiment) suggests that its neural locus is relatively early (pre-attentive) in visual processing (Clifford, 2014). While it is certainly possible, ultimately even desirable, to construct a model that spans all levels of visual processing, it is difficult to constrain such a model with currently available experimental data.

In summary, in Quiroga et al. (2016) we proposed that recurrent network connections could underlie tuning curve shifts in V1 and supported this model with electrophysiological data. Here we used the recurrent network model, fully constrained by neural data, to generate novel predictions about orientation perception. Our experiments confirmed the predicted attractive TAE. Because the model uses only well-supported patterns of recurrent connectivity, it is a parsimonious, mechanistic explanation of repulsive shifts in short-term tuning curves and the short-term attractive TAE. We emphasize, however, that neither the electrophysiological nor the current behavioral data prove that the model is correct, or that recurrent connections are necessary to explain these phenomena. Such proofs of necessity are fundamentally beyond the purview of models. Instead,

model value derives from the ability to generate conceptually novel understanding of neural processing and experimentally testable hypotheses.

## DATA AVAILABILITY STATEMENT

The datasets generated for this study are available on request to the corresponding author.

## ETHICS STATEMENT

The studies involving human participants were reviewed and approved by The Institutional Review Board of Rutgers University. The patients/participants provided their written informed consent to participate in this study.

## AUTHOR CONTRIBUTIONS

MQ, AM, and BK designed experiments and edited the manuscript. MQ performed the experiments. MQ and BK developed the model, performed model simulations, and analyzed the data. BK wrote the manuscript.

## FUNDING

The National Eye Institute [EY017605], the Charles and Johanna Busch Memorial Fund, and the Behavioral and Neural Sciences Graduate Program at Rutgers, The State University of New Jersey, supported this research. The funding sources were not involved in study design, data collection and interpretation, or the decision to submit the work for publication. The content is solely the responsibility of the authors and does not necessarily represent the official views of the funding agencies.

## ACKNOWLEDGMENTS

We thank Minal Patel, Kiran Wattamwar, Mina Henaen, Jasmine Siegel, and Benjamin Maas for their assistance with data collection.

## REFERENCES

- Benucci, A., Ringach, D. L., and Carandini, M. (2009). Coding of stimulus sequences by population responses in visual cortex. *Nat. Neurosci.* 12, 1317–1324. doi: 10.1038/nn.2398
- Carandini, M., and Ringach, D. L. (1997). Predictions of a recurrent model of orientation selectivity. *Vision Res.* 37, 3061–3071. doi: 10.1016/S0042-6989(97)00100-4
- Chelaru, M. I., and Dragoi, V. (2008). Asymmetric synaptic depression in cortical networks. *Cereb. Cortex* 18, 771–788. doi: 10.1093/cercor/bhm119
- Chopin, A., and Mamassian, P. (2012). Predictive properties of visual adaptation. *Curr. Biol.* 22, 622–626. doi: 10.1016/j.cub.2012.02.021
- Clifford, C. W. G. (2014). The tilt illusion: phenomenology and functional implications. *Vision Res.* 104, 3–11. doi: 10.1016/j.visres.2014.06.009
- Clifford, C. W. G., Wenderoth, P., and Spehar, B. (2000). A functional angle on some after-effects in cortical vision. *Proc. R. Soc. B Biol. Sci.* 267, 1705–1710. doi: 10.1098/rspb.2000.1198
- Deneve, S., Latham, P. E., and Pouget, A. (2001). Efficient computation and cue integration with noisy population codes. *Nat. Neurosci.* 4, 826–831. doi: 10.1038/90541
- Dragoi, V., Sharma, J., and Sur, M. (2000). Adaptation-induced plasticity of orientation tuning in adult visual cortex. *Neuron* 28, 287–298. doi: 10.1016/S0896-6273(00)00103-3
- Felsen, G., Shen, Y. S., Yao, H., Spor, G., Li, C., and Dan, Y. (2002). Dynamic modification of cortical orientation tuning mediated by recurrent connections. *Neuron* 36, 945–954. doi: 10.1016/S0896-6273(02)01011-5
- Fischer, J., and Whitney, D. (2014). Serial dependence in visual perception. *Nat. Neurosci.* 17, 2569–2574. doi: 10.1038/nn.3689
- Ghose, G. M., Yang, T., and Maunsell, J. H. R. (2002). Physiological correlates of perceptual learning in monkey V1 and V2. *J. Neurophysiol.* 87, 1867–1888. doi: 10.1152/jn.00690.2001
- Gibson, J. J. (1933). Adaptation, after-effect and contrast in the perception of curved lines. *J. Exp. Psychol.* 16, 1–31. doi: 10.1037/h0074626

- Gibson, J. J., and Radner, M. (1937). Adaptation, after-effect and contrast in the perception of tilted lines. I. Quantitative studies. *J. Exp. Psychol.* 20, 453–467. doi: 10.1037/h0059826
- Gilbert, C. D., and Wiesel, T. N. (1990). The influence of contextual stimuli on the orientation selectivity of cells in primary visual cortex of the cat. *Vision Res.* 30, 1689–1701. doi: 10.1016/0042-6989(90)90153-C
- Hahnloser, R. H. R., Douglas, R. J., and Hepp, K. (2002). Attentional recruitment of inter-areal recurrent networks for selective gain control. *Neural Comput.* 14, 1669–1689. doi: 10.1162/08997660260028665
- Harris, J. P., and Calvert, J. E. (1989). Contrast, spatial frequency and test duration effects on the tilt aftereffect: implications for underlying mechanisms. *Vision Res.* 29, 129–135. doi: 10.1016/0042-6989(89)90179-X
- He, S., and MacLeod, D. I. A. (2001). Orientation-selective adaptation and tilt after-effect from invisible patterns. *Nature* 411, 473–476. doi: 10.1038/35078072
- Hegd , J. (2009). How reliable is the pattern adaptation technique? A modeling study. *J. Neurophysiol.* 102, 2245–2252. doi: 10.1152/jn.00216.2009
- Heinrich, T. S., and Bach, M. (2001). Contrast adaptation in human retina and cortex. *Investig. Ophthalmol. Vis. Sci.* 42, 2721–2727. Available online at: <https://iovs.arvojournals.org/article.aspx?articleid=2200085>
- Ibbotson, M., and Krekelberg, B. (2011). Visual perception and saccadic eye movements. *Curr. Opin. Neurobiol.* 21, 553–558. doi: 10.1016/j.conb.2011.05.012
- Jin, D. Z., Dragoi, V., Sur, M., and Seung, H. S. (2005). Tilt aftereffect and adaptation-induced changes in orientation tuning in visual cortex. *J. Neurophysiol.* 94, 4038–4050. doi: 10.1152/jn.00571.2004
- Joukes, J., Hartmann, T. S., and Krekelberg, B. (2014). Motion detection based on recurrent network dynamics. *Front. Syst. Neurosci.* 8:239. doi: 10.3389/fnsys.2014.00239
- Joukes, J., Yu, Y., Victor, J. D., and Krekelberg, B. (2017). Recurrent network dynamics; a link between form and motion. *Front. Syst. Neurosci.* 11:12. doi: 10.3389/fnsys.2017.00012
- Kanai, R., and Verstraten, F. A. J. (2005). Perceptual manifestations of fast neural plasticity: motion priming, rapid motion aftereffect and perceptual sensitization. *Vision Res.* 45, 3109–3116. doi: 10.1016/j.visres.2005.05.014
- Kar, K., and Krekelberg, B. (2016). Testing the assumptions underlying fMRI adaptation using intracortical recordings in area MT. *Cortex* 80, 1–14. doi: 10.1016/j.cortex.2015.12.011
- Kohn, A. (2007). Visual adaptation: physiology, mechanisms, and functional benefits. *J. Neurophysiol.* 97, 3155–3164. doi: 10.1152/jn.00086.2007
- Kontsevich, L. L., and Tyler, C. W. (1999). Bayesian adaptive estimation of psychometric slope and threshold. *Vision Res.* 39, 2729–2737. doi: 10.1016/S0042-6989(98)00285-5
- Kourtzi, Z., Krekelberg, B., and van Wezel, R. J. A. R. J. A. (2008). Linking form and motion in the primate brain. *Trends Cogn. Sci.* 12, 230–236. doi: 10.1016/j.tics.2008.02.013
- Krekelberg, B. (2001). The persistence of position. *Vision Res.* 41, 529–539. doi: 10.1016/S0042-6989(00)00281-9
- Krekelberg, B., Boynton, G. M., and van Wezel, R. J. A. (2006a). Adaptation: from single cells to BOLD signals. *Trends Neurosci.* 29, 250–256. doi: 10.1016/j.tins.2006.02.008
- Krekelberg, B., Dannenberg, S., Hoffmann, K.-P., Bremmer, F., and Ross, J. (2003). Neural correlates of implied motion. *Nature* 424, 674–677. doi: 10.1038/nature01852
- Krekelberg, B., and Lappe, M. (2001). Neuronal latencies and the position of moving objects. *Trends Neurosci.* 24, 335–339. doi: 10.1016/S0166-2236(00)01795-1
- Krekelberg, B., Van Wezel, R. J. A., and Albright, T. D. (2006b). Interactions between speed and contrast tuning in the middle temporal area: implications for the neural code for speed. *J. Neurosci.* 26, 8988–8998. doi: 10.1523/JNEUROSCI.1983-06.2006
- Kristjansson, A. (2011). The functional benefits of tilt adaptation. *Seeing Perceiving* 24, 37–51. doi: 10.1163/187847511X555283
- Magnussen, S., and Johnsen, T. (1986). Temporal aspects of spatial adaptation. A study of the tilt aftereffect. *Vision Res.* 26, 661–672. doi: 10.1016/0042-6989(86)90014-3
- Malach, R., Amir, Y., Harel, M., and Grinvald, A. (1993). Relationship between intrinsic connections and functional architecture revealed by optical imaging and *in vivo* targeted biocytin injections in primate striate cortex. *Proc. Natl. Acad. Sci. U.S.A.* 90, 10469–10473. doi: 10.1073/pnas.90.22.10469
- Mineiro, P., and Zipser, D. (1998). Analysis of direction selectivity arising from recurrent cortical interactions. *Neural Comput.* 10, 353–371. doi: 10.1162/089976698300017791
- M ller, J. R., Metha, a. B., Krauskopf, J., and Lennie, P. (1999). Rapid adaptation in visual cortex to the structure of images. *Science* 285, 1405–1408. doi: 10.1126/science.285.5432.1405
- M sseler, J., Stork, S., and Kerzel, D. (2002). Comparing mislocalizations with moving stimuli: the Fr hlich effect, the flash-lag, and representational momentum. *Vis. Cogn.* 9, 120–138. doi: 10.1080/13506280143000359
- Pachitariu, M., and Sahani, M. (2017). Visual motion computation in recurrent neural networks. *bioRxiv [Preprint]*. doi: 10.1101/099101
- Patterson, C. A., Duijnhouwer, J., Wissig, S. C., Krekelberg, B., and Kohn, A. (2014). Similar adaptation effects in primary visual cortex and area MT of the macaque monkey under matched stimulus conditions. *J. Neurophysiol.* 111, 1203–1213. doi: 10.1152/jn.00030.2013
- Patterson, C. A., Wissig, S. C., and Kohn, A. (2013). Distinct effects of brief and prolonged adaptation on orientation tuning in primary visual cortex. *J. Neurosci.* 33, 532–543. doi: 10.1523/JNEUROSCI.3345-12.2013
- Quiroga, M., Morris, A. P., and Krekelberg, B. (2016). Adaptation without plasticity. *Cell Rep.* 17, 58–68. doi: 10.1016/j.celrep.2016.08.089
- Rajimehr, R. (2004). Unconscious orientation processing. *Neuron* 41, 663–673. doi: 10.1016/S0896-6273(04)00041-8
- Rezec, A., Krekelberg, B., and Dobkins, K. R. (2004). Attention enhances adaptability: evidence from motion adaptation experiments. *Vision Res.* 44, 3035–3044. doi: 10.1016/j.visres.2004.07.020
- Rutishauser, U., and Douglas, R. (2009). State-dependent computation using coupled recurrent networks. *Neural Comput.* 21, 478–509. doi: 10.1162/neco.2008.03-08-734
- Sanchez-Vives, M. V., Nowak, L. G., and McCormick, D. A. (2000b). Cellular mechanisms of long-lasting adaptation in visual cortical neurons *in vitro*. *J. Neurosci.* 20, 4286–4299. doi: 10.1523/JNEUROSCI.20-11-04286.2000
- Sanchez-Vives, M. V., Nowak, L. G., and McCormick, D. A. (2000a). Membrane mechanisms underlying contrast adaptation in cat area 17 *in vivo*. *J. Neurosci.* 20, 4267–4285. doi: 10.1523/JNEUROSCI.20-11-04267.2000
- Sawamura, H., Orban, G. A., and Vogels, R. (2006). Selectivity of neuronal adaptation does not match response selectivity: a single-cell study of the fMRI adaptation paradigm. *Neuron* 49, 307–318. doi: 10.1016/j.neuron.2005.11.028
- Schoups, A., Vogels, R., Qian, N., and Orban, G. (2001). Practising orientation identification improves orientation coding in V1 neurons. *Nature* 412, 549–553. doi: 10.1038/35087601
- Schwartz, O., Hsu, A., and Dayan, P. (2007). Space and time in visual context. *Nat. Rev. Neurosci.* 8, 522–535. doi: 10.1038/nrn2155
- Sekuler, R., and Littlejohn, J. (1974). Tilt aftereffect following very brief exposures. *Vision Res.* 14, 151–152. doi: 10.1016/0042-6989(74)90133-3
- Shapley, R. M., and Victor, J. D. (1978). The effect of contrast on the transfer properties of cat retinal ganglion cells. *J. Physiol.* 285, 275–298. doi: 10.1113/jphysiol.1978.sp012571
- Solomon, S. G., and Kohn, A. (2014). Moving sensory adaptation beyond suppressive effects in single neurons. *Curr. Biol.* 24, R1012–R1022. doi: 10.1016/j.cub.2014.09.001
- Teich, A. F., and Qian, N. (2003). Learning and adaptation in a recurrent model of V1 orientation selectivity. *J. Neurophysiol.* 89, 2086–2100. doi: 10.1152/jn.00970.2002
- Ts'o, D. Y., Gilbert, C. D., and Wiesel, T. N. (1986). Relationships between horizontal interactions and functional architecture in cat striate cortex as revealed by cross-correlation analysis. *J. Neurosci.* 6, 1160–1170. doi: 10.1523/JNEUROSCI.06-04-01160.1986
- Ursino, M., Magosso, E., and Cuppini, C. (2008). Possible mechanisms underlying tilt aftereffect in the primary visual cortex: a critical analysis with the aid of simple computational models. *Vision Res.* 48, 1456–1470. doi: 10.1016/j.visres.2008.04.002
- Watanabe, T., and Sasaki, Y. (2015). Perceptual learning: toward a comprehensive theory. *Annu. Rev. Psychol.* 66, 197–221. doi: 10.1146/annurev-psych-010814-015214

- Wenderoth, P., and van der Zwan, R. (1989). The effects of exposure duration and surrounding frames on direct and indirect tilt aftereffects and illusions. *Percept. Psychophys.* 46, 338–344. doi: 10.3758/BF03204987
- Wichmann, F. A., and Hill, N. J. (2001a). The psychometric function: I. Fitting, sampling, and goodness of fit. *Percept. Psychophys.* 63, 1293–1313. doi: 10.3758/BF03194544
- Wichmann, F. A., and Hill, N. J. (2001b). The psychometric function: II. Bootstrap-based confidence intervals and sampling. *Percept. Psychophys.* 63, 1314–1329. doi: 10.3758/BF03194545
- Wissig, S. C., and Kohn, A. (2012). The influence of surround suppression on adaptation effects in primary visual cortex. *J. Neurophysiol.* 107, 3370–3384. doi: 10.1152/jn.00739.2011
- Wolfe, J. M. (1984). Short test flashes produce large tilt aftereffects. *Vision Res.* 24, 1959–1964. doi: 10.1016/0042-6989(84)90030-0
- Yao, H., and Dan, Y. (2001). Stimulus timing-dependent plasticity in cortical processing of orientation. *Neuron* 32, 315–323. doi: 10.1016/S0896-6273(01)00460-3

**Conflict of Interest:** The authors declare that the research was conducted in the absence of any commercial or financial relationships that could be construed as a potential conflict of interest.

Copyright © 2019 Quiroga, Morris and Krekelberg. This is an open-access article distributed under the terms of the Creative Commons Attribution License (CC BY). The use, distribution or reproduction in other forums is permitted, provided the original author(s) and the copyright owner(s) are credited and that the original publication in this journal is cited, in accordance with accepted academic practice. No use, distribution or reproduction is permitted which does not comply with these terms.



# Similar Expectation Effects for Immediate and Delayed Stimulus Repetitions

Catarina Amado<sup>1</sup>, Sophie-Marie Rostalski<sup>2\*</sup>, Mareike Grotheer<sup>3</sup>, Nadine Wanke<sup>4</sup> and Gyula Kovács<sup>2</sup>

<sup>1</sup> Experimental Cognitive Science, Eberhard Karls Universität Tübingen, Tübingen, Germany, <sup>2</sup> Biological Psychology and Cognitive Neurosciences, Institute of Psychology, Friedrich Schiller University Jena, Jena, Germany, <sup>3</sup> Department of Psychology, Stanford University, Stanford, CA, United States, <sup>4</sup> Institute of Psychology, University of Hamburg, Hamburg, Germany

## OPEN ACCESS

### Edited by:

Colin W. G. Clifford,  
University of New South Wales,  
Australia

### Reviewed by:

Szonya Durant,  
Royal Holloway, University of London,  
United Kingdom  
Mark W. Greenlee,  
University of Regensburg, Germany

### \*Correspondence:

Sophie-Marie Rostalski  
sophie-marie.rostalski@uni-jena.de

### Specialty section:

This article was submitted to  
Perception Science,  
a section of the journal  
Frontiers in Neuroscience

**Received:** 26 September 2019

**Accepted:** 05 December 2019

**Published:** 20 December 2019

### Citation:

Amado C, Rostalski S-M,  
Grotheer M, Wanke N and Kovács G  
(2019) Similar Expectation Effects  
for Immediate and Delayed Stimulus  
Repetitions.  
Front. Neurosci. 13:1379.  
doi: 10.3389/fnins.2019.01379

A prior cue or stimulus allows prediction of the future occurrence of an event and therefore reduces the associated neural activity in several cortical areas. This phenomenon is labeled expectation suppression (ES) and has recently been shown to be independent of the generally observed effects of stimulus repetitions (repetition suppression, RS: reduced neuronal response after the repetition of a given stimulus). While it has been shown that attentional cueing is strongly affected by the length of the cue-target delay, we have no information on the temporal dynamics of expectation effects, as in most prior studies of ES the delay between the predictive cue and the target (i.e., the inter-stimulus interval, ISI) was in the range of a few hundred milliseconds. Hence, we presented participants with pairs of faces where the first face could be used to build expectations regarding the second one, in the sense that one gender indicated repetition of the same face while the other gender predicted the occurrence of novel faces. In addition, we presented the stimulus pairs with two different ISIs (0.5 s for Immediate and 1.75 or 3.75 s for Delayed ISIs). We found significant RS as well as a reduced response for correctly predicted when compared to surprising trials in the fusiform face area. Importantly, the effects of repetition and expectation were both independent of the length of the ISI period. This implies that Immediate and Delayed cue-target stimulus arrangements lead to similar expectation effects in the face sensitive-visual cortex.

**Keywords:** expectation, fMRI adaptation, prediction, repetition suppression, inter-stimulus interval

## INTRODUCTION

Repetition related phenomena have been widely studied using both electrophysiological and neuroimaging techniques. Typically these studies report suppression of the neural signal for repeated when compared to alternating stimuli (repetition suppression, RS; Henson and Rugg, 2003; for review see Grill-Spector et al., 2006). RS has been explained in many ways (i.e., synaptic depression, network dynamics, and facilitation of the neural response) and has become one of the most intensively studied phenomena in cognitive neurosciences. Further, it is broadly applied as a

tool to investigate the selective properties of neuronal populations in neuroimaging experiments (fMRI adaptation; Malach, 2012).

Recently, the neural mechanisms of RS have been connected to predictive coding theories of sensory perception (PC, see Friston, 2005; Auksztulewicz and Friston, 2016). According to models of PC, the brain constantly generates predictions about sensory inputs and then computes the difference between these predictions and the actual sensory input. Therefore, surprising/incorrectly predicted events cause higher neural activity than expected/correctly predicted events (Friston, 2005, 2010; Friston and Kiebel, 2009). In other words, the occurrence of an expected event can also lead to reduced neuronal activity when compared to incorrect predictions, i.e., to surprising events. This phenomenon was recently labeled expectation suppression (ES, Todorovic and de Lange, 2012).

In an influential study, Summerfield et al. (2008) presented participants with pairs of faces that could either repeat or alternate. These faces were grouped into blocks with either high (75%, RB) or low (25%, AB) repetition probabilities ( $P(\text{rep})$ ). The results revealed larger RS in the fusiform face area (FFA; Kanwisher et al., 1997) in blocks with more repetitions (RB), and hence more expected when compared to blocks with fewer repetitions, and thus surprising repetitions (AB). Therefore, the authors suggested that higher-order contextual expectations modulated repetition-related processes. Other studies confirmed the existence of such  $P(\text{rep})$  modulations of RS for faces (Kovács et al., 2012, 2013; Larsson and Smith, 2012; Grotheer et al., 2014) and Roman letters (Grotheer and Kovács, 2014). While no such modulations were found for chairs (Kovács et al., 2013) or unfamiliar characters (Grotheer and Kovács, 2014), but for a different conclusion see Mayrhauser et al. (2014). All of these studies used a factorial design in which repetition and repetition probability varied orthogonally. However, they did not allow the independent testing of expectation and repetition effects due to the use of high and low repetition blocks to manipulate expectations.

Other studies have induced explicit perceptual expectations on a trial-by-trial basis by associating a given stimulus with a preceding schematic cue or image (Egner et al., 2010; Meyer and Olson, 2011). Current MEG and neuroimaging studies have combined such paradigms with stimulus repetitions, in the sense that the first stimulus of a pair signals the likelihood of repetitions or alternations, and found both ES and RS to be present in the target-related signal (Todorovic and de Lange, 2012; Grotheer and Kovács, 2015; Amado and Kovács, 2016). Importantly, both the MEG and the neuroimaging studies have found that the effects of expectation and repetition are independent and additive processes in the human brain. Moreover, a recent EEG study (Feuerriegel et al., 2018) also investigated whether repetition effects are influenced by perceptual expectations and found distinct spatiotemporal patterns of repetition and expectation effects, supporting the idea of separable mechanisms underlying these phenomena.

Earlier studies have explored the influence of the inter-stimulus interval (ISI) length on RS and showed similarities between short and long-lagged repetition effects

(Henson et al., 2004; Sayres and Grill-Spector, 2006), but it has also been suggested that different neuronal mechanisms explain RS for long and short ISIs (Epstein et al., 2008; Kouider et al., 2009; Weiner et al., 2010; Larsson and Smith, 2012). Additionally, both electrophysiological (Feuerriegel et al., 2015) and behavioral (Matthews, 2015) studies of RS and repetition priming, describing behavioral response improvements for repeatedly presented stimuli, have reported distinct effects of stimulus duration and ISI variability.

Moreover, it is also known that ISI length affects attentional cueing (Hansen and Hillyard, 1980; Busse et al., 2006). Briefly, attentional cueing experiments rely on the flexible allocation of attention to specific aspects of the sensory stimulation, such as certain features of the stimuli, as well as their temporal or spatial properties. In general, attention can be driven both by top-down (i.e., cognitive expectations, called “endogenous” attention) or bottom-up (i.e., sensory events, called “exogenous” attention) processes (Hopfinger and West, 2006). The nature of the cue determines the type of attentional process (see Posner and Cohen, 1984). Interestingly, the ISI length seems to interfere with exogenous and endogenous attention in a different manner. At short durations (at around 2 s), endogenous attention enhances perceptual sensitivity (through an improvement in the accuracy of the responses). However, at longer durations (typically larger than 4 s) endogenous attention can actually impair stimulus sensitivity (Ling and Carrasco, 2006). In the case of exogenous attentional processes, the responses are faster and more accurate when valid cues are presented with short intervals between the cue and the target. If, however, the ISI length is large the participants’ reactions for valid cues will be slower (i.e., larger than 300 ms; see Posner and Cohen, 1984) and less accurate (Handy et al., 1999) than for invalid cues. Also, Busse et al. (2006) found facilitation of the behavioral response (in terms of shorter RTs) with short cue-target ISIs, only when both location and feature cues were valid. Longer ISIs induced the opposite effect, as the RTs were longer when the targets appeared at the cued location.

In terms of the PC theory expectations are probability-based top-down information that are tested against sensory input. Endogenous attention can be connected to the term perceptual expectation as both can rely on cues on a trial-by-trial basis (Meyer and Olson, 2011). In spite of the demonstrated effects of ISI on RS and on attentional cueing, previous studies which have investigated ES have invariably used short (in the range of few hundred milliseconds) delay-intervals between the predictive cue and the target (Egner et al., 2010; Grotheer and Kovács, 2015; Amado and Kovács, 2016).

Since we have no information on the temporal dynamics of cue-based expectation effects (Matthews and Gheorghiu, 2016), the current study aimed to investigate whether additive effects of RS and ES are consistent across changes of the presentation delay. To this end, we used the methods, task, and paradigm of Grotheer and Kovács (2015) with different ISI lengths. To anticipate our results, we observed significant RS and ES in the FFA, but we did not find any interaction between ES and RS for either ISI conditions, suggesting that the length of ISI does not influence the neural mechanisms of ES and RS.

## MATERIALS AND METHODS

### Participants

Twenty-six healthy Caucasian volunteers participated in the experiment. The number of participants was chosen based on our prior published works. In our previous papers testing RS (Grotheer et al., 2014:  $n = 26$ ; Grotheer and Kovács, 2014:  $n = 17$ ; Grotheer and Kovács, 2015:  $n = 25$ ; Amado et al., 2016:  $n = 22$ ; Hermann et al., 2016:  $n = 29$ ) we invariably tested similar number of participants and observed always strong and reliable RS as well as probability-based modulations of RS. Therefore, we did not use any specific way to estimate the sample sizes here. No participant reported any neurological or psychiatric illnesses and all subjects had normal or corrected to normal visual acuity and gave written informed consent in accordance with the protocols approved by the Ethical Committee of the Friedrich-Schiller-University Jena by following the Declaration of Helsinki. Overall, three participants were excluded from the final analysis. One was excluded due to excessive head-movements (i.e., translation/rotation of  $> 5$  mm/degrees) during the recording, while another participant failed to perform the experimental task properly (the performance was below 50% in one experimental run) and one participant interrupted the recording session. Therefore, the current report is based on the data of 23 participants (17 females; 20 right-handed, mean age ( $\pm$ SD): 21.6 (0.7) years).

### Stimulation and Procedure

Stimuli were 300 gray-scale, digital photos of full-frontal Caucasian faces ( $2.75^\circ$  visual angle), identical to those of Grotheer and Kovács (2015). Briefly, stimuli were fit behind a circular mask, placed in the center of the screen on a uniform black background. Stimulus pairs were presented, with 250 ms presentation time for each stimulus. We only used Caucasian faces as it is known that the own-race bias results in differences regarding the perceptual expertise with own when compared to other-race faces (for review see: Meissner and Brigham, 2001). Two ISI conditions were used. In the *Immediate* condition, the ISI was 500 ms, and hence identical to that of previous publications (Grotheer and Kovács, 2015; Amado and Kovács, 2016). In the *Delayed* condition, the ISI was varied randomly between 1.75 and 3.75 s (this temporal jitter was introduced to help the separation of the BOLD response, related to S1 and S2 as these two are not presented within one TR anymore). The two ISI trial types (*Immediate* and *Delayed*) were presented in two separate runs in an order randomized across participants. The inter-trial intervals were randomized between 1 and 3 s or between 3.75 and 5.75 s for the *Immediate* and *Delayed* conditions, respectively (see **Figure 1**). This relatively short time-range for the *Delayed* ISI condition was chosen because the further elongation of the ISI (to the order of minutes) would have led to an experiment-duration up to 2 h. Two runs were recorded from each participant (one for each ISI condition) and no stimulus occurred in more than one trial during a given run (i.e., the same stimulus could occur in two different runs). The runs contained 180 trials and lasted for about 11 and 25 min for

the *Immediate* and *Delayed* conditions, respectively. Stimuli were back-projected via an LCD video projector (NEC GT 1150, NEC Deutschland GmbH, Ismaning, Germany, with modified lens for short focal point) onto a translucent circular screen, placed inside the scanner bore [stimulus presentation was controlled by Matlab R2013a (The MathWorks, Natick, MA, United States), using Psychtoolbox (Version 3.0.9)].

Trial structure and design were identical to those of Grotheer and Kovács (2015) and Amado and Kovács (2016). We used a paired stimulus presentation where the predictive cue, the first stimulus (S1), could either be different [Alternation Trial (Alt)] or identical [Repetition Trial (Rep)] to the second, target stimulus (S2). To reduce local feature adaptation the size of either S1 or S2 (chosen randomly) was reduced by 18%. Both stimuli of a pair were either female or male and participants were presented with 50% female/male trials randomly. The gender of S1 cued stimulus repetition or alternation to the participants probabilistically, meaning high (75%) or low (25%) probabilities of repetition/alternation of the target stimulus (S2). For example, for half of the subjects, female faces signaled high repetition probability (75%), while male faces signaled high alternation probability (75%). This way, participants could form expectations regarding the likelihood of repetitions and alternations. Correctly predicted trials correspond to a congruence between the given cue (S1) and the repetition/alternation occurrence during S2 (75% of the trials), whereas the incorrectly predicted, or surprising trials correspond to an incongruency between the given cue (S1) and the repetition/alternation occurrence during S2 (25% of the trials). The relationship between face gender and repetition probability was counterbalanced across participants (11 participants in one version and 12 in the other one), in a way that for the other half of the subjects ( $N = 11$ ) the gender cueing high repetition probability was male and the relative repetition probabilities were reversed accordingly. Participants were informed about the relative repetition/alternation probabilities as well as about their contingencies on the face gender of S1 prior to the scanning sessions. In addition, participants performed a 5-min long training session (using stimuli that were different from those used in the main experiment) immediately prior to the fMRI recordings.

Briefly, a trial started with a yellow fixation cross, which was presented for 1 or 3 s in the *Immediate* ISI condition and 3.75 or 5.75 s in the *Delayed* ISI condition. Participants were asked to fixate it. The cross was followed by the predictive cue, S1, which was shown for 250 ms. During the ISI a small white circle appeared on the screen. The ISI conditions correspond to *Immediate* and *Delayed* lengths of fix 500 ms and varying 1.75/3.75 s, respectively. Finally, the target, S2, was presented for 250 ms.

Moreover, following the method of Larsson and Smith (2012), 20 (11.1% of the trials) additional blank trials were included in each run to enable the estimation of the average response time course to the target stimulus (S2) alone. In these trials, S1 was normally displayed and instead of S2, a blank screen was presented. This way, an estimate of the average response time course to S2 alone was obtained by performing a subtraction between the blank trials and the experimental conditions which

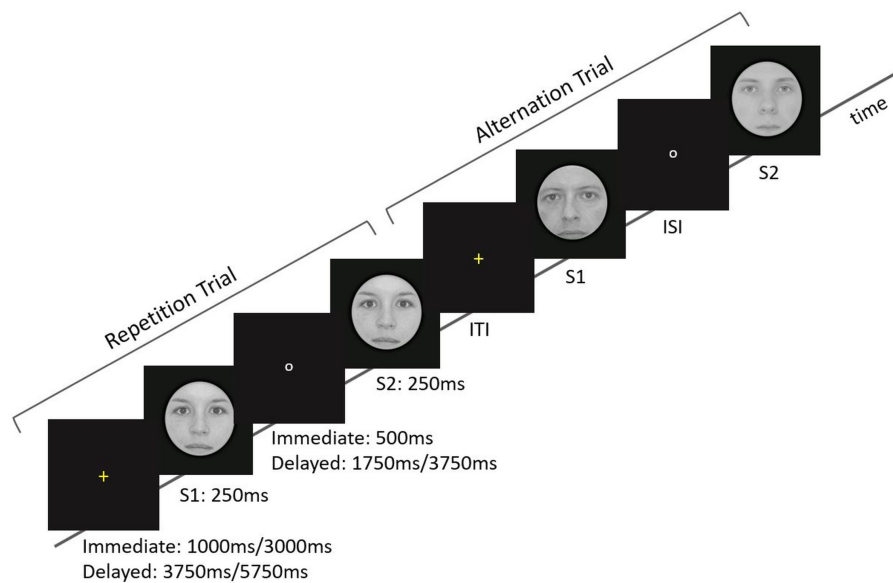


**FIGURE 1 |** Overview of the stimulation parameters and arrangements. At the beginning of each trial, a yellow fixation cross was presented for 1 or 3 s in the *Immediate* ISI condition and for 3.75 or 5.75 s in the *Delayed* ISI condition. The cross was followed by the predictive cue, S1, which was shown for 250 ms. During the ISI a small white circle appeared on the screen. The ISI conditions correspond to *Immediate* and *Delayed* lengths of fix 500 ms and varying 1.75/3.75 s, respectively. Finally, the target, S2, was presented for 250 ms. Note that *Immediate* and *Delayed* trials were given in separate runs.

included S2 and S1 as well. In order not to bias the predictions of participants, these trials had an equal amount of female and male faces for S1. Importantly, the overall probabilities for the correctly predicted and surprising conditions were 66.7 and 22.2%, respectively. As the introduction of the blank trials made the separation of subsequent trials perceptually more difficult, the color of the fixation cross was changed to yellow before the presentation of S1, to clearly mark the beginning of trials.

In total, we had five different experimental conditions, presented randomly within a run: expected repetition (E\_Rep), expected alternation (E\_Alt), surprising repetition (S\_Rep), surprising alternation (S\_Alt), and blank (Blank) trials. **Figure 2** illustrates the experimental design.

To control participants' attention and to confirm that they are able to judge the stimulus gender effectively, 18% of the trials were target trials in which subjects had to report whether the S1 had been a female or male face by pressing a button (Todorovic and de Lange, 2012). Therefore, for these target trials, a choice-screen was presented for 2 s centrally showing either the text "*female? male*" or "*male? female*," randomly. The choice-screen appeared 1 s after S2 was blanked out. A small color change of the fixation cross functioned as feedback regarding their answers (green for correct and red for incorrect responses).

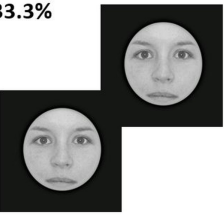
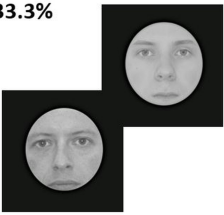
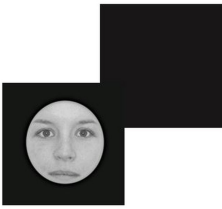
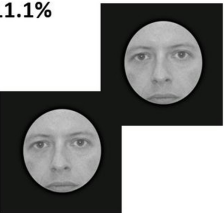
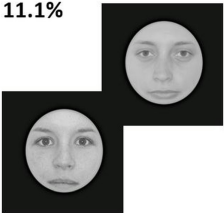
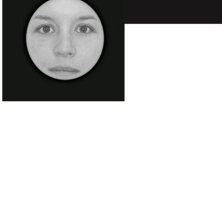
## Imaging Parameters and Data Analysis

Imaging was done with a 3-Tesla MR scanner (Siemens MAGNETOM Prisma fit, Erlangen, Germany). T2\* weighted images were collected using an EPI sequence (35 slices, 10° tilted relative to axial, TR = 2000 ms; TE = 30 ms; flip angle = 90°; 64 × 64 matrices; 3 mm isotropic voxel size). A high-resolution T1-weighted 3D anatomical image was acquired using

an MP-RAGE sequence (TR = 2300 ms; TE = 3.03 ms; 192 slices; 1 mm isotropic voxel size).

Details of preprocessing and statistical analysis were described previously (Cziraki et al., 2010). The functional images were realigned, normalized to the MNI-152 space, resampled to 2 × 2 × 2 mm resolution and spatially smoothed with a Gaussian kernel of 8 mm FWHM (SPM12, Wellcome Department of Imaging Neuroscience, London, United Kingdom). A separate functional localizer run (640 s long, 20-s epochs of faces, objects and Fourier randomized versions of faces, interleaved with 10 s of blank periods, 2 Hz stimulus repetition rate; 300 ms exposure; 200 ms blank) served as a basis for Regions of Interest (ROIs) detection. ROI creation was performed with MARSBAR 0.44 toolbox for SPM (Brett et al., 2002). Only those individuals in whom the respective ROIs could be identified in both hemispheres were included in the further analyses. The FFA was determined individually as an area responding more intensely to faces than to objects and Fourier randomized versions of faces ( $p < 0.0001_{\text{UNCORRECTED}}$ ). Its location could be identified reliably and bilaterally in 20 participants [average MNI coordinates ( $\pm$ SE): 41 (0.6), -54 (1.3), -19 (0.8), and -41 (1.4), -57 (1.7), -18 (0.7); average cluster size ( $\pm$ SE): 72(7), 52(5) voxels; for the right and left hemispheres, respectively].

A time series of the mean voxel value within the areas of interest was calculated and extracted from our event-related sessions using custom made scripts and Marsbar. The convolution of each of the five experimental conditions (E\_Rep, E\_Alt, S\_Rep, S\_Alt, Blank) with the canonical hemodynamic response function (HRF) of SPM12 (Wellcome Department of Imaging Neuroscience, London, United Kingdom) was used to define predictors for a General Linear Model (GLM) analysis

	REPETITION	ALTERNATION	BLANK
Expected (E)	33.3% 	33.3% 	11.1% 
Surprising (S)	11.1% 	11.1% 	

**FIGURE 2 |** Experimental design and conditions. Each face gender signaled different repetition/alternation probabilities (high or low) randomly for every participant. Here we present an example where the face gender signaling high repetition probability was female (E\_Rep), while male faces cued high probability of alternations (E\_Alt). Male/female faces signaled low probability of repetitions/alternations (S\_Rep/S\_Alt). Blank trials contained either female or male faces, randomly.

of the data. Target trials were not modeled separately, as there was sufficient time (1 s) between the end of the trial and the choice-screen presentation. Thus, the BOLD signal of the S2 was not affected by the button presses or by the choice-screens. Note that the subtraction between blank trials and the other experimental conditions (E\_Rep, E\_Alt, S\_Rep, S\_Alt) was executed to estimate the average response time course to S2 alone (Larsson and Smith, 2012). The peak values of the BOLD signal elicited by S2 only were submitted to the following statistical analysis. We performed repeated measures ANOVAs for the FFA activity separately with hemisphere (2), expectation level (2, E and S), trial type (2, Alt and Rep) and ISI condition (2, Immediate and Delayed) as factors. *Post hoc* analyses were executed using Fisher LSD tests. We also performed a *t*-test and calculated Bayes factor (e.g., Dienes, 2011) to test the independence of RS/ES from the ISI length and denoted evidence according to the thresholds proposed by Jeffreys (1940). We used the following prior hypothesis: RS and ES effects are larger in the Immediate ISI condition than in the Delayed one, therefore the reported results show how much more likely our hypothesis is when compared with the null hypothesis. In order to perform a *t*-test and directly compare the effects of repetition and expectation suppression for the two ISI conditions, we calculated the repetition suppression index (RSI = Alt-Rep) and the expectation suppression index (ESI = Sur-Exp).

As there is evidence that prediction error units of FFA can be activated by a positive prediction error (i.e., the occurrence of an unexpected face), but not by a negative one (i.e., the unexpected omission of a face; see Egner et al., 2010). We decided to test the influence of stimulus omission in this experiment by performing a repeated measures ANOVAs for the FFA activity separately with ISI condition (2, Immediate and Delayed) and omission level

(2, Blanked and Non-blanked trials) as factors. *Post hoc* analyses were executed using Fisher LSD tests.

## RESULTS

### Behavior

Participants required on average 981 ms ( $\pm$ SD: 45 ms) to determine the gender of the presented S1 faces. Reaction times did not differ significantly between trial types ( $F(1,22) = 1.15$ ,  $p = 0.29$ ,  $\eta_p^2 = 0.05$ ), expectation levels ( $F(1,22) = 0.24$ ,  $p = 0.63$ ,  $\eta_p^2 = 0.01$ ) or ISI conditions ( $F(1,22) = 2.22$ ,  $p = 0.15$ ,  $\eta_p^2 = 0.09$ ). Similarly, only tendencies were observed for any of the interactions ( $p > 0.08$  for all comparisons). We found a tendency for an interaction between expectation levels and ISI conditions ( $F(1,22) = 3.18$ ,  $p = 0.088$ ,  $\eta_p^2 = 0.126$ ), showing that correctly predicted trials differed between ISI conditions [being faster for *Immediate* trials ( $M(\pm$ SD) = 927 (39)ms) as compared to *Delayed* ones ( $M(\pm$ SD) = 1018 (35)ms),  $p = 0.003$ ], while incorrect predictions did not show any difference.

Mean accuracy for gender judgment was 86% ( $\pm$ SD: 3%) across all experimental conditions. The participants' accuracies did not differ between trial types ( $F(1,22) = 1.53$ ,  $p = 0.22$ ,  $\eta_p^2 = 0.07$ ) and ISI conditions ( $F(1,22) = 1.62$ ,  $p = 0.22$ ,  $\eta_p^2 = 0.07$ ). Further, no significant interactions were observed ( $p > 0.08$  for all comparisons). Interestingly, and confirming previous results (Grotheer and Kovács, 2015; Amado and Kovács, 2016), there was weak evidence for a main effect of expectation level ( $F(1,22) = 3.4$ ,  $p = 0.08$ ,  $\eta_p^2 = 0.13$ ), showing an enhanced accuracy for correctly predicted ( $M(\pm$ SD) = 88 (3)%) when compared to surprising ( $M(\pm$ SD) = 82 (5)%) trials.

The similar accuracy rates and response times suggest a similar allocation of attention to the different experimental conditions.

## Fusiform Face Area

Overall, the results confirmed those of our prior studies (Grotheer and Kovács, 2015; Amado and Kovács, 2016). We observed a significant main effect of trial type (i.e., significant RS; **Figure 3**;  $F(1,19) = 25.09$ ,  $p = 0.0008$ ,  $\eta_p^2 = 0.57$ ) with an average signal reduction of 0.1% (equivalent to an average relative signal reduction of 27%). We also found a main effect of expectation level (i.e., significantly higher responses for surprising as compared to correctly predicted events:  $F(1,19) = 5.65$ ,  $p = 0.028$ ,  $\eta_p^2 = 0.23$ ). On average the correct predictions led to a signal reduction of 0.05% (corresponding to an average relative signal decrease of 16%) when compared to the incorrect predictions. No main effect of hemisphere was found ( $F(1,19) = 1.27$ ,  $p = 0.27$ ,  $\eta_p^2 = 0.06$ ). Additionally, the effects of trial type and expectation level did not interact with each other ( $F(1,19) = 3.08$ ,  $p = 0.10$ ,  $\eta_p^2 = 0.14$ ), but were additive (**Figure 3**).

More important to the aims of the current study, we did not find a significant main effect of ISI condition ( $F(1,19) = 1.68$ ,  $p = 0.21$ ,  $\eta_p^2 = 0.08$ ). There was neither an interaction of ISI condition with the effect of trial type ( $F(1,19) = 0.37$ ,  $p = 0.54$ ,  $\eta_p^2 = 0.02$ ) nor with the effect of expectation ( $F(1,19) = 1.2$ ,  $p = 0.28$ ,  $\eta_p^2 = 0.06$ ). The four-way interaction of the hemisphere, ISI condition, trial type and expectation was not significant either ( $F(1,19) = 0.53$ ,  $p = 0.48$ ,  $\eta_p^2 = 0.03$ ). None of the remaining two-way and three-way interactions are significant. This suggests that both RS and ES are independent of the length of the ISI period. The Bayesian  $t$ -test revealed that both effects of neuronal response suppression, i.e., RS ( $B_{10} < 0.2$ ) and ES ( $B_{10} < 0.2$ ) are independent of the ISI length.

We found a significant main effect of omission level [i.e., larger BOLD responses to the non-blank trials when compared to blank trials;  $F(1,19) = 53.95$ ,  $p = 0.000001$ ,  $\eta_p^2 = 0.59$ ]. No interaction was found between the ISI condition and the omission level ( $F(1,19) = 1.44$ ,  $p = 0.23$ ,  $\eta_p^2 = 0.074$ ).

Importantly, the two ISI conditions of this study differ in terms of ISI variability characteristics and predictability. Although we included blank trials in both ISI condition blocks, in the *Immediate* ISI condition, there is only one possible ISI length (500 ms), and therefore the stimulus onset is nearly fully predictable in time. While, in the *Delayed* ISI condition, there are two possible ISIs (long – 5.75 s and short – 3.75 s). In this condition, the longer one is nearly fully predictable, as it will occur whenever there was no stimulus after 3.75 s and the current trial isn't a blank trial. The short ISI in the *Delayed* condition is only expected in 44, 45% of the trials. To test whether the results were affected by these differences in the variability and predictability characteristics of the ISI length of the *Immediate* (constant and fully predictable) and the *Delayed* ISI condition (variable and semi-predictable, i.e., long – 5.75 s and short – 3.75 s), we performed a repeated measures ANOVA to compare the BOLD responses of the two fully predictable conditions, i.e., the longer *Delayed* ISI lengths and the *Immediate* ISI condition. This extra analysis only revealed to be significant in two main effects: repetition suppression ( $F(1,19) = 15.63$ ;  $p = 0.0009$ ;  $\eta_p^2 = 0.45$ ) and ISI (in a way that the *Immediate* ISI length elicited larger BOLD responses when compared with the longer *Delayed* ISI condition;  $F(1,19) = 18.88$ ;  $p = 0.0004$ ;  $\eta_p^2 = 0.47$ ).

## Whole-Brain Analysis

It is theoretically possible that expectation and repetition effects are encoded elsewhere in the brain. Hence, we performed a second level whole-brain analysis testing for the main effects of RS, ES, ISI and the interaction of these factors, using a fixed threshold of  $p < 0.05_{\text{FWE}}$ , with a cluster size  $> 50$  voxels. Testing the main effect of ISI (*Delayed*  $>$  *Immediate*) revealed an active cluster in the early visual cortex (MNI  $[x,y,z]$ : 4, –86, 20; cluster size: 288), while the opposite contrast (*Immediate*  $>$  *Delayed*) led to several regions with significant activations (**Figure 4**). The whole-brain analysis did not reveal additional active clusters when testing for the main effects of RS and ES or the interactions between ES, ISI, and RS.

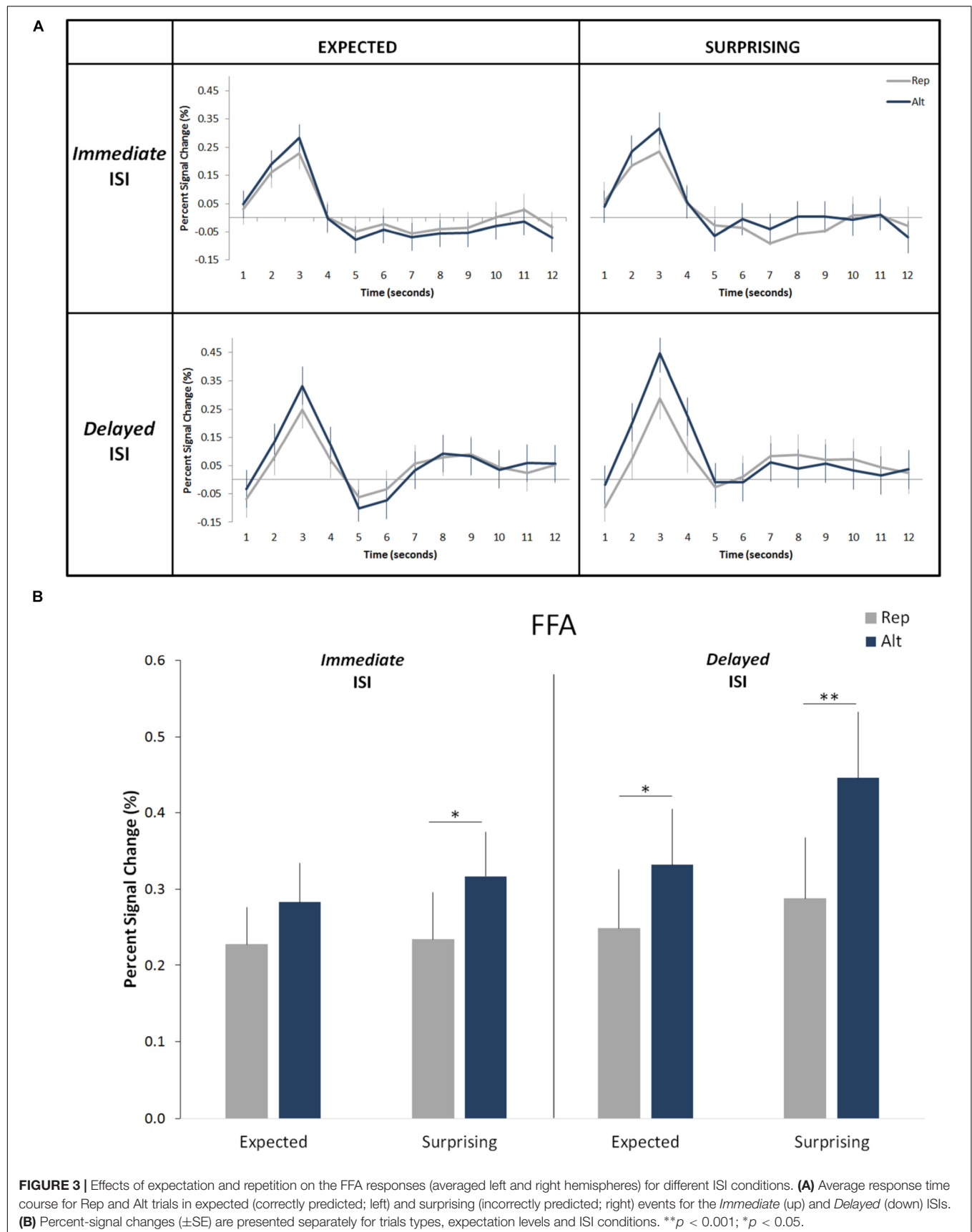
In order not to overlook any activation on the whole-brain level (however, see the recent discussion, initiated by Eklund et al. (2016) about the inflated false-positive rates of such cluster analyses) we also applied a more liberal  $p < 0.0001_{\text{uncorrected}}$  threshold with a smaller cluster size ( $> 20$  voxels). Both the *Immediate*  $>$  *Delayed* and the *Delayed*  $>$  *Immediate* contrasts showed some additional regions with significant activations (**Table 1**). Yet, once again, no additional active clusters were found when testing for the main effects of RS and ES or for the interactions between ES, ISI and RS, supporting the results of the ROI analysis. In principle, one would expect the FFA to be activated in the whole-brain analysis when testing for the main effects of RS and ES as well. Still, it is likely that the lower sensitivity of the whole-brain, when compared to the ROI based analysis (Nieto-Castanon et al., 2003), as well as the large inter-individual difference in the peak location of the FFA (Zhen et al., 2015) accounts for the lack of such an observation.

## DISCUSSION

We observed significant repetition and expectation effects in the FFA in the form of reduced responses for repeated and expected stimuli, respectively. These effects were found to be additive and independent of the length of ISI and imply that *Immediate* and *Delayed* predictive cueing produce similar effects of expectation related response suppression in the FFA, suggesting that the observed expectation effects survive a several second-long time-interval. The fact that RS and ES were found to be additive and thereby independent from each other for both ISI lengths confirms the results of recent studies that used short ISIs (Todorovic and de Lange, 2012; Grotheer and Kovács, 2015; Amado et al., 2016).

## Repetition Suppression

Earlier RS studies, using different ISI lengths, have suggested that RS is stable over short cue-target periods (in the range of 250 ms to 4 s) for object stimuli in an fMRI experiment (Henson et al., 2004; Sayres and Grill-Spector, 2006), which is in accordance with our results showing no difference in RS across ISI lengths. However, if ISIs are prolonged further (maximum of 8 min) several studies propose that the neural mechanisms underlying RS with short ISIs (less than 3 s) are different from those underlying RS with long ISIs (Henson et al., 2004; Sayres and Grill-Spector, 2006).



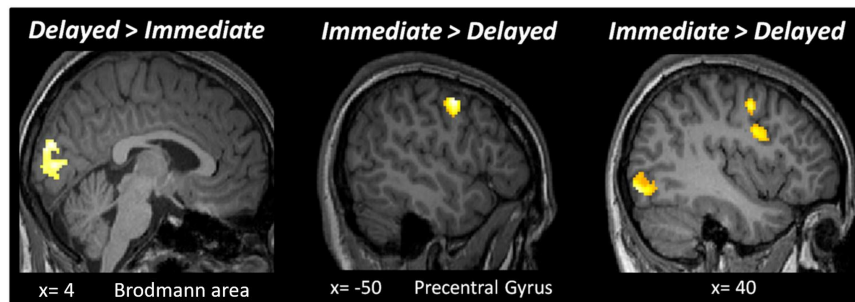


**FIGURE 4 |** Results of the whole-brain analysis with a fixed threshold of  $p < 0.05_{\text{FWE}}$ , with a cluster size bigger than 50 voxels for the following contrasts: *Delayed > Immediate* and *Immediate > Delayed*.

**TABLE 1 |** Summary of significant activations in the whole-brain analysis.

Contrast	Brain region	Coordinates	Cluster size	Threshold
<i>Delayed &gt; Immediate</i>	Brodman area 18	4, -86, 20	288	( $p < 0.05$ FWE)
<i>Delayed &gt; Immediate</i>	Inter-Hemispheric	0, -62, 56	57	( $p < 0.0001$ unc)
<i>Delayed &gt; Immediate</i>	Brodman area 6	56, -4, 6	23	( $p < 0.0001$ unc)
<i>Immediate &gt; Delayed</i>	Precentral Gyrus	-50, -4, 48	241	( $p < 0.05$ FWE)
<i>Immediate &gt; Delayed</i>	Inferior Occipital Gyrus	40, -84, -10	405	( $p < 0.05$ FWE)
<i>Immediate &gt; Delayed</i>	Brodman area 6	50, 2, 48	481	( $p < 0.05$ FWE)
		6, 8, 54	143	( $p < 0.05$ FWE)
<i>Immediate &gt; Delayed</i>	Sub-Gyral	28, -50, 46	67	( $p < 0.05$ FWE)
<i>Immediate &gt; Delayed</i>	Lingual Gyrus	-18, -88, -8	211	( $p < 0.05$ FWE)
<i>Immediate &gt; Delayed</i>	Middle Frontal Gyrus	-28, -5, 54	61	( $p < 0.0001$ unc)

For example, Epstein et al. (2008) reported that the effect of ISI on RS for visual scenes measured in the fMRI depends on scene viewpoint (in the range of 500 ms to 8 min, for short and long ISIs, respectively), in other words, short-interval RS was only significant when scenes were repeated from the same viewpoint, while long-interval RS was less viewpoint-dependent. Also, long- and short-interval RS effects did not interact at all. Furthermore, Weiner et al. (2010) used objects as stimuli and showed that RS varies quantitatively across time periods in the ventral temporal cortex. This study used ISI categories which are somewhat different from those used in the current study: the short and the long ISI periods were 500 ms to 3 s and of 1 to 174 s, respectively. Therefore, in the study of Weiner et al. (2010) there was an overlap of durations in the short and long ISI conditions, which was not present in the current study. Additionally, the maximum length of their “short” ISI is comparable to our *Delayed* condition and they did not study RS on a trial by trial basis. Please note that Weiner et al. (2010), as well as Epstein et al. (2008) and Henson et al. (2004) used object stimuli and therefore also tested different regions. All these facts make the comparison to the current study difficult.

Face studies have found that with long ISIs (in the range of 7 min), the effects of repetition depend on familiarity such that RS only occurs for familiar faces (Kouider et al., 2009). In this study, participants had to judge face familiarity. The results revealed that face-processing occurs even without perceptual awareness. Furthermore, different face viewpoints were also investigated for the short-lagged (subliminal priming) condition, yet no effects of

viewpoint were found for either the familiar or unfamiliar faces. Note that the minimum duration for the long-lagged condition was 7 min in their study, which is considerably larger than the 3.75 s applied in the current study. Importantly, instead of a blank screen, in this study, a mask was presented between S1 and S2 to manipulate perceptual awareness. The use of shorter lengths and the absence of this mask in the ISI period might explain why we found RS effects with unfamiliar faces for the *Delayed* condition as well. Also, the current study did not include familiarity as a factor. It will be important to determine what role familiarity plays in expectations and RS with specifically designed future experiments that are comparable to those of the study of Kouider et al. (2009). Another study using face stimuli and examining the impact of different cue-target intervals is from Larsson and Smith (2012). They investigated how probability-based expectations affect RS with longer ISIs and showed that P(rep) modulation of RS exists with longer (4 s) cue-target periods but that this effect depends on attention. These findings are in accordance with our results, despite the fact that Larsson and Smith (2012) induced expectations implicitly, based on the differential probabilities of trials within blocks, while here expectations were manipulated explicitly, with a cue, on a trial-by-trial basis. Please note, that the main goal in their study was to show the effect of attention on probability-based RS modulation.

A recent electrophysiological study has investigated not only how RS varies with different ISI periods but also how it is influenced by diverse stimulus presentation durations of S1 (Feuerriegel et al., 2015). Their results indicate no effect of ISI

period on the N170 amplitudes for faces or chairs. However, the amplitude of the positive P2 component was lowest when the ISI was short (200 ms). As is known, electroencephalography has better temporal resolution than fMRI, and this fact can possibly explain incongruences between that and the current studies. Also, the ISI periods of this study varied from 200 to 500 ms, which is in the range of our *Immediate* condition and makes comparison difficult. Anyway, further electrophysiological studies are also necessary to evaluate how expectation effects modulate RS in different cue-target stimulation periods.

## Expectation

Notably, no ISI effects on ES were observed on the behavioral data or on the BOLD signal in the current study, whereas Busse et al. (2006) reported reaction time facilitation for expected events that were presented with short cue-target stimulus periods. In other words, if expectations are fulfilled (the target can be predicted) and the cue and the target appear in a narrow time window response times are shortened (which fits the predictive coding framework). The discrepant results of Busse et al. (2006) and our current study can easily be explained by the lower number of trials in our study [360 vs. 500 in Busse et al. (2006)] and the application of different stimuli (moving dots vs. faces). Also, Busse et al. (2006) used an exogenous cue, whereas we applied endogenous cues, signaling the appearance of subsequent images.

Another behavioral study inspected how time perception depends on different durations of stimulus presentation and ISI (Matthews, 2015). Following the paradigm of previous studies (Summerfield et al., 2008; Larsson and Smith, 2012), this behavioral study used the probabilities of repetitions in each block to manipulate expectations. Interestingly, repeats were judged longer than novel items for shorter ISIs, but this effect was more pronounced when the repetitions were rare. For the longer ISI condition repeated and novel images were judged the same.

The fact that we found similar ES for the *Immediate* and *Delayed* conditions is in line with theories of predictive coding (Friston and Kiebel, 2009, PC). PC explains the brain as a cascading system of parallel feed-forward and feedback processes in which the sensory information is continuously compared to the current expectations of the system, based on prior experiences, and only the difference of the two, the predictive error, is propagated to higher-level areas (Friston, 2010). The predictive error is calculated and updated continuously in such a system. Whether there is an upper time-limit of the influence of the predictive stimuli is still an open question. Our results, however, suggest that the effect of the calculated predictions is not only manifest for immediate subsequent phenomena but also extends to a time range of several seconds, increasing the stability of the system. Recently, the processing of sensory information and most of the neuronal phenomena, such as RS and ES is explained under the predictive coding framework more and more widely. This framework assumes that, for example, visual processing occurs in a hierarchical manner in which lower-level areas receive predictions about the incoming sensory input from higher-order areas through feedback connections (Friston, 2005). Consequently, when the sensory input coincides with the created

high-level expectations, there is a suppression of the predicted neural responses in lower level areas, due to an inhibited response of these neuronal populations in the form of an efficient encoding mechanism (Friston and Kiebel, 2009).

Given the universal nature of PC, it is rather surprising that some recent findings disagree with the PC explanations of the neuronal response suppression. Evidence comes from studies that used non-face stimuli (fractals and chairs) and found no repetition probability modulations of RS in macaques' inferior temporal (Kaliukhovich and Vogels, 2011) and humans' lateral occipital cortices (Kovács et al., 2013) (but see Mayrhauser et al., 2014 for a different conclusion). These results are in contrast to what had been found for faces and voices, i.e., a strong modulation of RS by P(rep) (Summerfield et al., 2008; Kovács et al., 2012; Larsson and Smith, 2012; Andics et al., 2013). Therefore, the question if the observed similarity of short and long-term ISI on P(rep) in our study is a general property of the visual processing network, or its validity is limited to the areas processing faces is open and requires further studies. The above described differences in the capacity of PC explaining RS led to the following question: are there several neuronal mechanisms underlying the effect of P(rep) in the different cortical areas or are there other crucial factors determining these differences? One possible factor could be the level of expertise or prior experience with the given stimulus category. In fact, the results of Grotheer and Kovács (2014) suggest that expertise influences the magnitude of P(rep) modulation effect on RS, in a way that expectation effects only occur for familiar (real Roman characters) but not novel objects (false Roman characters). Since we assume that we are experts on faces, this could be a possible explanation for the different results. However, a more recent fMRIa study using face stimuli (Olkkonen et al., 2017) could show that expectation facilitates recognition behaviorally, but these modulatory effects could not be found in the BOLD signal of face-sensitive regions. Also, a recent study (Vinken et al., 2018) tested the effects of repetition probability in RS of the macaque inferotemporal cortex and found no interaction of P(rep) and RS on the spiking activity even though repetitions were task-relevant and repetition probability affected behavioral decisions. Again, in the current study, the sensory stimuli were of high expertise, i.e., faces. Therefore, future experiments will be needed in order to clearly understand whether the time window between cue and target stimuli lead to similar expectation effects for novel and familiar stimuli equally.

Furthermore, Larsson and Smith (2012) showed that perceptual expectation requires attention, specifically the P(rep) modulation effect on RS was only present if participants' attention was directed toward the stimuli. Note that the experimental design of Larsson and Smith (2012) study focused on probabilistic, implicit expectations. Hence, it would be worthwhile to manipulate the subjects' spatial and/or object-based attention, repetitions and expectations orthogonally, possibly applying a paradigm similar to Todorovic and de Lange (2012) or Grotheer and Kovács (2015). It is likely that the attentional state of the participants and therefore the applied task also plays a role in the fact that different results were obtained in the previous studies.

However, as it has been mentioned above, Kovács et al. (2013) did not observe P(rep) effects for every-day objects and the participants performed the same task (i.e., to signal the occurrence of a target trial, where the size difference between S1 and S2 was 55% by pressing a button) as in those prior studies, which reported significant P(rep) effects on RS for faces (Kovács et al., 2012; Grotheer et al., 2014). These findings suggest that differences in the attentional state alone are unlikely to induce such dissimilar perceptual expectation effects unless the given stimuli attract different attentional resources *per se*. In fact, there is evidence that faces recruit more attention than inanimate objects (Mack et al., 2002; New et al., 2007), which might explain the differences in P(rep) modulation effects on RS previously observed (Summerfield et al., 2008; Kovács et al., 2013). Still, to the best of our knowledge, there is no evidence that real Roman characters draw more attention than false Roman characters. Also, Olkkonen et al. (2017) could not find a P(rep) modulation effect on RS magnitude even though they used faces. Still, in this case, attentional effects could have caused the differences between the behavioral and neuroimaging data, as for the behavioral experiment attention was drawn to the images, whereas in the fMRI experiment participants performed an orthogonal task on target trials. Even though attention cannot be completely ruled out to explain previous findings, it is very unlikely as the source of the stability in terms of the ISI of expectation effect observed in the current study.

Importantly, in the current study there is a methodological asymmetry between the two expected experimental conditions, i.e., expected repetition (E\_Rep) and the expected alternation (E\_Alt). In the expected alternation condition the participants can only predict that the S2 is a previously unseen face, while in the expected repetition condition the predictions are that the S2 face is equal to S1. In other words, in the expected alternation condition participants can predict what the stimulus is not, but not what it is. Note that predictive theories argue that prediction updates occur repeatedly, and beliefs are gradually refined until the sensory system settles on the most likely interpretation of the inputs. Considering this, one can reason that if the statistical regularities of an environment are against our “default” predictions (i.e., learned based on experience), the strength of those predictions would be continuously diminished, due to constant updates. There is, therefore, a gap in the precision level of the predictions created in these two conditions. Still, there is an expectation effect on the alternation trials for both Immediate and Delayed ISI lengths (see **Figure 3**), in a way that the BOLD response is larger for surprising alternation than for the expected one. Following this line of thought, one question arises: what would happen if the alternation is predictable? Pajani et al. (2017) employed the influential Summerfield paradigm (2008) with an additional alternating block type where alternations were predictable. Participants could predict the S2 face based on S1, as S2 was specifically paired with S1. The participants were not aware of the contingencies but learned those in a preceding training session on the day before the scanning session. The authors found that predictable alternation trials elicited reduced FFA responses, as compared to unpredictable faces. Interestingly, repetition trials showed similar neuronal activation when presented in alternation blocks to when

presented in the predictable alternation blocks. In other words, even though these repetition trials are surprising FFA responses were more suppressed than for predictable. In fact, repetition is always expected as it is the default expectation and, therefore, even with the alternating trials being predictable and expected, default expectations of repetition maintain and are stronger than the experimentally induced perceptually expectations. Still, it is not yet known how the predictable alternation affects cue-based, explicit expectations. Thus, future training studies will be necessary.

The gender-identification task used in the current study requires attention to S1 and not to S2 (Todorovic and de Lange, 2012), which can lead to different attentional states between S1 and S2. Prior studies using this task (Grotheer and Kovács, 2015; Amado et al., 2016) revealed that subjects utilized different repetition probabilities to perform the task. In other words, even if they did not know or remember the gender of the first face, they could expect the faces to be repeated or alternating, congruent on the gender of S1. If so, then participants should show perfect performance and faster reaction times for expected trials. Interestingly, the results of the current study do not show any behavioral facilitation response for expected trials, a result similar to those of Todorovic and de Lange (2012). One possible explanation is that the gender-identification of S1 is less dependent on the effects of expectation and surprise than that of S2. We decided the behavioral task relied on the discrimination of the S1 gender, to make sure participants directed their attention to the S1 in a way that expectations were induced and to ensure those expectations were not incorrect due to wrong discrimination of the S1 gender. It is possible that the chosen behavioral task might have directed attention toward S1 and away from S2, still, we found RS and ES effects in the FFA. A very recent study (Olkkonen et al., 2017), on the other hand, found a strong behavioral modulation of a priming effect (shorter RT for repeated as compared to alternating trials) depending on the likelihood of repetitions (larger modulation for expected as compared to unexpected trials). Surprisingly and contrary to many prior studies, the fMRI was not modulated by expectation in this study, suggesting the relative independence of behavioral and neuroimaging correlates of expectation and urging further experiments, testing the issue.

## Possible ISI Variability Effects

In addition, we also know that the frequency or pace of events is a crucial parameter for the creation of expectations. A central timing system also referred to as “pacemaker,” describes that the pace/frequency of the event occurrences enables the creation of temporal perception units (Zakay and Block, 1997). Furthermore, it has been proposed that these local temporal perception units feed information to central systems (Matthews, 2015) and probably have an important role in prediction generation as well. Summerfield et al. (2011) investigated in an electrophysiological study how the consistency of stimulus repetition influences the effects of expectation and RS using stable (30–40 trial long) and volatile (10 trial long) blocks of stimulus presentations. Note that expectation was manipulated using different repetition probabilities in these blocks. Their results showed that RS was modulated by expectations at central electrodes for the stable,

long blocks, while no modulation was present for the volatile, shorter blocks. As stability over time (sometimes labeled as “time-variability,” see Friston, 2010) can play a role in forming expectations, it will be important to test possible effects of ISI variability and the ISI length, independently. This relates to the major limitation of the current experiment, i.e., the fact that the two ISIs had different variability characteristics, as we, due to methodological constraints, only had one long ISI but variable and one short and at the same time constant ISI condition. Furthermore, the possibility that activation differences found between the *Immediate* and the *Delayed* ISIs are dependent on the different synchrony levels cannot be excluded as the additionally longer ITIs we used for the *Delayed* condition might also contribute to different overall temporal patterns. Therefore, further experiments are necessary to disentangle these two distinct effects (variability and length).

## Whole-Brain Analysis

The results obtained by the whole-brain analysis are in line with the previous studies that propose different neuronal mechanisms for short and long lagged cue-target stimulation periods. The results show several brain activation differences between the *Immediate* and the *Delayed* ISIs. Yet no significant differences between these two conditions were found in the FFA. Moreover, the whole-brain analysis did not elicit main effects of trial or expectation conditions which were previously found by Grotheer and Kovács (2015), Amado et al. (2016). The lack of these effects in the present study might be due to the lower number of trials in comparison with the former studies. Furthermore, the possibility that activation differences found between the *Immediate* and the *Delayed* ISIs are dependent on the different variability levels (constant and variable) cannot be excluded.

## CONCLUSION

In conclusion, this study shows that RS and expectation effects in the FFA are independent and additive processes for both *Immediate* and *Delayed* ISIs. As no significant difference was

found between the two ISI lengths in the FFA, we can conclude the effects of repetition and expectation are maintained for several seconds in the FFA.

## DATA AVAILABILITY STATEMENT

The datasets generated for this study are available on request to the corresponding author.

## ETHICS STATEMENT

The studies involving human participants were reviewed and approved by the Ethics Committee of the Faculty of Social and Behavioural Sciences of the University of Jena. The patients/participants provided their written informed consent to participate in this study. Written informed consent was obtained from the individual(s) for the publication of any potentially identifiable images or data included in this manuscript.

## AUTHOR CONTRIBUTIONS

CA, MG, and GK designed the concept of the manuscript. MG and NW ran the experiments and analyzed the data together with CA. CA, S-MR, and GK wrote the manuscript.

## FUNDING

This work was supported by grants from the Deutsche Forschungsgemeinschaft (KO 3918/5-1).

## ACKNOWLEDGMENTS

We would like to clarify that this manuscript is part of the dissertation of CA (Amado, 2017).

## REFERENCES

- Amado, C. (2017). *Prediction Related Phenomena of Visual Perception*. Ph.D. thesis, Friedrich-Schiller-University, Jena.
- Amado, C., and Kovács, G. (2016). Does surprise enhancement or repetition suppression explain visual mismatch negativity? *Eur. J. Neurosci.* 43, 1590–1600. doi: 10.1111/ejn.13263
- Amado, C., Hermann, P., Kovács, P., Grotheer, M., Vidnyánszky, Z., and Kovács, G. (2016). The contribution of surprise to the prediction based modulation of fMRI responses. *Neuropsychologia* 84, 105–112. doi: 10.1016/j.neuropsychologia.2016.02.003
- Andics, A., Gál, V., Vicsi, K., Rudas, G., and Vidnyánszky, Z. (2013). FMRI repetition suppression for voices is modulated by stimulus expectations. *NeuroImage* 69, 277–283. doi: 10.1016/j.neuroimage.2012.12.033
- Auksztulewicz, R., and Friston, K. (2016). Repetition suppression and its contextual determinants in predictive coding. *Cortex* 80, 125–140. doi: 10.1016/j.cortex.2015.11.024
- Brett, M., Johnsrude, I. S., and Owen, A. M. (2002). The problem of functional localization in the human brain. *Nat. Rev. Neurosci.* 3, 243–249. doi: 10.1038/nrn756
- Busse, L., Katzner, S., and Treue, S. (2006). Spatial and feature-based effects of exogenous cueing on visual motion processing. *Vis. Res.* 46, 2019–2027. doi: 10.1016/j.visres.2005.12.016
- Cziraki, C., Greenlee, M. W., and Kovács, G. (2010). Neural correlates of high-level adaptation-related aftereffects. *J. Neurophysiol.* 103, 1410–1417. doi: 10.1152/jn.00582.2009
- Dienes, Z. (2011). Bayesian versus orthodox statistics: which side are you on? *Perspect. Psychol. Sci.* 6, 274–290. doi: 10.1177/1745691611406920
- Egner, T., Monti, J. M., and Summerfield, C. (2010). Expectation and surprise determine neural population responses in the ventral visual stream. *J. Neurosci.* 30, 16601–16608. doi: 10.1523/JNEUROSCI.2770-10.2010
- Eklund, A., Nichols, T. E., and Knutsson, H. (2016). Cluster failure: why fMRI inferences for spatial extent have inflated false-positive rates. *Proc. Natl. Acad. Sci. U.S.A.* 113, 7900–7905. doi: 10.1073/pnas.1602413113
- Epstein, R. A., Parker, W. E., and Feiler, A. M. (2008). Two kinds of FMRI repetition suppression? Evidence for dissociable neural mechanisms. *J. Neurophysiol.* 99, 2877–2886. doi: 10.1152/jn.90376.2008
- Feuerriegel, D., Churches, O., Coussens, S., and Keage, H. A. D. (2018). Evidence for spatiotemporally distinct effects of image repetition and perceptual

- expectations as measured by event-related potentials. *Neuroimage* 169, 94–105. doi: 10.1016/j.neuroimage.2017.12.029
- Feuerriegel, D., Churches, O. F., and Keage, H. A. D. (2015). Is neural adaptation of the N170 category-specific? Effects of adaptor stimulus duration and interstimulus interval. *Int. J. Psychophysiol.* 96, 8–15. doi: 10.1016/j.ijpsycho.2015.02.030
- Friston, K. (2005). A theory of cortical responses. *Philos. Trans. R. Soc. Lond. B Biol. Sci.* 360, 815–836. doi: 10.1098/rstb.2005.1622
- Friston, K. (2010). The free-energy principle: a unified brain theory? *Nat. Rev. Neurosci.* 11, 127–138. doi: 10.1038/nrn2787
- Friston, K., and Kiebel, S. (2009). Predictive coding under the free-energy principle. *Philos. Trans. R. Soc. Lond. B Biol. Sci.* 364, 1211–1221. doi: 10.1098/rstb.2008.0300
- Grill-Spector, K., Henson, R., and Martin, A. (2006). Repetition and the brain: neural models of stimulus-specific effects. *Trends Cogn. Sci.* 10, 14–23. doi: 10.1016/j.tics.2005.11.006
- Grotheer, M., Hermann, P., Vidnyánszky, Z., and Kovács, G. (2014). Repetition probability effects for inverted faces. *Neuroimage* 102(Pt 2), 416–423. doi: 10.1016/j.neuroimage.2014.08.006
- Grotheer, M., and Kovács, G. (2014). Repetition probability effects depend on prior experiences. *J. Neurosci.* 34, 6640–6646. doi: 10.1523/JNEUROSCI.5326-13.2014
- Grotheer, M., and Kovács, G. (2015). The relationship between stimulus repetitions and fulfilled expectations. *Neuropsychologia* 67, 175–182. doi: 10.1016/j.neuropsychologia.2014.12.017
- Handy, T. C., Jha, A. P., and Mangun, G. R. (1999). Promoting novelty in vision: inhibition of return modulates perceptual-level processing. *Psychol. Sci.* 10, 157–161. doi: 10.1111/1467-9280.00124
- Hansen, J. C., and Hillyard, S. A. (1980). Endogenous brain potentials associated with selective auditory attention. *Electroencephalogr. Clin. Neurophysiol.* 49, 277–290. doi: 10.1016/0013-4694(80)90222-9
- Henson, R. N., Rylands, A., Ross, E., Vuilleumier, P., and Rugg, M. D. (2004). The effect of repetition lag on electrophysiological and haemodynamic correlates of visual object priming. *Neuroimage* 21, 1674–1689. doi: 10.1016/j.neuroimage.2003.12.020
- Henson, R. N. A., and Rugg, M. D. (2003). Neural response suppression, haemodynamic repetition effects, and behavioural priming. *Neuropsychologia* 41, 263–270. doi: 10.1016/S0028-3932(02)00159-8
- Hermann, P., Grotheer, M., Kovács, G., and Vidnyánszky, Z. (2016). The relationship between repetition suppression and face perception. *Brain Imaging Behav.* 11, 1018–1028. doi: 10.1007/s11682-016-9575-9
- Hopfinger, J. B., and West, V. M. (2006). Interactions between endogenous and exogenous attention on cortical visual processing. *Neuroimage* 31, 774–789. doi: 10.1016/j.NEUROIMAGE.2005.12.049
- Jeffreys, H. (1940). Theory of probability. *J. Philos.* 37, 524–528.
- Kaliukhovich, D. A., and Vogels, R. (2011). Stimulus repetition probability does not affect repetition suppression in macaque inferior temporal cortex. *Cereb. Cortex* 21, 1547–1558. doi: 10.1093/cercor/bhq207
- Kanwisher, N., McDermott, J., and Chun, M. M. (1997). The fusiform face area: a module in human extrastriate cortex specialized for face perception. *J. Neurosci.* 17, 4302–4311. doi: 10.1523/jneurosci.17-11-04302.1997
- Kouider, S., Eger, E., Dolan, R., and Henson, R. N. (2009). Activity in face-responsive brain regions is modulated by invisible, attended faces: evidence from masked priming. *Cereb. Cortex* 19, 13–23. doi: 10.1093/cercor/bhn048
- Kovács, G., Iffland, L., Vidnyánszky, Z., and Greenlee, M. W. (2012). Stimulus repetition probability effects on repetition suppression are position invariant for faces. *Neuroimage* 60, 2128–2135. doi: 10.1016/j.neuroimage.2012.02.038
- Kovács, G., Kaiser, D., Kaliukhovich, D. A., Vidnyánszky, Z., and Vogels, R. (2013). Repetition probability does not affect fMRI repetition suppression for objects. *J. Neurosci.* 33, 9805–9812. doi: 10.1523/JNEUROSCI.3423-12.2013
- Larsson, J., and Smith, A. T. (2012). fMRI repetition suppression: neuronal adaptation or stimulus expectation? *Cereb. Cortex* 22, 567–576. doi: 10.1093/cercor/bhr119
- Ling, S., and Carrasco, M. (2006). When sustained attention impairs perception. *Nat. Neurosci.* 9, 1243–1245. doi: 10.1038/nn1761
- Mack, A., Pappas, Z., Silverman, M., and Gay, R. (2002). What we see: inattention and the capture of attention by meaning. *Conscious. Cogn.* 11, 488–506. doi: 10.1016/S1053-8100(02)00028-4
- Malach, R. (2012). Targeting the functional properties of cortical neurons using fMR-adaptation. *Neuroimage* 62, 1163–1169. doi: 10.1016/j.neuroimage.2012.01.002
- Matthews, W. J. (2015). Time perception: the surprising effects of surprising stimuli. *J. Exp. Psychol. Gen.* 144, 172–197. doi: 10.1037/xge0000041
- Matthews, W. J., and Gheorghiu, A. I. (2016). Repetition, expectation, and the perception of time. *Curr. Opin. Behav. Sci.* 8, 110–116. doi: 10.1016/j.cobeha.2016.02.019
- Mayrhauser, L., Bergmann, J., Crone, J., and Kronbichler, M. (2014). Neural repetition suppression: evidence for perceptual expectation in object-selective regions. *Front. Hum. Neurosci.* 8:225. doi: 10.3389/fnhum.2014.00225
- Meissner, C. A., and Brigham, J. C. (2001). Thirty years of investigating the own-race bias in memory for faces: a meta-analytic review. *Presented Psychol. Public Policy Law* 7, 3–35. doi: 10.1037//1076-8971.7.1.3
- Meyer, T., and Olson, C. R. (2011). Statistical learning of visual transitions in monkey inferotemporal cortex. *Proc. Natl. Acad. Sci. U.S.A.* 108, 19401–19406. doi: 10.1073/pnas.1112895108
- New, J., Cosmides, L., and Tooby, J. (2007). Category-specific attention for animals reflects ancestral priorities, not expertise. *Proc. Natl. Acad. Sci. U.S.A.* 104, 16598–16603. doi: 10.1073/pnas.0703913104
- Nieto-Castanon, A., Ghosh, S. S., Tourville, J. A., and Guenther, F. H. (2003). Region of interest based analysis of functional imaging data. *Neuroimage* 19, 1303–1316. doi: 10.1016/S1053-8119(03)00188-5
- Olkkonen, M., Aguirre, G. K., and Epstein, R. A. (2017). Expectation modulates repetition priming under high stimulus variability. *J. Vis.* 17:10. doi: 10.1167/17.6.10
- Pajani, A., Kouider, S., Roux, P., and de Gardelle, V. (2017). Unsuppressible repetition suppression and exemplar-specific expectation suppression in the fusiform face area. *Sci. Rep.* 7:160. doi: 10.1038/s41598-017-00243-3
- Posner, M. I., and Cohen, Y. (1984). Components of visual orienting. *Atten. Perform. X* 32, 531–556.
- Sayres, R., and Grill-Spector, K. (2006). Object-selective cortex exhibits performance-independent repetition suppression. *J. Neurophysiol.* 95, 995–1007. doi: 10.1152/jn.00500.2005
- Summerfield, C., Trittschuh, E. H., Monti, J. M., Mesulam, M.-M., and Egner, T. (2008). Neural repetition suppression reflects fulfilled perceptual expectations. *Nat. Neurosci.* 11, 1004–1006. doi: 10.1038/nn.2163
- Summerfield, C., Wyart, V., Mareike Johnen, V., and de Gardelle, V. (2011). Human scalp electroencephalography reveals that repetition suppression varies with expectation. *Front. Hum. Neurosci.* 5:67. doi: 10.3389/fnhum.2011.00067
- Todorovic, A., and de Lange, F. P. (2012). Repetition suppression and expectation suppression are dissociable in time in early auditory evoked fields. *J. Neurosci.* 32, 13389–13395. doi: 10.1523/JNEUROSCI.2227-12.2012
- Vinken, K., Op de Beeck, H. P., and Vogels, R. (2018). Face repetition probability does not affect repetition suppression in macaque inferotemporal cortex. *J. Neurosci.* 38, 7492–7504. doi: 10.1523/JNEUROSCI.0462-18.2018
- Weiner, K. S., Sayres, R., Vinberg, J., and Grill-Spector, K. (2010). fMRI-adaptation and category selectivity in human ventral temporal cortex: regional differences across time scales. *J. Neurophysiol.* 103, 3349–3365. doi: 10.1152/jn.01108.2009
- Zakay, D., and Block, R. A. (1997). Temporal cognition. *Curr. Dir. Psychol. Sci.* 6, 12–16.
- Zhen, Z., Yang, Z., Huang, L., Kong, X. Z., Wang, X., Dang, X., et al. (2015). Quantifying interindividual variability and asymmetry of face-selective regions: a probabilistic functional atlas. *Neuroimage* 113, 13–25. doi: 10.1016/j.neuroimage.2015.03.010

**Conflict of Interest:** The authors declare that the research was conducted in the absence of any commercial or financial relationships that could be construed as a potential conflict of interest.

Copyright © 2019 Amado, Rostalski, Grotheer, Wanke and Kovács. This is an open-access article distributed under the terms of the Creative Commons Attribution License (CC BY). The use, distribution or reproduction in other forums is permitted, provided the original author(s) and the copyright owner(s) are credited and that the original publication in this journal is cited, in accordance with accepted academic practice. No use, distribution or reproduction is permitted which does not comply with these terms.



# Face Adaptation and Face Priming as Tools for Getting Insights Into the Quality of Face Space

Ronja Mueller<sup>1,2\*</sup>, Sandra Utz<sup>2,3,4</sup>, Claus-Christian Carbon<sup>2,3,4</sup> and Tilo Strobach<sup>1</sup>

<sup>1</sup> Medical School Hamburg, Hamburg, Germany, <sup>2</sup> Bamberg Graduate School of Affective and Cognitive Sciences, University of Bamberg, Bamberg, Germany, <sup>3</sup> Department of General Psychology and Methodology, University of Bamberg, Bamberg, Germany, <sup>4</sup> Research Group EPAEG (Ergonomics, Psychological Aesthetics, Gestalt), Bamberg, Germany

## OPEN ACCESS

### Edited by:

Colin W. G. Clifford,  
University of New South Wales,  
Australia

### Reviewed by:

Jessie J. Peissig,  
California State University, Fullerton,  
United States  
Nuala Brady,  
University College Dublin, Ireland

### \*Correspondence:

Ronja Mueller  
ronja.mueller@medicalschoo-  
hamburg.de

### Specialty section:

This article was submitted to  
Perception Science,  
a section of the journal  
Frontiers in Psychology

**Received:** 30 September 2019

**Accepted:** 22 January 2020

**Published:** 07 February 2020

### Citation:

Mueller R, Utz S, Carbon C-C and  
Strobach T (2020) Face Adaptation  
and Face Priming as Tools for Getting  
Insights Into the Quality of Face  
Space. *Front. Psychol.* 11:166.  
doi: 10.3389/fpsyg.2020.00166

During the recognition of faces, the incoming perceptual information is matched against mental representations of familiar faces stored in memory. Face space models describe an abstract concept of face representations and their mental organization, in which facial representations are located on various characteristic dimensions, depending on their specific facial characteristics. However, these models are defined just as incompletely as the general understanding of face recognition. We took two phenomena from face processing to better understand face recognition, and so the nature of face space: face adaptation and face priming. The face literature has mainly focused on face adaptation, largely neglecting face priming when trying to integrate outcomes regarding face recognition into the face space framework. Consequently, the present paper aims to review both phenomena and their contributions to face recognition, representation, and face space.

**Keywords:** face space, face adaptation, face priming, mental representation, face perception, face processing model

## INTRODUCTION

It is a common assumption that familiar faces are encoded and recognized by matching the incoming perceptual information against facial representations stored in memory (Bruce and Young, 1986). To discriminate faces from each other, these stored representations must contain a large variety of characteristics, continuously differing from each other along many dimensions (Lee et al., 2000). The ‘face space,’ according to Valentine (1991), describes an abstract concept, that considers these dimensional relationships among mental representations. Valentine proposes a multidimensional space, in which each facial representation is located, depending on its characteristic value on each dimension. According to this model, face representations that are located close to each other are similar, whereas representations that are further apart, share fewer similarities. The facial information these dimensions contain and on which the representations vary is not further specified. They could be global properties (e.g., age, gender, or ethnicity) or more specific facial parameters, such as the eye–mouth distance or the size of the head (Valentine et al., 2016). How many dimensions are needed to encode all human faces one encounters, is not known exactly. Through computational modeling, Lewis (2004) was able to narrow down the number of dimensions to between 15 and 22 (other authors, however, estimate the number of dimensions to be much higher; see, Meytlis and Sirovich, 2007).

Within the face space framework several models about its specific structure exist. The two most well-known versions of the face space, the norm-based face space and the exemplar model, mainly differ in how the faces are arranged in space and in relation to each other (Valentine, 2001; Lewis, 2004; Valentine et al., 2016). The norm-based model assumes that faces are encoded relative to a specific prototypical face or central-norm face. Thus, a face must be located within the face space in relation to the norm. The deviation from the norm can be seen as a vector, in which the direction and the magnitude represent the distinctiveness and identity of a face (**Figure 1**). Within the exemplar model, however, faces are located in the face space without any reference to a norm or prototype. The distances between the face representations define the level of similarity (faces that are closer to each other are more similar; regarding facial similarity see also Tredoux, 2002). The distribution of the representations provide information about the distinctiveness (very distinct exemplars are located in areas of low representation density; Lewis, 2004; Valentine et al., 2016).

Studies investigating the perception, processing, and storage of faces can provide essential information about the functioning and structure of the face space. Two paradigms that are frequently used in this context are face adaptation and priming. In experimental settings, face adaptation effects are usually assessed by presenting familiar faces that were initially inspected as manipulated versions. In a subsequent test phase, participants

are then asked to determine the veridical face out of the original and slightly altered faces. Results typically show a bias of the participants' selection toward the previously inspected, manipulated version. This implies that the original face seems to be perceived as altered in the direction opposite to the adaptor face (Strobach and Carbon, 2013). Unlike basic, low-level adaptation effects on, e.g., color, motion or orientation, face adaptation effects seem to be very robust over time and thus suggest a high-level processing and an adaptation on a representational memory basis (Carbon and Ditye, 2011; Walther et al., 2013).

Priming is another phenomenon often used to demonstrate how recent perceptual experiences can alter the perception and recognition of faces. While adaptation usually leads to a perceptual bias opposite to the adaptor (i.e., original face versions are shifted away from the adaptation faces), priming often results in faster and/or more accurate responses in facial recognition after inspecting the same or similar faces (Ellis et al., 1987; Walther et al., 2013). Different priming paradigms can be distinguished, each addressing different mental concepts. For instance, repetition priming describes a paradigm in which a stimulus is initially presented as a prime and presented again in the subsequent test phase next to alternative stimuli. Repetition priming can facilitate the processing of that initially presented stimulus through activating its specific mental representation. Thus, the presentation of a face can facilitate the subsequent perception and recognition of the same face by activating its mental face representation (Ellis et al., 1993; Schweinberger et al., 1995). Semantic or associative priming characterizes a paradigm in which a stimulus is initially presented and an associated or unrelated stimulus is shown in the subsequent test phase. Associate priming can facilitate the processing of semantically related stimuli through activating a semantic network or an associated concept (Schweinberger et al., 1995; McNamara, 2005). Thus, the presentation of a person's face can facilitate the recognition of an associated person (e.g., Barack and Michelle Obama) by activating a semantic network.

Both phenomena (i.e., face adaptation and priming) seem to differ substantially from each other and even seem to cause opposite effects (priming usually leads to an improvement of recognition and identification, whereas a correct facial identification becomes more difficult through adaptation). Nevertheless, they generally lead to a similar result: in one way or another, they both alter subsequent face recognition by either activating or altering mental representations of faces. Thus, both phenomena could potentially be used to gain insights into the structure and the characteristics of the face space. However, previous studies have so far mainly focused on adaptation when trying to integrate outcomes regarding face perception into the face space framework. Although priming could contribute as well to the understanding of the face space, this phenomenon has been mostly neglected in the face space literature. Consequently, the present paper aims to review both phenomena and their contributions to facial perception, processing and storage and thus also to the face space. To enable a systematic evaluation and categorization of the face adaptation and priming literature, both

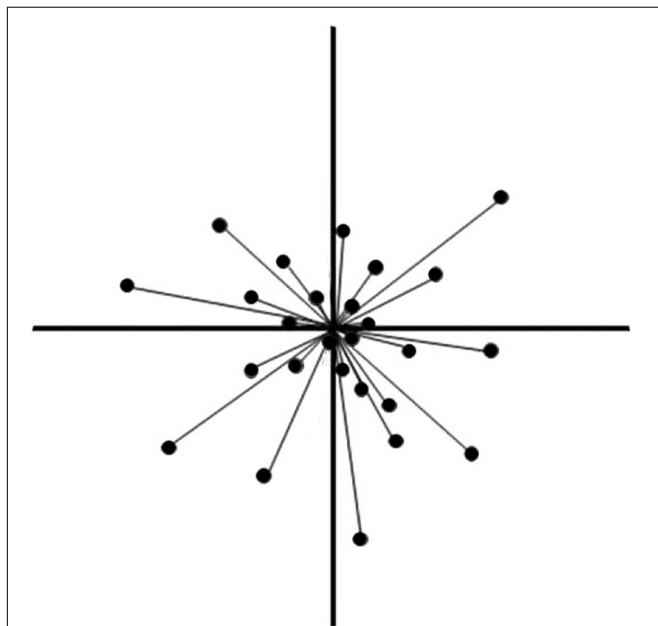


**FIGURE 1** | A two-dimensional illustration of the norm-based model of the face space proposed by Valentine (1991). The two dimensions are used for illustrative purpose only. The actual model contains multiple dimensions, on which faces can be distinguished. The points in the illustration represent the mental representations of familiar faces, which are located depending on their expressions on each dimension. The center represents the general face norm. The graph is based on the ideas of Valentine (1991). The permission and figure license has been obtained from the copyright holder [© SAGE Publications].

phenomena will be examined by taking into account two different dimensions: temporal aspects of the paradigms (*timing*) and the transferability of the effects to other face images or identities (*transfer*; Strobach and Carbon, 2013).

## TEMPORAL CHARACTERISTICS

The dimension *timing* categorizes adaptation and priming effects according to different temporal information. The first temporal information type *adaptor/prime duration* focuses on the length of the presentation time of the adaptor or prime. It reveals the impact the presentation duration can have on the adaptability or priming ability of faces. The second type of temporal information focuses on the *test duration*, the time span of the presented test stimuli. Similar to the *adaptor/prime duration*, this temporal information type provides insights into how the duration of the presentation of test faces can modulate the size of the adaptation or priming effects. Finally, we focus on the *delay*, the time interval between the adaptation or priming stimuli and the test phase. Here we distinguish between two general test designs: (1) a design in which a test stimulus is presented trial-wise after an adaptation or priming stimulus; and (2) a block-wise design in which there is first an adaptation or priming phase with several trials and then a separate test phase. The temporal information type *delay* provides essential information about the robustness and sustainability of adaptation or priming effects. It also gives us information about the recalibration ability of the visual system (meaning a recalibration back to the previous state of the visual

system; Carbon and Ditye, 2011; Strobach and Carbon, 2013). The different temporal characteristics of all studies reported in this chapter, are summarized in **Table 1**.

## Adaptor/Prime Duration

### Adaptor Duration

Different presentation durations of the adaptor can cause differences in the strength of the adaptation effects. An increase in the presentation duration of the adaptation stimuli, for example, usually results in a stronger adaptation effect. For relatively short time intervals between adaptation and test phases Leopold et al. (2005) and Rhodes et al. (2007) have investigated adaptation effects on identity alterations (features of identities, who were unknown before starting the adaptation phase, were altered by morphing identities or by increasing or decreasing the identity strength through synthetically altering the person's features) and adaptation to (initially unknown) distorted faces, by varying the presentation duration of the adaptation stimulus (1,000, 2,000, 4,000, 8,000, 16,000 ms). They demonstrated stronger effects for longer adaptation durations. In fact, this relation can be expressed by a logarithmic function between adaptation duration and effect size. Thus, the adaptation effect constantly increases with longer presentation durations, but the size of the increase progressively decreases. However, it remains unanswered to what extent the approach to the adaptor can proceed. Hence, it is also an open question whether a complete adaptation (meaning a complete adjustment of the mental representation to the perceived face) could be possible with sufficiently long adaptation duration. For long-term adaptation effects (i.e., a

**TABLE 1** | Adaptation/prime duration, delay and test duration in the selected face adaptation and priming studies, reported in this paper.

Phenomenon	Study	Adaptor/prime duration	Delay	Test duration
Adaptation	Carbon and Ditye, 2011	2000, 3000, 4000 ms (+200 ms feedback)	5 min, 24 h, 1 week	Unlimited
	Carbon and Leder, 2006	30 s	80 min	Unlimited
	Carbon et al., 2007	81 s	5 min, 24 h	Unlimited
	Webster and MacLin, 1999	5 min (+8 s top-up)	500 ms	8 s
	Leopold et al., 2001	5,000 ms	150, 300, 600, 1,200, 2,400 ms	200 ms
	Kloth and Schweinberger, 2008	1 min, 24 s (+3.5 s top-up in the first test block)	0–10 min	400 ms
	Leopold et al., 2001	5,000 ms	150, 300, 600, 1,200, 2,400 ms	200 ms
	Leopold et al., 2005	1, 2, 4, 8, 16 s	<i>nr</i>	100, 200, 400, 800, 1,600 ms
	Rhodes et al., 2007	1, 2, 4, 8, 16 s	1000 ms	100, 200, 400, 800, 1,600, 3,200 ms
	Rhodes et al., 2003	4,000 ms (+8 s top-up)	500 ms	1,500 ms
	Walther et al., 2013	500 ms	50 ms	300 ms
Priming	Barbot and Kouider, 2012	60, 1,000 ms	0 min	700 ms
	Ellis et al., 1997	5 s	5 min	2.5 s
	Ellis et al., 1993	Unlimited	5 min	Unlimited
	Johnston and Barry, 2006	Unlimited	3–5 min	Unlimited
	Lewis and Ellis, 1999	<i>nr</i>	24 h, 7 and 60 days	<i>nr</i>
	Maylor, 1998	10 s	4 min, 22 months	10 s
	Rieth and Huber, 2010	17, 50, 150, 400, 2,000 ms	0 min	33, 50, 100 ms
	Walther et al., 2013	500 ms	50 ms	300 ms

*Delay* = interval between adaptation and test; *feedback* = additional adaptor presentation following the adaptation trial and a cover task; *top-up* = additional adaptation stimulus preceding each test trial; *nr* = not reported.

break between the adaptation and test phase of 5 min and 24 h) Strobach et al. (2011) found a positive correlation between the presentation duration (comparing durations of 1,000, 2,000, and 3,000 ms) of adaptation stimuli with manipulated eye–mouth distances and the adaptation effect.

### Prime Duration

For priming, previous studies show rather ambiguous results. Barbot and Kouider (2012), for example, compared a relatively brief duration (60 ms) with a longer duration (1,000 ms) of prime stimulation and found for both durations facilitation in later recognition for initially presented visible face prime stimuli (using familiar faces). However, for stimuli that were invisible to the participants, due to inter-ocular suppression, the authors could demonstrate a facilitated recognition of the primed test stimuli for the short prime duration while the longer prime duration led to a negative priming effect in the test phase, reflecting recognition impairments. Rieth and Huber (2010) systematically investigated priming effects of visible face primes, using face stimuli that were unfamiliar at the beginning of the experiment. By continuously varying the presentation duration of the prime stimuli (17, 50, 150, 400, and 2,000 ms), the authors were able to demonstrate that brief prime durations (up to 50 ms) provoke a facilitation effect while longer prime durations lead to a continuous decrease in performance and again to a negative priming effect (a negative priming effect was reported only for the prime duration of 2,000 ms). Referring to the study of Barbot and Kouider (2012), it might be possible that a negative priming effect would also have been observed for visible familiar face primes if the authors had increased the prime duration.

Study results investigating the priming duration by alternative means, should be taken into account as well. Lewis and Ellis (1999) for example, found a relationship between the number of prime repetitions (using familiar face primes) and the reaction time (to identify a subsequent face), which fits a negative power curve. Thus, the priming effect constantly increases with more prime repetitions (i.e., an increased prime duration), but the size of the increase progressively decreased. Negative priming effects, however, could not be detected in this study. Hence, it can be concluded that prolonged priming in the way of longer presentation durations are qualitatively different from a prolonged priming due to an increase of prime repetitions.

### Implications of Adaptation and Prime Duration for the Face Space

Different adaptor and prime durations have very different effects on both phenomena. While a longer presentation duration of the adaptor seems to cause an increasing adaptation effect, a longer presentation duration of a prime leads to a continuous decrease of the effect and can even result in negative priming. In an adaptation process, the representation continuously changes in the direction of the adaptor (Strobach and Carbon, 2013): the longer the presentation duration, the larger the adaptation effect and thus the approximation of the representation to the adaptor. As a result of this approximation, the representation would change its position in face space (along a continuum between the original and the adaptor), in such a way that a

greater approximation leads to a larger position shift in face space (Valentine et al., 2016; see **Figure 2** for an illustration).

In contrast to adaptation, a positive priming effect does not lead to a shift of the representation within the face space but to an activation increase of the representation. For the greatest possible priming effect, a prime should be presented briefly. This is probably the most effective way to achieve the greatest possible activation of its representation within the face space and a faster processing of the subsequent face stimulus. Rieth and Huber (2010) assumed that a longer prime presentation duration results in a neural habituation and thus leads to a continuous activation reduction of the representation of the previously inspected stimulus. The authors argued that by inhibiting the representation of the previously seen face, a confusion with subsequent faces will be avoided and hence the identification of them will be facilitated. Thus, an accumulation of activations of different representations within the face space does not seem possible.

Furthermore, the reversal into negative priming could be seen as an activation inhibition of face space representations (by habituation of the corresponding neuronal networks; Rieth and Huber, 2010). However, it is open as to whether this negative priming effect could also be explained by an adaptation mechanism and thus a change of the face representation's position in the face space. The negative priming effect is at least very similar to the effect of a facial adaptation process; both phenomena lead to slower or more difficult recognition of an original face. If one assumes that a mental facial representation never corresponds exactly to what one sees on the presented stimuli (even if the stimuli have not been manipulated), an adaptation process should occur due to the lack of fit between both images (e.g., Clifford et al., 2000; Clifford and Rhodes, 2005). Following this assumption, a longer prime presentation could probably trigger an adaptation process. It therefore remains unclear whether the effect of an extended presentation duration demonstrated by Rieth and Huber (2010) is rather that of a negative priming or that of an adaptation mechanism, or whether both phenomena may be used synonymously in this case.

While longer prime durations lead to a negative priming effect (or adaptation effect) prolonged priming due to an increase of prime repetitions also show a progressive decrease of improvement but no reverse into negative priming (Lewis and Ellis, 1999; Rieth and Huber, 2010). Thus, just like longer prime durations, repeated priming somehow seems to trigger a habituation process as well, leading to a continuous activation reduction of the representation in face space and hence to a decrease in performance. Nevertheless, compared to longer prime durations a high number of repetitions does not lead to negative priming effects. This might be explained by a dishabituation process, caused by interfering sensations (which can be mental or real) in between the prime repetitions. Thus, a previous habituation triggered by a prime could be diminished by the time interval between the prime repetitions, so that further repetitions continue to lead to a positive (although weakened) priming effect. Whether an even higher number of repetitions (even higher than reported by Lewis and Ellis, 1999) could lead to negative priming remains unanswered.

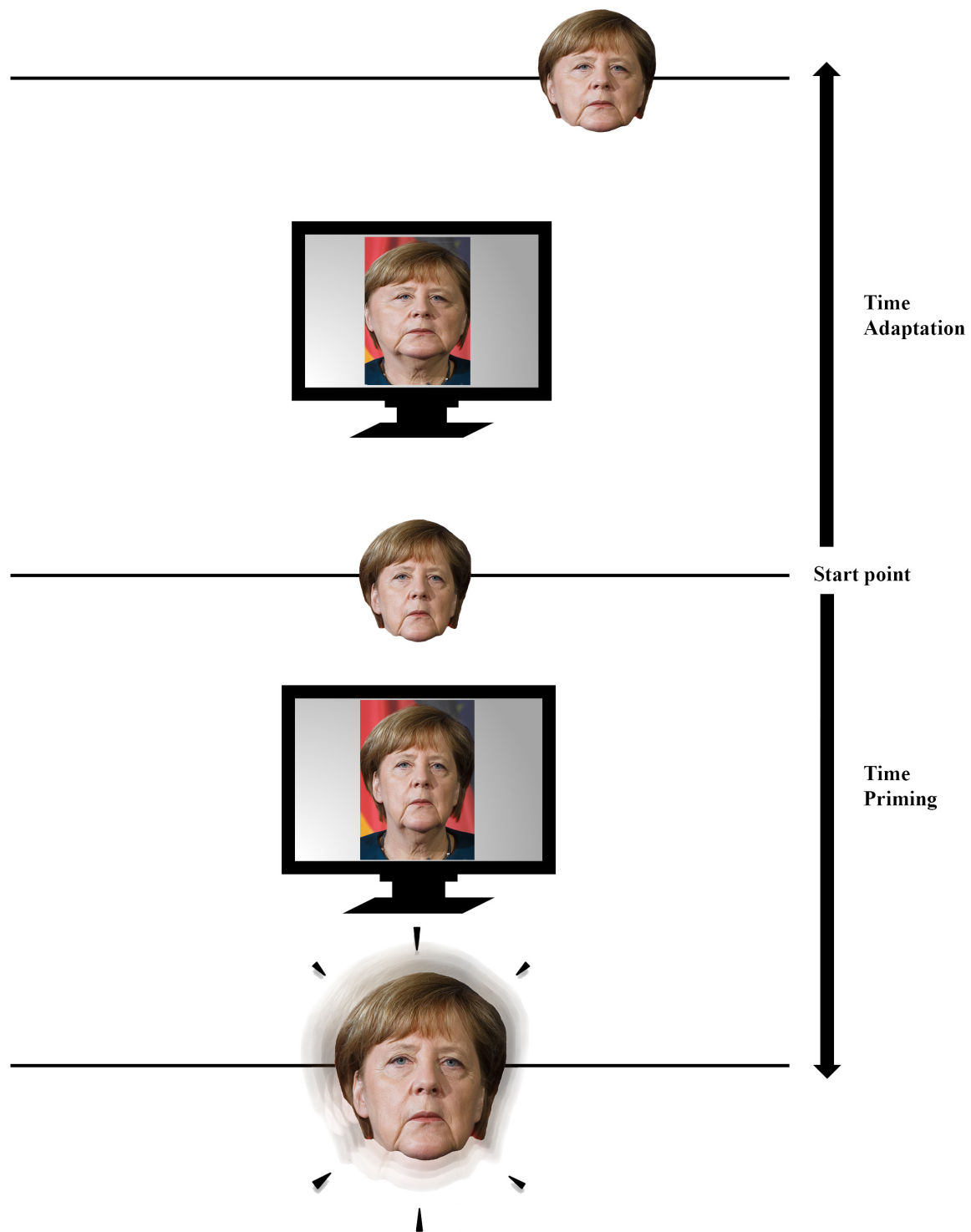


**FIGURE 2 |** A basic illustration of the processes that occur in face space during adaptation and priming. A picture of German chancellor Angela Merkel is used as an example. Both processes have the same starting point: a mental representation located in face space on a specific face dimension on which a face can vary. During an adaptation process (upwards from center), a strongly manipulated version of the person is then presented on a monitor (in this case a manipulation of the face width was performed). The adaptation to the extreme version subsequently leads to a position shift of the representation toward the adaptor. During a priming process (downwards from center), however, a non-manipulated picture of the person is presented as a prime on a monitor. Although the prime subsequently leads to an activation of the representation within the face space (represented by the “glow” and the enlargement of the image), it does not lead to a position shift. The presented images are used for illustrative purpose only. Permissions and image licenses have been obtained from the copyright holders [Source: © Drop of Light/Shutterstock.com].

## Test Duration

### Adaptation Test Duration

The presentation duration of a test stimulus can, similar to the adaptor presentation duration, modulate the magnitude of adaptation effects. An increase of the test duration usually leads to a decrease of the adaptation effect. Using familiarized face stimuli (by implementing a discrimination training before starting the adaptation phase), Leopold et al. (2005) and Rhodes et al. (2007) have investigated facial adaptation effects, varying the presentation duration of the test stimulus (i.e., 100, 200, 400, 800, 1,600, and 3,200 ms). The study results indicate an exponential decay of the adaptation effect, so that the adaptation effect constantly decreases with longer test stimulus presentation duration, but the size of the decrease is progressively reduced.

### Priming Test Duration

Presenting face stimuli that were unfamiliar at the beginning of the experiment and by using no time interval between adaptation and test phase, Rieth and Huber (2010) investigated the relationship between test stimulus presentation duration and face priming and were able to demonstrate that longer test durations lead to a decrease of the priming effect (employing test durations of 33, 50, and 100 ms). However, to the best of the authors' knowledge, there is no systematic investigation of this issue using familiar faces or longer test durations than 100 ms (for results in the adaptation area see, Leopold et al., 2005; Rhodes et al., 2007). This under-representation of studies could be caused by the generally preferred test design. Usually a design is chosen where the test duration depends on the onset of the response the participant is executing, which makes a systematic analysis of the relation between test duration and priming effect difficult. Future research should therefore focus on studies that use a design in which test durations are controlled and determined in advance. In addition, investigations should also include familiar face stimuli, to see if the observed pattern by Rieth and Huber (2010; a decrease of the priming effect due to extended test durations) can also be observed for familiar face stimuli.

### Implications of Adaptation and Prime Test Duration for the Face Space

It seems that the alteration of the test duration modulates the magnitude of the effects of both phenomena in similar ways. Adaptation studies have shown that an increase in the test duration leads to a decrease in the adaptation effect. In an adaptation process, a longer presentation duration of the test stimulus probably leads to a continuous decrease of the previously generated adaptation effect, due to a readjustment (or re-adaptation) of the representation to the original face (Carbon et al., 2007), since the test stimulus either corresponds to the original face or differs only slightly from the original face (compared to the adaptation stimulus). Referring to the face space this would mean that the adaptation to the adaptor leads to a position shift of the representation within the face space, but a longer test duration reduces this shift by provoking a re-adaptation to the original face and thus a shift of the representation back to the original face space position.

According to Rieth and Huber (2010) not only a prime should be presented briefly, but also the test stimulus, to achieve the greatest possible activation of its representation within the face space and thus the greatest possible priming effect. As mentioned before, a longer prime duration causes a decrease in the priming effect by a decrease of the representation activation due to a neuronal habituation. Because the test stimulus addresses the representation again (regardless of whether it corresponds exactly to the prime stimulus or not), a longer test duration probably has a similar effect as a longer prime duration and leads, as an overstimulation of the representation, to neuronal habituation and thus a decrease in the priming effect as well.

## Delay

### Delay Within the Adaptation Paradigm

In the early days of face adaptation research, adaptation effects were tested with a time delay of a few seconds or even less between the adaptation and test trials (Webster and MacLin, 1999; Leopold et al., 2001; Rhodes et al., 2003). Such a short delay, however, does not provide much information about the robustness of the effect. Kloth and Schweinberger (2008) conducted one of the first studies to systematically investigate the delay characteristics (using intervals of 1 s up to 539 s) of face adaptation effects with gaze direction information (i.e., the direction the presented identity is looking toward with the eyes while the head is orientated frontally). Although the effects continuously decreased over time, the authors were able to demonstrate those effects on gaze information up to 385 s. Carbon and colleagues extended this research to configural information of the eye–mouth distance and were able to demonstrate (weaker but still significant) adaptation effects even up to a delay of hours and even 1 week (Carbon and Leder, 2006; Carbon et al., 2007; Carbon and Ditye, 2011; Strobach et al., 2011). Thus, face adaptation effects seem to be extremely robust. However, it is still an open issue as to how long exactly an adaptation effect can last and whether these durations vary between different types of facial information (e.g., local information, age, gender, or emotion).

### Delay Within the Priming Paradigm

The robustness of priming effects in faces is already represented by an adequate number of studies. Face priming effects could be demonstrated in a trial-wise test design for rather short delays (such as milliseconds, seconds, or minutes) between priming and test trials (see, e.g., Ellis et al., 1993, 1997; Johnston and Barry, 2006; Rieth and Huber, 2010; Barbot and Kouider, 2012; Walther et al., 2013) and also for very long delays (such as days, months, or even years) in a design in which both phases were separated (Maylor, 1998; Lewis and Ellis, 1999). Although the face priming effects also become weaker with increasing delays (e.g., Lewis and Ellis, 1999), these effects appear to be similarly robust as face adaptation effects.

### Implications of the Adaptation and Prime Delay for the Face Space

Both phenomena seem to have a similar robustness and a similar decay pattern of the effects. For adaptation effects, the

longest delay between adaptation and test phase investigated so far has been 1 week (Carbon and Ditye, 2011, 2012), which suggests an extremely robust effect. Referring to the face space, these results indicate that changes of the representation are 'sticky' and that the shift of representations within the face space is very persistent. However, the continuous decrease of the effect suggests that a readjustment of the representation to the preadaptation status is being performed. Moreover, little is known about the possible reasons for this readjustment to the original representation status before adaptation. It could be that a longer delay between adaptation and test phase provides more opportunities for an exposure (whether mental or real) to the presented identity; because changes of the adaptation stimuli are usually artificial, perceptual experiences outside the experimental setting will mostly contain original faces. This could lead to a re-adaptation process to the original representation in face space, resulting in a continuous reduction of the adaptation effect. Another possible explanation for a re-adaptation could be that to integrate the changes of the adaptation stimuli into the representation permanently, a more frequent and/or longer exposure to the change is necessary (probably in the sense of a threshold that must be overcome). This would indicate that the representations within the face space are extremely stable, so that with adaptation shorter than a potential threshold, a continuous re-adaptation back to the original is performed automatically.

Face priming effects seem to be similar or even more robust than adaptation effects. Studies were still able to demonstrate face priming effects after months or even years (Maylor, 1998; Lewis and Ellis, 1999). Hence, the prime either seems to cause a very stable and long-term activation of the representation located in the face space or it must somehow facilitate a reactivation of it. The latter may appear more likely, since the reactivation of a representation probably consumes fewer cognitive resources and capacities than maintaining an activation over a longer period of time. The continuous decrease of the effect over time is likely to be caused either by a constant decrease of the activation or by a constant decrease of the reactivation capability of the representation located in the face space.

## TRANSFERABILITY

The dimension *transfer* categorizes adaptation and priming effects according to their transferability between different versions of the same image or between different face images and identities. Hence, two approaches can be distinguished: (1) an investigation of the transfer across different changes of specific image dimensions (e.g., orientation, position, or size) or (2) a transfer across different images of the same or different identities (Carbon et al., 2007; Strobach and Carbon, 2013). Studies investigating the transferability of adaptation and priming effects will be discussed according to these approaches.

The first approach (transferability between images differing in specific image dimensions) is often used to exclude low-level, retinal effects and to understand the role of the altered face dimensions in the storage of faces. This approach is

less informative about the identity-specific transfer but rather focuses on image-specific characteristics and their role within the face representations and thus the face space. The second approach compares the identity specificity of the adaptation or priming effects. Here we have three different categories to systemize and compare the transferability (transfer levels). The first category (*pictorial level*) describes an experimental design where the identical image is presented in the adaptation/priming as well as in the test phase. Effects from this category can be contrasted with effects from the second category (*structural level*) in which the adaptation/priming and test image differ from each other but still show the same identity and the third category (*cross-identity level*), in which different identities are shown in the adaptation/priming and test phase (see **Figure 3** for an illustration). By comparing the results of these three categories, it can be determined to what extent adaptation or priming effects are image- or identity-specific. Within the *cross-identity* condition, the strength of divergence between the adaptation/priming and test stimuli can be further varied by investigating the adaptation/priming effects to different groups of individuals, such as gender, ethnicity, age groups, or family members.

In general, the transfer dimension provides important information about the nature of face processing. It reflects the plasticity and flexibility of representations stored in memory, it can reveal common coding principles of faces within different levels of visual processing (from sensory, more retinotopic processing, to a high-level and probably face-specific processing) and can therefore offer important information on the organization of the representations in face space (Webster, 2011; Webster and MacLeod, 2011; Strobach and Carbon, 2013). The different transfer characteristics of all studies reported in this chapter, are summarized in **Table 2**.

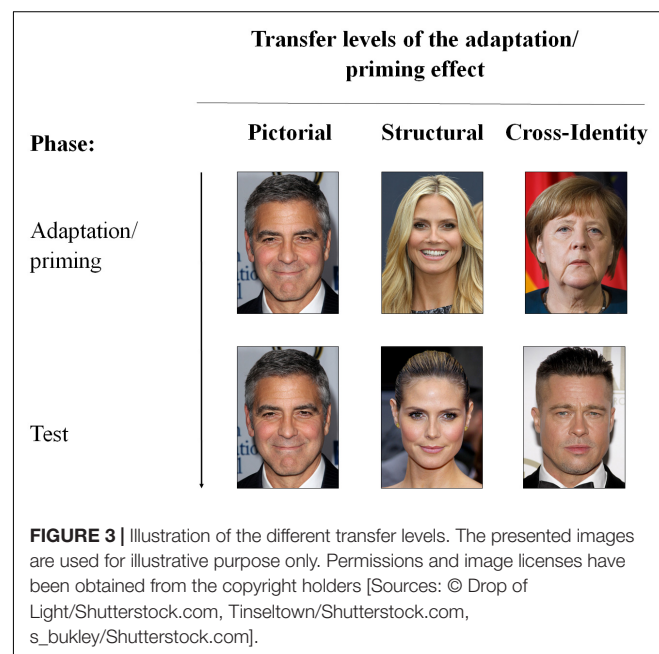


**TABLE 2 |** Adaptation dimension or priming task, image transfer dimension and identity transfer dimensions in the selected face adaptation and priming studies reported in this paper.

Phenomenon	Study	Adaptation dimension/ priming task	Image transfer dimensions	Identity transfer dimensions
Adaptation	Afraz and Cavanagh, 2008	Identity	Position	Cross-identity
	Anderson and Wilson, 2005	Identity	Size, viewpoint	Cross-identity
	Barrett and O'Toole, 2009	Gender	<i>nr</i>	Cross-identity
	Carbon and Ditye, 2011	Distortion	Position	Pictorial, structural, cross-identity
	Carbon and Ditye, 2012	Distortion	Position	Pictorial, structural, cross-identity
	Carbon and Leder, 2005	Distortion	<i>nr</i>	Pictorial, structural
	Carbon et al., 2007	Distortion	<i>nr</i>	Pictorial, structural, cross-identity
	Fox and Barton, 2007	Expression	<i>nr</i>	Pictorial, structural, cross-identity
	Fox et al., 2008	Identity	Expression	Inter-identity transfer
	Guo et al., 2009	Contrast	Inversion	Pictorial, cross-identity
	Hole, 2011	Identity	Inversion, viewpoint, stretched image	Cross-identity
	Jaquet and Rhodes, 2008	Distortion	Size	Cross-identity
	Jaquet et al., 2008	Distortion	<i>nr</i>	Cross-identity
	Jiang et al., 2006	Identity	Viewpoint, face shape, reflectance	Cross-identity
	Kovács et al., 2007	Gender	Position	Cross-identity
	Lai et al., 2012	Age	<i>nr</i>	Structural, cross-identity
	Leopold et al., 2001	Identity	Position; size	Cross-identity
	Otten and Banaji, 2012	Expression	<i>nr</i>	Structural, cross-identity
	Rhodes et al., 2003	Distortion	Rotation of 45° or 90°	Cross-identity
	Rhodes et al., 2004	Distortion, gender	Size, inversion	Cross-identity
	Strobach et al., 2011	Distortion	<i>nr</i>	Pictorial, structural, cross-identity
	Watson and Clifford, 2003	Distortion	Rotation of 45° or 90°, inversion	Pictorial
	Watson and Clifford, 2006	Gender	Rotation of 45° or 90°, inversion, size	Cross-identity
	Webster et al., 2004	Gender, ethnicity, expression	<i>nr</i>	Structural, cross-identity
	Yamashita et al., 2005	Distortion	Size, spatial frequency content, contrast, color	Pictorial, cross-identity
	Zhao and Chubb, 2001	Distortion	Size, inversion	Pictorial
Priming	Boehm et al., 2006	Familiarity decision	Inversion	Pictorial
	Bourne et al., 2009	Familiarity decision	Blurring, configural, position	Pictorial
	Brooks et al., 2002	Identification	Inversion, size, position, mirror reversal	Pictorial, structural transfer
	Bruce et al., 1994	Familiarity decision	Color alterations, cartoons	Pictorial
	Bruce and Valentine, 1985	Identification, familiarity decision	<i>nr</i>	Pictorial, structural transfer
	Bruce and Valentine, 1986	Familiarity decision	Blurring	Cross-identity
	Ellis et al., 1990	Occupation, familiarity, expression, and gender decision	<i>nr</i>	Pictorial, cross-identity
	Ellis et al., 1987	Identification, familiarity decision	<i>nr</i>	Pictorial, structural transfer
	Ellis et al., 1993	Identification, expression identification, gender decision	<i>nr</i>	Pictorial, structural, cross-identity
	Ellis et al., 1979	Familiarity decision	Trimming to internal or external features	Pictorial
	Goshen-Gottstein and Ganel, 2000	Gender decision	<i>nr</i>	Pictorial, structural transfer
	Johnston and Barry, 2006	Occupation and nationality decision	<i>nr</i>	Pictorial, cross-identity
	Kaiser et al., 2013	Gender decision	Size	Pictorial, cross-identity
	Rostamirad et al., 2009	Identification	<i>nr</i>	Pictorial, cross-identity
	Walther et al., 2013	Identification	Size	Cross-identity
	Young et al., 1994	Identification, familiarity, and gender decision	<i>nr</i>	Cross-identity
	Zarate and Sanders, 1999	Gender and ethnicity decision	<i>nr</i>	Pictorial, cross-identity

*Adaptation dimension = facial dimension examined within the adaptation paradigm; priming task = identification or classification task within the priming or test phase; image transfer dimension = investigated transferability across specific image dimensions; identity transfer dimensions = investigated transferability according to the three different identity-specific transfer categories; nr = not reported.*

## Transfer Between Images Differing in Specific Dimensions

### Transfer Within the Adaptation Paradigm

Several authors were able to demonstrate adaptation effects regarding the identity or gender of the presented image (features of the identity were altered by morphing the identity with other identities or by increasing or decreasing the identity strength, through synthetically altering the person's features), despite changes in the (retinal) location of the presented test stimulus (Leopold et al., 2001; Kovács et al., 2007; Afraz and Cavanagh, 2008). The authors either used faces that were unfamiliar (Kovács et al., 2007) when starting the adaptation phase or that were learned in an initial training session (Leopold et al., 2001; Afraz and Cavanagh, 2008). The studies by Kovács et al. (2007) and Afraz and Cavanagh (2008) revealed a reduction of the adaptation effects when changing the position of the test image, suggesting that the effects must include both position-variant and position-specific components.

Furthermore, transfer effects across differences of the (retinal) size between the adapting and test image seem to be possible (at least for faces that were unfamiliar at the beginning of the adaptation phase; Leopold et al., 2001; Zhao and Chubb, 2001; Rhodes et al., 2004; Anderson and Wilson, 2005; Yamashita et al., 2005). However, the study results of Zhao and Chubb (2001), Rhodes et al. (2004), and Yamashita et al. (2005) indicate that the adaptive processes are not insensitive to changes in size but also show some kind of size specificity within the adaptation effect (which is indicated by a reduction of the adaptation effect when changing the size). A similar pattern could also be found for a transfer across different orientations in picture plane. Using faces that were unfamiliar when starting the adaptation phase, Rhodes et al. (2003) and Watson and Clifford (2003, 2006) were able to demonstrate adaptation effects regarding the gender or distortions (e.g., vertically or horizontally, expanded or contracted faces) despite a rotation of the adapting stimuli to either 45 or 90° to the right or the left side. Nevertheless, the study results of Watson and Clifford (2003, 2006) indicate a significantly weaker adaptation effect, when the adaptation and test stimuli were rotated in different directions from the upright position compared to when both were rotated identically. These results suggest again that there must be an invariant component and a dimension-specificity within the adaptation effect.

Previous studies applying an even larger rotation of images by 180° (i.e., an inversion) are very ambivalent in their results. Hole (2011), using familiar face stimuli, and Rhodes et al. (2004), presenting faces that were unfamiliar when starting the adaptation phase, were able to induce similar adaptation effects for upright and inverted faces regarding distortions or the identity of the presented personalities. While Hole (2011) inverted just the adaptation image, Rhodes et al. (2004) demonstrated a transfer of the adaptation effect from (1) inverted adaptation to upright test images and (2) from upright adaptation images to inverted test images. Rhodes et al. (2004), however, used a test design in which those opposite conditions were induced simultaneously (e.g., presenting a contracted,

upright face simultaneously with a stretched inverted face in the adaptation phase). Other authors, however, detected an asymmetric pattern. By also presenting faces that were unfamiliar at the beginning of the adaptation phase, they either found much weaker (Watson and Clifford, 2003) or no effects (Watson and Clifford, 2006; Guo et al., 2009) when using inverted adaptation and upright test images, but equally strong effects (compared to no inversion at all) when presenting an upright adaptation and an inverted test stimulus.

Further transfer effects were also observed across alterations of the image relations (e.g., stretching the image vertically) and surface reflectance (i.e., albedo; Jiang et al., 2006; Hole, 2011). Moreover, Yamashita et al. (2005) looked at the transferability of adaptation effects to changes in spatial frequency content, contrast, color and size. While they found strong adaptation effects across changes in contrast, color and size, there was only a weak transferability of the effects to changes in contrast polarity and spatial frequency.

In general, the relation of invariant and variant components of the adaptation effect can vary tremendously for the different images or facial dimensions. For adaptation, alterations on dimensions that are known to affect the recognizability of a face (e.g., contrast and spatial frequency) seem to have a greater influence on the magnitude of the adaptation effect compared to alterations that only marginally affect the recognizability of a face (e.g., size or position; Yamashita et al., 2005; Hole, 2011). However, even for dimensions that affect the recognizability, adaptation effects can still be detected, indicating that although a considerable part of these effects appear to be retinotopic, the effects also indicate an involvement of higher, face-specific processing mechanisms (Hole, 2011). The asymmetric pattern regarding the inversion of the adaptation images observed by Watson and Clifford (2003, 2006) and Guo et al. (2009) might have been obtained due to the use of faces that were initially unfamiliar, since Hole (2011) was able to demonstrate adaptation effects inverting the adaptor by using highly familiar faces. However, it is open as to why Rhodes et al. (2004) were able to prove strong adaptation effects applying an inversion of the adaptor, even though they used faces that were initially unfamiliar. It might be the very different test design the authors used (simultaneously induced opposite adaptation effects) that led to these results.

### Transfer Within the Priming Paradigm

For priming, Kaiser et al. (2013) and Walther et al. (2013) found effects regarding the recognition of familiar faces, despite differences in the size between the priming and test stimulus. Priming effects could also be generated with a 180-degree rotation (i.e., an inversion) of the prime, using face stimuli with which the participants familiarized themselves in a 1-h training session (Boehm et al., 2006). However, these effects were much weaker compared to the upright prime condition. Similar results could also be observed by Brooks et al. (2002) using familiar face stimuli. They systematically investigated invariances in priming to various metric transformations and found equally strong priming effects when stimuli differed in

size, position, and reflectional orientation (mirror reversal). Interestingly, they showed significantly reduced effects when the test stimuli were inverted, pointing to face expert-processing (Schwaninger et al., 2003).

Bruce et al. (1994) were able to demonstrate priming effects from different grayscale images (two levels of gray [black and white] or four levels of gray [black, dark gray, light gray, and white]) on the same colored images (using familiar faces), although these priming effects were much weaker than those that could be detected from one colored image to the next. They also found a similar reduction of priming effects when computer-drawn photographs were presented as the prime and the original photograph as the test stimulus, or vice versa (compared to the condition in which the original images were presented in both phases). By manipulating facial features in the priming phase through blurring, Bourne et al. (2009) were able to show a transfer of identity priming (the task included a popularity rating of the presented famous identities), although here again effects were reduced compared to the unmanipulated condition. Furthermore, identity priming effects seem to be possible even when the test image is trimmed to just the internal features of a familiar (and also initially unfamiliar) face (Ellis et al., 1979).

In general, for priming the pattern seems to be similar to the one seen in the adaptation area: a transfer across manipulations is possible but to some extent the manipulations do affect the magnitude of the priming effect, suggesting invariant and variant components within the priming effect. Whether there is also a similar pattern regarding those dimensions that affect the recognizability of faces more strongly (i.e., dimensions that influence the priming effect more strongly than dimensions that do not have an influence on the recognizability) has not yet been investigated very intensively. The study by Brooks et al. (2002) might suggest a similar pattern to that of adaptation, since an inversion (which is known to impair recognition) generated significantly weaker priming effects than other metric changes (such as size, position, and reflectional orientation).

### Implications of the Transfer Between Different Image Versions for the Face Space

Altogether, the listed results on adaptation and priming show that the effects are not entirely retinotopic but that there is a component of face-specific processing. The systematic investigation of these face-specific components provides important information about which factors are generally involved in face representations and thus also which dimensions define the face space. Further research could eventually identify and specify the 15 to 22 dimensions of the face space, determined by Lewis (2004) at some point. The above results on adaptation and priming might indicate that factors that qualitatively change faces (and thus affect face recognition, such as contrast polarity) are more likely to be represented in face space than factors that are of a more quantitative or metric nature and thus do not affect recognition, such as size or position.

However, by applying an inversion of a face (which is known to impair recognition and even might lead to non-expert processing of faces, see Schwaninger et al., 2003), very ambiguous results were obtained. Within the adaptation area, Watson and Clifford

(2003, 2006) and Guo et al. (2009) observed reduced adaptation effects, by using face stimuli that were unfamiliar at the beginning of the adaptation phase and by inverting the adaptor. Hole (2011), however, also inverted the adaptor but used familiar faces and found adaptation effects were as equally strong as those in upright face stimuli. Thus, an inversion does not seem to affect the perception and processing of familiar faces as much as the perception and processing of initially unfamiliar faces. The facilitated recognition of familiar faces despite an inversion of the face stimulus might be due to a high flexibility (i.e., for example wide-ranging information about the identity) of the representations stored in memory and face space. The high flexibility could allow the identification of a person (and thus also an adaptation of the representation) despite large alterations of the orientation. Unfamiliar faces, on the other hand, are not yet stored in memory as highly flexible representations, so that large alterations of the orientation can be less easily ignored.

However, applying an inversion within the priming paradigm, weaker effects were also observed using familiar faces (Brooks et al., 2002). This may be explained by the differences between the two paradigms priming and adaptation. Within the priming paradigm the presentation duration of the prime is usually much shorter compared to the presentation duration of the adaptor (see section “Implications of the Transfer Between Different Image Versions for the Face Space”). When applying an inversion, the shorter presentation duration could lead to additional recognition difficulties, since more time might be needed to compensate the inversion of the image and to recognize the presented identity and then activate its representation within the face space. Within the adaptation paradigm, on the other hand, the adaptor is usually presented for longer to achieve the greatest possible effect, so that recognition might be easier despite an inversion of the stimuli.

### Transfer on an Identity Level Transfer Within the Adaptation Paradigm

Most studies investigating the transfer of adaptation effects from one image of a familiar identity to a different image of the same identity (*structural level*) were focused on distortions when manipulating the adaptor (e.g., alterations of the eyes–mouth distance; Carbon and Leder, 2005; Carbon et al., 2007; Carbon and Ditye, 2011, 2012; Strobach et al., 2011). All of them were able to find strong transfer effects even though the transfer on the *structural level* often led to a small decrease of the adaptation effect compared to the adaptation effect on a *pictorial level* (Carbon and Leder, 2005; Carbon and Ditye, 2012). Using face stimuli that were unfamiliar at the beginning of the adaptation phase, Fox and Barton (2007) on the other hand, observed equally robust adaptation effects on the *pictorial* and *structural level*. However, they did not distort the presented stimuli but investigated adaptation effects to different emotional expressions.

The same authors were also able to transfer the demonstrated effects across different identities (*cross-identity level*), irrespective of the gender of the presented identities (Fox and Barton, 2007). Although these adaptation effects on a *cross-identity level* were significant, they were weaker compared to the effects on the *pictorial* or *structural level*, suggesting that the generated

effects are at least partially identity-specific. Fox et al. (2008) reversed this paradigm by investigating adaptation effects on identity alterations and their modulation by congruency of facial expressions (using familiar as well as initially unfamiliar face stimuli). Interestingly, they did not find any impact of expression congruency on the identity effects, which indicates that identity perception is independent of emotional expressions (Fox et al., 2008). However, other authors who also investigated adaptation effects on different emotional expressions found limitations in the transferability of the effects. Using faces that were unfamiliar when starting the adaptation phase, Otten and Banaji (2012) reported a robust transferability of expression effects across images of the same identity and across images of a different identity but significantly weaker effects for images of individuals of a different ethnicity.

For configurally distorted famous faces, several studies were able to demonstrate a robust transfer to other identities, even though the magnitude of the effects decreased compared to the *pictorial* or *structural level* (Carbon et al., 2007; Carbon and Ditye, 2011, 2012; Strobach et al., 2011). However, also for configurally distorted (initially unfamiliar) faces, a limited transferability to other ethnicities could be observed (Jaquet et al., 2008), indicating an ethnic specific component within the effect. Additionally, Jaquet and Rhodes (2008) investigated the transferability of adaptation effects on configural alterations (presenting face stimuli that were initially unfamiliar) across gender and found a partial transfer (i.e., a weaker but still significant effect for the different-gender condition than for the same-gender condition), suggesting both common and gender-specific components within the adaptation effect. A gender adaptation effect (using as well-initially unfamiliar faces), on the other hand, was largely transferable across different identities and thus did not seem to have an identity-specific component (Webster et al., 2004). Moreover, the study also revealed differences in category boundaries selected in the preadaptation assessment (observers categorized images of a gender-morph-continuum to estimate the category boundary of male and female), indicating that observers tended to select a category boundary that was shifted to their own gender. These differences in category boundary were also observed with different ethnicities (Asian and Caucasian), leading to a shift of the observer's boundary toward their own ethnicity. However, this shift was not as intense when observers had already been exposed to the other race for a longer time (e.g., Asians living in the US for at least 1 year). Additionally, other authors have found an impaired identification of the face's gender in other race faces (O'Toole et al., 1996).

A transfer of adaptation effects between other social groups was found by Barrett and O'Toole (2009). They investigated adaptation effects (using face stimuli that were unfamiliar at the beginning of the experiment) on gender and demonstrated a transfer of these effects across different age groups (Barrett and O'Toole, 2009). However, by presenting familiar face stimuli, Lai et al. (2012) investigated adaptation effects on age differences and observed that they were just partly transferable across different identities, suggesting both identity-variant and identity-specific components within the adaptation effect.

## Transfer Within the Priming Paradigm

Face priming effects seem to be equally transferable to different images of the same identity (*structural level*) as adaptation effects (Bruce and Valentine, 1985; Ellis et al., 1987, 1993), although the priming effects seem to decrease the more dissimilar the prime and the test images are. Ellis et al. (1987) systematically investigated the transferability of priming (using famous faces) by applying a three-level differentiation regarding the similarity of the presented test stimuli to the prime: identical, similar, and dissimilar (the similarity of the stimuli was rated in advance by an independent jury). The priming effect seemed to be greatest when the prime and the test image were identical, less when they were similar, and least when they were dissimilar (but still representing the same person).

Several studies investigating priming effects on a *cross-identity level* focused on associate priming and thus compared highly associated couples (e.g., Siegfried and Roy) with less associated identities (e.g., Angela Merkel and George Clooney). In these studies, Bruce and Valentine (1986) and Young et al. (1994) observed strong priming effects on famous highly associated identities. While a transfer of the priming effect to a highly associated identity seems to be successful, a transfer to other ethnically related identities apparently does not work. By using face primes that were unfamiliar at the beginning of the experiment, Rostamirad et al. (2009) demonstrated a facilitation effect in recognition when the test face was preceded by the same priming face, an inhibition effect when it was a different face and an even greater inhibition when the face belonged to the same ethnic group as the prime. Zarate and Sanders (1999) also investigated priming effects (using faces that were initially unfamiliar) across different ethnicities and gender. They could not find a relation between the strength of the priming effect and ethnic and gender similarity of the prime and test image, but observed that the magnitude of the priming effect was rather modulated by the general similarity of the stimuli. The authors suggest that the facilitation effect is not generated through the activation of a superordinate abstract concept (e.g., gender or ethnicity), but that the priming effect is rather prime-specific and depends on the inter-item similarity.

In line with these results, Ellis et al. (1990) found that, by systematically investigating the transferability of priming effects (using familiar and initially unfamiliar face stimuli) to different categorization tasks (familiarity, occupation, gender, and expression tasks), priming effects only occur for decisions in the test phase that require an identification of a face and not a classification according to a higher concept. Thus, a priming effect was observed for familiarity and occupation tasks in the test phase but not for gender or expression tasks. On the other hand, any encounter with a face seems to be sufficient to cause priming (meaning that the magnitude of a priming effect does not depend on the task given in the priming phase, but obviously does depend on the task given in the test phase). Nevertheless, the study results of Johnston and Barry (2006) do not seem to fully fit into this picture. As in the study by Ellis et al. (1990), the authors found repetition priming effects for an occupation decision task. However, by using familiar faces, Johnston and Barry (2006) were also able to demonstrate a priming effect for

a nationality decision task in the test phase, which, according to the Ellis et al. (1990) argumentation (that only tasks that require an identification of the face show priming effects), should actually not exist. Other authors also disagreed with the argumentation of Ellis and colleagues, since they were able to find priming effects (using face stimuli that were unfamiliar at the beginning of the experiment) for a gender decision task (Goshen-Gottstein and Ganel, 2000). However, Ellis et al. (1990), Goshen-Gottstein and Ganel (2000), and Johnston and Barry (2006) investigated priming effects across different categorization tasks only on a *pictorial level*. They did not consider the transferability of the effects on a *structural* or *cross-identity level*. Hence, in their test design higher concepts (such as gender) could only be addressed by the categorization of the stimuli (in, e.g., female or male). However, since a systematic comparison of the categories on a *cross-identity level* [i.e., comparing the transferability of priming effects of an identity of one category (e.g., female) to either a different identity of the same category or an identity of the opposite category (e.g., male)] was not performed, the results give little assurance as to whether higher concepts were really primed or not.

### Implications of Identity Transfer for the Face Space

Both phenomena, adaptation and priming, seem to transfer quite well across different images of the same identity and thus provide further evidence that adaptation as well as priming effects do have an identity-specific component. Furthermore, the results regarding the transferability on a *structural level* suggest a high flexibility of the representations stored in memory and face space, since they seem to be altered and activated despite significant alterations of the images presented in the adaptation and priming paradigms. Thus, they must somehow contain either wide-ranging information about the identity or stable, basic and minimalistic face structures that allow an identification of a person despite large and diverse changes. The basis on which the recognition of a person's face occurs is not clear yet. However, the fact that adaptation effects can be generated through altering very diverse information might indicate that the representations rather contain a wide range of different face information than just a very basic structure.

Regarding transferability on a *cross-identity level*, the reported findings on adaptation provide clear evidence that adaptation effects are transferable to different identities. This suggests a hierarchical processing of faces, where adaptation also affects superordinate face categories, indicating a distinction of different social groups (e.g., different ethnicities, gender, etc.) in facial processing. Referring to the face space, this would mean that adaptation not only alters the representation of the presented identity but also the representation of the social group(s) to which the person belongs. This suggests that either different modules or sub-face spaces must exist (that probably show some overlap between each other) or different prototypes for each social group, which can be altered through adaptation. Thus, adaptation would alter the common underlying face structures and lead to an alteration not just of that identity presented in the adaptation paradigm but also of all other faces located close to the identity or within the same social group. The reported

results regarding the category boundary further suggest that there are stronger adaptation effects to the sub-face spaces individuals encounter most and also that these more familiar sub-face spaces are more differentiated.

Furthermore, there seem to be differences in the transferability of adaptation effects depending on the type of adaptation information. Face information that is more transient or more variable (such as facial expression or age) appears to transfer more easily (see the reported results of, Fox and Barton, 2007; Fox et al., 2008; Barrett and O'Toole, 2009; Lai et al., 2012) than information that is invariant (such as configural face information, gender, or ethnicity), suggesting that this information type has a more subordinate role in facial perception and processing and thus also in the face space. However, on a *cross-identity level* (i.e., a transfer to other identities) more variable information also shows slight limitations of the transfer to other identities (Fox and Barton, 2007; Lai et al., 2012), indicating that it cannot be neglected completely when investigating face-specific adaptation effects. Thus, it does have a face-specific component within the adaptation effect and therefore must also be somehow represented in face space. However, the face-specific component of the effect seems to be somehow smaller compared to the level of face specificity within the adaptation effects obtained with more invariant information. This indicates that the representation of more variable information in face space must also be somehow weaker compared to the representation of more invariant information.

For priming, the picture regarding the transferability on a *cross-identity level* seems to be more ambiguous than for adaptation. Many of the reported results indicate transferability to different identities but this transfer rather depends on the similarity of the presented images than on belonging to the same or a different superordinate social group. Thus, referring to the face space, an activation of a representation of an identity might not automatically lead to an activation of a higher-level prototype or a sub-space. The results rather indicate that, within the face space, just those identities that are located very close to the primed identity (due to their similarity on many face dimensions) might also be affected through priming. However, the outcomes regarding the transferability of priming effects to associated individuals suggest that an activation of representations that are more distant to the primed identity within the face space is also possible. Thus, the activation of a representation might automatically lead to an activation of the representation of the associated person, due to the strong associative and exclusive bond between them. Another explanation could be that by activating a representation, a higher concept under which both associated persons are to be classified is activated as well. As a result, not only the representations of the associated persons would be activated, but also representations of possible other persons belonging to this concept. Although this idea would clearly contradict the results of Zarate and Sanders (1999; demonstrating that the priming effects rather depend on the inter-item similarity than on the belonging to the same concept), it would support the results of Goshen-Gottstein and Ganel (2000) and Johnston and Barry (2006), who demonstrated priming effects for nationality and gender tasks. However, the

results of these studies should be taken into account with caution, since it is not clear yet whether the implemented categorization tasks can really address higher concepts.

## DISCUSSION

Adaptation and priming are two established paradigms in the face literature. Both paradigms and their associated phenomena can assist a better understanding of face recognition and face representation. Regarding the face space framework, up to now the literature has mainly focused on face adaptation while largely neglecting face priming. By reviewing and comparing the literature on face adaptation and face priming within one paper, this work aims to create an overall picture of both phenomena and their contributions to the face space. While face adaptation is a phenomenon that seems to alter a representation, leading to a shift of the representation within the face space, face priming mainly activates such a representation. The reported studies show that these effects can be influenced by modifications of the temporal components of adaptation and priming.

### Summary of the Temporal Characteristics of Adaptation and Priming and the Consequences for the Face Space

A longer adaptation duration causes an increasing adaptation effect (Rhodes et al., 2007; Strobach et al., 2011) and therefore a larger position shift of the representation within the face space. A longer prime duration, however, leads to a decrease of the priming effect (Rieth and Huber, 2010) and therefore to an activation reduction of the facial representation within the face space. This activation reduction might be an automatized mechanism to avoid a confusion with other faces presented afterward. However, a longer prime duration can sometimes even cause a negative priming effect (Rieth and Huber, 2010; Barbot and Kouider, 2012). Since negative priming and adaptation seem to be identical regarding their behavioral outcome (they both lead to a slower or more difficult recognition), the negative priming effect could also be that of an adaptation process (evoked due to the lack of fit between the presented facial stimulus and the mental representation). Thus, a longer prime duration might function as an adaptor and might lead to a shift of the facial representation within the face space toward the prime.

Compared to the adaptation duration, a longer presentation of the adaptation test stimulus does not cause a greater adaptation effect but rather decreases it Leopold et al. (2005) and Rhodes et al. (2007), since it leads to a re-adaptation process and thus to a shift of the facial representation within the face space back to the original position. A longer presentation of the prime test stimulus also causes a decrease of the priming effect (Rieth and Huber, 2010), probably because the test stimulus addresses, just like the prime, the mental face space representation and thus leads, as an overstimulation of the representation, to a neuronal habituation and activation reduction.

The effects of both phenomena, however, can be equally robust, since they can last up to a week or (at least priming effects) up to several months (Maylor, 1998; Lewis and Ellis, 1999; Carbon and Ditye, 2011, 2012). Thus, an adaptation can probably lead to a very persistent shift of the mental representation within the face space, whereas priming causes a long-lasting activation or a facilitated reactivation of the facial representation. However, the effects of both phenomena decrease, the more time elapses between the adaptation/priming and the test phase. Within the context of adaptation, a possible explanation for the continuous decrease of the effect might be an increased possibility of exposure to the presented identity (which possibly causes a re-adaptation back to the original representation and thus decreases the effect), during a long delay. Another possible explanation could be that the re-adaptation process is an automatic process due to the robustness of the original facial representation (which presumably is built up over a longer period of time) and which does not integrate transient alterations permanently unless they are presented for longer and/or more frequently. The continuous decrease of priming effects over time, however, might be caused by either a constant decrease of the activation of the representation or a decrease of the reactivation capability of the representation located in face space. Since a longer priming duration seems to lead to an activation reduction to inhibit a confusion with other faces seen subsequently, a long-term maintenance of activation does not seem plausible (also for shorter priming durations). A facilitated reactivation, however, would probably not inhibit the recognition of subsequent faces (since it would only lead to a full reactivation of the representation, if the identity is presented again) and thus might be more likely.

### Summary of the Transfer Characteristics of Adaptation and Priming and the Consequences for the Face Space

Not only the temporal components of adaptation and priming give us information about the facial perception, the storage and thus the face space, but also the transferability of adaptation and priming effects contribute to the understanding of it. The listed study results reveal that a transfer of adaptation and priming effects across alterations of specific image dimensions is possible, but to some extent the alterations do affect the magnitude of the effects (meaning that the effects usually decrease when they are transferred; see, e.g., Bruce et al., 1994; Brooks et al., 2002; Yamashita et al., 2005; Kovács et al., 2007). This indicates that although a considerable part of the effects seems to be retinotopic, there does exist some kind of face-specific component too. Nevertheless, the results also show that dimensions that qualitatively change faces and thus affect their recognition (e.g., contrast polarity or spatial frequency) have a greater impact on the adaptation and priming effects than dimensions that are of a more quantitative or metric nature (e.g., size or position) and do not affect the recognition as much (see, e.g., Brooks et al., 2002; Yamashita et al., 2005). Thus, the dimensions that have a greater impact show a greater face specificity and are therefore more likely to be represented in

face space than dimensions that do not affect the adaptation and priming effects as much.

Adaptation and priming effects can be observed not only despite changes in specific image dimensions, but also despite a presentation of a completely different image of the identity in the test phase (Bruce and Valentine, 1985; Ellis et al., 1987; Carbon and Leder, 2005; Carbon et al., 2007). Thus, the representations within the face space must somehow be very flexible. They must either contain wide-ranging information about the identity or stable but minimalistic face structures that allow an identification of an identity despite large and diverse changes. Since adaptation effects can be evoked by altering very diverse face information, the latter might be more likely.

Adaptation and priming effects regarding the transferability on a *cross-identity level* reveal that both kinds of effects are (at least partly) transferable to different identities (Bruce and Valentine, 1986; Carbon et al., 2007; Strobach et al., 2011). The reported findings on adaptation indicate a hierarchical processing of faces, where adaptation not only alters the representation of the presented identity but also affects superordinate concepts (see, e.g., Jaquet and Rhodes, 2008; Jaquet et al., 2008). This suggests that there must exist different sub-face spaces or different prototypes for each superordinate concept within the face space. Thus, by altering the representation of a specific identity, underlying face structures of superordinate concepts would be altered toward the adaptor too. The findings further suggest that there are stronger adaptation effects for the sub-face spaces individuals encounter most and that these sub-face spaces are more differentiated than more unfamiliar ones (O'Toole et al., 1996; Webster et al., 2004). The listed results on priming, on the other hand, are ambiguous. Some studies indicate that the transferability of priming effects to other identities rather depends on the similarity of the presented images than on the belonging to (and thus activation of) a common sub-face space (Zarate and Sanders, 1999). Other study results, however, suggest, that priming is able to activate representations of identities that are strongly associated with the primed identity (e.g., Young et al., 1994). However, it is not clear yet whether this activation of other representations occurs due to an activation of a higher sub-face space under which the associated persons are to be classified or due to an associative and exclusive bond between these identities.

## Future Adaptation and Priming Studies and the Face Space

The two phenomena adaptation and priming demonstrate that perceived faces can change our facial perception and storage and hence our face space significantly. Adaptation and priming studies manipulating the temporal factors help identify the best temporal structure of both paradigms (in the way of generating the greatest possible effects; e.g., for adaptation a long adaptor and a short test stimulus, for priming both: a short prime and a short test stimulus). A systematic manipulation of temporal parameters may also provide information about the underlying mechanisms of the two phenomena. It seems that the presentation of a stimulus could initially lead to a priming effect. However, prolonging the presentation of the

stimulus might possibly induce an adaptation effect (see the results on negative priming). Thus, it could be assumed, that it depends on the presentation duration of the adaptor/prime, which phenomenon occurs.

However, the study by Walther et al. (2013) indicates that the ambiguity of the test stimulus should rather be considered as the decisive factor. The authors were able to demonstrate both phenomena within one paradigm. While adaptation effects were induced by presenting very ambiguous test stimuli, unambiguous test stimuli provoked priming effects. Thus, it still seems unclear which specific parameters (e.g., temporal parameters or the ambiguity of the test stimuli) are crucial for the occurrence of one or the other phenomenon. Future studies should therefore focus more on the investigation of specific parameters using combined (adaptation and priming) paradigms to better understand and distinguish both phenomena.

Furthermore, studies on temporal characteristics provide important information about the robustness of the adaptation and priming effects and the hereby-created long-term transformation of the face space (i.e., persistent shifts of representations and sub-face spaces, a permanent facilitation of activation as well as the pattern of decay of those alterations). However, it is still unclear which mechanisms are causing the continuous decrease of the effects over time, at least for adaptation. Future studies should therefore specifically investigate the two possible mechanisms responsible for the re-adaptation (i.e., increased exposure to the original image of the presented identity or automatic re-adaptation process due to the robustness of the original facial representation).

The investigations on the image dimensions of adaptation and priming stimuli reveal that some face information is more important and thus probably more likely represented in the face space than other facial characteristics (e.g., invariant information, such as gender, ethnicity, etc. is more likely included in face space than variant information, such as size or location). However, due to a lack of systematic studies on this topic, the dimensions on which all faces vary within the face space [according to Lewis (2004) there should be from 15 up to 22 dimensions] could not yet be determined. Nevertheless, the view that only an exclusive number of dimensions exist in face space and thus facial information other than those dimensions is not considered in facial perception, should be questioned. The reported studies show that facial information that seems to be less important for facial perception (since it has a weaker impact on adaptation and priming effects) still affects the perception of faces and thus also the face space. Perhaps this categorical view of the face space dimensions should be reconsidered and it should be further investigated whether the very diverse facial information is just represented with a different weighting within the face space. Future research should therefore systematically compare adaptation and priming effects on variant and invariant facial information.

The reported studies investigating the transferability of effects further show that the facial representations located in face space are very flexible (i.e., a recognition is possible despite large alterations of the presented face) and that there must be some kind of sub-face spaces representing higher concepts. While

adaptation clearly has an effect on these sub-face spaces, no final conclusion can be drawn yet as to whether priming also activates higher concepts. Thus, future studies should focus on a systematic investigation of priming effects on different superordinate concepts to further clarify this topic.

Finally, it can be stated that priming probably can add as much to the understanding of face space as adaptation. It would therefore be recommendable to consider priming more closely in this still challenging field of face research in the future.

## RÉSUMÉ

Face adaptation and priming are two phenomena that seem to differ tremendously. While adaptation leads to a shift of representations within the face space, priming rather activates these representations without shifting them (see **Figure 2**). However, both paradigms alter subsequent face recognition and thus, can be used to gain a better understanding of face recognition, representation and hence the face space. By analyzing the characteristics of the two different effects, both phenomena can give us detailed information about the content, the structure and the flexibility of the face space. The adaptability or priming of specific face information, for example, provide insight into what facial dimensions are stored in face space. The comparison of different facial information may also reveal a different weighting of the information stored in face space (e.g., invariant information seems to be more relevant than variant information). The transferability of effects can reveal information about the structure of the face

space (e.g., division into sub-face spaces). The robustness and decay of effects, however, give insight into how flexible or stable representations are within the face space. Furthermore, the specific temporal characteristics of the two paradigms (e.g., adaptor/prime duration) might reveal information about the underlying mechanism of both phenomena. Thus the presentation of a stimulus may initially lead to a priming effect (i.e., a pure activation of the representation). However, if the stimulus is presented for a longer time, an adaptation effect might be induced. The systematic evaluation of the adaptation and priming literature presented here, highlights the valuableness of both paradigms for the investigation of face recognition and representation. It also reveals that priming (although often neglected by face-space literature) is an equally useful tool as adaptation to explore the face space.

## AUTHOR CONTRIBUTIONS

C-CC and TS conceived of the conceptual idea. RM wrote the manuscript with input from all coauthors (C-CC, SU, and TS). TS supervised the process of writing. All authors provided critical feedback and helped in shaping the manuscript.

## FUNDING

This research was supported by a grant to C-CC and TS from the Deutsche Forschungsgemeinschaft (DFG, CA 917/7-1; STR 1223/4-1).

## REFERENCES

- Afraz, S. R., and Cavanagh, P. (2008). Retinotopy of the face aftereffect. *Vision Res.* 48, 42–54. doi: 10.1016/j.visres.2007.10.028
- Anderson, N. D., and Wilson, H. R. (2005). The nature of synthetic face adaptation. *Vision Res.* 45, 1815–1828. doi: 10.1016/j.visres.2005.01.012
- Barbot, A., and Kouider, S. (2012). Longer is not better: nonconscious overstimulation reverses priming influences under interocular suppression. *Atten. Percept. Psychophys.* 74, 174–184. doi: 10.3758/s13414-011-0226-3
- Barrett, S. E., and O'Toole, A. J. (2009). Face adaptation to gender: does adaptation transfer across age categories? *Vis. Cogn.* 17, 700–715. doi: 10.1080/13506280802332197
- Boehm, S. G., Klostermann, E. C., Sommer, W., and Paller, K. A. (2006). Dissociating perceptual and representation-based contributions to priming of face recognition. *Conscious. Cogn.* 15, 163–174. doi: 10.1016/j.concog.2005.06.001
- Bourne, V. J., Vladeanu, M., and Hole, G. J. (2009). Lateralised repetition priming for featurally and configurally manipulated familiar faces: evidence for differentially lateralised processing mechanisms. *Laterality* 14, 287–299. doi: 10.1080/13576500802383709
- Brooks, B. E., Rosielle, L. J., and Cooper, E. E. (2002). The priming of face recognition after metric transformations. *Perception* 31, 297–313. doi: 10.1068/p3283
- Bruce, V., Burton, A. M., Carson, D., Hanna, E., and Mason, O. (1994). "Repetition priming of face recognition," in *Attention and Performance XV: Conscious and Nonconscious Information Processing*, eds C. Umiltà, and M. Moscovitch (London: The MIT Press), 179–202.
- Bruce, V., and Valentine, T. (1985). Identity priming in the recognition of familiar faces. *Br. J. Psychol.* 76, 373–383. doi: 10.1111/j.2044-8295.1985.tb01960.x
- Bruce, V., and Valentine, T. (1986). Semantic priming of familiar faces. *Q. J. Exp. Psychol. A* 38, 125–150. doi: 10.1080/14640748608401588
- Bruce, V., and Young, A. (1986). Understanding face recognition. *Br. J. Psychol.* 77, 305–327. doi: 10.1111/j.2044-8295.1986.tb02199.x
- Carbon, C.-C., and Ditye, T. (2011). Sustained effects of adaptation on the perception of familiar faces. *J. Exp. Psychol. Hum. Percept. Perform.* 37, 615–625. doi: 10.1037/a0019949
- Carbon, C.-C., and Ditye, T. (2012). Face adaptation effects show strong and long-lasting transfer from lab to more ecological contexts. *Front. Psychol.* 3:3. doi: 10.3389/fpsyg.2012.00003
- Carbon, C.-C., and Leder, H. (2005). Face adaptation: changing stable representations of familiar faces within minutes? *Adv. Cogn. Psychol.* 1, 1–7. doi: 10.2478/v10053-008-0038-8
- Carbon, C.-C., and Leder, H. (2006). The Mona Lisa effect: is 'our' Lisa fame or fake? *Perception* 35, 411–414. doi: 10.1068/p5452
- Carbon, C.-C., Strobach, T., Langton, S. R. H., Harsányi, G., Leder, H., and Kovács, G. (2007). Adaptation effects of highly familiar faces: immediate and long lasting. *Mem. Cognit.* 35, 1966–1976. doi: 10.3758/bf03192929
- Clifford, C. W. G., and Rhodes, G. (2005). *Fitting the Mind to the World: Adaptation and Aftereffects in High Level Vision*. Oxford: Oxford University Press.
- Clifford, C. W. G., Wenderoth, P., and Spehar, B. (2000). A functional angle on some aftereffects in cortical vision. *Proc. R. Soc. Lond. B Biol. Sci.* 267, 1705–1710. doi: 10.1098/rspb.2000.1198
- Ellis, A. W., Burton, A. M., Young, A., and Flude, B. M. (1997). Repetition priming between parts and wholes: tests of a computational model of familiar face recognition. *Br. J. Psychol.* 88, 579–608. doi: 10.1111/j.2044-8295.1997.tb02659.x
- Ellis, A. W., Young, A. W., and Flude, B. M. (1990). Repetition priming and face processing: priming occurs within the system that responds to the identity of a face. *Q. J. Exp. Psychol. A* 42, 495–512. doi: 10.1080/14640749008401234

- Ellis, A. W., Young, A. W., Flude, B. M., and Hay, D. C. (1987). Repetition priming of face recognition. *Q. J. Exp. Psychol. A* 39, 193–210. doi: 10.1080/14640748708401784
- Ellis, H. D., Ellis, D. M., and Hosie, J. A. (1993). Priming effects in children's face recognition. *Br. J. Psychol.* 84, 101–110. doi: 10.1111/j.2044-8295.1993.tb02465.x
- Ellis, H. D., Shepherd, J. W., and Davies, G. M. (1979). Identification of familiar and unfamiliar faces from internal and external features: some implications for theories of face recognition. *Perception* 8, 431–439. doi: 10.1068/p080431
- Fox, C. J., and Barton, J. J. S. (2007). What is adapted in face adaptation? The neural representations of expression in the human visual system. *Brain Res.* 1127, 80–89. doi: 10.1016/j.brainres.2006.09.104
- Fox, C. J., Oruc, I., and Barton, J. J. (2008). It doesn't matter how you feel. The facial identity aftereffect is invariant to changes in facial expression. *J. Vis.* 8, 11.1–11.13. doi: 10.1167/8.3.11
- Goshen-Gottstein, Y., and Ganel, T. (2000). Repetition priming for familiar and unfamiliar faces in a sex-judgment task: evidence for a common route for the processing of sex and identity. *J. Exp. Psychol. Learn. Mem. Cogn.* 26, 1198–1214. doi: 10.1037/0278-7393.26.5.1198
- Guo, X. M., Oruç, Y., and Barton, J. J. S. (2009). Cross-orientation transfer of adaptation for facial identity is asymmetric: a study using contrast-based recognition thresholds. *Vision Res.* 49, 2254–2260. doi: 10.1016/j.visres.2009.06.012
- Hole, G. (2011). Identity-specific face adaptation effects: evidence for abstractive face representations. *Cognition* 119, 216–228. doi: 10.1016/j.cognition.2011.01.011
- Jaquet, E., and Rhodes, G. (2008). Face aftereffects indicate dissociable, but not distinct, coding of male and female faces. *J. Exp. Psychol. Hum. Percept. Perform.* 34, 101–112. doi: 10.1037/0096-1523.34.1.101
- Jaquet, E., Rhodes, G., and Hayward, W. G. (2008). Race-contingent aftereffects suggest distinct perceptual norms for different race faces. *Vis. Cogn.* 16, 734–753. doi: 10.1080/13506280701350647
- Jiang, F., Blanz, V., and O'Toole, A. J. (2006). Probing the visual representation of faces with adaptation: a view from the other side of the mean. *Psychol. Sci.* 17, 493–500. doi: 10.1111/j.1467-9280.2006.01734.x
- Johnston, R. A., and Barry, C. (2006). Repetition priming of access to biographical information from faces. *Q. J. Exp. Psychol.* 59, 326–339. doi: 10.1080/02724980443000791
- Kaiser, D., Walther, C., Schweinberger, S. R., and Kovacs, G. (2013). Dissociating the neural bases of repetition-priming and adaptation in the human brain for faces. *J. Neurophysiol.* 110, 2727–2738. doi: 10.1152/jn.00277.2013
- Kloth, N., and Schweinberger, S. R. (2008). The temporal decay of eye gaze adaptation effects. *J. Vis.* 8, 1–11. doi: 10.1167/8.11.4
- Kovács, G., Zimmer, M., Harza, I., and Vidnyánszky, Z. (2007). Adaptation duration affects the spatial selectivity of facial aftereffects. *Vision Res.* 47, 3141–3149. doi: 10.1016/j.visres.2007.08.019
- Lai, M., Oruc, I., and Barton, J. J. (2012). Facial age after-effects show partial identity invariance and transfer from hands to faces. *Cortex* 48, 477–486. doi: 10.1016/j.cortex.2010.11.014
- Lee, K., Byatt, G., and Rhodes, G. (2000). Caricature effects, distinctiveness, and identification: testing the face-space framework. *Psychol. Sci.* 11, 379–385. doi: 10.1111/1467-9280.00274
- Leopold, D. A., O'Toole, A. J., Vetter, T., and Blanz, V. (2001). Prototype-referenced shape encoding revealed by high-level aftereffects. *Nat. Neurosci.* 4, 89–94. doi: 10.1038/82947
- Leopold, D. A., Rhodes, G., Müller, K. M., and Jeffery, L. (2005). The dynamics of visual adaptation to faces. *Proc. R. Soc. Lond. B Bio. Sci.* 272, 897–904. doi: 10.1098/rspb.2004.3022
- Lewis, M. (2004). Face-space—R: towards a unified account of face recognition. *Vis. Cogn.* 11, 29–69. doi: 10.1080/13506280344000194
- Lewis, M. B., and Ellis, H. D. (1999). Repeated repetition priming in face recognition. *Q. J. Exp. Psychol. A* 52, 927–955. doi: 10.1080/027249899390873
- Maylor, E. A. (1998). Retrieving names in old age: short- and (very) long-term effects of repetition. *Mem. Cognit.* 26, 309–319. doi: 10.3758/BF03201142
- McNamara, T. P. (2005). *Semantic Priming: Perspectives from Memory and Word Recognition*. New York: Psychology Press.
- Meytlis, M., and Sirovich, L. (2007). On the dimensionality of face space. *IEEE Trans. Pattern Anal. Mach. Intell.* 29, 1262–1267. doi: 10.1109/TPAMI.2007.1033
- O'Toole, A. J., Peterson, J., and Deffenbacher, K. A. (1996). An 'other-race effect' for categorizing faces by sex. *Perception* 25, 669–676. doi: 10.1068/p250669
- Otten, M., and Banaji, M. R. (2012). Social categories shape the neural representation of emotion: evidence from a visual face adaptation task. *Front. Integr. Neurosci.* 6:9. doi: 10.3389/fnint.2012.00009
- Rhodes, G., Jeffery, L., Clifford, C. W. G., and Leopold, D. A. (2007). The timecourse of higher-level face aftereffects. *Vision Res.* 47, 2291–2296. doi: 10.1016/j.visres.2007.05.012
- Rhodes, G., Jeffery, L., Watson, T. L., Clifford, C. W. G., and Nakayama, K. (2003). Fitting the mind to the world: face adaptation and attractiveness aftereffects. *Psychol. Sci.* 14, 558–566. doi: 10.1046/j.0956-7976.2003.psci\_1465.x
- Rhodes, G., Jeffery, L., Watson, T. L., Jaquet, E., Winkler, C., and Clifford, C. W. (2004). Orientation-contingent face aftereffects and implications for face-coding mechanisms. *Curr. Biol.* 14, 2119–2123. doi: 10.1016/j.cub.2004.11.053
- Rieth, C. A., and Huber, D. E. (2010). Priming and habituation for faces: individual differences and inversion effects. *J. Exp. Psychol. Hum. Percept. Perform.* 36, 596–618. doi: 10.1037/a0018737
- Rostamirad, S., Barton, J. J. S., and Oruc, I. (2009). Center-surround organization of face-space: evidence from contrast-based face-priming. *Neuroreport* 20, 1177–1182. doi: 10.1097/WNR.0b013e32832f078d
- Schwaninger, A., Carbon, C. C., and Leder, H. (2003). "Expert face processing: specialization and constraints," in *The Development of Face Processing*, eds G. Schwarzer, and H. Leder (Göttingen: Hogrefe & Huber), 81–97.
- Schweinberger, S. R., Pfütze, E.-M., and Sommer, W. (1995). Repetition priming and associative priming of face recognition: evidence from event-related potentials. *J. Exp. Psychol. Learn. Mem. Cogn.* 21, 722–736. doi: 10.1037//0278-7393.21.3.722
- Strobach, T., and Carbon, C. C. (2013). Face adaptation effects: reviewing the impact of adapting information, time, and transfer. *Front. Psychol.* 4:318. doi: 10.3389/fpsyg.2013.00318
- Strobach, T., Ditye, T., and Carbon, C.-C. (2011). Long-term adaptation effects of highly familiar faces are modulated by adaptation duration. *Perception* 40, 1000–1004. doi: 10.1068/p6986
- Tredoux, C. (2002). A direct measure of facial similarity and its relation to human similarity perceptions. *J. Exp. Psychol. Appl.* 8, 180–193. doi: 10.1037/1076-898x.8.3.180
- Valentine, T. (1991). A unified account of the effects of distinctiveness, inversion, and race in face recognition. *Q. J. Exp. Psychol. A* 43, 161–204. doi: 10.1080/14640749108400966
- Valentine, T. (2001). "Face-space models of face recognition," in *Computational, Geometric, and Process Perspectives on Facial Cognition: Contexts and Challenges*, eds M. J. Wenger, and J. T. Townsend (Mahwah, NJ: Lawrence Erlbaum Associates), 83–113.
- Valentine, T., Lewis, M. B., and Hills, P. J. (2016). Face-space: a unifying concept in face recognition research. *Q. J. Exp. Psychol.* 69, 1996–2019. doi: 10.1080/17470218.2014.990392
- Walther, C., Schweinberger, S. R., Kaiser, D., and Kovacs, G. (2013). Neural correlates of priming and adaptation in familiar face perception. *Cortex* 49, 1963–1977. doi: 10.1016/j.cortex.2012.08.012
- Watson, T. L., and Clifford, C. W. (2003). Pulling faces: an investigation of the face-distortion aftereffect. *Perception* 32, 1109–1116. doi: 10.1068/p5082
- Watson, T. L., and Clifford, C. W. (2006). Orientation dependence of the orientation-contingent face aftereffect. *Vision Res.* 46, 3422–3429. doi: 10.1016/j.visres.2006.03.026
- Webster, M. A. (2011). Adaptation and visual coding. *J. Vis.* 11, 3. doi: 10.1167/11.5.3
- Webster, M. A., Kaping, D., Mizokami, Y., and Duhamel, P. (2004). Adaptation to natural facial categories. *Nature* 428, 557–561. doi: 10.1038/nature02420
- Webster, M. A., and MacLeod, D. I. (2011). Visual adaptation and face perception. *Philos. Trans. R. Soc. Lond. Series B Biol. Sci.* 366, 1702–1725. doi: 10.1098/rstb.2010.0360
- Webster, M. A., and MacLin, O. H. (1999). Figural aftereffects in the perception of faces. *Psychon. Bull. Rev.* 6, 647–653. doi: 10.3758/BF03212974

- Yamashita, J. A., Hardy, J. L., De Valois, K. K., and Webster, M. A. (2005). Stimulus selectivity of figural aftereffects for faces. *J. Exp. Psychol. Hum. Percept. Perform.* 31, 420–437. doi: 10.1037/0096-1523.31.3.420
- Young, A. W., Flude, B. M., Hellowell, D. J., and Ellis, A. W. (1994). The nature of semantic priming effects in the recognition of familiar people. *Br. J. Psychol.* 85, 393–411. doi: 10.1111/j.2044-8295.1994.tb02531.x
- Zarate, M. A., and Sanders, J. D. (1999). Face categorization, graded priming, and the mediating influences of similarity. *Soc. Cogn.* 17, 367–389. doi: 10.1521/soco.1999.17.4.367
- Zhao, L., and Chubb, C. (2001). The size-tuning of the face-distortion after-effect. *Vision Res.* 41, 2979–2994. doi: 10.1016/S0042-6989(01)00202-4

**Conflict of Interest:** The authors declare that the research was conducted in the absence of any commercial or financial relationships that could be construed as a potential conflict of interest.

Copyright © 2020 Mueller, Utz, Carbon and Strobach. This is an open-access article distributed under the terms of the Creative Commons Attribution License (CC BY). The use, distribution or reproduction in other forums is permitted, provided the original author(s) and the copyright owner(s) are credited and that the original publication in this journal is cited, in accordance with accepted academic practice. No use, distribution or reproduction is permitted which does not comply with these terms.



# Cortical Microcircuit Mechanisms of Mismatch Negativity and Its Underlying Subcomponents

Jordan M. Ross<sup>1,2</sup> and Jordan P. Hamm<sup>1,2,3\*</sup>

<sup>1</sup>Neuroscience Institute, Georgia State University, Atlanta, GA, United States, <sup>2</sup>Center for Behavioral Neuroscience, Georgia State University, Atlanta, GA, United States, <sup>3</sup>Center for Neuroinflammation and Cardiometabolic Diseases, Georgia State University, Atlanta, GA, United States

## OPEN ACCESS

### Edited by:

Mehdi Adibi,  
University of New South Wales,  
Australia

### Reviewed by:

Stanislav S. Zakharenko,  
St. Jude Children's Research  
Hospital, United States  
Behtash Babadi,  
University of Maryland, College Park,  
United States

### \*Correspondence:

Jordan P. Hamm  
jhamm1@gsu.edu

**Received:** 30 September 2019

**Accepted:** 17 March 2020

**Published:** 31 March 2020

### Citation:

Ross JM and Hamm JP  
(2020) Cortical Microcircuit  
Mechanisms of Mismatch Negativity  
and Its Underlying Subcomponents.  
*Front. Neural Circuits* 14:13.  
doi: 10.3389/fncir.2020.00013

In the neocortex, neuronal processing of sensory events is significantly influenced by context. For instance, responses in sensory cortices are suppressed to repetitive or redundant stimuli, a phenomenon termed “stimulus-specific adaptation” (SSA). However, in a context in which that same stimulus is novel, or deviates from expectations, neuronal responses are augmented. This augmentation is termed “deviance detection” (DD). This contextual modulation of neural responses is fundamental for how the brain efficiently processes the sensory world to guide immediate and future behaviors. Notably, context modulation is deficient in some neuropsychiatric disorders such as schizophrenia (SZ), as quantified by reduced “mismatch negativity” (MMN), an electroencephalography waveform reflecting a combination of SSA and DD in sensory cortex. Although the role of NMDA-receptor function and other neuromodulatory systems on MMN is established, the precise microcircuit mechanisms of MMN and its underlying components, SSA and DD, remain unknown. When coupled with animal models, the development of powerful precision neurotechnologies over the past decade carries significant promise for making new progress into understanding the neurobiology of MMN with previously unreachable spatial resolution. Currently, rodent models represent the best tool for mechanistic study due to the vast genetic tools available. While quantifying human-like MMN waveforms in rodents is not straightforward, the “oddball” paradigms used to study it in humans and its underlying subcomponents (SSA/DD) are highly translatable across species. Here we summarize efforts published so far, with a focus on cortically measured SSA and DD in animals to maintain relevance to the classically measured MMN, which has cortical origins. While mechanistic studies that measure and contrast both components are sparse, we synthesize a potential set of microcircuit mechanisms from the existing rodent, primate, and human literature. While MMN and its subcomponents likely reflect several mechanisms across multiple brain regions, understanding fundamental microcircuit mechanisms is an important step to understand MMN as a whole. We hypothesize that SSA reflects adaptations occurring at synapses along the sensory-thalamocortical pathways, while DD depends on both SSA inherited from afferent inputs and resulting disinhibition of non-adapted neurons arising from the distinct physiology and wiring properties of local interneuronal subpopulations and NMDA-receptor function.

**Keywords:** adaptation, deviance detection, interneuron, NMDA, somatostatin, parvalbumin, cortex, schizophrenia

## INTRODUCTION

Organisms are continuously inundated with sensory information. Given that the majority of incoming information is redundant or behaviorally unimportant, organisms need to be able to suppress the neural processing of irrelevant stimuli to conserve resources. Such adjustments are made possible by a process referred to as stimulus-specific adaptation (SSA; Adrian, 1926a,b; Adrian and Zotterman, 1926a,b; Nomoto et al., 1964; Pérez-González and Malmierca, 2014). Neurons can adapt to repetitive sensory information, reducing their firing responses at various stages of processing, from initial sensation to higher-order encoding, a phenomenon that occurs across all sensory modalities (McLaughlin and Kelly, 1993; Dalton, 2000; Wagner et al., 2006; Kohn, 2007; Pérez-González and Malmierca, 2014; Heil and Peterson, 2015). However, the sensory world is dynamic and the ability to perceive changes and adjust behavior accordingly determines the success of the organism. While organisms must be able to undergo SSA, they must also be able to quickly detect changes that differ from what has recently been experienced (or what can thereby be predicted), as it may signal salient information. This ability of neurons and neural systems to detect abrupt, unexpected variation from the constant, expected sensory milieu (or a set of presented stimuli) is known as deviance detection (DD) and typically involves an increase in firing responses (Malmierca et al., 2009; Antunes et al., 2010; Hamm and Yuste, 2016; Musall et al., 2017; Parras et al., 2017; Polterovich et al., 2018).

Together, SSA and DD represent important, complementary phenomena—the ability to adapt to contextually redundant information (SSA) while maintaining the ability to detect when a change occurs (DD) that might signal relevant, important information. Notably, most of the research regarding these phenomena has been carried out in the auditory and visual systems, and thoughtful experimental design efforts to differentiate SSA and DD (**Figure 1**) are an emerging trend in the study of sensory context processing (Harms et al., 2014; Chen et al., 2015; Hamm and Yuste, 2016; Wiens et al., 2019). For example, sensory “oddball” paradigms involve the presentation of a repetitive, highly probable “standard” (or “redundant”) stimulus typically occurring between 75–95% of trials (which occur rapidly, at least once every second) with a rarer interspersed “target” (or “deviant”) stimulus (**Figure 1A**). Studies employing a single “oddball” paradigm are the most common, yet alone they cannot differentiate SSA and DD. A simple difference wave (in the EEG) or difference in neuronal spike rate between “redundants” and “deviants” conflate these two components. Control paradigms such as “flip flop” sequences (**Figure 1A**; i.e., two back to back oddball runs where the deviant and the redundant are swapped) ensure DD is not a function of physical stimulus characteristics. Another commonly used technique, the “many standards” control (**Figure 1B**) allows researchers to determine whether DD signatures are due to the relative rarity of “deviant” stimuli or result from true detection of deviations from expected patterns (Schröger and Wolff, 1996; Jacobsen and Schröger, 2001, 2003; Jacobsen et al., 2003b). Further,

“cascade” sequences (**Figure 1C**) are used to ensure that the ordering effects in basic “oddball” presentations do not contribute to apparent DD. Stimuli in the cascade control are always preceded by the same stimulus, like the typical oddball sequence, and unlike the many-standards control. Also unlike the many-standards control, the cascade sequence establishes a pattern of stimulus presentations with (overall) less influence of SSA.

While SSA and DD are typically measured at the neuronal level, they likely reflect circuit-level computations (Natan et al., 2015, 2017; Hamm and Yuste, 2016), and are robust when measured with gross-electrophysiological techniques reflecting summed activity within a neocortical region (local field potential, LFP; electroencephalogram, EEG). Thus, SSA and DD can be assessed at multiple levels in multiple species, including humans where non-invasive measurements of neurophysiology remain constrained to a more gross, macro-level (i.e., EEG or MEG). Despite their presence across species, human EEG studies, especially in clinical and neuropsychiatric research, have focused instead on an aggregate measure of context processing: the mismatch negativity (MMN; Näätänen, 1995; Näätänen and Alho, 1995b; Tiitinen et al., 1997). MMN is an event-related potential (ERP) wherein a more negative scalp potential (occurring about 150 ms post-stimulus onset) is elicited by the “deviant” stimulus than by the “redundant” stimulus in an oddball paradigm (**Figures 2A–C**). Diminished or absent MMN is a classic, highly replicated biomarker for sensory context processing deficits common in schizophrenia (SZ) and other psychotic disorders (Näätänen et al., 2011, 2014; Lavoie et al., 2019; Tada et al., 2019), so efforts to describe the biological substrates and mechanisms of human MMN remain paramount. Indeed, some progress has been made to understand MMN generation (Garrido et al., 2009), but confoundingly, MMN comprises both SSA and DD (**Figure 2E**). These subcomponents are rarely assessed separately in human clinical studies (which often just involve a single “oddball” paradigm), and if these subcomponents depend on different neurobiology or circuit functions, a direct interpretation of the neural underpinnings of SZ-MMN deficits will remain challenging.

This review aims to examine recent studies regarding the mechanisms of SSA and DD in animals and, when appropriate, compare them to human studies of MMN. Unfortunately, it remains unclear whether human SZ populations exhibit deficits in SSA, DD, both, neither, and/or some additional MMN-relevant component, yet the fact that DD, in particular, may depend on some neuronal functions with known SZ relevance (e.g., interneurons) merits consideration (Hamm and Yuste, 2016). Here we show that the emerging literature demonstrates that, indeed, SSA and DD can be separated experimentally at the cellular and circuit level in rodents, but it remains unclear how they are related mechanistically and concerning the underlying cells and circuits which generate them. Therefore, we aim to discuss the underlying circuits identified through animal experimentation, proposing a hypothetical model of these circuits in layer 2/3 of the neocortex (**Figure 3**). Our model, though limited by virtue (Box et al., 2005),

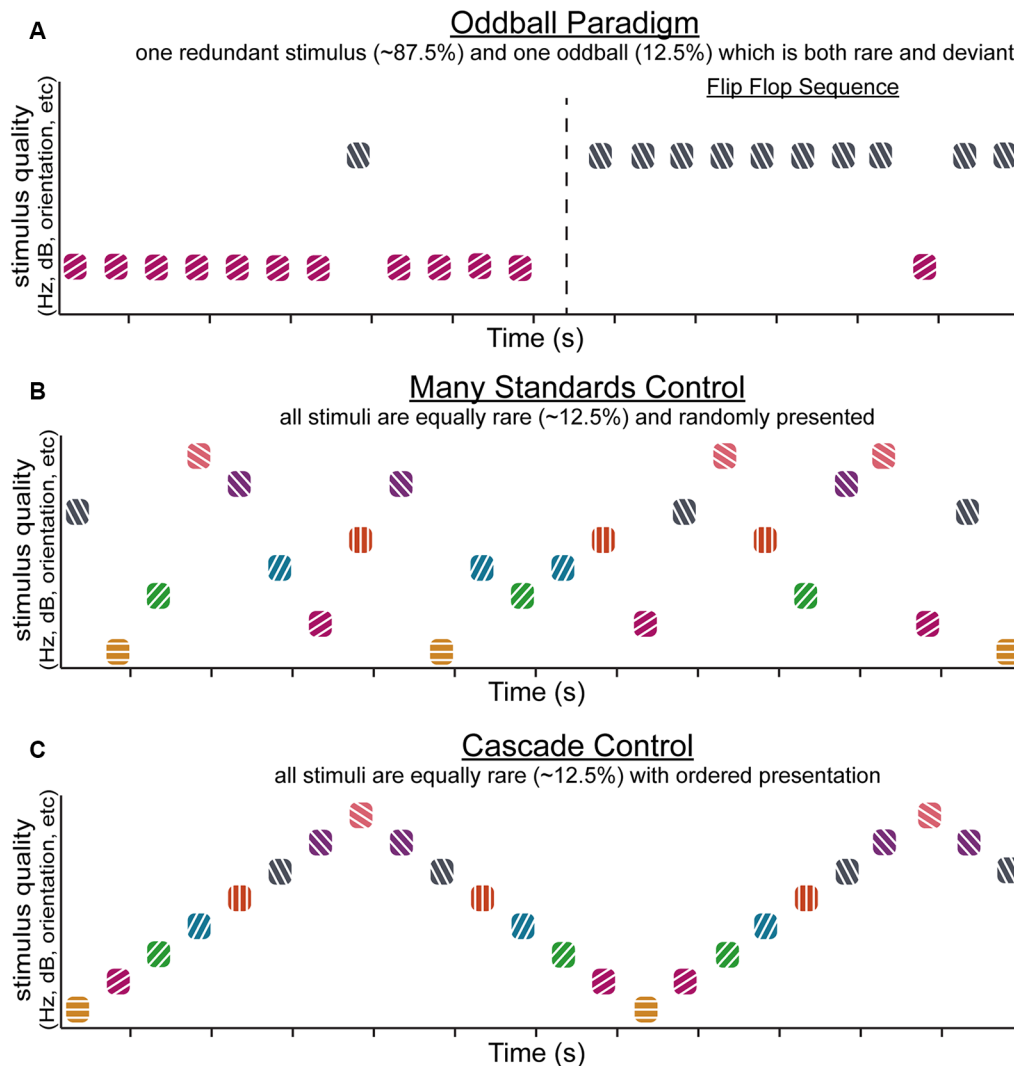


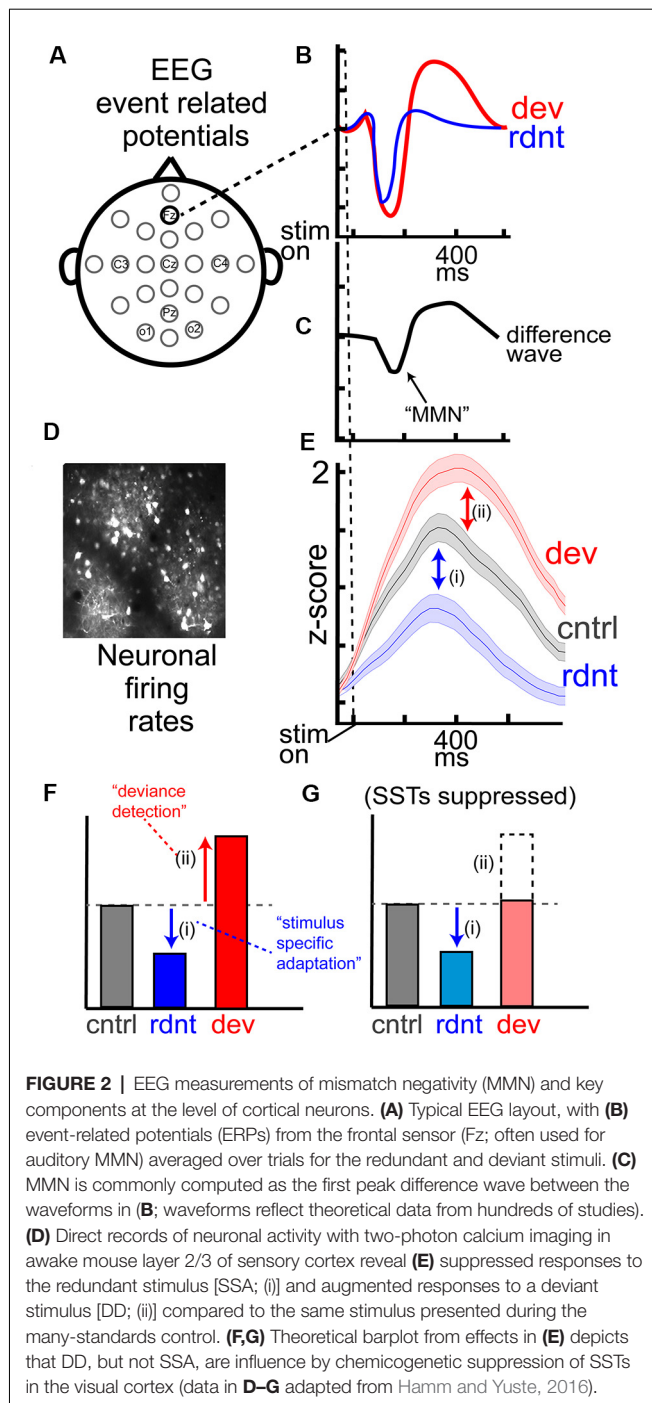
**FIGURE 1 |** The oddball paradigm and commonly associated control sequences. Simplified schematics demonstrating various stimulus sequences that can be used to investigate stimulus-specific adaptation (SSA) and deviance detection (DD). The typical oddball sequence (**A**, left) utilizes two stimuli that differ in stimulus quality. One of the stimuli is designated the “redundant” and accounts for the majority of the presentations (in this case ~90%). The overabundance of redundant presentations establishes a regular pattern that is violated by “oddball” (or “deviant”) stimuli, which rarely occur (in this case ~10% of presentations). An extension of the oddball paradigm, the flip flop sequence (**A**, right) flips the redundant and oddball stimuli to control for differences in neural responses that might arise due to the physical characteristics of the stimuli. The many standards control sequence (**B**) presents several stimuli within a sensory modality that differ in terms of stimulus quality so that each appears with equally rare probability, in this case, ~12.5% of the time. There is no established pattern of stimulus presentations. The stimuli in the many standards sequence are presented randomly, unlike stimuli in a cascade control sequence (**C**), where several stimuli appear with equally rare probability (again, in this case, ~12.5%) but are presented in ascending or descending order such that the difference in stimulus quality is the same for each presentation.

will hopefully prove useful for future investigations of sensory context processing in the neocortex.

## THE “ODDBALL” PARADIGM

To quantify sensory context processing in human participant samples, researchers often record EEG and employ an “oddball” paradigm (**Figures 1, 2A–C**). This paradigm and related studies have been thoroughly reviewed elsewhere (Picton, 1992; Näätänen, 1995), and the basic structure of stimulus presentation

is described above (**Figure 1**). Importantly, these stimuli can be virtually of any sensory modality, all of which have produced MMN analogs in the EEG (Tiitinen et al., 1997; Shinzaki et al., 1998; Pause and Krauel, 2000; Rosburg et al., 2007; Escera et al., 2014; Kremlacek et al., 2016). One of the strengths of the MMN is that it is independent and unaffected by active attention to the presented stimuli (Schröger et al., 1992; Näätänen and Alho, 1995a; Marshall et al., 1996; Tiitinen et al., 1997; Fischer et al., 2000; Näätänen, 2000; Ibáñez et al., 2009; Näätänen et al., 2010), unlike, for example, the P300, which requires an



ongoing target detection task, occurs 150 ms later than the MMN, and likely involves synchronized activity across many sensory and non-sensory cortical and subcortical brain areas. This added complexity makes P300 less valuable for a pure assessment of contextual modulation of sensory processing (Picton, 1992; Näätänen, 1995; Ethridge et al., 2015). This is especially important given that people with SZ often have both attentional and pre-attentive processing deficits (Rabinowicz et al., 2000; Schechter et al., 2006; Elshaikh et al., 2015; Hamm

et al., 2015; Javitt and Freedman, 2015), and, thus, a marker of pre-attentive context processing like the MMN is advantageous for animal experimentation where attention may be difficult to obtain or gauge.

In general, the fact that “deviant” stimuli in the “oddball” paradigm elicit an enhanced response in sensory cortex matches well with results obtained across multiple sensory modalities and from several species (Featherstone et al., 2018; Tada et al., 2019) including non-human primates (Javitt et al., 1992; Ueno et al., 2008; Komatsu et al., 2015), rats (Nakamura et al., 2011; Shiramatsu et al., 2013; Harms et al., 2014), and mice (Umbricht et al., 2005; Ehrlichman et al., 2008; Chen et al., 2015), suggesting that the oddball paradigm is well suited for studying contextual modulation of sensory cortical responses in both human and animal studies and that underlying mechanisms are likely conserved across sensory modality. Still, establishing a one-to-one correspondence of gross-level brain potentials/waves (such as the N1, P2, and MMN) between humans and animals (Ehrlichman et al., 2008), and even between sensory modality within human samples (Kremlacek et al., 2016), has not been straightforward. The latencies and shapes of ERPs within and across species depend on several factors not directly related to the fundamental sensory or cognitive “computation,” including the speed of neuronal transmission from primary sensory afferents to neocortex and the location of recording electrodes with regards to the generator of the ERP waveform (Luck and Kappenman, 2013).

On the other hand, animal studies do offer a direct measure of the firing responses of individual neurons within the sensory cortex, and enable deeper, more direct insight into biological mechanisms (**Figures 2D,E**). An additional advantage presented by animal models is that virtually all experimental practices employed in human studies have homologs for animal experimentation, allowing for direct comparison while simultaneously offering more mechanistic insight. For instance, ketamine, along with another N-methyl-D-aspartate receptor (NMDAR) antagonists, is known to reduce the MMN in humans as well as rodents and non-human primates (Ehrlichman et al., 2008; Gil-Da-Costa et al., 2013; Chen et al., 2015; Haaf et al., 2018; Schuelert et al., 2018).

Furthermore, the oddball task applies to a wide variety of experimental assays in animal research. In addition to the standard scalp and intracranial LFP recordings (Ayala et al., 2012; Ayala and Malmierca, 2015) that are relatable to human EEG measures, mouse models, in particular, are compatible with more cutting-edge methods that allow direct visualization and/or manipulation of neural activity, such as electrophysiological cell recordings (Taaseh et al., 2011; Chen et al., 2015; Duque et al., 2016; Parras et al., 2017), two-photon (2P) imaging, and Opto/chemico-genetics (Natan et al., 2015; Hamm and Yuste, 2016). These newer imaging techniques provide significantly improved spatial resolution over traditional methods. For example, recent work using a combination of two-photon microscopy and LFP recordings verified the presence of an MMN-like LFP response and established that both SSA and DD could be reliably measured at the level of individual neurons (Hamm and Yuste, 2016).

Mice also allow for genetic dissection of specific cell populations. This represents a significant improvement over traditional methods that were only able to measure from a heterogeneous population with limited spatial resolution. Recent studies have focused on principal neuron populations as well as inhibitory interneurons and are beginning to yield significant insights into the mechanisms of MMN and sensory context processing (Natan et al., 2015; Duque et al., 2016; Hamm and Yuste, 2016; Musall et al., 2017). Additionally, the oddball paradigm has been used in conjunction with pharmacology (Ehrlichman et al., 2008, 2009; Bristow et al., 2016; Aleksandrov et al., 2018; Harms et al., 2018; Lee et al., 2018), optogenetics (Natan et al., 2015, 2017), and chemogenetics (Hamm and Yuste, 2016) to isolate mechanisms responsible for the components of MMN. The genetic access along with the available manipulations that animal models afford allows significant insights to the mechanisms of MMN in human populations, both basic and clinical.

Yet, because the correspondence of mouse responses to human-like MMN potentials measured at the scalp is unclear, animal studies of MMN-like processing have been typically held to the additional criterion of differentiating true DD from SSA (Harms et al., 2016). As described above, this requires at least two additional stimulus presentation paradigms, the flip flop and the many-standards paradigm (Figure 1; Hamm and Yuste, 2016), enabling the researcher to separate DD in a neuron's augmented response to the "oddball" from its simple preference to that stimulus and the absence of SSA (Harms et al., 2016). Indeed, mouse sensory cortices do display both SSA (i.e., response to stimulus in many-standards control is greater than the response to the same stimulus when presented repetitively in oddball) and DD (response to stimulus in oddball is greater than the response to the same stimulus in many-standards control), and the ability to apply the above-mentioned technologies is leading to important inferences about the mechanisms of SSA and DD (Hamm and Yuste, 2016; Musall et al., 2017; Parras et al., 2017; Polterovich et al., 2018), which we will describe below. It remains unknown whether SSA and DD are distinct processes and whether they are dependent on one another—in other words, must a neuronal circuit undergo adaptation to detect deviations from previous stimulation, and vice versa, is DD necessary for maintaining stimulus adaptation?

## SPECIFIC STIMULUS ADAPTATION

Adaptation or reduced neuronal responsivity, selective to repeated stimuli occurs in all primary sensory cortices (Figures 2D–F) but is also measurable in some subcortical structures (Nelken, 2014). For example, in auditory processing SSA can be detected in the inferior colliculus, a midbrain structure involved in auditory processing that lies upstream of both primary thalamic nuclei and auditory cortex. GABA, primarily through GABA<sub>A</sub> receptors, appears to exert its effects through overall gain-control in the inferior colliculus, by regulating the magnitude of neural excitation to repeated stimulation (Duque et al., 2014). The local inhibition accounts for a significant proportion of SSA but cannot completely

explain the altered neural responses (Ayala and Malmierca, 2018), indicating other mechanisms play a role as well. Similarly, cholinergic and endocannabinoid systems act to modulate SSA subcortical auditory and olfactory responses *en masse* but are not responsible for generating SSA (Ayala and Malmierca, 2015; Valdés-Baizabal et al., 2017; Ogg et al., 2018). Iontophoretic application of both acetylcholine and cannabinoid agonists appear to increase responses (through muscarinic receptors and cannabinoid receptors type 1, respectively) specifically to repetitive stimulations, thereby reducing SSA, without affecting neural responses to the deviant tone (Ayala and Malmierca, 2015; Valdés-Baizabal et al., 2017). All together these effects likely propagate to downstream primary cortices, thus altering the input to these regions in a stimulus specific manner and driving behavioral responses. There is indirect evidence to suggest that this is the case as stimulation of cholinergic release in the olfactory bulb is sufficient to reinstate olfactory bulb responses to repetitive stimuli (in both anesthetized and awake conditions) and is sufficient to reinstate behavioral investigatory behaviors to repetitive olfactory stimuli (Ogg et al., 2018); however, it remains unclear the extent to which these processes directly contribute to SSA in primary sensory cortices to contribute to cortical SSA and perceptual adaptation.

At the level of individual neurons, SSA can occur at the input-output stage by changing the intrinsic response properties of presynaptic neurons, such as spike frequency (Fairhall et al., 2001; Wilent and Contreras, 2005; Pozzorini et al., 2013; Ogg et al., 2015), or by modulating the strength of input onto postsynaptic neurons *via* synaptic depression (Abbott et al., 1997; Tsodyks and Markram, 1997; Anwar et al., 2017; Musall et al., 2017). For example, across all sensory cortices, repetitive stimulation induces spike frequency adaptation, an increase in neuronal firing threshold following an initial response that reduces the firing frequency of the neuron. Spike frequency adaptation is long-lasting in neocortical pyramidal cells (PYRs) and can cause temporal decorrelation of output spikes (Pozzorini et al., 2013). Such mechanisms at the level of individual neurons or populations of neurons are putative mechanisms by which SSA occurs in the global cortical system. Single synapses can also change in response to repeated stimulation, demonstrating short-term facilitation, depression, or a combination of the two which acts to dynamically filter sensory input (Suzuki and Bekkers, 2006; Kuo and Trussell, 2011; Nikolaev et al., 2013). In essence, sensory input activates a specific population of neurons that are all tuned towards that specific input. Continual presentations of that stimulus ultimately lead to synaptic depression of those neurons, which in turn reduces the excitatory drive onto downstream cortical neurons (Mill et al., 2011). While this adaptation is measurable in single neurons, individual neurons participate in larger networks so changes in a population of neurons propagate throughout the sensory system, which is relevant to wide-scale sensory coding. It is important to remember that networks of neurons rather than individual neurons are responsible for sensory adaptation, even though adaptive processes of individual neurons likely contribute to cortical SSA, as SSA cannot be explained by intrinsic properties of

single neurons alone (Mill et al., 2011; Solomon and Kohn, 2014; Malmierca et al., 2015).

Cortical SSA has also been measured in the absence of cortico-cortical synaptic depression, instead finding that repeated sensory stimulation reduces thalamocortical input (Chung et al., 2002). This suggests that decreased thalamic input to cortical regions contributes to cortical SSA during repeated stimulation, such as during an oddball paradigm (Natan et al., 2015). Thalamocortical synaptic depression was once thought to exist only during development but evidence demonstrates it is conserved in adults (Blundon et al., 2011), making it an attractive candidate for an underlying mechanism of cortical SSA. Given that afferent projections from thalamus represent the primary pathway for most sensory information to sensory cortical regions, altered thalamic input to the cortex, or thalamocortical gating, likely plays an important role in controlling cortical responses to sensory input (Hillenbrand and van Hemmen, 2002; Wang et al., 2010; Whitmire et al., 2016). While nearly all sensory information is relayed through the thalamus to sensory cortices, olfactory information bypass the thalamus entirely but olfactory cortices still exhibit SSA (McCollum et al., 1991; Wilson, 1998a,b; 2000; Best and Wilson, 2004), suggesting that SSA is a combination of cortical synaptic depression as well as thalamocortical gating (Lundstrom et al., 2010; Blundon and Zakharenko, 2013; Nelken, 2014).

While the role of SSA specifically in SZ-related MMN deficits remains to be demonstrated (Michie et al., 2016), people with SZ can manifest what appears to be reduced cortical adaptation (Javitt and Freedman, 2015; Javitt and Sweet, 2015; Andrade et al., 2016) and thalamocortical gating (Adler et al., 1998). Thalamocortical gating alone cannot explain SSA (Lundstrom et al., 2010; Nelken, 2014), and ERP studies in general in SZ, including the “P50 gating” ERP, often cannot disentangle true deficits in ERP adaptation from simply reduced baseline ERPs (i.e., reduced cortical response to the initial stimulus vs. the repeated one (Clementz et al., 1998; Hamm et al., 2014). Still, the evidence linking SZ to altered thalamocortical connectivity extends beyond MMN and P50 paradigms and this disconnect is thought to underlie several aspects of symptomatology (Sodhi et al., 2011; Klingner et al., 2014; Chen et al., 2019; Hua et al., 2019; Huang et al., 2019; Tu et al., 2019). It is noteworthy that some genetic SZ animal models possess altered thalamocortical networks (Chun et al., 2014; Kröcher et al., 2015), and administering ketamine, which blocks NMDARs to produce SZ-like phenotypes in healthy patients and animals alike, alters thalamocortical connectivity (Höflich et al., 2015; Becker et al., 2016; Furth et al., 2017). If reduced SSA does exist in SZ, it would remain difficult to determine the extent to which this is related to reduced thalamocortical connectivity, since reduced signaling would lead to smaller baseline responses to stimuli in sensory cortex (which has been demonstrated in SZ; Rosburg et al., 2008; Hamm et al., 2014). Reduced drive, to begin with, would effectively appear to reduce adaption when normalized (Clementz et al., 1998; Patterson et al., 2008). Additionally, from a cognitive perspective encoding “redundancy” or sensory context would be weaker when the signals are weaker in general.

One point to consider in this problem is that NMDAR blockade, a face-valid model of SZ sensory processing features, also reduces MMN in humans and animals (Ehrlichman et al., 2008; Gil-Da-Costa et al., 2013; Haaf et al., 2018; Schuelert et al., 2018). The nature of how NMDAR blockade affects the time-course and oscillatory aspects of auditory MMN has led to the interpretation that DD specifically is NMDAR-dependent (Javitt et al., 1996; Lee et al., 2018). There remains some discrepancy regarding whether and how NMDARs are involved in SSA (Farley et al., 2010; Chen et al., 2015). Farley et al. (2010) recorded multiunit activity in the auditory cortex of anesthetized rats and showed that systemic NMDAR blockade with MK801 did not affect gross SSA. On the other hand, Chen et al. (2015) report a significant effect of direct MK801 infusion on SSA in excitatory neurons based on whole-cell recordings in the auditory cortex of anesthetized mice. Interestingly, this effect effectively eliminated all stimulus-driven firing responses, so it remains unclear whether some aspects of SSA may have survived in excitatory neurons with lower doses of NMDAR blockade and/or in awake preparations, perhaps inherited from upstream sources. Additional work will be needed involving local NMDAR block at different concentrations.

It is important to note that sensory adaptation can be broadly defined as any stimulus- or context-dependent modulation of sensation or perception, and is a phenomenon that has been described across all modalities and all stages of sensory encoding and processing. One such form of sensory adaptation is forward suppression, in which processing of a stimulus can be modulated by a different immediately preceding stimulus (Plomp, 1964; Relkin and Turner, 1988; Scholes et al., 2011). Work in the auditory system has isolated two separate mechanisms that produce suppressed cortical responses on different timescales. Forward suppression in auditory cortex can last for hundreds of milliseconds; however, suppression in the first 100 ms seems to be a result of GABAergic postsynaptic inhibition whereas suppression beyond the first 100 ms is mediated by synaptic depression at thalamocortical projections due to a switch from burst firing to single action potential firing (Calford and Semple, 1995; Brosch and Schreiner, 1997; Wehr and Zador, 2005; Bayazitov et al., 2013). In this review, we refer to SSA, which can be thought of as a stimulus-specific, repetition-dependent form of forward suppression. The bursting switch which underlies auditory cortex forward suppression is also thought to explain part, but not all, of SSA (Bayazitov et al., 2013); however, this has not been systematically tested. Forward suppression as well as other forms of sensory adaptation, such as sensory gating, may be embedded in SSA and the oddball paradigm (Boutros et al., 1995; Wang et al., 2010); however, they likely affect all stimuli (redundant, deviant, and/or control stimuli) equally.

SSA can also operate on different timescales, with cortical responses exhibiting reduced responses to experienced stimuli for milliseconds to days (Condon and Weinberger, 1991; Ulanovsky et al., 2004; Kato et al., 2015). As with forward suppression, the different timescales of SSA are thought to rely on separate mechanisms. For example, long-lasting multiday adaptation appears to reflect increased recruitment of inhibitory

interneurons, which can be reversed if the stimulus becomes behaviorally relevant (Kato et al., 2015). Therefore, the timing of both stimulus presentation and length of experimental paradigms represent important methodological considerations for further dissecting mechanisms of SSA.

## DEVIANCE DETECTION

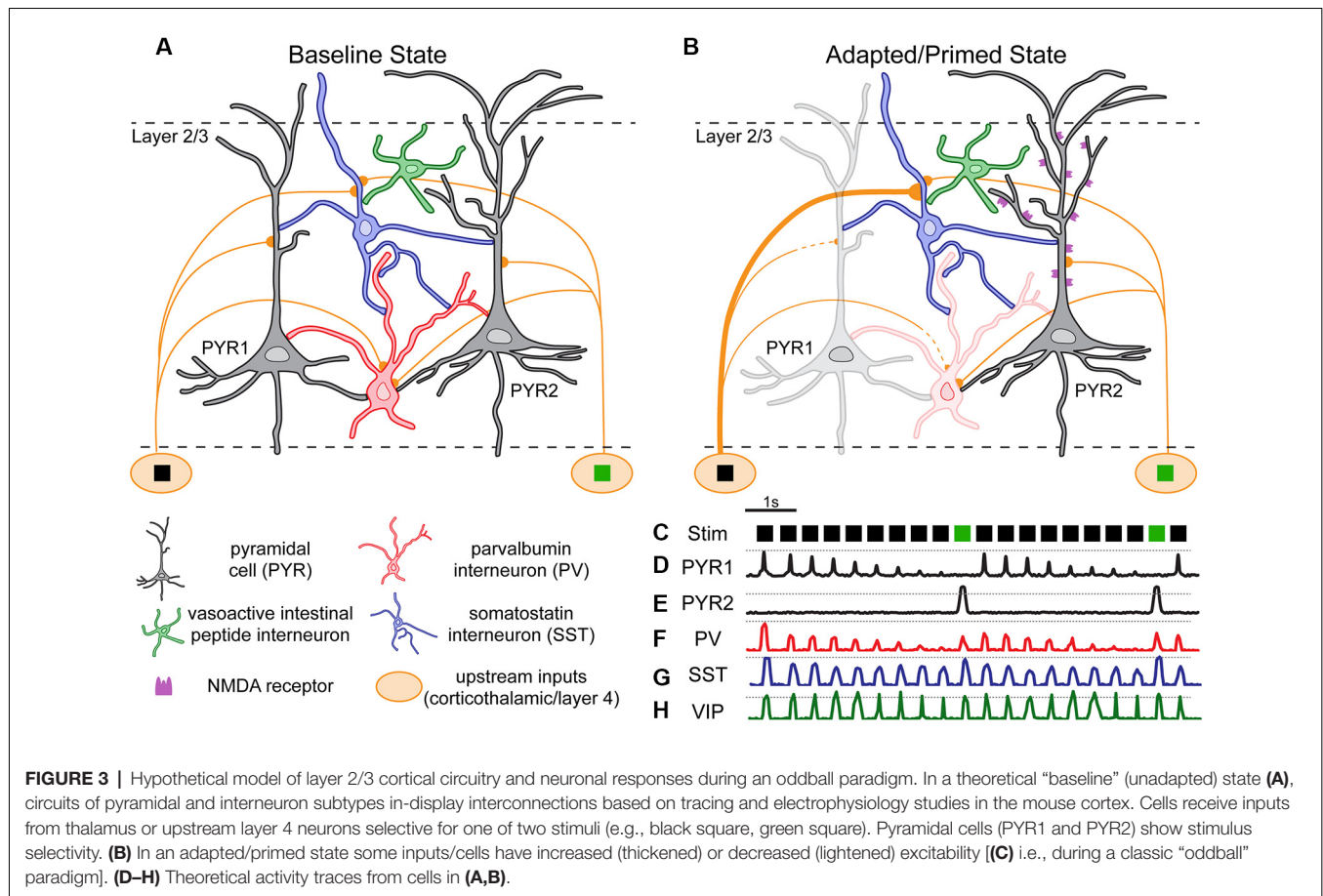
Like SSA, DD occurs in primary cortices (**Figures 2E,F**; Hamm and Yuste, 2016; Musall et al., 2017; Parras et al., 2017; Polterovich et al., 2018) as well as sub-cortical structures (Kohn, 2007; Anderson et al., 2009; Malmierca et al., 2009; Antunes et al., 2010) and measurable DD is seemingly stronger at subsequent downstream processing stages (Parras et al., 2017). Notably, in auditory paradigms brainstem nuclei do not appear to contribute to SSA or DD; however, subcortical neurons exhibiting SSA and DD receive strong input from the primary auditory cortex (Ayala et al., 2015). Therefore, it was previously postulated that DD measured in sub-cortical structures was a reflection of DD in primary sensory cortices backpropagating to lower regions (Nelken and Ulanovsky, 2007). However, deactivating sensory cortices does not appear to affect subcortical DD (Antunes and Malmierca, 2011; Anderson and Malmierca, 2013; Malmierca et al., 2015), suggesting DD may be independently generated or enhanced at each stage (Ayala and Malmierca, 2012). Recent work in the somatosensory cortex indicates cortical DD is due primarily to intracortical circuitry at specific cortical layers that may be enhanced by input from subcortical structures (Musall et al., 2017). In the visual cortex, DD may not be present in initial thalamic inputs at all, originating within intracortical circuits entirely (Hamm et al., 2018).

Intracortical circuits comprise complex excitatory-inhibitory interactions to shape sensory processing (Wood et al., 2017). The activity of excitatory neurons is sculpted by feedback from inhibitory interneurons, which makes them an interesting focus for understanding information processing within the circuit. Two of the largest populations of GABAergic inhibitory interneurons, parvalbumin- (PV) and somatostatin- (SST) positive interneurons, have gained significant attention in studies of DD, especially in the auditory cortex where they are known to influence representations of auditory stimuli. Interestingly, optogenetic stimulation of PVs in the auditory cortex increases the functional connectivity of the thalamocortical circuit (Hamilton et al., 2013), which may enhance processing, and even perception, of sensory inputs. In support of this, stimulation of PVs in the auditory cortex has been shown to enhance behavioral performance on tone frequency detection tasks, while suppression decreases behavioral auditory discrimination (Aizenberg et al., 2015). However, optogenetic stimulation of both PVs and SSTs in the auditory cortex can cause contradictory and confounding results when viewing the single-unit activity of aspects of auditory processing (Seybold et al., 2015; Phillips and Hasenstaub, 2016). Future work should include careful design and interpretation of causal manipulations of interneuron populations to dissect how interneurons function (both in isolation and in concert) to control cortical functions and sensory processing. Besides, other classes and sub-classes of neocortical

inhibitory neurons, such as vasoactive intestinal polypeptide (VIP) neurons which often inhibit other inhibitory interneurons, have yet to be studied in this context and future studies should aim to include this unique and comparatively understudied class of interneurons.

Beyond understanding how cortical interneuron populations contribute to basic sensory processing, it is of interest to understand how they contribute to SSA and DD specifically. The use of transgenic animal models (Feil et al., 2009) allows for specific investigation and manipulation of subpopulations of neurons during the oddball paradigm to characterize neural activity. For example, studies using electrophysiological recordings of excitatory PYRs as well as PV and SST interneurons in auditory cortex supports evidence that each of these cell types demonstrate oddball driven responses (Chen et al., 2015; Natan et al., 2015). That is, these significant effects were computed between responses to deviants vs. redundants, potentially involving both SSA and DD. While Chen et al. (2015) included a separate analysis of genuine DD (i.e., responses to deviants vs. a many-standards control), PYRs, SSTs, and PVs all lacked significant DD in their spiking output (an effect potentially influenced by anesthesia). PYRs nevertheless demonstrated both early (0–100 ms after tone onset) and late (200–400 ms after tone onset) phase oddball effects (Chen et al., 2015), which align with the late component signals detected in human MMN and supports the use of oddball paradigms in mouse models as translationally applicable to humans. Other studies using mouse models have also demonstrated neuronal predictive activity that gives rise to large mismatch responses when expected patterns are violated, which mimics human MMN responses (Parras et al., 2017). Characterizing and understanding the contribution of interneuron activity during oddball paradigms may reveal physiological mechanisms of SSA, DD, and composite MMN that are relevant to understanding these phenomena in humans.

The fact that interneurons show oddball and other prediction error-driven activity (Chen et al., 2015; Garrett et al., 2020), suggests GABAergic interneurons may play a role in modulating DD in PYRs, which putatively gives rise to a perception of novelty or deviance. By recording from excitatory PYRs while opto-/chemogenetically modulating PVs and SSTs, researchers have been able to dissect contributions of these interneurons to DD in excitatory neocortical cells. Optogenetically silencing PVs in the auditory cortex results in loss of overall gain control, equally enhancing responses to repeated stimuli, thereby reducing SSA, and deviant stimuli. However, silencing SSTs enhanced the firing rate of excitatory cells only in response to repeated stimuli (i.e. “redundants”), without altering the firing rate in response to deviant stimuli (Natan et al., 2015). While this auditory cortex study did not specifically dissect DD from SSA with control paradigms, another study did and found that chemogenetic suppression of SSTs in the visual cortex reduces DD in excitatory neurons (**Figure 2G**; Hamm and Yuste, 2016). While differences in the use of control paradigms preclude a direct comparison of these effects, it's important to note that, in both studies, SSTs



appear to impart context selective inhibition on PYRs (while PVs do not). Further, the apparent differences on which stimulus type SSTs appear to exert the largest effect (redundant vs. deviant) could arise from differences in experimental paradigm [inclusion of control paradigms; optogenetic (Natan et al., 2015) vs. chemogenetic (Hamm and Yuste, 2016) manipulation of SSTs; sensory cortex studied]. Methods of interneuron silencing are important to consider as optogenetic suppression offers temporally precise and highly transient inactivation of desired cells, while chemogenetic suppression lasts several minutes to hours. This methodological difference means that chemogenetic suppression may affect all aspects of the oddball paradigm, affecting the overall encoding of the context or even giving rise to an adaptive rebalancing of inhibition/excitation ratios, for instance, while optogenetic suppression can be induced at discrete phases of the paradigm, which could contribute to the differences reported here. Despite contradictory results, these studies suggest a conserved role of SST interneurons in the contextual processing of stimuli in V1 and A1 cortices. Interestingly, postmortem analysis of SZ brain tissue demonstrates reduced and aberrant SST activity in the neocortex (Hashimoto et al., 2008a,b; Fung et al., 2010, 2014; Volk and Lewis, 2013), which poses an exciting link between the role of SSTs in SSA and/or DD and deficient MMN in SZ patients.

## TWO SIDES OF THE SAME COIN?

As mentioned above, MMN and the use of oddball paradigms without additional controls have resulted in composite studies of SSA and DD, with DD often being assumed to be the simple absence of SSA in neural populations. However, using standard and deviant auditory stimuli of the same frequency but different intensities or localization is still capable of provoking an MMN response in humans, demonstrating that DD occurs in adapted populations and is not simply the absence of SSA (Schröger and Wolff, 1996; Jacobsen et al., 2003a; Althen et al., 2011; Shestopalova et al., 2018). Therefore, more focus has been on determining whether DD truly reflects a violation of expected patterns or rarity of an event. If DD reflects rarity, the magnitude of the response to the deviant stimulus would be the same whether the stimulus was deviant or simply rare. Alternatively, if DD reflects violation of expectations, truly deviant stimuli, those that disrupt expected patterns, would elicit a larger response than rare stimuli. Teasing these hypotheses apart has been of recent focus in animal models, as numerous paradigmatic controls have been implemented (Jacobsen and Schröger, 2001, 2003; Jacobsen et al., 2003b; Harms et al., 2014; Harms, 2016).

In addition to paradigm controls, researchers are using cell- and circuit-based manipulations to separate SSA and DD (Strelnikov, 2007). For example, in the inferior colliculus

cholinergic modulation appears to affect SSA to repetitive auditory stimuli without altering DD (Ayala and Malmierca, 2015). Cholinergic modulation has also been shown to affect the MMN in neurotypical humans (Caldenhove et al., 2017); however, whether this is due to basic stimulus processing or novelty detection requires further investigation. In contrast, DD, but seemingly not SSA, depends on signaling from SST interneurons, at least in the primary visual cortex, as inhibiting them abolishes DD while sparing SSA in principal neurons of primary visual cortex (Hamm and Yuste, 2016). Additionally, NMDA receptors may support oddball-driven responses and/or DD as blockade of NMDA receptors reduces MMN (Ehrlichman et al., 2008; Chen et al., 2015; Harms, 2016; Chien et al., 2019) but proper controls still need to be employed to determine if this reduction is due to altered DD or SSA (Harms, 2016). Again, there is conflicting evidence regarding the extent to which the NMDAR function contributes to SSA, making it difficult to discern its relationship to DD (Farley et al., 2010; Chen et al., 2015).

Taken together the evidence supports conclusions drawn from human MMN studies and suggests that DD is a complex process that is separable from SSA in neural recordings (Csépe, 1995; Ruusuvirta et al., 1998; Jung et al., 2013; Shiramatsu et al., 2013; Harms et al., 2014; Chen et al., 2015; Hamm and Yuste, 2016; Kum et al., 2019); however, additional work is required to truly dissect individual mechanisms of each process. It has yet to be demonstrated whether DD in the cortex can exist without the presence of a locally, alternatively “adapted” population of neurons (or at least adapted upstream inputs). We have combined findings across several human and animal studies to build a theoretical model of cortical MMN wherein DD and SSA are separable, but wherein DD would depend on SSA (but not the reverse).

The basic model of layer 2/3 is laid out in **Figure 3**. In a baseline state (**Figure 3A**), upstream inputs synapse onto inhibitory interneurons (PV/SST) and PYRs. During an oddball paradigm (**Figure 3B**), the neocortical circuit enters a state which is both adapted and primed for DD. Repetitive stimulation (i.e., the same stimulus; **Figure 3C**) results in synaptic depression of inputs from upstream neurons selective for the redundant stimulus (black square) to PYRs (Hamm et al., 2018; in this case PYR1) and PVs (Chen et al., 2015). We propose that this synaptic depression on PYRs, inherited from multiple upstream synapses (e.g., onto thalamic relays) underlies SSA (Khatri et al., 2004; Yarden and Nelken, 2017), as depicted by the PYR1 trace. Indeed, SSA is present in thalamocortical inputs (**Figure 3D**; Khatri et al., 2004; Asari and Zador, 2009). PYR1 initially responds at a non-adapted level (**Figure 3D**; hashed line) but decreases response amplitude with each subsequent presentation. Similar adaptation has been observed in PYRs and PVs (**Figure 3F**; Reyes et al., 1998; Chen et al., 2015; Natan et al., 2017). In contrast, synaptic facilitation occurs on SSTs (Reyes et al., 1998), but since the inputs themselves may carry adaptation from further upstream, these effects lead to SSA which is present but less dramatic in SSTs (**Figure 3G**; Chen et al., 2015). Upstream input selective for the deviant stimulus (green square) remains unadapted, and presentations of the deviant stimulus induce

PYR2 responses above the non-adapted level (**Figure 3E**; hashed line), i.e., classic “DD.”

This is due to at least three additional processes: (1) to open-state NMDA receptors, as pharmacological blockade of NMDA receptors diminishes MMN and oddball-drive responses/DD (Javitt et al., 1996; Chen et al., 2015). (2) DD also appears to depend on the action of SSTs, as inhibiting them selectively reduces DD (Natan et al., 2015; Hamm and Yuste, 2016). And (3) SSTs provide stronger inhibitory drive onto PVs than they do onto PYRs, and PVs impart stronger inhibition onto PYRs than SSTs do (Ma et al., 2010, 2012; Cottam et al., 2013; Natan et al., 2015; Safari et al., 2017). Thus (relatively) increased activity of SSTs throughout the paradigm leads to inhibition of PVs, which disinhibits all PYRs non-selectively, leading to the opening of NMDARs and supralinear responses (i.e., DD) in PYRs which are not adapted (i.e., PYR2 in this figure). Interestingly, a subset of SSTs is known to mediate disinaptic inhibition between PYRs (Silberberg and Markram, 2007). So alternatively, decreased activity of PYR1s, and thus reduced drive on mediating SSTs which inhibit PYR2s, may also contribute to the disinhibition (and opening of NMDARs) in PYR2s in the oddball paradigm before the presentation of the deviant. VIPs and other interneuron subtypes are an integral part of the neocortical circuit (Karnani et al., 2014), but as of now, little is known about their role in SSA or DD.

Notably, a number of the premises in **Figure 3** come from studies of layer 2/3 neurons in primary sensory regions, so our confidence is strongest in this supragranular circuitry. Overall, like all models ours in **Figure 3** is incomplete. For example, in another version of the oddball paradigm, DD has been reported in auditory cortex when a single auditory tone is used but the duration of the tone differs between the redundant and the deviant, known as “duration” mismatch (Schall et al., 2003; Colin et al., 2009; Peter et al., 2010; Schirmer et al., 2015). Duration MMN is also affected in SZ (Koshiyama et al., 2020). Although our model (**Figure 3**) is conceived with separate pitch or orientation-selective cortical ensembles, duration sensitive neurons have been identified in the auditory cortex (Beukes et al., 2009; Wang et al., 2016). Therefore, possibly, the dynamics among separate ensembles selective for the duration (or other non-identity stimulus features such as intensity, source localization, etc; Frey et al., 2015) may contribute to duration MMN and DD through similar intracortical circuit described in our model. Whether DD can exist in the absence of two separate PYR ensembles is unclear, although it could be apparent that it arises this way locally *via* feedback. For example, perhaps the interplay between duration selective neurons in a down-stream region (e.g., down-stream to A1) could effectively give rise to DD and send it back up-stream (e.g., as feedback to A1). Such an experiment constitutes an important test for our model.

Further, much of the SSA and DD work on which it is based, for instance, come from different sensory modalities (e.g., visual, auditory, and somatosensory), which may (Latimer et al., 2019) or may not (Kremlacek et al., 2016) exhibit distinct local circuitry for processing context. Further, distinct subpopulations exist

within the SST-interneuron class which exhibit net inhibitory or net disinhibitory effects on PYRs (e.g., layer 4  $\times$  94 cells; Muñoz et al., 2017). It remains possible that distinct subpopulations of interneurons, even within the same interneuron class (e.g., SSTs) differentially contribute to SSA and DD. Finally, it does not directly account for top-down influences nor information inherited from subcortical structures (Nelken and Ulanovsky, 2007; Stefanics et al., 2014, 2016; Carbajal and Malmierca, 2018). More rigorous studies across sensory systems are necessary to develop a cohesive and complete model of SSA and DD.

## FUTURE STUDIES

Though incomplete, the proposed model may prove useful in guiding specific experiments in future work, especially in mice, where access to interneuron subpopulations is significant. First, a clearer picture of how SSTs, VIPs, PVs, and PYRs respond during oddball experiments in awake animals needs to be established. In particular, direct VIPs recordings in this paradigm have not been reported. Additional work should establish whether VIPs exhibit dynamics as hypothesized in **Figure 3H**, and/or SSA, DD, or some repetition facilitation (an inverse SSA).

Second, causal roles for PVs and VIPs have not been thoroughly examined in the context of DD (refer to Natan et al., 2015, 2017; regarding a role for PVs in auditory SSA Opto- or chemicogenetic experiments to target these populations while monitoring DD/SSA/MMN in the local cortex, like e.g., Hamm and Yuste (2016), are warranted.

Third, interactions between interneuron subtypes, namely that SSTs, PVs, and VIPs inhibit each other during specific parts of the oddball paradigm to effectively disinhibit subsets of PYRs, is key to this model. Imaging one population (e.g., PVs) while stimulating/inhibiting another (e.g., SSTs) and measuring gross LFP output would be a suitable test of these aspects of the model, and such an experiment is possible through the use of double transgenic strategies involving both Cre- and Flp- dependent gene expression in a complementary fashion (He et al., 2016).

Fourth, whether upstream inputs onto SSTs vs. PYRs are facilitated during this paradigm should be directly explored. This is a challenging experiment, but it is theoretically possible using 2P calcium imaging of axon boutons (Hamm et al., 2018), a combination of retrograde viral and cre-dependent expression (to express GCaMP in only upstream neurons synapsing on SSTs), and dual-color imaging (to colocalize boutons on SST dendrites).

Finally, a strong test of this model would be a demonstration that DD-like computations can be generated in isolated cortical circuits. *In vivo* recordings in the sensory cortex during an oddball paradigm followed by precise subsequent *ex vivo* recordings of the same neuronal populations in slices (Karnani et al., 2016) combined with patterned optogenetic stimulation (Carrillo-Reid et al., 2019) of two separate input populations (simulating the redundant and deviant preferring neurons) to generate and test adaptation and DD-like facilitation is possible, though, again, challenging. If SSA-like and DD-like processing are identified in such a setup, this would not only open the

door for highly precise circuit-level investigations but could also revolutionize how MMN-deficits are understood.

## CONCLUSIONS AND CLINICAL SIGNIFICANCE

Recent results obtained from animals using the oddball and various control sequences demonstrates SSA and DD are not only separable, but likely arise due to different mechanisms. Our synthesis of this data and hypothesized model (**Figure 3**) suggests that DD in layer 2/3 of neocortex depends on the presence of adaptation in a subset of the local network and/or in afferents from the thalamus or layer 4, but this requires additional investigation. In both humans and animals, it appears DD is facilitated by and functionally related to the degree of SSA (Taaseh et al., 2011; Chien et al., 2019). Together these results highlight the complementary but distinct nature of SSA and DD. Furthermore, while the two processes have separable mechanisms, they also have mechanistic commonalities. For example, both are regulated by overall excitatory-inhibitory tone but different neuromodulators exert independent effects (Garrido et al., 2009). Future work is required to further elucidate the pathways and mechanisms required to generate adaptation and detection of deviation from expected patterns, especially when contexts become more complex than e.g., an “oddball paradigm.”

Both SSA and DD are co-represented in the human neurophysiological MMN response. While MMN is known to be altered relative to neurotypical controls in several neuropsychiatric diseases, such as SZ, autism spectrum disorders, and major depressive disorder among several others, many of these exhibit shared and distinct genetic risk (Brainstorm et al., 2018), neural pathophysiology (Mitelman, 2019), and symptoms of attentive or pre-attentive deficits that may lead to altered MMN for similar and distinct reasons. Animal research to understand the (likely) myriad neural circuit mechanisms underlying MMN will help in interpreting this biomarker in a neuropsychiatric setting (e.g., linking specific interneuron pathology to specific aspects of the MMN), but without differentiating the components of SSA and DD within the MMN measure during human experimentation, translational leaps will be difficult. Besides, such information would broaden our greater understanding of how the brain recognizes the change in its environment, a function with significant basic survival implications.

## AUTHOR CONTRIBUTIONS

JR and JH discussed and contributed to the final manuscript.

## FUNDING

This work was supported by the Georgia State University Next Generation Postdoctoral Scholars Fellowship (JR), National Institutes of Mental Health (R00MH115082; JH) and the Whitehall Foundation (2019-05-44; JH).

## REFERENCES

- Abbott, L. F., Varela, J. A., Sen, K., and Nelson, S. B. (1997). Synaptic depression and cortical gain control. *Science* 275, 220–224. doi: 10.1126/science.275.5297.221
- Adler, L. E., Olincy, A., Waldo, M., Harris, J. G., Griffith, J., Stevens, K., et al. (1998). Schizophrenia, sensory gating and nicotinic receptors. *Schizophr. Bull.* 24, 189–202. doi: 10.1093/oxfordjournals.schbul.a033320
- Adrian, E. D. (1926a). The impulses produced by sensory nerve endings: part I. *J. Physiol.* 61, 49–72. doi: 10.1113/jphysiol.1926.sp002273
- Adrian, E. D. (1926b). The impulses produced by sensory nerve-endings: part 4. Impulses from Pain Receptors. *J. Physiol.* 62, 33–51. doi: 10.1113/jphysiol.1926.sp002334
- Adrian, E. D., and Zotterman, Y. (1926a). The impulses produced by sensory nerve endings: part 3. Impulses set up by Touch and Pressure. *J. Physiol.* 61, 465–483. doi: 10.1113/jphysiol.1926.sp002308
- Adrian, E. D., and Zotterman, Y. (1926b). The impulses produced by sensory nerve-endings: part II. The response of a Single End-Organ. *J. Physiol.* 61, 151–171. doi: 10.1113/jphysiol.1926.sp002281
- Aizenberg, M., Mwila-bwe-Tshilobo, L., Briguglio, J. J., Natan, R. G., and Geffen, M. N. (2015). Bidirectional regulation of innate and learned behaviors that rely on frequency discrimination by cortical inhibitory neurons. *PLoS Biol.* 13:e1002308. doi: 10.1371/journal.pbio.1002308
- Aleksandrov, A. A., Knyazeva, V. M., Volnova, A. B., Dmitrieva, E. S., Korenkova, O., Espinoza, S., et al. (2018). Identification of TAAR5 agonist activity of  $\alpha$ -NETA and its effect on mismatch negativity amplitude in awake rats. *Neurotox. Res.* 34, 442–451. doi: 10.1007/s12640-018-9902-6
- Althen, H., Grimm, S., and Escera, C. (2011). Fast detection of unexpected sound intensity decrements as revealed by human evoked potentials. *PLoS One* 6:e28522. doi: 10.1371/journal.pone.0028522
- Anderson, L. A., Christianson, G. B., and Linden, J. F. (2009). Stimulus-specific adaptation occurs in the auditory thalamus. *J. Neurosci.* 29, 7359–7363. doi: 10.1523/JNEUROSCI.0793-09.2009
- Anderson, L. A., and Malmierca, M. S. (2013). The effect of auditory cortex deactivation on stimulus-specific adaptation in the inferior colliculus of the rat. *Eur. J. Neurosci.* 37, 52–62. doi: 10.1111/ejn.12018
- Andrade, G. N., Butler, J. S., Peters, G. A., Molholm, S., and Foxe, J. J. (2016). Atypical visual and somatosensory adaptation in schizophrenia-spectrum disorders. *Transl. Psychiatry* 6:e804. doi: 10.1038/tp.2016.63
- Antunes, F. M., and Malmierca, M. S. (2011). Effect of auditory cortex deactivation on stimulus-specific adaptation in the medial geniculate body. *J. Neurosci.* 31, 17306–17316. doi: 10.1523/JNEUROSCI.1915-11.2011
- Antunes, F. M., Nelken, I., Covey, E., and Malmierca, M. S. (2010). Stimulus-specific adaptation in the auditory thalamus of the anesthetized rat. *PLoS One* 5:e14071. doi: 10.1371/journal.pone.0014071
- Anwar, H., Li, X., Bucher, D., and Nadim, F. (2017). Functional roles of short-term synaptic plasticity with an emphasis on inhibition. *Curr. Opin. Neurobiol.* 43, 71–78. doi: 10.1016/j.conb.2017.01.002
- Asari, H., and Zador, A. M. (2009). Long-lasting context dependence constrains neural encoding models in rodent auditory cortex. *J. Neurophysiol.* 102, 2638–2656. doi: 10.1152/jn.00577.2009
- Ayala, Y. A., and Malmierca, M. S. (2012). Stimulus-specific adaptation and deviance detection in the inferior colliculus. *Front. Neural Circuits* 6:89. doi: 10.3389/fncir.2012.00089
- Ayala, Y. A., and Malmierca, M. S. (2015). Cholinergic modulation of stimulus-specific adaptation in the inferior colliculus. *J. Neurosci.* 35, 12261–12272. doi: 10.1523/JNEUROSCI.0909-15.2015
- Ayala, Y. A., and Malmierca, M. S. (2018). The effect of inhibition on stimulus-specific adaptation in the inferior colliculus. *Brain Struct. Funct.* 223, 1391–1407. doi: 10.1007/s00429-017-1546-4
- Ayala, Y. A., Pérez-González, D., Duque, D., Nelken, I., and Malmierca, M. S. (2012). Frequency discrimination and stimulus deviance in the inferior colliculus and cochlear nucleus. *Front. Neural Circuits* 6:119. doi: 10.3389/fncir.2012.00119
- Ayala, Y. A., Udeh, A., Dutta, K., Bishop, D., Malmierca, M. S., and Oliver, D. L. (2015). Differences in the strength of cortical and brainstem inputs to SSA and non-SSA neurons in the inferior colliculus. *Sci. Rep.* 5:10383. doi: 10.1038/srep10383
- Bayazitov, I. T., Westmoreland, J. J., and Zakharenko, S. S. (2013). Forward suppression in the auditory cortex is caused by the  $\text{Ca}_v3.1$  calcium channel-mediated switch from bursting to tonic firing at thalamocortical projections. *J. Neurosci.* 33, 18940–18950. doi: 10.1523/JNEUROSCI.3335-13.2013
- Becker, R., Braun, U., Schwarz, A. J., Gass, N., Schweiger, J. I., Weber-Fahr, W., et al. (2016). Species-conserved reconfigurations of brain network topology induced by ketamine. *Transl. Psychiatry* 6:e786. doi: 10.1038/tp.2016.53
- Best, A. R., and Wilson, D. A. (2004). Coordinate synaptic mechanisms contributing to olfactory cortical adaptation. *J. Neurosci.* 24, 652–660. doi: 10.1523/JNEUROSCI.4220-03.2004
- Beukes, E. W., Munro, K. J., and Purdy, S. C. (2009). Duration-sensitive neurons in the auditory cortex. *Neuroreport* 20, 1129–1133. doi: 10.1097/wnr.0b013e32832ea601
- Blundon, J. A., and Zakharenko, S. S. (2013). Presynaptic gating of postsynaptic synaptic plasticity: a plasticity filter in the adult auditory cortex. *Neuroscientist* 19, 465–478. doi: 10.1177/1073858413482983
- Blundon, J. A., Bayazitov, I. T., and Zakharenko, S. S. (2011). Presynaptic gating of postsynaptically expressed plasticity at mature thalamocortical synapses. *J. Neurosci.* 31, 16012–16025. doi: 10.1523/JNEUROSCI.3281-11.2011
- Boutros, N. N., Torello, M. W., Barker, B. A., Tueting, P. A., Wu, S. C., and Nasrallah, H. A. (1995). The P50 evoked potential component and mismatch detection in normal volunteers: implications for the study of sensory gating. *Psychiatry Res.* 57, 83–88. doi: 10.1016/0165-1781(95)02637-c
- Box, G. E. P., Hunter, J. S., and Hunter, W. G. (2005). *Statistics for Experimenters: Design, Innovation, and Discovery*. Hoboken, NJ: Wiley-Interscience.
- Brainstorm, C., Anttila, V., Bulik-Sullivan, B., Finucane, H. K., Walters, R. K., Bras, J., et al. (2018). Analysis of shared heritability in common disorders of the brain. *Science* 360:eap8757. doi: 10.1126/science.aap8757
- Bristow, L. J., Easton, A. E., Li, Y. W., Sivarao, D. V., Lidge, R., Jones, K. M., et al. (2016). The novel, nicotinic  $\alpha 7$  receptor partial agonist, BMS-933043, improves cognition and sensory processing in preclinical models of schizophrenia. *PLoS One* 11:e0159996. doi: 10.1371/journal.pone.0159996
- Brosch, M., and Schreiner, C. E. (1997). Time course of forward masking tuning curves in cat primary auditory cortex. *J. Neurophysiol.* 77, 923–943. doi: 10.1152/jn.1997.77.2.923
- Caldenhove, S., Borghans, L., Blokland, A., and Sambeth, A. (2017). Role of acetylcholine and serotonin in novelty processing using an oddball paradigm. *Behav. Brain Res.* 331, 199–204. doi: 10.1016/j.bbr.2017.05.031
- Calford, M. B., and Semple, M. N. (1995). Monaural inhibition in cat auditory cortex. *J. Neurophysiol.* 73, 1876–1891. doi: 10.1152/jn.1995.73.5.1876
- Carbajal, G. V., and Malmierca, M. S. (2018). The neuronal basis of predictive coding along the auditory pathway: from the subcortical roots to cortical deviance detection. *Trends Hear.* 22:2331216518784822. doi: 10.1177/2331216518784822
- Carrillo-Reid, L., Han, S., Yang, W., Akrouh, A., and Yuste, R. (2019). Controlling visually guided behavior by holographic recalling of cortical ensembles. *Cell* 178, 447.e5–457.e5. doi: 10.1016/j.cell.2019.05.045
- Chen, I. W., Helmchen, F., and Lutcke, H. (2015). Specific early and late oddball-evoked responses in excitatory and inhibitory neurons of mouse auditory cortex. *J. Neurosci.* 35, 12560–12573. doi: 10.1523/JNEUROSCI.2240-15.2015
- Chen, P., Ye, E., Jin, X., Zhu, Y., and Wang, L. (2019). Association between thalamocortical functional connectivity abnormalities and cognitive deficits in schizophrenia. *Sci. Rep.* 9:2952. doi: 10.1038/s41598-019-39367-z
- Chien, V. S. C., Maess, B., and Knösche, T. R. (2019). A generic deviance detection principle for cortical On/Off responses, omission response, and mismatch negativity. *Biol. Cybern.* 113, 475–494. doi: 10.1007/s00422-019-00804-x
- Chun, S., Westmoreland, J. J., Bayazitov, I. T., Eddins, D., Pani, A. K., Smeyne, R. J., et al. (2014). Specific disruption of thalamic inputs to the auditory cortex in schizophrenia models. *Science* 344, 1178–1182. doi: 10.1126/science.1253895
- Chung, S., Li, X., and Nelson, S. B. (2002). Short-term depression at thalamocortical synapses contributes to rapid adaptation of cortical sensory responses *in vivo*. *Neuron* 34, 437–446. doi: 10.1016/s0896-6273(02)00659-1
- Clementz, B. A., Geyer, M. A., and Braff, D. L. (1998). Poor P50 suppression among schizophrenia patients and their first-degree biological relatives. *Am. J. Psychiatry* 155, 1691–1694. doi: 10.1176/ajp.155.12.1691
- Colin, C., Hoonhorst, I., Markessis, E., Radeau, M., De Tourtchaninoff, M., Foucher, A., et al. (2009). Mismatch negativity (MMN) evoked by sound duration contrasts: an unexpected major effect of deviance direction

- on amplitudes. *Clin. Neurophysiol.* 120, 51–59. doi: 10.1016/j.clinph.2008.10.002
- Condon, C. D., and Weinberger, N. M. (1991). Habituation produces frequency-specific plasticity of receptive fields in the auditory cortex. *Behav. Neurosci.* 105, 416–430. doi: 10.1037/0735-7044.105.3.416
- Cottam, J. C., Smith, S. L., and Haussner, M. (2013). Target-specific effects of somatostatin-expressing interneurons on neocortical visual processing. *J. Neurosci.* 33, 19567–19578. doi: 10.1523/JNEUROSCI.2624-13.2013
- Csépe, V. (1995). On the origin and development of the mismatch negativity. *Ear Hear.* 16, 91–104. doi: 10.1097/00003446-199502000-00007
- Dalton, P. (2000). Psychophysical and behavioral characteristics of olfactory adaptation. *Chem. Senses* 25, 487–492. doi: 10.1093/chemse/25.4.487
- Duque, D., Malmierca, M. S., and Caspary, D. M. (2014). Modulation of stimulus-specific adaptation by GABA<sub>A</sub> receptor activation or blockade in the medial geniculate body of the anesthetized rat. *J. Physiol.* 592, 729–743. doi: 10.1113/jphysiol.2013.261941
- Duque, D., Wang, X., Nieto-Diego, J., Krumbholz, K., and Malmierca, M. S. (2016). Neurons in the inferior colliculus of the rat show stimulus-specific adaptation for frequency, but not for intensity. *Sci. Rep.* 6:24114. doi: 10.1038/srep24114
- Ehrlichman, R. S., Gandal, M. J., Maxwell, C. R., Lazarewicz, M. T., Finkel, L. H., Contreras, D., et al. (2009). N-methyl-D-aspartic acid receptor antagonist-induced frequency oscillations in mice recreate pattern of electrophysiological deficits in schizophrenia. *Neuroscience* 158, 705–712. doi: 10.1016/j.neuroscience.2008.10.031
- Ehrlichman, R. S., Maxwell, C. R., Majumdar, S., and Siegel, S. J. (2008). Deviance-elicited changes in event-related potentials are attenuated by ketamine in mice. *J. Cogn. Neurosci.* 20, 1403–1414. doi: 10.1162/jocn.2008.20097
- Elshahk, A. A., Sponheim, S. R., Chafee, M. V., and MacDonald, A. W. (2015). Spatial attentional control is not impaired in schizophrenia: dissociating specific deficits from generalized impairments. *J. Abnorm. Psychol.* 124, 302–308. doi: 10.1037/a0038537
- Escera, C., Leung, S., and Grimm, S. (2014). Deviance detection based on regularity encoding along the auditory hierarchy: electrophysiological evidence in humans. *Brain Topogr.* 27, 527–538. doi: 10.1007/s10548-013-0328-4
- Ethridge, L. E., Hamm, J. P., Pearlson, G. D., Tamminga, C. A., Sweeney, J. A., Keshavan, M. S., et al. (2015). Event-related potential and time-frequency endophenotypes for schizophrenia and psychotic bipolar disorder. *Biol. Psychiatry* 77, 127–136. doi: 10.1016/j.biopsych.2014.03.032
- Fairhall, A. L., Lewen, G. D., Bialek, W., and de Ruyter van Steveninck, R. R. (2001). Efficiency and ambiguity in an adaptive neural code. *Nature* 412, 787–792. doi: 10.1038/35090500
- Farley, B. J., Quirk, M. C., Doherty, J. J., and Christian, E. P. (2010). Stimulus-specific adaptation in auditory cortex is an NMDA-independent process distinct from the sensory novelty encoded by the mismatch negativity. *J. Neurosci.* 30, 16475–16484. doi: 10.1523/JNEUROSCI.2793-10.2010
- Featherstone, R. E., Melnychenko, O., and Siegel, S. J. (2018). Mismatch negativity in preclinical models of schizophrenia. *Schizophr. Res.* 191, 35–42. doi: 10.1016/j.schres.2017.07.039
- Feil, S., Valtcheva, N., and Feil, R. (2009). Inducible Cre mice. *Methods Mol. Biol.* 530, 343–363. doi: 10.1007/978-1-59745-471-1\_18
- Fischer, C., Morlet, D., and Giard, M. (2000). Mismatch negativity and N100 in comatose patients. *Audiol. Neurotol.* 5, 192–197. doi: 10.1159/000013880
- Frey, J. D., Wendt, M., and Jacobsen, T. (2015). Automatic detection of unattended changes in room acoustics. *Neurosci. Lett.* 584, 162–167. doi: 10.1016/j.neulet.2014.09.050
- Fung, S. J., Fillman, S. G., Webster, M. J., and Shannon Weickert, C. (2014). Schizophrenia and bipolar disorder show both common and distinct changes in cortical interneuron markers. *Schizophr. Res.* 155, 26–30. doi: 10.1016/j.schres.2014.02.021
- Fung, S. J., Webster, M. J., Sivagnanasundaram, S., Duncan, C., Elashoff, M., and Weickert, C. S. (2010). Expression of interneuron markers in the dorsolateral prefrontal cortex of the developing human and in schizophrenia. *Am. J. Psychiatry* 167, 1479–1488. doi: 10.1176/appi.ajp.2010.09060784
- Furth, K. E., McCoy, A. J., Dodge, C., Walters, J. R., Buonanno, A., and Delaville, C. (2017). Neuronal correlates of ketamine and walking induced  $\gamma$  oscillations in the medial prefrontal cortex and mediodorsal thalamus. *PLoS One* 12:e0186732. doi: 10.1371/journal.pone.0186732
- Garrett, M., Manavi, S., Roll, K., Ollerenshaw, D. R., Groblewski, P. A., Ponvert, N. D., et al. (2020). Experience shapes activity dynamics and stimulus coding of VIP inhibitory cells. *Elife* 9:e50340. doi: 10.7554/eLife.50340
- Garrido, M. I., Kilner, J. M., Stephan, K. E., and Friston, K. J. (2009). The mismatch negativity: a review of underlying mechanisms. *Clin. Neurophysiol.* 120, 453–463. doi: 10.1016/j.clinph.2008.11.029
- Gil-Da-Costa, R., Stoner, G. R., Fung, R., and Albright, T. D. (2013). Nonhuman primate model of schizophrenia using a noninvasive EEG method. *Proc. Natl. Acad. Sci. U S A* 110, 15425–15430. doi: 10.1073/pnas.1312264110
- Haaf, M., Leicht, G., Curic, S., and Mülert, C. (2018). Glutamatergic deficits in schizophrenia—biomarkers and pharmacological interventions within the ketamine model. *Curr. Pharm. Biotechnol.* 19, 293–307. doi: 10.2174/1389201019666180620112528
- Hamilton, L. S., Sohl-Dickstein, J., Huth, A. G., Carels, V. M., Deisseroth, K., and Bao, S. (2013). Optogenetic activation of an inhibitory network enhances feedforward functional connectivity in auditory cortex. *Neuron* 80, 1066–1076. doi: 10.1016/j.neuron.2013.08.017
- Hamm, J. P., Bobilev, A. M., Hayrynen, L. K., Hudgens-Haney, M. E., Oliver, W. T., Parker, D. A., et al. (2015). Stimulus train duration but not attention moderates  $\gamma$ -band entrainment abnormalities in schizophrenia. *Schizophr. Res.* 165, 97–102. doi: 10.1016/j.schres.2015.02.016
- Hamm, J. P., Ethridge, L. E., Boutros, N. N., Keshavan, M. S., Sweeney, J. A., Pearlson, G. D., et al. (2014). Diagnostic specificity and familiarity of early versus late evoked potentials to auditory paired stimuli across the schizophrenia-bipolar psychosis spectrum. *Psychophysiology* 51, 348–357. doi: 10.1111/psyp.12185
- Hamm, J. P., Shymkiv, Y., Han, S., Yang, W., and Yuste, R. (2018). Cortical subnetworks encode context of visual stimulus. *bioRxiv* [Preprint]. doi: 10.1101/452219
- Hamm, J. P., and Yuste, R. (2016). Somatostatin interneurons control a key component of mismatch negativity in mouse visual cortex. *Cell Rep.* 16, 597–604. doi: 10.1016/j.celrep.2016.06.037
- Harms, L. (2016). Mismatch responses and deviance detection in N-methyl-D-aspartate (NMDA) receptor hypofunction and developmental models of schizophrenia. *Biol. Psychol.* 116, 75–81. doi: 10.1016/j.biopsycho.2015.06.015
- Harms, L., Fulham, W. R., Todd, J., Budd, T. W., Hunter, M., Meehan, C., et al. (2014). Mismatch negativity (MMN) in freely-moving rats with several experimental controls. *PLoS One* 9:e110892. doi: 10.1371/journal.pone.0110892
- Harms, L., Fulham, W. R., Todd, J., Meehan, C., Schall, U., Hodgson, D. M., et al. (2018). Late deviance detection in rats is reduced, while early deviance detection is augmented by the NMDA receptor antagonist MK-801. *Schizophr. Res.* 191, 43–50. doi: 10.1016/j.schres.2017.03.042
- Harms, L., Michie, P. T., and Näätänen, R. (2016). Criteria for determining whether mismatch responses exist in animal models: focus on rodents. *Biol. Psychol.* 116, 28–35. doi: 10.1016/j.biopsycho.2015.07.006
- Hashimoto, T., Arion, D., Unger, T., Maldonado-Avilés, J. G., Morris, H. M., Volk, D. W., et al. (2008a). Alterations in GABA-related transcriptome in the dorsolateral prefrontal cortex of subjects with schizophrenia. *Mol. Psychiatry* 13, 147–161. doi: 10.1038/sj.mp.4002011
- Hashimoto, T., Bazmi, H. H., Mirnics, K., Wu, Q., Sampson, A. R., and Lewis, D. A. (2008b). Conserved regional patterns of GABA-related transcript expression in the neocortex of subjects with schizophrenia. *Am. J. Psychiatry* 165, 479–489. doi: 10.1176/appi.ajp.2007.07081223
- He, M., Tucciarone, J., Lee, S., Nigro, M. J., Kim, Y., Levine, J. M., et al. (2016). Strategies and tools for combinatorial targeting of GABAergic neurons in mouse cerebral cortex. *Neuron* 91, 1228–1243. doi: 10.1016/j.neuron.2016.08.021
- Heil, P., and Peterson, A. J. (2015). Basic response properties of auditory nerve fibers: a review. *Cell Tissue Res.* 361, 129–158. doi: 10.1007/s00441-015-2177-9
- Hillenbrand, U., and van Hemmen, J. L. (2002). Adaptation in the corticothalamic loop: computational prospects of tuning the senses. *Philos. Trans. R. Soc. Lond. B Biol. Sci.* 357, 1859–1867. doi: 10.1098/rstb.2002.1174
- Höflich, A., Hahn, A., Küblböck, M., Kranz, G. S., Vanicek, T., Windischberger, C., et al. (2015). Ketamine-induced modulation of the thalamo-cortical network in healthy volunteers as a model for schizophrenia. *Int. J. Neuropsychopharmacol.* 18:pyv040. doi: 10.1093/ijnp/pyv040
- Hua, J., Blair, N. I. S., Paez, A., Choe, A., Barber, A. D., Brandt, A., et al. (2019). Altered functional connectivity between sub-regions in the thalamus

- and cortex in schizophrenia patients measured by resting state BOLD fMRI at 7T. *Schizophr. Res.* 206, 370–377. doi: 10.1016/j.schres.2018.10.016
- Huang, A. S., Rogers, B. P., and Woodward, N. D. (2019). Disrupted modulation of thalamus activation and thalamocortical connectivity during dual task performance in schizophrenia. *Schizophr. Res.* 210, 270–277. doi: 10.1016/j.schres.2018.12.022
- Ibáñez, A. M., Martín, R. S., Hurtado, E., and López, V. (2009). ERPs studies of cognitive processing during sleep. *Int. J. Psychol.* 44, 290–304. doi: 10.1080/00207590802194234
- Jacobsen, T., Horenkamp, T., and Schröger, E. (2003a). Preattentive memory-based comparison of sound intensity. *Audiol. Neurotol.* 8, 338–346. doi: 10.1159/000073518
- Jacobsen, T., Schröger, E., Horenkamp, T., and Winkler, I. (2003b). Mismatch negativity to pitch change: varied stimulus proportions in controlling effects of neural refractoriness on human auditory event-related brain potentials. *Neurosci. Lett.* 344, 79–82. doi: 10.1016/s0304-3940(03)00408-7
- Jacobsen, T., and Schröger, E. (2001). Is there pre-attentive memory-based comparison of pitch? *Psychophysiology* 38, 723–727. doi: 10.1111/1469-8986.3840723
- Jacobsen, T., and Schröger, E. (2003). Measuring duration mismatch negativity. *Clin. Neurophysiol.* 114, 1133–1143. doi: 10.1016/s1388-2457(03)00043-9
- Javitt, D. C., and Freedman, R. (2015). Sensory processing dysfunction in the personal experience and neuronal machinery of schizophrenia. *Am. J. Psychiatry* 172, 17–31. doi: 10.1176/appi.ajp.2014.13121691
- Javitt, D. C., Schroeder, C. E., Steinschneider, M., Arezzo, J. C., and Vaughan, H. G. Jr. (1992). Demonstration of mismatch negativity in the monkey. *Electroencephalogr. Clin. Neurophysiol.* 83, 87–90. doi: 10.1016/0013-4694(92)90137-7
- Javitt, D. C., Steinschneider, M., Schroeder, C. E., and Arezzo, J. C. (1996). Role of cortical N-methyl-D-aspartate receptors in auditory sensory memory and mismatch negativity generation: implications for schizophrenia. *Proc. Natl. Acad. Sci. U S A* 93, 11962–11967. doi: 10.1073/pnas.93.21.11962
- Javitt, D. C., and Sweet, R. A. (2015). Auditory dysfunction in schizophrenia: integrating clinical and basic features. *Nat. Rev. Neurosci.* 16, 535–550. doi: 10.1038/nrn4002
- Jung, F., Stephan, K. E., Backes, H., Moran, R., Gramer, M., Kumagai, T., et al. (2013). Mismatch responses in the awake rat: evidence from epidural recordings of auditory cortical fields. *PLoS One* 8:e63203. doi: 10.1371/journal.pone.0063203
- Karnani, M. M., Agetsuma, M., and Yuste, R. (2014). A blanket of inhibition: functional inferences from dense inhibitory connectivity. *Curr. Opin. Neurobiol.* 26, 96–102. doi: 10.1016/j.conb.2013.12.015
- Karnani, M. M., Jackson, J., Ayzenshtat, I., Tucciarone, J., Manoocheri, K., Snider, W. G., et al. (2016). Cooperative subnetworks of molecularly similar interneurons in mouse neocortex. *Neuron* 90, 86–100. doi: 10.1016/j.neuron.2016.02.037
- Kato, H. K., Gillet, S. N., and Isaacson, J. S. (2015). Flexible sensory representations in auditory cortex driven by behavioral relevance. *Neuron* 88, 1027–1039. doi: 10.1016/j.neuron.2015.10.024
- Khatri, V., Hartings, J. A., and Simons, D. J. (2004). Adaptation in thalamic barreloid and cortical barrel neurons to periodic whisker deflections varying in frequency and velocity. *J. Neurophysiol.* 92, 3244–3254. doi: 10.1152/jn.00257.2004
- Klingner, C. M., Langbein, K., Dietzek, M., Smesny, S., Witte, O. W., Sauer, H., et al. (2014). Thalamocortical connectivity during resting state in schizophrenia. *Eur. Arch. Psychiatry Clin. Neurosci.* 264, 111–119. doi: 10.1007/s00406-013-0417-0
- Kohn, A. (2007). Visual adaptation: physiology, mechanisms, and functional benefits. *J. Neurophysiol.* 97, 3155–3164. doi: 10.1152/jn.00086.2007
- Komatsu, M., Takaura, K., and Fujii, N. (2015). Mismatch negativity in common marmosets: whole-cortical recordings with multi-channel electrocorticograms. *Sci. Rep.* 5:15006. doi: 10.1038/srep15006
- Koshiyama, D., Kirihaara, K., Tada, M., Nagai, T., Fujioka, M., Usui, K., et al. (2020). Reduced auditory mismatch negativity reflects impaired deviance detection in schizophrenia. *Schizophr. Bull.* doi: 10.1093/schbul/sbaa006 [Epub ahead of print].
- Kremelacke, J., Kreegipuu, K., Tales, A., Astikainen, P., Poldver, N., Näätänen, R., et al. (2016). Visual mismatch negativity (vMMN): a review and meta-analysis of studies in psychiatric and neurological disorders. *Cortex* 80, 76–112. doi: 10.1016/j.cortex.2016.03.017
- Kröcher, T., Malinovskaja, K., Jürgenson, M., Aonurm-Helm, A., Zharkovskaya, T., Kalda, A., et al. (2015). Schizophrenia-like phenotype of polysialyltransferase ST8SIA2-deficient mice. *Brain Struct. Funct.* 220, 71–83. doi: 10.1007/s00429-013-0638-z
- Kum, J., Kim, J. W., Braubach, O., Ha, J. G., Cho, H. J., Kim, C. H., et al. (2019). Neural dynamics of olfactory perception: low- and high-frequency modulations of local field potential spectra in mice revealed by an oddball stimulus. *Front. Neurosci.* 13:478. doi: 10.3389/fnins.2019.00478
- Kuo, S. P., and Trussell, L. O. (2011). Spontaneous spiking and synaptic depression underlie noradrenergic control of feed-forward inhibition. *Neuron* 71, 306–318. doi: 10.1016/j.neuron.2011.05.039
- Latimer, K. W., Barbera, D., Sokoletsky, M., Awwad, B., Katz, Y., Nelken, I., et al. (2019). Multiple timescales account for adaptive responses across sensory cortices. *J. Neurosci.* 39, 10019–10033. doi: 10.1523/JNEUROSCI.1642-19.2019
- Lavoie, S., Polari, A. R., Goldstone, S., Nelson, B., and McGorry, P. D. (2019). Staging model in psychiatry: review of the evolution of electroencephalography abnormalities in major psychiatric disorders. *Early Interv. Psychiatry* 13, 1319–1328. doi: 10.1111/eip.12792
- Lee, M., Balla, A., Sershen, H., Sehatpour, P., Lakatos, P., and Javitt, D. C. (2018). Rodent mismatch negativity/theta neuro-oscillatory response as a translational neurophysiological biomarker for N-methyl-D-aspartate receptor-based new treatment development in schizophrenia. *Neuropsychopharmacology* 43, 571–582. doi: 10.1038/npp.2017.176
- Luck, S. J., and Kappenman, E. S. (2013). *The Oxford Handbook of Event-Related Potential Components*. Oxford; New York, NY: Oxford University Press.
- Lundstrom, B. N., Fairhall, A. L., and Maravall, M. (2010). Multiple timescale encoding of slowly varying whisker stimulus envelope in cortical and thalamic neurons *in vivo*. *J. Neurosci.* 30, 5071–5077. doi: 10.1523/JNEUROSCI.2193-09.2010
- Ma, Y., Hu, H., and Agmon, A. (2012). Short-term plasticity of unitary inhibitory-to-inhibitory synapses depends on the presynaptic interneuron subtype. *J. Neurosci.* 32, 983–988. doi: 10.1523/JNEUROSCI.5007-11.2012
- Ma, W. P., Liu, B. H., Li, Y. T., Huang, Z. J., Zhang, L. I., and Tao, H. W. (2010). Visual representations by cortical somatostatin inhibitory neurons—selective but with weak and delayed responses. *J. Neurosci.* 30, 14371–14379. doi: 10.1523/JNEUROSCI.3248-10.2010
- Malmierca, M. S., Anderson, L. A., and Antunes, F. M. (2015). The cortical modulation of stimulus-specific adaptation in the auditory midbrain and thalamus: a potential neuronal correlate for predictive coding. *Front. Syst. Neurosci.* 9:19. doi: 10.3389/fnsys.2015.00019
- Malmierca, M. S., Cristaudo, S., Pérez-González, D., and Covey, E. (2009). Stimulus-specific adaptation in the inferior colliculus of the anesthetized rat. *J. Neurosci.* 29, 5483–5493. doi: 10.1523/JNEUROSCI.4153-08.2009
- Marshall, L., Molle, M., and Bartsch, P. (1996). Event-related  $\gamma$  band activity during passive and active oddball tasks. *Neuroreport* 7, 1517–1520. doi: 10.1097/00001756-199606170-00016
- McCollum, J., Larson, J., Otto, T., Schottler, F., Granger, R., and Lynch, G. (1991). Short-latency single unit processing in olfactory cortex. *J. Cogn. Neurosci.* 3, 293–299. doi: 10.1162/jocn.1991.3.3.293
- McLaughlin, D. F., and Kelly, E. F. (1993). Evoked potentials as indices of adaptation in the somatosensory system in humans: a review and prospectus. *Brain Res. Rev.* 18, 151–206. doi: 10.1016/0165-0173(93)90001-g
- Michie, P. T., Malmierca, M. S., Harms, L., and Todd, J. (2016). The neurobiology of MMN and implications for schizophrenia. *Biol. Psychol.* 116, 90–97. doi: 10.1016/j.biopsycho.2016.01.011
- Mill, R., Coath, M., Wenekers, T., and Denham, S. L. (2011). A neurocomputational model of stimulus-specific adaptation to oddball and Markov sequences. *PLoS Comput. Biol.* 7:e1002117. doi: 10.1371/journal.pcbi.1002117
- Mitelman, S. A. (2019). Transdiagnostic neuroimaging in psychiatry: a review. *Psychiatry Res.* 277, 23–38. doi: 10.1016/j.psychres.2019.01.026
- Muñoz, W., Tremblay, R., Levenstein, D., and Rudy, B. (2017). Layer-specific modulation of neocortical dendritic inhibition during active wakefulness. *Science* 355, 954–959. doi: 10.1126/science.aag2599

- Musall, S., Haiss, F., Weber, B., and von der Behrens, W. (2017). Deviant processing in the primary somatosensory cortex. *Cereb. Cortex* 27, 863–876. doi: 10.1093/cercor/bhv283
- Näätänen, R. (1995). The mismatch negativity: a powerful tool for cognitive neuroscience. *Ear Hear.* 16, 6–18. doi: 10.1097/00003446-199502000-00002
- Näätänen, R. (2000). Mismatch negativity (MMN): perspectives for application. *Int. J. Psychophysiol.* 37, 3–10. doi: 10.1016/s0167-8760(00)00091-x
- Näätänen, R., and Alho, K. (1995a). Generators of electrical and magnetic mismatch responses in humans. *Brain Topogr.* 7, 315–320. doi: 10.1007/bf01195257
- Näätänen, R., and Alho, K. (1995b). Mismatch negativity—a unique measure of sensory processing in audition. *Int. J. Neurosci.* 80, 317–337. doi: 10.3109/00207459508986107
- Näätänen, R., Astikainen, P., Ruusuvirta, T., and Huottilainen, M. (2010). Automatic auditory intelligence: an expression of the sensory-cognitive core of cognitive processes. *Brain Res. Rev.* 64, 123–136. doi: 10.1016/j.brainresrev.2010.03.001
- Näätänen, R., Kujala, T., Kreegipuu, K., Carlson, S., Escera, C., Baldeweg, T., et al. (2011). The mismatch negativity: an index of cognitive decline in neuropsychiatric and neurological diseases and in ageing. *Brain* 134, 3435–3453. doi: 10.1093/brain/awr064
- Näätänen, R., Sussman, E. S., Salisbury, D., and Shafer, V. L. (2014). Mismatch negativity (MMN) as an index of cognitive dysfunction. *Brain Topogr.* 27, 451–466. doi: 10.1007/s10548-014-0374-6
- Nakamura, T., Michie, P. T., Fulham, W. R., Todd, J., Budd, T. W., Schall, U., et al. (2011). Epidural auditory event-related potentials in the rat to frequency and duration deviants: evidence of mismatch negativity? *Front. Psychol.* 2:367. doi: 10.3389/fpsyg.2011.00367
- Natan, R. G., Briguglio, J. J., Mwilambwe-Tshilobo, L., Jones, S. I., Aizenberg, M., Goldberg, E. M., et al. (2015). Complementary control of sensory adaptation by two types of cortical interneurons. *Elife* 4:e09868. doi: 10.7554/eLife.09868
- Natan, R. G., Rao, W., and Geffen, M. N. (2017). Cortical interneurons differentially shape frequency tuning following adaptation. *Cell Rep.* 21, 878–890. doi: 10.1016/j.celrep.2017.10.012
- Nelken, I. (2014). Stimulus-specific adaptation and deviance detection in the auditory system: experiments and models. *Biol. Cybern.* 108, 655–663. doi: 10.1007/s00422-014-0585-7
- Nelken, I., and Ulanovsky, N. (2007). Mismatch negativity and stimulus-specific adaptation in animal models. *J. Psychophysiol.* 21, 214–223. doi: 10.1027/0269-8803.21.34.214
- Nikolaev, A., Leung, K. M., Odermatt, B., and Lagnado, L. (2013). Synaptic mechanisms of adaptation and sensitization in the retina. *Nat. Neurosci.* 16, 934–941. doi: 10.1038/nn.3408
- Nomoto, M., Suga, N., and Katsuki, Y. (1964). Discharge pattern and inhibition of primary auditory nerve fibers in the monkey. *J. Neurophysiol.* 27, 768–787. doi: 10.1152/jn.1964.27.5.768
- Ogg, M. C., Bendahmane, M., and Fletcher, M. L. (2015). Habituation of glomerular responses in the olfactory bulb following prolonged odor stimulation reflects reduced peripheral input. *Front. Mol. Neurosci.* 8:53. doi: 10.3389/fnmol.2015.00053
- Ogg, M. C., Ross, J. M., Bendahmane, M., and Fletcher, M. L. (2018). Olfactory bulb acetylcholine release dishabituates odor responses and reinstates odor investigation. *Nat. Commun.* 9:1868. doi: 10.1038/s41467-018-04371-w
- Parras, G. G., Nieto-Diego, J., Carbajal, G. V., Valdés-Baizabal, C., Escera, C., and Malmierca, M. S. (2017). Neurons along the auditory pathway exhibit a hierarchical organization of prediction error. *Nat. Commun.* 8:2148. doi: 10.1038/s41467-017-02038-6
- Patterson, J. V., Hetrick, W. P., Boutros, N. N., Jin, Y., Sandman, C., Stern, H., et al. (2008). P50 sensory gating ratios in schizophrenics and controls: a review and data analysis. *Psychiatry Res.* 158, 226–247. doi: 10.1016/j.psychres.2007.02.009
- Pause, B. M., and Krauel, K. (2000). Chemosensory event-related potentials (CSERP) as a key to the psychology of odors. *Int. J. Psychophysiol.* 36, 105–122. doi: 10.1016/s0167-8760(99)00105-1
- Pérez-González, D., and Malmierca, M. S. (2014). Adaptation in the auditory system: an overview. *Front. Integr. Neurosci.* 8:19. doi: 10.3389/fnint.2014.00019
- Peter, V., McArthur, G., and Thompson, W. F. (2010). Effect of deviance direction and calculation method on duration and frequency mismatch negativity (MMN). *Neurosci. Lett.* 482, 71–75. doi: 10.1016/j.neulet.2010.07.010
- Phillips, E. A., and Hasenstaub, A. R. (2016). Asymmetric effects of activating and inactivating cortical interneurons. *Elife* 5:e18383. doi: 10.7554/eLife.18383
- Picton, T. W. (1992). The P300 wave of the human event-related potential. *J. Clin. Neurophysiol.* 9, 456–479. doi: 10.1097/00004691-199210000-00002
- Plomp, R. (1964). Rate of decay of auditory sensation. *J. Acoust. Soc. Am.* 36, 277–282. doi: 10.1121/1.1918946
- Polterovich, A., Jankowski, M. M., and Nelken, I. (2018). Deviance sensitivity in the auditory cortex of freely moving rats. *PLoS One* 13:e0197678. doi: 10.1371/journal.pone.0197678
- Pozzorini, C., Naud, R., Mensi, S., and Gerstner, W. (2013). Temporal whitening by power-law adaptation in neocortical neurons. *Nat. Neurosci.* 16, 942–948. doi: 10.1038/nn.3431
- Rabinowicz, E. F., Silipo, G., Goldman, R., and Javitt, D. C. (2000). Auditory sensory dysfunction in schizophrenia: imprecision or distractibility? *Arch. Gen. Psychiatry* 57, 1149–1155. doi: 10.1001/archpsyc.57.12.1149
- Relkin, E. M., and Turner, C. W. (1988). A reexamination of forward masking in the auditory nerve. *J. Acoust. Soc. Am.* 84, 584–591. doi: 10.1121/1.396836
- Reyes, A., Lujan, R., Rozov, A., Burnashev, N., Somogyi, P., and Sakmann, B. (1998). Target-cell-specific facilitation and depression in neocortical circuits. *Nat. Neurosci.* 1, 279–285. doi: 10.1038/1092
- Rosburg, T., Boutros, N. N., and Ford, J. M. (2008). Reduced auditory evoked potential component N100 in schizophrenia—a critical review. *Psychiatry Res.* 161, 259–274. doi: 10.1016/j.psychres.2008.03.017
- Rosburg, T., Trautner, P., Ludwig, E., Schaller, C., Kurthen, M., Elger, C. E., et al. (2007). Hippocampal event-related potentials to tone duration deviance in a passive oddball paradigm in humans. *NeuroImage* 37, 274–281. doi: 10.1016/j.neuroimage.2007.05.002
- Ruusuvirta, T., Penttonen, M., and Korhonen, T. (1998). Auditory cortical event-related potentials to pitch deviances in rats. *Neurosci. Lett.* 248, 45–48. doi: 10.1016/s0304-3940(98)00330-9
- Safari, M. S., Mirnajafi-Zadeh, J., Hioki, H., and Tsumoto, T. (2017). Parvalbumin-expressing interneurons can act solo while somatostatin-expressing interneurons act in chorus in most cases on cortical pyramidal cells. *Sci. Rep.* 7:12764. doi: 10.1038/s41598-017-12958-4
- Schall, U., Johnston, P., Todd, J., Ward, P. B., and Michie, P. T. (2003). Functional neuroanatomy of auditory mismatch processing: an event-related fMRI study of duration-deviant oddballs. *NeuroImage* 20, 729–736. doi: 10.1016/s1053-8119(03)00398-7
- Schecter, I., Butler, P. D., Jalbrzikowski, M., Pasternak, R., Saperstein, A. M., and Javitt, D. C. (2006). A new dimension of sensory dysfunction: stereopsis deficits in schizophrenia. *Biol. Psychiatry* 60, 1282–1284. doi: 10.1016/j.biopsych.2006.03.064
- Schirmer, A., Escoffier, N., Cheng, X., Feng, Y., and Penney, T. B. (2015). Detecting temporal change in dynamic sounds: on the role of stimulus duration, speed, and emotion. *Front. Psychol.* 6:2055. doi: 10.3389/fpsyg.2015.02055
- Scholes, C., Palmer, A. R., and Sumner, C. J. (2011). Forward suppression in the auditory cortex is frequency-specific. *Eur. J. Neurosci.* 33, 1240–1251. doi: 10.1111/j.1460-9568.2010.07568.x
- Schröger, E., Näätänen, R., and Paavilainen, P. (1992). Event-related potentials reveal how non-attended complex sound patterns are represented by the human brain. *Neurosci. Lett.* 146, 183–186. doi: 10.1016/0304-3940(92)90073-g
- Schröger, E., and Wolff, C. (1996). Mismatch response of the human brain to changes in sound location. *Neuroreport* 7, 3005–3008. doi: 10.1097/00001756-199611250-00041
- Schuelert, N., Dorner-Ciossek, C., Brendel, M., and Rosenbrock, H. (2018). A comprehensive analysis of auditory event-related potentials and network oscillations in an NMDA receptor antagonist mouse model using a novel wireless recording technology. *Physiol. Rep.* 6:e13782. doi: 10.14814/phy2.13782
- Seybold, B. A., Phillips, E. A. K., Schreiner, C. E., and Hasenstaub, A. R. (2015). Inhibitory actions unified by network integration. *Neuron* 87, 1181–1192. doi: 10.1016/j.neuron.2015.09.013
- Shestopalova, L. B., Petropavlovskaya, E. A., Semenova, V. V., and Nikitin, N. I. (2018). Mismatch negativity and psychophysical detection of rising and falling

- intensity sounds. *Biol. Psychol.* 133, 99–111. doi: 10.1016/j.biopsycho.2018.01.018
- Shinozaki, N., Yabe, H., Sutoh, T., Hiruma, T., and Kaneko, S. (1998). Somatosensory automatic responses to deviant stimuli. *Cogn. Brain Res.* 7, 165–171. doi: 10.1016/s0926-6410(98)00020-2
- Shiramatsu, T. I., Kanzaki, R., and Takahashi, H. (2013). Cortical mapping of mismatch negativity with deviance detection property in rat. *PLoS One* 8:e82663. doi: 10.1371/journal.pone.0082663
- Silberberg, G., and Markram, H. (2007). Disynaptic inhibition between neocortical pyramidal cells mediated by Martinotti cells. *Neuron* 53, 735–746. doi: 10.1016/j.neuron.2007.02.012
- Sodhi, M. S., Simmons, M., McCullumsmith, R., Haroutunian, V., and Meador-Woodruff, J. H. (2011). Glutamatergic gene expression is specifically reduced in thalamocortical projecting relay neurons in schizophrenia. *Biol. Psychiatry* 70, 646–654. doi: 10.1016/j.biopsych.2011.02.022
- Solomon, S. G., and Kohn, A. (2014). Moving sensory adaptation beyond suppressive effects in single neurons. *Curr. Biol.* 24, R1012–R1022. doi: 10.1016/j.cub.2014.09.001
- Stefanics, G., Kremláček, J., and Czigler, I. (2014). Visual mismatch negativity: a predictive coding view. *Front. Hum. Neurosci.* 8:666. doi: 10.3389/fnhum.2014.00666
- Stefanics, G., Kremláček, J., and Czigler, I. (2016). Mismatch negativity and neural adaptation: two sides of the same coin. Response: commentary: visual mismatch negativity: a predictive coding view. *Front. Hum. Neurosci.* 10:13. doi: 10.3389/fnhum.2016.00013
- Strelnikov, K. (2007). Can mismatch negativity be linked to synaptic processes? A glutamatergic approach to deviance detection. *Brain Cogn.* 65, 244–251. doi: 10.1016/j.bandc.2007.04.002
- Suzuki, N., and Bekkers, J. M. (2006). Neural coding by two classes of principal cells in the mouse piriform cortex. *J. Neurosci.* 26, 11938–11947. doi: 10.1523/JNEUROSCI.3473-06.2006
- Taaseh, N., Yaron, A., and Nelken, I. (2011). Stimulus-specific adaptation and deviance detection in the rat auditory cortex. *PLoS One* 6:e23369. doi: 10.1371/journal.pone.0023369
- Tada, M., Kiriha, K., Mizutani, S., Uka, T., Kunii, N., Koshiyama, D., et al. (2019). Mismatch negativity (MMN) as a tool for translational investigations into early psychosis: a review. *Int. J. Psychophysiol.* 145, 5–14. doi: 10.1016/j.ijpsycho.2019.02.009
- Tiitinen, H., May, P., and Näätänen, R. (1997). The transient 40-Hz response, mismatch negativity, and attentional processes in humans. *Prog. Neuropsychopharmacol. Biol. Psychiatry* 21, 751–771. doi: 10.1016/s0278-5846(97)00077-8
- Tsodyks, M. V., and Markram, H. (1997). The neural code between neocortical pyramidal neurons depends on neurotransmitter release probability. *Proc. Natl. Acad. Sci. U S A* 94, 719–723. doi: 10.1073/pnas.94.2.719
- Tu, P. C., Bai, Y. M., Li, C. T., Chen, M. H., Lin, W. C., Chang, W. C., et al. (2019). Identification of common thalamocortical dysconnectivity in four major psychiatric disorders. *Schizophr. Bull.* 45, 1143–1151. doi: 10.1093/schbul/sby166
- Ueno, A., Hirata, S., Fuwa, K., Sugama, K., Kusunoki, K., Matsuda, G., et al. (2008). Auditory ERPs to stimulus deviance in an awake chimpanzee (*Pan troglodytes*): towards hominid cognitive neurosciences. *PLoS One* 3:e1442. doi: 10.1371/journal.pone.0001442
- Ulanovsky, N., Las, L., Farkas, D., and Nelken, I. (2004). Multiple time scales of adaptation in auditory cortex neurons. *J. Neurosci.* 24, 10440–10453. doi: 10.1523/JNEUROSCI.1905-04.2004
- Umbricht, D., Vyssotski, D., Latanov, A., Nitsch, R., and Lipp, H. P. (2005). Deviance-related electrophysiological activity in mice: is there mismatch negativity in mice? *Clin. Neurophysiol.* 116, 353–363. doi: 10.1016/j.clinph.2004.08.015
- Valdés-Baizabal, C., Parras, G. G., Ayala, Y. A., and Malmierca, M. S. (2017). Endocannabinoid modulation of stimulus-specific adaptation in inferior colliculus neurons of the rat. *Sci. Rep.* 7:6997. doi: 10.1038/s41598-017-07460-w
- Volk, D. W., and Lewis, D. A. (2013). Prenatal ontogeny as a susceptibility period for cortical GABA neuron disturbances in schizophrenia. *Neuroscience* 248, 154–164. doi: 10.1016/j.neuroscience.2013.06.008
- Wagner, A., Aizenstein, H., Frank, G. K., Figurski, J., May, J. C., Putnam, K., et al. (2006). Neural correlates of habituation to taste stimuli in healthy women. *Psychiatry Res.* 147, 57–67. doi: 10.1016/j.psychres.2005.11.005
- Wang, X., Qi, Q., Huang, C., Chomiak, T., and Luo, F. (2016). Duration sensitivity of neurons in the primary auditory cortex of albino mouse. *Hear. Res.* 332, 160–169. doi: 10.1016/j.heares.2015.10.018
- Wang, Q., Webber, R. M., and Stanley, G. B. (2010). Thalamic synchrony and the adaptive gating of information flow to cortex. *Nat. Neurosci.* 13, 1534–1541. doi: 10.1038/nn.2670
- Wehr, M., and Zador, A. M. (2005). Synaptic mechanisms of forward suppression in rat auditory cortex. *Neuron* 47, 437–445. doi: 10.1016/j.neuron.2005.06.009
- Whitmire, C. J., Waiblinger, C., Schwarz, C., and Stanley, G. B. (2016). Information coding through adaptive gating of synchronized thalamic bursting. *Cell Rep.* 14, 795–807. doi: 10.1016/j.celrep.2015.12.068
- Wiens, S., Szychowska, M., Eklund, R., and van Berlekom, E. (2019). Cascade and no-repetition rules are comparable controls for the auditory frequency mismatch negativity in oddball tasks. *Psychophysiology* 56:e13280. doi: 10.1111/psyp.13280
- Wilent, W. B., and Contreras, D. (2005). Stimulus-dependent changes in spike threshold enhance feature selectivity in rat barrel cortex neurons. *J. Neurosci.* 25, 2983–2991. doi: 10.1523/JNEUROSCI.4906-04.2005
- Wilson, D. A. (1998a). Habituation of odor responses in the rat anterior piriform cortex. *J. Neurophysiol.* 79, 1425–1440. doi: 10.1152/jn.1998.79.3.1425
- Wilson, D. A. (1998b). Synaptic correlates of odor habituation in the rat anterior piriform cortex. *J. Neurophysiol.* 80, 998–1001. doi: 10.1152/jn.1998.80.2.998
- Wilson, D. A. (2000). Comparison of odor receptive field plasticity in the rat olfactory bulb and anterior piriform cortex. *J. Neurophysiol.* 84, 3036–3042. doi: 10.1152/jn.2000.84.6.3036
- Wood, K. C., Blackwell, J. M., and Geffen, M. N. (2017). Cortical inhibitory interneurons control sensory processing. *Curr. Opin. Neurobiol.* 46, 200–207. doi: 10.1016/j.conb.2017.08.018
- Yarden, T. S., and Nelken, I. (2017). Stimulus-specific adaptation in a recurrent network model of primary auditory cortex. *PLoS Comput. Biol.* 13:e1005437. doi: 10.1371/journal.pcbi.1005437

**Conflict of Interest:** The authors declare that the research was conducted in the absence of any commercial or financial relationships that could be construed as a potential conflict of interest.

Copyright © 2020 Ross and Hamm. This is an open-access article distributed under the terms of the Creative Commons Attribution License (CC BY). The use, distribution or reproduction in other forums is permitted, provided the original author(s) and the copyright owner(s) are credited and that the original publication in this journal is cited, in accordance with accepted academic practice. No use, distribution or reproduction is permitted which does not comply with these terms.



# The Role of Temporal and Spatial Attention in Size Adaptation

Alessia Tonelli<sup>1,2\*</sup>, Arezoo Pooresmaeili<sup>3</sup> and Roberto Arrighi<sup>4\*</sup>

<sup>1</sup> Department of Translational Research of New Technologies in Medicine and Surgery, University of Pisa, Pisa, Italy, <sup>2</sup> Univip, Unit for Visually Impaired People, Istituto Italiano di Tecnologia, Genoa, Italy, <sup>3</sup> Perception and Cognition Group, European Neuroscience Institute, Göttingen, Germany, <sup>4</sup> Department of Neuroscience, Psychology, Pharmacology and Child Health (NEUROFARBA), University of Florence, Florence, Italy

## OPEN ACCESS

### Edited by:

Colin W. G. Clifford,  
University of New South Wales,  
Australia

### Reviewed by:

Jason Bell,  
University of Western Australia,  
Australia  
Regan Mathew Gallagher,  
University of Queensland, Australia

### \*Correspondence:

Alessia Tonelli  
tonelli.alessia@gmail.com  
Roberto Arrighi  
roberto.arrighi@gmail.com

### Specialty section:

This article was submitted to  
Perception Science,  
a section of the journal  
Frontiers in Neuroscience

**Received:** 29 January 2020

**Accepted:** 01 May 2020

**Published:** 03 June 2020

### Citation:

Tonelli A, Pooresmaeili A and  
Arrighi R (2020) The Role of Temporal  
and Spatial Attention in Size  
Adaptation. *Front. Neurosci.* 14:539.  
doi: 10.3389/fnins.2020.00539

One of the most important tasks for the visual system is to construct an internal representation of the spatial properties of objects, including their size. Size perception includes a combination of bottom-up (retinal inputs) and top-down (e.g., expectations) information, which makes the estimates of object size malleable and susceptible to numerous contextual cues. For example, it has been shown that size perception is prone to adaptation: brief previous presentations of larger or smaller adapting stimuli at the same region of space changes the perceived size of a subsequent test stimulus. Large adapting stimuli cause the test to appear smaller than its veridical size and vice versa. Here, we investigated whether size adaptation is susceptible to attentional modulation. First, we measured the magnitude of adaptation aftereffects for a size discrimination task. Then, we compared these aftereffects (on average 15–20%) with those measured while participants were engaged, during the adaptation phase, in one of the two highly demanding central visual tasks: Multiple Object Tracking (MOT) or Rapid Serial Visual Presentation (RSVP). Our results indicate that deploying visual attention away from the adapters did not significantly affect the distortions of perceived size induced by adaptation, with accuracy and precision in the discrimination task being almost identical in all experimental conditions. Taken together, these results suggest that visual attention does not play a key role in size adaptation, in line with the idea that this phenomenon can be accounted for by local gain control mechanisms within area V1.

**Keywords:** size perception, visual adaptation, spatial attention, multiple object tracking, rapid serial visual presentation

## INTRODUCTION

Achieving a reliable representation of the surrounding space is one of the most critical tasks that the animals' brain (including humans) has to accomplish. For example, accurate judgment of the size or distance of the objects in the environment is critical for survival as it allows to successfully interact with them. Accordingly, much research has been dedicated to unveil the brain mechanisms underpinning objects' size perception. Nevertheless, the exact mechanisms that underlie size perception are yet poorly understood (Schwarzkopf et al., 2010).

One important characteristic of size perception demonstrated by many studies is its susceptibility to contextual effects. For example, in the Ebbinghaus illusion (Massaro and Anderson, 1971), two identical circles surrounded by large and small stimuli are perceived as having

different sizes. The stimulus surrounded by large flankers appears smaller compared to the other. Mario Ponzo reported another well-known illusion (i.e., Ponzo Illusion), where two identical horizontal lines drawn across a pair of converging lines, one on top and one below, appear to have different lengths; with the one above looking longer than the one below (Leibowitz et al., 1969).

In light of this evidence showing robust contextual modulations of the perceived objects' size, it has been proposed that stimulus size is represented in high-level, associative visual areas such as occipitotemporal cortex where multiple cues related to the objects' identity are combined together (Eger et al., 2008; Konkle and Oliva, 2012). Another related line of evidence supporting this idea is that objects' size is coded in terms of their abstract, real-world as opposed to retinal size, i.e., an elephant is judged to be bigger than a table even when both are presented as images with identical sizes (Konkle and Oliva, 2012; Henik et al., 2017). However, a series of recent studies (Murray et al., 2006; Sperandio et al., 2012; Pooresmaeili et al., 2013) suggested instead that size perception may occur at even earlier stages of visual processing, for instance at the level of the primary visual cortex (area V1). In a fMRI study, Murray et al. (2006) leveraged pictorial cues to manipulate the perceived position of two identical objects in depth (i.e., Ponzo illusion) while recording participants brain activity in area V1. The results show that V1 activation scaled with the perceived size of the objects despite their physical size remaining constant. This suggests that V1 activation combines the incoming retinal signals representing the physical size of the objects with feedbacks from higher-level areas processing objects' position in depth (see also Fang et al., 2008). Similarly, Sperandio et al. (2012) measured V1 activity when participants perceived afterimages of different sizes caused by the projection of the same object on surfaces that were at different viewing distances. The results clearly indicated that V1 activity changed in accordance with the perceived and not the physical size of the afterimage.

Despite these studies suggesting a key role of V1 in constructing an internal representation of objects size, the use of perspective pictorial cues to manipulate perceived size may lead to the involvement of extra-striate cortex where such cues are most reliably coded (Trotter and Celebrini, 1999; Andersson et al., 2007). To overcome such possible effects, size perception has been recently investigated by employing a contextual manipulation that does not use any perspective cue, i.e., perceptual adaptation (Pooresmaeili et al., 2013; Tonelli et al., 2017). After a prolonged exposure to a stimulus of a given size (adapter), the perceived size of a subsequent stimulus presented in the same position of the visual field (test) was found to be robustly distorted according to the classical rebound adaptation effects: larger adapting stimuli caused the test to appear smaller and vice versa. The computational model proposed to account for such adaptation aftereffects was based on a gain control mechanism in which perceived size is influenced by a mechanistic combination of inhibitory and excitatory cortical signals induced by the adapter and test stimuli. In detail, after a sustained presentation of the adapting stimulus, the activity of the V1 regions representing the adapter edges is reduced, changing

the gain of responses of the nearby regions of the striate cortex. When the target stimulus is subsequently presented, the typical cortical activation to this stimulus is distorted by the gain modulation produced by the adapter. In conclusion, the distortion of objects sizes was proposed to arise from gain control mechanisms occurring locally at the level of area V1, whereby the area V1 neural activity matched the perceived, and not the physical size of the object. Although local gain modulation mechanisms at the level of area V1 could sufficiently explain size adaptation effects observed in these previous studies (Sperandio et al., 2012; and in particularly Pooresmaeili et al., 2013), it is still possible that top-down, feedback mechanisms arising from extra-striate cortex (area V2, V3, or V4), higher-level visual areas (such as lateral occipital cortex, area LO) or the fronto-parietal attentional network also influence the strength of the putative local interactions (Schwabe et al., 2006; Gilbert and Li, 2013). To investigate this possibility, Sperandio et al. (2012) tested BOLD responses in retinotopic visual areas beyond area V1. BOLD responses in the areas V2 and V3 showed no modulation in relation to the size of afterimages, which casts doubt on the involvement of these extra-striate areas in the representation of objects' perceived size. Pooresmaeili et al. (2013), however, found that the strongest size adaptation effect across all tested conditions (i.e., with the adapter being larger, identical, or smaller in size than the test stimulus) occurred in areas V1–V3, whereas in area V4 only a trend was found that did not reach statistical significance. In area LO (Lateral Occipital Cortex) the adaptation effect was only observed when the adapter and the test had an identical size, which is in line with the role of this area in object categorization (Grill-Spector et al., 1999). Therefore, in both studies, the most robust correlates of perceived size were found in area V1. Is it possible that these correlates of size perception at the level of area V1 reflect mechanisms that are stirred by the allocation of visual attention? This is a plausible question given that attention can influence almost all aspects of visual processing. As demonstrated by a host of previous research, the deployment of spatial attention not only increases sensitivity, shortens reaction times and induces a more accurate performance (Posner et al., 1980; Doshier et al., 1986; Yeshurun and Carrasco, 1998), but also alters stimulus appearance (for a review see Gobell and Carrasco, 2005). Indeed, attention has been reported to increase apparent contrast (Carrasco et al., 2004), spatial frequency (Lamb and Yund, 1996), motion coherence (Liu et al., 2006), and perceived speed (Anton-Erxleben et al., 2013). Moreover, the relationship between visual attention and the perception of object size has been also directly investigated. On one hand, it has been shown that attention alters the perceived objects size (Anton-Erxleben et al., 2007), while on the other hand, objects' size has been demonstrated to interact with the way that visual attention is allocated (Collegio et al., 2019).

Many influential models of attention maintain that modulation of visual processing by attention relies on top-down feedback signals that originate from a fronto-parietal network (Corbetta and Shulman, 2002) and influence upstream visual areas such as area V1, possibly through a gain-control mechanism (Reynolds and Chelazzi, 2004). Inspired by

this theoretical framework, some studies have employed manipulations of visual attention as a means to investigate whether the perceived objects' size is genuinely coded at the level of the primary visual areas or it originates from feedback pathways conveying contextual information from higher visual areas. For instance, exploiting a paradigm similar to Murray et al. (2006) and Fang et al. (2008) reported that the focus of visual attention alters the representation of objects size in V1. Specifically, while spatial distribution of V1 activity represented the perceived rather than physical size of the stimuli – activities induced by a stimulus perceived to be located further away yielded a more eccentric representation than those evoked by a stimulus perceived as being closer – directing attention elsewhere significantly reduced this effect. This result is consistent with the idea that diverting the focus of visual attention attenuates the top-down influence of higher visual areas on V1, thereby dampening V1's capacity to integrate 3D depth cues. In a complementary study, Kreutzer et al. (2015) reported a significant role of selective attention in contextual modulation of object size perception even when they did not entail high-level perspective cues. Taken together, the picture emerging from these latter studies suggests that the local gain control mechanisms proposed by Pooremaeili et al. (2013) might in fact result from long-distance feedback signals originating from elsewhere in the visual hierarchy.

In the current study, we try to resolve this controversy by directly testing whether visual attention mediates the visual size adaptation effects observed in our previous work (Pooremaeili et al., 2013). We asked participants to perform a size discrimination task in the periphery of the visual field while, during visual adaptation, they performed one of the two sustained attentional tasks (tested in separated sessions) at fovea. These tasks comprised either a rapid serial visual presentation (RSVP – Broadbent and Broadbent, 1987), or a multiple object-tracking task (MOT – Pylyshyn and Storm, 1988) engaging temporal or spatio-temporal attention, respectively. Participants' performance was assessed in terms of accuracy (Point of Subjective Equality: PSE) as well as precision (Weber Fractions: WFs), that is the discrimination threshold normalized by the PSE. If the effects of adaptation on the processing of objects' size tap on automatic, pre-attentive processes, withdrawing attention from the adapter location and allocating it elsewhere should not affect subjects' size estimations. Conversely, the involvement of attention-dependent mechanisms will predict a reduction or disappearance of size adaptation effects when attention is diverted away from the adapter.

## MATERIALS AND METHODS

### Participants

Nine healthy adults (three males, six females, average age: 27.7 years of age –  $SD = 0.97$ ) with normal or corrected to normal vision participated in the experiments. All participants have been recruited from the faculty of psychology of the local university and have not been compensated to participate in the study. The local ethics committee (Comitato

Etico Pediatrico Regionale, Azienda Ospedaliera-universitaria Meyer, Florence) approved all experimental procedures. The study was carried out in accordance with the Declaration of Helsinki and each participant gave informed consent before participation.

### Stimuli

All visual stimuli were generated in MATLAB, using the Psychophysics Toolbox version extensions and displayed on a Mitsubishi Diamond Plus 220 monitor (resolution of  $1,280 \times 1,024$  corresponding to  $41^\circ \times 31.2^\circ$  from participants' viewing distance of 57 cm) with a refresh rate of 85 Hz. In the size discrimination task, stimuli consisted of Craik–O'Brien–Cornsweet circles defined by high-pass Gaussian filters (with a 50% cutoff at spatial frequency of 0.5 cyc/deg). The polarity of the stimuli was reversed at a rate of 10 Hz to avoid afterimages and the presentation time was always set to 500 ms (see **Figure 1A**). Stimuli for the MOT task consisted of 12 dots with a diameter of  $0.4^\circ$ . The dots moved at a speed of about 2 deg/sec in straight lines, and when colliding with other dots bounced appropriately with their motion constrained within a central invisible circular area of  $5^\circ$  of radius (**Figure 1B**). In the rapid serial visual presentation task (RSVP), participants were presented with small red or white alphabetic letters subtending  $2^\circ \times 2^\circ$  displayed at the center of the screen at a rate of about 10 Hz within the 6 s of the adaptation phase (**Figure 1C**).

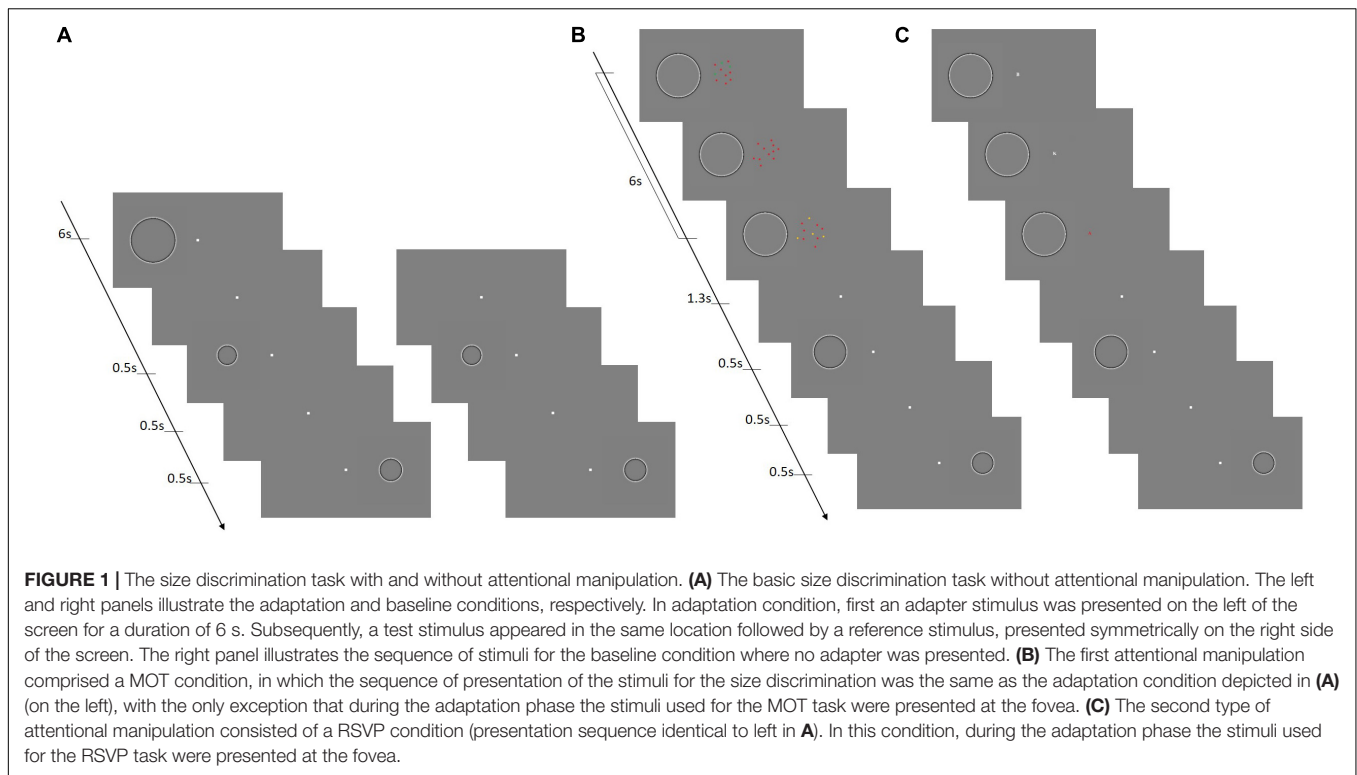
## Procedures

### Size Discrimination

A sequences of two Craik–O'Brien–Cornsweet circles were displayed at two diametrically opposite positions along the monitor horizontal midline at an eccentricity of  $10^\circ$  from the monitor center. In each trial, the size (diameter) of the reference stimulus (displayed on the right) was kept constant at  $5^\circ$  whilst the size of the test stimulus (displayed on the left) varied according to an adaptive staircase QUEST (Watson and Pelli, 1983) with the test size constrained to appear within  $\pm 50\%$  of the size of the reference (**Figure 1**). The participants' task consisted of indicating which stimulus was larger by pressing a key on a PC keyboard. In the adaptation trials, the presentation of the test and reference stimuli was preceded by a large Craik–O'Brien–Cornsweet circle ( $10^\circ$  diameter so that the physical size of the adapter was always larger than the test) displayed on the left-hand side. At the end of the adaptation phase (6 s) the adapter disappeared and the sequence of test and reference stimulus started after 1,300 ms (i.e., inter-trial interval, ITI = 1,500 ms). Each time the discrimination task was carried out, each participant completed 100 trials.

### Rapid Serial Visual Presentation (RSVP)

In this condition, during adaptation, a sequence of red and white letters was presented in the center of the screen. Participant had to indicate whether the number of red letters was more or less than 10 by pressing a key within a 1.3 s interval from the sequence offset (all slower responses were excluded from the



analyses). Each participant performed 100 trials each time the task was performed.

### Multiple Object Tracking (MOT)

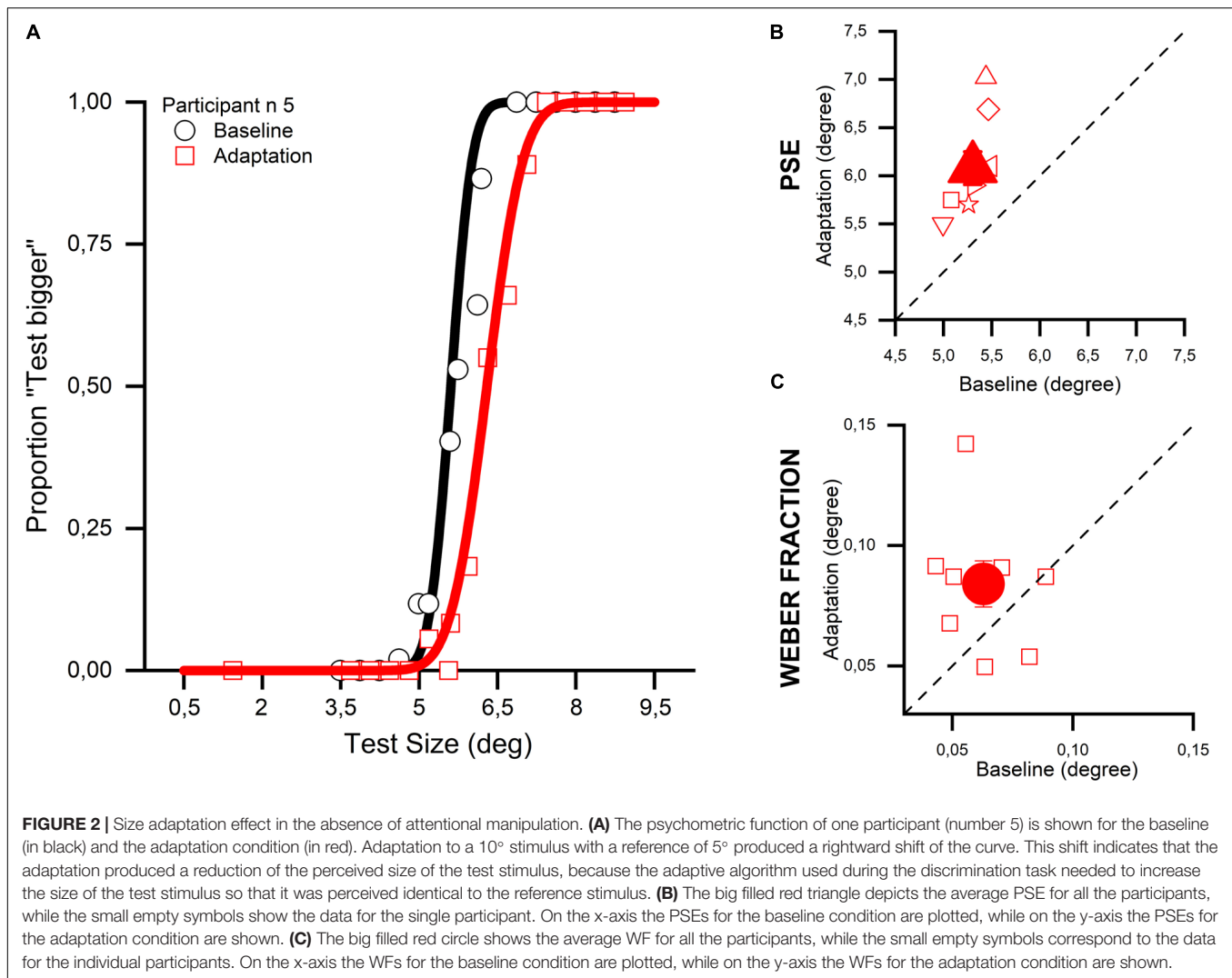
In this condition, during adaptation, participants were presented with 12 randomly moving dots: nine red (distractors) and three green (targets). Participants had 2 s to lock their attention on the target dots, and then these turned to red and became undistinguishable from the distractors. At the end of this tracking phase lasting 4 s, four out of the twelve dots became orange and the task was to indicate whether one of the orange dots was green at the beginning by pressing a key within 1.3 s. Again, all slower responses were excluded from the following analyses. Each participant performed 100 trials each time the task was performed.

At the beginning of the experiment, participants' performance for RSVP and MOT task was measured for several rates of letter presentation (RSVP) and dots speed (MOT). The aim of this procedure was to adjust the difficulty of the two tasks for each participant so that a correct rate of around 70–75% could be achieved for each individual. This procedure allows assessing an increase or a decrease in performance when these tasks were performed during the presentation of the adapting stimuli and concurrent with the size discrimination task.

Subsequently, each participant performed the task of discrimination in baseline and after that where performed three conditions of adaptation in random order between the adaptations with or without attending the MOT or RSVP stimuli and whether or not had to paid attention to the attentional stimuli.

## RESULTS

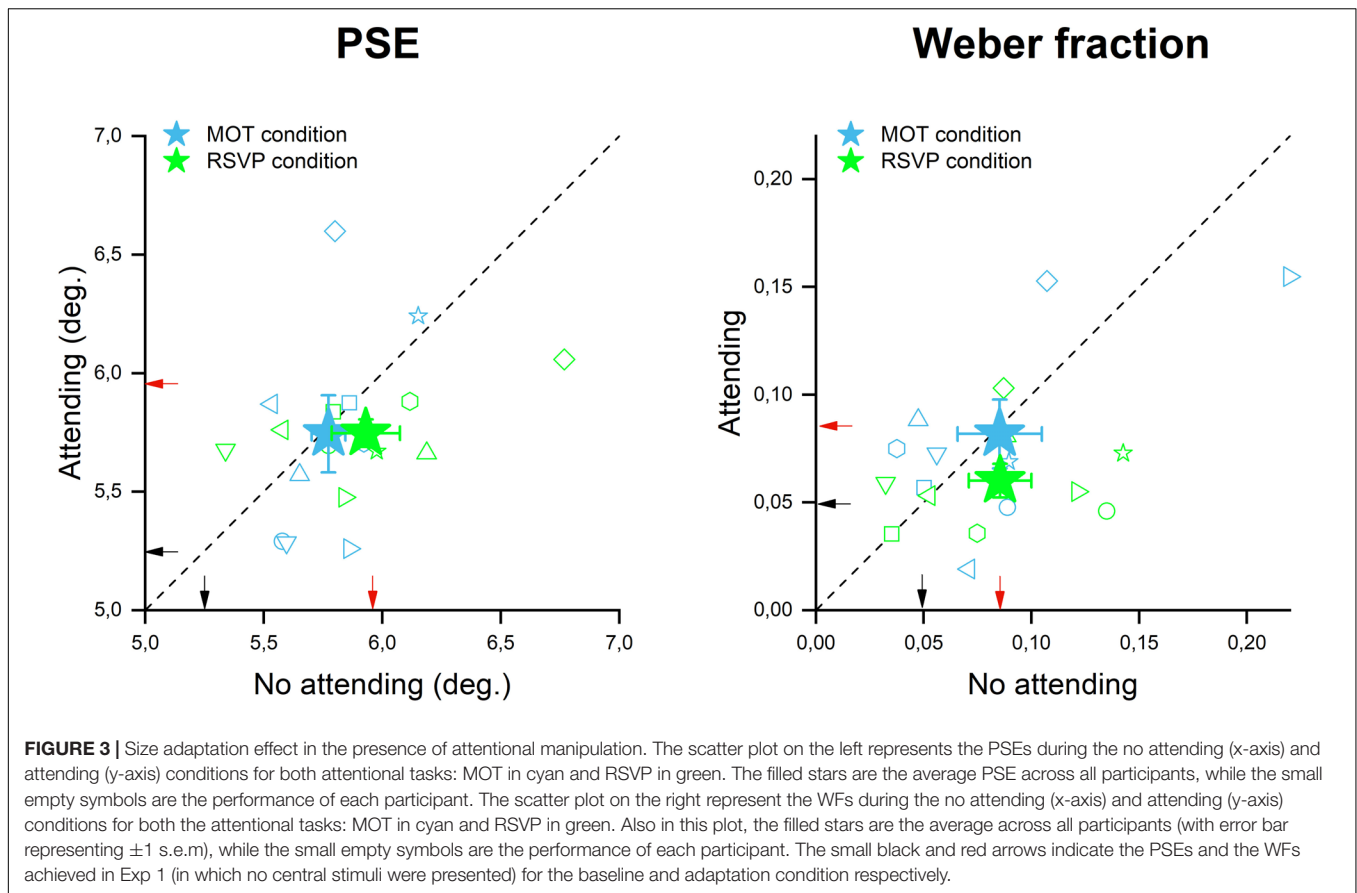
In the first experiment (Exp. 1), we measured the effect of a sustained exposure to a large stimulus (adapter) on the perception of the size of a smaller stimulus subsequently displayed at the adapted location. We measured the physical size of the adapted stimulus (test) needed to make it appear as large as the reference stimulus displayed in a neutral location (PSEs) and compared them with those obtained when size discrimination was performed without adaptation. **Figure 2A** shows how the percentage of “test stimulus larger” responses varied relative to the physical size of the test stimulus for a representative subject. In the baseline condition (no-adaptation), estimates for the test stimulus were rather veridical with the PSEs close to 5° (i.e., physical size of the reference). However, when the presentation of the test stimulus was preceded by a large adapting stimulus, its perceived size was robustly compressed as shown by the rightward shift of the red psychometric function. All participants showed robust adaptation aftereffects (see **Figure 2B**) making the difference between the baseline and adaptation condition highly statistically significant (two-tailed paired-sample *t*-test,  $t_8 = 6.204$ ,  $p < 0.001$ , 95% CI [0.49, 1.07]), a result that replicates previous studies exploiting a similar paradigm (Pooresmaeli et al., 2013; Tonelli et al., 2017). Moreover, a close inspection of the psychometric functions shown in **Figure 2A** suggests that the slope of the curve of the adaptation condition (red) was shallower than that for the no-adaptation (black) condition. Such difference opens up the possibility that adaptation not only affects the *accuracy* of size estimates (as shown by shifts of the PSEs) but also their *precision* to yield lower thresholds



to discriminate between the test and reference. To test this hypothesis, we performed an analysis where for each participant the precision of stimulus size discrimination was measured in terms of Weber Fractions (WFs – discrimination thresholds normalized by PSEs), in both the baseline and adaptation conditions (**Figure 2C**). WFs for the adaptation condition were found to be, on average, slightly higher than in the baseline condition indicating that the exposure to the adapting stimuli lowered the size discrimination sensitivity; a result at odds with the hypothesis that sensory adaptation is aimed to increase the discriminability of similar stimuli (Barlow's efficient coding hypothesis, see Barlow, 1961; Simoncelli, 2003). However, due to the high variability amongst participants, this difference turned out to be just marginally significant (two-tailed paired-sample *t*-test,  $t_8 = 1.843$ ,  $p = 0.1$ , 95% CI  $[-0.005, 0.047]$ ), thus a definitive statement cannot be made about this result at the present stage.

To assess the role of the focus of attention in the size adaptation phenomenon, we devised two new versions of Exp. 1 in which during the adaptation phase, participants were

presented with a central stimulus corresponding to either a temporal (RSVP) or a spatio-temporal (MOT) attentional task. In one case (i.e., central attention condition), participants were required to perform a task on this central display while in the other case (no central attention condition) they passively viewed this display but performed no task on it. The rationale was to compare participants' accuracy and precision in the size discrimination task between these two conditions, which were identical in terms of sensory loads but differed in terms of the allocation of attention. **Figure 3** shows the participants' accuracy and precision of size discrimination when a RSVP or MOT task was performed during adaptation. The perceived size of the test stimulus was quite similar when RSVP stimuli were displayed but subjects were instructed to ignore them (no attending- mean 5.9,  $SD = 0.4$ ) relative to the condition in which RSVP had to be accomplished and thus attention was withdrawn from the adapting stimulus location (mean 5.74,  $SD = 0.17$ , see green stars in **Figure 3A**). This result suggests that shifting the focus of attention away from the adapting stimuli – via a temporal attentional task – did not significantly

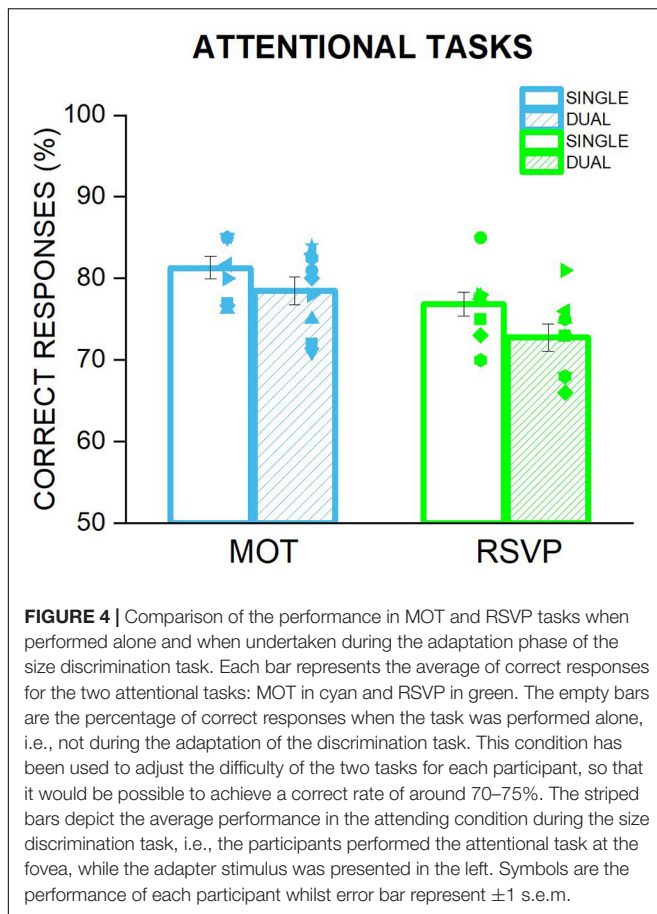


affect the amount of size adaptation induced by them. Indeed, both conditions (attending and not attending to the central RSVP task) turned out to be not significantly different from the adaptation condition of Exp. 1 where no central stimulus was displayed at all [a one-way ANOVA:  $F_{(2,16)} = 3.35$ ,  $p = 0.07$ ,  $ges = 0.127$ ]. One possibility for this lack of interference between size adaptation and the deployment of attentional resources away from the adapters might be that the RSVP task did not involve any spatial processing, which is at the core of objects' size perception. To test for this hypothesis, we replicated the previous experiment by using MOT as the central task as it implies a dynamic allocation of attention to a different spatial location, over time, to track multiple moving targets. However, even in this case, the magnitude of size adaptation indicated by the averaged PSEs achieved when participants were engaged with the central task (y axis position of cyan star in **Figure 3A**, mean 5.74,  $SD = 0.46$ ) was found to be similar to the condition in which no central task was performed (x axis of the cyan star in **Figure 3A**, mean 5.77,  $SD = 0.2$ ). This adaptation magnitude also turned out to be similar to those achieved in Exp. 1 when no central stimuli were displayed at all [a one-way ANOVA:  $F_{(2,16)} = 2.3$ ,  $p = 0.31$ ,  $ges = 0.137$ ]. Taken together these results suggest that neither the increase of sensory load induced by the mere presentation of the central stimuli (the no attending to central task condition), nor the shift of attentional resources away from the adapters (attending to the

central task condition) significantly affect the magnitude of size adaptation aftereffects.

However, even if sensory or attentional load did not affect the accuracy of stimulus size estimates (PSEs); they might still have significantly affected discrimination precision. To test this hypothesis, we measured WFs for the "not attending" and "attending" to the central task conditions for both RSVP and MOT task. WFs measured with the MOT as a central task (**Figure 3B**, in cyan) were found to be almost identical between the "attending" (mean 0.08,  $SD = 0.04$ ) and "not attending" (mean 0.08,  $SD = 0.05$ ) to the central task conditions with these values also being very similar to those achieved in Exp. 1 [a one-way ANOVA:  $F_{(2,16)} = 0.02$ ,  $p = 0.97$ ,  $ges = 0.001$ ]. On the other hand, WFs measured when participants performed RSVP as a central task turned out to be slightly smaller in the "attending" condition (see the green star **Figure 3B**) than in the "not attending" and the no-central stimuli Exp. 1 condition. However, due to the rather substantial variability amongst participants, this difference was not statistically significant [a one-way ANOVA:  $F_{(2,16)} = 2.9$ ,  $p = 0.09$ ,  $ges = 0.135$ ; no attending mean 0.08,  $SD = 0.02$ ; attending mean 0.06,  $SD = 0.04$ ].

One possibility to account for the lack of a significant change in accuracy or precision when the focus of attention is manipulated might be that participants preserved adaptation aftereffects by deploying a negligible amount of their attentional resources to the central task either voluntarily or due to the peripheral flickering



of the adapters automatically capturing their attention. In other words, it might be that performance in the size discrimination task was preserved at the cost of the central task. If so, participants' performance in the RSVP or MOT task when they were performed on their own should be higher than when they were performed during the size discrimination task. However, as shown in **Figure 4**, the percentage of correct responses for the RSVP or the MOT task when the central stimuli were presented simultaneously with the peripheral adapters were almost identical to those measured when these tasks were performed alone (RSVP:  $t = 1.62$ ,  $p = 0.12$ ; MOT:  $t_8 = 1.35$ ,  $p = 0.2$ ). These results clearly rule out the possibility that attention did not affect size adaptation because it was not sufficiently engaged by the central task. Therefore an insufficient deployment of attentional resources on the central tasks cannot account for the similar magnitude of adaptation aftereffects found for the condition in which subjects were engaged in a central task and those where they were not.

## DISCUSSION

In this study, we investigated the role of attention in mediating size adaptation aftereffects, i.e., distortions of perceived size of visual objects induced by the relative size of stimuli previously

displayed in the same area of the visual field. Our results replicate previous findings showing that as a consequence of a prolonged exposure to a given visual stimulus, perceived size of the patterns subsequently presented in that area are distorted as follows: larger adapting stimuli cause the test to appear smaller than its veridical size and vice versa (Pooresmaeili et al., 2013; Tonelli et al., 2017). However, the main goal of the present study was to assess whether, and to what extent, attentional manipulations (such as deploying attention away from the adapters during the adaptation phase) affect size adaptation aftereffects. The results clearly demonstrated that attention *did not* affect either the accuracy or the precision of subject's performance in the discrimination task, suggesting that size adaptation occurs independently from attentional mechanisms. In particular, neither the PSEs (physical size of the adapted stimulus perceived as large as the reference) nor the Weber Fractions (the just noticeable physical difference between the test and reference stimulus) of subjects was significantly changed by engaging in a central perceptual task during exposure to adapting stimuli.

We used two different central attentional tasks (tested in separate sessions), a RSVP mainly engaging temporal attention and a MOT task primarily requiring spatio-temporal attentional resources to track moving stimuli. The rationale was to test for a possible role of "similarity" between the type of attentional resources engaged in the central task and the perceptual processes engaged by size adaptation. The reasoning we followed here to use two types of attentional manipulation was inspired by previous cross-modal studies investigating whether attentional resources for different sensory modalities are shared or independent. Several studies support the latter hypothesis by showing that subjects' performance in a given perceptual task (i.e., visual or auditory) remained unchanged when they concurrently performed a second task in a different sensory modality. However, as brilliantly demonstrated by Wahn and König (2015a,b), this independence only occurred when the primary and the secondary task engaged two different types of attention (i.e., object-based vs. spatial). On the other hand, if the primary and the secondary task both engaged the same type of attentional resources (i.e., spatial attention), subjects' performance in one task impaired performance in the other task suggesting shared attentional resources across different sensory modalities.

Based on these previous observations, we employed two tasks, which involved different degrees of similarity with the type of putative attentional mechanisms that could underlie size perception. Neither the RSVP task that engaged attention across time, nor the MOT task which relied on allocation of attention across space and time yielded significant changes in size adaptation aftereffects (see **Figure 3**) pointing to an almost complete independence of size adaptation from both temporal and spatio-temporal attentional processes. Importantly, we also ruled out the possibility that size discrimination performance was preserved *at the cost* of the central task as subject's performance in both RSVP and MOT tasks during adaptation phase of the size discrimination task did not significantly differ from when they were performed alone (see for details **Figure 4**). Moreover,

we were able to disentangle the effects of attentional deployment from those induced by a change in the sensory load, due to the mere presence of the stimuli of the central task. To this end, we measured the accuracy and precision of the size discrimination task under two conditions. In one condition, subjects were required to attend to the central stimuli while in the other condition they were instructed not to do so (see **Figure 3**). However, keeping the amount of sensory information the same, we found that engaging subjects in a central attentional task during adaptation did not yield any significant effect pointing again to the independence of mechanisms underlying size adaptation from attention.

Interestingly, although attention has been reported to affect many aspects of visual perception, such as apparent contrast (Carrasco et al., 2004), spatial frequency (Lamb and Yund, 1996), motion coherence (Liu et al., 2006), or perceived speed (Anton-Erxleben et al., 2013) and to robustly affect population receptive fields (pRFs) in all areas along the visual hierarchy (Klein et al., 2014), conflicting results have been reported regarding its role in mediating adaptation aftereffects. On one side, attention has been reported to affect adaptation to high level stimuli such as faces (Rhodes et al., 2011) or body size (Stephen et al., 2018). On the other side, however, adaptation aftereffects for low-level visual features have been reported to be attention-independent. For example, Morgan (2012) reported a significant adaptation of stimulus perceived velocity that was completely independent of the amount of attention deployed to the test stimulus. The same author also demonstrated that motion aftereffects induced by adaptation occur independently from subjects' attentional load during the task. In other words, Morgan's results support the idea that visual adaptation for features that are encoded at the early stages of visual processing hierarchy, might be primarily attention-independent. Size adaptation is likely to be one of these processes given that its aftereffects have been successfully modeled in terms of a simple gain control mechanism in which perceived size is retrieved through a combination of inhibitory and excitatory cortical signals induced by the adapter and test stimuli (Pooresmaeili et al., 2013).

However, not all the results in the literature on perception of objects' size are in line with this interpretation. For example, it has been demonstrated that the representation of objects' size in the primary visual area (V1) is attention-dependent (Fang et al., 2008). The authors showed that cortical activations to the same object depicted at two different "depth positions" of a rendered three-dimensional hallway (a version of the well-known Ponzo illusion; Leibowitz et al., 1969) differed according to the perceived object size (Murray et al., 2006). This perceptual illusion was, however, strongly attenuated when spatial attention was diverted away from the test stimuli. It is important to note that in this experiment perceived objects size was manipulated via complex 3D contextual information that are likely to tap on the feedback projections from extra-striate visual areas (involved in processing 3D pictorial cues) down to the V1. Given that these processes are, in turn, likely to be mediated by attentional mechanisms, the difference in the contextual information used in Fang et al. (2008) and Murray et al. (2006) studies (prospective 3D), and the ones employed in the present study (relative size

of 2D objects) might explain the differences in obtained results. Lastly, we note another study, which reported a significant effect of spatial attention in mediating size adaptation without using prospective cues (Kreutzer et al., 2015). The role of attention was investigated by presenting a single adapting stimulus containing both a large and a small adapter, and requiring subjects to selectively direct their attention to one of the adapters before performing a size discrimination task. The results showed that the perceived size of a subsequently displayed test stimulus inversely covaried with the size of the attended adapter suggesting that attention mediates size adaptation aftereffects. However, the simultaneous presentation of flickering stimuli defining the large and the small adapters at a relatively close distance from each other might have made it difficult for the subjects to deploy selectively attention to one of the two adapters. In line with this, the reported size of adaptation aftereffects was quite small (changes of perceived size induced by the small adapter were about 3%) as well as asymmetrical (large adapter not affecting the perceived size of the test stimulus), contrary to other reports investigating size adaptation (Pooresmaeili et al., 2013; Tonelli et al., 2017). Future studies are needed to test these speculations and clarify in which conditions attention mediates size adaptation and in which conditions size adaptation aftereffects are attention-independent.

## DATA AVAILABILITY STATEMENT

The datasets generated for this study are available at the following link <http://doi.org/10.5281/zenodo.3831328>.

## ETHICS STATEMENT

The studies involving human participants were reviewed and approved by Comitato Etico Pediatrico Regionale, Azienda Ospedaliero-universitaria Meyer, Florence (FI). Written informed consent to participate in this study was provided by the patient/participants.

## AUTHOR CONTRIBUTIONS

AT and RA contributed conception, design of the study, and wrote the first draft of the manuscript. AT collected the data and performed the statistical analysis. All authors contributed to manuscript revision, read, and approved the submitted version.

## FUNDING

This project has received funding from the European Research Council (ERC) under the European Union's Horizon 2020 Research and Innovation Program (Grant Agreement No. 801715 – PUPILTRAITS) and from the Italian Ministry of Education, University, and Research under the PRIN2017 program (Grant Agreement No. 2017XBJN4F – ENVIRONMAG).

## REFERENCES

- Andersson, F., Joliot, M., Percey, G., and Petit, L. (2007). Eye position-dependent activity in the primary visual area as revealed by fMRI. *Hum. Brain Mapp.* 28, 673–680. doi: 10.1002/hbm.20296
- Anton-Erxleben, K., Henrich, C., and Treue, S. (2007). Attention changes perceived size of moving visual patterns. *J. Vis.* 7, 1–9. doi: 10.1167/7.11.5
- Anton-Erxleben, K., Herrmann, K., and Carrasco, M. (2013). Independent effects of adaptation and attention on perceived speed. *Psychol. Sci.* 24, 150–159. doi: 10.1177/0956797612449178
- Barlow, H. B. (1961). “Possible principles underlying the transformations of sensory messages,” in *Sensory Communication*, (Cambridge, MA: The MIT Press), 216–234. doi: 10.7551/mitpress/9780262518420.003.0013
- Broadbent, D. E., and Broadbent, M. H. P. (1987). From detection to identification: response to multiple targets in rapid serial visual presentation. *Percept. Psychophys.* 42, 105–113. doi: 10.3758/bf03210498
- Carrasco, M., Ling, S., Gobel, J., Fuller, S., and Read, S. (2004). Attention alters appearance in early vision: contrast sensitivity, spatial resolution, and color saturation. *J. Vis.* 4:67.
- Collegio, A. J., Nah, J. C., Scotti, P. S., and Shomstein, S. (2019). Attention scales according to inferred real-world object size. *Nat. Hum. Behav.* 3:40. doi: 10.1038/s41562-018-0485-2
- Corbetta, M., and Shulman, G. L. (2002). Control of goal-directed and stimulus-driven attention in the brain. *Nat. Rev. Neurosci.* 3:201.
- Dosher, B. A., Sperling, G., and Wurst, S. A. (1986). Tradeoffs between stereopsis and proximity luminance covariance as determinants of perceived 3D structure. *Vis. Res.* 26, 973–990.
- Eger, E., Ashburner, J., Haynes, J.-D., Dolan, R. J., and Rees, G. (2008). fMRI activity patterns in human LOC carry information about object exemplars within category. *J. Cogn. Neurosci.* 20, 356–370. doi: 10.1162/jocn.2008.20019
- Fang, F., Boyaci, H., Kersten, D., and Murray, S. O. (2008). Attention-dependent representation of a size illusion in human V1. *Curr. Biol.* 18, 1707–1712. doi: 10.1016/j.cub.2008.09.025
- Gilbert, C. D., and Li, W. (2013). Top-down influences on visual processing. *Nat. Rev. Neurosci.* 14:350.
- Gobell, J., and Carrasco, M. (2005). Attention alters the appearance of spatial frequency and gap size. *Psychol. Sci.* 16, 644–651. doi: 10.1111/j.1467-9280.2005.01588.x
- Grill-Spector, K., Kushnir, T., Edelman, S., Avidan, G., Itzhak, Y., and Malach, R. (1999). Differential processing of objects under various viewing conditions in the human lateral occipital complex. *Neuron* 24, 187–203. doi: 10.1016/S0896-6273(00)80832-80836
- Henik, A., Glikson, Y., Kallai, A., and Leibovich, T. (2017). Size perception and the foundation of numerical processing. *Curr. Dir. Psychol. Sci.* 26, 45–51.
- Klein, B. P., Harvey, B. M., and Dumoulin, S. O. (2014). Attraction of position preference by spatial attention throughout human visual cortex. *Neuron* 84, 227–237.
- Konkle, T., and Oliva, A. (2012). A real-world size organization of object responses in occipitotemporal cortex. *Neuron* 74, 1114–1124. doi: 10.1016/j.neuron.2012.04.036
- Kreutzer, S., Fink, G. R., and Weidner, R. (2015). Attention modulates visual size adaptation. *J. Vis.* 15:10.
- Lamb, M. R., and Yund, E. W. (1996). Spatial frequency and attention: effects of level-, target-, and location-repetition on the processing of global and local forms. *Percept. Psychophys.* 58, 363–373.
- Leibowitz, H., Brislin, R., Perlmutter, L., and Hennessy, R. (1969). Ponzo perspective illusion as a manifestation of space perception. *Science* 166, 1174–1176. doi: 10.1126/science.166.3909.1174
- Liu, T., Fuller, S., and Carrasco, M. (2006). Attention alters the appearance of motion coherence. *Psychon. Bull. Rev.* 13, 1091–1096.
- Massaro, D. W., and Anderson, N. H. (1971). Judgmental model of the ebbinghaus illusion. *J. Exp. Psychol.* 89, 147–151. doi: 10.1037/h0031158
- Morgan, M. J. (2012). Motion adaptation does not depend on attention to the adaptor. *Vis. Res.* 55, 47–51. doi: 10.1016/j.visres.2011.12.009
- Murray, S. O., Boyaci, H., and Kersten, D. (2006). The representation of perceived angular size in human primary visual cortex. *Nat. Neurosci.* 9, 429–434.
- Pooresmaeli, A., Arrighi, R., Biagi, L., and Morrone, M. C. (2013). Blood oxygen level-dependent activation of the primary visual cortex predicts size adaptation illusion. *J. Neurosci.* 33, 15999–16008. doi: 10.1523/JNEUROSCI.1770-13.2013
- Posner, M. I., Snyder, C. R., and Davidson, B. J. (1980). Attention and the detection of signals. *J. Exp. Psychol. Gen.* 109:160.
- Pylyshyn, Z. W., and Storm, R. W. (1988). Tracking multiple independent targets: evidence for a parallel tracking mechanism. *Spat. Vis.* 3, 179–197.
- Reynolds, J. H., and Chelazzi, L. (2004). Attentional modulation of visual processing. *Annu. Rev. Neurosci.* 27, 611–647.
- Rhodes, G., Jeffery, L., Evangelista, E., Ewing, L., Peters, M., and Taylor, L. (2011). Enhanced attention amplifies face adaptation. *Vis. Res.* 51, 1811–1819.
- Schwabe, L., Obermayer, K., Angelucci, A., and Bressloff, P. C. (2006). The role of feedback in shaping the extra-classical receptive field of cortical neurons: a recurrent network model. *J. Neurosci.* 26, 9117–9129.
- Schwarzkopf, D., Song, C., and Rees, G. (2010). The surface area of human V1 predicts the subjective experience of object size. *Nat. Neurosci.* 14, 28–30. doi: 10.1038/nn.2706
- Simoncelli, E. P. (2003). Vision and the statistics of the visual environment. *Curr. Opin. Neurobiol.* 13, 144–149. doi: 10.1016/S0959-4388(03)00047-43
- Sperandio, I., Chouinard, P. A., and Goodale, M. A. (2012). Retinotopic activity in V1 reflects the perceived and not the retinal size of an afterimage. *Nat. Neurosci.* 15, 540–542. doi: 10.1038/nn.3069
- Stephen, I. D., Sturman, D., Stevenson, R. J., Mond, J., and Brooks, K. R. (2018). Visual attention mediates the relationship between body satisfaction and susceptibility to the body size adaptation effect. *PLoS One* 13:e0189855. doi: 10.1371/journal.pone.0189855
- Tonelli, A., Cuturi, L. F., and Gori, M. (2017). The influence of auditory information on visual size adaptation. *Front. Neurosci.* 11:594. doi: 10.3389/fnins.2017.00594
- Trotter, Y., and Celebrini, S. (1999). Gaze direction controls response gain in primary visual-cortex neurons. *Nature* 398, 239–242. doi: 10.1038/18444
- Wahn, B., and König, P. (2015a). Audition and vision share spatial attentional resources, yet attentional load does not disrupt audiovisual integration. *Front. Psychol.* 6:1084. doi: 10.3389/fpsyg.2015.01084
- Wahn, B., and König, P. (2015b). Vision and haptics share spatial attentional resources and visuotactile integration is not affected by high attentional load. *Multisens. Res.* 28, 371–392. doi: 10.1163/22134808-22132482
- Watson, A. B., and Pelli, D. G. (1983). QUEST: a bayesian adaptive psychometric method. *Percept. Psychophys.* 33, 113–120.
- Yeshurun, Y., and Carrasco, M. (1998). Attention improves or impairs visual performance by enhancing spatial resolution. *Nature* 396:72.

**Conflict of Interest:** The authors declare that the research was conducted in the absence of any commercial or financial relationships that could be construed as a potential conflict of interest.

Copyright © 2020 Tonelli, Pooresmaeli and Arrighi. This is an open-access article distributed under the terms of the Creative Commons Attribution License (CC BY). The use, distribution or reproduction in other forums is permitted, provided the original author(s) and the copyright owner(s) are credited and that the original publication in this journal is cited, in accordance with accepted academic practice. No use, distribution or reproduction is permitted which does not comply with these terms.



# Adaptation Modulates Spike-Phase Coupling Tuning Curve in the Rat Primary Auditory Cortex

Mohammad Zarei<sup>1,2\*†</sup>, Mohsen Parto Dezfouli<sup>1,3\*†</sup>, Mehran Jahed<sup>2\*‡</sup> and Mohammad Reza Daliri<sup>1,3\*‡</sup>

<sup>1</sup> School of Cognitive Sciences (SCS), Institute for Research in Fundamental Sciences (IPM), Tehran, Iran, <sup>2</sup> School of Electrical Engineering, Sharif University of Technology (SUT), Tehran, Iran, <sup>3</sup> Neuroscience and Neuroengineering Research Laboratory, Department of Biomedical Engineering, School of Electrical Engineering, Iran University of Science and Technology (IUST), Tehran, Iran

## OPEN ACCESS

### Edited by:

Davide Zoccolan,  
International School for Advanced  
Studies (SISSA), Italy

### Reviewed by:

Nikolay Grigorievich Bibikov,  
N. N. Andreyev Acoustics Institute,  
Russia  
Marco Cambiaghi,  
University of Verona, Italy

### \*Correspondence:

Mohammad Zarei  
zarej\_mohammad@ee.sharif.edu  
Mohsen Parto Dezfouli  
moh3nparto@ipm.ir  
Mehran Jahed  
jahed@sharif.edu  
Mohammad Reza Daliri  
daliri@iust.ac.ir

<sup>†</sup>These authors share first authorship

<sup>‡</sup>These authors share senior  
authorship

**Received:** 07 April 2020

**Accepted:** 13 July 2020

**Published:** 03 August 2020

### Citation:

Zarei M, Parto Dezfouli M,  
Jahed M and Daliri MR (2020)  
Adaptation Modulates Spike-Phase  
Coupling Tuning Curve in the Rat  
Primary Auditory Cortex.  
*Front. Syst. Neurosci.* 14:55.  
doi: 10.3389/fnsys.2020.00055

Adaptation is an important mechanism that causes a decrease in the neural response both in terms of local field potentials (LFP) and spiking activity. We previously showed this reduction effect in the tuning curve of the primary auditory cortex. Moreover, we revealed that a repeated stimulus reduces the neural response in terms of spike-phase coupling (SPC). In the current study, we examined the effect of adaptation on the SPC tuning curve. To this end, employing the phase-locking value (PLV) method, we estimated the spike-LFP coupling. The data was obtained by a simultaneous recording from four single-electrodes in the primary auditory cortex of 15 rats. We first investigated whether the neural system may use spike-LFP phase coupling in the primary auditory cortex to encode sensory information. Secondly, we investigated the effect of adaptation on this potential SPC tuning. Our data showed that the coupling between spikes' times and the LFP phase in beta oscillations represents sensory information (different stimulus frequencies), with an inverted bell-shaped tuning curve. Furthermore, we showed that adaptation to a specific frequency modulates SPC tuning curve of the adapter and its neighboring frequencies. These findings could be useful for interpretation of feature representation in terms of SPC and the underlying neural mechanism of adaptation.

**Keywords:** neural adaptation, spike-LFP coupling, auditory cortex, sensory coding, tuning curve

## INTRODUCTION

Neural adaptation is a brain mechanism that observed in various sensory systems of mammals and amphibians, including the visual (Müller, 1999; Kayser et al., 2009), auditory (Bibikov, 1977; Dean et al., 2005; Anderson et al., 2009; Malmierca et al., 2009; Hagan et al., 2012; Parto Dezfouli and Daliri, 2015), and somatosensory (Katz et al., 2006; Adibi et al., 2013, 2014; Ahmadi et al., 2019) systems. Earlier studies have reported an interesting adaptation behavior in certain neurons, including in the auditory system, so-called as stimulus-specific adaptation (SSA) (Ulanovsky et al., 2003, 2004; Nelken and Ulanovsky, 2007; Szymanski et al., 2009; Ayala and Malmierca, 2012; Khouri and Nelken, 2015; Parto Dezfouli and Daliri, 2015), here on referred to as "Adaptation." SSA leads to a significant decline in the corresponding responses of frequent stimuli. For example, an oddball sound releases a stronger response compared to the common one. Initially, researches believed that this phenomenon was related to cortical processes, but additional evidence revealed

similar behavior in other subcortical routes, such as medial geniculate body (MGB) (Anderson et al., 2009), and Inferior Colliculus (IC) (Ayala and Malmierca, 2012).

Adaptation decreases the neuronal activities in the sensory areas and leads to a system that is not disturbed in exposure to frequent stimuli (Dean et al., 2005; Adibi et al., 2013). Also, adaptation changes the system sensitivity during the action of the stimulus (Chen et al., 2010). To suppress the attention to repeated stimuli, the adaptation mechanism alters several neural properties. For instance, it helps to better detect deviance by increasing the neural sensitivity related to an unexpected change (Ulanovsky et al., 2003). In the auditory system, different parameters of a stimulus such as intensity, tone frequency distance, and Inter-Stimulus Interval is affected by adaptation. Additionally, it has been shown that presenting an audio sequence in a random pattern significantly affects the neural responses (Yaron et al., 2012).

Synchronous neural activity, alongside neural desynchrony, has been vastly studied in neuroscience, with implications for sensory information encoding and decoding, memory, attention, adaptation, and high cognitive process (Eckhorn and Obermueller, 1993; Galarreta and Hestrin, 2001; Uhlhaas et al., 2009; Pipa and Munk, 2011; van Wijk et al., 2012; Mendoza-Halliday et al., 2014; Li et al., 2015; Merrikhi et al., 2017, 2018). Local field potentials (LFPs), as the low-frequency part of neural signal, reflect the common synaptic activity of a population of neighboring neurons (Buzsáki and Draguhn, 2004; Buzsáki et al., 2012; Jansen et al., 2015), while spikes are short-timed high-frequency content signals reflecting more individual activity. Neuronal synchronization can be addressed by temporally relating spiking activities to the background oscillations of LFPs (Salinas and Sejnowski, 2001; Pikovsky et al., 2002; Tiesinga et al., 2008; Fries, 2009). This relationship has been observed in various cognitive functions and within different brain regions, including the prefrontal cortex, cortical area, and hippocampus (Siegel et al., 2009; Cutsuridis and Hasselmo, 2011). The relationship further reveals information on the neuronal synchronization in each frequency band. For instance, the relation between spikes and its corresponding theta fluctuations of LFP in hippocampus neurons reflects spatial memory information (Cutsuridis and Hasselmo, 2011). Also, spike-LFP Phase Coupling (SPC) can provide information about cell type and firing rate, and avoids volume conduction complications (Canolty et al., 2010; Hoerzer et al., 2010; Womelsdorf et al., 2010; Hansen and Dragoi, 2011; Vinck et al., 2012; Xu et al., 2013; Herreras, 2016). There are different measures for estimating spike-LFP synchronization, including coherence coefficient and cross-correlation (Carter et al., 1973; Carter, 1987; Zeitler et al., 2006; Srinath and Ray, 2014), spike-triggered correlation matrix synchronization (SCMS) (Li et al., 2016), phase-locking value (PLV) (Lachaux et al., 1999), and spike field coherence (SFC) (Fries et al., 2001, 2002; Curtis et al., 2009; Grasse and Moxon, 2010; Hagan et al., 2012). PLV is considered as one of the fundamental approaches to estimate synchronization. However, this measure is highly biased and dependent on spike rates. Accordingly, before using PLV method, spikes should be matched at a specified rate. Therefore, using a scheme, the spikes equalized to a specific threshold  $T$ ;

trials with a number of spikes below  $T$  are discarded, and those with spike rate more than  $T$ , are randomly equalized down to the number of  $T$ .

It is known that the sensory information, namely various stimuli tuning curves, represent by spiking activity or LFPs. The power variation of LFPs could reflect various features of stimuli like tone frequency, orientation, motion, etc (Siegel and König, 2003; Henrie and Shapley, 2005; Ray et al., 2008; Kayser et al., 2009; Ince et al., 2012; García-Rosales et al., 2018a,b). Neuronal spiking activity is also able to reveal stimuli information. Relating these two signals (spike and LFP) provides a comprehensive explanation about the neural activities (Quiroga and Panzeri, 2009; Perge et al., 2014). Considering the information of spike times together with the LFP phase reveals different features in various cognitive functions (Lachaux et al., 1999; Pesaran et al., 2002, 2008; Ray and Maunsell, 2010; Vinck et al., 2010; Li et al., 2017). In fact, the coupling of spikes of single neurons to the phase of LFPs (spike-LFP phase coupling) has been a useful measure to decode the sensory information and behaviors in low and high-frequency bands (Mehring et al., 2003; Mollazadeh et al., 2009). Furthermore, a recent study revealed the spike-LFP coupling within and between areas, i.e., spikes-LFP relation in V1, spikes-LFP relation in V4, and the relation between spikes of V4 and LFP of V1 (Li et al., 2019).

We previously showed that SSA suppresses the coupling of spikes to the beta phase of LFP oscillations (Parto Dezfouli et al., 2019). Here, we sought to investigate the effect of SSA on neighboring frequencies in terms of SPC responses. To this end, we first assessed whether the spike-LFP phase coupling has a tuned response for encoding sensory information, here in the rat primary auditory cortex. In other words, we examined a potential link between the spike-LFP signals and stimuli in terms of the tone frequency tuning curves (frequency selectivity). Notably, in this study, we used the term “tuning curve” for frequency tuning curve. Second, we explored how this adaptation would alter the SPC response.

## MATERIALS AND METHODS

The surgery procedure, experimental recording, and data preprocessing are described in Parto Dezfouli and Daliri (2015). Further details, employed in the current study, are provided below.

### Recording

The data was collected from the primary auditory cortex of 15 anesthetized rats. The adult Wistar rats weight ranges between 250 and 350 g. The recording was done using tungsten electrodes (FHC, 5M, United States). The parallel electrodes (tip diameter of ~5–10  $\mu$ m) were placed with 200  $\mu$ m distance from each other. The recording electrodes were inserted into the desired location by a Microdrive (SM-21, Narishige, Japan). Multi-unit activity (MUA) and LFP were collected over A1 area with 10 kHz sampling rate (recording system: USB-ME64-PGA; Multichannel System, Germany). Through the experiment using “MCRack” software, the data was visualized online. We used

an eight-channel miniature preamplifier to pre-amplify the raw signals. Next, a band-pass filtered from 1 to 5 kHz was applied to them and amplified again with a gain of 1000. Finally, the recorded data was stored for subsequent offline analyses.

## Experimental Paradigm

First, we characterized the selective neuron by presenting 300 ms broad-band noise bursts with 500 ms interval between them. Next, for each selected recording site, we identified the characteristic frequency and four frequencies around it (in the range of 200 Hz–20 kHz). These five desired tone frequencies (namely  $f_1$ – $f_5$ ) were presented in four intensities 40, 50, 60, and 70 dB SPL in a quasi-random pattern. Each tone was presented for 50 ms duration with a 300 ms inter-stimulus interval (**Figure 1A**).

The main task consists of two control and adapting sequences. In the control sequence, 20 selected combinations were uniformly presented (30 trials of each combination). In the adapting sequence, a similar procedure was conducted but with different likelihood of stimuli presentation. In this sequence, the characteristic frequency ( $f_3$ ) in the level of 60 dB SPL (as the adaptor) was presented for 80% of all sequence likelihood. Accordingly, each frequency of pure tones was presented with the same probability of 20% in the control sequence, while that probability was 80% for the adaptor and 5% for neighboring frequencies in the adapting sequence.

## Data Analysis

All preprocessing and analyses were implemented in MATLAB 2016b (Mathworks, Natick, MA, United States). LFP signals, were filtered between the ranges of 1–300 Hz. Subsequently, using 300–3000 Hz band-pass filtered MUAs were extracted. Next, we employed a threshold method to detect spike times. The threshold may be set based on the standard deviation (SD) of the whole trace, namely as twice the SD, as considered in this study (Pouzat et al., 2002). The resulting spike trains were smoothed using a 10 ms Hamming window and aligning to the stimulus onset. For LFPs, after 1–300 Hz filtering, the baseline correction was applied to each trace (Parto Dezfouli et al., 2014). Subsequently, the preprocessed data were divided to different canonical frequency bands using band-pass filters and non-causal finite impulse response (FIR) filter. We used the time between 0 and 100 ms after the stimulus onset for the main analysis.

## SPC Based on the PLV Method

Here, we utilized PLV to quantify SPC (Lachaux et al., 1999). PLV method calculates the power of dependability or linking of LFP phases in spike times, by computing the angular summation between spikes to beta range LFP fluctuations. We used the following equation:

$$M = \frac{1}{N} \left| \sum_{n=1}^N \exp(j\phi_n) \right| \quad (1)$$

where  $N$  shows the number of spikes,  $\phi_n$  is related to the instantaneous phase (here in the beta-band) at the time of  $n$ th

spike which is determined by Hilbert transform, and  $\exp(j\phi_n)$  is the complex exponential function of  $\phi_n$ . The amplitude of vector  $M$  ( $|M|$ ) indicates the SPC power and its angle ( $\angle M$ ) shows the phases of LFPs in the time of spikes occurrence. A larger value for vector  $M$  indicates that the occurrence of spikes are more likely to a specific phase of LFP, and the smaller value is related to distributed spikes across different phases. PLV alters between 0 and 1.

As noted, the dependency of SPC value to the spike numbers is considered as one limitation of SPC estimation. For example, two neurons with various firing rates, it is distinctly possible that the neuron with a greater firing rate results in a lower SPC. This problem was targeted to address in previous studies on SPC (Vinck et al., 2012; Zarei et al., 2018).

In this study, to calculate the SPC by PLV, an equalizing strategy was used in order to find the spike counts based on a threshold. Here we reach an optimal compromise between spike rates and trial numbers using an optimal thresholding scheme (Zarei et al., 2018). Accordingly, the trials with spike rates greater than the threshold were equalized to that threshold (by randomly removing), and the trials whose number of spikes were less the threshold, were removed.

To overcome this problem, we matched the firing rates in the control and adapting conditions. Therefore, after finding a threshold  $T$  for the mean firing rates, trials with firing rates less than the  $T$  were removed and spikes in trials with firing rates greater than the  $T$  were reduced to the  $T$  value. Especially, in order to produce normalized LFP signals, the LFP strength for each neuron was standardized by deducting the average and dividing the result by the SD.

In order to quantify the adaptation effect, we computed the difference between the firing-rate/SPC strength of control and adapting conditions. We measured the adaptation changes using Adaptation Index (AI) in an analysis similar to SSA index (SI) that was employed in earlier studies (Ulanovsky et al., 2003, 2004), and is defined as,

$$AI = \frac{C(f_i) - A(f_i)}{C(f_i) + A(f_i)} \quad (2)$$

where the parameters  $C(f_i)$  and  $A(f_i)$  are the response (firing-rate/SPC) strength related to the frequency  $f_i$  in the control and adapting sequences, respectively. The AI denotes the difference between control and adapting sequences within each stimulus tone frequency. Therefore, the AI value shows the difference between control and adapting responses (firing-rate/SPC).

## Fitting Model

In many signal processing subjects fitting Gaussian functions to neural data is very essential, that a Gaussian function is of the following form:

$$y = Ae^{-\frac{(x - \mu)^2}{2\sigma^2}}$$

This function can be mapped with a symmetrical bell-shaped curve positioned at the place  $x = \mu$ , with  $A$  being the altitude of the peak and  $\sigma$  utilizing its width.

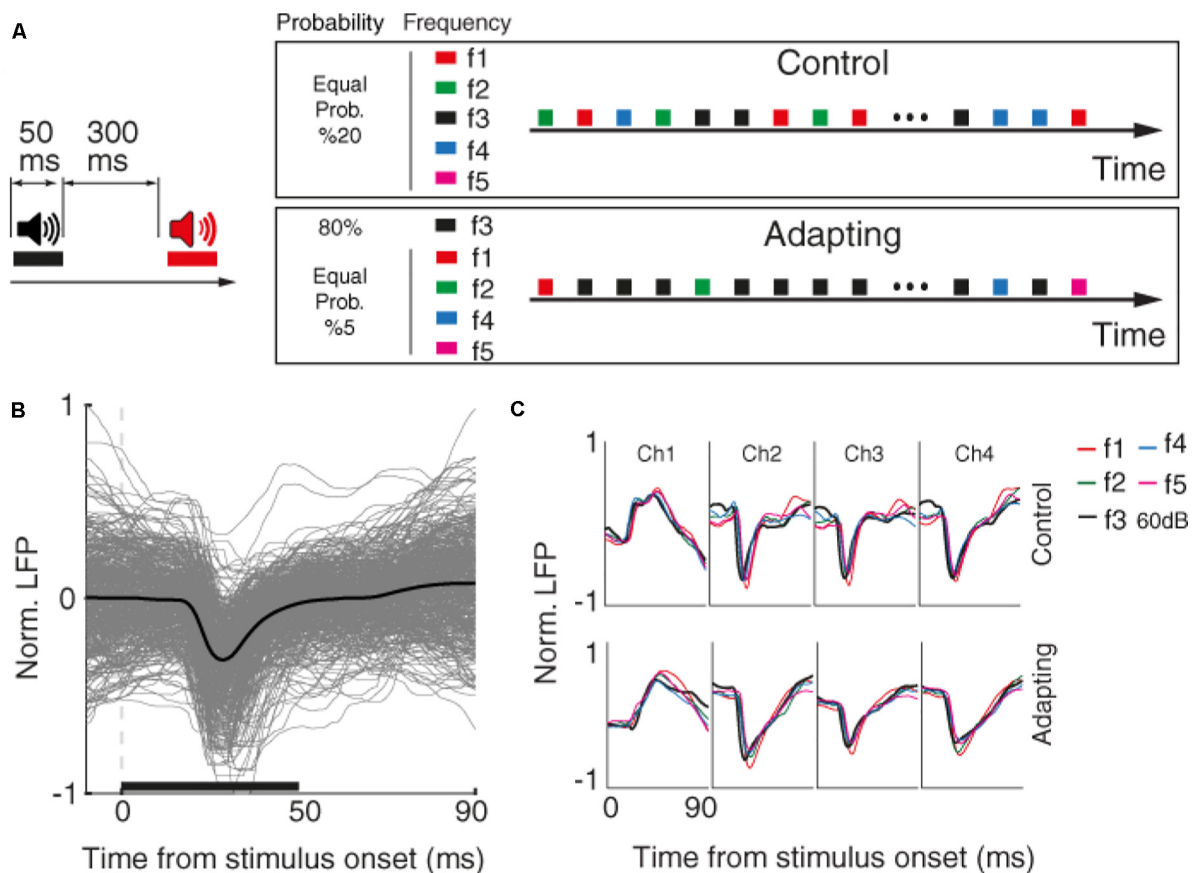


**FIGURE 1 |** Behavioral task and raw data. **(A)** Timeline of the stimulus presentation in two control and adapting sequences. Left: pure tone stimuli with the duration of 50 and 300 ms inter-stimulus interval were presented. Right: stimuli were presented in two adapting and control sequences. Within the control sequence, stimuli were presented with an identical probability. Within the adapting sequence, the same combinations as the control sequence were presented such that the adapter and rest frequencies were presented with the likelihood of 80 and 20% of the whole sequence, respectively. **(B)** Raw LFP for a sample recording site. The x-axis shows the time from stimulus onset, and the y-axis is normalized LFP amplitude. Gray lines show LFP trace of different trials and black line denotes the average response. The horizontal bar shows the stimulus period. **(C)** Average raw LFPs of five frequencies of pure tones at 60 dB SPL level for a sample recording site (site 14) during the time following stimulus onset, in control (top panel), and adapting (bottom panel) conditions.

## Quantification and Statistical Analyses

### Wilcoxon Rank-Sum

We employed the Wilcoxon rank-sum test for statistical assessment of the firing rate and SPC between the characteristic frequency and its neighboring frequencies across neurons (**Figures 4A,B**).

### Standard Error of Mean (SEM) and Standard Deviation (SD)

Standard error of mean (SEM) and SD were used to convey variability through different measures, where SEM exemplify uncertainty in the assessment of the mean and SD illustrates a scattering of the data from the mean (**Figures 3A, 4A,B, 5**).

### Correlation

In this study, the Pearson's correlation was used between the mean firing rate and SPC strength (**Figure 4B**). Pearson's correlation is a statistical measure that quantifies linear correlation between two variables. It assumes a value between

(−1 and +1), where −1 depicts a negative correlation, 0 shows no correlation, and +1 represents a positive correlation.

## RESULTS

We investigated sensory information coding in terms of SPC tuning curve and then explored how adaptation could alter this potential SPC-based tuning curve. To this end, we used data of an auditory task consisting of two usual and adapted conditions. **Figure 1A** depicts the timeline and phases of the auditory task made up of two sequences; control and adapting. Pure tones in 20 arrangements of five frequencies and four intensity levels were employed in the experiment. In the control sequence, stimuli were randomly presented with an equal likelihood of 5% for each combination. The adapting sequence is constituted of the same stimuli but with different probabilities of stimuli presentation. In this sequence, an adapter (characteristic frequency, f3, at 60 dB SPL intensity) was presented with 80% probability of the

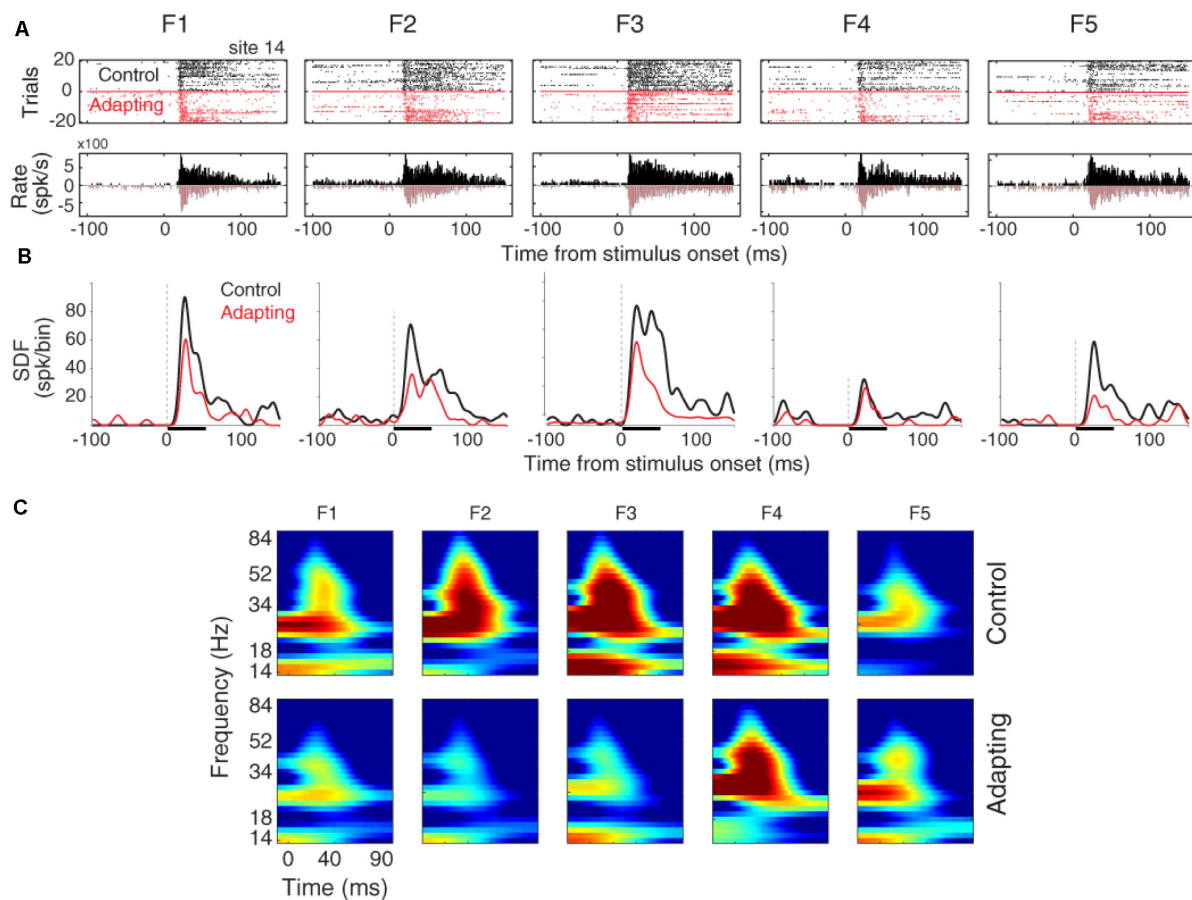


**FIGURE 2 |** Adaptation impacts on the neuronal spiking activity and LFP responses. **(A)** Raster plot and peristimulus time histogram (PSTH) of the adapter (tone frequency f3) and its neighboring frequencies at 60 dB SPL intensity for a sample recording site (site 14) in control (black) and adapting (red) sequences. **(B)** Comparison of spike density function (SDF) between control (black) and adapting (red) sequences for the five respective frequencies of pure tones at 60 dB SPL intensity. **(C)** Time-frequency representation of the LFP power for different stimuli in a sample recording site (site 14). Color bars show the mean normalized LFP power, as a function of time (x-axis) and LFP frequency (y-axis) in the control (top panels) and adaptation (bottom panels) sequences.

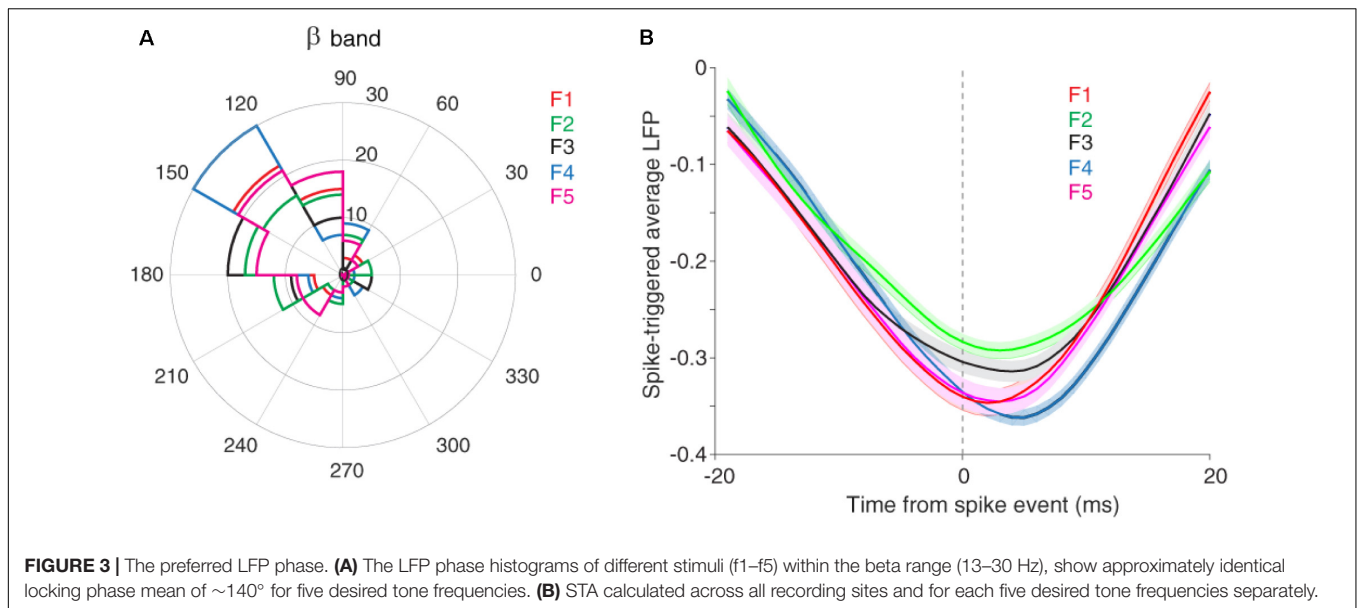
whole sequence and other four frequencies were occupied the rest 20% of the sequence. During the experiment, neural data (LFP and MUA) were collected from 96 sites over the primary auditory cortex (A1). Raw LFPs of a sample recording site and the average of these raw LFPs for each of the five tone frequencies are shown in **Figures 1B,C**, respectively.

The raster plots and peristimulus time histograms of the five desired tone frequencies related to a sample recording site are shown for the control and adapting conditions, separately (**Figure 2A**). Consistent with previous findings (Ulanovsky et al., 2003; Nelken and Ulanovsky, 2007), spiking activity shows a suppression due to the adapting effect (**Figure 2A**). To have a better estimation of neural responses, we convolved a Gaussian Kernel (with  $\sigma = 10$ ) with the spikes (Hill et al., 2015). This resulted in a continuous probability density function as illustrated in **Figure 2B**. **Figure 2C** shows the time-frequency representation of the adapter (f3) and the neighboring frequencies (f1, f2, f4, f5), for site 14. Consistent with **Figure 2A**, the adaptation caused suppression in the LFP power of the adapter and the neighboring frequencies. This adaptation effect is shown to be

stronger in the characteristic frequency (f3), as compared to the neighboring frequencies.

## Sensory Representation Based on Spike-LFP Coupling

It has been shown that the neuronal spiking activity and cortical LFP are attenuated due to adaptation (Taaseh et al., 2011; Parto Dezfouli and Daliri, 2015). Recently, we showed that adaptation decreases the spike to LFP phase coupling within beta range but not in other frequency bands (Parto Dezfouli et al., 2019). To this end, we divided LFP to six canonical frequency bands, namely delta, theta, alpha, beta, low and high gamma. Results indicated a significant difference in the SPC values between control and adaptation conditions within the beta range, but not in other bands (Parto Dezfouli et al., 2019). Therefore, here, we focused our analyses within the beta range (13–30 Hz). Based on our previous findings, the primary auditory system may further use this SPC within the beta range to encode sensory information. We considered the phase with dominant



occurrence of spikes as the preferred, as the preferred phase ( $\alpha$ ) and the phase with  $180^\circ$  distance from it ( $180-\alpha$ ) as the anti-preferred phase. The preferred phase was identified by calculating the histogram of LFP phases in spike times. The LFP phase histograms (in the beta range) for different stimuli, namely conditions of five desired tone frequencies (f1–f5) were shown in **Figure 3A**. As described, the LFP phase distributions at different stimulus frequencies differ significantly from the uniform distribution. The different locking phases for the five desired tone frequencies (f1–f5) amount to almost identical locking phase means of about  $140^\circ$ , with no significant statistical difference ( $p = 0.3$ ,  $t$ -test). This shows that auditory neurons tend to fire more likely in a specific phase within the beta range (13–30 Hz) of LFPs. This effect is observed in both adapting or control conditions, and independent of different stimulus frequencies.

We also estimated the preferred LFP phase using the spike-triggered average (STA) method. For this purpose, after detecting the spike times, the LFPs within a window ( $\pm 20$  ms) around spike times were averaged. **Figure 3B** shows that the coupling strength, defined as the difference between the peak and trough of the STA curve, is different in the certain phase (phase of the coupling) for various stimuli (f1, f5). In other words, the strength of coupling in the primary auditory cortex neurons encodes sensory information. Moreover, **Figure 3B** indicates the falling phase ( $\sim 160^\circ$ ) as the preferred phase in which spikes are coupled to (consistent with **Figure 3A**). In the following, we examine this discrimination of sensory information for different stimuli in the format of a tuning curve (TC).

## SPC Follows an Inverted Bell-Shaped Tuning Curve

To investigate if the coupling between spikes and LFP phase encodes sensory information in the rat primary auditory cortex, we measured the coupling between spikes and the phase of

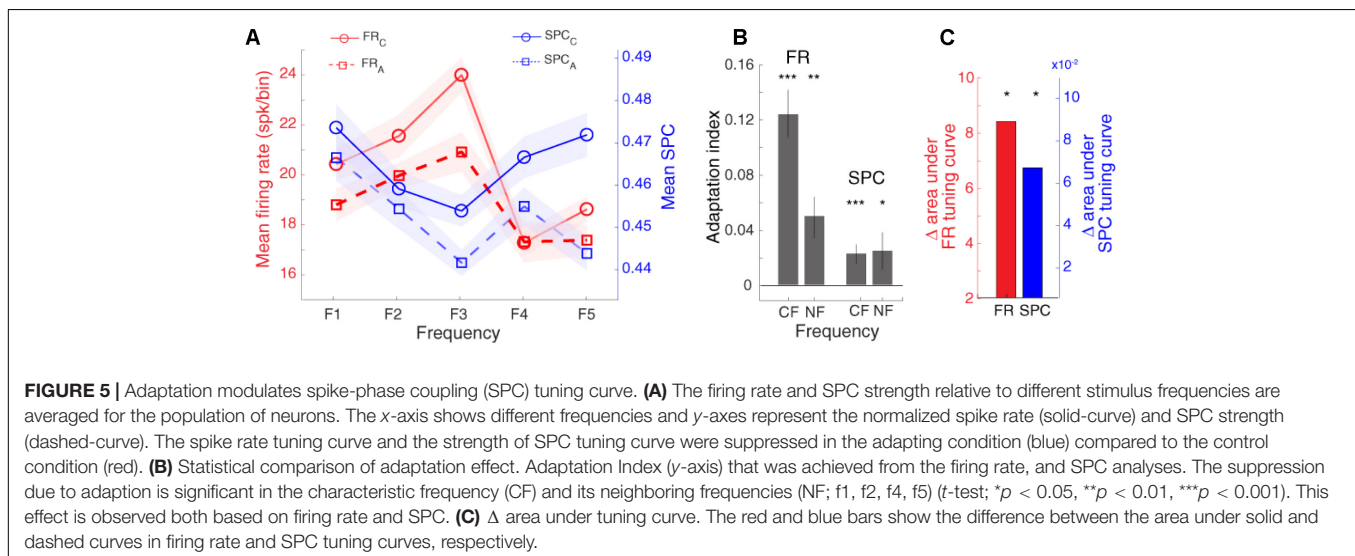
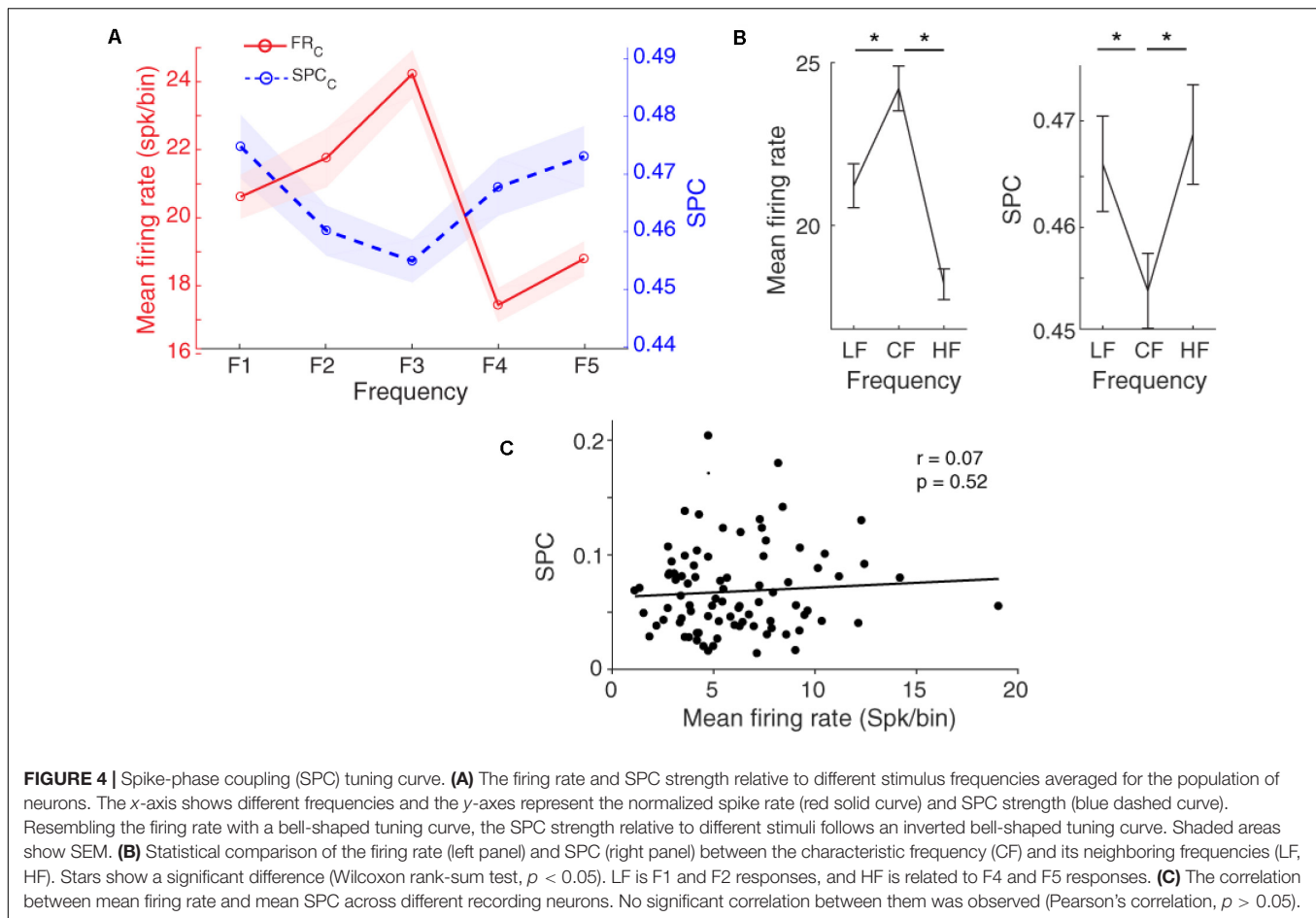
beta-frequency oscillations of LFP as a function of different stimulus frequencies.

**Figure 4A** shows that the locking of spikes to the LFP phase follows a tuning curve based on the different frequencies of the presented stimulus. Statistical comparison between the characteristic frequency and its lower and higher neighboring frequencies (LF and HF, respectively) shows a significant difference between them (**Figure 4B**, Wilcoxon rank-sum test,  $p < 0.05$ ), averaged across neurons ( $n = 96$ ) within the 13–30 Hz band. The SPC strength follows a shape of an inverted bell tuning curve relative to the different tone stimulus frequencies (using fitting model Piecewise linear interpolation). This tuning curve is inverted compared to the tuning based on the spike rate. That is, the least SPC occurs for the characteristic frequency as determined based on the spike rate, while the largest spike-LFP phase coupling is induced by the neighboring frequencies.

To evaluate the relation of SPC (based on LFP phase at the beta range) and spike rate in the tuning curve, we computed the correlation between mean spike rate and mean SPC for characteristic frequency and neighboring frequencies in all individual neurons. Results show no significant correlation between the mean firing rate and SPC strength (**Figure 4C**; Pearson correlation,  $r = 0.07$ ,  $p = 0.52$ ). It shows that SPC is mechanistically independent of the spike rate.

## Adaptation Modulates SPC Tuning Curve

As expected, **Figure 5** shows that the spike rate tuning curve (SR-TC) is attenuated in the adapting condition in comparison to the control condition (Taaseh et al., 2011; Parto Dezfouli and Daliri, 2015). Furthermore, as mentioned in **Figure 4A**, SPC strength relative to different stimuli follows a tuning curve (SPC-TC) across neurons. Importantly, adaptation modulates this SPC tuning curve across sites, in both control (blue dashed line), and adapting (red dashed-line) sequences (**Figure 5**). The SPC strength was decreased in the adapting sequence compared to the



control sequence. This index quantifies the difference between neural responses of the two desired sequences (control and adapting). Due to the nonsymmetrical tuning curve and a non-monotonic trend of the neighboring responses, we computed AI for responses (firing-rate/SPC) of two conditions; characteristic

frequency (CF) and its neighboring frequencies (NF; f1, f2, f4, f5) (**Figure 5B**). Also, the  $\Delta$  area under tuning curve is performed using the difference between the area under control (solid) and adapting (dashed) curves in firing rate and SPC tuning curves, respectively (**Figure 5C**). As a result, the adaptation caused a

suppression in the spiking activity and SPC of the characteristic frequency and the neighboring frequencies. In other words, adaptation shifts down both tuning curves.

Notable, the range of AI values change between  $-1$  and  $+1$ . The positive value indicates a lower response strength for adapting compared to the control condition.

## DISCUSSION

In this study, we found a tuning link between the sensory information and the coupling of spike times to the LFP phase. Furthermore, we revealed that the adaptation mechanism modulates this SPC tuning curve.

Stimulus-specific adaptation understood as an interesting phenomenon in the neural system, including the auditory cortical neurons, (Ulanovsky et al., 2003, 2004; Ayala and Malmierca, 2012), here on denoted to as “Adaptation.” SSA affects a major decrease in neural responses to frequent stimuli. Adaptation has a tendency to conceal neuronal activities in the sensory systems, leading to a system that is not distracted in exposure to frequent stimuli (Dean et al., 2005; Adibi et al., 2013) from the world such as light, smell, and sound. To decrease attention to frequent stimuli, the adaptation mechanism affects certain variations in neural properties.

As aforementioned, SPC indicates how spikes are harmonized in the LFPs for various functions of the brain such as attention, adaptation, perception, and maintaining information. This relationship has pointed to various brain areas, such as the visual cortex, prefrontal cortex, and the hippocampus (Siegel et al., 2009; Cutsuridis and Hasselmo, 2011). It is known that the sensory information, namely various stimuli tuning curves, represent by LFPs or spike activities (Snowden et al., 1992; Liu and Newsome, 2006; Ray and Maunsell, 2010). Importantly, relating these two signals, namely spike-LFP, provides a comprehensive explanation regarding neural activities (Quiroga and Panzeri, 2009; Perge et al., 2014). Indeed, SPC is a useful measure to decode the sensory information and behaviors in low and high-frequency bands as well as parietal and frontal cortex for alpha and beta bands (Mehring et al., 2003; Mollazadeh et al., 2009). Furthermore, LFP phase-locking was observed in the secondary auditory cortex during remote memory recall (Cambiaghi et al., 2016), where phase-locking was associated with a specific behavioral outcome.

Moreover, in line with sensory information findings, Uhlhaas et al. (2009) found that the SFC is boosted for preferred stimulus neurons in gamma band while it is reduced for the non-preferred stimulus. Belitski et al. (2010) documented the spike LFP relation may convey sensory properties in the low-frequency range and Kevan et al. revealed that the spike LFP behavior may be distinguished in reaction to various stimulus conditions (Martin and Schröder, 2016). A number of SPC quantities are studied, where the major synchronization quantities are the SCMS, pairwise phase consistency, SFC, and PLV (Lachaux et al., 1999; Grasse and Moxon, 2010; Vinck et al., 2010; Li et al., 2016). PLV technique calculates the amplitude of the average variation between spikes and LFP phases as the power

of coupling. To overcome the limitation of the PLV method (bias on the number of spikes), researches that utilize this technique usually match the firing at a specific spike number using the optimal thresholding method.

The main purposes of this study were to (i) evaluate the potential of the tone frequency tuning curve (sensory information) based on SPC, and (ii) examine the effect of adaptation on this tuning curve. In a recent study, we showed that SSA reduces the SPC strength significantly in the beta range (Parto Dezfouli et al., 2019). Resembling previous procedure, in this work, we analyzed the power of SPC in terms of tuning curve for sensory information coding. Our results indicate that the SPC follows a shape of an inverted bell curve relative to the different stimulus frequencies (using fitting model Gaussian function), averaged across neurons ( $n = 96$ ) within the 13–30 Hz band (**Figure 4A**). Importantly, to evaluate the relation of SPC (based on the LFP phase at the beta range) and establish that it is mechanistically independent of firing rate, the correlation computed between mean spike rate and mean SPC within the characteristic frequency and neighboring frequencies for all individual neurons. Our results show no considerable correlation between the SPC strength and mean spike rate (**Figure 4B**).

Previous studies revealed different tuning curves such as V shape, O shape, and bimodal peak, for the neurons in the primary auditory cortex (Sutter, 2000). Therefore, the shape of the neurons' tuning curves is not necessarily bell-shaped or symmetrical. Therefore, instead of investigating the adaptation effect on each of the frequencies, we performed the adaptation on the whole frequencies. Namely, we computed for responses (firing-rate/SPC) of characteristic frequency (CF) and neighboring frequencies (NF;  $f_1$ ,  $f_2$ ,  $f_4$ ,  $f_5$ ) (**Figure 5B**). Also, the  $\Delta$  area under tuning curve is performed using the difference between the area under of the solid and dashed curves in firing rate and SPC tuning curves, respectively (in terms of area under tuning curve, **Figure 5C**). As a result, the adaptation leads to a reduction in the spiking activity and SPC of the characteristic frequency and neighboring frequencies. Moreover, this selective function (SPC tuning) is inverted compared to the spike rate tuning. Our results illustrate that additional spikes evoked by the characteristic frequency, (compared to the neighboring frequencies) occur more frequently at the preferred compared to the anti-preferred phase of LFP. Furthermore, spikes evoked by the characteristic frequency depict a probability distribution that is less non-uniform than of the spikes induced by the neighboring frequencies. This may cause such stronger neural discrimination at the preferred compared to the anti-preferred phase of LFP, namely SPC tuning curve is inverted compared to the tuning based on the spike rate. Furthermore, we found that the adaptation modulates SPC tuning curve of the adapter and the neighboring frequencies and shift it toward lower values.

## CONCLUSION

This study indicates three main findings. First, the strength of SPC is selective for sensory information in the primary auditory cortex. Second, the locking of spikes to the LFP phase

follows an inverted bell-shaped tuning curve relative to the different stimulus frequencies. Third, the adaptation modulates SPC tuning curve of the adapter and its neighboring frequencies.

## DATA AVAILABILITY STATEMENT

The data analyzed in this study is subject to the following licenses/restrictions: The datasets analyzed in this article are not publicly available. Requests to access these datasets should be directed to MD, daliri@iust.ac.ir (upon reasonable request).

## ETHICS STATEMENT

In the current study, we aimed to investigate sensory information tuning in terms of spike-phase coupling and examine the effect of adaptation on this potential tuning curve. We conducted all procedures of this experiment in Iran Neural Technology Center (INTC) at Iran University of Science and Technology (IUST) using standards and conforming methods of the ministry of health and medical education. Animals are kept in the standard cages in animal facilities of the Neural Technology Center. All animals care, surgical procedures and experiments reviewed and approved and performed according to the protocols of the committee of Neuroscience Research Laboratory, Iran University of Science and Technology in

strict accordance with the recommendations in the Guide for the Care and Use of Laboratory Animals of the National Institutes of Health. All surgeries were conducted under urethane pentobarbital anesthesia, and all protocols were considered to minimize suffering. At the final step after the experiment, the animal was sacrificed under ether anesthesia (Parto Dezfouli and Daliri, 2015).

## AUTHOR CONTRIBUTIONS

All authors contributed to the concept of the work, drafting, and revising the manuscript. MP performed the experimental recording. MZ and MP analyzed and interpreted the data.

## FUNDING

The project was supported by the Iran Neural Technology Center (INTC).

## ACKNOWLEDGMENTS

We would like to thank Prof. Abbas Erfanian for his support for the experimental recording of the data and helpful inputs.

## REFERENCES

- Adibi, M., McDonald, J. S., Clifford, C. W., and Arabzadeh, E. (2014). Population decoding in rat barrel cortex: optimizing the linear readout of correlated population responses. *PLoS Computat. Biol.* 10:e1003415. doi: 10.1371/journal.pcbi.1003415
- Adibi, M., McDonald, J. S., Clifford, C. W. G., and Arabzadeh, E. (2013). Adaptation improves neural coding efficiency despite increasing correlations in variability. *J. Neurosci.* 33, 2108–2120. doi: 10.1523/JNEUROSCI.3449-12.2013
- Ahmadi, A., Behrooz, M., Shalchyan, V., and Daliri, M. R. (2019). Rat navigation by stimulating somatosensory cortex. *J. Bionic Eng.* 16, 931–942. doi: 10.1007/s42235-019-0107-3
- Anderson, L. A., Christianson, G. B., and Linden, J. F. (2009). Stimulus-specific adaptation occurs in the auditory thalamus. *J. Neurosci.* 29, 7359–7363. doi: 10.1523/JNEUROSCI.0793-09.2009
- Ayala, Y. A., and Malmierca, M. S. (2012). Stimulus-specific adaptation and deviance detection in the inferior colliculus. *Front. Neural Circuits* 6:89. doi: 10.3389/fncir.2012.00089
- Belitski, A., Panzeri, S., Magri, C., Logothetis, N. K., and Kayser, C. (2010). Sensory information in local field potentials and spikes from visual and auditory cortices: time scales and frequency bands. *J. Comput. Neurosci.* 29, 533–545. doi: 10.1007/s10827-010-0230-y
- Bibikov, N. G. (1977). "Novelty" neurons in the frog auditory system. *Z. Vyssh. Nerv. Deiat. Im. Pavlova* 27, 1075–1082.
- Buzsáki, G., Anastassiou, C. A., and Koch, C. (2012). The origin of extracellular fields and currents — EEG, ECoG, LFP and spikes. *Nat. Rev. Neurosci.* 13, 407–420. doi: 10.1038/nrn3241
- Buzsáki, G., and Draguhn, A. (2004). Neuronal oscillations in cortical networks. *Science* 304, 1926–1929. doi: 10.1126/science.1099745
- Cambiaghi, M., Grosso, A., Likhtik, E., Mazziotti, R., Concina, G., Renna, A., et al. (2016). Higher-order sensory cortex drives basolateral amygdala activity during the recall of remote, but not recently learned fearful memories. *J. Neurosci.* 36, 1647–1659. doi: 10.1523/JNEUROSCI.2351-15.2016
- Canolty, R. T., Ganguly, K., Kennerley, S. W., Cadieu, C. F., Koepsell, K., Wallis, J. D., et al. (2010). Oscillatory phase coupling coordinates anatomically dispersed functional cell assemblies. *Proc. Natl. Acad. Sci. U.S.A.* 107, 17356–17361. doi: 10.1073/pnas.1008306107
- Carter, G., Knapp, C., and Nuttall, A. (1973). Estimation of the magnitude-squared coherence function via overlapped fast Fourier transform processing. *IEEE Trans. Audio Electroacoust.* 21, 337–344. doi: 10.1109/TAU.1973.1162496
- Carter, G. C. (1987). Coherence and time delay estimation. *Proc. IEEE* 75, 236–255. doi: 10.1109/PROC.1987.13723
- Chen, J., Yang, H., Wang, A., and Fang, F. (2010). Perceptual consequences of face viewpoint adaptation: face viewpoint aftereffect, changes of differential sensitivity to face view, and their relationship. *J. Vis.* 10, 1–11. doi: 10.1167/10.3.12
- Curtis, J., Mitchell, J., and Reynolds, J. (2009). Estimates of spike-LFP coherence based on finite spiking data vary with mean firing rate. *Front. Syst. Neurosci.* 6:03.333. doi: 10.3389/conf.neuro.06.2009.03.333
- Cutsuridis, V., and Hasselmo, M. (2011). Spatial memory sequence encoding and replay during modeled theta and ripple oscillations. *Cognit. Comput.* 3, 554–574. doi: 10.1007/s12559-011-9114-3
- Dean, I., Harper, N. S., and McAlpine, D. (2005). Neural population coding of sound level adapts to stimulus statistics. *Nat. Neurosci.* 8, 1684–1689. doi: 10.1038/nn1541
- Eckhorn, R., and Obermueller, A. (1993). Single neurons are differently involved in stimulus-specific oscillations in cat visual cortex. *Exp. Brain Res.* 95, 177–182. doi: 10.1007/BF00229667
- Fries, P. (2009). Neuronal gamma-band synchronization as a fundamental process in cortical computation. *Annu. Rev. Neurosci.* 32, 209–224. doi: 10.1146/annurev.neuro.051508.135603
- Fries, P., Reynolds, J. H., Rorie, A. E., and Desimone, R. (2001). Modulation of oscillatory neuronal synchronization by selective visual attention. *Science* 291, 1560–1563. doi: 10.1126/science.291.5508.1560
- Fries, P., Schröder, J.-H., Roelfsema, P. R., Singer, W., and Engel, A. K. (2002). Oscillatory neuronal synchronization in primary visual cortex as a correlate of stimulus selection. *J. Neurosci.* 22, 3739–3754.

- Galarreta, M., and Hestrin, S. (2001). Spike transmission and synchrony detection in networks of GABAergic interneurons. *Science* 292, 2295–2299. doi: 10.1126/science.1061395
- García-Rosales, F., Beetz, M. J., Cabral-Calderin, Y., Kössl, M., and Hechavarria, J. C. (2018a). Neuronal coding of multiscale temporal features in communication sequences within the bat auditory cortex. *Commun. Biol.* 1, 1–14. doi: 10.1038/s42003-018-0205-5
- García-Rosales, F., Martin, L. M., Beetz, M. J., Cabral-Calderin, Y., Kössl, M., and Hechavarria, J. C. (2018b). Low-frequency spike-field coherence is a fingerprint of periodicity coding in the auditory cortex. *iScience* 9, 47–62. doi: 10.1016/j.isci.2018.10.009
- Grasse, D. W., and Moxon, K. A. (2010). Correcting the bias of spike field coherence estimators due to a finite number of spikes. *J. Neurophysiol.* 104, 548–558. doi: 10.1152/jn.00610.2009
- Hagan, M. A., Dean, H. L., and Pesaran, B. (2012). Spike-field activity in parietal area LIP during coordinated reach and saccade movements. *J. Neurophysiol.* 107, 1275–1290. doi: 10.1152/jn.00867.2011
- Hansen, B. J., and Dragoi, V. (2011). Adaptation-induced synchronization in laminar cortical circuits. *Proc. Natl. Acad. Sci. U.S.A.* 108, 10720–10725. doi: 10.1073/pnas.1102017108
- Henrie, J. A., and Shapley, R. (2005). LFP power spectra in V1 cortex: the graded effect of stimulus contrast. *J. Neurophysiol.* 94, 479–490. doi: 10.1152/jn.00919.2004
- Herreras, O. (2016). Local field potentials: myths and misunderstandings. *Front. Neural Circ.* 10:101. doi: 10.3389/fncir.2016.00101
- Hill, M. R. H., Fried, I., and Koch, C. (2015). Quantification and classification of neuronal responses in kernel-smoothed peristimulus time histograms. *J. Neurophysiol.* 113, 1260–1274. doi: 10.1152/jn.00595.2014
- Hoerzer, G. M., Liebe, S., Schloegl, A., Logothetis, N. K., and Rainer, G. (2010). Directed coupling in local field potentials of macaque V4 during visual short-term memory revealed by multivariate autoregressive models. *Front. Comput. Neurosci.* 4:14. doi: 10.3389/fncom.2010.00014
- Ince, R. A. A., Mazzoni, A., Bartels, A., Logothetis, N. K., and Panzeri, S. (2012). A novel test to determine the significance of neural selectivity to single and multiple potentially correlated stimulus features. *J. Neurosci. Methods* 210, 49–65. doi: 10.1016/j.jneumeth.2011.11.013
- Jansen, M., Li, X., Lashgari, R., Kremkow, J., Bereshpolova, Y., Swadlow, H. A., et al. (2015). Chromatic and achromatic spatial resolution of local field potentials in awake cortex. *Cereb. Cortex* 25, 3877–3893. doi: 10.1093/cercor/bhu270
- Katz, Y., Heiss, J. E., and Lampl, I. (2006). Cross-whisker adaptation of neurons in the rat barrel cortex. *J. Neurosci.* 26, 13363–13372. doi: 10.1523/JNEUROSCI.4056-06.2006
- Kayser, C., Montemurro, M. A., Logothetis, N. K., and Panzeri, S. (2009). Spike-phase coding boosts and stabilizes information carried by spatial and temporal spike patterns. *Neuron* 61, 597–608. doi: 10.1016/j.neuron.2009.01.008
- Khoury, L., and Nelken, I. (2015). Detecting the unexpected. *Curr. Opin. Neurobiol.* 35, 142–147. doi: 10.1016/j.conb.2015.08.003
- Lachaux, J.-P., Rodriguez, E., Martinerie, J., and Varela, F. J. (1999). Measuring phase synchrony in brain signals. *Hum. Brain Mapp.* 8, 194–208.
- Li, X., Chen, Y., Lashgari, R., Bereshpolova, Y., Swadlow, H. A., Lee, B. B., et al. (2015). Mixing of chromatic and luminance retinal signals in primate area V1. *Cereb. Cortex* 25, 1920–1937. doi: 10.1093/cercor/bhu002
- Li, Y., Yu, C., Zhou, Z. C., Stitt, I., Sellers, K. K., Gilmore, J. H., et al. (2017). Early development of network oscillations in the ferret visual cortex. *Sci. Rep.* 7:17766. doi: 10.1038/s41598-017-17502-y
- Li, Z., Cui, D., and Li, X. (2016). Unbiased and robust quantification of synchronization between spikes and local field potential. *J. Neurosci. Methods* 269, 33–38.
- Li, Z., Gao, M., and Wang, Y. (2019). The orientation selectivity of spike-LFP synchronization in macaque V1 and V4. *Front. Comput. Neurosci.* 13:47. doi: 10.3389/fncom.2019.00047
- Liu, J., and Newsome, W. T. (2006). Local field potential in cortical area MT: stimulus tuning and behavioral correlations. *J. Neurosci.* 26, 7779–7790. doi: 10.1523/JNEUROSCI.5052-05.2006
- Malmierca, M. S., Cristaudo, S., Perez-Gonzalez, D., and Covey, E. (2009). Stimulus-specific adaptation in the inferior colliculus of the anesthetized rat. *J. Neurosci.* 29, 5483–5493. doi: 10.1523/JNEUROSCI.4153-08.2009
- Martin, K. A. C., and Schröder, S. (2016). Phase locking of multiple single neurons to the local field potential in Cat V1. *J. Neurosci.* 36, 2494–2502. doi: 10.1523/JNEUROSCI.2547-14.2016
- Mehring, C., Rickert, J., Vaadia, E., De Oliveira, S. C., Aertsen, A., and Rotter, S. (2003). Inference of hand movements from local field potentials in monkey motor cortex. *Nat. Neurosci.* 6, 1253–1254. doi: 10.1038/nn1158
- Mendoza-Halliday, D., Torres, S., and Martinez-Trujillo, J. C. (2014). Sharp emergence of feature-selective sustained activity along the dorsal visual pathway. *Nat. Neurosci.* 17, 1255–1262. doi: 10.1038/nn.3785
- Merrikhi, Y., Clark, K., Albarran, E., Parsa, M., Zirnsak, M., Moore, T., et al. (2017). Spatial working memory alters the efficacy of input to visual cortex. *Nat. Commun.* 8:15041. doi: 10.1038/ncomms15041
- Merrikhi, Y., Clark, K., and Noudoost, B. (2018). Concurrent influence of top-down and bottom-up inputs on correlated activity of Macaque extrastriate neurons. *Nat. Commun.* 9:5393. doi: 10.1038/s41467-018-07816-4
- Mollazadeh, M., Aggarwal, V., Thakor, N. V., Law, A. J., Davidson, A., and Schieber, M. H. (2009). “Coherency between spike and LFP activity in M1 during hand movements,” in *Proceedings of the 4th International IEEE/EMBS Conference on Neural Engineering, NER 09*, Antalya, 506–509. doi: 10.1109/NER.2009.5109344
- Müller, J. R. (1999). Rapid adaptation in visual cortex to the structure of images. *Science* (80-) 285, 1405–1408. doi: 10.1126/science.285.5432.1405
- Nelken, I., and Ulanovsky, N. (2007). Mismatch negativity and stimulus-specific adaptation in animal models. *J. Psychophysiol.* 21, 214–223. doi: 10.1027/0269-8803.21.34.214
- Parto Dezfooli, M., and Daliri, M. R. (2015). The effect of adaptation on the tuning curves of rat auditory cortex. *PLoS ONE* 10:e0115621. doi: 10.1371/journal.pone.0115621
- Parto Dezfooli, M., Zarei, M., Jahed, M., and Daliri, M. R. (2019). Stimulus-specific adaptation decreases the coupling of spikes to LFP phase. *Front. Neural Circ.* 13:44. doi: 10.3389/fncir.2019.00044
- Parto Dezfooli, M. A., Dezfooli, M. P., and Rad, H. S. (2014). A novel approach for baseline correction in 1H-MRS signals based on ensemble empirical mode decomposition. *Conf. IEEE Eng. Med. Biol.* 2014, 3196–3199. doi: 10.1109/EMBC.2014.6944302
- Perge, J. A., Zhang, S., Malik, W. Q., Homer, M. L., Cash, S., Friehs, G., et al. (2014). Reliability of directional information in unsorted spikes and local field potentials recorded in human motor cortex. *J. Neural Eng.* 11:046007. doi: 10.1088/1741-2560/11/4/046007
- Pesaran, B., Nelson, M. J., and Andersen, R. A. (2008). Free choice activates a decision circuit between frontal and parietal cortex. *Nature* 453, 406–409. doi: 10.1038/nature06849
- Pesaran, B., Pezaris, J. S., Sahani, M., Mitra, P. P., and Andersen, R. A. (2002). Temporal structure in neuronal activity during working memory in macaque parietal cortex. *Nat. Neurosci.* 5, 805–811. doi: 10.1038/nn890
- Pikovsky, A., Rosenblum, M., Kurths, J., and Hilborn, R. C. (2002). Synchronization: a universal concept in nonlinear science. *Am. J. Phys.* 70, 655–655. doi: 10.1119/1.1475332
- Pipa, G., and Munk, M. H. J. (2011). Higher order spike synchrony in prefrontal cortex during visual memory. *Front. Comput. Neurosci.* 5:23. doi: 10.3389/fncom.2011.00023
- Pouzat, C., Mazor, O., and Laurent, G. (2002). Using noise signature to optimize spike-sorting and to assess neuronal classification quality. *J. Neurosci. Methods* 122, 43–57. doi: 10.1016/S0165-0270(02)00276-5
- Quiroga, R. Q., and Panzeri, S. (2009). Extracting information from neuronal populations: information theory and decoding approaches. *Nat. Rev. Neurosci.* 10, 173–185.
- Ray, S., Hsiao, S. S., Crone, N. E., Franaszczuk, P. J., and Niebur, E. (2008). Effect of stimulus intensity on the spike-local field potential relationship in the secondary somatosensory cortex. *J. Neurosci.* 28, 7334–7343. doi: 10.1523/JNEUROSCI.1588-08.2008
- Ray, S., and Maunsell, J. H. R. (2010). Differences in gamma frequencies across visual cortex restrict their possible use in computation. *Neuron* 67, 885–896. doi: 10.1016/j.neuron.2010.08.004
- Salinas, E., and Sejnowski, T. J. (2001). Correlated neuronal activity and the flow of neural information. *Nat. Rev. Neurosci.* 2, 539–550. doi: 10.1038/35086012
- Siegel, M., and König, P. (2003). A functional gamma-band defined by stimulus-dependent synchronization in area 18 of awake behaving cats. *J. Neurosci.* 23, 4251–4260. doi: 10.1523/jneurosci.23-10-04251.2003

- Siegel, M., Warden, M. R., and Miller, E. K. (2009). Phase-dependent neuronal coding of objects in short-term memory. *Proc. Natl. Acad. Sci. U.S.A.* 106, 21341–21346. doi: 10.1073/pnas.0908193106
- Snowden, R. J., Treue, S., and Andersen, R. A. (1992). The response of neurons in areas V1 and MT of the alert rhesus monkey to moving random dot patterns. *Exp. Brain Res.* 88, 389–400.
- Srinath, R., and Ray, S. (2014). Effect of amplitude correlations on coherence in the local field potential. *J. Neurophysiol.* 112, 741–751. doi: 10.1152/jn.00851.2013
- Sutter, M. L. (2000). Shapes and level tolerances of frequency tuning curves in primary auditory cortex: quantitative measures and population codes. *J. Neurophysiol.* 84, 1012–1025. doi: 10.1152/jn.2000.84.2.1012
- Szymanski, F. D., Garcia-Lazaro, J. A., and Schnupp, J. W. H. (2009). Current source density profiles of stimulus-specific adaptation in rat auditory cortex. *J. Neurophysiol.* 102, 1483–1490. doi: 10.1152/jn.00240.2009
- Taaseh, N., Yaron, A., and Nelken, I. (2011). Stimulus-specific adaptation and deviance detection in the rat auditory cortex. *PLoS ONE* 6:e23369. doi: 10.1371/journal.pone.0023369
- Tiesinga, P., Fellous, J.-M., and Sejnowski, T. J. (2008). Regulation of spike timing in visual cortical circuits. *Nat. Rev. Neurosci.* 9, 97–107. doi: 10.1038/nrn2315
- Uhlhaas, P., Pipa, G., Lima, B., Melloni, L., Neuenschwander, S., Nikolić, D., et al. (2009). Neural synchrony in cortical networks: history, concept and current status. *Front. Integr. Neurosci.* 3:17. doi: 10.3389/neuro.07.017.2009
- Ulanovsky, N., Las, L., Farkas, D., and Nelken, I. (2004). Multiple time scales of adaptation in auditory cortex neurons. *J. Neurosci.* 24, 10440–10453. doi: 10.1523/JNEUROSCI.1905-04.2004
- Ulanovsky, N., Las, L., and Nelken, I. (2003). Processing of low-probability sounds by cortical neurons. *Nat. Neurosci.* 6, 391–398. doi: 10.1038/nn1032
- van Wijk, B. C. M., Beek, P. J., and Daffertshofer, A. (2012). Neural synchrony within the motor system: what have we learned so far? *Front. Hum. Neurosci.* 6:252. doi: 10.3389/fnhum.2012.00252
- Vinck, M., Battaglia, F. P., Womelsdorf, T., and Pennartz, C. (2012). Improved measures of phase-coupling between spikes and the Local field potential. *J. Comput. Neurosci.* 33, 53–75. doi: 10.1007/s10827-011-0374-4
- Vinck, M., van Wingerden, M., Womelsdorf, T., Fries, P., and Pennartz, C. M. A. (2010). The pairwise phase consistency: a bias-free measure of rhythmic neuronal synchronization. *Neuroimage* 51, 112–122. doi: 10.1016/j.neuroimage.2010.01.073
- Womelsdorf, T., Johnston, K., Vinck, M., and Everling, S. (2010). Theta-activity in anterior cingulate cortex predicts task rules and their adjustments following errors. *Proc. Natl. Acad. Sci. U.S.A.* 107, 5248–5253. doi: 10.1073/pnas.0906194107
- Xu, X., Zheng, C., and Zhang, T. (2013). Reduction in LFP cross-frequency coupling between theta and gamma rhythms associated with impaired STP and LTP in a rat model of brain ischemia. *Front. Comput. Neurosci.* 7:27. doi: 10.3389/fncom.2013.00027
- Yaron, A., Hershenhoren, I., and Nelken, I. (2012). Sensitivity to complex statistical regularities in rat auditory cortex. *Neuron* 76, 603–615. doi: 10.1016/j.neuron.2012.08.025
- Zarei, M., Jahed, M., and Daliri, M. R. (2018). Introducing a comprehensive framework to measure spike-LFP coupling. *Front. Comput. Neurosci.* 12:78. doi: 10.3389/fncom.2018.00078
- Zeitler, M., Fries, P., and Gielen, S. (2006). Assessing neuronal coherence with single-unit, multi-unit, and local field potentials. *Neural Comput.* 18, 2256–2281. doi: 10.1162/neco.2006.18.9.2256

**Conflict of Interest:** The authors declare that the research was conducted in the absence of any commercial or financial relationships that could be construed as a potential conflict of interest.

Copyright © 2020 Zarei, Parto Dezfouli, Jahed and Daliri. This is an open-access article distributed under the terms of the Creative Commons Attribution License (CC BY). The use, distribution or reproduction in other forums is permitted, provided the original author(s) and the copyright owner(s) are credited and that the original publication in this journal is cited, in accordance with accepted academic practice. No use, distribution or reproduction is permitted which does not comply with these terms.



# Capturing Multiple Timescales of Adaptation to Second-Order Statistics With Generalized Linear Models: Gain Scaling and Fractional Differentiation

Kenneth W. Latimer<sup>1\*</sup> and Adrienne L. Fairhall<sup>2</sup>

<sup>1</sup> Department of Neurobiology, University of Chicago, Chicago, IL, United States; <sup>2</sup> Department of Physiology & Biophysics, University of Washington, Seattle, WA, United States

## OPEN ACCESS

### Edited by:

Colin W. G. Clifford,  
University of New South Wales,  
Australia

### Reviewed by:

Paul Miller,  
Brandeis University, United States  
Joshua A. Goldberg,  
Hebrew University of Jerusalem, Israel

### \*Correspondence:

Kenneth W. Latimer  
latimerk@uchicago.edu

**Received:** 13 January 2020

**Accepted:** 23 July 2020

**Published:** 09 September 2020

### Citation:

Latimer KW and Fairhall AL (2020)  
Capturing Multiple Timescales of  
Adaptation to Second-Order Statistics  
With Generalized Linear Models: Gain  
Scaling and Fractional Differentiation.  
*Front. Syst. Neurosci.* 14:60.  
doi: 10.3389/fnsys.2020.00060

Single neurons can dynamically change the gain of their spiking responses to take into account shifts in stimulus variance. Moreover, gain adaptation can occur across multiple timescales. Here, we examine the ability of a simple statistical model of spike trains, the generalized linear model (GLM), to account for these adaptive effects. The GLM describes spiking as a Poisson process whose rate depends on a linear combination of the stimulus and recent spike history. The GLM successfully replicates gain scaling observed in Hodgkin-Huxley simulations of cortical neurons that occurs when the ratio of spike-generating potassium and sodium conductances approaches one. Gain scaling in the GLM depends on the length and shape of the spike history filter. Additionally, the GLM captures adaptation that occurs over multiple timescales as a fractional derivative of the stimulus envelope, which has been observed in neurons that include long timescale afterhyperpolarization conductances. Fractional differentiation in GLMs requires long spike history that span several seconds. Together, these results demonstrate that the GLM provides a tractable statistical approach for examining single-neuron adaptive computations in response to changes in stimulus variance.

**Keywords:** adaptation, gain scaling, fractional differentiation, generalized linear model (GLM), Hodgkin and Huxley model

## 1. INTRODUCTION

Neurons adapt their spiking responses in a number of ways to the statistics of their inputs (Fairhall, 2014; Weber and Fairhall, 2019). A particularly well-studied example is adaptation to the stimulus variance, which can provide important computational properties. First, neurons can show gain scaling, such that the input is scaled by the stimulus standard deviation (Fairhall et al., 2001a; Mease et al., 2013). Scaling of the gain by the stimulus standard deviation implies that single spikes maintain the same information about the stimulus independent of its overall amplitude. This adaptation of the “input gain” with stimulus standard deviation can occur very rapidly. Second, the mean firing rate can adapt to variations in the stimulus variance across multiple timescales (Fairhall et al., 2001b; Wark et al., 2007). This form of spike frequency adaptation can in some cases have power-law properties (Pozzorini et al., 2013) and serve to compute the fractional derivative of the variance (Anastasio, 1998; Lundstrom et al., 2008).

One approach to studying such adaptation is to use Hodgkin-Huxley style (HH) conductance based models to explore potential single-neuron mechanisms underlying these computations (Lundstrom et al., 2008; Mease et al., 2013). Although HH models can indeed capture such behavior, the mechanistic HH framework is not ideally suited to reveal its dynamical basis as HH model parameters are difficult to interpret in terms of computation and coding. Moreover, fitting HH models to intracellular data is difficult (Buhry et al., 2011; Csersik et al., 2012; Vavoulis et al., 2012; Lankarany et al., 2014), and only recently methods that fit HH models to spike trains alone have been gaining success (Meng et al., 2011, 2014).

In contrast, statistical point-process models based on the generalized linear model (GLM) framework have provided a tractable tool for modeling spiking responses of neurons in sensory systems (Truccolo et al., 2005; Pillow et al., 2008). Previous work has shown the utility of finding linear features that can explain the spiking behavior of HH models (Agüera y Arcas and Fairhall, 2003; Agüera y Arcas et al., 2003; Weber and Pillow, 2017). Unlike simple linear/non-linear models, GLMs also incorporate a dependence on the history of activity, potentially providing a helpful interpretative framework for adaptation (Mease et al., 2014; Latimer et al., 2019a). We therefore fit GLMs to spike trains generated from HH neurons. Here, we considered gain scaling and fractional differentiation individually by using one set of HH neurons that showed gain scaling and another that produced fractional differentiation. Our goal here is not to analyze the details of these models to explain the adaptation phenomena, but to use these models as a source of “experimental” data with which to test the ability of the GLM to capture the same phenomena. We found that the GLMs could reproduce the single-neuron adaptive computations of gain scaling or fractional differentiation. Capturing gain scaling across a range of HH active conductance parameters depended both on the choice of link function and spike history length. As the length of the spike history filter increased, the stimulus dependency of neurons changed from differentiating to integrating (Stevenson, 2018). Capturing adaptation as a fractional derivative required a history filter that could account for long timescale effects: on the order of 10 s. Together these results demonstrate that the GLM provides a tractable statistical framework for modeling adaptation that occurs at the single-neuron level.

## 2. MATERIALS AND METHODS

To generate spike train data that display the two types of adaptation we study, we use Hodgkin-Huxley neuron models with parameter choices and channel dynamics previously shown to reproduce effects seen in experimental data. In principle we could use a single model that incorporates both gain scaling and fractional differentiation. While both types of adaptation have been observed in fly neuron H1 (Fairhall et al., 2001b), they have not been reported to occur in the same cortical cells. We therefore choose here to separate the two effects by considering two previously proposed HH models: one that has been applied to model gain scaling (Mease et al., 2013) and a second which

exhibits fractional differentiation (Lundstrom et al., 2008). We verified (data not shown) that both effects can be obtained within the same model, but with slight quantitative differences.

### 2.1. Gain Scaling

Gain scaling refers to the case when for an input-output function of a neuron, the input gain is proportional to the standard deviation (SD) of the stimulus ( $\sigma$ ). Thus, the gain depends on the recent context. If a neuron achieves perfect gain scaling, the firing rate  $R$  given a particular stimulus value,  $s$ , and input standard deviation can be written as:

$$R_{\sigma}(s) = \bar{R}_{\sigma} \hat{R}\left(\frac{s}{\sigma}\right) \quad (1)$$

where the normalized stimulus  $\hat{s} = \frac{s}{\sigma}$ , and the output gain,  $\bar{R}_{\sigma}$ , is constant in  $s$ .

To quantify the degree of gain scaling in a neuron's spiking output, we measure the firing rate function in response to a white-noise input,  $x(t)$ , at different SDs and constant mean  $\mu$  (Figure 1A). For each standard deviation, we compute the normalized spike-triggered average (STA; Figure 1B) (Rieke et al., 1999). We then compute the stimulus as the convolution  $s(t) = \int_0^t \text{STA}(t')(x(t-t') - \mu)dt'$ . The spike rate function is then defined probabilistically as

$$R_{\sigma}(s)\Delta_t = p_{\sigma}(\text{spk}|\hat{s}) = \frac{p_{\sigma}(\hat{s}|\text{spk})}{p_{\sigma}(\hat{s})} p_{\sigma}(\text{spk}) \quad (2)$$

where the right side follows from Bayes' rule. The average firing rate in time bin of width  $\Delta_t$  is  $p_{\sigma}(\text{spk})$ . Thus, we get  $\bar{R}_{\sigma}\Delta_t = p_{\sigma}(\text{spk})$  and  $\hat{R}\left(\frac{s}{\sigma}\right) = \frac{p_{\sigma}(\hat{s}|\text{spk})}{p_{\sigma}(\hat{s})}$ . The spike-triggered stimulus distribution,  $p_{\sigma}(\hat{s}|\text{spk})$ , is the probability of the stimulus given that a spike occurred in the bin. By definition the marginal stimulus distribution,  $p_{\sigma}(\hat{s})$ , is a standard normal distribution which does not depend on  $\sigma$ . Therefore, if  $p_{\sigma}(\hat{s}|\text{spk})$  is similar across different values of  $\sigma$ , gain scaling is achieved because  $\hat{R}(\hat{s})$  does not depend on  $\sigma$ .

We measure gain scaling in terms of the spike-triggered distribution. We do so using the 1st Wasserstein, or earth-mover's metric (Rubner et al., 1998) (we obtained qualitatively similar results using the symmetrized Kullback-Leibler divergence and Jensen-Shannon divergence). The Wasserstein metric is a distance function between two probability distributions. Intuitively, it can be thought of as the minimum work needed to transform one distribution into the other by moving probability mass as if the distributions are piles of sand (Supplementary Figure 1). Formally, it is defined as

$$W_1(\mu, \nu) = \inf_{\gamma \in \Gamma(\mu, \nu)} \int_{M \times M} d(x, y) d\gamma(x, y) \quad (3)$$

where  $\nu$  and  $\mu$  are probability measures on a metric space  $M$  with metric  $d(\cdot, \cdot)$ . The infimum is taken over the collection of measures,  $\Gamma(\mu, \nu)$ , on  $M \times M$  with  $\mu$  and  $\nu$  marginal distributions. We compute the gain scaling score at  $\sigma$  as

$$D_{\sigma} = W_1(p_1(\hat{s}|\text{spk}), p_{\sigma}(\hat{s}|\text{spk})). \quad (4)$$

A distance close to 0 indicates that the spike-triggered distributions are similar, and therefore the cell is gain scaling its input (**Figures 1C,D**). Larger values of  $D_\sigma$  indicate that the input-output function does not scale with  $\sigma$  (**Figures 1E–G**). We computed the spike-triggered distribution using a histogram with bins of width 0.1.

### 2.1.1. Gain Scaling in Hodgkin-Huxley Neurons

A previous study by Mease et al. (2013) found that Hodgkin-Huxley models could account for gain scaling observed in pyramidal neurons. Thus we simulated spikes from single-compartment Hodgkin-Huxley style models of pyramidal neurons, providing a source of data with which to explore the expression of this property using GLMs. In this model, the membrane voltage depends on voltage-gated sodium and potassium conductances ( $G_{Na}$  and  $G_K$ ) and a passive leak conductance ( $G_L$ ). The voltage and gating dynamics followed the equations (Mainen et al., 1995)

$$C \frac{dV}{dt} = I_{stim}(t) - G_{Na} m^3 h (V - E_{Na}) - G_K n (V - E_K) - G_L (V - E_L) \quad (5)$$

such that for each gate  $x \in \{n, m, h\}$

$$\tau_x(V) \frac{dx}{dt} = x_\infty(V) - x, \quad \tau_x(V) = \frac{1}{\alpha_x(V) + \beta_x(V)} \quad (6)$$

$$n_\infty(V) = \alpha_n(V) \tau_n(V), \quad m_\infty(V) = \alpha_m(V) \tau_m(V), \quad h_\infty(V) = \frac{1}{1 + \exp\left(\frac{V+65}{6.2}\right)} \quad (7)$$

$$\alpha_n(V) = \frac{20(V-20)}{1 - \exp\left(-\frac{V-20}{9}\right)}, \quad \beta_n(V) = \frac{-2(V-20)}{1 - \exp\left(\frac{V-20}{9}\right)} \quad (8)$$

$$\alpha_m(V) = \frac{182(V+35)}{1 - \exp\left(-\frac{V+35}{9}\right)}, \quad \beta_m(V) = \frac{-124(V+35)}{1 - \exp\left(\frac{V+35}{9}\right)}$$

$$\alpha_h(V) = \frac{24(V+50)}{1 - \exp\left(-\frac{V+50}{5}\right)}, \quad \beta_h(V) = \frac{-9.1(V+75)}{1 - \exp\left(\frac{V+75}{5}\right)}$$

The parameters of the model were the same as in Mease et al. (2013). The reversal potentials were  $E_{Na} = 50$ ,  $E_K = -77$ , and  $E_L = -70$  mV and the capacitance was  $C = 1 \mu F/cm^2$ . The leak conductance was set to  $0.4 pS/\mu m^2$  so that the resting membrane had a time constant of  $\sim 25$  ms. As in Mease et al. (2013), we explored a range of values for the active conductances  $G_{Na}$  and  $G_K$ : from 600 to 2,000  $pS/\mu m^2$  in increments of  $100 pS/\mu m^2$ . Simulations were performed in MATLAB using a fourth-order Runge-Kutta method with step size 0.01 ms. Spike times were defined as upward crossings of the voltage trace at -10 mV separated by at least 2 ms.

The input was constructed as independent Gaussian draws every 1 ms with parameters  $\mathcal{N}(\mu, (4\mu\sigma)^2)$  where  $\sigma$  was set to 1.0, 1.3, 1.6, or 2.0. The mean was constrained to be proportional to the standard deviation similarly the current-clamp protocol used to study gain scaling in Mease et al. (2013). For each value of  $G_{Na}$  and  $G_K$ , the mean input,  $\mu$ , was tuned so that at baseline,

where  $\sigma = 1$ , each simulation produced  $\sim 10$  spk/s using a 100 s simulation. We did not consider values of  $G_{Na}$  and  $G_K$  that spiked spontaneously (i.e., spiked when  $\mu = 0$ ). We simulated 2,000 s of spiking activity at each stimulus level (generating  $\sim 20,000$  spikes at  $\sigma = 1$ ).

## 2.2. Fractional Differentiation

We next looked at periodic modulations of the stimulus standard deviation to model long timescale adaptive effects. We applied stimuli consisting of Gaussian noise with sinusoidal or square wave modulation of the variance between 1 and  $\sigma$  with  $\sigma$  again taking values of 1.3, 1.6, or 2.0, at a number of different frequencies. We analyzed simulated spike trains across seven noise modulations periods: 1, 2, 4, 8, 16, 32, and 64 s. The simulations were 3,200 s for each period, giving a minimum of 50 cycles per period.

Lundstrom et al. (2008) found that pyramidal neurons can act as fractional differentiators of the stimulus amplitude envelope for this type of input. Fractional derivatives generalize the derivative operator such that, analogous to taking the first derivative of a function twice to obtain the second derivative, taking the fractional derivative of order  $\alpha = 1/2$  twice results in the first derivative (Oldham and Spanier, 1974). Fractional differential filters respond to a square stimulus as an exponential-like decay with a time constant that depends on  $\alpha$  (**Figures 2A,B**). Fractionally differentiating a sinusoidal stimulus produces a frequency dependent gain change (**Figure 2C**)

$$\text{gain} \propto f^\alpha \quad (9)$$

where  $f$  is the frequency. Additionally, fractionally differentiating the sine function gives a frequency independent phase shift,  $\phi$ , of the stimulus (**Figure 2D**):

$$\phi = \alpha \frac{\pi}{2}. \quad (10)$$

These three measures can be combined to estimate approximate fractional differentiation by neurons.

To compute the fractional derivative order, we computed cycle-averaged responses obtained using 30 bins per cycle at each stimulus amplitude modulation frequency. We fit the cycle-averaged square-wave responses across all modulation frequencies as the best fitting fractional derivative of the stimulus amplitude (plus a baseline rate) using least-squares. To fit  $\alpha$  to the phase lead of the sine-wave responses, we computed mean phase lead ( $\phi$ ) across frequencies and applied Equation (10). To fit  $\alpha$  to the gain of the sine-wave responses, we applied Equation (9) by fitting a least-squares regression between the frequency of modulation and the logarithm of the gain.

### 2.2.1. Fractional Differentiation by Hodgkin-Huxley Neurons

We simulated neurons from the standard HH model with three additional afterhyperpolarization (AHP) currents with time constants ranging from 0.3 to 6 s as was done by Lundstrom et al.

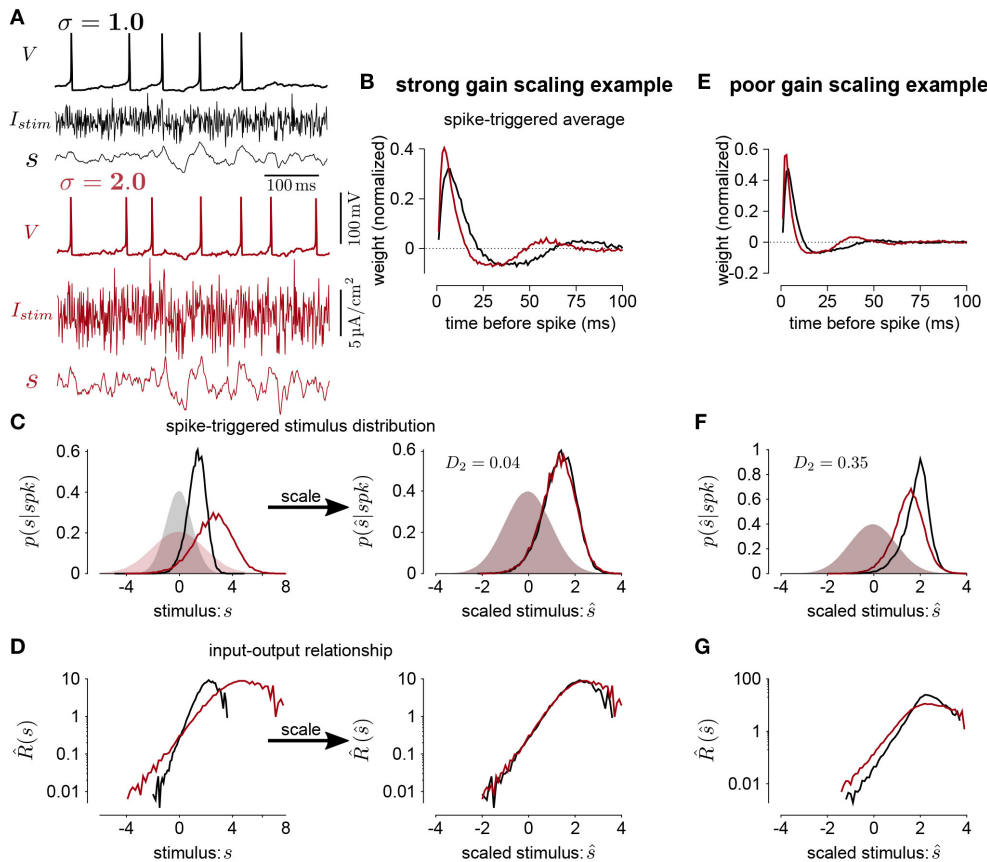


**FIGURE 1 | (A)** The voltage ( $V$ ), stimulus current ( $I_{stim}$ ), and stimulus filtered by the STA ( $s$ ) for Hodgkin-Huxley simulations of a neuron stimulated with white noise at two different standard deviation levels (black  $\sigma = 1$ ; red  $\sigma = 2$ ). In this simulation, the total sodium and potassium conductances were equal ( $G_{Na} = G_K = 1,000 \text{ pS}/\mu\text{m}^2$ ). **(B)** The STAs measured at the two stimulus standard deviations. **(C)** Left shows the spike-triggered distributions of the STA filtered input ( $s$ ) and right shows the distributions over the STA filtered input scaled by the standard deviation ( $\hat{s}$ ). The shaded areas show the prior stimulus distributions, which are Gaussian distributed with standard deviation  $\sigma$ . **(D)** The input-output functions of the stimulation at each stimulus level. Scaling the input by the standard deviation shows that the simulated neuron scales the gain of the input by the stimulus standard deviation (right). **(E)** The STAs measured at two standard deviations from a Hodgkin-Huxley simulation with high potassium and low sodium total conductances ( $G_{Na} = 600$  and  $G_K = 2,000 \text{ pS}/\mu\text{m}^2$ ). The spike-triggered stimulus distribution **(F)** and scaled input-output function **(G)** for this simulation does not show gain scaling.

(2008). The equations for the HH neurons were

$$C \frac{dV}{dt} = I_{stim}(t) - G_{Na} m^3 h (V - E_{Na}) - G_K n^4 (V - E_K) - G_L (V - E_L) - \sum_{i=1}^3 G_{AHP,i} a_i (V - E_{AHP}) \quad (11)$$

The gates  $x \in n, m, h$  follow the dynamics

$$\tau_x(V) \frac{dn}{dt} = x_\infty(V) - x, \quad \tau_x(V) = \frac{1}{\alpha_x(V) + \beta_x(V)}, \quad x_\infty(V) = \alpha_x(V) \tau_x(V) \quad (12)$$

$$\begin{aligned} \alpha_n(V) &= \frac{0.01(V + 55)}{1 - \exp(-0.1(V + 55))}, \\ \beta_n(V) &= 0.125 \exp(-(V + 65)/80) \\ \alpha_m(V) &= \frac{0.1(V + 40)}{1 - \exp(-0.1(V + 40))}, \\ \beta_m(V) &= 4 \exp(-(V + 65)/18) \\ \alpha_h(V) &= 0.07 \exp(-(V + 65)/20), \\ \beta_h(V) &= \frac{1}{1 + \exp(-0.1(V + 35))}. \end{aligned} \quad (13)$$

The AHP currents have linear dynamics and are incremented by 1 at spike times ( $t_{spk,i}$ ):

$$\frac{da_i}{dt} = -\frac{a_i}{\tau_i} + \sum_i \delta(t - t_{spk,i}) \quad (14)$$

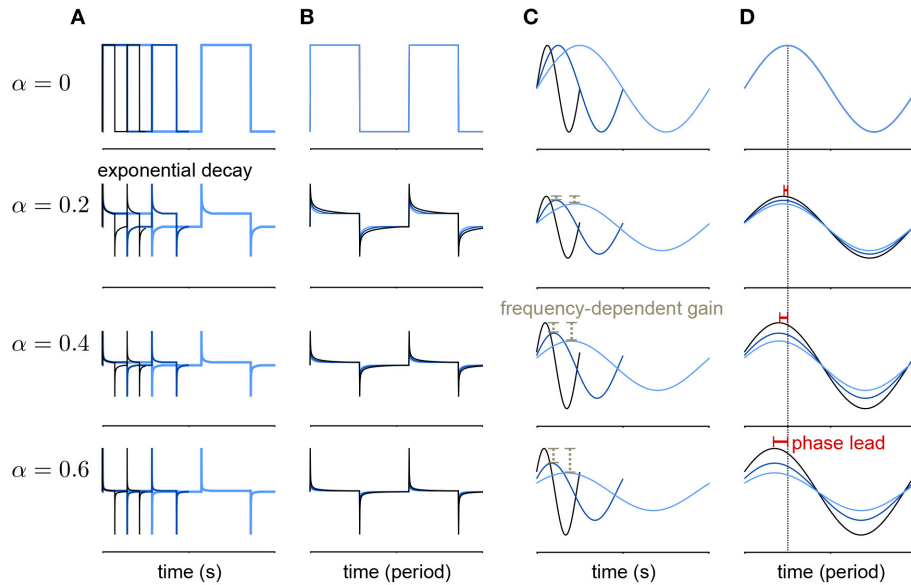


**FIGURE 2 |** Example of a fractional derivative of several orders. Each row shows a different fractional order ( $\alpha$ ) of the function in the top row. **(A)** The fractional derivatives of a step function with three different periods (colors) shows exponential filtering with an  $\alpha$  dependent timescale. **(B)** The fractional derivatives in **(A)** scaled by period. **(C)** The fractional derivatives of a sine function for three different periods. As  $\alpha$  increases, the fractional derivative shows greater frequency-dependent gain. **(D)** The same function as in **(B)** with the sine functions scaled by period. At higher orders, the phase lead of the fractional derivative relative to the signal increases equally over frequencies.

where  $\delta$  is the Dirac delta function. The parameters standard were:  $G_{Na} = 120$ ,  $G_K = 36$ ,  $G_L = 0.3 \text{ mS/cm}^2$ ;  $E_{Na} = 50$ ,  $E_K = -77$ ,  $E_L = -54.4 \text{ mV}$ ; and  $C = 1 \mu\text{F/cm}^2$ . The AHP conductances were set relative to the leak conductance:  $G_{AHP} = (0.05, 0.006 \text{ and } 0.004)G_L$ . The AHP reversal potential was  $E_{AHP} = -100 \text{ mV}$  and the AHP timescales were set to  $\tau_i = (0.3, 1, \text{ and } 6) \text{ s}$ .

Similarly to the gain scaling simulations, the stimulus was sampled independently in each 1ms bin from a normal distribution with mean  $\mu$ . The time-dependent variance given  $\sigma$  and the period  $p$  was  $4\mu f_p(t, \sigma)$ . The time-dependent modulation function for the square-wave stimulus was

$$f_p(t, \sigma) = 1 + (\sigma - 1) \left\lfloor \frac{1}{2} \sin\left(\frac{2t\pi}{p}\right) + 1 \right\rfloor \quad (15)$$

where  $\lfloor \cdot \rfloor$  denotes the floor operator, and the function for the sine-wave stimulus was similarly defined as

$$f_p(t, \sigma) = 1 + (\sigma - 1) \left( \frac{1}{2} \sin\left(\frac{2t\pi}{p}\right) + \frac{1}{2} \right). \quad (16)$$

The parameter  $\mu$  was calibrated so that with no variance modulation (i.e.,  $\sigma = 1$ ), the simulated cells produced  $\sim 10 \text{ spk/s}$ .

### 2.3. Generalized Linear Models

The GLM defines the spiking activity as an autoregressive Poisson process with (Figure 3A). The spike rate at time  $t$  is given as a linear–nonlinear function of the stimulus and the spike history

$$\lambda_t = f(\mathbf{k}_{stim}^\top \mathbf{x}_t + \mathbf{h}_{spk}^\top \mathbf{y}_{hist,t} + b) \quad (17)$$

where  $\mathbf{x}_t$  is the stimulus vector preceding time  $t$  (the values of  $I_s \text{ tim}$ ), and  $\mathbf{y}_{hist}$  is the spike history vector. The parameters of the GLM are the stimulus filter ( $\mathbf{k}_{stim}$ ), the spike history filter ( $\mathbf{h}_{spk}$ ), and baseline rate ( $b$ ). For the inverse-link function,  $f$ , we used the canonical exponential function except where otherwise noted.

The log-likelihood of a binned spike train,  $\mathbf{y}$ , given the model parameters is then

$$\log p(\mathbf{y} | \mathbf{k}_{stim}, \mathbf{h}_{spk}, b) = \sum_{t=1}^T -\lambda_t \Delta_t + y_t \log(\lambda_t) + \text{const.} \quad (18)$$

For all model fits and simulations, we set  $\Delta_t = 1 \text{ ms}$ . We numerically maximized the log-likelihood using conjugate-gradient methods.

To reduce the number of model parameters, we parameterized the filters using smooth basis functions (Figure 3B). The stimulus filter was parameterized using 15 raised cosine basis functions:

$$\mathbf{k}_{stim}(t) = \sum_{j=1}^{15} z_j \mathbf{g}_j(t), \quad \mathbf{g}_j(t) = \begin{cases} \frac{1}{2} \cos\left(\frac{\log[t+c]-\phi_j}{a}\right) + \frac{1}{2} & \text{for } \frac{\log[t+c]-\phi_j}{a} \in [-\pi, \pi] \\ 0 & \text{otherwise} \end{cases} \quad (19)$$

where  $t$  is in seconds. To fit  $\mathbf{k}_{stim}$ , we optimized the weights  $z_j$ . We set  $c = 0.02$  and  $a = 2(\phi_2 - \phi_1)/\pi$ . The  $\phi_j$  were evenly spaced from  $\phi_1 = \log(T_0/1000 + c)$ ,  $\phi_{15} = \log(T_{end}/1000 + c)$  where the peaks of the filters are in the range  $T_0 = 0$  and  $T_{end} = 100 \text{ ms}$ .

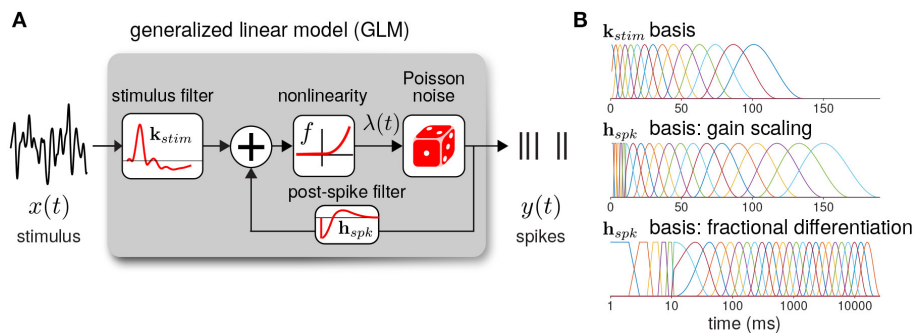


**FIGURE 3 | (A)** Diagram of the neural GLM that describes spiking as an autoregressive Poisson process. **(B)** The basis functions used to parameterize the GLM filters. (top) The stimulus basis used for all GLMs. (middle) The spike history basis used for the gain scaling simulations. (bottom) The spike history basis used for the fractional differentiation simulations. Due to the length of the spike history filters needed to capture fractional differentiation, the time axis is shown in log scale.

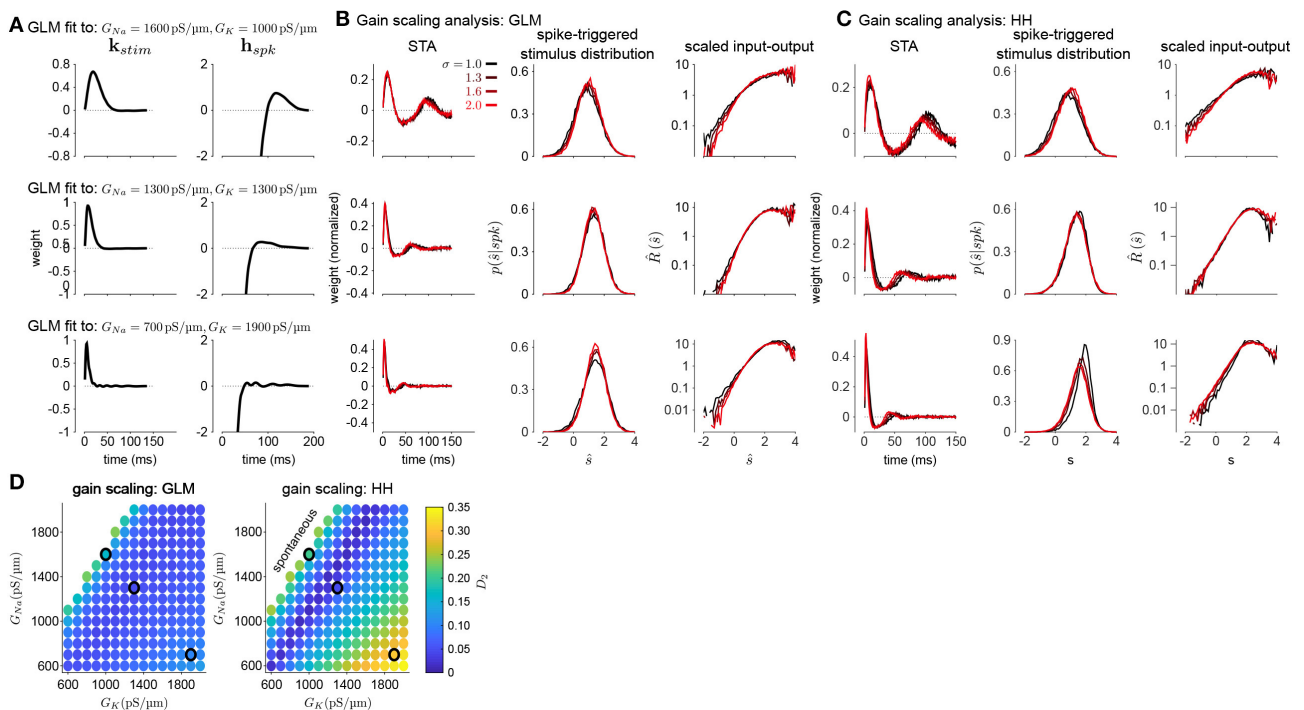
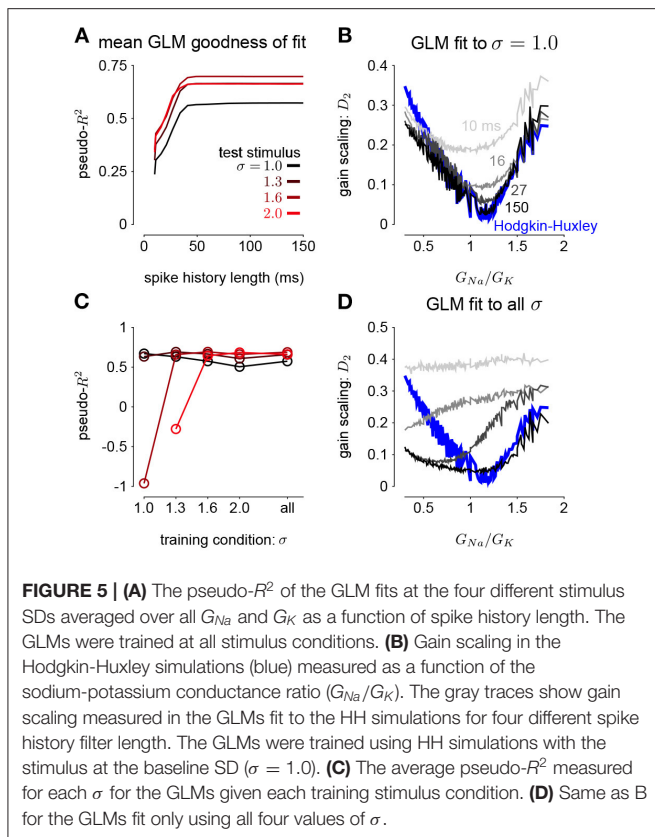


**FIGURE 4 | (A)** Example filters from GLM fits to HH simulations with three different spiking conductance levels (rows). Large negative values driving the refractory period in the spike history filter (right) have been truncated. **(B)** The spike-triggered averages (left), scaled spike-triggered stimulus distributions (right), and scaled input-output functions (right) for the GLM fits in A for all four stimulus SDs. **(C)** Same as B for the HH simulations. **(D)** Gain scaling ( $D_2$  from Equation (4), Wasserstein distance between the spike-triggered distributions at  $\sigma = 1$  and  $\sigma = 2$ ) at all the spiking conductance levels explored for the GLM simulations (top) and the Hodgkin-Huxley simulations (bottom). Lower values of  $D_2$  correspond to stronger gain scaling. The three black circles indicate the conductance levels for the GLM examples in A and B. Gain scaling was not computed for values of  $G_{Na}$  and  $G_K$  that resulted in spontaneous spiking in the Hodgkin-Huxley simulations.

The spike history filter bases were constructed in two parts. To account for the absolute refractory period, we used 5 box car filters of width 2 ms for the first 10 ms of the spike history. The remaining spike history filter was parameterized using raised cosine basis functions with the parameter  $c = 0.05$ . For the gain scaling simulations,  $N = 15$  cosine basis functions were used with spacing  $T_0 = 10$  and  $T_{end} = 150$  ms. For the fractional differentiation simulations,  $N = 25$  cosine basis functions were

used with spacing  $T_0 = 10$  and  $T_{end} = 16,000$  ms. To explore how the timescale of spike history affected adaptation in the GLM, for each model we fit the GLM using only the first  $i$  cosine basis functions for each  $i = 0$  (using only the refractory box-car functions) to  $i = N$ . Thus, we obtained  $N + 1$  nested model fits across a range of spike history lengths. When stated, the length of the spike history filter,  $T_{hist}$ , denotes the time of the peak of the  $i$ th basis function.



### 2.3.1. Evaluating Model Performance

We evaluated the GLM performance by assessing the ability of the GLM to predict the HH model response to a 32 s novel stimulus. For the gain scaling simulations, we tested the response to the test stimulus at each stimulus SD ( $\sigma$ ). For the fractional differentiation simulations, the stimulus SD was modulated by a sine or square wave with a 4 s period and a modulation height of  $\sigma = 2.0$ . Predictive performance was evaluated using the pseudo- $R^2$  score (Cameron and Windmeijer, 1997). We selected this measure because it can be applied to Poisson process observations instead of trial-averaged firing rates as is required by the standard  $R^2$  measure of explained variance (Benjamin et al., 2018). Thus, it is especially appropriate for comparing the stochastic GLM to a spike train simulated by the deterministic HH model. The pseudo- $R^2$  is written as the ratio of deviances:

$$\begin{aligned} \text{pseudo} - R^2 &= 1 - \frac{D(\mathbf{y}^*, \text{GLM})}{D(\mathbf{y}^*, \text{null})} \\ &= 1 - \frac{\log(p_{\text{GLM}}(\mathbf{y}^* | \mathbf{k}_{\text{stim}}, \mathbf{h}_{\text{spk}}, b)) - \log(p_{\text{sat}}(\mathbf{y}^*))}{\log(p_{\text{null}}(\mathbf{y}^* | \bar{\mathbf{y}}^*)) - \log(p_{\text{sat}}(\mathbf{y}^*))} \end{aligned} \quad (20)$$

where  $\mathbf{y}^*$  is the test spike train. The GLM likelihood is  $p_{\text{GLM}}(\mathbf{y}^* | \mathbf{k}_{\text{stim}}, \mathbf{h}_{\text{spk}}, b)$  and the likelihood of the null model ( $p_{\text{null}}(\mathbf{y}^* | \bar{\mathbf{y}}^*)$ ) is the probability of the spike train given only the mean firing rate,  $\bar{\mathbf{y}}^*$ . The saturated model likelihood ( $p_{\text{sat}}(\mathbf{y}^*)$ ) is the probability of observing  $\mathbf{y}^*$  given one parameter per bin:

that is, the Poisson probability of observing  $\mathbf{y}^*$  given a model with rate  $\lambda = 1$  in each bin in which the HH model spiked and rate  $\lambda = 0$  in each bin that the HH did not spike. Thus, the pseudo- $R^2$  measures the fraction of explainable log-likelihood captured by the GLM.

## 3. RESULTS

### 3.1. GLMs Capture Gain Scaling Behavior

To investigate how GLMs can capture biophysically realistic gain scaling, we fit the Hodgkin-Huxley simulations with GLMs (Figure 4A). We fit a unique GLM for each value of  $G_{Na}$  and  $G_K$  in the HH model, and the GLMs were fit using the entire range of stimulus SDs ( $\sigma = 1.0, 1.3, 1.6$ , and  $2.0$ ). Applying the STA analysis at the four stimulus SDs, we quantified gain scaling in GLM fits and compared the gain scaling in the GLM simulations to the HH neurons (Figures 4B,C). Across the range of spiking conductance values, we found that the GLM fits consistently showed gain scaling (Figure 4D). The HH neurons showed the greatest degree of gain scaling when the  $G_{Na}/G_K$  ratio was close to one, with the lowest  $D_2$  score occurring at a ratio of 1.17 (Mease et al., 2013). We observed the same pattern in the GLM simulations, but the GLM fits generally exhibited stronger gain scaling when  $G_{Na}/G_K < 1$  than the HH neurons. We note that in general the optimal  $G_{Na}/G_K$  ratio depends on the leak conductance; however, here we assumed a fixed leak for simplicity.

The GLM's characterization of the HH neurons depended on the spike history filter. This is revealed by comparing the stimulus filters (Figure 4A) to the stimulus features extracted by spike-triggered averaging (Figure 4B): While the STA showed multiphasic responses, the GLM stimulus filter was consistent with a simple, monophasic integration. This demonstrates that the STA reflects the combination of stimulus and spike history effects (Agüera y Arcas and Fairhall, 2003; Stevenson, 2018). A spike history filter of sufficient length was necessary to achieve accurate model fits across all stimulus SDs (Figures 5A,B). A possible interpretation of this finding is that the spike history is acting as a measure of the “context” that serves to normalize the stimulus response, and that a sufficiently long sampling of the spiking output is needed in order to perform this normalization appropriately.

We also explored how the stimulus conditions used to fit the GLM determined the model's ability to capture gain scaling. Remarkably, we found that the GLM fit only to the baseline stimulus SD ( $\sigma = 1.0$ ) captured the gain scaling pattern seen in the HH neuron (Figure 5B). The gain scaling observed in the GLMs required a sufficiently long spike history filter, on the order of at least 50 ms. With shorter spike history, the GLM did not obtain the same level of gain scaling at the optimal  $G_{Na}/G_K$  ratio. However, these GLM fits failed to generalize across stimulus SDs. The GLM trained only at  $\sigma = 1.0$  explained less variance in the spiking responses to a stimulus at  $\sigma = 2.0$  than a model capturing only the mean firing rate for all values of  $G_{Na}$  and  $G_K$  (predictive pseudo- $R^2 < 0$ ; Figure 5C). Therefore, the GLM trained at  $\sigma = 1.0$  does not accurately characterize the HH responses despite accurately predicting gain scaling in

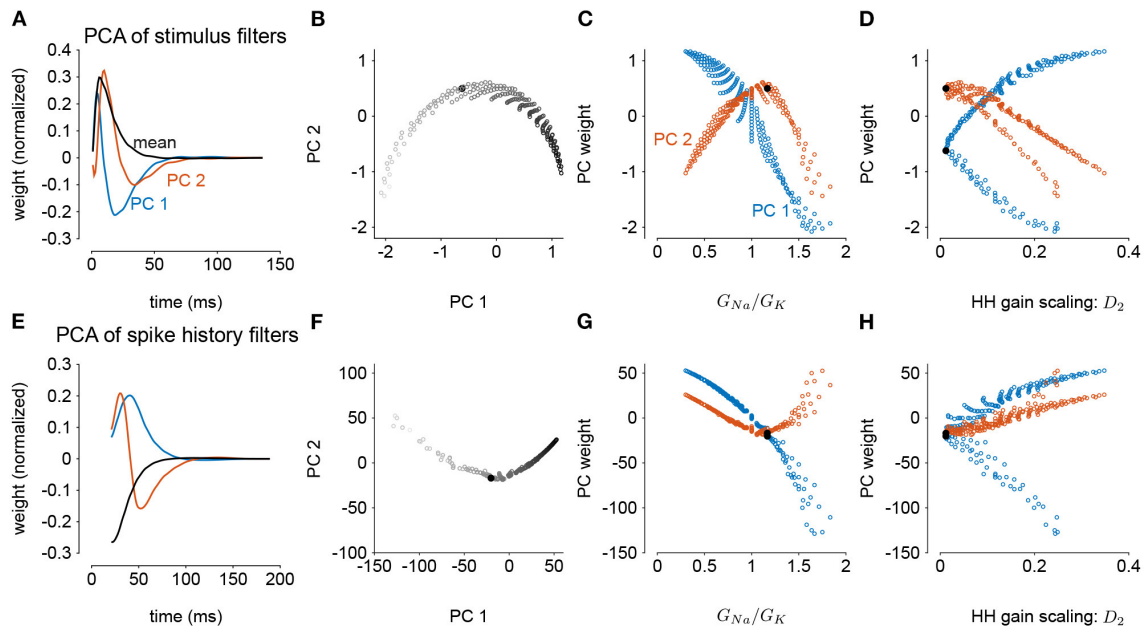


**FIGURE 6 |** Principal component analysis of the GLM stimulus and spike history filters trained across all values of  $G_{Na}$  and  $G_K$ . The GLMs were trained on all  $\sigma$  values with a spike history length of 150 ms. **(A)** The first two PCs (blue and red) of the stimulus filter. The normalized mean filter is given in black. **(B)** The projections of the stimulus filters onto the first two PCs. The shade of the points corresponds to  $G_{Na}/G_K$  where lighter indicates a higher ratio. The black points in **(B,C,E,F)** indicates GLM fit to the HH model with the best gain scaling (i.e., lowest  $D_2$ ). **(C)** The stimulus filter PC weights (same as in **B**) as a function of the  $G_{Na}/G_K$  ratio. **(D)** The stimulus filter PC weights as a function of the gain scaling factor ( $D_2$ ) observed in the HH simulation fit by the GLM. **(E–H)** Same as **(A–D)** for the GLMs' spike history filters. The first 20 ms of the spike history filters were excluded from analysis to avoid effects from the strong refractory period.

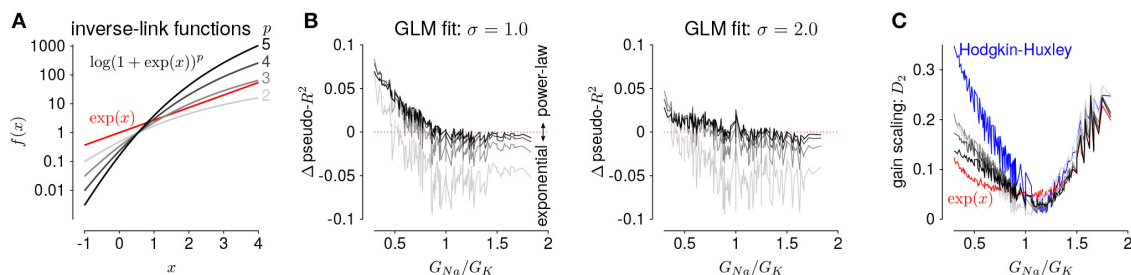


**FIGURE 7 | (A)** The five inverse-link functions tested in the GLM. The red trace shows the canonical exponential inverse-link function used in **Figures 4, 5**. The gray traces show the soft-power function for different exponents,  $p$ . **(B)** The difference in predictive performance (measured as pseudo- $R^2$ ) between the exponential GLMs and the power-law GLMs for  $p \in \{2, 3, 4, 5\}$  for a test stimulus of  $\sigma = 1.0$  (left) and  $\sigma = 2.0$  (right). Positive values indicate the GLM with a power-law non-linearity had greater predictive performance than the exponential GLM. The GLMs were fit to all  $\sigma$ . **(C)** Gain scaling predicted by the power-law GLMs (gray traces) compared to the exponential GLMs (red) and the HH simulations (blue).

those cells. In contrast, GLMs trained at all four  $\sigma$  values failed to capture the lack of gain scaling at low  $G_{Na}/G_K$  values despite showing improved model fit across all  $\sigma$  (**Figure 5D**; a detailed example is provided in **Supplementary Figure 2A**). Because the GLM trained on all  $\sigma$  showed both consistent generalization performance and strong gain scaling behavior, the remaining analyses considered only that training condition.

We next considered how the GLM parameters related to the gain scaling computation and the space of  $G_{Na}$  and  $G_K$  in the HH models. To visualize the geometry of the model parameters, we performed PCA on the stimulus and

spike history filters (**Figures 6A,E**). The filters produced across the two HH parameters spanned a two-dimensional subspace (variance explained: stimulus 98.8%, spike history 97.3%). The PCA reconstructions for example stimulus filters are given in **Supplementary Figure 3**. This decomposition of the stimulus filter shows that the first mode is primarily an integrator, while the second acts as a derivative, and will serve to adjust the timescale of the filter's integration window. The inflection point for the second mode suggests that there may be an optimal time constant of stimulus and spike history integration needed to support the gain scaling property (**Figures 6B,F**). The first

component for both filters correlated with the  $G_{Na}/G_K$  ratio (Figures 6C,G; stimulus PC1  $r = -0.97, p < 10^{-4}$ ; spike history PC2  $r = 0.97, p < 10^{-4}$ ). The second PC correlates with the gain scaling value observed in the corresponding HH model (Figures 6D,H; stimulus PC2  $r = -0.89, p < 10^{-4}$ ; spike history PC2  $r = 0.90, p < 10^{-4}$ ).

### 3.1.1. Power-Law Firing Rate Nonlinearities

The GLMs we considered used the canonical inverse-link function, the exponential nonlinearity (McCullagh and Nelder, 1989), to transform the filtered stimulus plus spike history into a firing rate. However, it is known that firing rate nonlinearities that instead have a power-law relationship of the input produce gain scaling (Miller and Troyer, 2002; Murphy and Miller, 2003). We therefore considered a range of soft-power nonlinearities over a range of exponents for the GLM firing rate (Figure 7A; Equation 17):

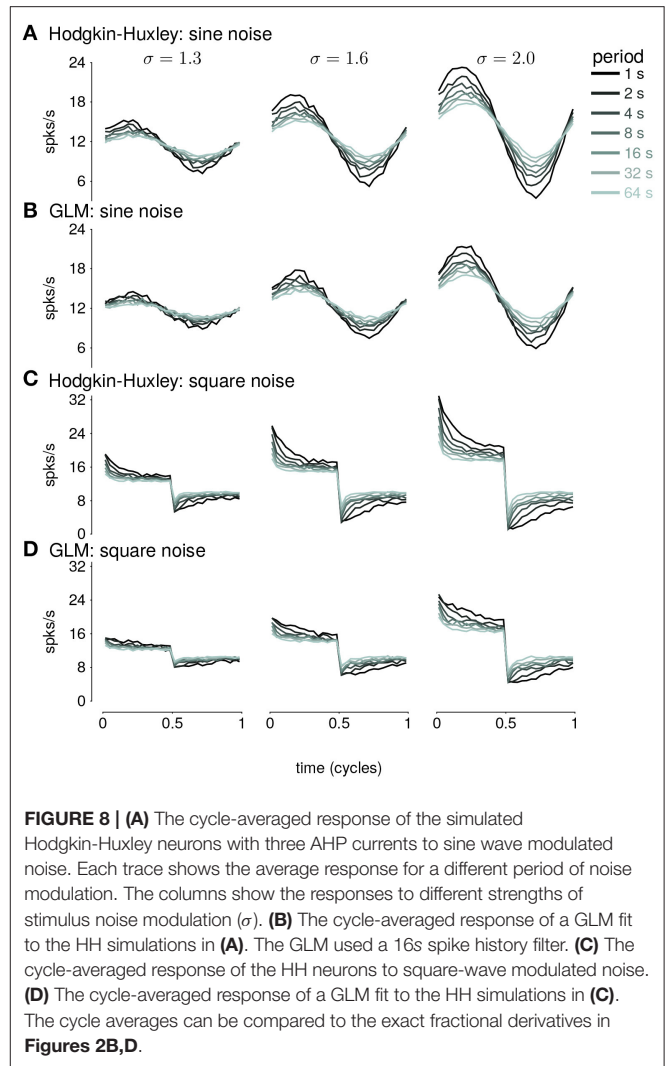
$$f(x) = \log(1 + \exp(x))^p \quad (21)$$

for  $p \in \{2, 3, 4, 5\}$  (for  $p = 1$ , the model performed poorly for all HH simulations and the results are not shown). We found that the power-law nonlinearity produced better predictive fit than the exponential for HH simulations with low  $G_{Na}/G_K$  ratios (Figure 7B). For those ratios, the exponential GLM in fact predicted *greater* gain scaling than the HH simulation actually showed (Figure 5A and Supplementary Figure 2A). We found the power-law nonlinearities showed *less* gain scaling in the low  $G_{Na}/G_K$  regime, which was more consistent with the HH simulations (Figure 7C). This perhaps counter-intuitive result is likely due to the temporal processing of the GLM: the spike history filter shapes the effective stimulus-response function over longer timescales. Thus, the instantaneous spike rate function need not be a power law to produce gain scaling and an instantaneous power-law function may not result in strong gain scaling in the presence of spike history dependencies.

## 3.2. GLMs Capture Fractional Differentiation With Long Timescales of Adaptation

In this section, we address adaptive computations occurring over multiple timescales spanning tens of seconds, instead of instantaneous gain. We consider adaptation to changes in stimulus variance in the responses of HH simulations with three AHP currents (Lundstrom et al., 2008). The neurons were injected with noise stimuli with a periodically modulated SD. The stimulus SD followed either a sine or square wave. We focused our analyses on the cycle-averaged firing rate to see how the neural responses reflect fractional differentiation of the stimulus SD envelope in the cycle-averages.

We fit GLMs to HH simulations in response to either sine- or square-wave SD modulation. The training data included simulations with noise modulation periods of 1–64s. We considered GLMs with different lengths of spike history filters. Cycle-averaged responses of HH and GLM simulations appear qualitatively similar (Figure 8), and thus we aimed to characterize how well the GLM fits captured the fractional



differentiation properties of the HH neuron. Although the AHP conductances act to provide a simple linear filtering of the spike train similar to the GLM's spike history filter, the GLM effectively assumes that the spike history is instead a current such that the total conductance of the cell remains constant (Latimer et al., 2019b). Therefore, it is not given that the GLM can replicate the computational effects of the AHP conductances.

The sinusoidal noise simulations show two properties of fractional differentiation. First, we estimated response gain (i.e., the strength of the sinusoidal modulation in the cycle-averaged response as a function of stimulus period; Figure 9A). In an ideal fractional differentiator, the log gain is proportional to the log of the stimulus period. The HH neuron shows a near linear response ( $r^2 = 0.99, p < 10^{-4}$ ). Although the GLM with short history shows an almost flat relationship, increasing the spike history length shows similar slope to the HH neuron. The second property was the phase lead of the cycle-averaged response relative to the stimulus (Figure 9B). The phase lead should be constant under perfect fractional differentiation. The

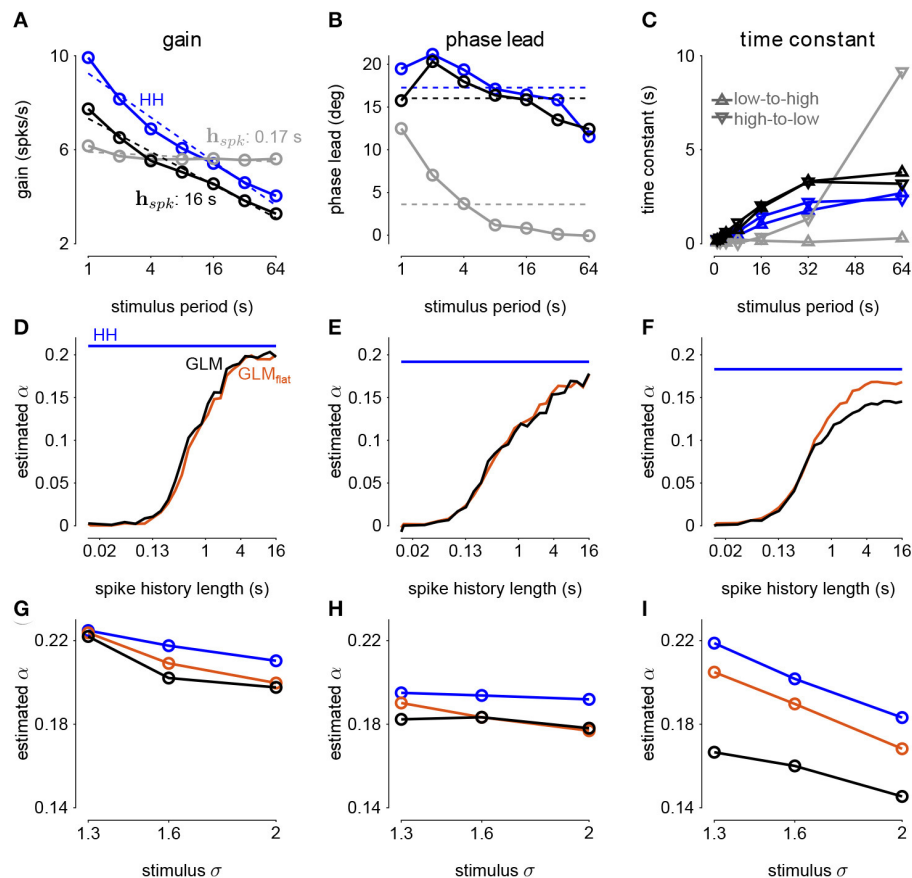


**FIGURE 9 | (A)** The gain of the average responses to sine-wave modulated noise as a function of stimulus period for the HH and GLMs (Figures 8A,B right). The GLM fit with a 0.17 s spike history filter (gray) is compared to the GLM with the full 16 s spike history (black). The HH simulation is given in blue. The noise stimulus was modulated with  $\sigma = 2$ . **(B)** The phase lead of the average responses to sine-wave modulated noise as a function of stimulus period for the HH and GLMs. The fraction of variance explained in the HH phase lead curve by the GLM with 16 s spike history was  $R^2 = 0.61$ . **(C)** The time constant of an exponential function fit to the cycle-averaged response to square wave noise for each stimulus period (Figures 8C,D right). The markers denote time constants estimated for steps from low to high variance or step from high to low variance. The fraction of variance explained of the log time constants of the HH simulation by the GLM with 16 s spike history was  $R^2 = 0.80$ . **(D)** The fractional differentiation order ( $\alpha$ ) of the GLM estimated by the slope of gain as a function of the log stimulus period in **(B)**. The value is estimated for each spike history lengths (black) and compared to  $\alpha$  estimated from the HH simulation (blue). The red trace shows  $\alpha$  estimated from the GLM fit only to unmodulated noise. **(E)**  $\alpha$  estimated by the average phase lead across stimulus periods. **(F)**  $\alpha$  estimated by fitting a the square-wave responses with a fractional differentiating filter. **(G–I)**  $\alpha$  estimated at different noise modulation strengths for the 16 s spike history GLM and HH simulation.

phase lead declines with longer period, but the HH simulation still shows strong phase lead in a 64 s period. Short spike history filter GLMs exhibit a phase lead that tends to zero with long SD periods. However, the GLM fit with a long spike history filter closely tracks the HH neuron's phase lead.

The final signature of fractional differentiation was the exponential decay of the cycle-averaged response under square-wave noise simulation (Figure 9C). We estimate the time constant of the decay on the square noise cycle average for both steps up and steps down in stimulus SD. The time constant increases approximately linearly with the SD period, and GLMs with long spike history showed time constants closely approximated the HH neuron.

From each signature, we estimated the order of the fractional differentiation ( $\alpha$ ) in both the HH neurons and the GLM fits. We estimated the order using the slope of log-period compared

to log-gain and mean phase lead across all stimulus periods for the sine-wave SD simulations (Figures 9D,E). A least-squares fit of FD filter of order  $\alpha$  was applied to the square noise stimuli (Figure 9F). We considered  $\alpha$  for the GLM fits as a function of the spike history length. The order estimates for the HH neuron, although slightly different for each signature, were approximately  $\alpha = 0.2$ . The GLM's FD order tends toward that of the HH neuron as the spike history length increases from below. Surprisingly, when we considered a GLM trained only to a flat noise stimulus (no sine or square modulation; stimulus SD  $\sigma = 1.0$ ) showed similar estimates of  $\alpha$  (Figures 9D–F, red traces). Thus, the response properties giving rise to fractional differentiation of the noise envelope could be detected by the GLM even without driving with long timescale noise modulation.

We then considered how the estimated fractional differentiation order depended on the strength of the SD

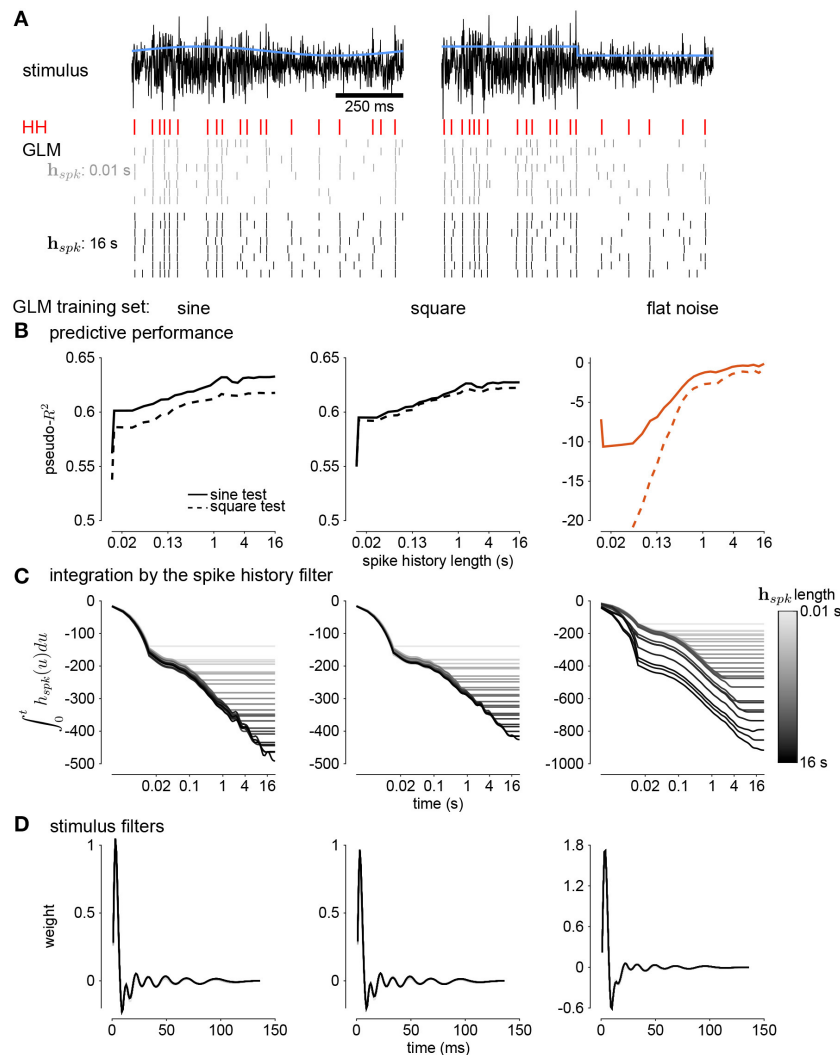


**FIGURE 10 | (A)** Comparing simulations of the HH model to sine wave modulated (left) and square wave modulated (right) noise. The black traces show the stimulus and the blue traces show the standard deviation envelope. The red raster denotes the HH spike response. Several repeated simulations of the GLM are shown for a GLM trained with only a 10ms spike history (gray raster) and a GLM trained with the full 16s spike history (black raster). **(B)** Assessing the model fitness for GLMs fit to sine wave modulated noise (left), square wave noise (middle), and unmodulated noise (right). The pseudo- $R^2$  measured on a withheld training set simulated from the HH model as a function of spike history length. The stimulus was sine (solid lines) or square (dashed lines) modulated noise with a 4s period and a modulation strength of  $\sigma = 2$ . **(C)** The integral over time (i.e., cumulative sums) of each spike history filter. **(D)** The stimulus filters for all GLM fits.

modulation. We found a slightly higher  $\alpha$  for lower stimulus SDs (note that  $\sigma = 2.0$  was used to fit the GLMs) for the gain and timescale estimates (Figures 9G–I). However, the phase lead estimate was fairly stable across SDs.

Next, we quantified how well the GLM predicted the HH responses to new stimuli (Figure 10A). Spike history filters with timescales of several seconds improved the GLM's ability to predict spike trains, and the improvement continued for spike histories of several seconds (Figure 10B). However, training only on unmodulated noise did not result in a good GLM fit despite predicting  $\alpha$  (Figure 10B).

We examined the parameter estimates in the GLM as a function of spike history length. We plotted the integral of

the spike history filter to show how the filter integrates spikes over time. The integrals show long timescales for the GLM fit to either sine- or square- wave noise (Figure 10C). The GLM fit to either type of noise predicted over 60% of the variance in the HH responses to both sine- and square-wave noise. The flat noise GLM also showed long timescales, but the integral changed substantially with changes in the length of spike history. This indicates that the combination of spike-history dependent timescales is not well-constrained in the flat noise condition despite predicting  $\alpha$ , perhaps due to biases present in the data without modulations (Stevenson, 2018). The stimulus filters are short timescale and showed little dependence on spike history length (Figure 10D). Thus, the GLM captured fractional

differentiation in the HH neuron by linearizing the long timescale AHP currents.

## 4. DISCUSSION

Individual neurons can adapt their responses to changes in input statistics. Here, we studied two adaptive computations to changes in the stimulus variance that are captured by biophysically realistic neurons. First, we examined gain scaling of the inputs so that the spike-triggered stimulus distribution was independent of the stimulus variance. The ability of the neuron to gain scale depended on the ratio of the spike-generating potassium and sodium conductances. Second, we considered spiking responses that approximate a fractional derivative of the stimulus standard deviation, which can be produced by a set of AHP currents with different timescales. Although HH neurons can produce these adaptive effects, it is difficult to fit the HH to data.

Our results demonstrate that the GLM provides a tractable statistical framework for modeling adaptation to stimulus variance in single-neurons. The GLM provides an alternative representation of the spiking responses as two linear filters (stimulus and spike history filters) with a fixed spiking non-linearity instead of a multidimensional (and potentially stochastic) dynamical system (Meng et al., 2011, 2014). Importantly, a single GLM could accurately approximate the responses of HH neurons across multiple levels of input variance or across multiple timescales of variance modulation. The GLM accomplished this by linearizing the effect of recent spiking into a non-linear and stochastic spiking mechanism to adjust for the current stimulus statistics, which can act as a measure of the current stimulus context. To reproduce gain scaling, around 150ms of spike history is required, in line with the rapid expression of the gain scaling property with changes in stimulus statistics (Fairhall et al., 2001a; Mease et al., 2013). In the fractional derivative case, the GLM summarized the multiple AHP currents of the HH models as a single linear autoregressive function with multiple timescale effects.

This approach shows that at least part of the spectrum of adaptive behaviors to stimuli with time-varying characteristics can be captured through a single linear spike history feedback. Effective alternative approaches have captured time-varying context with a multiplicity of filters acting on different timescales of the stimulus alone (Kass and Ventura, 2001; McFarland et al., 2013; Qian et al., 2018; Latimer et al., 2019a).

## REFERENCES

- Agüera y Arcas, B., and Fairhall, A. L. (2003). What causes a neuron to spike? *Neural Comput.* 15, 1789–1807. doi: 10.1162/08997660360675044
- Agüera y Arcas, B., Fairhall, A. L., and Bialek, W. (2003). Computation in a single neuron: Hodgkin and huxley revisited. *Neural Comput.* 15, 1715–1749. doi: 10.1162/08997660360675017
- Anastasio, T. J. (1998). Nonuniformity in the linear network model of the oculomotor integrator produces approximately fractional-order dynamics and more realistic neuron behavior. *Biol. Cybernet.* 79, 377–391. doi: 10.1007/s004220050487
- Benjamin, A. S., Fernandes, H. L., Tomlinson, T., Ramkumar, P., VerSteeg, C., Chowdhury, R. H., et al. (2018). Modern machine learning as a

The simulations explored here assumed the input to a cell was an injected current generated from a Gaussian distribution. However, neurons receive input as excitatory and inhibitory conductances, which can be integrated across complex dendritic processes (Ozuysal et al., 2018; Latimer et al., 2019b). Additionally, realistic input statistics may not follow a Gaussian distribution (Heitman et al., 2016; Maheswaranathan et al., 2018). Further work toward understanding the adaptive computations performed by single neurons should consider the inputs the neuron receives within a broader network and should consider non-linear stimulus processing (McFarland et al., 2013; Benjamin et al., 2018).

Neural coding and computations that occur across a wide range of input levels depend heavily on adaptation to the stimulus variance (Wark et al., 2007). The GLM, despite being a simple approximation, can provide a good representation of adaptive computations in biophysically realistic neurons.

## DATA AVAILABILITY STATEMENT

All simulations are publicly available at <https://github.com/latimerk/GainScalingGLM>.

## AUTHOR CONTRIBUTIONS

KL and AF designed the study and wrote the manuscript. KL performed the simulations and statistical analysis. All authors contributed to the article and approved the submitted version.

## FUNDING

This work was supported by the Human Frontiers in Science Program to AF. KL was supported by a Chicago Fellowship.

## ACKNOWLEDGMENTS

We thank Jonathan Pillow and Misha Proskurin for their help in developing this project.

## SUPPLEMENTARY MATERIAL

The Supplementary Material for this article can be found online at: <https://www.frontiersin.org/articles/10.3389/fnsys.2020.00060/full#supplementary-material>

benchmark for fitting neural responses. *Front. Comput. Neurosci.* 12:56. doi: 10.3389/fncom.2018.00056

- Buhry, L., Grassia, F., Giremus, A., Grivel, E., Renaud, S., and Saïghi, S. (2011). Automated parameter estimation of the hodgkin-huxley model using the differential evolution algorithm: application to neuromimetic analog integrated circuits. *Neural Comput.* 23, 2599–2625. doi: 10.1162/NECO\_a\_00170
- Cameron, A. C., and Windmeijer, F. A. (1997). An R-squared measure of goodness of fit for some common nonlinear regression models. *J. Econometr.* 77, 329–342. doi: 10.1016/S0304-4076(96)01818-0
- Csersik, D., Hangos, K. M., and Szederkényi, G. (2012). Identifiability analysis and parameter estimation of a single hodgkin-huxley type voltage dependent ion channel under voltage step measurement conditions. *Neurocomputing* 77, 178–188. doi: 10.1016/j.neucom.2011.09.006

- Fairhall, A. (2014). "Adaptation and natural stimulus statistics," in *The Cognitive Neurosciences, Chapter 26*, eds S. M. Gazzaniga and R. G. Mangun (Cambridge, MA: MIT Press), 283–293.
- Fairhall, A. L., Lewen, G. D., Bialek, W., and de Ruyter van Steveninck, R. R. (2001a). Efficiency and ambiguity in an adaptive neural code. *Nature* 412:787. doi: 10.1038/35090500
- Fairhall, A. L., Lewen, G. D., Bialek, W., and de Ruyter van Steveninck, R. R. (2001b). "Multiple timescales of adaptation in a neural code," in *Advances in Neural Information Processing Systems*, eds T. K. Leen, T. G. Dietterich, and V. Tresp (Cambridge MA: MIT Press), 124–130.
- Heitman, A., Brackbill, N., Greschner, M., Sher, A., Litke, A. M., and Chichilnisky, E. (2016). Testing pseudo-linear models of responses to natural scenes in primate retina. *bioRxiv* 045336. doi: 10.1101/045336
- Kass, R. E., and Ventura, V. (2001). A spike-train probability model. *Neural Comput.* 13, 1713–1720. doi: 10.1162/08997660152469314
- Lankarany, M., Zhu, W.-P., and Swamy, M. (2014). Joint estimation of states and parameters of Hodgkin-Huxley neuronal model using Kalman filtering. *Neurocomputing* 136, 289–299. doi: 10.1016/j.neucom.2014.01.003
- Latimer, K. W., Barbera, D., Sokoletsky, M., Awad, B., Katz, Y., Nelken, I., et al. (2019a). Multiple timescales account for adaptive responses across sensory cortices. *J. Neurosci.* 39, 10019–10033. doi: 10.1523/JNEUROSCI.1642-19.2019
- Latimer, K. W., Rieke, F., and Pillow, J. W. (2019b). Inferring synaptic inputs from spikes with a conductance-based neural encoding model. *eLife* 8:e47012. doi: 10.7554/eLife.47012
- Lundstrom, B. N., Higgs, M. H., Spain, W. J., and Fairhall, A. L. (2008). Fractional differentiation by neocortical pyramidal neurons. *Nat. Neurosci.* 11:1335. doi: 10.1038/nn.2212
- Maheswaranathan, N., Kastner, D. B., Baccus, S. A., and Ganguli, S. (2018). Inferring hidden structure in multilayered neural circuits. *PLoS Comput. Biol.* 14:e1006291. doi: 10.1371/journal.pcbi.1006291
- Mainen, Z. F., Joerges, J., Huguenard, J. R., and Sejnowski, T. J. (1995). A model of spike initiation in neocortical pyramidal neurons. *Neuron* 15, 1427–1439. doi: 10.1016/0896-6273(95)90020-9
- McCullagh, P., and Nelder, J. A. (1989). *Generalized Linear Models, Volume 37 of Monographs on Statistics and Applied Probability, 2nd Edn.* London: Chapman & Hall; CRC.
- McFarland, J. M., Cui, Y., and Butts, D. A. (2013). Inferring nonlinear neuronal computation based on physiologically plausible inputs. *PLoS Comput. Biol.* 9:e1003143. doi: 10.1371/journal.pcbi.1003143
- Mease, R. A., Famulare, M., Gjorgjieva, J., Moody, W. J., and Fairhall, A. L. (2013). Emergence of adaptive computation by single neurons in the developing cortex. *J. Neurosci.* 33, 12154–12170. doi: 10.1523/JNEUROSCI.3263-12.2013
- Mease, R. A., Lee, S., Moritz, A. T., Powers, R. K., Binder, M. D., and Fairhall, A. L. (2014). Context-dependent coding in single neurons. *J. Comput. Neurosci.* 37, 459–480. doi: 10.1007/s10827-014-0513-9
- Meng, L., Kramer, M. A., and Eden, U. T. (2011). A sequential monte carlo approach to estimate biophysical neural models from spikes. *J. Neural Eng.* 8:065006. doi: 10.1088/1741-2560/8/6/065006
- Meng, L., Kramer, M. A., Middleton, S. J., Whittington, M. A., and Eden, U. T. (2014). A unified approach to linking experimental, statistical and computational analysis of spike train data. *PLoS ONE* 9:e85269. doi: 10.1371/journal.pone.0085269
- Miller, K. D., and Troyer, T. W. (2002). Neural noise can explain expansive, power-law nonlinearities in neural response functions. *J. Neurophysiol.* 87, 653–659. doi: 10.1152/jn.00425.2001
- Murphy, B. K., and Miller, K. D. (2003). Multiplicative gain changes are induced by excitation or inhibition alone. *J. Neurosci.* 23, 10040–10051. doi: 10.1523/JNEUROSCI.23-31-10040.2003
- Oldham, K., and Spanier, J. (1974). *The Fractional Calculus Theory and Applications of Differentiation and Integration to Arbitrary Order*, Vol. 111. New York, NY: Elsevier.
- Ozysal, Y., Kastner, D. B., and Baccus, S. A. (2018). Adaptive feature detection from differential processing in parallel retinal pathways. *PLoS Comput. Biol.* 14:e1006560. doi: 10.1371/journal.pcbi.1006560
- Pillow, J. W., Shlens, J., Paninski, L., Sher, A., Litke, A. M., Chichilnisky, E., et al. (2008). Spatio-temporal correlations and visual signalling in a complete neuronal population. *Nature* 454:995. doi: 10.1038/nature07140
- Pozzorini, C., Naud, R., Mensi, S., and Gerstner, W. (2013). Temporal whitening by power-law adaptation in neocortical neurons. *Nat. Neurosci.* 16, 942–948. doi: 10.1038/nn.3431
- Qian, C., Sun, X., Zhang, S., Xing, D., Li, H., Zheng, X., et al. (2018). Nonlinear modeling of neural interaction for spike prediction using the staged point-process model. *Neural Comput.* 30, 3189–3226. doi: 10.1162/neco\_a\_01137
- Rieke, F., Warland, D., de Ruyter van Steveninck, R., and Bialek, W. (1999). *Spikes: Exploring the Neural Code*. Cambridge, MA: MIT Press.
- Rubner, Y., Tomasi, C., and Guibas, L. J. (1998). "A metric for distributions with applications to image databases," in *Sixth International Conference on Computer Vision (IEEE Cat. No. 98CH36271)* (Mumbai: IEEE), 59–66. doi: 10.1109/ICCV.1998.710701
- Stevenson, I. H. (2018). Omitted variable bias in GLMs of neural spiking activity. *Neural Comput.* 30, 3227–3258. doi: 10.1162/neco\_a\_01138
- Truccolo, W., Eden, U. T., Fellows, M. R., Donoghue, J. P., and Brown, E. N. (2005). A point process framework for relating neural spiking activity to spiking history, neural ensemble, and extrinsic covariate effects. *J. Neurophysiol.* 93, 1074–1089. doi: 10.1152/jn.00697.2004
- Vavoulis, D. V., Straub, V. A., Aston, J. A., and Feng, J. (2012). A self-organizing state-space-model approach for parameter estimation in Hodgkin-Huxley-type models of single neurons. *PLoS Comput. Biol.* 8:e1002401. doi: 10.1371/journal.pcbi.1002401
- Wark, B., Lundstrom, B. N., and Fairhall, A. (2007). Sensory adaptation. *Curr. Opin. Neurobiol.* 17, 423–429. doi: 10.1016/j.conb.2007.07.001
- Weber, A. I., and Fairhall, A. L. (2019). The role of adaptation in neural coding. *Curr. Opin. Neurobiol.* 58, 135–140. doi: 10.1016/j.conb.2019.09.013
- Weber, A. I., and Pillow, J. W. (2017). Capturing the dynamical repertoire of single neurons with generalized linear models. *Neural Comput.* 29, 3260–3289. doi: 10.1162/neco\_a\_01021

**Conflict of Interest:** The authors declare that the research was conducted in the absence of any commercial or financial relationships that could be construed as a potential conflict of interest.

Copyright © 2020 Latimer and Fairhall. This is an open-access article distributed under the terms of the Creative Commons Attribution License (CC BY). The use, distribution or reproduction in other forums is permitted, provided the original author(s) and the copyright owner(s) are credited and that the original publication in this journal is cited, in accordance with accepted academic practice. No use, distribution or reproduction is permitted which does not comply with these terms.



# Cross-Whisker Adaptation of Neurons in Layer 2/3 of the Rat Barrel Cortex

Yonatan Katz\* and Ilan Lampl

Department of Neurobiology, The Weizmann Institute of Science, Rehovot, Israel

Neurons in the barrel cortex respond preferentially to stimulation of one principal whisker and weakly to several adjacent whiskers. Such integration exists already in layer 4, the pivotal recipient layer of thalamic inputs. Previous studies show that cortical neurons gradually adapt to repeated whisker stimulations and that layer 4 neurons exhibit whisker specific adaptation and no apparent interactions with other whiskers. This study aimed to study the specificity of adaptation of layer 2/3 cortical cells. Towards this aim, we compared the synaptic response of neurons to either repetitive stimulation of one of two responsive whiskers or when repetitive stimulation of the two whiskers was interleaved. We found that in most layer 2/3 cells adaptation is whisker-specific. These findings indicate that despite the multi-whisker receptive fields in the cortex, the adaptation process for each whisker-pathway is mostly independent of other whiskers. A mechanism allowing high responsiveness in complex environments.

## OPEN ACCESS

### Edited by:

Mehdi Adibi,  
University of Padua, Italy

### Reviewed by:

Robert N. S. Sachdev,  
Humboldt University of Berlin,  
Germany  
Arash Fassihizakeri,  
University of California, San Diego,  
United States

### \*Correspondence:

Yonatan Katz  
yonatan.katz@weizmann.ac.il

**Received:** 27 December 2020

**Accepted:** 06 April 2021

**Published:** 28 April 2021

### Citation:

Katz Y and Lampl I (2021)  
Cross-Whisker Adaptation of Neurons  
in Layer 2/3 of the Rat Barrel Cortex.  
*Front. Syst. Neurosci.* 15:646563.  
doi: 10.3389/fnsys.2021.646563

**Keywords:** barrel cortex, whisker stimulation, layer 2/3 cortex, receptive fields, integration, intracellular, *in vivo*

## INTRODUCTION

The organization of receptive fields in layer 2/3 of the barrel cortex has been studied in rodents mainly using passive stimulation of individual whiskers. In the barrel cortex neurons typically respond primarily to stimulation of a single whisker and somewhat less to neighboring whiskers (Simons, 1985; Simons and Carvell, 1989; Armstrong-James et al., 1992; Bruno and Simons, 2002). Layer 4 cells typically have wider receptive fields than layer 2/3 cells (Bureau et al., 2006; Viaene et al., 2011). Vertically directed axons project excitation from layer 4 cells into layer 2/3 cells of the same column (Lübke et al., 2000). Hence the response in layer 2/3 cells to whisker stimulation is delayed by 2–3 ms relative to the response in layer 4 cells (Armstrong-James et al., 1992). This additional delay supports the notion that layer 2/3 are innervated mostly by cortical cells. However, their response to multiple whiskers may reflect inputs from layer 4 or neighboring columns (Simons, 1985).

Assuming that the synthesis of the wider receptive fields of layer 2/3 emerges in the cortex, the adjacent whisker response of these cells can reflect inputs from the same column via multi-whisker layer 4 cells and/or from adjacent barrels through horizontal connections. Some proposed that the whisker-trigeminal system is a labeled-line pathway, where subcortical structures relay to layer 4 cortex only principal whisker (PW) inputs and adjacent whisker (AW) responses are therefore synthesized by intracortical interactions (Armstrong-James and Callahan, 1991; Armstrong-James et al., 1991; Fox et al., 2003). Others found that AW responses in layer 4 are independent of

intracortical interactions, reflecting direct thalamic inputs that relay both PW and AW inputs (Simons and Carvell, 1989; Goldreich et al., 1999; Urbain and Deschênes, 2007). For layer 2/3 cells, most studies agreed that suprathreshold excitation spreads horizontally within layer 2/3 into the adjacent cortical columns and subsequently across the entire barrel field. *In vivo* whole-cell recordings suggest that most layer 2/3 pyramidal cells respond with large EPSPs upon deflection of a single whisker and have subthreshold receptive fields broader than those of layer 4 spiny neurons (Brecht and Sakmann, 2002; Brecht et al., 2003), suggesting intracortical integration. Based on this hypothesis, the adjacent whisker response is independent of layer 4 activity of the principal column. In other words, if adjacent whisker response in layer 2/3 emerges from a neighboring barrel, applying repetitive stimulation to the PW, which leads to adaptation, should not affect the cell's response to stimulation of an adjacent whisker. On the other hand, if the multi-whisker receptive field is inherited from layer 4 cells, a cross-adaptation effect should be observed, leading to attenuation of the response to AW stimulation following adaptive stimulation of the PW. Considering the latter possibility, cross-whisker adaptation might not be always observed: when a test AW stimulation is applied after several stimuli were applied to the PW, due to their low firing response, the synapses connecting layer 4 to layer 2/3 may recover from the adaptation process, leading to a large response to the test stimulation. To overcome this issue we examine the adaptive interactions using an interleaved stimulation of the PW and AW. We assume that such interleaved stimulation leads to a high level of activity in layer 4, maintaining synapses common to the two stimulated whiskers at a depressed state. Such stimulation therefore allowed us to track the interactions over time as adaptation progresses. We hypothesized that the convergence of different whiskers' pathways at the level of layer 4 should result in a stronger interaction during adaptation compared to the expected interactions when a synthesis of the receptive fields occurs at the level of layer 2/3.

We intracellularly recorded the response of layer 2/3 neurons to interleaved whisker stimulation of the PW and AW and evaluated the degree of interactions between them due to adaptation. We found no interactions for most layer 2/3 cells. Significant interactions were found only in about one-quarter of the tested whiskers, where profound adaptation induced by repetitive stimulation of one whisker caused a significant reduction in the response of a second whisker. No physiological parameters such as latency or response amplitude were related to the level of interactions.

## MATERIALS AND METHODS

### Ethics Statement

All surgical and experimental procedures were performed in accordance with the regulations of The Weizmann Institute Animal Care and Use Committee (IACUC App.Num. 00470109-1).

## General

Adult female Sprague–Dawley rats ( $n = 18$ ) were anesthetized with halothane (0.5–1.0%), tracheotomized, and ventilated. Heart rate, temperature, and expired  $\text{CO}_2$  were monitored continuously. Intracellular recordings were made from barrel cortex layer 2/3 neurons using glass micropipettes (5–9 M $\Omega$ ) filled with an intracellular solution containing in mM: K-gluconate, 136; KCl, 10; NaCl, 5; HEPES, 10; MgATP, 1; NaGTP, 0.3; phosphocreatine, 10; mOsm, 310. For each recording, the principal whisker (PW) and the adjacent whisker (AW) having the highest amplitude were mechanically deflected in the PW preferred direction using a piezoelectric stimulator (for details see Katz et al., 2006).

In these experiments, intracellular whole-cell patch recordings were used and membrane potential was not compensated for the junction potential ( $\sim 12$  mV). Signals were amplified using Axoclamp-2B (Molecular Devices, Palo Alto, CA, United States) and low passed at 4 kHz before being digitized at 10 kHz.

## Stimulation Protocol

For control stimulation, a 5/10 Hz train of 10/20 stimuli was used for each of the two whiskers. To estimate the interaction between whiskers, 10 Hz interleaved-stimulation was presented where each whisker was actually stimulated at 5 Hz (see **Figure 1**). These responses were compared to either 5 Hz or 10 Hz stimulation trains delivered to each whisker alone. During each trial, a 3 s inter-train interval was used.

## Response Quantification and Adaptation Index

We have quantified a number of response properties such as the amplitude, latency, rise-time, and adaptation index. The response amplitude was defined as the maximal amplitude relative to baseline within a 50 ms window following the stimulation. The latency to response was defined as the time from stimulus onset to 10% deviation of the averaged membrane potential from baseline (PSP onset) was defined as the latency to the response. The response rise-time was quantified as the time measured from 10% to 90% of the response amplitude.

The adaptation index (AI) was quantified according to the following equation:

$$AI = 1 - \frac{\text{mean}(R_{(n-1)} : R_n)}{R_1}$$

Explicitly, this is one minus the ratio between the mean of the last two responses [ $R_{(n-1)}$  and  $R_n$ ] and the first responses ( $R_1$ ) was calculated. The number of stimulations during 5 and 10 Hz was 10 and 20, respectively.

## Calculation of the Interactions Between Whiskers and Adapted-State Response

Here we define the cross-whisker adaptation under interleaved stimulation. When a response of a cell to the deflection of one whisker is affected by the preceding whisker deflection of another whisker, it is defined as an interaction. The interaction can either

be facilitatory or inhibitory. To measure the interaction for a given stimulation ( $i$ ), the given formula was used:

$$\text{Interaction}(i) = 1 - \frac{R_{\text{interleaved}}(i) - R_{10\text{Hz}}(i * 2)}{R_{5\text{Hz}}(i) - R_{10\text{Hz}}(i * 2)}$$

$R$  = Averaged EPSP

where  $R_{\text{interleaved}}(i)$  denotes the  $i$ th response of the cell to the stimulated whisker during the interleaved stimulation of the relevant whisker.  $R_{10\text{Hz}}(i * 2)$  denotes the response of the cell during 10 Hz whisker stimulation; because the stimulation frequency is double that during 5 Hz stimulation, the response to the ( $i * 2$ ) stimulation is measured.  $R_{5\text{Hz}}$  denotes the control response during 5 Hz stimulation. The change in response from 5 Hz to 10 Hz provides a reference for the interactions.

An index of 1 will be obtained for full interaction (the amount of adaptation for the interleaved stimulation is identical to that expected from a single whisker stimulation) and 0 if the response was not affected by interleaving it with stimulating the other whisker. If the response to 10 Hz stimulation is weaker than the response to 5 Hz stimulation and the interleaved response has an intermediate value in between, then the interaction value can vary between 0 when there is no interaction to 1 for a strong interaction. Thus, response to whisker stimulation which was significantly suppressed during interleaved stimulation was termed “interacting.” According to the level of interactions of cells for responses to stimulation of the two whiskers, cells were divided into three groups: 1. Interacting, 2. Non-interacting, 3. Unidirectional-interacting when only one whisker affected the response of the other one and not vice versa.

The adapted-state response was defined as the mean response of the last two deflections in 5 Hz or 10 Hz train stimuli.

## RESULTS

### Recorded Population

Intracellular whole-cell patch recordings were performed in layer 2/3 of the barrel cortex of anesthetized rats. Overall, 28 cells were recorded in 18 animals. For each cell, the principal whisker (PW) and most responsive adjacent whisker (AW) were stimulated. The average recording depth was  $411 \pm 117 \mu\text{m}$  and the mean latency whisker responses were  $7.7 \pm 0.3$  and  $8.7 \pm 0.3$  ms (for PW and AW), corresponding to layers 2/3 in the rat (Katz et al., 2006).

### The Response of Layer 2/3 Cells to 5 Hz, 10 Hz, and Interleaved Stimulation of the Principal and Adjacent Whiskers

Feed-forward inputs to layer 2/3 ascend mainly from layer 4 (Fanselow et al., 2001; Helmstaedter et al., 2009). If layer 4 cells integrate inputs from different whiskers and if adaptation results from local mechanisms such as short-term synaptic plasticity, strong interactions are expected in response to the interleaved stimulation. However, our former results from layer 2/3 recordings showed only weak, but significant, interactions between the inputs from two different whiskers (Katz et al., 2006).

In this former study, test stimulation to a whisker was delivered following repetitive stimulation of its neighboring whisker. We reasoned that due to the low firing rate of layer 4 cells, in particular toward the end of the stimulation train, the ascending synapses to layer 2/3, common to the two whiskers, will recover from depression and thus restore the ability to respond upon subsequent stimulation of the neighboring whisker. Here we used an interleaved stimulation protocol to keep the ascending pathway at a depressed state and thus allow evaluation of the interactions while stimulating the two whiskers. Hence, this form of stimulation allows testing the interactions between whiskers pathways during the adaptation process, well before the response is fully adapted. For each cell, we tested the adaptation to PW or AW stimulation at two frequencies. An example cell is shown in **Figure 1**. Neuronal responses of this cell to 5 Hz stimulation were weakly adapted ( $AI = 0.22 \pm 0.03$ , **Figures 1A,E**). Adaptation was more pronounced at 10 Hz stimulation ( $p < 0.005$ ,  $AI = 0.47 \pm 0.02$ , **Figures 1B,F**). To test for interactions, we used interleaved stimulation. Each of the two whiskers was stimulated at 5 Hz with half a cycle shift between the trains resulting in effective 10 Hz stimulation input at the recorded cell (**Figures 1C,G**).

Interleaved stimulation in this example only weakly affected the adaptation pattern that is expected from single whisker stimulation at 5 Hz. This was observed by comparing the responses to stimulation of each whisker in the interleaved average response to those evoked by the 5 Hz stimulation (compare traces in **Figures 1A,E,C,G**, the pattern of stimulation is depicted below the averaged membrane potential traces). The amplitude of the responses during interleaved stimulation closely matched the response to 5 Hz stimulation, indicating that the presence of stimulation of the neighboring whisker did not affect the time course and magnitude of the adaptation when considering stimulation of each whisker alone. The average peak response amplitudes during each stimulation protocol were measured (**Figures 1D,H**), and used for population analysis. Since the number of whisker deflections during 10 Hz stimulation was double that during 5 Hz, only response amplitudes for odd deflections are presented.

The population peak response amplitudes to 5 Hz (**Figure 2A** blue line), 10 Hz (**Figure 2A**, green line), and the interleaved stimuli (**Figure 2A**, cyan line) were averaged across the population ( $n = 56$  whiskers, 28 cells). The responses to 10 Hz stimulation were reduced by 50% and were significantly smaller than the responses to 5 Hz (27% reduction) or interleaved stimulations (36% reduction), (rank-sum  $p < 0.05$ ). Hence, on average the responses to the two whiskers interacted, but the effect was not significant and much smaller than from the expected full interaction.

If inputs evoked by stimulation of one whisker undergo adaptation independently of those evoked by the other whisker, stimulation of a second whisker will not affect its response as previously found in layer 4 cells (Katz et al., 2006). In that case, one would expect that the responses during the interleaved stimulation will be equal to the responses during 5 Hz stimulation, having no interactions. On the other hand, if inputs from both whiskers ascend along the same pathway

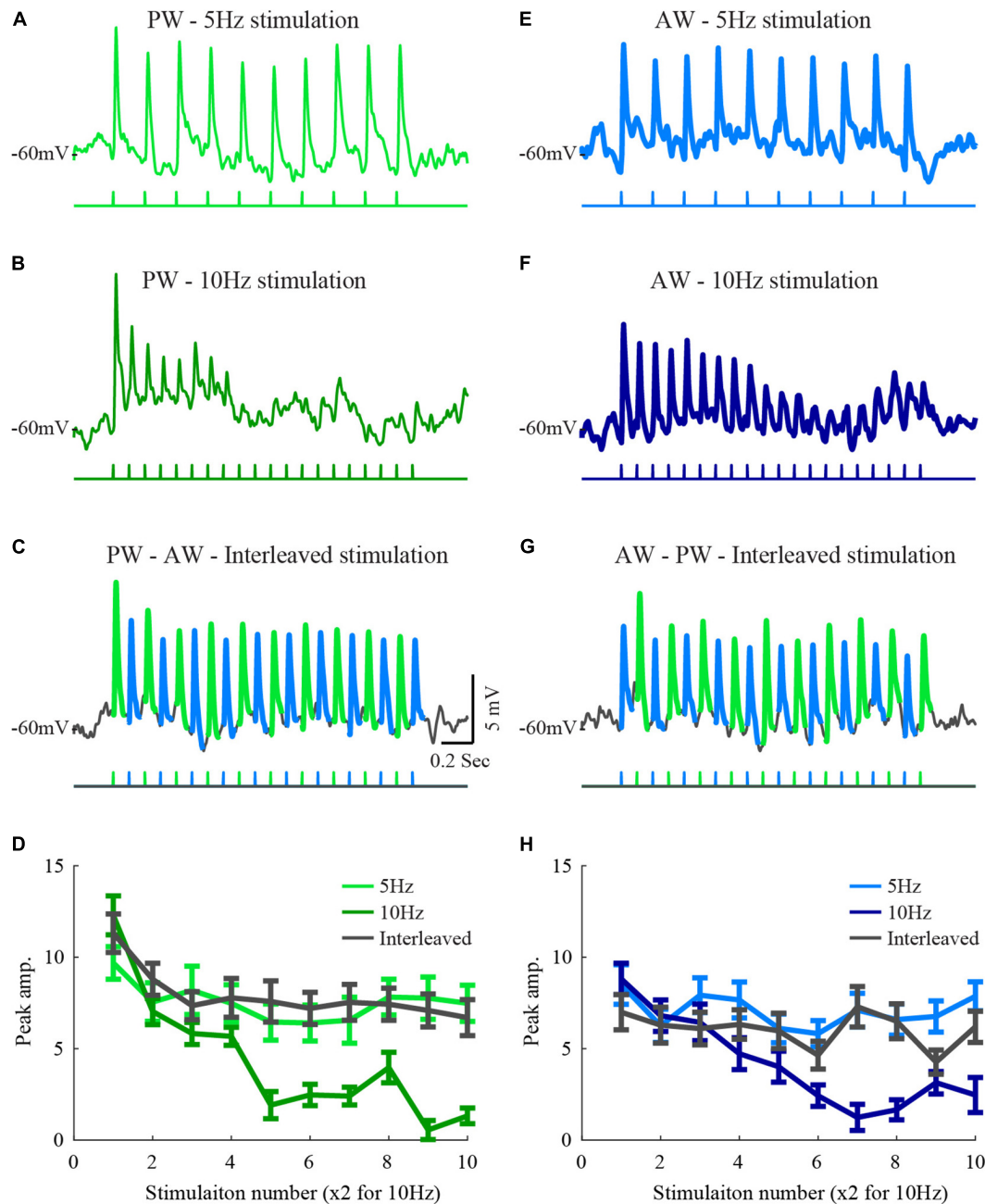
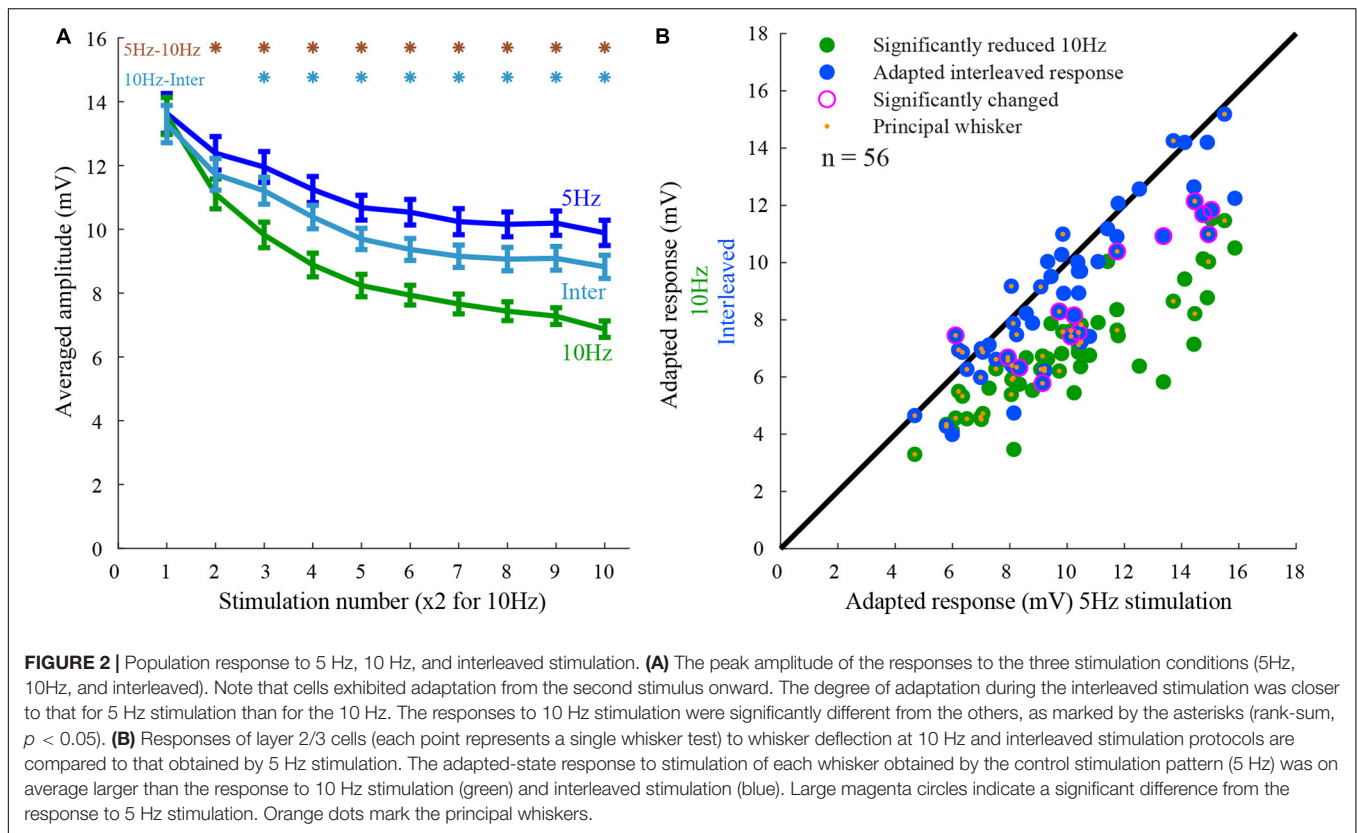


**FIGURE 1 |** Responses of a layer 2/3 cell to stimulation of two whiskers during interleaved stimulation. **(A)** The average response of a layer 2/3 cell to 5 Hz stimulation of the principal whisker (stimulation pattern is depicted below the trace). **(B)** The average response of the same cell to 10 Hz stimulation of the PW principal whisker. **(C)** The average response to stimulation of the principal whisker and to the adjacent whisker under interleaved stimulation (the trace was segmented by colors to depict the response to the two stimulated whiskers). **(D)** The average peak amplitudes of the three stimulation patterns in **(A–C)** are depicted in light-blue for the 5 Hz stimulation, blue for the 10 Hz, and in dark gray for the response to the principal whisker during the interleaved stimulation. **(E–H)** Same conventions as in **(A–D)** for responses to the adjacent whisker. The scales are similar for all plots.

and undergo adaptation after the two pathways converged, the interleaved response will be similar to the response during 10 Hz stimulation, exhibiting strong interactions. We evaluated the interactions during adapted-state responses (see section “Materials and Methods”). Surprisingly, on average, cross-whisker interactions during adapted-state responses were not

significantly different from the average control response to 5 Hz stimulation (**Figure 2A**). The interleaved responses were significantly different in only 14 out of 56 stimulated whiskers (rank-sum  $p < 0.05$ , 28 cells). All but one of these responses were significantly smaller than the control responses (**Figure 2B**, outer purple circles).



For whisker-inputs exhibiting significant interacting responses ( $n = 14$ ), synaptic inputs might have different properties compared to those that exhibit no interactions ( $n = 42$ ). For example, two interacting whisker-inputs might have similar synaptic response properties, suggesting that they share the same pathway and thus undergo adaptation after the point of convergence. Alternatively, the affected input might evoke a smaller response due to the recruitment of a subpopulation of afferents evoked by stimulation of the other input. In this case, such a difference will lead to an asymmetrical cross-whisker adaptation effect. Thus, various properties such as the amplitude, rise-time, and latency of interacting versus non-interacting inputs were measured (Figure 3). The response amplitudes of interacting whisker-inputs were not significantly different from that of non-interacting whisker-inputs (rank-sum,  $p > 0.05$ ), even though during train stimulation only the responses of non-interacting whisker-inputs were significantly reduced (Figure 3A, rank-sum,  $p < 0.005$ ).

The rise time of both groups was not significantly different (except for the sixth stimulus). Still, during repeated stimulation, non-interacting inputs had a significant increase in the rise time (Figure 3B). Another essential property of the responses is latency. If the input of either group arrives via different pathways, then their latency might be different. However, the average latency for both groups' responses was similar ( $10.7 \pm 0.8$  and  $9.6 \pm 0.3$  ms, respectively, rank-sum,  $p > 0.05$ ).

The division into groups causes information loss (Felsenstein and Pötzelberger, 1998; Taylor and Yu, 2002;

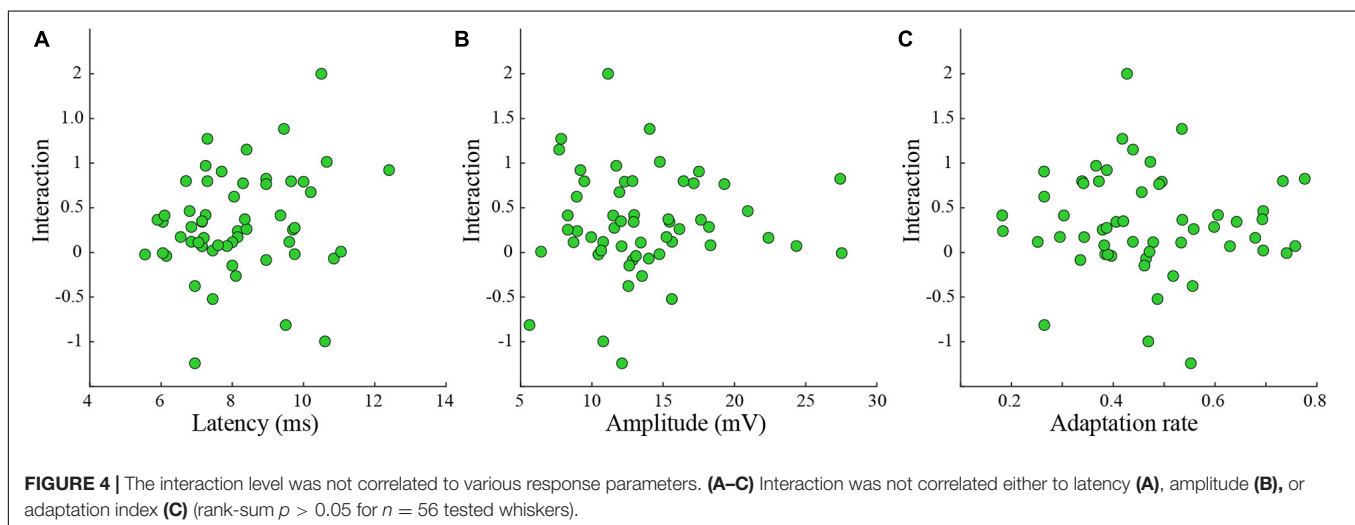
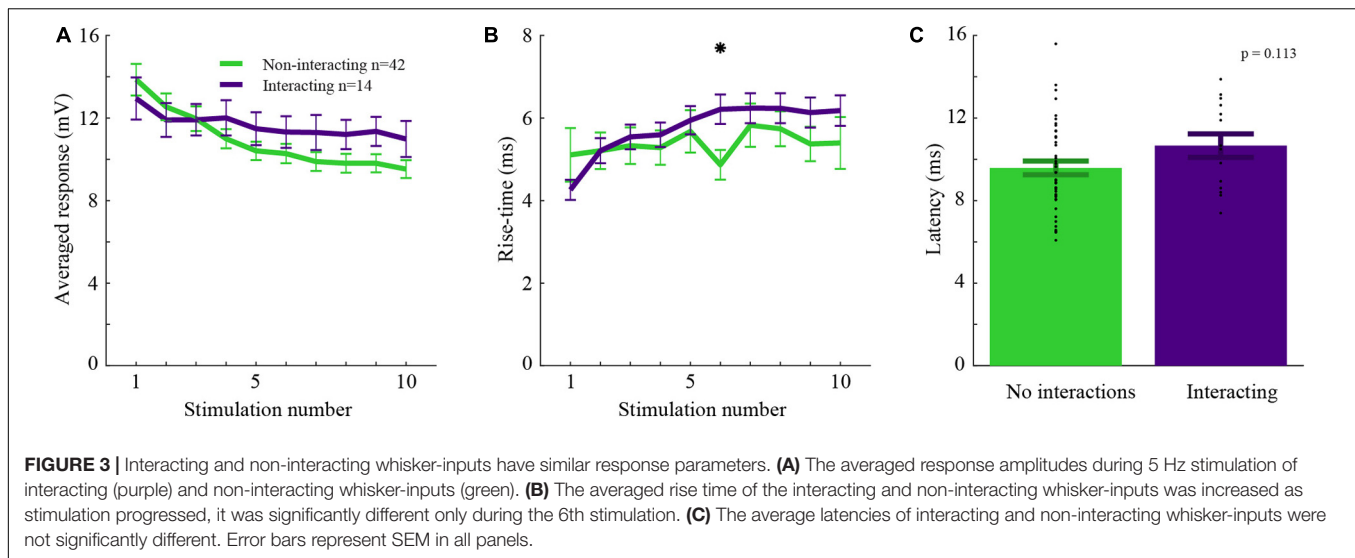
Altman and Royston, 2006; Bennette and Vickers, 2012). Hence the statistical power to detect a relationship between the variable (i.e., latency, amplitude, and adaptation rate) and the interaction is reduced. Thus, we tested if the interaction level was related to the latency, the amplitude, or the adaptation rate of the response (Figure 4). Again, we found that the interaction was not correlated to any of these parameters (Figures 4A–C).

In an attempt to understand the interactions on a single cell level, cells with interactions were divided into two groups by the type of the input-interactions. Cells in which the responses were reciprocally affected (Figure 5, green dots) and cells in which interactions were unidirectional, namely where only one whisker-input was affected (green encircled by purple). Since amplitude and latency might be related to the level of interactions, the ratios of these properties were calculated within the groups. Neither the amplitudes nor the latencies were different between the groups (rank-sum  $p > 0.05$ ).

Specifically, in unidirectional cells (Figures 5A,B green dots encircled by purple), the response amplitude and latency of the non-interacting responses (abscissa) were similar to those of their paired responses (rank-sum,  $p > 0.05$ , in both properties).

To evaluate whether the level of interactions depends on the amplitude of the response, the level of input interaction between each pair was reciprocally quantified. The level of interaction was found not to be dependent on the response amplitude ( $0.32 \pm 0.4$ ,  $p > 0.5$ ).

To further check if the level of the interaction is related to the identity of the stimulated whisker (PW/AW), we compared



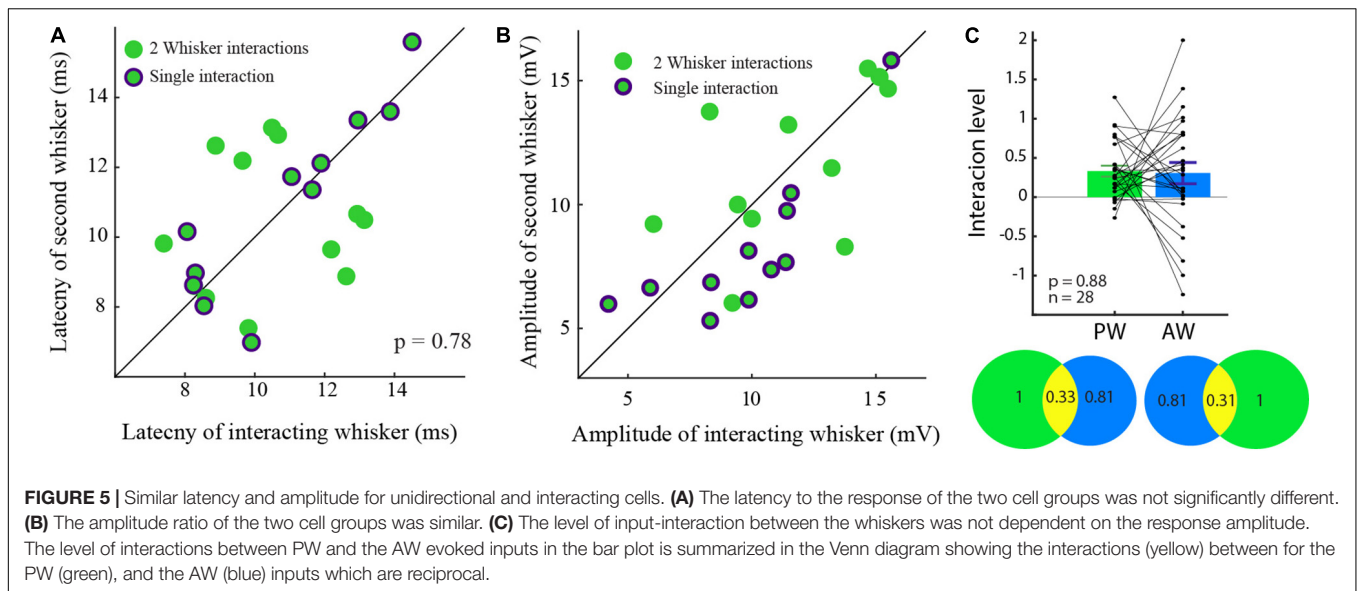
the level of interaction between the inputs evoked by stimulation of the PW and the AW. We found that the interactions of the PWs and the AWs inputs were similar and reciprocal (**Figure 5C**; rank-sum  $p > 0.5$ ). On the Venn diagram, one can see that stimulation of the PW reduced the AW whisker responses by 33% on average (**Figure 5C**, bottom left circles) and stimulation of the AW reduced the response to stimulation of the PW by 31% (right) on average.

## DISCUSSION

We evaluated the synaptic interactions between inputs arriving from the principal and the adjacent whisker in layer 2/3 cortical cells of anesthetized rats. Interleaved stimulation interactions were assessed according to the expected interactions from the adaptation of the responses to 5 and 10 Hz stimulation of each whisker alone. If the response to interleaved stimulation resembles the one that is expected from 5 Hz, no interactions are

observed, whereas if it is similar to that obtained under 10 Hz, the two adaptation processes strongly interact. We found that in  $\sim 75\%$  of the tested whiskers, evoked synaptic inputs were not affected by the stimulation of a neighboring whisker, indicating whisker-specific adaptation.

Inputs that were affected had no specific property (such as latency to response, amplitude, or adaptation level) that can predict the existence of the interactions (although some tendency for a longer response latency was found for the interacting, affected whiskers as shown in **Figure 3C**). The results suggest that the adaptation to whisker stimulation in layer 2/3 cortical cells is primarily independent, further strengthening our previous study (Katz et al., 2006). Yet, the functional role of whisker-specific adaptation in the detection and discriminability of sensory stimuli is unclear. We suggest that during natural whisking behavior, this specificity enhances both aspects of perception by routing sensory signals independently to a different population of neurons, without being affected by the recent history of stimulation of neighboring whiskers.



The implications for synthesis of receptive fields in layer 4 are less clear. Still, our findings strongly support the notion that the multi-whisker receptive fields of layer 2/3 cells emerge due to integration at the cortical level, either by integration of independent ascending inputs from layer 4 cells or integration of inputs from layer 2/3 cells of neighboring barrels. Supposing that multi-whisker receptive fields of layer 2/3 cells are inherited from layer 4 cells, we strongly suggest that at the stimulation rate we used in our study (i.e., 10 Hz), no additional adapting mechanisms act in the layer 4 to layer 2/3 pathway. Whether or not adaptation of cortical cells to other types of mechanical stimulation (Lottem and Azouz, 2008; Maravall et al., 2013; Sachidhanandam et al., 2013) exhibits a similar degree of specificity is not clear and remains to be studied.

Nevertheless, our results do not support early convergence of pathways at the thalamic level (Jubran et al., 2016). In such a case, we would expect that a significant portion of whiskers would exhibit strong interactions. The finding that there are asymmetrical interactions, which the depression of the synaptic input cannot explain, raises the possibility that inhibition might participate in the interactions. Still, the validity of our results in awake animals needs to be further studied.

## Possible Mechanisms for Interactions

At least three central mechanisms can be responsible for the interactions between inputs arriving from different whiskers; intrinsic adaptation (Carandini and Ferster, 1997), short-term synaptic depression (Gabernet et al., 2005; Kheradpezhrouh et al., 2017), and cross-whisker inhibition (Brumberg et al., 1996; Moore and Nelson, 1998).

Suppose synaptic depression would explain the adaptation of cortical cells to whisker stimulation. In that case, it is reasonable to expect a reduction in response to both whiskers during interleaved stimulation as both inputs from the whiskers ascend through the same pathway. This indeed was the case in ~20% of

interacting cells (6/28 cells). On the other hand, unidirectional interactions in which only one whisker suppresses the other can be attributed to suppression between the pathways. Layer 4 cells efficiently recruit interneurons in layer 2/3 (Armstrong-James et al., 1992; Feldmeyer et al., 2002; Shepherd and Svoboda, 2005; Helmstaedter et al., 2008). Thus, during unidirectional interactions, the principal whisker's response can activate layer 2/3 interneurons that later shunt the adjacent whisker's response. However, to obtain a conclusive decision about the involvement of inhibition in unidirectional interaction, two properties for such inhibition are required. First, the typical time course of IPSCs in layer 2/3 terminates approximately at the same time as the interleaved stimulation ISI (100 ms) (Ling and Benardo, 1995; Heiss et al., 2008) allowing the shunting of following responses. Second, stimulation of the adjacent whisker is not supposed to recruit a significant inhibition since it evokes a relatively weak and slow response. This is feasible if the response of the adjacent whisker arrives from the adjacent barrel, or from the same subset of synapses but is weaker and slower and recruits fewer interneurons (Kapfer et al., 2007). Our data do not meet this condition since the amplitudes or latencies to responses of the affecting whiskers in unidirectional cells are not stronger than those of the affected whiskers (Figure 5B). Another pathway for inhibition can be mediated via the horizontal connections of the neurogliaform cells. During whisker movements, Martinotti cells reduce their tonic inhibition (Gentet et al., 2012), resulting in increased inhibition of neurogliaform cells via horizontal connections (Tamás et al., 2003; Gentet, 2012) that can mediate slow inter-barrel inhibition.

Yet, the inability to predict the interaction level between inputs from different whiskers arriving at the same cell by their amplitude and latency suggests no canonical circuit in layer 2/3 in which the interactions between inputs from two whiskers can be deduced by their response properties. It is possible that future experiments in which recordings will

be targeted to specific types of cortical cells using various CRE-lines will reveal more structure across the population in the adaptation pattern and its specificity to whisker identity.

## Possible Implications for Synthesis of Multi-Whisker Receptive Fields in Layer 2/3

During interleaved stimulation, responses were significantly reduced only in 25% (14/56) of inputs evoked by stimulation of the tested whiskers. The reduction in the response of layer 2/3 neurons suggests that some afferents are common to both inputs. This is in favor of the 'inherited receptive field hypothesis' which claims that barrel cortex neurons inherit their RF from their thalamic afferents (Goldreich et al., 1999; Lübke et al., 2000; Kwegyir-Afful et al., 2005), in this case from layer 4 cells. On the other hand, in 75% of the inputs, the responses did not show any interactions, which is evidence in favor of the 'cortical integration hypothesis' which claims that inputs from adjacent whiskers are transferred via cortico-cortical interactions (Armstrong-James et al., 1991; Fox et al., 2003).

There are (at least) two parallel cortical pathways for the ascending inputs from the adjacent whiskers. One pathway enters layer 2/3 from the adjacent barrel whereas the second arrives from multi-whisker layer 4 barrel cells and thus shares the same synapse with the principal whisker. If the interactions result from depletion of synaptic resources (i.e., synaptic depression Lampl and Katz, 2017), then interactions between inputs evoked by stimulation of two whiskers should depend on the response amplitudes. For example, a very weak response when stimulating one whisker will not affect the response evoked by stimulating the second whisker since it almost does not use mutual resources. On the other hand, input from whiskers with similar amplitudes and latencies probably arriving from the same pathway are expected to show strong interactions. Therefore, it was suggested that the amplitude ratio of responses when stimulating two whiskers and the latency differences can predict the significance of the interactions. On a single cell level, we found that these two predictors were not related to the measured interactions (Figure 4). One possible reason for the indistinguishable results might be the small sampled population and lack of cellular identity (barrel- or septa-related).

Another option is the lack of consistency in the exact recording position relative to the center of each barrel column. Few studies point toward an internal barrel map in which the adjacent-whisker would have a broader representation closer to its border (Andermann and Moore, 2006), affecting the response properties and circuitry. Hence the location of the cell within the barrel might set the degree of the interactions. Though we did not find a relation between the amplitude and the interaction, it is possible that a careful mapping of the recording position within the barrel might produce a different result.

Although the source of the interactions could not be revealed in this study, the various types of interactions favor both hypotheses for receptive field integration in layer 2/3.

Many cells did not show any interactions between inputs arriving from the two whiskers, suggesting that layer 2/3 neurons integrate them. Another option for the weak interactions due to synaptic depression during adaptation is the possibility that the firing rate of individual input cells is low, leading to weak synaptic depression (Lampl and Katz, 2017). In that case, input arriving at layer 2/3 is inherited from many layer 4 cells having low firing probability, and the adaptation seen at a layer 2/3 cell results from synaptic adaptation of the previous thalamocortical synapse (Gil et al., 1999; Chung et al., 2002; Jubran et al., 2016) of the stimulated whisker. Yet, because layer 4 cells exhibit multi-whisker receptive fields, we strongly suggest that layer 2/3 cells integrate inputs from different whiskers due to cortico-cortical interactions.

## CONCLUSION

Our results show complex integration in layer 2/3 cells. For most cells the response to interleaved stimulation of two whiskers mostly shows no interactions, but in a small number of cases, it can result in strong reciprocal interactions or asymmetrical unidirectional interactions. Our results thus combine contrasting studies by supporting both cortico-cortical and inherited receptive fields.

## DATA AVAILABILITY STATEMENT

Custom code in MATLAB and data are available at the Open Science Framework - <https://osf.io/f4mnb/>.

## ETHICS STATEMENT

The animal study was reviewed and approved by the Weizmann Institute Animal Care and Use Committee. Written informed consent was obtained from the owners for the participation of their animals in this study.

## AUTHOR CONTRIBUTIONS

IL and YK designed the experiments, carried out the analysis, and wrote the manuscript. YK carried out the electrophysiology experiments. Both authors contributed to the article and approved the submitted version.

## FUNDING

IL is the incumbent of the Norman and Helen Asher Professorial Chair at the Weizmann Institute of Science. YK is incumbent of the Marianne Manoville Beck Research Fellow Chair in Brain Research. This research was supported by DFG (SFB 1089) to IL and Israel Science Foundation (ISF 1539/17) to IL. This research was also supported by Marianne Manoville Beck Laboratory for Research.

## REFERENCES

- Altman, D. G., and Royston, P. (2006). The cost of dichotomising continuous variables. *BMJ* 332, 1080.
- Andermann, M. L., and Moore, C. I. (2006). A somatotopic map of vibrissa motion direction within a barrel column. *Nat. Neurosci.* 9, 543–551. doi: 10.1038/n1671
- Armstrong-James, M., and Callahan, C. A. (1991). Thalamo-cortical processing of vibrissal information in the rat. II. spatiotemporal convergence in the thalamic ventroposterior medial nucleus (VPM) and its relevance to generation of receptive fields of S1 cortical “barrel” neurones. *J. Comp. Neurol.* 303, 211–224. doi: 10.1002/cne.903030204
- Armstrong-James, M., Callahan, C. A., and Friedman, M. A. (1991). Thalamo-cortical processing of vibrissal information in the rat. I. Intracortical origins of surround but not centre-receptive fields of layer IV neurones in the rat S1 barrel field cortex. *J. Comp. Neurol.* 303, 193–210. doi: 10.1002/cne.903030203
- Armstrong-James, M., Fox, K., and Das-Gupta, A. (1992). Flow of excitation within rat barrel cortex on striking a single vibrissa. *J. Neurophysiol.* 68, 1345–1358. doi: 10.1152/jn.1992.68.4.1345
- Bennette, C., and Vickers, A. (2012). Against quantiles: categorization of continuous variables in epidemiologic research, and its discontents. *BMC Med. Res. Methodol.* 12:21. doi: 10.1186/1471-2288-12-21
- Brecht, M., Roth, A., and Sakmann, B. (2003). Dynamic receptive fields of reconstructed pyramidal cells in layers 3 and 2 of rat somatosensory barrel cortex. *J. Physiol.* 553, 243–265. doi: 10.1113/jphysiol.2003.044222
- Brecht, M., and Sakmann, B. (2002). Dynamic representation of whisker deflection by synaptic potentials in spiny stellate and pyramidal cells in the barrels and septa of layer 4 rat somatosensory cortex. *J. Physiol.* 543, 49–70. doi: 10.1113/jphysiol.2002.018465
- Brumberg, J. C., Pinto, D. J., and Simons, D. J. (1996). Spatial gradients and inhibitory summation in the rat whisker barrel system. *J. Neurophysiol.* 76, 130–140. doi: 10.1152/jn.1996.76.1.130
- Bruno, R. M., and Simons, D. J. (2002). Feedforward mechanisms of excitatory and inhibitory cortical receptive fields. *J. Neurosci.* 22, 10966–10975. doi: 10.1523/jneurosci.22-24-10966.2002
- Bureau, I., von Saint Paul, F., and Svoboda, K. (2006). Interdigitated paralemniscal and lemniscal pathways in the mouse barrel cortex. *PLoS Biol.* 4:e382. doi: 10.1371/journal.pbio.0040382
- Carandini, M., and Ferster, D. (1997). A tonic hyperpolarization underlying contrast adaptation in cat visual cortex. *Science* 276, 949–952. doi: 10.1126/science.276.5314.949
- Chung, S., Li, X., and Nelson, S. B. (2002). Short-term depression at thalamocortical synapses contributes to rapid adaptation of cortical sensory responses in vivo. *Neuron* 34, 437–446. doi: 10.1016/s0896-6273(02)00659-1
- Fanselow, E. E., Sameshima, K., Baccala, L. A., and Nicolelis, M. A. (2001). Thalamic bursting in rats during different awake behavioral states. *Proc. Natl. Acad. Sci. U.S.A.* 98, 15330–15335. doi: 10.1073/pnas.261273898
- Feldmeyer, D., Lübke, J., Silver, R. A., and Sakmann, B. (2002). Synaptic connections between layer 4 spiny neurone-layer 2/3 pyramidal cell pairs in juvenile rat barrel cortex: physiology and anatomy of interlaminar signalling within a cortical column. *J. Physiol.* 538, 803–822. doi: 10.1113/jphysiol.2001.012959
- Felsenstein, K., and Pötzlberger, K. (1998). The Asymptotic Loss of Information for Grouped Data. *J. Multivar. Anal.* 67, 99–127. doi: 10.1006/jmva.1998.1759
- Fox, K., Wright, N., Wallace, H., and Glazewski, S. (2003). The origin of cortical surround receptive fields studied in the barrel cortex. *J. Neurosci.* 23, 8380–8391. doi: 10.1523/jneurosci.23-23-08380.2003
- Gabernet, L., Jadhav, S. P., Feldman, D. E., Carandini, M., and Scanziani, M. (2005). Somatosensory integration controlled by dynamic thalamocortical feed-forward inhibition. *Neuron* 48, 315–327. doi: 10.1016/j.neuron.2005.09.022
- Gentet, L. J. (2012). Functional diversity of supragranular GABAergic neurons in the barrel cortex. *Front. Neural. Circuits* 6:52. doi: 10.3389/fncir.2012.00052
- Gentet, L. J., Kremer, Y., Taniguchi, H., Huang, Z. J., Staiger, J. F., and Petersen, C. C. H. (2012). Unique functional properties of somatostatin-expressing GABAergic neurons in mouse barrel cortex. *Nat. Neurosci.* 15, 607–612. doi: 10.1038/nn.3051
- Gil, Z., Connors, B. W., and Amitai, Y. (1999). Efficacy of thalamocortical and intracortical synaptic connections: quanta, innervation, and reliability. *Neuron* 23, 385–397. doi: 10.1016/s0896-6273(00)80788-6
- Goldreich, D., Kyriazi, H. T., and Simons, D. J. (1999). Functional independence of layer IV barrels in rodent somatosensory cortex. *J. Neurophysiol.* 82, 1311–1316. doi: 10.1152/jn.1999.82.3.1311
- Heiss, J. E., Katz, Y., Ganmor, E., and Lampl, I. (2008). Shift in the balance between excitation and inhibition during sensory adaptation of S1 neurons. *J. Neurosci. Off. J. Soc. Neurosci.* 28, 13320–13330. doi: 10.1523/JNEUROSCI.2646-08.2008
- Helmstaedter, M., Sakmann, B., and Feldmeyer, D. (2009). L2/3 interneuron groups defined by multiparameter analysis of axonal projection, dendritic geometry, and electrical excitability. *Cereb. Cortex* 19, 951–962. doi: 10.1093/cercor/bhn130
- Helmstaedter, M., Staiger, J. F., Sakmann, B., and Feldmeyer, D. (2008). Efficient recruitment of layer 2/3 interneurons by layer 4 input in single columns of rat somatosensory cortex. *J. Neurosci. Off. J. Soc. Neurosci.* 28, 8273–8284. doi: 10.1523/JNEUROSCI.5701-07.2008
- Jubran, M., Mohar, B., and Lampl, I. (2016). The Transformation of Adaptation Specificity to Whisker Identity from Brainstem to Thalamus. *Front. Syst. Neurosci.* 10:56. doi: 10.3389/fnsys.2016.00056
- Kapfer, C., Glickfeld, L. L., Atallah, B. V., and Scanziani, M. (2007). Supralinear increase of recurrent inhibition during sparse activity in the somatosensory cortex. *Nat. Neurosci.* 10, 743–753. doi: 10.1038/nn1909
- Katz, Y., Heiss, J. E., and Lampl, I. (2006). Cross-whisker adaptation of neurons in the rat barrel cortex. *J. Neurosci. Off. J. Soc. Neurosci.* 26, 13363–13372. doi: 10.1523/JNEUROSCI.4056-06.2006
- Kheradpezhough, E., Adibi, M., and Arabzadeh, E. (2017). Response dynamics of rat barrel cortex neurons to repeated sensory stimulation. *Sci. Rep.* 7, 11445. doi: 10.1038/s41598-017-11477-6
- Kwegyir-Afful, E. E., Bruno, R. M., Simons, D. J., and Keller, A. (2005). The role of thalamic inputs in surround receptive fields of barrel neurons. *J. Neurosci. Off. J. Soc. Neurosci.* 25, 5926–5934. doi: 10.1523/JNEUROSCI.1360-05.2005
- Lampl, I., and Katz, Y. (2017). Neuronal adaptation in the somatosensory system of rodents. *Neuroscience* 343, 66–76. doi: 10.1016/j.neuroscience.2016.11.043
- Ling, D. S., and Benardo, L. S. (1995). Recruitment of GABAA inhibition in rat neocortex is limited and not NMDA dependent. *J. Neurophysiol.* 74, 2329–2335. doi: 10.1152/jn.1995.74.6.2329
- Lottem, E., and Azouz, R. (2008). Dynamic translation of surface coarseness into whisker vibrations. *J. Neurophysiol.* 100, 2852–2865. doi: 10.1152/jn.90302.2008
- Lübke, J., Egger, V., Sakmann, B., and Feldmeyer, D. (2000). Columnar organization of dendrites and axons of single and synaptically coupled excitatory spiny neurons in layer 4 of the rat barrel cortex. *J. Neurosci. Off. J. Soc. Neurosci.* 20, 5300–5311. doi: 10.1523/jneurosci.20-14-05300.2000
- Maravall, M., Alenda, A., Bale, M. R., and Petersen, R. S. (2013). Transformation of adaptation and gain rescaling along the whisker sensory pathway. *PLoS One* 8:e82418. doi: 10.1371/journal.pone.0082418
- Moore, C. I., and Nelson, S. B. (1998). Spatio-temporal subthreshold receptive fields in the vibrissa representation of rat primary somatosensory cortex. *J. Neurophysiol.* 80, 2882–2892. doi: 10.1152/jn.1998.80.6.2882
- Sachidhanandam, S., Sreenivasan, V., Kyriakatos, A., Kremer, Y., and Petersen, C. C. H. (2013). Membrane potential correlates of sensory perception in mouse barrel cortex. *Nat. Neurosci.* 16, 1671–1677. doi: 10.1038/nn.3532
- Shepherd, G. M. G., and Svoboda, K. (2005). Laminar and columnar organization of ascending excitatory projections to layer 2/3 pyramidal neurons in rat barrel cortex. *J. Neurosci. Off. J. Soc. Neurosci.* 25, 5670–5679. doi: 10.1523/JNEUROSCI.1173-05.2005

- Simons, D. J. (1985). Temporal and spatial integration in the rat SI vibrissa cortex. *J. Neurophysiol.* 54, 615–635. doi: 10.1152/jn.1985.54.3.615
- Simons, D. J., and Carvell, G. E. (1989). Thalamocortical response transformation in the rat vibrissa/barrel system. *J. Neurophysiol.* 61, 311–330. doi: 10.1152/jn.1989.61.2.311
- Tamás, G., Lorincz, A., Simon, A., and Szabadics, J. (2003). Identified sources and targets of slow inhibition in the neocortex. *Science* 299, 1902–1905. doi: 10.1126/science.1082053
- Taylor, J. M. G., and Yu, M. (2002). Bias and Efficiency Loss Due to Categorizing an Explanatory Variable. *J. Multivar. Anal.* 83, 248–263. doi: 10.1006/jmva.2001.2045
- Urbain, N., and Deschênes, M. (2007). A new thalamic pathway of vibrissal information modulated by the motor cortex. *J. Neurosci. Off. J. Soc. Neurosci.* 27, 12407–12412. doi: 10.1523/JNEUROSCI.2914-07.2007
- Viaene, A. N., Petrof, I., and Sherman, S. M. (2011). Synaptic properties of thalamic input to layers 2/3 and 4 of primary somatosensory and auditory cortices. *J. Neurophysiol.* 105, 279–292. doi: 10.1152/jn.00747.2010

**Conflict of Interest:** The authors declare that the research was conducted in the absence of any commercial or financial relationships that could be construed as a potential conflict of interest.

Copyright © 2021 Katz and Lampl. This is an open-access article distributed under the terms of the Creative Commons Attribution License (CC BY). The use, distribution or reproduction in other forums is permitted, provided the original author(s) and the copyright owner(s) are credited and that the original publication in this journal is cited, in accordance with accepted academic practice. No use, distribution or reproduction is permitted which does not comply with these terms.



# Disentangling of Local and Wide-Field Motion Adaptation

Jinglin Li<sup>†</sup>, Miriam Niemeier<sup>†</sup>, Roland Kern and Martin Egelhaaf\*

Neurobiology, Bielefeld University, Bielefeld, Germany

## OPEN ACCESS

### Edited by:

Davide Zoccolan,  
International School for Advanced  
Studies (SISSA), Italy

### Reviewed by:

Anna Lisa Stöckl,  
Julius Maximilian University  
of Würzburg, Germany  
Iris Salecker,  
INSERM U1024 Institut de Biologie  
de l'Ecole Normale Supérieure,  
France

### \*Correspondence:

Martin Egelhaaf  
martin.egelhaaf@uni-bielefeld.de

<sup>†</sup>These authors have contributed  
equally to this work and share first  
authorship

**Received:** 22 May 2021

**Accepted:** 11 August 2021

**Published:** 31 August 2021

### Citation:

Li J, Niemeier M, Kern R and  
Egelhaaf M (2021) Disentangling  
of Local and Wide-Field Motion  
Adaptation.  
Front. Neural Circuits 15:713285.  
doi: 10.3389/fncir.2021.713285

Motion adaptation has been attributed in flying insects a pivotal functional role in spatial vision based on optic flow. Ongoing motion enhances in the visual pathway the representation of spatial discontinuities, which manifest themselves as velocity discontinuities in the retinal optic flow pattern during translational locomotion. There is evidence for different spatial scales of motion adaptation at the different visual processing stages. Motion adaptation is supposed to take place, on the one hand, on a retinotopic basis at the level of local motion detecting neurons and, on the other hand, at the level of wide-field neurons pooling the output of many of these local motion detectors. So far, local and wide-field adaptation could not be analyzed separately, since conventional motion stimuli jointly affect both adaptive processes. Therefore, we designed a novel stimulus paradigm based on two types of motion stimuli that had the same overall strength but differed in that one led to local motion adaptation while the other did not. We recorded intracellularly the activity of a particular wide-field motion-sensitive neuron, the horizontal system equatorial cell (HSE) in blowflies. The experimental data were interpreted based on a computational model of the visual motion pathway, which included the spatially pooling HSE-cell. By comparing the difference between the recorded and modeled HSE-cell responses induced by the two types of motion adaptation, the major characteristics of local and wide-field adaptation could be pinpointed. Wide-field adaptation could be shown to strongly depend on the activation level of the cell and, thus, on the direction of motion. In contrast, the response gain is reduced by local motion adaptation to a similar extent independent of the direction of motion. This direction-independent adaptation differs fundamentally from the well-known adaptive adjustment of response gain according to the prevailing overall stimulus level that is considered essential for an efficient signal representation by neurons with a limited operating range. Direction-independent adaptation is discussed to result from the joint activity of local motion-sensitive neurons of different preferred directions and to lead to a representation of the local motion direction that is independent of the overall direction of global motion.

**Keywords:** optic flow, motion adaptation, fly, LPTC, local adaptation, global adaptation, electrophysiology, computational modeling

## INTRODUCTION

Neuronal adaptation, i.e., the adjustment of the response properties of neurons according to their recent stimulus history, is a general feature of neurons (Kohn, 2007; Rieke and Rudd, 2009). Motion adaptation in the fly visual motion pathway has been particularly well characterized in a variety of electrophysiological studies (Maddess and Laughlin, 1985; Harris, 1999; Harris et al., 2000; Neri and Laughlin, 2005; Kurtz, 2007, 2009; Kalb et al., 2008a,b; Liang et al., 2008, 2011; Nordström and O'Carroll, 2009; Liang, 2010). For the fly visual motion pathway at least two sites of adaptation have been pinpointed: at the level of retinotopically organized local motion detectors, on the one hand, and at the more downstream level of directionally selective cells with large receptive fields, the lobula plate tangential cells (LPTCs) that pool the outputs of many local motion detecting neurons, on the other hand.

From a functional perspective, adaptive processes in sensory systems often come into play when a very large stimulus range must be mapped onto the operating range of neurons limited by the underlying biophysical mechanisms. Adaptation then leads to the neuron's working range being adjusted to the prevailing stimulus conditions. Although this functional aspect might play a role, various other functional consequences were also discussed with regard to movement adaptation. These range from the energy required for signal representation (Brenner et al., 2000; Fairhall et al., 2001; Heitwerth et al., 2005) to an enhancement of the differential sensitivity to speed, the direction of motion and discontinuities in the motion stimuli (Maddess and Laughlin, 1985; Neri and Laughlin, 2005; Liang et al., 2008; Kurtz et al., 2009b). During translatory locomotion in cluttered natural environments such velocity discontinuities may result from changes in the depth structure of the environment. Their representation in the visual motion pathway could be shown to be enhanced as a consequence of motion adaptation (Liang et al., 2008; Ullrich et al., 2015; Li et al., 2016, 2017).

The experimental evidence for all these conclusions is based for methodological reasons mainly on electrophysiological recordings from LPTCs, i.e., at a processing stage where the local movement detectors sensing motion in a retinotopic way across the entire visual field have already been spatially pooled to a large extent (reviews: Egelhaaf, 2009; Borst et al., 2020). Whereas LPTCs are accessible to electrophysiological recording because of their relatively large size, this is hardly possible in a systematic way for their small local motion-sensitive input neurons (Gruntman et al., 2018). Therefore, most inferences about motion adaptation at the level of local motion-sensitive neurons have been drawn only indirectly. Since most stimuli employed in previous studies led to adaptation at both the level of local motion-sensitive neurons and the level of LPTCs, local and wide-field adaptation mechanisms could not easily be disentangled.

Therefore, we designed a novel stimulus paradigm, which allowed us to exclude largely the effects of local motion adaptation and to compare the consequences of adaptation with motion stimuli that avoided local motion adaptation to those evoked by stimulus conditions that are identical in all other

aspects, except that local motion adaptation was not excluded. In this way, we could pinpoint by intracellular recording from a prominent LPTC, the HSE-cell (Hausen and Egelhaaf, 1989), for the first time the adaptive effects caused at the level of LPTCs, as well as, by comparing the responses obtained with and without local adaptation, the adaptive effects that are a consequence of local motion adaptation. The experimental results will be interpreted on the basis of a computational model of the fly's visual motion pathway that has been proposed in previous studies (Li et al., 2016, 2017), but is now extended to include motion adaptation at both the level of local movement detectors as well as the LPTCs.

## MATERIALS AND METHODS

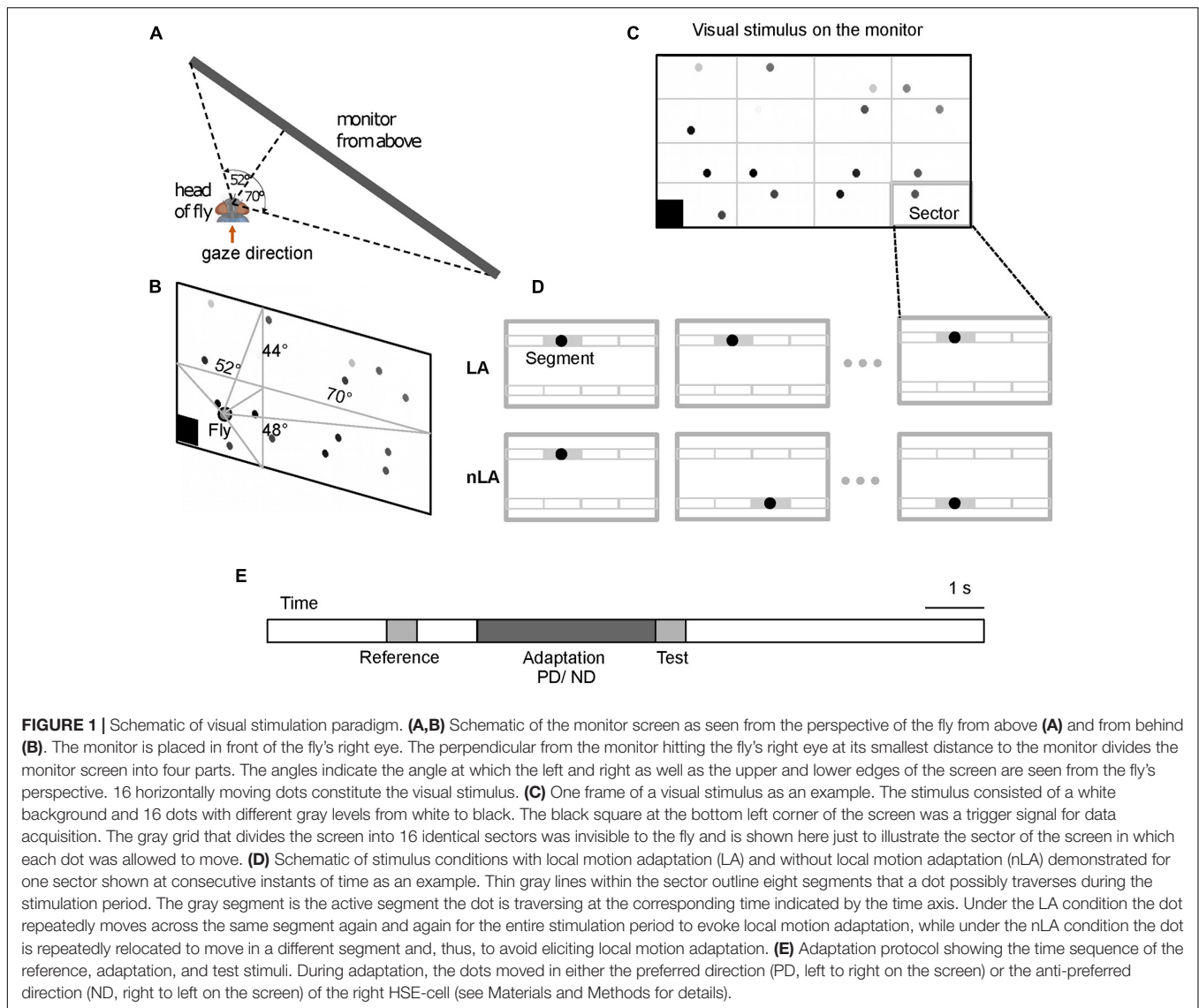
### Visual Stimulation

Stimulus movies were presented to the animal on a monitor (Acer LCD monitor GN246HL) at a rate of 144 fps and a luminance of white and black stimulus areas of 250 and 2 cd/m<sup>2</sup>, respectively. To stimulate the right eye, the monitor was placed at the right side of the animal. The perpendicular from the fly's eye to the monitor screen was 12.7 cm and virtually divided the screen into four quadrants of different size (for the angular size and location of the monitor screen from the perspective of the fly see **Figures 1A,B**). The stimulus field was located well within the large receptive field of the HSE-cell (Hausen, 1982b; Krapp et al., 2001). The position and the orientation of the fly were adjusted according to the fly's deep pseudopupil (Franceschini, 1975). The stimulus movies were generated with a custom program written in Matlab, 2017b (The Mathworks, Inc., Natick, MA, United States) and displayed by the command line version of the VLC media player<sup>1</sup> under control of custom scripts on Ubuntu Linux.

To investigate the impact of adaptive motion on the response gain of the HSE-cell, a 500 ms reference and a 500 ms test stimulus were presented before and after a 3 s adaptation motion stimulus, respectively. A 1 s interval without any motion separated the end of the reference stimulus and the start of the adaptation period; the last frame of the reference stimulus was constantly shown in this interval. In contrast, the test stimulus directly followed the adaptation period (**Figure 1E**). Two seconds before and 5 s after the reference and test stimulus, respectively, neuronal responses were recorded with the stimulus pattern stationary so that the adaptive effects in the cell can subside.

To disentangle the adaptive effects caused by local motion adaptation from those caused by global adaptation, we designed two types of motion stimuli, which had identical overall stimulus strength, but only differed in the adaptation they induced: one elicited local motion adaptation (LA conditions), while the other avoided local motion adaptation (nLA conditions). This means that it had to be ensured that in the LA case the same areas in the visual field were repeatedly stimulated and in the nLA case exactly that had to be prevented, whereby the overall stimulus was not allowed to differ—apart from statistical details. This was accomplished by subdividing for both stimulus types

<sup>1</sup><https://www.videolan.org>



the 3 s adaptation period into six consecutive 500 ms time intervals and by using stimulus patterns composed of black dots on a white background (**Figures 1B–D**), with all dots moving in small segments in the same direction and with the same speed. Both types of stimuli comprised the same number of dots and the same dot velocity, i.e., both types of stimuli were characterized at each instant of time by the same overall strength of motion. The only difference was that under the LA condition, dots moved repeatedly across the same small segments (**Figure 1D** upper diagrams), while under the nLA condition dots moved always across different segments in successive 500 ms intervals without trajectory overlap during the entire stimulus period (**Figure 1D** bottom diagrams). More precisely, the white background of the screen (1,920 px × 960 px) was invisibly subdivided into 16 equally sized sectors (480 px azimuth × 240 px elevation) (**Figure 1C**); each sector confined the moving area of a single dot. The sectors were subdivided into 4 by 2 invisible non-overlapping 120 px × 120 px segments (**Figure 1D**). A 48

px-diameter black dot moved horizontally for 500 ms within a given segment at a velocity of 240 px/s. Dot size (speed) was  $7^\circ \times 7^\circ$  (35 deg/s) perpendicular to the fly ( $0^\circ/0^\circ$ ) and—as a consequence of systematic perspective distortions due to the flat monitor screen— $1.6^\circ \times 2.5^\circ$  (8 deg/s) at the right margin of the screen stimulating the lateral visual field ( $70^\circ/0^\circ$ ). A dot moving repeatedly in just one of the eight randomly chosen segments allowed local adaptation to PD or ND (LA stimulus). Alternatively, a dot could move for 500 ms consecutively in one of the eight different segments of a given sector in random order and, thus, did not elicit local motion adaptation (nLA stimulus). Note that the strength of the responses induced by the individual dots in the different sectors may differ for two reasons: (a) the sensitivity gradient within the HSE-cell's receptive field (Hausen, 1982b; Krapp et al., 2001) and (b) the decrement of retinal dot size and velocity toward the lateral part of the stimulus screen as a consequence of perspective distortions (see above). Within each sector, however, these gradients are rather small, so that

there should be only negligible differences between the response strengths to dot movement in the different segments of a given sector and thus to LA and nLA adaptation.

To reduce flicker responses of the recorded neuron due to a synchronous appearance and disappearance of the different dots when they begin and end their movements, each started and ended moving at a different phase randomly chosen from 16 phases equally distributed within the 500 ms interval. The flickering effects were further reduced by gradually increasing and decreasing the gray values (black and gray dots in **Figures 1B,C**) of the dots in three steps during the initial and the final 90 ms of each 500 ms movement period.

For both the LA and nLA conditions, motion adaptation was either directed in the preferred direction (PD, left to right on the screen) or the null direction (ND, right to left) of the right HSE-cell. Accordingly, the fly was confronted with four different stimulus conditions: LA and nLA with motion during the adaptation period in the preferred direction and null direction, respectively. To adapt the same location for the two adaptation directions, under the PD and ND condition a dot traversed the same segment in the opposite direction. For the LA condition, the segments traversed by the dots were identical for the reference, adaptation, and test phase. Since for the nLA condition repetition of movement in the same segment was avoided, the segments that the dots traversed never matched over the entire reference, adaptation, and test phases. As a consequence, the traversed segments had to differ between the reference and test stimuli during nLA motion. Therefore, pairs of nLA motion stimuli were generated where the reference and test patterns were exchanged between consecutive stimulus presentations to ensure that the test and the reference stimulus were overall the same apart from their temporal order. Eight pairs of stimuli of different dot constellations were generated to reduce the effect of pattern-specific modulations in the average neuronal response that can be observed in LPTCs if stimuli contain low spatial frequency components (Meyer et al., 2011).

## Animal Preparation and Electrophysiological Experiments

One-day-old female blowflies (*Calliphora vicina*) from our laboratory stock were dissected according to standard procedures for intracellular recording of HSE-cells (Dürr and Egelhaaf, 1999). Briefly, a blowfly was anesthetized with CO<sub>2</sub> and fixed with wax on a microscope glass slide at the dorsal thorax, the wing bases, and the abdomen. The legs were removed, and wounds were waxed. The head was pitched down and fixed to the thorax to make its rear accessible. The head capsule of both hemispheres was opened from the back, the right opening for the intracellular recording of the HSE-cell, and the left opening for the indifferent electrode. Ringer's solution (composition in mM: NaCl 128.3, NaHCO<sub>3</sub> 1.67, CaCl<sub>2</sub> 1.89, KCl 4.69, Glucose 12.6, KH<sub>2</sub>PO<sub>4</sub> 3.38, Na<sub>2</sub>HPO<sub>4</sub> 3.3; all chemicals from Merck and Fisher Scientific, Germany) was applied *via* the indifferent electrode, which was connected *via* an electrode holder and a silicone tube to a syringe, to prevent the brain from drying out. The proboscis and the antennae were removed. Tissues bridging both hemispheres were

partially removed to make the esophagus accessible, which was pulled out of the head and fixed to the dorsal part of the thorax with wax. The wounds were waxed. Air sacks, fat bodies, and part of tracheas were removed to make the axon of the HSE-cell accessible. The electrode for intracellular recording was pulled from a borosilicate thin-walled glass pipette (OD = 1.00 mm, Warner Instruments) with a Flaming/Brown Micropipette Puller (Model P-1000, Sutter Instrument). The electrodes were filled with 1 M KCl and had resistances ranging from 27 to 45 MΩ. Intracellular recordings were obtained from the axon of the right HSE-cell. The cell could be identified unambiguously by its characteristic response properties (Hausen, 1982a) using both a search stimulus on the monitor as well as a hand-held light probe. Graded changes in their membrane potential are the main response mode of HS-cells, even if recorded in their axons (Hausen, 1982a). The membrane potential was recorded with a bridge amplifier (BA-03x, npi, Germany). The membrane potential was sampled at a frequency of 25 kHz and an amplitude resolution of about 0.3 mV (National Instruments PCIe-6251, 16-bit-ADC resolution). Digitized data were collected by a program based on the Matlab data acquisition toolbox (program written by Jens-Peter Lindemann) and stored on a hard disk for offline data analysis. All experiments were carried out at temperatures ranging between 22.3 and 24.5°C.

## Data Analysis

The analysis of recorded neuronal responses, the statistics as well as the model simulations were done with programs written in Matlab, 2019b. 13 HSE-neurons from different flies were recorded (550 sweeps in total; at least between 4 and 24 trials for each of the four stimulus conditions, median number of sweeps per condition: 9). Another set of recordings using the same design, but not exactly the same stimuli, were obtained in the Ph.D. project of Li, 2019; this data led to the same overall conclusion as the more recent data obtained in the present study. The resting potential as determined by the time-averaged membrane potential over 2 s before the start of the motion stimuli was subtracted from the responses. Only cells/trials were included into the analysis, if the resting potential was more negative than -40 mV, less membrane potential drift than 1 mV between the beginning and end of the responses and if responses of at least four repetitions under the same stimulus condition could be recorded. The responses were for- and backward low-pass filtered with a time constant 180 ms to focus our analysis on the graded component of the HSE-cell response. The reference response ( $R_{ref}$ ) and the test response ( $R_{test}$ ) were calculated as time-average over the respective last 400 ms of the stimulation period, thus not taking into account the initial 100 ms response transients. Similarly, the responses at the beginning and the end of the adaptation period ( $R_{badp}$ ,  $R_{eadp}$ ) were calculated as an average over 400 ms with the averaging starting only 100 ms after motion onset. Changes in the HSE-cell response evoked by motion adaption were assessed in two ways:

- (1) The relative amplitude reduction of the response during adaptation ( $RAR_{adpt}$ ) was calculated as the difference between average response at the end of adaptation ( $R_{eadp}$ )

and the average response at the beginning of the adaptation period ( $R_{badp}$ ) and normalized to the average reference response:

$$RAR_{adpt} = (R_{eadpt} - R_{badpt})/R_{ref} \quad (1)$$

- (2) How much the test response was smaller than the reference response was determined in a similar way as the normalized difference between the test and reference response:

$$RAR_{test} = (R_{test} - R_{ref})/R_{ref} \quad (2)$$

To determine the time constant for the decay in the response amplitude during the adaptation period, the HSE-cell responses were fitted by the formula

$$R_{HSE} = a \cdot \exp(-t/\tau) + b \quad (3)$$

with  $R_{HSE}$  being the average membrane potential of 13 HSE-cells,  $t$  the time,  $\tau$  the approximated time constant, and  $a$ ,  $b$  are parameters for curve fitting with the scaling factor  $a$  and  $b$  the level where the exponential curve settles.

## Modeling

The experimental data were interpreted on the basis of a computational model of the visual motion pathway of flies, which has been developed in two previous studies (Li et al., 2016, 2017) apart from one extension accounting for the adaptation properties of the HSE-cell. This kind of computational model, which has a long tradition in the field of insect motion vision (Borst and Egelhaaf, 1989; Borst, 2000), is not intended to mimic the cellular circuits that could be identified in recent years through sophisticated anatomical, molecular, and genetic approaches often combined with functional imaging (Mauss et al., 2017; Yang and Clandinin, 2018; Borst et al., 2020). Rather, the aim was to functionally characterize the crucial computational processes at each of the stages of the visual motion pathway. A one-to-one mapping of these processing steps to specific cellular elements is neither intended nor appropriate.

According to the overall structure of the fly visual system, the model of the visual motion pathway is composed of successive layers of retinotopic arrays of model photoreceptors (PRs), the lamina with its characteristic large monopolar cells (LMCs), the medulla with the elementary motion detectors (EMDs), and the lobula plate with a characteristic LPTC, the HSE-cell, integrating the output signals of a large array of EMDs (Figure 2). The model parameters were tuned in the previous studies by a systematic search to qualitatively capture adaptive features revealed in previous electrophysiological studies (Laughlin and Hardie, 1978; Maddess and Laughlin, 1985; Juusola et al., 1995; Harris et al., 2000; Kurtz et al., 2009b) as well as the experimental results presented in the present study.

The peripheral visual system of the model consisted of PRs with low-pass-like temporal characteristics and the LMCs with their high-pass-like temporal characteristics. It was modeled

according to Li et al. (2016). The LMC output was half-wave rectified and split into an ON and an OFF pathway according to its biological counterparts in the fly visual system (Figure 2C; Haag et al., 2017). Brightness adaptation of the photoreceptors was accomplished essentially by dividing a fast signal branch representing fast fluctuations in the input signal by a slow signal branch representing signal fluctuations on a much slower timescale. The fast and slow time constants amounted to 9 and 250 ms, respectively.

In the medulla, the outputs of the ON and OFF pathways, respectively, were fed into the adaptive motion detector model. This motion detector model was of the correlation-type consisting of two mirror symmetric half-detectors sensitive to motion in opposite directions (Figure 2C). Motion adaptation was implemented at the level of the half-detector output by a mechanism similar to that of brightness adaptation of the photoreceptors (see above), i.e., by dividing a fast signal branch representing fast fluctuations in the motion signal by a slow signal branch representing pattern velocities on a much slower timescale. Since motion adaptation takes much longer than brightness adaptation in the peripheral visual system, the “fast” and “slow” time constants were chosen to be much larger, 20 and 4,000 ms, respectively, than the time constants characteristic of brightness adaptation (see above). While the fast branches were the different half-detector outputs after being low-pass filtered with a small time constant, the slow branch was the average of the outputs of the PD and ND half-detectors of both the ON and OFF pathways after being low-pass filtered with a large time constant, leading to a direction-independent motion adaptation (Figure 2C). Except for two parameters, all parameter settings characterizing the peripheral visual system (photoreceptors and LMCs) as well as the adaptive local motion detector are identical to those as specified in the legend of Figure 1 in Li et al. (2017). To obtain a slightly better fit with the electrophysiological data recorded in the current study, just two parameters determining the speed of recovery and the strength of local adaptation were further adjusted:  $p1 = 50$  ms (instead of 30 ms) and  $p2 = 500$  ms (instead of 150 ms) (Li et al., 2017).

In the LPTC model, for simplicity, we assumed that the outputs of the local motion detectors are linearly summated in the lobula plate. Here, both half-detectors, i.e., ON and OFF, responding best to preferred-direction motion of the LPTC contributed to the sum with a positive sign, whereas both half-detectors responding best to null-direction motion of the LPTC contributed with a negative sign (Figure 2C). The simplification of linearly summating the motion detector outputs instead of implementing a dynamic gain control at this processing stage (Borst et al., 1995; Lindemann et al., 2005) is justified in the context of the current paper, since the pattern size in all model simulations was kept constant. Adaptation at the LPTC level was concluded in a previous study (Kurtz, 2007) to be directionally selective and elicited exclusively during depolarization of the cell and mimicked here in a computationally parsimonious way by subtracting from the summated EMD responses ( $R_{EMD}$ ) a low-pass filtered version of them. During hyperpolarization the

summated EMD response was just scaled to the membrane potential as has been measured in the experiment:

$$R_{HSE} = \left\{ \begin{array}{l} F_{mV} * F_{ratio} * (\sum R_{EMD} - F_{adapt} * LPF(\max(\sum R_{EMD}, 0))) \\ \text{for } \sum R_{EMD} \geq 0 \\ F_{mV} * \sum R_{EMD} \text{ for } \sum R_{EMD} < 0 \end{array} \right\} \quad (4)$$

with  $F_{mV}$  representing the scaling factor transforming the model response into mV, and  $F_{ratio}$  representing the ratio between the asymmetric depolarizing and hyperpolarizing response amplitude—as averaged across all neurons used for our analysis—to a given stimulus moving in the preferred and null direction, respectively.  $F_{mV} = 842$  and  $F_{ratio} = 1.97$  were determined by scaling the  $R_{ref}$  of the model under nLA conditions to that of the cell. The time constant of the first-order low-pass filter (indicated by LPF in eq.4) was 1,170 ms as determined from the neural responses averaged across all cells used for our analysis under the condition without local motion adaptation (see Eq. 3).  $F_{adapt} = 0.32$ , the scaling factor for the magnitude of the adaptive decay was determined by scanning through the parameter space in steps of 0.01 for the minimal difference between the model response and the cell response.

## RESULTS

To pinpoint the role of local vs. wide-field motion adaptation for shaping the responses of LPTCs we specifically designed a visual stimulus paradigm, which allowed us, while stimuli being identical with respect to their overall motion strength, to include (LA) or exclude (nLA) local adaptation. The graded membrane potential changes of the HSE-cell, recorded intracellularly under our nLA conditions were, therefore, shaped only by wide-field motion adaptation at the level of this LPTC. However, since wide-field motion adaptation cannot be avoided when analyzing motion adaptation on the basis of HSE-cell responses, the responses obtained under the LA conditions were not only the consequence of local motion adaptation, but inevitably also of wide-field adaptation. Therefore, we inferred the characteristics of local motion adaptation presynaptic to the HSE-cell indirectly by comparing the corresponding responses obtained under nLA and LA conditions.

**Figure 3** displays the average time-dependent membrane potential changes of 13 HSE-cells for LA or nLA motion either in the preferred (PD, **Figure 3A**) or null (ND, **Figure 3B**) direction. The experimentally determined response curves are superimposed by the corresponding model responses. Since under both stimulus conditions, LA and nLA, the reference stimuli were apart from statistical differences the same, the HSE-cell and its model analog depolarized in a very similar way during the reference phases.

During PD motion adaptation (**Figure 3A**) the responses declined on median by slightly more than 20% even if local adaptation was prevented (nLA, magenta curve; **Figure 4A**, left).

The decay in the response amplitude during PD adaptation under the nLA condition can be interpreted as reflecting the *time constant of wide-field adaptation*; it was estimated on this basis and approximates 1.17 s (see gray curve in **Figure 3A**). The consequences of PD adaptation were also reflected by an on median about 20% smaller test response in comparison to the reference response (**Figure 3A**, magenta curve; **Figure 4B**, left). The median response decay during LA is about 36% (**Figure 3A**, cyan curve) and thus significantly larger than during nLA (**Figure 4C**, left; Wilcoxon Rank Sum Test,  $p = 3.31 \times 10^{-4} < 0.001$ ). Accordingly, also the test response for LA (**Figure 3A**, cyan curve) is much smaller for the LA compared to the nLA condition (**Figure 4D**, left; Wilcoxon Rank Sum Test,  $p = 1.65 \times 10^{-5} < 0.001$ ). This difference between the HSE-cell responses obtained under the nLA and LA conditions, respectively, reflects the consequences of local motion adaptation. The time-dependent response profiles and mean adaptation-dependent response changes of the HSE-cell are qualitatively well reflected by the corresponding model responses (**Figures 3A, 4**, black curves/symbols). Note, that the periodic modulations in the model responses to LA are due to sensitivity gradients within the areas stimulated by the moving dots. Since during nLA they are presented in each trial in different parts of the overall stimulation area, these modulations are largely averaged out (for details on pattern-dependent response modulations in LPTCs, see Meyer et al., 2011). In the experimental data, these relatively small pattern-dependent response modulations are largely camouflaged by noise.

During adapting motion in the ND (**Figure 3B**), the HSE-cells hyperpolarized compared to their resting potential. With local motion adaptation being largely prevented (nLA) the hyperpolarization declined during the 3 s time interval on median by about 14% (**Figure 3B**, magenta curve; **Figures 4A,C** center). If the HSE-cell was adapted with ND motion of the same overall strength, but now allowing for local motion adaptation, the hyperpolarizing response amplitude decreased on median by about 17% (**Figure 3B**, cyan curve; **Figure 4C** center) and thus more than without local adaptation (Wilcoxon Rank Sum Test,  $p = 0.014 < 0.05$ ). Without local motion adaptation it even increased slightly by about 7% in relation to the reference phase (**Figure 3B**, magenta curve; **Figures 4A,B**) and decreased on median by about 23% as a consequence of LA (**Figure 3B**, cyan curve; **Figure 4D** center). Consequently, the reference and test response after ND motion adaptation with and without local motion adaptation differed much (Wilcoxon Rank Sum Test,  $p = 2.08 \times 10^{-5} < 0.001$ ).

Since the effects of PD adaptation are much larger than those of ND adaptation for the nLA condition (**Figures 4A,B**; Wilcoxon Rank Sum Test: response decline during motion adaptation  $p = 7.13 \times 10^{-4} < 0.001$ , test response  $p = 9.72 \times 10^{-5} < 0.001$ ), it is suggested that wide-field motion adaptation is strongly direction dependent. This might be a direct or indirect consequence of the depolarization level of the cell. In contrast to wide-field motion adaptation, which can be characterized with our stimulus paradigm largely uncontaminated by local motion adaptation, this is not possible for local motion adaptation. As a proxy for the properties of

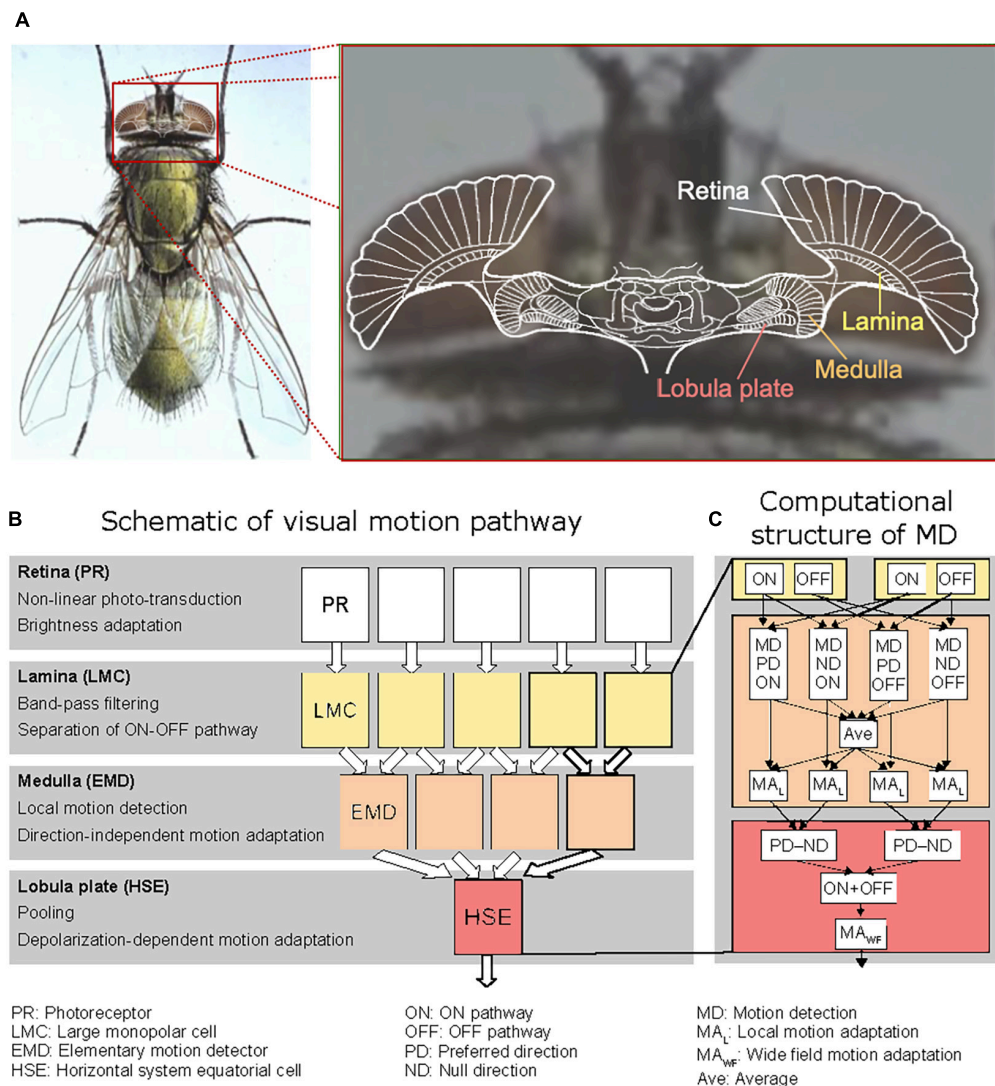


**FIGURE 2 |** Organization of the processing stages of the fly's visual motion pathway. **(A)** Sketch of a horizontal section of the brain of the blowfly projected onto a photograph of its head, with the retina and the three main visual neuropiles labeled. The colors correspond to those used to mark the corresponding processing stages in the computational model shown in panels **(B,C)**. **(B)** Schematic illustration of the visual motion pathway with its consecutive processing stages and its retinotopic columnar organization (up to the level of the Lobula plate). The computations performed at the individual processing stages are briefly characterized at the left of the diagram. **(C)** Sketch of the different computations performed in two neighboring channels of the model Lamina and of the motion detection (MD) processing in the Medulla, as well as the computations performed at the HSE level. The non-linearly transformed photoreceptor signals are temporally band-pass filtered in each Lamina column by the Large Monopolar Cells (LMC), half-wave rectified and split into an ON and an OFF channel. The Lamina output signals are fed into a model of an elaborated elementary movement detector (EMD) of the correlation type. The signals are processed separately at the EMD stage for the ON and OFF channels as well as for preferred direction (PD) and null direction motion (ND), respectively. For motion adaptation, the outputs of the resulting four channels, shown here for horizontal motion, are averaged (AVE); the average also includes the signals of the corresponding four vertically oriented movement detecting elements (not shown) leading to a direction-independent signal representing the overall motion at the respective location in the visual field. Local motion adaptation (MA<sub>L</sub>) is accomplished by dividing the outputs of the movement detection channels by the averaged motion signal after low-pass filtering. The movement detector channel outputs are then summated according to their respective sign (PD positive, ND negative) by the model HSE-cell. For the details of the different computational steps, see Materials and Methods.

local adaptation, we determined the difference in adaptive effects between LA and nLA stimulation based on the simplifying assumption that the two adaptive components superpose linearly (**Figure 4**, gray boxes). Since the differences are relatively small for PD and ND adaptation, although they differ significantly for the test responses (Wilcoxon Rank Sum Test: response

decline during motion adaptation  $p = 0.41$  i.e., nonsignificant; test response  $p = 0.008 < 0.01$ ), local motion adaptation can be suggested to be largely independent of the direction of motion, unlike the highly direction dependent wide-field motion adaptation. since there was only little wide-field ND motion adaptation, if local adaptation was largely prevented (**Figure 3B**,

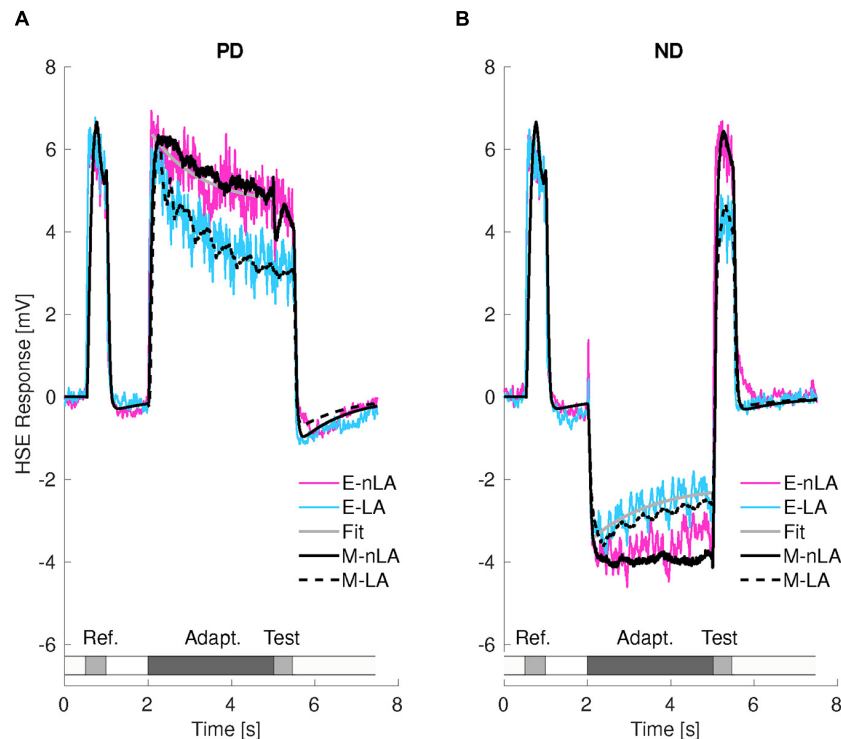


**FIGURE 3 |** Consequences of motion adaptation for the HSE-cell and the adaptive model of the visual motion pathway. **(A)** Average time-dependent responses of 13 HSE-cells for preferred direction (PD) motion with local motion adaptation (LA, cyan trace) and without local motion adaptation (nLA, magenta trace). Smooth gray line is the fitted curve used for estimating the time constant of wide-field motion adaptation (see Methods). The black traces represent the corresponding responses of the adaptive model of the visual motion pathway. The stimulation protocol is schematically illustrated below the cell response. **(B)** Same as in panel **(A)**, however, for null direction (ND) adaptation. Smooth gray line is the fitted curve used for estimating the time constant of local motion adaptation (see section “Materials and Methods”). The resting potential was subtracted from the responses for the experimental results, which were for- and backward low-pass filtered with a time constant of 180 ms.

magenta curve), the decay in the response amplitude during ND adaptation under the LA condition (**Figure 3B**, cyan curve) was essentially due to local motion adaptation. Therefore, the *time constant of local motion adaptation* can be estimated under this stimulus condition (see Methods). The time constant was estimated as 1.47 s (gray line in **Figure 3B**).

For both PD and ND motion adaptation as well as the corresponding nLA and LA conditions, the model responses (black lines in **Figure 3** and black dots in **Figure 4**) match their experimental counterpart at least qualitatively. This finding indicates that the relatively simple computational model of the fly visual motion pathway with its two adaptive stages is sufficient to account for most of our experimental data. The only difference is that ND nLA leads to a slight decrease in response in the HSE-cell, i.e., it gets less hyperpolarized, which is not reflected in the model because of the assumption of strict directionality of wide-field adaptation (compare black and magenta lines in **Figure 3B**).

## DISCUSSION

Motion adaptation in insects has been proposed to be a multi-stage process taking place at several levels in the visual motion

pathway. The two most prominent adaptation stages are the array of retinotopically organized local motion-sensitive elements and their postsynaptic wide-field lobula plate tangential cells (LPTCs) that pool the outputs of local motion-sensitive cells from large parts of the visual field (Hausen, 1984; Egelhaaf, 2009, 2020; Borst, 2014). By intracellularly recording the graded membrane potential changes of a particular LPTC, the HSE-cell, we could unravel the role of the individual consecutive adaptation stages and their contribution to overall motion adaptation as it manifests itself at the level of LPTCs. This could only be achieved by using a novel stimulus design that allowed the local movement adaptation to be either included or excluded while the total stimulus strength was kept constant. Thus, wide-field adaptation could be analyzed either in isolation or together with local adaptation, the characteristics of which could then be indirectly inferred by comparing the cellular responses to the two stimulus conditions. Thus, our study is distinguished from previous studies of motion adaptation based on LPTC recordings (Maddess and Laughlin, 1985; de Ruyter van Steveninck et al., 1986; Borst and Egelhaaf, 1987; Harris et al., 2000; Reisenman et al., 2003; Neri and Laughlin, 2005; Kalb et al., 2008a) that could only characterize the joint effects of the different consecutive adaptation processes. Our

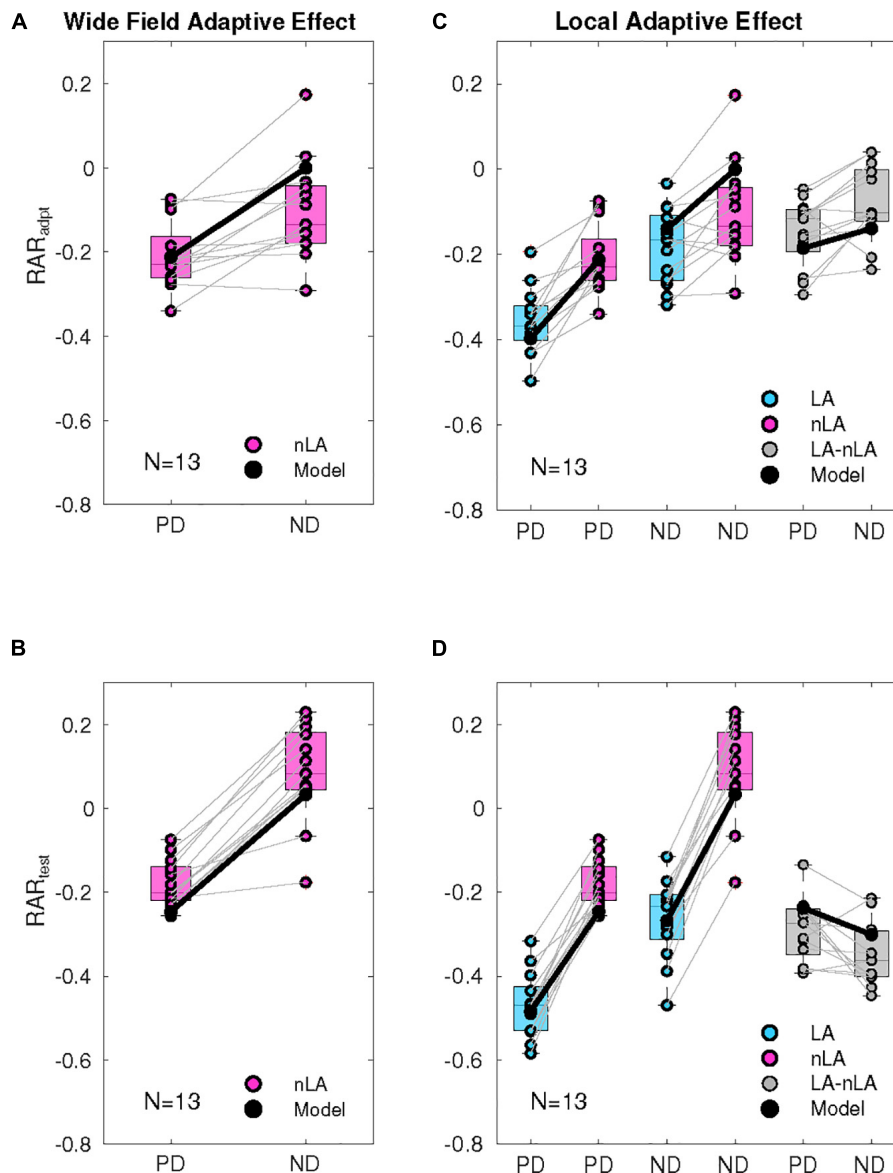


**FIGURE 4 |** Quantification of wide-field and local adaptation. **(A)** Relative amplitude reduction of the response during motion adaptation ( $RAR_{adpt}$ ): Consequences of wide-field adaptation determined by comparing the response at the end and beginning of the adaptation phase. The response level at the beginning and end of the wide-field motion adaptation period (nLA) was determined by averaging over 400 ms periods starting 100 ms after the start of the adaptation period or terminating at its end. The response decrement during the adaptation period was normalized by the average reference response. The model responses (black dots) were treated in the same way. The adaptive effects are shown both pairwise for PD and ND adaptation of all 13 cells (magenta dots) and as box plots (mid-line, median, magenta box, 25–75 percentile). **(B)** Consequences of wide-field adaptation determined by comparing the test and reference responses and normalizing them to the average reference response. The averages were taken for the last 400 ms of the reference and test response, respectively. The first 100 ms were not included because of the initial response transient of the reference response. The model responses (black dots) were treated in the same way. The adaptive effects are shown both pairwise for PD and ND adaptation (nLA) for all 13 cells (magenta dots) and as box plots (mid-line, median, magenta box, 25–75 percentile). **(C)** Consequences of local adaptation during the adaptation period by comparing the responses obtained for both nLA (magenta) and LA (cyan). The responses under the LA condition were determined in the way as described in panel **(A)** for the nLA condition. The model responses (black dots) were treated in the same way as the experimentally determined responses. The adaptive effects for the LA and nLA conditions are shown pairwise [nLA: same data as in panel **(A)**] and as box plots (mid-line, median, box, 25–75 percentile). The data for PD adaptation are shown in the left, those for ND adaptation in the middle. On the right, the corresponding differences between the adaptive effects obtained under the LA and nLA conditions, respectively, are shown in gray along with the model equivalents for both PD and ND adaptation. **(D)** Consequences of local adaptation by comparing the corresponding test and reference responses obtained for both nLA (magenta) and LA (cyan). The adaptive effects were normalized to the average reference response. The responses under the LA condition were determined in the way as described in panel **(B)** for the nLA condition. The model responses (black dots) were treated in the same way as the experimentally determined responses. The adaptive effects for the LA and nLA conditions are shown pairwise [nLA: same data as in panel **(B)**] and as box plots (mid-line, median, box, 25–75 percentile). The data for PD adaptation are shown in the left, those for ND adaptation in the middle. On the right, the corresponding differences between the adaptive effects obtained under the LA and nLA conditions, respectively, are shown in gray along with the model equivalents for both PD and ND adaptation.

results suggest, in line with previous studies (Harris et al., 1999; Kurtz et al., 2000, 2009a; Kurtz, 2007), that wide-field motion adaptation strongly depends on the motion direction. We further concluded that, in contrast, local motion adaptation is largely direction independent. We hypothesize that this independence aims at a robust representation of the direction of local motion, independent of local motion history, by the population activity of local motion-sensitive neurons with different preferred directions at a given point in the retinotopic array.

## Relation to Previous Research

Various aspects of motion adaptation have been characterized in other contexts and with different types of stimuli leading to a variety of interpretations. How do these concepts relate to our conclusions? Harris et al. (2000) suggested that motion adaptation induces three components of contrast gain modulation: (1) a contrast gain reduction as described by a shift of the contrast-response function toward higher contrasts, (2) a subtractive effect leading to a hyperpolarizing shift of the contrast-response function, and (3) a contraction of response range. Further, Harris et al. (2000) provided evidence that the contrast gain reduction was independent of the motion direction of the adapting stimulus. Based on our results, this phenomenon can be concluded to be caused by local motion adaptation. In principle, local adaptation can take place at different stages of the visual motion pathway. Since, according to Harris et al. (2000), flicker stimulation induced a much weaker contrast gain reduction than motion in any direction, contrast gain reduction is probably located after the computation of motion. Contrast gain reduction may, in agreement with our model simulations (see also Li et al., 2017), involve the pooled outputs of different subtypes of the local motion-sensitive neurons with different preferred directions to adapt each subtype equally. The adaptive reduction of the response amplitude to constant-velocity motion goes along with an enhancement of the sensitivity to velocity transients (Kurtz et al., 2009a), which has been suggested to be the consequence local adaptive mechanisms (Maddess and Laughlin, 1985) and is probably based on the process described by Harris et al. (2000) as contrast gain control. We accounted for this adaptive feature by direction independent local motion adaptation. Both the contrast gain reduction and the enhancement of the sensitivity to velocity transients could be modeled by a specific local motion adaptation mechanism (Li et al., 2017). Whether further adaptive effects of enhancing the sensitivity to other stimulus transients resulting from sudden contrast, orientation, or spatial frequency changes (Kurtz et al., 2009b) can also be explained by this mechanism needs to be further investigated. The subtractive, hyperpolarizing shift induced by motion adaptation is highly direction-dependent (Harris et al., 1999, 2000) corresponding well to the wide-field motion adaptation at the level of the HSE-cell we revealed in our study. This hyperpolarizing shift is likely associated with  $\text{Ca}^{2+}$  accumulation in the dendrite of the HSE-cell (Kurtz et al., 2000; Kurtz, 2007) and caused by the opening of specific potassium channels (Kurtz et al., 2009a).

In the previous studies, contrast gain modulation induced by motion adaptation has been assessed by varying the pattern

contrast of the reference and the test stimuli presented before and after a strong preferred direction adaptation and by comparing the response amplitude for each contrast condition before and after adaptation (Harris et al., 2000). The directional gain modulation has been determined in a similar way by altering the motion direction of the reference and the test stimuli and comparing the response amplitudes before and after motion adaptation (Neri and Laughlin, 2005; Kalb et al., 2008a). Whether the adaptive components that contribute to the contrast gain modulation (Harris et al., 2000) can explain without further assumptions the local and global adaptive effects in directional sensitivity (Neri and Laughlin, 2005) needs to be clarified. Our novel stimulus paradigm allows us to further investigate the parameter space of pattern contrast and motion direction to explicitly address these issues in order to support further understanding of the mechanisms and potential functional significance of motion adaptation.

While motion adaptation has originally been suggested to be a consequence of the adaptation of the motion detector time constant (de Ruyter van Steveninck et al., 1986; Clifford and Langley, 1996), later experimental studies (Harris et al., 1999) did not support this suggestion. In a previous study (Li et al., 2017) we suggested a motion adaptation model based on a similar adaptation mechanism as accounting for brightness adaptation in the peripheral visual system (Li et al., 2016). This mechanism can reproduce direction-independent reduction of response sensitivity of local motion-sensitive neurons without causing a change in the motion detector time constant (Li et al., 2017).

## Functional Significance of Motion Adaptation

Motion adaptation in the insect visual motion pathway has been studied mostly based on recordings of wide-field motion-sensitive LPTCs. These studies used either relatively simple system-analytical stimuli (Maddess and Laughlin, 1985; de Ruyter van Steveninck et al., 1986; Borst and Egelhaaf, 1987; Harris et al., 1999, 2000; Neri and Laughlin, 2005; Kalb et al., 2008a; Kurtz et al., 2009b; Nordström and O'Carroll, 2009), or more naturalistic motion stimuli (Liang et al., 2008, 2011). Motion adaptation has usually been considered to be beneficial for enhancing the sensitivity to changes in the speed (Maddess and Laughlin, 1985), direction (Neri and Laughlin, 2005), or other stimulus or environmental features (Liang et al., 2008; Kurtz et al., 2009a). As a consequence of this kind of adaptation (Neri and Laughlin, 2005), information about the absolute value of the relevant stimulus feature (e.g., velocity) is lost for the benefit of an increased sensitivity to stimulus changes. Further studies demonstrated based on information-theoretical methods how motion adaptation facilitates efficient information transmission (Brenner et al., 2000), saves coding energy without losing information (Heitwerth et al., 2005), or even adapts without the cost of losing information about the absolute value of the prevailing level of the corresponding parameter (Fairhall et al., 2001). These functional benefits of motion adaptation are very similar to the functional aspects discussed in the context of brightness adaptation.

However, the neuronal representation of brightness and motion differ in at least one fundamental aspect, leading us to suggest an additional novel functional role of motion adaptation. Unlike local brightness, local motion is represented by four subtypes of local motion-sensitive neurons each tuned to one of four cardinal directions (Borst, 2014; Borst et al., 2020). If motion adaptation were strongly dependent on the direction of motion, the sensitivity of the different subtypes of neurons would be affected in different ways depending on the direction of self-motion of the animal and the resulting optical flow. The direction of motion represented by these neurons would shift, even if the retinal motion vector remained the same. According to the results presented, local motion adaptation is induced by both preferred and null-direction motion of the movement detectors. In other experiments it has been shown that strong motion adaptation is also induced by motion orthogonal to these directions (Harris et al., 2000; Li, 2019; Niemeier, unpublished results). Therefore, these experiments together with those of the current study, all based on the activity of the spatially pooling HSE-cell, suggest that local motion adaptation is largely direction independent. Based on the modeling results of our present and previous studies (Li et al., 2017), this conclusion can be interpreted computationally by assuming that local motion adaptation takes place at the level of the half-detectors, which are direction sensitive to some extent. The direction independence of the adaptation is assumed to be accomplished by dividing the half-detector outputs by the temporally low-pass filtered and summated output signals of the PD and ND half-detectors of the ON and OFF pathways for both horizontal and vertical motion (see **Figure 2C** right panel). Accordingly, the adaptive state of the four half-detectors and, thus, the direction of the movement vector (though not its length) signaled by their joint activity would be invariant against the adaptive state of the motion vision pathway up to the level of local movement detection. The direct consequence would be a robust representation of the direction of local motion by the horizontal and vertical movement detectors irrespective of the overall direction of the optic flow generated by self-motion of the animal. This hypothesis needs to be further validated by experimental as well as simulation evidence.

We have refrained here from assigning the individual elements of the computational model to specific local interneurons in the visual motion pathway. Although the properties of important cellular elements involved in motion detection is increasingly being elucidated thanks to innovative genetic, imaging, and electrophysiological approaches (Mauss et al., 2017; Yang and Clandinin, 2018; Borst et al., 2020) mapping the individual computations of motion detection to anatomically and partly physiologically characterized local interneurons would currently be highly speculative. However, such a mapping is not necessary for our functional conclusions with regard to local or global movement adaptation.

The local motion-sensitive cells are then spatially pooled by the population of LTPCs, which have either a predominantly horizontal or vertical preferred direction (Hausen, 1984). Because of the strong direction dependent adaptation component operating at the level of LTPCs, the adaptive state of the

population of these neurons is not adjusted in the same way by motion adaptation but depends on the way the animal has been moving. Hence, the self-motion vector represented by these neurons is not robust but depends on the way the animal moved before. The functional significance of this feature is not yet clear. It might be hypothesized that representing the direction of the vector of self-motion by the population of LTPCs is not of great functional relevance, as these cells are thought to mediate under closed-loop compensatory adjustments of the flight course after a disturbance. However, these cells have also been suggested to play a role in spatial vision, since they represent information about the spatial layout of the environment during the straight flight sections, i.e., during translatory motion. Then the responses of these cells do not only depend on the animal's speed of locomotion, but also on the spatial profile of the environment. The responses increase when the animal passes nearby objects, because these lead to a larger retinal velocity than background structures in the environment. Note, that as a consequence of the saccadic flight and gaze strategy of flies and other insects translatory flight sections make up approximately 80% of flight time, whereas changes in flight directions are squeezed into rapid saccadic turns (reviews: Egelhaaf et al., 2012; Egelhaaf et al., 2014). Further analyses are required to clarify whether direction dependent motion adaptation of LTPCs plays a functional role in spatial vision.

## DATA AVAILABILITY STATEMENT

The raw data supporting the conclusions of this article will be made available by the authors, without undue reservation.

## AUTHOR CONTRIBUTIONS

JL, MN, RK, and ME conceptualized and designed the project and wrote the manuscript. JL performed the preliminary electrophysiological experiments, developed the model, and conducted the model simulations. MN collected the electrophysiological data shown in this study. JL and MN analyzed the data. All authors contributed to the article and approved the submitted version.

## FUNDING

This work was supported by the Deutsche Forschungsgemeinschaft (DFG). We acknowledge the financial support of the German Research Foundation (DFG) and the Open Access Publication Fund of Bielefeld University for the article processing charge.

## ACKNOWLEDGMENTS

We would like to thank Jens-Peter Lindemann for writing programs for stimulus presentation and data acquisition.

## REFERENCES

- Borst, A. (2000). Models of motion detection. *Nat. Neurosci.* 3:1168. doi: 10.1038/81435
- Borst, A. (2014). Fly visual course control: behaviour, algorithms and circuits. *Nat. Rev. Neurosci.* 15, 590–599. doi: 10.1038/nrn3799
- Borst, A., and Egelhaaf, M. (1987). Temporal modulation of luminance adapts time constant of fly movement detectors. *Biol. Cybern.* 56, 209–215. doi: 10.1007/bf00365215
- Borst, A., and Egelhaaf, M. (1989). Principles of visual motion detection. *Trends Neurosci.* 12, 297–306. doi: 10.1016/0166-2236(89)90010-6
- Borst, A., Egelhaaf, M., and Haag, J. (1995). Mechanisms of dendritic integration underlying gain control in fly motion-sensitive interneurons. *J. Comput. Neurosci.* 2, 5–18. doi: 10.1007/bf00962705
- Borst, A., Haag, J., and Mauss, A. S. (2020). How fly neurons compute the direction of visual motion. *J. Comp. Physiol. A* 206, 109–124. doi: 10.1007/s00359-019-01375-9
- Brenner, N., Bialek, W., and de Ruyter van Steveninck, R. R. (2000). Adaptive rescaling maximizes information transmission. *Neuron* 26, 695–702. doi: 10.1016/s0896-6273(00)81205-2
- Clifford, C. W. G., and Langley, K. (1996). A model of temporal adaptation in fly motion vision. *Vis. Res.* 36, 2595–2608. doi: 10.1016/0042-6989(95)00301-0
- de Ruyter van Steveninck, R. R., Zaagman, W. H., and Mastebroek, H. A. K. (1986). Adaptation of transient responses of a movement-sensitive neuron in the visual system of the blowfly, *Calliphora erythrocephala*. *Biol. Cybern.* 54, 223–236. doi: 10.1007/bf00318418
- Dürr, V., and Egelhaaf, M. (1999). *In vivo* calcium accumulation in presynaptic and postsynaptic dendrites of visual interneurons. *J. Neurophysiol.* 82, 3327–3338. doi: 10.1152/jn.1999.82.6.3327
- Egelhaaf, M. (2009). Insect motion vision. *Scholarpedia* 4:1671. doi: 10.4249/scholarpedia.1671
- Egelhaaf, M. (2020). "Visual Processing in Free Flight," in *Encyclopedia of Computational Neuroscience*, eds D. Jaeger and R. Jung (New York: Springer), 1–23. doi: 10.1007/978-1-4614-7320-6\_343-15
- Egelhaaf, M., Boeddeker, N., Kern, R., and Lindemann, J. P. (2012). Spatial vision in insects is facilitated by shaping the dynamics of visual input through behavioral action. *Front. Neural Circ.* 6:108. doi: 10.3389/fncir.2012.00108
- Egelhaaf, M., Kern, R., and Lindemann, J. P. (2014). Motion as a source of environmental information: a fresh view on biological motion computation by insect brains. *Front. Neural Circ.* 8:127. doi: 10.3389/fncir.2014.00127
- Fairhall, A. L., Lewen, G. D., Bialek, W., and de Ruyter van Steveninck, R. R. (2001). Efficiency and ambiguity in an adaptive neural code. *Nature* 412, 787–792. doi: 10.1038/35090500
- Franceschini, N. (1975). "Sampling of the visual environment by the compound eye of the fly: fundamentals and applications," in *Photoreceptor Optics*, eds A. W. Snyder & R. Menzel. (Berlin: Springer), 98–125. doi: 10.1007/978-3-642-80934-7\_6
- Gruntman, E., Romani, S., and Reiser, M. B. (2018). Simple integration of fast excitation and offset, delayed inhibition computes directional selectivity in *Drosophila*. *Nat. Neurosci.* 21, 250–257. doi: 10.1038/s41593-017-0046-4
- Haag, J., Mishra, A., and Borst, A. (2017). A common directional tuning mechanism of *Drosophila* motion-sensing neurons in the ON and in the OFF pathway. *Elife* 6:e29044. doi: 10.7554/eLife.29044
- Harris, R. (1999). *Motion Adaptation in an Insect Visual System*. Cambridge: University of Cambridge.
- Harris, R. A., O'carroll, D. C., and Laughlin, S. B. (1999). Adaptation and the temporal delay filter of fly motion detectors. *Vis. Res.* 39, 2603–2613. doi: 10.1016/s0042-6989(98)00297-1
- Harris, R. A., O'carroll, D. C., and Laughlin, S. B. (2000). Contrast gain reduction in fly motion adaptation. *Neuron* 28, 595–606. doi: 10.1016/s0896-6273(00)00136-7
- Hausen, K. (1982a). Motion-sensitive interneurons in the optomotor system of the fly. I. The Horizontal Cells: structure and signals. *Biol. Cybern.* 45, 143–156. doi: 10.1007/bf00335241
- Hausen, K. (1982b). Motion sensitive interneurons in the optomotor system of the fly. II. The Horizontal Cells: receptive field organization and response characteristics. *Biol. Cybern.* 46, 67–79. doi: 10.1007/bf00335352
- Hausen, K. (1984). "The lobula-complex of the fly: structure, function and significance in visual behaviour," in *Photoreception and Vision in Invertebrates*, ed. M. A. Ali (New York: Plenum Press), 523–559. doi: 10.1007/978-1-4613-2743-1\_15
- Hausen, K., and Egelhaaf, M. (1989). "Neural mechanisms of visual course control in insects," in *Facets of Vision*, eds D. G. Stavenga and R. C. Hardie (Berlin: Springer), 391–424. doi: 10.1007/978-3-642-74082-4\_18
- Heitwerth, J., Kern, R., van Hateren, J. H., and Egelhaaf, M. (2005). Motion adaptation leads to parsimonious encoding of natural optic flow by blowfly motion vision system. *J. Neurophysiol.* 94, 1761–1769. doi: 10.1152/jn.00308.2005
- Juusola, M., Uusitalo, R. O., and Weckström, M. (1995). Transfer of graded potentials at the photoreceptor-interneuron synapse. *J. Gen. Physiol.* 103, 117–148. doi: 10.1085/jgp.105.1.117
- Kalb, J., Egelhaaf, M., and Kurtz, R. (2008a). Adaptation changes directional sensitivity in a visual motion-sensitive neuron of the fly. *Vis. Res.* 48, 1735–1742. doi: 10.1016/j.visres.2008.05.004
- Kalb, J., Egelhaaf, M., and Kurtz, R. (2008b). Adaptation of velocity encoding in synaptically coupled neurons in the fly visual system. *J. Neurosci.* 10, 9183–9193. doi: 10.1523/jneurosci.1936-08.2008
- Kohn, A. (2007). Visual adaptation: physiology, mechanisms, and functional benefits. *J. Neurophysiol.* 97, 3155–3164. doi: 10.1152/jn.00086.2007
- Krapp, H. G., Hengstenberg, R., and Egelhaaf, M. (2001). Binocular contribution to optic flow processing in the fly visual system. *J. Neurophysiol.* 85, 724–734. doi: 10.1152/jn.2001.85.2.724
- Kurtz, R. (2007). Direction-selective adaptation in fly visual motion-sensitive neurons is generated by an intrinsic conductance-based mechanism. *Neuroscience* 146, 573–583. doi: 10.1016/j.neuroscience.2007.01.058
- Kurtz, R. (2009). The many facets of adaptation in fly visual motion processing. *Commun. Integr. Biol.* 2, 1–3.
- Kurtz, R., Beckers, U., Hundsdoerfer, B., and Egelhaaf, M. (2009a). Mechanisms of after-hyperpolarization following activation of fly visual motion-sensitive neurons. *Eur. J. Neurosci.* 30, 567–577. doi: 10.1111/j.1460-9568.2009.06854.x
- Kurtz, R., Dürr, V., and Egelhaaf, M. (2000). Dendritic calcium accumulation associated with direction selective adaptation in visual motion-sensitive neurons *in vivo*. *J. Neurophysiol.* 84, 1914–1923. doi: 10.1152/jn.2000.84.4.1914
- Kurtz, R., Egelhaaf, M., Meyer, H. G., and Kern, R. (2009b). Adaptation accentuates responses of fly motion-sensitive visual neurons to sudden stimulus changes. *Proc. R. Soc. B Biol. Sci.* 276, 3711–3719. doi: 10.1098/rspb.2009.0596
- Laughlin, S. B., and Hardie, R. C. (1978). Common strategies for light adaptation in the peripheral visual systems of fly and dragonfly. *J. Comp. Physiol. A* 128, 319–340. doi: 10.1007/bf00657606
- Li, J. (2019). *Functional Significance of Adaption in Optic Flow-Based Spatial Vision in Flies*. Ph.D. thesis. Germany: Bielefeld University.
- Li, J., Lindemann, J. P., and Egelhaaf, M. (2016). Peripheral Processing Facilitates Optic Flow-Based Depth Perception. *Front. Comput. Neurosci.* 10:111. doi: 10.3389/fncom.2016.00111
- Li, J., Lindemann, J. P., and Egelhaaf, M. (2017). Local motion adaptation enhances the representation of spatial structure at EMD arrays. *PLoS Comput. Biol.* 13:e1005919. doi: 10.1371/journal.pcbi.1005919
- Liang, P. (2010). *Object and Background Coding by Different Neurons of Blowflies and the Benefit of Motion Adaptation*. Ph.D. thesis. Germany: Bielefeld University.
- Liang, P., Kern, R., and Egelhaaf, M. (2008). Motion adaptation enhances object-induced neural activity in three-dimensional virtual environment. *J. Neurosci.* 28, 11328–11332. doi: 10.1523/jneurosci.0203-08.2008
- Liang, P., Kern, R., Kurtz, R., and Egelhaaf, M. (2011). Impact of visual motion adaptation on neural responses to objects and its dependence on the temporal characteristics of optic flow. *J. Neurophysiol.* 105, 1825–1834. doi: 10.1152/jn.00359.2010
- Lindemann, J. P., Kern, R., Van Hateren, J. H., Ritter, H., and Egelhaaf, M. (2005). On the computations analysing natural optic flow: quantitative model analysis of the blowfly motion vision pathway. *J. Neurosci.* 25, 6435–6448. doi: 10.1523/jneurosci.1132-05.2005
- Maddess, T., and Laughlin, S. B. (1985). Adaptation of the motion-sensitive neuron H1 is generated locally and governed by contrast frequency. *Proc. R. Soc. Lond. B Biol. Sci.* 225, 251–275. doi: 10.1098/rspb.1985.0061

- Mauss, A. S., Vlasits, A., Borst, A., and Feller, M. (2017). Visual Circuits for Direction Selectivity. *Annu. Rev. Neurosci.* 40, 211–230. doi: 10.1146/annurev-neuro-072116-031335
- Meyer, H. G., Lindemann, J. P., and Egelhaaf, M. (2011). Pattern-Dependent Response Modulations in Motion-Sensitive Visual Interneurons—A Model Study. *PLoS One* 6:e21488. doi: 10.1371/journal.pone.0021488
- Neri, P., and Laughlin, S. B. (2005). Global versus local adaptation in fly motion-sensitive neurons. *Proc. R. Soc. Lond. B Biol. Sci.* 272, 2243–2249. doi: 10.1098/rspb.2005.3191
- Nordström, K., and O'Carroll, D. C. (2009). The motion after-effect: local and global contributions to contrast sensitivity. *Proc. R. Soc. B Biol. Sci.* 276, 1545–1554. doi: 10.1098/rspb.2008.1932
- Reisenman, C., Haag, J., and Borst, A. (2003). Adaptation of response transients in fly motion vision. I. Experiments. *Vis. Res.* 43, 1291–1307.
- Rieke, F., and Rudd, M. E. (2009). The Challenges Natural Images Pose for Visual Adaptation. *Neuron* 64, 605–616. doi: 10.1016/j.neuron.2009.11.028
- Ullrich, T. W., Kern, R., and Egelhaaf, M. (2015). Influence of environmental information in natural scenes and the effects of motion adaptation on a fly motion-sensitive neuron during simulated flight. *Biol. Open* 4, 13–21. doi: 10.1242/bio.20149449
- Yang, H. H., and Clandinin, T. R. (2018). Elementary motion detection in *Drosophila*: algorithms and mechanisms. *Ann. Rev. Vis. Sci.* 4, 143–163. doi: 10.1146/annurev-vision-091517-034153

**Conflict of Interest:** The authors declare that the research was conducted in the absence of any commercial or financial relationships that could be construed as a potential conflict of interest.

**Publisher's Note:** All claims expressed in this article are solely those of the authors and do not necessarily represent those of their affiliated organizations, or those of the publisher, the editors and the reviewers. Any product that may be evaluated in this article, or claim that may be made by its manufacturer, is not guaranteed or endorsed by the publisher.

Copyright © 2021 Li, Niemeier, Kern and Egelhaaf. This is an open-access article distributed under the terms of the Creative Commons Attribution License (CC BY). The use, distribution or reproduction in other forums is permitted, provided the original author(s) and the copyright owner(s) are credited and that the original publication in this journal is cited, in accordance with accepted academic practice. No use, distribution or reproduction is permitted which does not comply with these terms.



# Sensory Adaptation in the Whisker-Mediated Tactile System: Physiology, Theory, and Function

Mehdi Adibi<sup>1,2\*</sup> and Ilan Lampl<sup>3</sup>

<sup>1</sup> Department of Physiology and Biomedicine Discovery Institute, Monash University, Clayton, VIC, Australia, <sup>2</sup> Department of Neuroscience and Padova Neuroscience Center (PNC), University of Padova, Padova, Italy, <sup>3</sup> Department of Brain Sciences, Weizmann Institute of Science, Rehovot, Israel

## OPEN ACCESS

### Edited by:

Birgitta Dresp-Langley,  
Centre National de la Recherche  
Scientifique (CNRS), France

### Reviewed by:

Luc Estebanez,  
UMR9197 Institut des Neurosciences  
Paris Saclay (Neuro-PSI), France  
Yves Boubenec,  
École Normale Supérieure, France

### \*Correspondence:

Mehdi Adibi  
mehdi.adibi@monash.edu

### Specialty section:

This article was submitted to  
Perception Science,  
a section of the journal  
Frontiers in Neuroscience

**Received:** 03 September 2021

**Accepted:** 30 September 2021

**Published:** 29 October 2021

### Citation:

Adibi M and Lampl I (2021) Sensory  
Adaptation in the Whisker-Mediated  
Tactile System: Physiology, Theory,  
and Function.  
Front. Neurosci. 15:770011.  
doi: 10.3389/fnins.2021.770011

In the natural environment, organisms are constantly exposed to a continuous stream of sensory input. The dynamics of sensory input changes with organism's behaviour and environmental context. The contextual variations may induce >100-fold change in the parameters of the stimulation that an animal experiences. Thus, it is vital for the organism to adapt to the new diet of stimulation. The response properties of neurons, in turn, dynamically adjust to the prevailing properties of sensory stimulation, a process known as "neuronal adaptation." Neuronal adaptation is a ubiquitous phenomenon across all sensory modalities and occurs at different stages of processing from periphery to cortex. In spite of the wealth of research on contextual modulation and neuronal adaptation in visual and auditory systems, the neuronal and computational basis of sensory adaptation in somatosensory system is less understood. Here, we summarise the recent finding and views about the neuronal adaptation in the rodent whisker-mediated tactile system and further summarise the functional effect of neuronal adaptation on the response dynamics and encoding efficiency of neurons at single cell and population levels along the whisker-mediated touch system in rodents. Based on direct and indirect pieces of evidence presented here, we suggest sensory adaptation provides context-dependent functional mechanisms for noise reduction in sensory processing, salience processing and deviant stimulus detection, shift between integration and coincidence detection, band-pass frequency filtering, adjusting neuronal receptive fields, enhancing neural coding and improving discriminability around adapting stimuli, energy conservation, and disambiguating encoding of principal features of tactile stimuli.

**Keywords:** rodent, whisker system, somatosensory, neuronal adaptation, noise correlation, neural coding, information theory, neural network

## 1. INTRODUCTION

In the natural environment, organisms are constantly exposed to a continuous stream of sensory input. The dynamics of sensory input changes with organism's behaviour and environmental context. The contextual variations may induce over 100-fold change in the stimulation physical parameters describing the sensory environment that an animal experiences. Thus, it is vital for the organism to adapt to the new diet of stimulation. The response properties of neurons, in turn,

dynamically adjust to the prevailing properties of sensory stimulation, a process known as “sensory adaptation.” Adaptation is a ubiquitous phenomenon across all sensory modalities and occurs at different stages of processing from periphery to cortex. The neuronal consequences of adaptation are conventionally characterised as suppression in responsiveness. However, the current view of adaptation is continuous retuning of neuronal response functions in the form of shifts or rescaling to compensate for the changes in the diet of stimulation (Fairhall et al., 2001; Dean et al., 2005; Sharpee et al., 2006; Adibi et al., 2013b). This adaptive recalibration is hypothesised to improve neural coding efficiency by changing neuronal response functions to match the statistics of the sensory environment (Barlow, 1961; Smirnakis et al., 1997; Kvale and Schreiner, 2004; Dean et al., 2005; Hosoya et al., 2005; Price et al., 2005; Nagel and Doupe, 2006; Maravall et al., 2007; Adibi et al., 2013a). The present article provides an analytic summary of current views and research findings within the last decade on sensory adaptation in the rodent whisker-mediated tactile system.

The rodent whisker system provides a suitable model system in systems neuroscience due to its functional efficiency and structural organisation (Brecht, 2007; Petersen, 2007; Feldmeyer, 2012; Feldmeyer et al., 2013; Adibi, 2019); known as nocturnal animals, rodents rely on their vibrissal sensorimotor system to garner information about their surrounding environment. Every stage of processing comprises anatomical and functional somato-topographic maps of whiskers: “barrelettes” in the brainstem nuclei, “barreloids” in the sensory thalamus ventral posteromedial nucleus (VPM), and “barrels” in the primary somatosensory cortex (S1). Behavioural studies demonstrated that rodents are able to perform texture discrimination (Carvell and Simons, 1990; von Heimendahl et al., 2007), vibration amplitude and frequency discrimination (Adibi and Arabzadeh, 2011; Morita et al., 2011; Adibi et al., 2012; Fassihi et al., 2014), object localisation (Mehta et al., 2007; O’Connor et al., 2010), gap crossing (Harris et al., 1999; Celikel and Sakmann, 2007) and aperture width discrimination (Krupa et al., 2001) tasks using their macro-vibrissae. In the whisker sensory pathway, sensory adaptation has been observed and quantified along various stages of sensory processing, from trigeminal ganglion through brainstem and sensory thalamic nuclei to somatosensory cortex. These quantifications are commonly in terms of a drop in neuronal responsiveness to sustained or repetitive whisker stimulation (Hartings et al., 2003; Khatri et al., 2004; Fraser et al., 2006; Ganmor et al., 2010; Adibi et al., 2013b; Mohar et al., 2013; Kheradpezhohu et al., 2017). However, adaptation operates in both ways. For instance, sensory adaptation enhances neuronal responses when the stimulation regime changes to a lower level of stimulation or lower adaptation. In this article, we focus on the fast/rapid neuronal adaptation to the immediate history of stimulus within the order of a few hundreds of milliseconds. We discuss key findings about the intensity-dependent properties of sensory adaptation and further summarise the effect of neuronal adaptation on response dynamics and encoding efficiency of neurons at single-cell and population levels along the whisker-mediated tactile system. Finally, we summarise the perceptual effects of adaptation, and its functional role from a cognitive and systems neuroscience point of view.

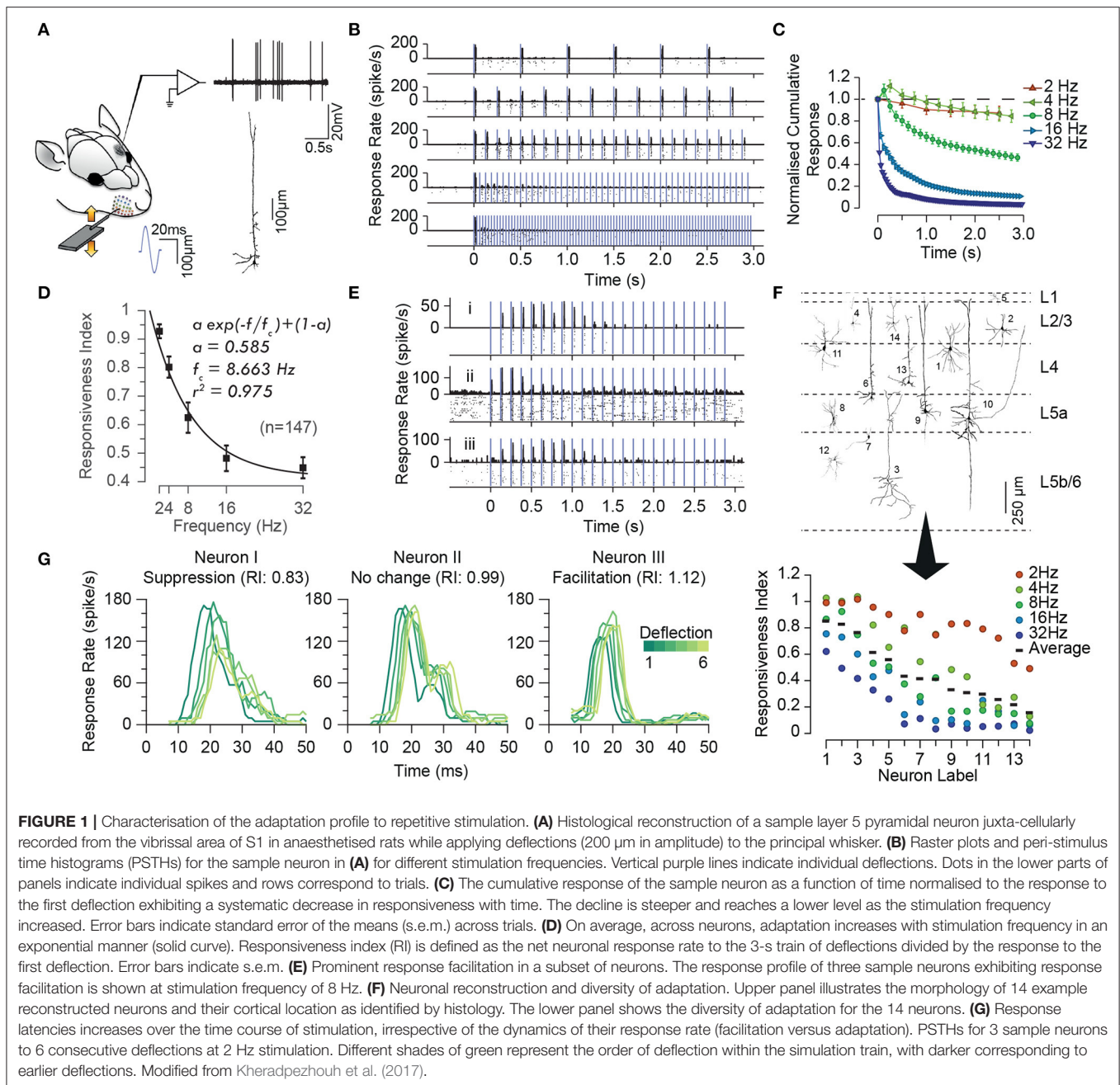
## 2. PHENOMENOLOGY OF SENSORY ADAPTATION

As in any sensory modality, neurons in the somatosensory pathway exhibit adaptation to repeated or sustained whisker stimulation. The degree of adaptation depends on the stimulation parameters such as the frequency (Ahissar et al., 2000; Khatri et al., 2004; Heiss et al., 2008; Kheradpezhohu et al., 2017, see **Figures 1A–D**), the amplitude and velocity of whisker stimulation (Ganmor et al., 2010; Adibi et al., 2013b; Mohar et al., 2013, see **Figures 2, 3**), and the cortical and behavioural states (Castro-Alamancos, 2004a; Katz et al., 2012). The most recognised characteristic of neuronal adaptation is in the form of an exponential decrease in the neuronal responses to repeated sensory stimulation with time (**Figures 1B,C**) as well as with the frequency of stimulation (**Figure 1D**, see also Hartings et al., 2003; Khatri et al., 2004; Heiss et al., 2008; Kheradpezhohu et al., 2017). However, juxta-cellular electrophysiology and labelling of neurons in the primary somatosensory cortex (Kheradpezhohu et al., 2017) revealed the diversity of adaptation profiles including facilitation and increased evoked responses over time (**Figure 1E**, also see below) and with the frequency of stimulation. This diversity was not found to be correlated with the morphology of cortical neurons or their location across cortical laminae (**Figure 1F**, also see Musall et al., 2014; Ramirez et al., 2014; Allitt et al., 2017). Interestingly, a ubiquitous effect of sensory adaptation is increased response latency with respect to the onset of each consecutive whisker stimulation (**Figure 1G**).

### 2.1. Sensory Adaptation Along the Pathway: From Periphery to Cortex

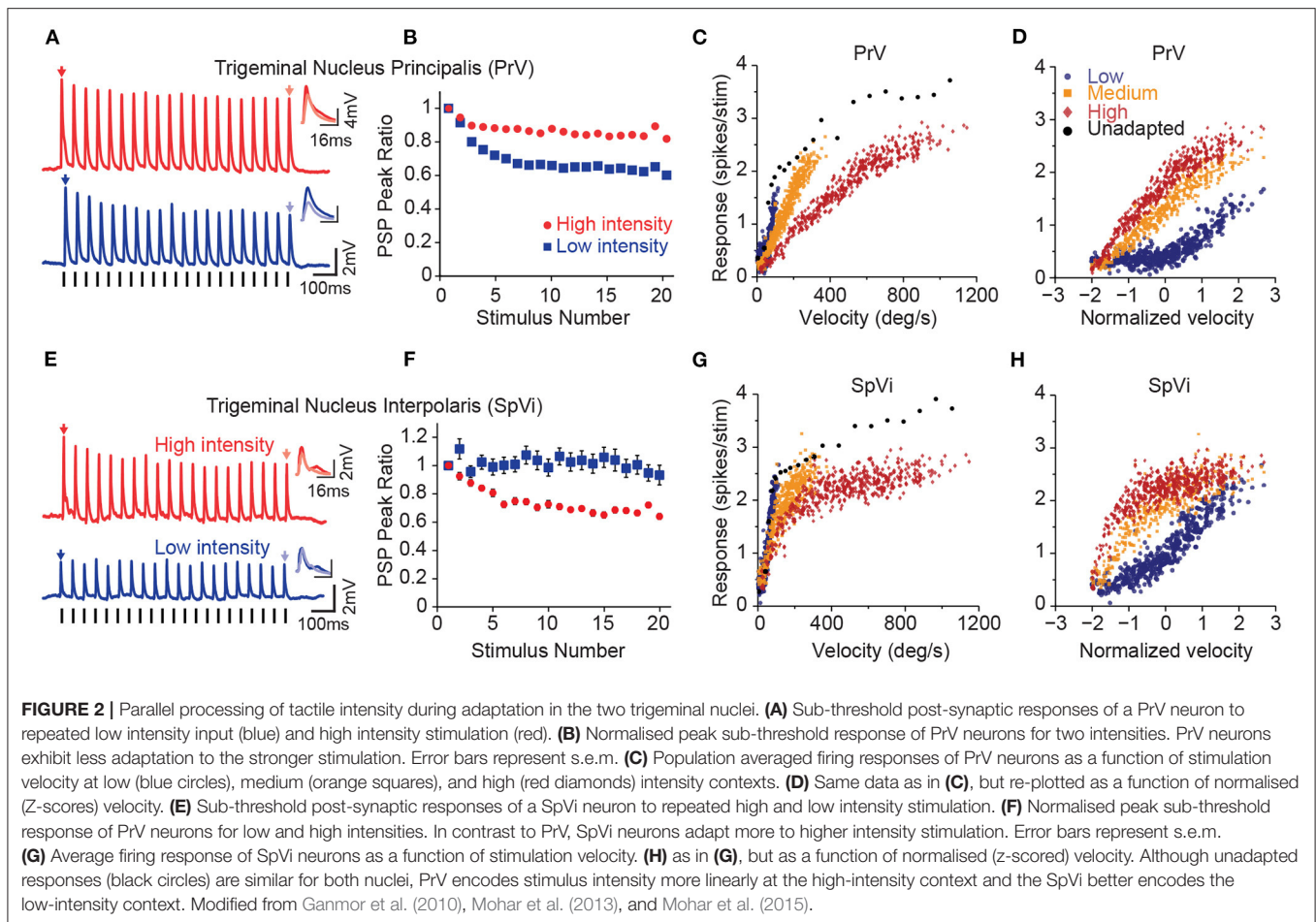
In the rodent whisker-mediated tactile system, neuronal adaptation is observed across all stages of sensory processing, from the whisker follicle through the brainstem and the thalamus to the somatosensory cortex. Vibrissae, or whiskers are the starting point of this system. The instantaneous velocity of whisker movement is one of the fundamental kinematic features of whisker-mediated sensation in both modes of sensation, the receptive (passive) mode and during whisking (active or generative mode). Whisker velocity has been shown to be related to the radial distance of stationary and moving objects during contact with whiskers (Bagdasarian et al., 2013; Lottem et al., 2015) as well as the speed of the moving object (Lottem et al., 2015). Additionally, profile of whisker velocity determines texture-specific kinetic signatures through sequence of stick-slip events—discrete high-velocity, high-acceleration whisker micro-motions—during contact with objects (Arabzadeh et al., 2005). As such, the body of the literature commonly characterises tactile stimuli in terms of the velocity of whisker movement.

The first stage of sensory processing, the trigeminal ganglion (also known as semilunar ganglion), consists of the cell bodies of pseudo-unipolar neurons with their distal axons arborising the vibrissae follicles and shaft of the mystacial whiskers as mechanosensory receptors (Vincent, 1913; Ma and Woolsey, 1984, for a review see Adibi, 2019). The proximal axons of trigeminal primary sensory neurons innervate the ipsilateral brainstem trigeminal complex



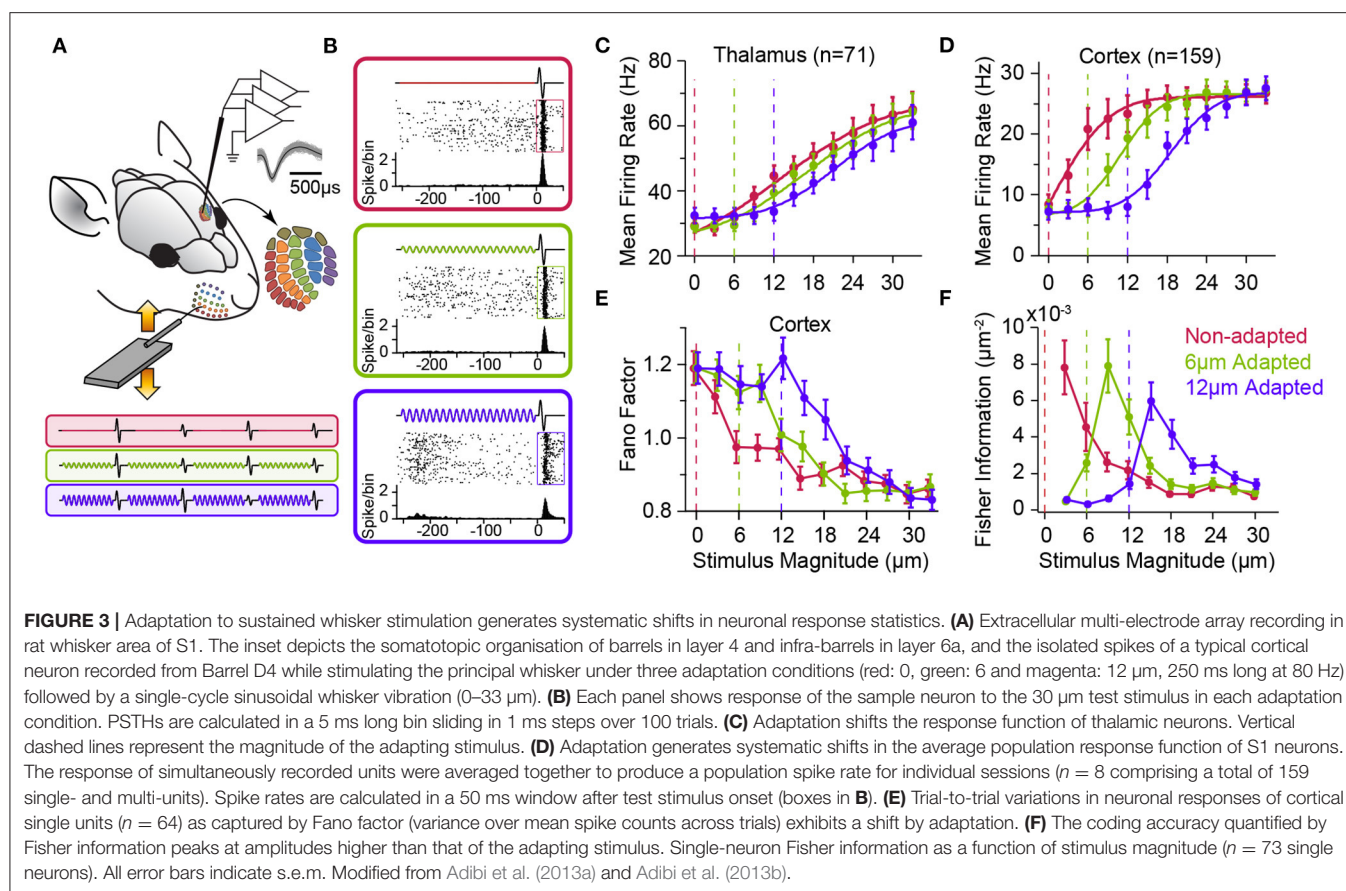
(Vincent, 1913; Ma and Woolsey, 1984). Each ganglion cell innervates only one whisker follicle (Fitzgerald, 1940; Zucker and Welker, 1969; Dykes, 1975; Gibson and Welker, 1983; Rice et al., 1986; Lichtenstein et al., 1990). Each follicle is innervated by 150–200 myelinated and around 100 unmyelinated distal axons of trigeminal ganglion neurons (Lee and Woolsey, 1975; Waite and Cragg, 1982; Renshan and Munger, 1986; Rice et al., 1986, 1997; Henderson and Jacquin, 1995). The nerve terminals and mechanoreceptors are of various types, morphologies and distributions (Melaragno and Montagna, 1953) such as Merkel cell-neurite complexes, lanceolate receptors, club-like endings,

Ruffini-like corpuscles—also referred to as reticular ending—and free nerve endings (Renshan and Munger, 1986; Rice et al., 1986; Ebara et al., 2002). Early studies classified the trigeminal ganglion neurons into slowly adapting and rapidly adapting based on their response profile within the first milliseconds to a rapid change in whisker angle. Rapidly adapting receptors do not elicit response to maintained whisker deflection, while slowly adapting receptors respond to sustained whisker deflection (Talbot et al., 1968; Kwegyir-Afful et al., 2008). The relative time interval between velocity-independent first spike latency of rapidly adapting neurons and velocity-dependent first spike latency of



slowly adapting neurons accurately and reliably encodes whisker movement velocity (Lottem et al., 2015). Whisker velocity is also encoded, although less robustly, by the firing rates of slowly adapting neurons (Shoykhet et al., 2000; Bale et al., 2013; Lottem et al., 2015). Merkel endings are the most prominent mechanoreceptors with slowly adapting characteristics (type I skin Merkel endings in mouse trunk and ring-sinus Merkel receptors in rat vibrissa follicles) (Iggo and Muir, 1969; Woodbury and Koerber, 2007; Furuta et al., 2020). Club-like, rete-ridge collar Merkel and lanceolate receptors are rapidly adapting while reticular-like type-I Ruffini endings exhibit slowly adapting characteristics (Li and Ginty, 2014; Tonomura et al., 2015; Furuta et al., 2020). Rapidly adapting ganglion cells have generally higher velocity thresholds (Zucker and Welker, 1969; Lichtenstein et al., 1990). The time course of adaptation in trigeminal ganglion neurons and mechanoreceptors is in the order of a few tens of milliseconds. In contrast to cortical (Khatri et al., 2004; Musall et al., 2014; Allitt et al., 2017; Kheradpezhough et al., 2017, see Figure 1), thalamic (Hartings et al., 2003; Khatri et al., 2004; Ganmor et al., 2010) and brainstem neurons (Mohar et al., 2013), the response of trigeminal ganglion neurons to repeated deflections at stimulation frequencies as high as 18 Hz exhibits little adaptation (Ganmor et al., 2010).

Proximal axons of the first-order trigeminal ganglion neurons innervate the two sensory nuclei in ipsilateral brainstem trigeminal complex: the principal sensory nucleus (PrV) and the spinal nucleus (SpV). The PrV and SpV interpolaris sub-nucleus (SpVi) provide the main sensory input to the thalamus forming the starting point of the two major parallel streams of somatosensory signals: the lemniscal and the paralemniscal pathways (Yu et al., 2006, for a review see Adibi, 2019). Neurons in these two sub-nuclei exhibit opposite intensity-dependent adaptation profiles to repeated deflections of the principal whisker (Figure 2); PrV neurons adapt less to higher intensity stimuli (Figures 2A,B), while neurons in SpVi exhibit increased adaptation as the intensity of deflections increases (Mohar et al., 2013, see Figures 2E,F). The intensity-dependent adaptation feature in PrV neurons is preserved at the level of VPM and cortical neurons (Ganmor et al., 2010; Mohar et al., 2013, 2015). While the neuronal mechanisms of intensity-dependent adaptation in SpVi and PrV neurons remain unknown, these findings suggest that neuronal adaptation in PrV may be due to the inter-subnuclear inhibition of PrV neurons by the SpVi (Furuta et al., 2008); as the intensity of stimulus increases, SpVi neurons adapt more causing a greater disinhibition of the PrV neurons. The disinhibition of PrV neurons to repeated



whisker deflections, in turn, decreases the level of adaptation at high-intensity stimulation regime; PrV neurons adapt less to higher intensity stimuli, while neurons in SpVi exhibit increased adaptation as the intensity of deflections increases (Mohar et al., 2013). The intensity-dependent pattern of adaptation in PrV neurons further is preserved at the level of VPM and cortical neurons (Ganmor et al., 2010; Mohar et al., 2013, 2015). Increasing the amplitude and velocity of whisker deflections does not increase the adaptation of synaptic responses in layer 4 neurons of the somatosensory cortex, but rather entails less adaptation (Ganmor et al., 2010). Importantly, previous studies (Timofeeva et al., 2004) suggested that inter-subnuclear interactions between SpVi inputs shape the receptive field size of PrV neurons. Indeed, the pattern of intensity-dependent adaptation in PrV neurons is reversed when the adjacent whisker is stimulated. That is, increasing the intensity of stimulation entails less adaptation when stimulation intensity increases.

Although the two trigeminal nuclei encode the intensity of whisker stimuli in a similar manner under non-adapted condition (Figures 2C,G), adaptation introduces distinct changes in the coding behaviour of these two nuclei (Mohar et al., 2015). Under adaptation, PrV neurons better encode the fluctuations of the stimulus at high intensity regimes (Figures 2C,D), whereas SpVi neurons better encode weak tactile stimuli (Figures 2G,H). A similar pattern was also

observed at the level of the subthreshold synaptic potentials (Mohar et al., 2015). As the neuronal adaptation linearises the response function of PrV neurons at high-intensity stimulation regime, it linearises the response function of SpVi neurons at low-intensity stimulation regime. Thus, the two parallel routes of stimulus intensity processing through PrV and SpVi together enhance the overall coding of stimulus intensity for a broader stimulation range. These findings suggest that neurons belonging to these two brainstem trigeminal nuclei may encode the intensity of stimulation together in a context-dependent manner untangling the coding ambiguity associated with response adaptation in different stimulation contexts.

Along the pathway from periphery to cortex, adaptation exhibits stronger effect on neuronal responses. Peripheral trigeminal ganglion neurons exhibit less adaptation than neurons in the principal nucleus of the brainstem trigeminal complex (PrV). Sensory thalamic neurons in the VPM, in turn, exhibit a higher level of adaptation than neurons in trigeminal complex, and less adaptation compared to cortical neurons (Khatri et al., 2004; Ganmor et al., 2010, also see Figures 3C,D). As mentioned earlier, the degree of adaptation depends on the frequency of whisker stimulation (Ahissar et al., 2000; Khatri et al., 2004; Heiss et al., 2008; Kheradpezhrouh et al., 2017; Latimer et al., 2019), the amplitude and velocity of deflections (Ganmor et al., 2010; Adibi et al., 2013b; Mohar et al., 2013), and the cortical state

(Castro-Alamancos, 2004a; Katz et al., 2012). The response of the neurons decreases to consecutive individual whisker deflections with an exponential decay (**Figure 1C**). As the stimulation frequency increases, neurons adapt stronger and at a faster rate (Khatri et al., 2004; Kheradpezhohu et al., 2017, also see **Figure 1D**). A significant subset of cortical neurons exhibit response facilitation over the course of repetitive stimulation at frequencies of 4–10 Hz (Brecht and Sakmann, 2002; Garabedian et al., 2003; Derdikman et al., 2006; Kheradpezhohu et al., 2017, see **Figure 1E**). The facilitation is then followed by a reduced responsiveness to further subsequent deflections (Kheradpezhohu et al., 2017). Similar facilitation effects are reported in response to repetitive optogenetic excitation of layer 6 corticothalamic neurons where the evoked response in layer 5a pyramidal neurons as well as fast-spiking inter-neurons in both layer 4 and 5a increased due to activation of facilitating synapses (Kim et al., 2014). Prolonged optogenetic activation of layer 6 corticothalamic neurons resulted in a hyper-polarisation of VPM neurons followed by depolarisation, shifting the mode of sensory responses from bursting to single-spike (Mease et al., 2014). Subsequently, VPM neurons exhibit reduced adaptation to 8 Hz repetitive whisker deflections during prolonged optogenetic stimulation of layer 6 neurons. This suggests corticothalamic feedback shapes both the gain and the temporal profile of sensory processing in cortex by controlling the gating of sensory information in VPM. Post-adaptation response facilitation was observed to stimulation at a few hundred milliseconds after the adapting repetitive stimulation in approximately a third of cortical neurons (Malina et al., 2013). Thalamic neurons, on the other hand, do not exhibit post-adaptation response facilitation revealing that facilitation does not emerge from thalamic neurons. Recordings at different holding currents revealed this facilitation is a result of a faster recovery of excitation compared to inhibition. Adaptation also is shown to decrease cross-whisker suppression, similar to the reduction in surround suppression in visual system (Higley and Contreras, 2006; Ramirez et al., 2014).

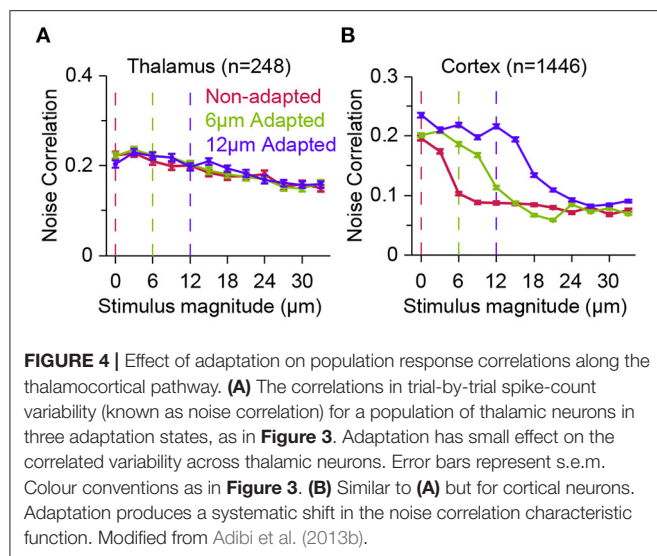
Early electrophysiology studies revealed that on average, neuronal responses from layers 2/3 and 5a exhibit stronger adaptation than cortical layers 4 and 5b (main lemniscal input layers) neurons (Ahissar et al., 2001; Derdikman et al., 2006). These findings are consistent with stronger adaptation in the posterior medial (POm) thalamus than in VPM (Diamond et al., 1992; Sosnik et al., 2001). In a detailed study of adaptation to sequences of stick-slip events across cortical laminae, Allitt et al. (2017) found stronger adaptation in supra-granular layers compared to layers 4 and 5. Lower layer 3 showed rates of adaptation that lie between that of layers 2/upper 3 and layers 4/5. Despite strong responses to high-speed protraction (at 654°/s) resulting in suppressed responses to the initial stick-slip event in the sequence, across all laminae, the rate of adaptation vs. frequency did not change with the speed of protraction (654°/s vs. 32.7°/s). However, layer 2 neurons represent initial texture-defining stick-slip events with temporal fidelity and relatively high firing rates irrespective of protraction speed, and only exhibit adaptation to the subsequent repetitive stick-slip stimuli, and not to the strong evoked responses by fast whisker protraction. Interestingly, stick-slip stimuli in Allitt et al. (2017)

drive weaker rates of adaptation at stimulation frequencies as high as 34 Hz compared to pulsatile whisker deflections at similar range of frequencies which disrupt texture encoding reported in previous studies (Ahissar et al., 2001; Chung et al., 2002; Khatri et al., 2004).

In the somatosensory cortex, both response latency and response peak time (to repeated whisker deflections) show a consistent increase over time with consecutive stimulations, irrespective of the direction and amount of the change in response rate (facilitation and suppression, as shown in **Figure 1G**, Allitt et al., 2017; Kheradpezhohu et al., 2017). This delayed response trend was also observed for neurons exhibiting little adaptation as well as those neurons exhibiting either decreased or increased responsiveness with repetitive stimulation. At stimulation frequencies >30 Hz, a large increase in latency from the 1st to 2nd stimulus was observed, followed by a decrease in response latency to a relative steady-state latency longer than that to the 1st stimulus and shorter than that for the 2nd stimulus (Allitt et al., 2017). These findings indicate that the context-dependent changes in the evoked response latency is governed by additional mechanisms than those underlying decrease or increase in the responsiveness.

## 2.2. Effect of Adaptation on Neuronal Response Characteristic Functions

As shown in **Figure 2**, adaptation exhibits differential effects depending on the intensity, frequency and potentially other physical parameters of sensory stimulation (also see Katz et al., 2006; Ganmor et al., 2010; Lampl and Katz, 2017; Katz and Lampl, 2021). Thus, it is important to characterise adaptation effects across a range of stimulus intensities. Using multi-electrode extracellular electrophysiology in anaesthetised rats (**Figure 3A**), Adibi et al. (2013b) quantified how neuronal adaptation modifies the input-output response function of neurons as a function of the whisker deflection intensity (amplitude). The neuronal input-output functions (also known as neurometric functions) typically exhibit an increase in the mean neuronal responses with stimulus amplitude (**Figures 3B–D**), along with decreased trial-by-trial variability (in terms of Fano factor, **Figure 3E**). Adibi et al. (2013b) delivered sustained sinusoidal vibrations at various amplitudes to whiskers to induce different levels of sensory adaptation, and then quantified the neuronal input-output function under each level of adaptation (**Figures 3A,B**). The findings revealed adaptation induces a rightward shift in the neuronal characteristic response functions (both the mean and variability against stimulus amplitude, **Figure 3**). The magnitude of the shift in neuronal responses depends on the magnitude of adapting stimulus; adaptation shifted the threshold of neuronal responses (the lowest stimulus intensity to which the evoked response is significantly higher than baseline activity) to stimulation amplitudes above that of adapting stimulus (**Figures 3C,D**). While adaptation shifts the neuronal characteristic functions (response rate and variability), it maintains the relationship between the two across different adaptation states. This was confirmed by a regression analysis between the response



variability and mean (Adibi et al., 2013b). Thus, adaptation transfers the operating point of neurons to lower rates with higher variability. It is worth to note that the lateral shift in response function lowers overall responsiveness (spike counts averaged across the whole stimulus range) which in turn, suggests a lower metabolic cost. Consequently, the coding accuracy (in terms of Fisher Information) peaks at amplitudes above the adapting stimulus (**Figure 3F**, see also Adibi et al., 2013a). Sensory adaptation produces systematic rightward shifts in the stimulus region with elevated coding efficiency consistent with the shift in the evoked neuronal response thresholds to amplitudes higher than that of the adapting stimulus (Adibi et al., 2013b).

## 2.3. Effect of Adaptation on the Network: Signal and Noise Correlations

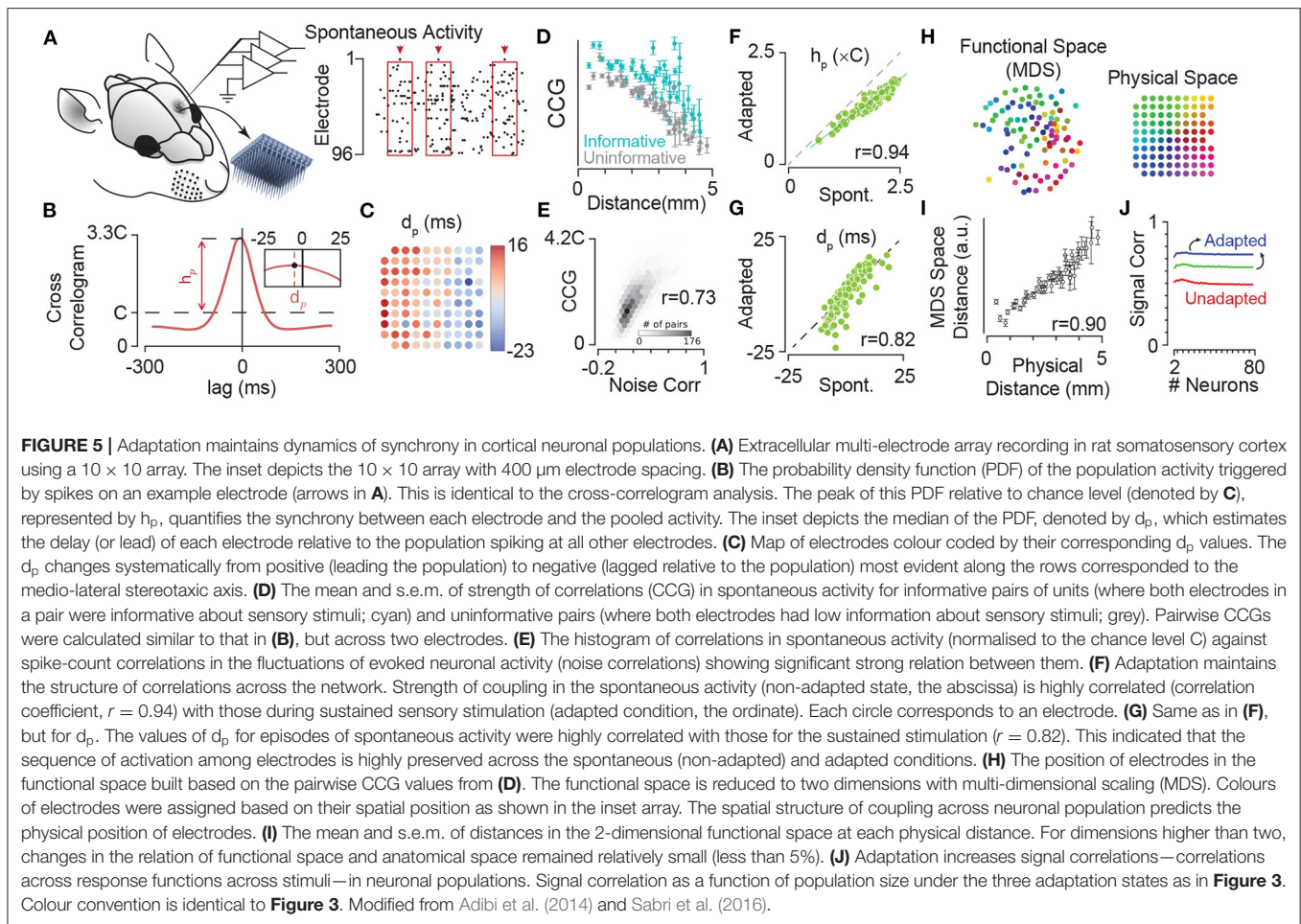
Shared neural variability is a ubiquitous phenomenon in neural networks. Conventionally, neuronal activity has been characterised by the average and variance of responses over multiple trials. However, single neuron statistics do not capture the stochastic and dynamic characteristics of a neural network. Correlated fluctuations across neurons—known as noise correlations—are one of the central bases of the recent theories of neural computation (Pouget et al., 2013). These correlations are shown to affect the information content of population activity in the cortex (Averbeck et al., 2006; Adibi et al., 2013a,b). Previous electrophysiology studies indicated sensory stimulation decorrelates the population responses in somatosensory cortex (Middleton et al., 2012; Adibi et al., 2013b). Similar stimulus-driven decorrelation was observed in the primary visual cortex of primates (Kohn and Smith, 2005), middle temporal (MT) cortex (Ponce-Alvarez et al., 2013) and anterior superior temporal sulcus of macaque monkeys (Oram, 2011). Sensory adaptation shifts the profile of noise correlations in cortex along the stimulus amplitude axis similar to the shift in the other response statistics including mean and variability of responses (**Figures 3, 4**). These parallel shifts

result in maintaining the relationship between noise correlations and the mean firing rate across different states of adaptation (Adibi et al., 2013b). Thus, the net effect of sensory adaptation in the cortex is to decrease the overall neuronal response rate across the stimuli while increasing the total variability as well as correlations in variability (noise correlation) across neurons in the cortex.

In contrast, at the upstream sensory stage to somatosensory cortex, in VPM, while thalamic neurons exhibit adaptation in form of a shift in the neurometric curves (**Figure 3C**), the noise correlation does not show visible difference across stimuli and adaptation states (**Figure 4A**). This was the case, even though the firing rate of thalamic neurons, on average, increased over two-fold from about 30 Hz at spontaneous level to 60 Hz with increasing the stimulus amplitude. In contrast, on average, a less than 25 Hz change in the response of cortical neurons to stimulation was accompanied by a halved level of noise correlations in the somatosensory cortex (**Figure 4B**).

By extracellular electrophysiology using a 10×10 electrode array from the somatosensory cortex (**Figures 5A,B**), Sabri et al. (2016) showed that neurons have a specific sequence of activation with respect to the population which is anatomically organised (**Figure 5C**). Additionally, the strength of pairwise correlations in the ongoing spontaneous activity of neuronal clusters decreases with the distance between the electrodes (**Figure 5D**), consistent with similar findings in other cortical areas (Smith and Kohn, 2008; Rothschild et al., 2010; Solomon et al., 2015). Correlations, on average, are stronger for units that better encode the sensory stimuli (**Figure 5D**), and predict the correlations in the evoked response fluctuations to sensory stimuli (i.e., noise correlations, **Figure 5E**) as well as signal correlations (see Sabri et al., 2016). The strength of correlations in spontaneous state (i.e., non-adapted) and adapted state (during sustained sensory stimulation) were highly correlated (**Figures 5F,G**, also see Sabri et al., 2016), indicating that neuronal adaptation maintains the spatiotemporal dynamics of population activity within the cortical networks; the functional connectivity map based on these correlations resembles the two-dimensional anatomical organisation of electrode locations (**Figures 5H,I**), and maintains its organisation across states of adaptation. Similarly, our unpublished data indicates neuronal adaptation maintains the spatial organisation of synchrony in the cortex as captured by the phase coupling of field potential oscillations (data not shown).

The shifts in the neuronal response functions by sensory adaptation cause an increased signal correlation (**Figure 5J**); sensory adaptation reduces the level of network heterogeneity by shifting the response function of neurons, aligning their responsive range with respect to the adaptor. Similar homeostatic effect of adaptation has been reported in the primary visual cortex of anaesthetised cats (Benucci et al., 2013). Benucci et al. (2013) observed that adaptation to a given orientation maintained the equality in responsiveness and the independence in orientation selectivity across the population.



## 2.4. Adaptation and Readout of Population Activity

How do the adaptation-induced shifts in characteristic functions (mean, variability and noise correlations) affect the efficiency of *readout* mechanisms of neuronal activity in downstream areas? A biologically plausible and efficient yet simple readout mechanism of the neuronal responses is a linear combination of the neuronal responses in a downstream neuron (decoder, see **Figure 6A**). The coefficients of the linear combination identify the synaptic weights between the neurons, and may be optimised to maximise the flow of sensory information or the decoder's discrimination performance (**Figure 6B**). The optimum weights depend on the amount of information each individual upstream neuron carries about the sensory stimuli (**Figure 6C**) and the structure of response co-variabilities across the population of downstream neurons (Adibi et al., 2014). This optimal linear readout determines an upper boundary of coding efficiency using the linear integration framework. Adibi et al. (2014) optimised the readout in two manners: (i) the pairwise-optimal readout scheme where for any pair of stimuli, the linear combination weights were optimised to maximise discriminability. And (ii) the groupwise-optimal readout scheme where an identical set of

weights were optimised to maximise the discrimination across all stimuli. The discriminability of neuronal responses under pairwise-optimal readout provides an upper bound for the performance of the groupwise-optimal readout. The groupwise-optimal readout approaches its upper bound when the neuronal responses to sensory stimuli are linearly correlated. This is equivalent to a maximal level of signal correlation in the population responses. In order to apply the appropriate set of weights, the pairwise-optimal readout scheme requires *a priori* knowledge about the pair of stimuli to be discriminated. Thus, the groupwise-optimal readout is arguably a more biologically plausible scheme.

Adibi et al. (2014) found that for either readout scheme, adaptation enhances the discriminability for stimuli higher in amplitude than the adaptor, while there is a decline in discriminability if both stimuli are lower than the adaptor (**Figure 6D**). The magnitude of the effect was larger for the groupwise-optimal readout compared to the pairwise-optimal readout. These findings represent a shift in discriminability from low amplitudes to amplitudes higher than the adapting stimulus, consistent with the observed rightward shift in the neuronal response functions in **Figure 3D**. Additionally,

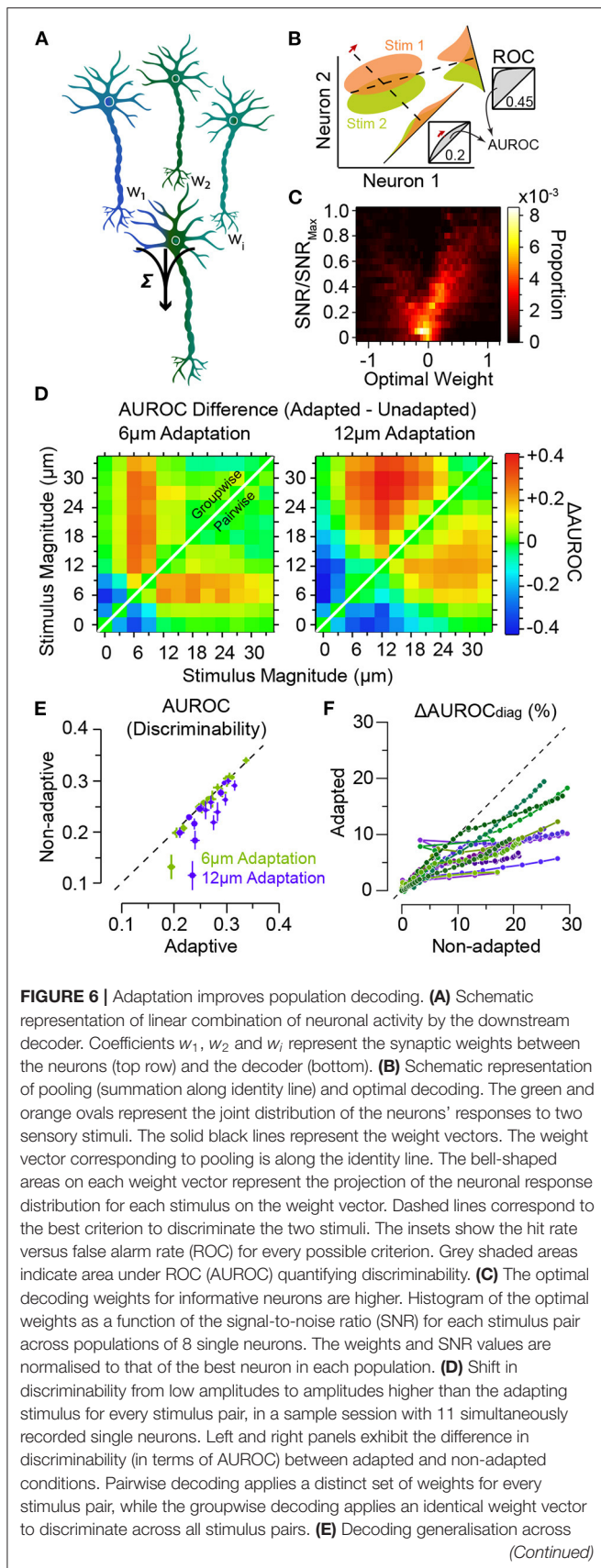


**FIGURE 6 |** adaptation states. The abscissa indicates the discriminability for the adaptive optimal decoder when optimised on half of the adapted responses and tested on the other half. The ordinate corresponds to discriminability for the non-adaptive optimal decoder when optimised on the non-adapted responses and tested on the adapted responses. Error bars indicate s.e.m. **(F)** The per cent drop in discriminability when ignoring noise correlations, denoted by  $\Delta\text{AUROC}_{\text{diag}}$ , for adaptation states, against the same measure in the non-adapted state. While noise correlations are higher in adapted states, the effect of ignoring these noise correlations under adaptation states is less compared to non-adapted state. Modified from Adibi et al. (2014).

adaptation increases the number of stimulus pairs with enhanced discriminability based on population responses (shades of red in **Figure 6D**).

As a result of the shifts in neuronal responses (**Figure 3**), the optimal readout weights which maximise discriminability between a pair of stimuli in the non-adapted state are expected to maximise discriminability between a new pair of stimuli that are in effect simply shifted by the adapting stimulus intensity. This predicts a high level of generalisation of the optimal readout across different states of adaptation. Adibi et al. (2014) verified this by quantifying the discriminability obtained from a non-adaptive readout—which its weights were optimised in the non-adapted state—relative to an adaptive readout—which its weights were optimised under the adaptation state. The results revealed that on average, the non-adaptive readout discriminability was 97 and 90% of that of the adaptive readout, for the 6  $\mu\text{m}$  and 12  $\mu\text{m}$  adaptation states, respectively (**Figure 6E**), indicating a markedly high level of generalisation of the optimal readout across different states of adaptation.

Noise correlations have been shown to depend on the stimulus features such as intensity-dependence in the somatosensory system (Adibi et al., 2013b) as well as in other sensory systems (Kohn and Smith, 2005; Oram, 2011; Middleton et al., 2012; Ponce-Alvarez et al., 2013). This suggests that instantaneous or short-term correlation structures may potentially provide an additional channel of information for sensory processing. The optimal linear readout scheme provides a framework for studying the effect of noise correlations on the efficiency of sensory processing in different adaptation conditions. Adibi et al. (2014) showed that neuronal adaptation increases signal (see **Figure 5J**) and noise correlations in population responses. By increasing signal and noise correlations, adaptation increases the redundancy of population responses. This adaptation-induced redundancy, can potentially limit the capacity of the cortical network to encode sensory information. The increased redundancy, in turn, may enhance the accuracy with which population responses represent sensory stimuli on trial-by-trial basis. The effect of noise correlation on information encoding/decoding depends on the direction of noise correlation (in the multi-dimensional space of joint population activity) relative to the direction of signal (Averbeck et al., 2006; Adibi et al., 2013b). In the non-adapted condition, noise correlations improve the accuracy of encoding/decoding for some populations and in some other populations, they were

detrimental to population coding (Adibi et al., 2014). Similar opposing effects of noise correlation were observed in awake animals performing a texture discrimination task (Safaai et al., 2013). The differential effects of noise correlation can be attributed to the heterogeneity of neuronal populations; in a heterogeneous population, different neurons may exhibit a variety of signal directions in their responses relative to noise. This leads to opposing effects of noise correlation in the non-adapted state. In the adapted state, however, with decreased level of heterogeneity (**Figure 5J**), the population responses are more homogenised, showing less diversity in their direction of signal relative to noise. This leads to entirely detrimental effect of noise correlations in the adapted states (Adibi et al., 2014). Compatible with this scenario, it has been observed that noise correlations under sensory adaptation were always detrimental to information encoding/decoding (Adibi et al., 2014). The magnitude of the effect of noise correlations was greater in adapted states than non-adapted condition.

Based on these results, one might predict that ignoring noise correlations would be more detrimental to the performance of the readout under adaptation. On the contrary, ignoring noise correlations in the readout by taking into account only the diagonal elements of the pairwise neuronal response covariance matrix (denoted by subscript “diag” in **Figure 6F**) was less detrimental under adaptation compared to the non-adapted state. This discrepancy can be explained in terms of a greater increase in signal correlations relative to noise correlations under adaptation (Adibi et al., 2014).

### 3. NEURONAL MECHANISMS UNDERLYING SENSORY ADAPTATION IN SOMATOSENSORY CORTEX

A potential neuronal mechanism for adaptation is based on normalisation models (Heeger, 1991, 1992): the net activity of a population of neighbouring neurons increases the input conductance of the excitatory synapses, and hence results in the division of the activity of the neuron by the pool activity of the network, or shunting inhibition. Prolonged stimulation leads to a steady network activity and hence a stable input conductance. The key assumption then is that the changes of the synaptic conductance have a time constant; after prolonged stimulation, this reduced input conductance does not abruptly return to its initial state, but to a transient state for a few hundreds of milliseconds. This model is consistent with the electrophysiological findings in cat and monkey striate visual cortex and magnocellular cells in monkey LGN under contrast adaptation: a lateral shift in response function along the logarithmic contrast axis (Ohzawa et al., 1982, 1985; Sclar et al., 1989; Solomon et al., 2004), and has psychophysical correlates in human (Pestilli et al., 2007). However, the rightward shift along the stimulus amplitude axis (as in **Figure 3D**) is difficult to interpret in terms of a pure normalisation model. Moreover, the normalisation model cannot explain the decreased responsiveness along with the shifts illustrated in the response function of neurons in cat visual cortex and auditory nerve

and inferior colliculus (Albrecht et al., 1984; Durant et al., 2007; Wen et al., 2009). An alternative mechanism is based on a tonic hyper-polarisation (Carandini et al., 1997) mainly due to decreased excitatory inputs (DeBruyn and Bonds, 1986; Vidyasagar, 1990; McLean and Palmer, 1996; Carandini et al., 1997), which is consistent with depression of synaptic excitation with repetitive electrical intracellular micro-stimulation of rat primary visual cortex neurons (Abbott et al., 1997). A general model consisting of these two mechanisms has been proposed for contrast adaptation in V1 neurons (Dhruv et al., 2011). Synaptic mechanisms, such as enhancement of inhibition (Dealy and Tolhurst, 1974) and depression of excitatory synapses (Finlayson and Cynader, 1995; Chance et al., 1998; Adorján et al., 1999; Carandini et al., 2002; Chung et al., 2002; Freeman et al., 2002; Wehr and Zador, 2005; Stevenson et al., 2010) have also been proposed as mechanisms underlying adaptation. *In vivo* experiments, however, demonstrated that suppression of inhibition by blockage of GABA<sub>A</sub> receptors did not block sensory adaptation (DeBruyn and Bonds, 1986; Nelson, 1991).

In the rat whisker-mediated tactile system, based on current views of sensory adaptation, this phenomenon is mainly a result of short-term thalamocortical synaptic depression (Chung et al., 2002; Castro-Alamancos, 2004b; Khatri et al., 2004; Higley and Contreras, 2006; Heiss et al., 2008). Whisker-specific adaptation at the level of cortex (Katz et al., 2006) supports this mechanism. Assuming that tactile adaptation results mostly from short-term depression of thalamocortical synapses give rise to a number of predictions. One prediction is that increasing the intensity of stimulation, which is followed by higher presynaptic firing probability, results in greater depression during sustained sensory stimulation due to depletion of synaptic resources and the relatively slower recovery processes. This prediction, however, is in contrast to the observed intensity-dependent profile of sensory adaptation along the lemniscal pathway (Ganmor et al., 2010, also see Lampl and Katz, 2017). Ganmor et al. (2010) found that increasing the amplitude and velocity of whisker deflection does not increase the adaptation of synaptic responses in layer 4 neurons in the primary somatosensory cortex, but rather entailed less adaptation. In a series of electrophysiology recordings along the entire lemniscal pathway and first order ganglion neurons, this study showed that the source for this unexpected profile of adaptation—reduced degree of adaptation with increased intensity of stimulation—lies in PrV neurons of the trigeminal complex in the brainstem. Another body of literature, implicates adaptation of the thalamic spike timing (Wang et al., 2010b; Whitmire et al., 2016; Wright et al., 2021), suggesting that cortical adaptation is mainly a result of reduced bursting and adaptive changes of evoked synchronous spikes in the VPM. Recent studies indicate that the strength of synaptic connections between individual thalamic and cortical neurons is insufficient to evoke action potentials in cortical neurons. Instead, the cortex is driven by synchronous activity of thalamic populations (Bruno and Sakmann, 2006; Zucca et al., 2019). This suggests that the level of synchrony across thalamic neurons is a mechanism in regulating the flow of information to the cortex. Optogenetic elevation of the baseline activity in VPM is shown that does not adapt cortical neurons,

and moderate level of sustained sensory stimulation has little effect on the response of cortical neurons to direct photo-stimulation of thalamocortical terminals in the cortex (Wright et al., 2021), suggesting little contribution of thalamocortical synaptic depression to sensory adaptation in the cortex in low and intermediate adaptation regimes. Further experiments are required to characterise the role of upstream structures such as thalamic sensory nuclei (Hartings et al., 2003; Khatri et al., 2004; Ganmor et al., 2010; Wang et al., 2010b), the laminar structure of the cortex (Allitt et al., 2017), intra-barrel and cross-barrel cortical circuitry (Katz et al., 2006) and the balance between excitatory and inhibitory connections (Higley and Contreras, 2006; Heiss et al., 2008; Malina et al., 2013) on sensory adaptation in the somatosensory system.

#### 4. ADAPTATION AND CODING EFFICIENCY: AN INFORMATION THEORETIC PERSPECTIVE

One of the current views of neuronal adaptation is that it is a mechanism by which neuronal responses adjust to the contextual changes in the environment in order to maintain the efficiency of neural codes. The efficiency can be quantified in relation to a given utility function (e.g., maximising discriminability or the rate of information) or a cost function (e.g., minimising the energy to transfer certain amount of information, or minimising the variance of estimation error).

##### 4.1. Fisher Information

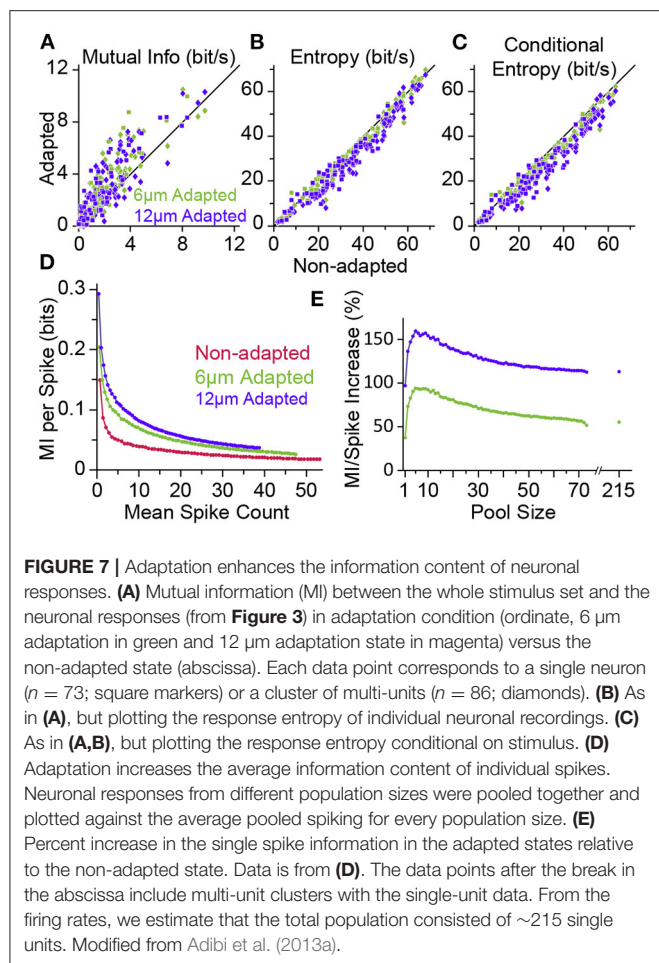
Fisher information (Fisher, 1922) is a well-known measure of coding accuracy that quantifies the amount of information that the neuronal responses carry about the sensory stimulus upon which the distribution of the neuronal responses depends. This measure has been used to characterise the effect of neuronal adaptation on the efficiency of coding in visual, auditory and somatosensory systems (Dean et al., 2005; Durant et al., 2007; Gutnisky and Dragoi, 2008; Adibi et al., 2013a). Adaptation can be considered as the procedure of matching the neuronal responses based on the distribution of the stimulus—a procedure known as ‘equalisation’ (Laughlin, 1981; Nadal and Parga, 1994)—in order to maintain the efficiency (or optimality) of neuronal code. For the biological case where the neuronal response variance is stimulus dependent (Churchland et al., 2010; Adibi et al., 2013b), the optimality will be obtained when the square root of the Fisher information function is equal to the distribution of the stimulus. Thus, the peak of Fisher information function should be aligned with the most frequent stimulus in the environment. This is compatible with the Linsker’s infomax principle (Linsker, 1988; van Hateren, 1992) and is equivalent to Barlow’s redundancy reduction principle (Barlow, 1961, 2001; Atick, 1992; Redlich, 1993).

In vision, neuronal adaptation is shown to maintain the efficiency of the neuronal responses by scaling the response function of neurons with changes in the variance of input (Brenner et al., 2000), or by shifting the neuronal response functions with changes in the mean of input distribution.

These adjustments have been reported in contrast adaptation in visual system (Ohzawa et al., 1982, 1985; Sclar et al., 1989; Solomon et al., 2004) and in sound level adaptation in auditory system (Dean et al., 2005) resulting in enhanced accuracy around the adapting (most frequent) stimulus (Dean et al., 2005; Durant et al., 2007). In somatosensory cortex, however, the shift in the coding accuracy to stimulus amplitudes above the adapting stimulus (Figure 3F) is not exactly consistent with the notion of equalisation or information maximisation. Equalisation predicts the peak of Fisher information aligns with the most frequent stimulus (here adapting stimulus). However, the Fisher information profile peaks at above adapting stimulus intensities (Figure 3F). As a result, neuronal adaptation filters out the most frequent features of the stimulus, and in turn, aligns the most sensitive portion of response curve (equivalent to peak of the Fisher information) to amplitudes above adapting stimulus. This potentially reflects a balance between homeostatic regulation of metabolic energy costs of spikes and maintenance of information content of neuronal responses, and in turn, tunes the network to the critical point of deviant detection. In the realm of whisker-mediated tactile world, for rodents, the most frequent stimuli may constitute the ambient noise in the surrounding environment, while behaviourally *significant* stimuli are those above the most frequent stimulus region. Adaptation can be considered as a mechanism to shift or scale the neuronal functions to maintain their accuracy for significant stimulus region by equalisation with respect to a “significance” function instead of the stimulus probability distribution function. In visual and auditory systems, however, adaptation tunes the neuronal responses to maintain the acuity for frequent stimuli. The more frequent stimuli, in these modalities, may be considered to constitute functionally or behaviourally significant stimuli.

##### 4.2. Shannon Information

The transformation of physical attributes of the sensory environment into spiking activity is analogous to the concept of an “encoder” in the framework of coding theory in the realm of communications. In this framework, the neuronal computation is analogous to either that of the “source coding” or “channel coding.” An efficient source code is the one that maximises its entropy according to the distribution of sensory input. It is equivalent to minimising the redundancy in the neural code. Channel coding, on the other hand, adds patterns of redundancy in the transmitted signal to reduce the decoding error rate at the receiver over transmission through an erroneous channel. In an information theoretic framework, Adibi et al. (2013a,b) showed the amount of information in the neuronal responses about the amplitude of the sensory stimuli (in terms of the mutual information between the neuronal response and stimulus amplitude) increases with adaptation, hence enhancing coding efficiency (Figure 7A). This leads to the prediction that the sensory cortex may act as an adaptive entropy maximiser that increases the entropy of its codes (spike rate) (Attneave, 1954; Barlow, 1961; Srinivasan et al., 1982; Atick, 1992) similar to an optimum source coder in the realm of communications (Shannon, 1948). To identify



the source of adaptation-induced enhancement in coding efficiency, Adibi et al. (2013a) decomposed the information content of neuronal responses (in terms of mutual information between neuronal responses and sensory stimuli) into its two fundamental components: the entropy of neuronal responses and the conditional response entropy given stimulus. Adaptation decreases the response entropy (**Figure 7B**) and the conditional response entropy (**Figure 7C**) at both the level of single neurons and the pooled activity of neuronal populations. The net effect of adaptation is to increase the mutual information between stimulus and neuronal responses. The information transmitted by a single spike also increases under adaptation, even when the overall rate of activity is matched across non-adapted and adaptation states (see **Figure 7D**).

The adaptation-induced increase in the information content of neuronal responses can be explained by a higher number of stimulus pairs for which adaptation increases Shannon information (and also discriminability) than the number of stimulus pairs (at amplitudes lower than adapting stimulus) of which adaptation reduces Shannon information (and discriminability) (**Figure 6D**, also see Adibi et al., 2013b). This lead to the net increase in the mutual information between neuronal responses and sensory stimuli and is consistent with the rightward shift in the Fisher information (**Figure 3F**).

## 5. FUNCTIONAL ROLES OF SENSORY ADAPTATION

In light of the recent findings and studies on the phenomenology and physiology of sensory adaptation summarised in the previous sections, here, we present a number of (potential) functions of neuronal adaptation in the whisker-mediated somatosensory system, some of which proposed in other sensory systems as well.

### 5.1. Noise Reduction

Sensory adaptation desensitises the tactile sensory system during exposure to sustained or continuous stimulation. After some time, we tend to not notice ongoing sensory stimulation such as the scratching of a shirt on our body. At the perceptual level, the perceived intensity of tactile stimuli exponentially decreases over time during adaptation (Berglund and Berglund, 1970). The response of sensory neurons also exhibit similar exponential reduction trend at multiple stages of sensory processing (Hartings et al., 2003; Khatri et al., 2004; Musall et al., 2014; Allitt et al., 2017; Kheradpezhough et al., 2017; Lampl and Katz, 2017). Consistently, as mentioned earlier, sensory stimuli with lower intensity than that of the adapting stimulus evoke little neuronal responses in the somatosensory cortex and thalamus (Adibi et al., 2013b, see also **Figure 3**). This reduced neuronal responsiveness to prevailing sensory stimuli, hence, provides a noise reduction mechanism to filter ambient stimuli at neuronal and cognitive levels.

### 5.2. Energy Conservation by Lowering Metabolic Costs

The fundamental basis of neural communication and brain function is through action potentials that neurons generate in order to transfer information to other neurons. The cost of a single action potential is high, with a net cost of  $\sim 2.4 \times 10^9$  ATP molecules per action potential (Lennie, 2003). The fraction of energy consumption in neocortex associated with neural signalling is estimated to be 52% of total energy expenditure (Attwell and Laughlin, 2001; Lennie, 2003). This severely limits the number of action potentials that neuronal populations may persistently generate in response to sustained or repeated sensory stimuli in the environment. In the somatosensory cortex, adaptation improves neural coding efficiency at a reduced metabolic cost associated with spiking, due to a net decrease in neuronal responses (Adibi et al., 2013b, also see **Figures 1B**, **3D**). Similarly, in the primary visual cortex, adaptation equalises population responses to stimulus orientations with different statistics, maintaining the overall rate of spiking averaged over time (Benucci et al., 2013).

### 5.3. Salience Processing and Deviance Detection

Survival in a dynamic and changing environment requires animals to detect unexpected sensory cues that signal necessary commodities (e.g., food and water), mates or danger from ambient sensory stimuli. For an urban rat searching for food in a dimly lit street, the tactile vibrations travelling through the asphalt from the movement of an approaching dog or car

provide accurate estimate of the distance from the impending danger. Namib Desert golden moles process seismic sensory signals to detect prey (Narins et al., 1997). An animal, hence, should efficiently and quickly identify salient stimuli from the continuous stream of sensory signals in changing environments and react with appropriate behavioural responses. In tactile, behaviourally relevant events are potentially those with a higher intensity/acceleration compared with the prevailing sensory stimuli. This is particularly true for the generative mode of the whisker-mediated sensory system where interactions with textures and objects produce changes in the whisker trajectory beyond the baseline whisking action (Adibi, 2019). Sensory adaptation serves as a neuronal mechanism for salient stimulus detection by adjusting the sensitive region of the neuronal response functions to stimulus intensities above the background level (Adibi et al., 2013b; Musall et al., 2014, also see **Figures 3 and 9**).

#### 5.4. Efficient Neural Coding and Improved Discrimination Around Adapting Stimulus

In the natural environment, the prevailing diet of sensory stimuli varies over time. An efficient neural code adaptively matches the limited discriminative range of neuronal responses according to the distribution of sensory stimuli (Barlow and Földiák, 1989). This constitutes scaling the discriminative region of neuronal responses according to the variance of sensory stimuli (variance adaptation), as well as shifting the most discriminative point of the neuronal responses to the most frequent sensory stimulus (mean adaptation). Previous studies observed that variance adaptation maintains the information content of neuronal responses (Maravall et al., 2007, 2013). As for the mean adaptation, at the neuronal level, adaptation enhances discriminability of neuronal responses to stimuli around the adapting stimulus (**Figure 6D**, also see Adibi et al., 2014). We predict that the enhanced neuronal discrimination improves perceptual discrimination performances. Similar improved perceptual effects have been observed in humans for vibrotactile amplitude (Goble and Hollins, 1993) and frequency (Goble and Hollins, 1994) discrimination. In animal literature, improved performance was observed in rats performing a spatial whisker discrimination task (**Figures 10E–H**, also see Ollerenshaw et al., 2014). Future studies are required to investigate the effect of adaptation on perceptual discriminability.

#### 5.5. Band-Pass Frequency Filtering Properties

During repetitive stimulation, adaptation leads to higher neuronal responsiveness at some frequencies than other frequencies, and therefore exhibiting frequency-filtering properties. Using different frequencies of whisker stimulation, Kheradpezhrouh et al. (2017) observed that the net evoked response of over 90% of cortical neurons was at stimulation frequencies other than the maximum frequency (see also **Figure 1**). This constitutes a low- and band-pass frequency filtering property of sensory adaptation. However, thalamic neurons show more high-pass frequency response properties

to sinusoidal stimulation at frequencies up to 40 Hz (Hartings et al., 2003). This could arise from lower spiking responses to sinusoidal stimuli at lower frequencies and hence at lower mean speed (Arabzadeh et al., 2003). A small yet significant subset of cortical neurons exhibit response facilitation (see **Figure 1E**) which is equivalent to high-pass filtering. Consistent with the diversity among cortical neurons in their frequency response profile (Allitt et al., 2017; Kheradpezhrouh et al., 2017), at synaptic level, also diverse filtering properties have been identified across neurons (Anwar et al., 2017). During synaptic plasticity, facilitating synapses serve as high-pass filters as they are stronger at high pre-synaptic spiking frequencies, while depressing synapses serve as low-pass filters as they are stronger at low pre-synaptic spiking frequencies.

A misconception in the literature is to consider adaptation as a high-pass filter due to its slow adaptive process (for instance see Benda, 2021). Based on this view, high-frequency stimulus components that change on time scales faster than the adaptation processes are transmitted with a higher gain than lower frequency components. The flaw in this interpretation is that a slow filter in the time domain—which is characterised by a long impulse response—is assumed to be a low-pass filter in the frequency domain. However, there are no direct links between the time domain characterisation of a filter (slow or fast) and its frequency-domain characterisations (in terms of the passband frequency range of the filter). In fact, the frequency passband of a slow filter (with long impulse response function) and a fast filter (with short impulse response function) can be around any frequency. Hence, irrespective of the length of impulse response function (slow vs. fast), a filter may exhibit various low-pass, band-pass or high-pass properties.

#### 5.6. Shift Between Integration and Coincidence Detection

Neurons conventionally are considered as coincidence detector or integrators depending on the time interval over which they accumulate and integrate input spikes (Abeles, 1982; König et al., 1996; Kisley and Gerstein, 1999). These modes of operation determine the way neural networks encode information; as rate coding scheme, or temporal coding scheme. Neuronal adaptation can be considered as a potential mechanism to shift the operating mode of the neuronal networks in a continuum between the two extreme modes of coincidence detector and temporal integrator. This can be implicated at the circuit level through different degrees of suppressive adaptation in either integrator or coincidence detector neurons within a neuronal population, or at single cell level through mechanisms of short term synaptic plasticity (Díaz-Quesada et al., 2014; Anwar et al., 2017) or through subthreshold adaptation modulation of the slope of the membrane potential (Kisley and Gerstein, 1999). Cortical layer 4 neurons including spiny stellate neurons which receive major thalamic input in barrel cortex have short integration intervals of a few milliseconds (Egger et al., 1999; Bruno, 2011; Adibi, 2019) and are driven by weak but synchronous thalamocortical input (Roy and Alloway, 2001; Bruno and Sakmann, 2006; Wang et al., 2010a,b). Varani et al. (2021) recently found that selective

optogenetic inhibition of layer 4 neurons decreases sub-threshold responses to whisker deflections in the preferred direction of layer 2/3 neurons, while it increases responses to deflections in the non-preferred direction, leading to a change in the direction tuning. This allows a broader integration of signals in these neurons. During adaptation, thalamo-cortical synapses in layer 4 exhibit short-term depression (Chung et al., 2002; Lundstrom et al., 2010; Díaz-Quesada et al., 2014), potentially moving the operation point of cortical circuits from coincidence detection of thalamic inputs toward integration of inter-laminar and cortico-cortical inputs in layer 2/3 or infragranular neurons (for instance, see Jordan and Keller, 2020). Consistently, our unpublished data indicates that circumventing the sensory input to layer 4 neurons through direct optogenetic stimulation of layer 2/3 pyramidal neurons results in little adaptation in neuronal responses across cortical layers in the primary somatosensory cortex of mice.

### 5.7. Disambiguating Principal Features of Vibrotactile Sensation: Frequency and Amplitude

Previous electrophysiological studies revealed that neurons in the primary somatosensory cortex of rats encode vibrotactile stimuli in terms of the mean speed of whisker movement (Arabzadeh et al., 2003, 2004). The mean speed is equivalent to the product of the two fundamental features of vibrotactile stimuli: frequency and amplitude. While an increase in either feature increases the activity of cortical neurons, no measure of neuronal response (firing rates or temporal patterns) explicitly encodes one principal feature independently of another. This representation forms the basis of whisker-mediated tactile sensation in awake rats as well (Adibi et al., 2012). Consequently, two distinct stimuli with identical products of their frequency and amplitude are indistinguishable based on cortical neuronal responses as well as at the perceptual level. Stimulus dependent properties of neuronal adaptation (Ganmor et al., 2010; Adibi et al., 2013b; Mohar et al., 2013, 2015) potentially provides a neuronal mechanism to disambiguate encoding of the principal features of tactile stimuli from one another. Increases in the frequency and amplitude of stimulation has differential effects on the adaptation profile of neuronal responses. Thalamic and cortical neurons exhibit a higher level of response depression with increases in the frequency of stimulation (Kheradpezhrouh et al., 2017). On the contrary, increased amplitude of stimulation results in lower level of adaptation (Ganmor et al., 2010; Mohar et al., 2013, 2015).

### 5.8. Parallel Processing of Stimulus Intensity

Adaptation alters the representation of external stimuli in a context-dependent manner, introducing response ambiguity. That is, an identical stimulus may evoke different responses depending on the context of stimulation, or conversely, different stimuli may evoke an identical response as context shifts. Under adaptation, PrV neurons better encode the fluctuations of the stimulus intensity when the intensity of stimuli is high, whereas neurons in the SpVi better encode weak tactile stimuli (Mohar et al., 2013, 2015). Together, the two nuclei provide and improve

the overall coding of stimulus intensity at different stimulation intensity regimes (Mohar et al., 2015). The differential stimulus-dependent adaptation properties in the two parallel pathways of tactile system, the lemniscal and paralemniscal pathways, hence, may help in reducing the inherent ambiguity of neural coding of stimulus features in different adaptation conditions.

### 5.9. Adjusting Neuronal Receptive Fields

Majority of cortical neurons across different layers of whisker area of the somatosensory cortex exhibit multi-whisker receptive fields (Simons, 1978; Armstrong-James and Fox, 1987; Moore and Nelson, 1998; Ghazanfar and Nicolelis, 1999; Brecht and Sakmann, 2002; Brecht et al., 2003). Various spatial properties of receptive fields including the principal whisker, size, response latency and centre of mass in majority of cortical neurons exhibit stimulus-dependent changes (Le Cam et al., 2011). Furthermore, feature encoding properties of cortical neurons changes with the level of spatial correlation in multi-whisker sensory stimuli (Estebanez et al., 2012). Analogously, temporal multi-whisker stimulation patterns (see **Figure 8**) through whisker-specific adaptation mechanisms in cortical neurons (Katz et al., 2006; Ramirez et al., 2014) can potentially adjust the receptive field properties of neurons during different modes of behaviour in the environment; while sustained stimulation of principal whisker reduces the responsiveness to that specific whisker, this adaptation does not transfer to adjacent whiskers (Katz et al., 2006). This specificity, thus, maintains the responsiveness to stimulation of adjacent whiskers. Consequently, in the adapted state, stimulation of adjacent whiskers evokes a higher level of response relative to adapted responses to principal whisker stimulation. These results in a broader spatial extent of functional receptive field compared to the non-adapted state. Consistently, Ramirez et al. (2014) showed that while surround inputs in the non-adapted state are suppressive, as previously reported in the literature (Simons, 1985; Simons and Carvell, 1989; Brumberg et al., 1996), under adaptation, they are facilitatory and enhance the evoked responses to deflections of the corresponding principal whisker at the level of sub-threshold (**Figures 8B–D**) and spiking activity (**Figure 8F**). The adaptation-induced facilitation was stronger in layer 4, 5, and 6 neurons (**Figure 8G**). Conversely, adaptation by stimulation of all whiskers causes narrowing of the receptive fields (Katz et al., 2006; Ramirez et al., 2014). Adaptation also has been shown to affect multi-whisker integration of tactile stimuli (**Figure 8E**); integration of unadapted sub-threshold neuronal responses (in terms of PSPs) and spiking activity to preferred multi-whisker stimuli were highly sub-linear (Mirabella et al., 2001; Ramirez et al., 2014). However, when presented in a background of multi-whisker stimulation (adapted state), multi-whisker integration of responses were more linear (Ramirez et al., 2014). Consistently, Ego-Stengel et al. (2005) found that when principal and adjacent whiskers were simulated together at 0.5Hz, 59% of cortical neurons exhibit significant suppressive interactions, whereas response facilitation was found in only 6% of neurons. In contrast, at 8 Hz, a significant supra-linear summation was observed in 19% of the cells, with stronger effect along an arc compared to along a row. Such dynamic

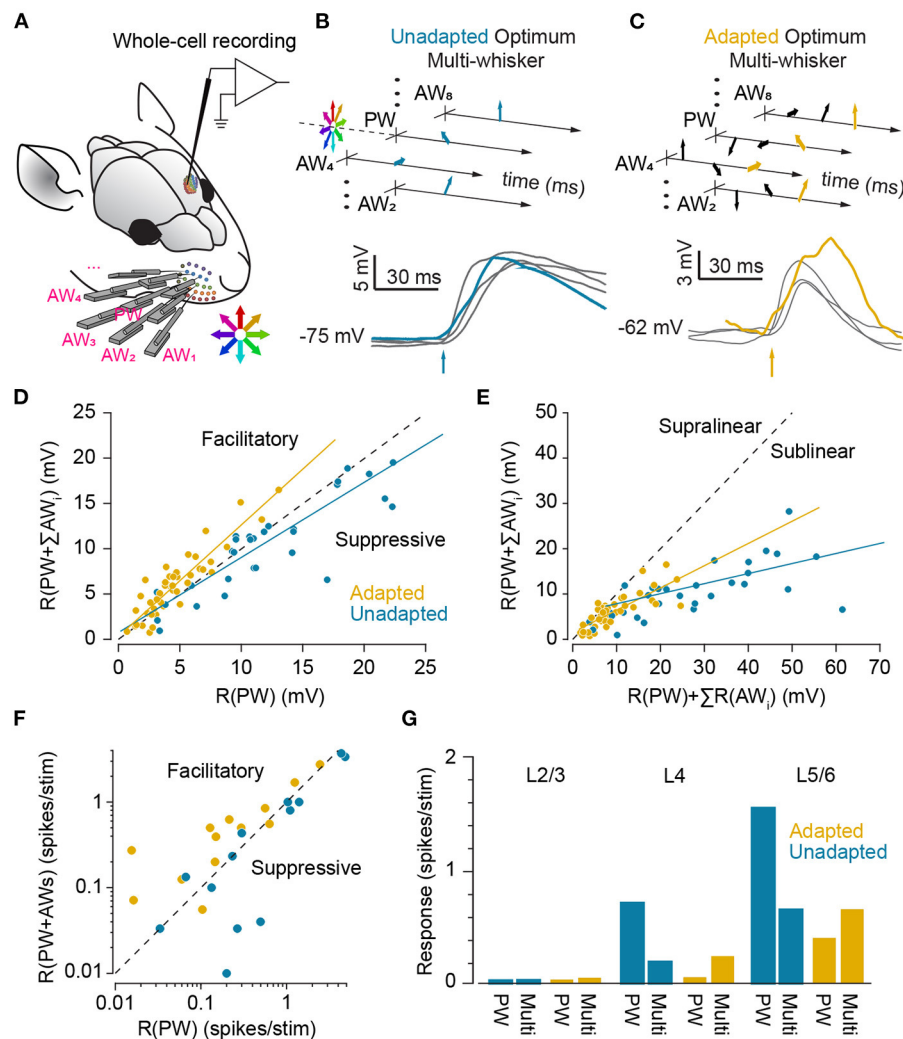


**FIGURE 8 |** Adaptation enhances summation of synaptic inputs and allows surround stimuli to facilitate responses. **(A)** Cortical neurons in the vibrissa area of S1 were recorded intra-cellularly during complex multi-whisker stimulation to nine whiskers. The principal whisker (PW) and each of the eight adjacent whiskers (AW) were stimulated with high-velocity deflections of fixed temporal structure (5-ms rise and 5-ms decay) in arbitrary angles. Deflections occurred stochastically in time and direction at a frequency of  $\sim 9.1$  Hz. The inset represents whisker directions in an eight angle-binned space. **(B)** The multi-whisker stimulus that evokes the maximum synaptic responses of a neuron to each of the nine whiskers,  $R(PW)$  or  $R(AW_i)$  are shown in black. The arrow indicates stimulus onset. The response to the multi-whisker stimuli,  $R(PW + \Sigma AW_i)$ , is shown in cyan (unadapted). **(C)** As in **(B)**, but the multi-whisker stimulus was embedded within random surround stimuli (adapted, amber). **(D)** Response to the multi-whisker stimuli,  $R(PW + \Sigma AW_i)$ , is plotted against the responses to principal whisker deflection,  $R(PW)$ . Surround inputs facilitated the PW response during adaptation by a factor of  $1.28 \pm 0.43$  ( $n = 36$ ,  $p < 10^{-9}$ , sign test), but suppressed activity in unadapted neurons by a factor of  $0.893 \pm 0.269$  ( $n = 33$ ,  $p = 0.36$ , sign test). **(E)** Data from **(D)**, but plotting response to the multi-whisker stimuli,  $R(PW + \Sigma AW_i)$ , against the sum of responses to individual deflections,  $R(PW) + \Sigma R(AW_i)$ . Multi-whisker summation was closer to linear during adaptation (amber, slope = 0.491,  $r = 0.631$ ,  $p < 10^{-7}$ ) compared to highly sublinear summation in unadapted condition (cyan, slope = 0.223,  $r = 0.442$ ,  $p < 10^{-9}$ ). **(F)** As in **(D)**, but for the spiking activity of neurons (13 out of  $n = 33$ ) that fired spikes in both conditions. Adaptation significantly facilitated spiking by a factor of  $1.78 \pm 1.04$  ( $p = 0.02$ ). In unadapted condition, responses were weakly suppressed or were not facilitated ( $0.85 \pm 0.3$ ,  $p = 0.30$ , sign test). **(G)** Same as **(F)**, but separated for layer 2 and 3 (L2/3), L4, and L5/6 neurons. The PW stimulation alone is the most effective driver of spiking activity in unadapted neurons in L4 and 5/6, but optimal multi-whisker stimuli were more effective under adaptation. Spiking activity in L2/3 remained sparse. Modified from Ramirez et al. (2014).

changes in the receptive fields could be a potential neuronal basis of invariant coding in whisker system. For instance, it might help to locate the position of whisker contact with respect to the head or the body instead of whiskers (for instance see Curtis and Kleinfeld, 2009). This position invariant information can potentially give rise to whisker-mediated coordination, and

contribute to spatio-topic representations such as those in grid cells in the entorhinal cortex (Hafting et al., 2005) or head-direction cells in classic Papez circuit (Taube, 1998). Further experiments in awake and anaesthetised animals are required to understand adaptive changes in the multi-whisker receptive field of cortical neurons and their functional role. The adaptive

adjustment of receptive fields forms the spatial dual of the adaptive shift between integration and coincidence detection modes in the time domain.

## 6. LINK TO PERCEPTION

Contextual modulations and adaptation are fundamental attributes of perceptual processing. Perceptual consequences of sensory adaptation have been commonly characterised in terms of repulsive after-effects. For instance, sustained exposure to lines at one orientation causes perceptual repulsion of the orientation of a subsequently viewed line, a phenomenon known as tilt after-effect (Gibson, 1933) with analogous repulsive effect observed in touch (Silver, 1969). Contextual effects of prolonged or repeated stimulation have been the subject of distinctly fewer studies in the tactile domain (Craig, 1993) while these effects are extensively studied in the visual system. The perceptual effects of sensory adaptation, and in particular whisker-mediated tactile system are still unknown, and limited to a few studies in the field. This is partly due to experimental challenges in training animals to withhold any action for the duration of adapting stimulus and further to isolate potential confounding effects of adapting stimuli on directly driving the behaviour. For a proportion of trials, animals may be distracted by the adapting stimulus. This, in turn, confounds measures of behaviour such as discrimination performance of the animals in a given sensory discrimination task. A solution to these challenges is to apply behavioural paradigms in which the adapting stimulus constitutes one of the stimuli based on which the animal makes perceptual judgements. For instance, in a discrimination task, one of the discriminanda could be the adapting stimulus. An example is a deviance or difference detection task in which the animals should detect a deviant stimulus in a repeated train of whisker deflections. The deviant stimulus could be a deviance in the location of the deflection (a different whisker), or in any physical feature of the stimulus including amplitude, duration or instantaneous frequency (inter-stimulus interval).

Using a similar behavioural approach, Musall et al. (2014) found rats performing a detection (**Figure 9A**) or frequency discrimination task (**Figure 9E**) exhibited reduced performance to detect or discriminate sequence of peripheral whisker stimulations compared to when the neuronal responses to subsequent stimuli were not adapted—using intensity-matched photo-stimulation, see **Figures 9B,C**—as shown in **Figures 9D,G**. Conversely, an optogenetic pattern of stimulation that mimicked sensory adaptation in cortical neurons replicated the whisker stimulation discrimination and detection performances (**Figures 9F,G**). Adaptation, however, enhanced the accuracy of rats detecting deviant whisker stimuli embedded within a series of whisker deflections at a lower amplitude (**Figures 9H–J**). This finding reveals that adaptation enhances perception of deviant stimuli with higher amplitudes than the prevailing stimuli while reducing the acuity under steady states of adaptation.

In another study, using a combination of single-whisker detection task and a two-whisker spatial discrimination

behavioural task (**Figures 10A,E**), Ollerenshaw et al. (2014) showed that sensory adaptation improves spatial discriminability of stimulation of either whisker in behaving animals at the expense of reduced detectability of whisker stimulation (**Figure 10B** vs. **Figure 10F**). These results are consistent with the performance of an ideal observer of neuronal activity from voltage sensitive dye (VSD) imaging of the somatosensory cortex in anaesthetised rats (**Figure 10**, Ollerenshaw et al., 2014); the non-adapted neuronal responses to deflection of each whisker were spatially wide-spread with significant spatial overlap (**Figure 10C** and inset in **Figure 10E**), while the adapted responses were spatially constrained with decreased spatial overlap (**Figures 10C,G**, also see Zheng et al., 2015). Accordingly, similar to behavioural results, while adaptation decreases the detection performance of the ideal observer of neuronal responses (**Figure 10D**), it enhances its discrimination performance (**Figure 10H**). These findings demonstrate a trade-off between detectability (detecting the presence or absence of stimulus) and spatial discriminability (distinguishing stimulus location) up to a moderate level of adaptation which is compatible with the frequency range of natural whisking. For higher levels of adaptation, however, suppression of neuronal responses causes decreased detectability and discriminability.

In contrast to vibration sensation (Hill, 2001), evidence that wild rodents use their vibrissae to distinguish tactile textures including roughness of surfaces in the natural world is yet to be found. In the laboratory environment, when trained, rats and mice are capable of distinguishing textures such as rough vs. smooth surfaces using their micro- and macro-vibrissae (Carvell and Simons, 1990; von Heimendahl et al., 2007), even by a single whisker (Park et al., 2020). The accuracy with which rats and mice distinguish textures is comparable to that of primate fingertips (Carvell and Simons, 1990). Tactile texture sensation requires the active mode of sensation when an animal's whiskers palpate an object/texture during exploratory whisking. The temporal profile of whisker stick-slip events is hypothesised to determine signatures of tactile textures (Arabzadeh et al., 2005) and forms the basis of whisker-mediated texture perception (Wolfe et al., 2008; Isett et al., 2018). High-speed whisker tracking during texture discrimination (Zuo and Diamond, 2019) revealed texture-informative whisker kinetics could be represented by three features respectively related to shape, motion, and angle of whisker during contact. These kinematic features account for the amount of evidence in each whisker touch and correlate with neuronal activity in the primary and secondary somatosensory cortices (Zuo and Diamond, 2019). Interestingly, an exponentially-decreasing weighted integration of sequential touches fits well the behavioural choices compared to a uniform integration or a recency model in which the most recent touch is weighted more. A similar exponentially-decreasing weighted integration of neuronal activity of the primary and secondary somatosensory cortical neurons with similar time constant as that of the whisker kinematic features accounts for behaviour (Zuo and Diamond, 2019). The exponentially-decreasing form of integration could potentially represent the perceptual weight of neuronal activity as they adapt and shape perception. As

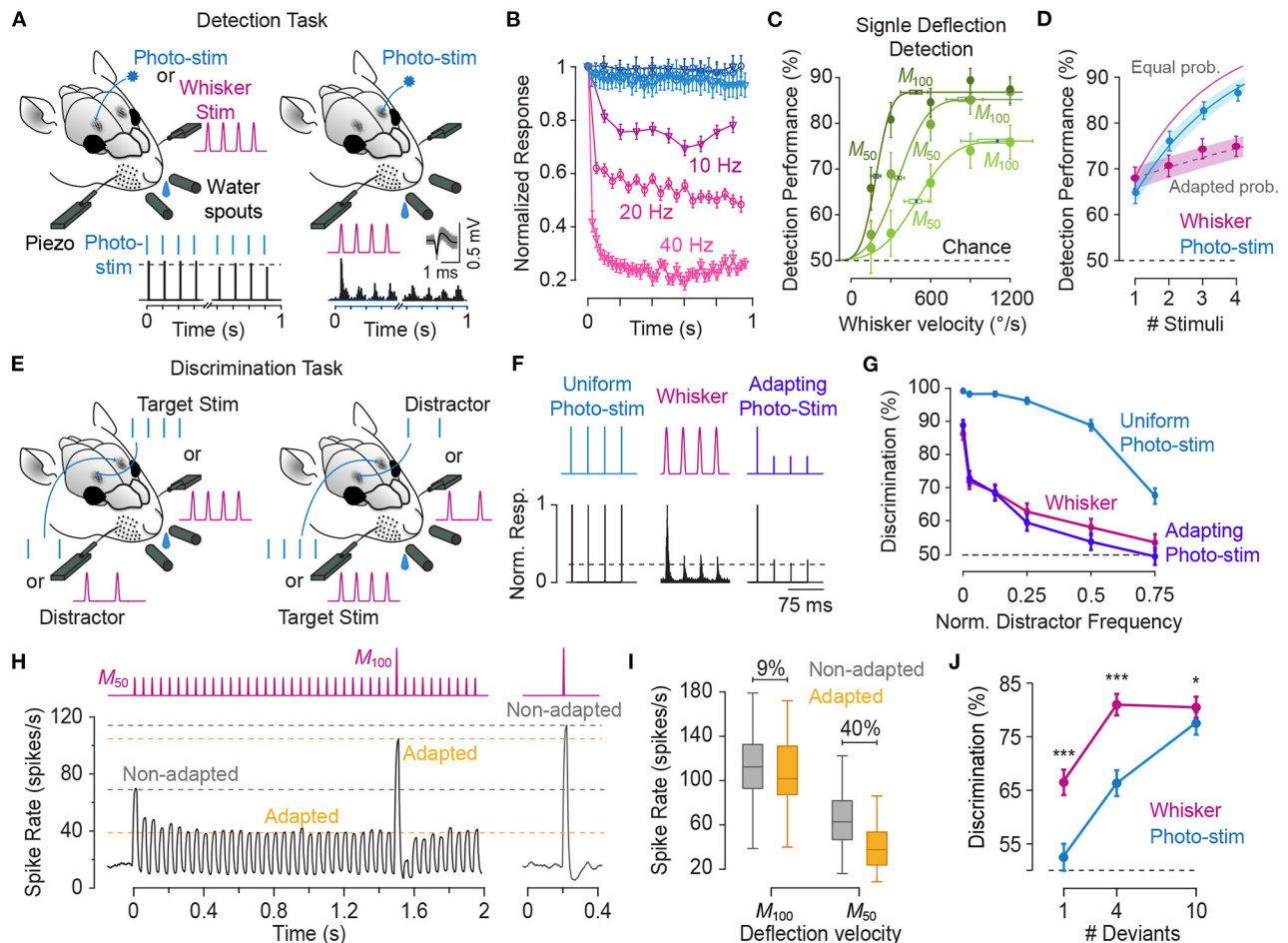
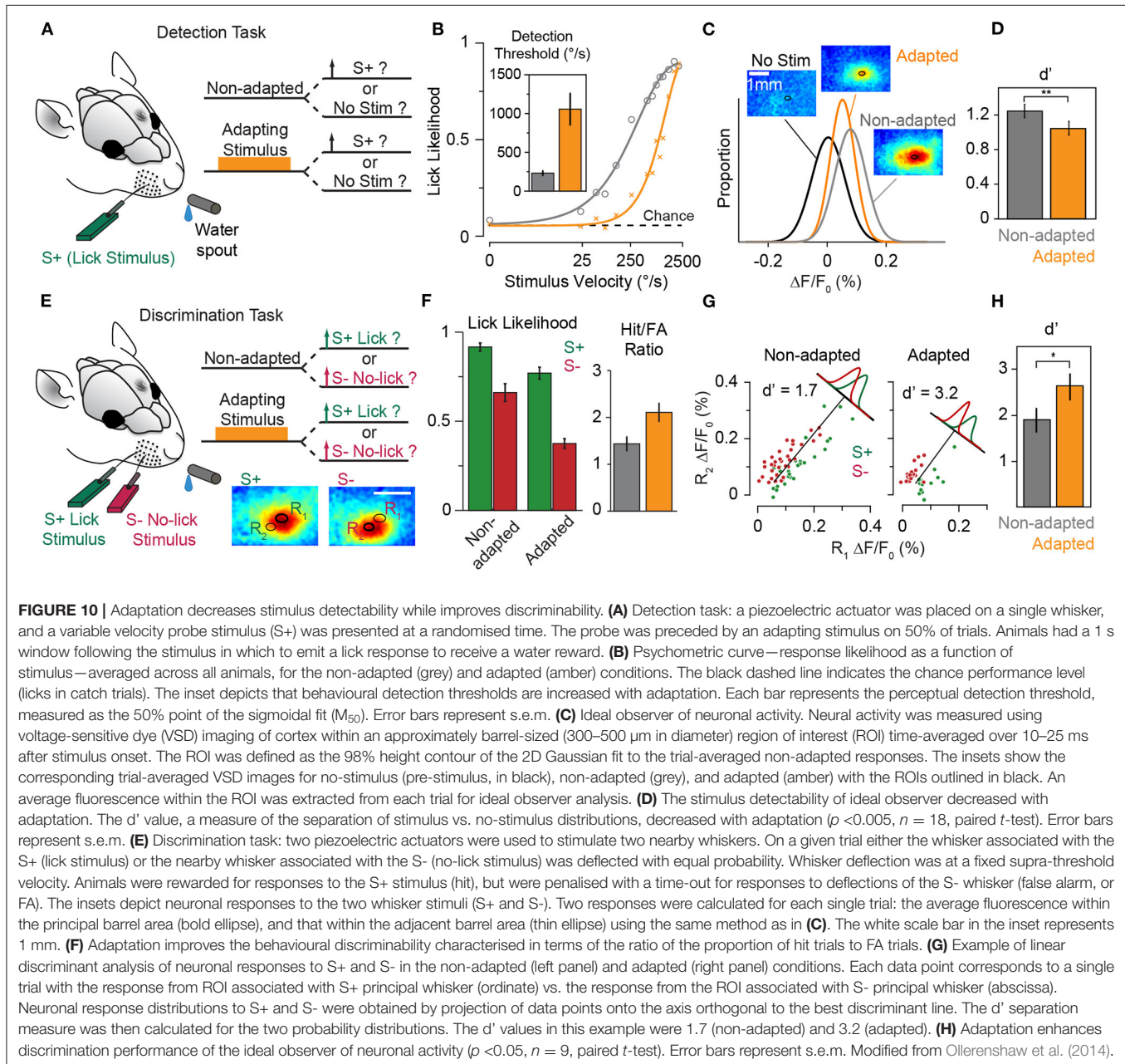


**FIGURE 9 |** Circumventing cortical adaptation enhances detection and frequency discrimination, while adaptation improves deviant detection. **(A)** Detection task: in a 2-alternative choice task, rats were trained to detect stimulus that applied to either the left or the right C1 whisker or its barrel column. A reward was given if the animal responded correctly by licking at one of two water spouts on the side associated with the stimulus side. Whisker stimuli (red) consisted of individual or uniform sequences of pulses (single-cycle 120-Hz sine-wave). Photo-stimuli (blue) consisted of individual or sequence of 1-ms square-wave pulses. Insets show extracellular recording from two neurons to 40-Hz photo-stimulation (left) and stimulation of the principal whisker (right). PSTHs with spike rates normalised to the initial response. **(B)** Normalised response to whisker pulses (shades of red, 33 neurons) and photo-stimulation (shades of blue, 15 neurons) at 5, 10, 20, and 40 Hz frequencies (darker corresponds to higher frequencies) showing frequency-dependent adaptation to whisker stimulation and little adaptation to photo-stimulation. **(C)** Velocity-response curves for detection of single-pulse whisker deflections for 3 rats.  $M_{50}$  and  $M_{100}$  correspond to the turning point and the asymptote of the cumulative Gaussian function fitted to each curve, respectively. **(D)** Circles represent detection performances for sequences of 1–4 stimuli (with 25 ms inter-pulse interval) at  $M_{50}$ . Detection of single whisker stimulus was 67.9%. However, detection rate increased by an average of  $2.3 \pm 0.93\%$  for every additional stimulus in the sequence. This is lower than the prediction that every stimulus had an equal perceptual detectability (equal probability model, solid curves). When adaptation was considered by reducing the detection probability of subsequent pulses according to observed neuronal adaptation in **(B)** (adapted probability model, dashed line), the predicted curve matched the behavioural detection performance. In contrast with whisker stimulation, detection performance of direct cortical photo-stimulation (in blue) was well-explained by equal detection probability of individual pulses (solid blue curve). This indicates that non-adaptive neural activation (as in **B**) results in uniform perceptual weight of individual pulses in a sequence. **(E)** Frequency discrimination task; as in **(A)**, but the animals were trained to discriminate between a target stimulus (1-s long sequence of stimuli at 20 or 40 Hz) and a distractor with a lower frequency. **(F)** Three stimuli used in the discrimination task, with the corresponding normalised PSTHs (lower panels). Dashed line represents the adaptation level to whisker stimulus at 40 Hz. The whisker stimuli and uniform photo-stimulation pulses were set at  $M_{100}$  level. For the adapting photo-stimulation, the irradiation level of the initial pulse was set to  $M_{100}$ , while the irradiation of subsequent pulses was reduced to that matching adaptation to whisker stimulation. **(G)** Frequency discrimination performances plotted against the frequency of distractor normalised to that of the target stimuli. Comparing discrimination performances for adaptation-free uniform photo-stimulation (blue) to whisker stimulation (red) reveals that adaptation reduces frequency discrimination performances. Adapting photo-stimulation (magenta) mimics whisker stimulation, resulting in reduced frequency discrimination performances. **(H)** Adaptation facilitates detection of deviant stimuli. The black trace shows average neural responses ( $n = 33$ ) to a 2-s long 20-Hz whisker stimulation sequence (at the mean  $M_{50}$  velocity of  $350^\circ/\text{s}$ ) with a single deviant (at  $M_{100}$ ,  $850^\circ/\text{s}$ ). Response amplitude to subsequent pulses was decreased by 40% relative to the initial pulse, whereas deviant response amplitude remained close to non-adapted single-pulse response. **(I)** As in **(H)**, but using whisker-box plot. The box shows

(Continued)

**FIGURE 9** | the first and third quartiles, the inner line is the median. Box whiskers represent minimum and maximum values. **(J)** Deviant stimulus detection performance as a function of number of deviant stimuli, was higher for whisker stimuli than photo-stimulation. Deviant detection task: two base sequences of either whisker or photo stimuli (at  $M_{50}$  amplitude, 20-Hz frequency and duration of 2 s) presented bilaterally. The target sequence (left or right) contained 1, 4, or 10 deviant pulses of  $M_{100}$  in amplitude at a random time after 1.5 s. Rats were rewarded upon successful identification of the deviant-containing target sequence. Error bars indicate s.e.m. **(B)** and 95% CI (elsewhere). Modified from Musall et al. (2014).



S1 neurons progressively adapt to the sequence of whisker contacts (Allitt et al., 2017), the amount of information/evidence in their responses decreases with adaptation over time, and hence, they contribute less to the perception. This is consistent with exponentially-decreased perceived intensity of repeated

tactile stimuli in human subjects (Berglund and Berglund, 1970) and in rats (Musall et al., 2014). Further experiments are required to understand the perceptual and neuronal effects of adaptation during the actively whisking mode of tactile sensation.

## AUTHOR CONTRIBUTIONS

MA drafted the manuscript. Both authors edited the manuscript and approved the final version.

## FUNDING

This work is supported by the University of Padua under the 2019 STARS Grants programme (CONTEXT, Context matters: from sensory processing to decision making) to MA. MA was supported by an Australian Research Council DECRA fellowship (DE200101468) and CJ Martin Early Career Fellowship (GNT1110421) from the Australian National Health and Medical Research Council (NHMRC). IL was supported by DFG (SFB 1089), Human Frontier Science Program Grant, Israel Science Foundation (ISF 1539/17), BSF Grant 2019251,

and the Marianne Manoville Beck Laboratory for Research in Neurobiology in Honor of her Parents Elisabeth and Miksa Manoville.

## ACKNOWLEDGMENTS

The authors would like to thank Mathew E. Diamond (International School for Advanced Studies - SISSA), Ramesh Rajan (Monash University) and Nelly Redolfi (University of Padua) for discussions and comments on the manuscript, and Garrett Stanley (Georgia Institute of Technology), Randy M. Bruno (Columbia University), Simon Musall (Forschungszentrum Jülich), and Florent Haiss (Institut Pasteur) for their support and providing materials used in **Figures 8–10**.

## REFERENCES

- Abbott, L., Varela, J., Sen, K., and Nelson, S. (1997). Synaptic depression and cortical gain control. *Science* 275, 221–224. doi: 10.1126/science.275.5297.221
- Abeles, M. (1982). Role of the cortical neuron: integrator or coincidence detector? *Israel J. Med. Sci.* 18, 83–92.
- Adibi, M. (2019). Whisker-mediated touch system in rodents: from neuron to behavior. *Front. Syst. Neurosci.* 13:40. doi: 10.3389/fnsys.2019.00040
- Adibi, M., and Arabzadeh, E. (2011). A comparison of neuronal and behavioral detection and discrimination performances in rat whisker system. *J. Neurophysiol.* 105:356. doi: 10.1152/jn.00794.2010
- Adibi, M., Clifford, C. W. G., and Arabzadeh, E. (2013a). Informational basis of sensory adaptation: entropy and single-spike efficiency in rat barrel cortex. *J. Neurosci.* 33, 14921–14926. doi: 10.1523/JNEUROSCI.1313-13.2013
- Adibi, M., Diamond, M., and Arabzadeh, E. (2012). Behavioral study of whisker-mediated vibration sensation in rats. *Proc. Natl. Acad. Sci. U.S.A.* 109, 971–976. doi: 10.1073/pnas.1116726109
- Adibi, M., McDonald, J. S., Clifford, C. W. G., and Arabzadeh, E. (2013b). Adaptation improves neural coding efficiency despite increasing correlations in variability. *J. Neurosci.* 33, 2108–2120. doi: 10.1523/JNEUROSCI.3449-12.2013
- Adibi, M., McDonald, J. S., Clifford, C. W. G., and Arabzadeh, E. (2014). Population decoding in rat barrel cortex: optimizing the linear readout of correlated population responses. *PLoS Comput. Biol.* 10:e1003415. doi: 10.1371/journal.pcbi.1003415
- Adorján, P., Piepenbrock, C., and Obermayer, K. (1999). Contrast adaptation and infomax in visual cortical neurons. *Rev. Neurosci.* 10, 181–200. doi: 10.1515/REVNEURO.1999.10.3-4.181
- Ahissar, E., Sosnik, R., Bagdasarian, K., and Haidarliu, S. (2001). Temporal frequency of whisker movement. II. Laminar organization of cortical representations. *J. Neurophysiol.* 86, 354–367. doi: 10.1152/jn.2001.86.1.354
- Ahissar, E., Sosnik, R., and Haidarliu, S. (2000). Transformation from temporal to rate coding in a somatosensory thalamocortical pathway. *Nature* 406, 302–306. doi: 10.1038/35018568
- Albrecht, D., Farrar, S., and Hamilton, D. (1984). Spatial contrast adaptation characteristics of neurones recorded in the cat's visual cortex. *J. Physiol.* 347, 713–739. doi: 10.1113/jphysiol.1984.sp015092
- Allitt, B. J., Alwis, D. S., and Rajan, R. (2017). Laminar-specific encoding of texture elements in rat barrel cortex. *J. Physiol.* 595, 7223–7247. doi: 10.1113/JP274865
- Anwar, H., Li, X., Bucher, D., and Nadim, F. (2017). Functional roles of short-term synaptic plasticity with an emphasis on inhibition. *Curr. Opin. Neurobiol.* 43, 71–78. doi: 10.1016/j.conb.2017.01.002
- Arabzadeh, E., Panzeri, S., and Diamond, M. E. (2004). Whisker vibration information carried by rat barrel cortex neurons. *J. Neurosci.* 24, 6011–6020. doi: 10.1523/JNEUROSCI.1389-04.2004
- Arabzadeh, E., Petersen, R. S., and Diamond, M. E. (2003). Encoding of whisker vibration by rat barrel cortex neurons: implications for texture discrimination. *J. Neurosci.* 23, 9146–9154. doi: 10.1523/JNEUROSCI.23-27-09146.2003
- Arabzadeh, E., Zorzin, E., and Diamond, M. E. (2005). Neuronal encoding of texture in the whisker sensory pathway. *PLoS Biol.* 3:e17. doi: 10.1371/journal.pbio.0030017
- Armstrong-James, M., and Fox, K. (1987). Spatiotemporal convergence and divergence in the rat S1 “barrel” cortex. *J. Comp. Neurol.* 263, 265–281. doi: 10.1002/cne.902630209
- Atick, J. (1992). Could information theory provide an ecological theory of sensory processing? *Network Comput. Neural Syst.* 3, 213–251. doi: 10.1088/0954-898X\_3\_2\_009
- Attneave, F. (1954). Some informational aspects of visual perception. *Psychol. Rev.* 61:183. doi: 10.1037/h0054663
- Attwell, D., and Laughlin, S. (2001). An energy budget for signaling in the grey matter of the brain. *J. Cereb. Blood Flow Metab.* 21, 1133–1145. doi: 10.1097/00004647-200110000-00001
- Averbeck, B., Latham, P., and Pouget, A. (2006). Neural correlations, population coding and computation. *Nat. Rev. Neurosci.* 7, 358–366. doi: 10.1038/nrn1888
- Bagdasarian, K., Szwed, M., Knutsen, P. M., Deutsch, D., Derdikman, D., Pietr, M., et al. (2013). Pre-neuronal morphological processing of object location by individual whiskers. *Nat. Neurosci.* 16, 622–631. doi: 10.1038/nn.3378
- Bale, M. R., Davies, K., Freeman, O. J., Ince, R. A., and Petersen, R. S. (2013). Low-dimensional sensory feature representation by trigeminal primary afferents. *J. Neurosci.* 33, 12003–12012. doi: 10.1523/JNEUROSCI.0925-13.2013
- Barlow, H. (1961). “The coding of sensory messages,” in *Current Problems in Animal Behaviour, 1st Edn.*, eds W. Thorpe and O. Zangwill (New York, NY: Cambridge University Press), 331–360.
- Barlow, H. (2001). Redundancy reduction revisited. *Network Comput. Neural Syst.* 12, 241–253. doi: 10.1080/net.12.3.241.253
- Barlow, H. B., and Földiák, P. (1989). “Adaptation and decorrelation in the cortex,” in *The Computing Neuron*, eds R. Durbin, C. Miall, and G. Mitchison (Boston, MA: Addison-Wesley Publishing Co., Inc.), 54–72.
- Benda, J. (2021). Neural adaptation. *Curr. Biol.* 31, R110–R116. doi: 10.1016/j.cub.2020.11.054
- Benucci, A., Saleem, A. B., and Carandini, M. (2013). Adaptation maintains population homeostasis in primary visual cortex. *Nat. Neurosci.* 16, 724–729. doi: 10.1038/nn.3382
- Berglund, U., and Berglund, B. (1970). Adaptation and recovery in vibrotactile perception. *Percept. Motor Skills* 30, 843–853. doi: 10.2466/pms.1970.30.3.843
- Brecht, M. (2007). Barrel cortex and whisker-mediated behaviors. *Curr. Opin. Neurobiol.* 17, 408–416. doi: 10.1016/j.conb.2007.07.008
- Brecht, M., Roth, A., and Sakmann, B. (2003). Dynamic receptive fields of reconstructed pyramidal cells in layers 3 and 2 of rat somatosensory barrel cortex. *J. Physiol.* 553, 243–265. doi: 10.1113/jphysiol.2003.044222

- Brecht, M., and Sakmann, B. (2002). Dynamic representation of whisker deflection by synaptic potentials in spiny stellate and pyramidal cells in the barrels and septa of layer 4 rat somatosensory cortex. *J. Physiol.* 543, 49–70. doi: 10.1113/jphysiol.2002.018465
- Brenner, N., Bialek, W., and de Ruyter van Steveninck, R. (2000). Adaptive rescaling maximizes information transmission. *Neuron* 26, 695–702. doi: 10.1016/S0896-6273(00)81205-2
- Brumberg, J. C., Pinto, D. J., and Simons, D. J. (1996). Spatial gradients and inhibitory summation in the rat whisker barrel system. *J. Neurophysiol.* 76, 130–140. doi: 10.1152/jn.1996.76.1.130
- Bruno, R. M. (2011). Synchrony in sensation. *Curr. Opin. Neurobiol.* 21, 701–708. doi: 10.1016/j.conb.2011.06.003
- Bruno, R. M., and Sakmann, B. (2006). Cortex is driven by weak but synchronously active thalamocortical synapses. *Science* 312, 1622–1627. doi: 10.1126/science.1124593
- Carandini, M., Barlow, H., O'keefe, L., Poirson, A., and Movshon, J. (1997). Adaptation to contingencies in macaque primary visual cortex. *Philos. Trans. R. Soc. B Biol. Sci.* 352:1149. doi: 10.1098/rstb.1997.0098
- Carandini, M., HEEGER, D. J., and Senn, W. (2002). A synaptic explanation of suppression in visual cortex. *J. Neurosci.* 22, 10053–10065. doi: 10.1523/JNEUROSCI.22-22-10053.2002
- Carvell, G. E., and Simons, D. J. (1990). Biometric analyses of vibrissal tactile discrimination in the rat. *J. Neurosci.* 10, 2638–2648. doi: 10.1523/JNEUROSCI.10-08-02638.1990
- Castro-Alamancos, M. A. (2004a). Absence of rapid sensory adaptation in neocortex during information processing states. *Neuron* 41, 455–464. doi: 10.1016/S0896-6273(03)00853-5
- Castro-Alamancos, M. A. (2004b). Dynamics of sensory thalamocortical synaptic networks during information processing states. *Prog. Neurobiol.* 74, 213–247. doi: 10.1016/j.pneurobio.2004.09.002
- Celikel, T., and Sakmann, B. (2007). Sensory integration across space and in time for decision making in the somatosensory system of rodents. *Proc. Natl. Acad. Sci. U.S.A.* 104, 1395–1400. doi: 10.1073/pnas.0610267104
- Chance, F. S., Nelson, S. B., and Abbott, L. F. (1998). Synaptic depression and the temporal response characteristics of V1 cells. *J. Neurosci.* 18, 4785–4799. doi: 10.1523/JNEUROSCI.18-12-04785.1998
- Chung, S., Li, X., and Nelson, S. B. (2002). Short-term depression at thalamocortical synapses contributes to rapid adaptation of cortical sensory responses *in vivo*. *Neuron* 34, 437–446. doi: 10.1016/S0896-6273(02)00659-1
- Churchland, M., Byron, M., Cunningham, J., Sugrue, L., Cohen, M., Corrado, G., et al. (2010). Stimulus onset quenches neural variability: a widespread cortical phenomenon. *Nat. Neurosci.* 13, 369–378. doi: 10.1038/nn.2501
- Craig, J. C. (1993). Anomalous sensations following prolonged tactile stimulation. *Neuropsychologia* 31, 277–291. doi: 10.1016/0028-3932(93)90092-E
- Curtis, J., and Kleinfeld, D. (2009). Phase-to-rate transformations encode touch in cortical neurons of a scanning sensorimotor system. *Nat. Neurosci.* 12, 492–501. doi: 10.1038/nn.2283
- Dealy, R. S., and Tolhurst, D. J. (1974). Is spatial adaptation an aftereffect of prolonged inhibition? *J. Physiol.* 241, 261–270. doi: 10.1113/jphysiol.1974.sp010652
- Dean, I., Harper, N. S., and McAlpine, D. (2005). Neural population coding of sound level adapts to stimulus statistics. *Nat. Neurosci.* 8, 1684–1689. doi: 10.1038/nn1541
- DeBruyn, E., and Bonds, A. (1986). Contrast adaptation in cat visual cortex is not mediated by GABA. *Brain Res.* 383, 339–342. doi: 10.1016/0006-8993(86)90036-3
- Derdikman, D., Yu, C., Haidarliu, S., Bagdasarian, K., Arieli, A., and Ahissar, E. (2006). Layer-specific touch-dependent facilitation and depression in the somatosensory cortex during active whisking. *J. Neurosci.* 26, 9538–9547. doi: 10.1523/JNEUROSCI.0918-06.2006
- Dhruv, N., Tailby, C., Sokol, S., and Lennie, P. (2011). Multiple adaptable mechanisms early in the primate visual pathway. *J. Neurosci.* 31, 15016–15025. doi: 10.1523/JNEUROSCI.0890-11.2011
- Diamond, M. E., Armstrong-James, M., and Ebner, F. F. (1992). Somatic sensory responses in the rostral sector of the posterior group (POM) and in the ventral posterior medial nucleus (VPM) of the rat thalamus. *J. Comp. Neurol.* 318, 462–476. doi: 10.1002/cne.903180410
- Díaz-Quesada, M., Martini, F. J., Ferrati, G., Bureau, I., and Maravall, M. (2014). Diverse thalamocortical short-term plasticity elicited by ongoing stimulation. *J. Neurosci.* 34, 515–526. doi: 10.1523/JNEUROSCI.2441-13.2014
- Durant, S., Clifford, C., Crowder, N., Price, N., and Ibbotson, M. (2007). Characterizing contrast adaptation in a population of cat primary visual cortical neurons using fisher information. *J. Optical Soc. Am. A* 24, 1529–1537. doi: 10.1364/JOSAA.24.001529
- Dykes, R. (1975). Afferent fibers from mystacial vibrissae of cats and seals. *J. Neurophysiol.* 38, 650–662. doi: 10.1152/jn.1975.38.3.650
- Ebara, S., Kumamoto, K., Matsuura, T., Mazurkiewicz, J. E., and Rice, F. L. (2002). Similarities and differences in the innervation of mystacial vibrissal follicle-sinus complexes in the rat and cat: a confocal microscopic study. *J. Comp. Neurol.* 449, 103–119. doi: 10.1002/cne.10277
- Egger, V., Feldmeyer, D., and Sakmann, B. (1999). Coincidence detection and changes of synaptic efficacy in spiny stellate neurons in rat barrel cortex. *Nat. Neurosci.* 2, 1098–1105. doi: 10.1038/16026
- Ego-Stengel, V., Mello E Souza, T., Jacob, V., and Shulz, D. E. (2005). Spatiotemporal characteristics of neuronal sensory integration in the barrel cortex of the rat. *J. Neurophysiol.* 93, 1450–1467. doi: 10.1152/jn.00912.2004
- Estebanez, L., El Boustani, S., Destexhe, A., and Shulz, D. E. (2012). Correlated input reveals coexisting coding schemes in a sensory cortex. *Nat. Neurosci.* 15, 1691–1699. doi: 10.1038/nn.3258
- Fairhall, A., Lewen, G., Bialek, W., and de Ruyter van Steveninck, R. (2001). Efficiency and ambiguity in an adaptive neural code. *Nature* 412, 787–792. doi: 10.1038/35090500
- Fassih, A., Akrami, A., Esmaili, V., and Diamond, M. E. (2014). Tactile perception and working memory in rats and humans. *Proc. Natl. Acad. Sci. U.S.A.* 111, 2331–2336. doi: 10.1073/pnas.1315171111
- Feldmeyer, D. (2012). Excitatory neuronal connectivity in the barrel cortex. *Front. Neuroanat.* 6:24. doi: 10.3389/fnana.2012.00024
- Feldmeyer, D., Brecht, M., Helmchen, F., Petersen, C. C., Poulet, J. F., Staiger, J. F., et al. (2013). Barrel cortex function. *Prog. Neurobiol.* 103, 3–27. doi: 10.1016/j.pneurobio.2012.11.002
- Finlayson, P. G., and Cynader, M. S. (1995). Synaptic depression in visual cortex tissue slices: an *in vitro* model for cortical neuron adaptation. *Exp. Brain Res.* 106, 145–155. doi: 10.1007/BF00241364
- Fisher, R. A. (1922). On the mathematical foundations of theoretical statistics. *Philos. Trans. R. Soc. Lond. Ser. A* 222, 309–368. doi: 10.1098/rsta.1922.0009
- Fitzgerald, O. (1940). Discharges from the sensory organs of the cat's vibrissae and the modification in their activity by ions. *J. Physiol.* 98, 163–178. doi: 10.1113/jphysiol.1940.sp003841
- Fraser, G., Hartings, J. A., and Simons, D. J. (2006). Adaptation of trigeminal ganglion cells to periodic whisker deflections. *Somatosens. Motor Res.* 23, 111–118. doi: 10.1080/08990220600906589
- Freeman, T. C. B., Durand, S., Kiper, D. C., and Carandini, M. (2002). Suppression without inhibition in visual cortex. *Neuron* 35, 759–771. doi: 10.1016/S0896-6273(02)00819-X
- Furuta, T., Bush, N. E., Yang, A. E.-T., Ebara, S., Miyazaki, N., Murata, K., et al. (2020). The cellular and mechanical basis for response characteristics of identified primary afferents in the rat vibrissal system. *Curr. Biol.* 30, 815.e5–826.e5. doi: 10.1016/j.cub.2019.12.068
- Furuta, T., Timofeeva, E., Nakamura, K., Okamoto-Furuta, K., Togo, M., Kaneko, T., et al. (2008). Inhibitory gating of vibrissal inputs in the brainstem. *J. Neurosci.* 28, 1789–1797. doi: 10.1523/JNEUROSCI.4627-07.2008
- Ganmor, E., Katz, Y., and Lampl, I. (2010). Intensity-dependent adaptation of cortical and thalamic neurons is controlled by brainstem circuits of the sensory pathway. *Neuron* 66, 273–286. doi: 10.1016/j.neuron.2010.03.032
- Garabedian, C. E., Jones, S. R., Merzenich, M. M., Dale, A., and Moore, C. I. (2003). Band-pass response properties of rat si neurons. *J. Neurophysiol.* 90, 1379–1391. doi: 10.1152/jn.01158.2002
- Ghazanfar, A. A., and Nicolelis, M. A. (1999). Spatiotemporal properties of layer V neurons of the rat primary somatosensory cortex. *Cereb. Cortex* 9, 348–361. doi: 10.1093/cercor/9.4.348
- Gibson, J. J. (1933). Adaptation, after-effect and contrast in the perception of curved lines. *J. Exp. Psychol.* 16:1. doi: 10.1037/h0074626
- Gibson, J. M., and Welker, W. I. (1983). Quantitative studies of stimulus coding in first-order vibrissa afferents of rats. 2. adaptation and

- coding of stimulus parameters. *Somatosens. Motor Res.* 1, 95–117. doi: 10.3109/07367228309144543
- Goble, A. K., and Hollins, M. (1993). Vibrotactile adaptation enhances amplitude discrimination. *J. Acoust. Soc. Am.* 93, 418–424. doi: 10.1121/1.405621
- Goble, A. K., and Hollins, M. (1994). Vibrotactile adaptation enhances frequency discrimination. *J. Acoust. Soc. Am.* 96, 771–780. doi: 10.1121/1.410314
- Gutnisky, D., and Dragoi, V. (2008). Adaptive coding of visual information in neural populations. *Nature* 452, 220–224. doi: 10.1038/nature06563
- Hafting, T., Fyhn, M., Molden, S., Moser, M., and Moser, E. (2005). Microstructure of a spatial map in the entorhinal cortex. *Nature* 436, 801–806. doi: 10.1038/nature03721
- Harris, J. A., Petersen, R. S., and Diamond, M. E. (1999). Distribution of tactile learning and its neural basis. *Proc. Natl. Acad. Sci. U.S.A.* 96, 7587–7591. doi: 10.1073/pnas.96.13.7587
- Hartings, J. A., Temereanca, S., and Simons, D. J. (2003). Processing of periodic whisker deflections by neurons in the ventroposterior medial and thalamic reticular nuclei. *J. Neurophysiol.* 90, 3087–3094. doi: 10.1152/jn.00469.2003
- HEEGer, D. (1991). “Nonlinear model of neural responses in cat visual cortex,” in *Computational Models of Visual Processing*, eds M. Landy and J. Movshon (Cambridge, MA: MIT Press), 119–133.
- HEEGer, D. (1992). Normalization of cell responses in cat striate cortex. *Visual Neurosci.* 9, 181–197. doi: 10.1017/S0952523800009640
- Heiss, J. E., Katz, Y., Ganmor, E., and Lampl, I. (2008). Shift in the balance between excitation and inhibition during sensory adaptation of s1 neurons. *J. Neurosci.* 28, 13320–13330. doi: 10.1523/JNEUROSCI.2646-08.2008
- Henderson, T., and Jacquin, M. (1995). What makes subcortical barrels. *Cereb. Cortex* 11, 123–187. doi: 10.1007/978-1-4757-9616-2\_3
- Higley, M. J., and Contreras, D. (2006). Balanced excitation and inhibition determine spike timing during frequency adaptation. *J. Neurosci.* 26, 448–457. doi: 10.1523/JNEUROSCI.3506-05.2006
- Hill, P. S. (2001). Vibration and animal communication: a review. *Am. Zool.* 41, 1135–1142. doi: 10.1093/icb/41.5.1135
- Hosoya, T., Baccus, S. A., and Meister, M. (2005). Dynamic predictive coding by the retina. *Nature* 436, 71–77. doi: 10.1038/nature03689
- Iggo, A., and Muir, A. (1969). The structure and function of a slowly adapting touch corpuscle in hairy skin. *J. Physiol.* 200:763. doi: 10.1113/jphysiol.1969.sp008721
- Isett, B. R., Feasel, S. H., Lane, M. A., and Feldman, D. E. (2018). Slip-based coding of local shape and texture in mouse s1. *Neuron* 97, 418–433. doi: 10.1016/j.neuron.2017.12.021
- Jordan, R., and Keller, G. B. (2020). Opposing influence of top-down and bottom-up input on excitatory layer 2/3 neurons in mouse primary visual cortex. *Neuron* 108, 1194–1206. doi: 10.1016/j.neuron.2020.09.024
- Katz, Y., Heiss, J., and Lampl, I. (2006). Cross-whisker adaptation of neurons in the rat barrel cortex. *J. Neurosci.* 26, 13363–13372. doi: 10.1523/JNEUROSCI.4056-06.2006
- Katz, Y., and Lampl, I. (2021). Cross-whisker adaptation of neurons in layer 2/3 of the rat barrel cortex. *Front. Syst. Neurosci.* 15:38. doi: 10.3389/fnsys.2021.646563
- Katz, Y., Okun, M., and Lampl, I. (2012). Trial-to-trial correlation between thalamic sensory response and global EEG activity. *Eur. J. Neurosci.* 35, 826–837. doi: 10.1111/j.1460-9568.2012.08006.x
- Khatri, V., Hartings, J., and Simons, D. (2004). Adaptation in thalamic barreloid and cortical barrel neurons to periodic whisker deflections varying in frequency and velocity. *J. Neurophysiol.* 92, 3244–3254. doi: 10.1152/jn.00257.2004
- Kheradpezhoh, E., Adibi, M., and Arabzadeh, E. (2017). Response dynamics of rat barrel cortex neurons to repeated sensory stimulation. *Sci. Rep.* 7:11445. doi: 10.1038/s41598-017-11477-6
- Kim, J., Matney, C. J., Blankenship, A., Hestrin, S., and Brown, S. P. (2014). Layer 6 corticothalamic neurons activate a cortical output layer, layer 5a. *J. Neurosci.* 34, 9656–9664. doi: 10.1523/JNEUROSCI.1325-14.2014
- Kisley, M. A., and Gerstein, G. L. (1999). The continuum of operating modes for a passive model neuron. *Neural Comput.* 11, 1139–1154. doi: 10.1162/089976699300016386
- Kohn, A., and Smith, M. (2005). Stimulus dependence of neuronal correlation in primary visual cortex of the macaque. *J. Neurosci.* 25, 3661–3673. doi: 10.1523/JNEUROSCI.5106-04.2005
- König, P., Engel, A. K., and Singer, W. (1996). Integrator or coincidence detector? The role of the cortical neuron revisited. *Trends Neurosci.* 19, 130–137. doi: 10.1016/S0166-2236(96)80019-1
- Krupa, D. J., Matell, M. S., Brisben, A. J., Oliveira, L. M., and Nicolelis, M. A. (2001). Behavioral properties of the trigeminal somatosensory system in rats performing whisker-dependent tactile discriminations. *J. Neurosci.* 21, 5752–5763. doi: 10.1523/JNEUROSCI.21-15-05752.2001
- Kvale, M. N., and Schreiner, C. E. (2004). Short-term adaptation of auditory receptive fields to dynamic stimuli. *J. Neurophysiol.* 91, 604–612. doi: 10.1152/jn.00484.2003
- Kwegyir-Afful, E. E., Marella, S., and Simons, D. J. (2008). Response properties of mouse trigeminal ganglion neurons. *Somatosens. Motor Res.* 25, 209–221. doi: 10.1080/08990220802467612
- Lampl, I., and Katz, Y. (2017). Neuronal adaptation in the somatosensory system of rodents. *Neuroscience* 343, 66–76. doi: 10.1016/j.neuroscience.2016.11.043
- Latimer, K. W., Barbera, D., Sokoletsky, M., Awwad, B., Katz, Y., Nelken, I., et al. (2019). Multiple timescales account for adaptive responses across sensory cortices. *J. Neurosci.* 39, 10019–10033. doi: 10.1523/JNEUROSCI.1642-19.2019
- Laughlin, S. (1981). A simple coding procedure enhances a neuron's information capacity. *Z Naturforschung* 36, 910–912. doi: 10.1515/znc-1981-9-1040
- Le Cam, J., Estebanez, L., Jacob, V., and Shulz, D. E. (2011). Spatial structure of multiwhisker receptive fields in the barrel cortex is stimulus dependent. *J. Neurophysiol.* 106, 986–998. doi: 10.1152/jn.00044.2011
- Lee, K. J., and Woolsey, T. A. (1975). A proportional relationship between peripheral innervation density and cortical neuron number in the somatosensory system of the mouse. *Brain Res.* 99, 349–353. doi: 10.1016/0006-8993(75)90035-9
- Lennie, P. (2003). The cost of cortical computation. *Curr. Biol.* 13, 493–497. doi: 10.1016/S0960-9822(03)00135-0
- Li, L., and Ginty, D. D. (2014). The structure and organization of lanceolate mechanosensory complexes at mouse hair follicles. *eLife* 3:e01901. doi: 10.7554/eLife.01901
- Lichtenstein, S., Carvell, G., and Simons, D. (1990). Responses of rat trigeminal ganglion neurons to movements of vibrissae in different directions. *Somatosens. Motor Res.* 7, 47–65. doi: 10.3109/08990229009144697
- Linsker, R. (1988). Self-organization in a perceptual network. *Computer* 21, 105–117. doi: 10.1109/2.36
- Lottem, E., Gugig, E., and Azouz, R. (2015). Parallel coding schemes of whisker velocity in the rat's somatosensory system. *J. Neurophysiol.* 113, 1784–1799. doi: 10.1152/jn.00485.2014
- Lundstrom, B. N., Fairhall, A. L., and Maravall, M. (2010). Multiple timescale encoding of slowly varying whisker stimulus envelope in cortical and thalamic neurons *in vivo*. *J. Neurosci.* 30, 5071–5077. doi: 10.1523/JNEUROSCI.2193-09.2010
- Ma, P., and Woolsey, T. (1984). Cytoarchitectonic correlates of the vibrissae in the medullary trigeminal complex of the mouse. *Brain Res.* 306:374. doi: 10.1016/0006-8993(84)90390-1
- Malina, K., Jubran, M., Katz, Y., and Lampl, I. (2013). Imbalance between excitation and inhibition in the somatosensory cortex produces postadaptation facilitation. *J. Neurosci.* 33, 8463–8471. doi: 10.1523/JNEUROSCI.4845-12.2013
- Maravall, M., Alenda, A., Bale, M. R., and Petersen, R. S. (2013). Transformation of adaptation and gain rescaling along the whisker sensory pathway. *PLoS ONE* 8:e82418. doi: 10.1371/journal.pone.0082418
- Maravall, M., Petersen, R. S., Fairhall, A. L., Arabzadeh, E., and Diamond, M. E. (2007). Shifts in coding properties and maintenance of information transmission during adaptation in barrel cortex. *PLoS Biology* 5:e19. doi: 10.1371/journal.pbio.0050019
- McLean, J., and Palmer, L. (1996). Contrast adaptation and excitatory amino acid receptors in cat striate cortex. *Visual Neurosci.* 13, 1069–1087. doi: 10.1017/S0952523800007720
- Mease, R. A., Krieger, P., and Groh, A. (2014). Cortical control of adaptation and sensory relay mode in the thalamus. *Proc. Natl. Acad. Sci. U.S.A.* 111, 6798–6803. doi: 10.1073/pnas.1318665111
- Mehta, S. B., Whitmer, D., Figueroa, R., Williams, B. A., and Kleinfeld, D. (2007). Active spatial perception in the vibrissa scanning sensorimotor system. *PLoS Biol.* 5:e15. doi: 10.1371/journal.pbio.0050015
- Melargno, H., and Montagna, W. (1953). The tactile hair follicles in the mouse. *Anatomical Rec.* 115, 129–149. doi: 10.1002/ar.1091150202

- Middleton, J. W., Omar, C., Doiron, B., and Simons, D. J. (2012). Neural correlation is stimulus modulated by feedforward inhibitory circuitry. *J. Neurosci.* 32, 506–518. doi: 10.1523/JNEUROSCI.3474-11.2012
- Mirabella, G., Battiston, S., and Diamond, M. E. (2001). Integration of multiple-whisker inputs in rat somatosensory cortex. *Cereb. Cortex* 11, 164–170. doi: 10.1093/cercor/11.2.164
- Mohar, B., Ganmor, E., and Lampl, I. (2015). Faithful representation of tactile intensity under different contexts emerges from the distinct adaptive properties of the first somatosensory relay stations. *J. Neurosci.* 35, 6997–7002. doi: 10.1523/JNEUROSCI.4358-14.2015
- Mohar, B., Katz, Y., and Lampl, I. (2013). Opposite adaptive processing of stimulus intensity in two major nuclei of the somatosensory brainstem. *J. Neurosci.* 33, 15394–15400. doi: 10.1523/JNEUROSCI.1886-13.2013
- Moore, C. I., and Nelson, S. B. (1998). Spatio-temporal subthreshold receptive fields in the vibrissa representation of rat primary somatosensory cortex. *J. Neurophysiol.* 80, 2882–2892. doi: 10.1152/jn.1998.80.6.2882
- Morita, T., Kang, H., Wolfe, J., Jadhav, S., and Feldman, D. (2011). Psychometric curve and behavioral strategies for whisker-based texture discrimination in rats. *PLoS ONE* 6:e20437. doi: 10.1371/journal.pone.0020437
- Musall, S., Von Der Behrens, W., Mayrhofer, J. M., Weber, B., Helmchen, F., and Haiss, F. (2014). Tactile frequency discrimination is enhanced by circumventing neocortical adaptation. *Nat. Neurosci.* 17:1567. doi: 10.1038/nn.3821
- Nadal, J.-P., and Parga, N. (1994). Nonlinear neurons in the low-noise limit: a factorial code maximizes information transfer. *Network Comput. Neural Syst.* 5, 565–581. doi: 10.1088/0954-898X\_5\_4\_008
- Nagel, K. I., and Doupe, A. J. (2006). Temporal processing and adaptation in the songbird auditory forebrain. *Neuron* 51, 845–859. doi: 10.1016/j.neuron.2006.08.030
- Narins, P. M., Lewis, E. R., Jarvis, J. J., and O’Riain, J. (1997). The use of seismic signals by fossorial southern african mammals: a neuroethological gold mine. *Brain Res. Bull.* 44, 641–646. doi: 10.1016/S0361-9230(97)00286-4
- Nelson, S. B. (1991). Temporal interactions in the cat visual system. III. Pharmacological studies of cortical suppression suggest a presynaptic mechanism. *J. Neurosci.* 11, 369–380. doi: 10.1523/JNEUROSCI.11-02-00369.1991
- O’Connor, D., Clack, N., Huber, D., Komiya, T., Myers, E., and Svoboda, K. (2010). Vibrissa-based object localization in head-fixed mice. *J. Neurosci.* 30:1947. doi: 10.1523/JNEUROSCI.3762-09.2010
- Ohzawa, I., Sclar, G., and Freeman, R. (1982). Contrast gain control in the cat visual cortex. *Nature* 298, 266–268. doi: 10.1038/298266a0
- Ohzawa, I., Sclar, G., and Freeman, R. (1985). Contrast gain control in the cat’s visual system. *J. Neurophysiol.* 54, 651–667. doi: 10.1152/jn.1985.54.3.651
- Ollerenshaw, D. R., Zheng, H. J., Millard, D. C., Wang, Q., and Stanley, G. B. (2014). The adaptive trade-off between detection and discrimination in cortical representations and behavior. *Neuron* 81, 1152–1164. doi: 10.1016/j.neuron.2014.01.025
- Oram, M. (2011). Visual stimulation decorrelates neuronal activity. *J. Neurophysiol.* 105, 942–957. doi: 10.1152/jn.00711.2009
- Park, J. M., Hong, Y. K., Rodgers, C. C., Dahan, J. B., Schmidt, E. R., and Bruno, R. M. (2020). Deep and superficial layers of the primary somatosensory cortex are critical for whisker-based texture discrimination in mice. *bioRxiv*. doi: 10.1101/2020.08.12.245381
- Pestilli, F., Viera, G., and Carrasco, M. (2007). How do attention and adaptation affect contrast sensitivity? *J. Vision* 7, 1–12. doi: 10.1167/7.7.9
- Petersen, C. C. H. (2007). The functional organization of the barrel cortex. *Neuron* 56, 339–355. doi: 10.1016/j.neuron.2007.09.017
- Ponce-Alvarez, A., Thiele, A., Albright, T. D., Stoner, G. R., and Deco, G. (2013). Stimulus-dependent variability and noise correlations in cortical MT neurons. *Proc. Natl. Acad. Sci. U.S.A.* 110, 13162–13167. doi: 10.1073/pnas.1300098110
- Pouget, A., Beck, J. M., Ma, W. J., and Latham, P. E. (2013). Probabilistic brains: knowns and unknowns. *Nat. Neurosci.* 16, 1170–1178. doi: 10.1038/nn.3495
- Price, N. S. C., Ono, S., Mustari, M. J., and Ibbotson, M. R. (2005). Comparing acceleration and speed tuning in macaque MT: physiology and modeling. *J. Neurophysiol.* 94, 3451–3464. doi: 10.1152/jn.00564.2005
- Ramirez, A., Pnevmatikakis, E. A., Merel, J., Paninski, L., Miller, K. D., and Bruno, R. M. (2014). Spatiotemporal receptive fields of barrel cortex revealed by reverse correlation of synaptic input. *Nat. Neurosci.* 17, 866–875. doi: 10.1038/nn.3720
- Redlich, A. N. (1993). Redundancy reduction as a strategy for unsupervised learning. *Neural Comput.* 5, 289–304. doi: 10.1162/neco.1993.5.2.289
- Renehan, W. E., and Munger, B. L. (1986). Degeneration and regeneration of peripheral nerve in the rat trigeminal system. I. Identification and characterization of the multiple afferent innervation of the mystacial vibrissae. *J. Comp. Neurol.* 246, 129–145. doi: 10.1002/cne.902460109
- Rice, F., Fundin, B., Arvidsson, J., Aldskogius, H., and Johansson, O. (1997). Comprehensive immunofluorescence and lectin binding analysis of vibrissa follicle sinus complex innervation in the mystacial pad of the rat. *J. Comp. Neurol.* 385, 149–184. doi: 10.1002/(SICI)1096-9861(19970825)385:2<149::AID-CNE1>3.0.CO;2-1
- Rice, F. L., Mance, A., and Munger, B. L. (1986). A comparative light microscopic analysis of the sensory innervation of the mystacial pad. I. Innervation of vibrissa follicle-sinus complexes. *J. Comp. Neurol.* 252, 154–174. doi: 10.1002/cne.902520203
- Rothschild, G., Nelken, I., and Mizrahi, A. (2010). Functional organization and population dynamics in the mouse primary auditory cortex. *Nat. Neurosci.* 13, 353–360. doi: 10.1038/nn.2484
- Roy, S. A., and Alloway, K. D. (2001). Coincidence detection or temporal integration? What the neurons in somatosensory cortex are doing. *J. Neurosci.* 21, 2462–2473. doi: 10.1523/JNEUROSCI.21-07-02462.2001
- Sabri, M. M., Adibi, M., and Arabzadeh, E. (2016). Dynamics of population activity in rat sensory cortex: network correlations predict anatomical arrangement and information content. *Front. Neural Circ.* 10:49. doi: 10.3389/fncir.2016.00049
- Safaii, H., von Heimendahl, M., Sorando, J. M., Diamond, M. E., and Maravall, M. (2013). Coordinated population activity underlying texture discrimination in rat barrel cortex. *J. Neurosci.* 33, 5843–5855. doi: 10.1523/JNEUROSCI.3486-12.2013
- Sclar, G., Lennie, P., and DePriest, D. (1989). Contrast adaptation in striate cortex of macaque. *Vision Res.* 29, 747–755. doi: 10.1016/0042-6989(89)90087-4
- Shannon, C. E. (1948). A mathematical theory of communication. *Bell Syst. Tech. J.* 27, 379–423. doi: 10.1002/j.1538-7305.1948.tb00917.x
- Sharpe, T. O., Sugihara, H., Kurgansky, A. V., Rebrik, S. P., Stryker, M. P., and Miller, K. D. (2006). Adaptive filtering enhances information transmission in visual cortex. *Nature* 439, 936–942. doi: 10.1038/nature04519
- Shoykhet, M., Doherty, D., and Simons, D. J. (2000). Coding of deflection velocity and amplitude by whisker primary afferent neurons: implications for higher level processing. *Somatosens. Motor Res.* 17, 171–180. doi: 10.1080/08990220050020580
- Silver, R. J. (1969). *Tilt after-effects in touch* (Ph.D. thesis). Brandeis University, Waltham, MA, United States.
- Simons, D., and Carvell, G. (1989). Thalamocortical response transformation in the rat vibrissa/barrel system. *J. Neurophysiol.* 61:311. doi: 10.1152/jn.1989.61.2.311
- Simons, D. J. (1978). Response properties of vibrissa units in rat SI somatosensory neocortex. *J. Neurophysiol.* 41, 798–820. doi: 10.1152/jn.1978.41.3.798
- Simons, D. J. (1985). Temporal and spatial integration in the rat SI vibrissa cortex. *J. Neurophysiol.* 54, 615–635. doi: 10.1152/jn.1985.54.3.615
- Smirnakis, S. M., Berry, M. J., Warland, D. K., Bialek, W., and Meister, M. (1997). Adaptation of retinal processing to image contrast and spatial scale. *Nature* 386, 69–73. doi: 10.1038/386069a0
- Smith, M., and Kohn, A. (2008). Spatial and temporal scales of neuronal correlation in primary visual cortex. *J. Neurosci.* 28, 12591–12603. doi: 10.1523/JNEUROSCI.2929-08.2008
- Solomon, S., Peirce, J., Dhruv, N., and Lennie, P. (2004). Profound contrast adaptation early in the visual pathway. *Neuron* 42, 155–162. doi: 10.1016/S0896-6273(04)00178-3
- Solomon, S. S., Chen, S. C., Morley, J. W., and Solomon, S. G. (2015). Local and global correlations between neurons in the middle temporal area of primate visual cortex. *Cereb. Cortex* 25, 3182–3196. doi: 10.1093/cercor/bhu111
- Sosnik, R., Haidarliu, S., and Ahissar, E. (2001). Temporal frequency of whisker movement. I. Representations in brain stem and thalamus. *J. Neurophysiol.* 86, 339–353. doi: 10.1152/jn.2001.86.1.339
- Srinivasan, M., Laughlin, S., and Dubs, A. (1982). Predictive coding: a fresh view of inhibition in the retina. *Proc. R. Soc. Lond. Ser. B Biol. Sci.* 216, 427–459. doi: 10.1098/rspb.1982.0085

- Stevenson, I. H., Cronin, B., Sur, M., and Kording, K. P. (2010). Sensory adaptation and short term plasticity as bayesian correction for a changing brain. *PLoS ONE* 5:e12436. doi: 10.1371/journal.pone.0012436
- Talbot, W. H., Darian-Smith, I., Kornhuber, H. H., and Mountcastle, V. B. (1968). The sense of flutter-vibration: comparison of the human capacity with response patterns of mechanoreceptive afferents from the monkey hand. *J. Neurophysiol.* 31:301. doi: 10.1152/jn.1968.31.2.301
- Taube, J. S. (1998). Head direction cells and the neurophysiological basis for a sense of direction. *Prog. Neurobiol.* 55, 225–256. doi: 10.1016/S0304-0082(98)00004-5
- Timofeeva, E., Lavallée, P., Arsenault, D., and Deschênes, M. (2004). Synthesis of multiwhisker-receptive fields in subcortical stations of the vibrissa system. *J. Neurophysiol.* 91, 1510–1515. doi: 10.1152/jn.01109.2003
- Tonomura, S., Ebara, S., Bagdasarian, K., Uta, D., Ahissar, E., Meir, I., et al. (2015). Structure-function correlations of rat trigeminal primary neurons: emphasis on club-like endings, a vibrissa mechanoreceptor. *Proc. Japan Acad. Ser. B* 91, 560–576. doi: 10.2183/pjab.91.560
- van Hateren, J. H. (1992). Theoretical predictions of spatiotemporal receptive fields of fly lms, and experimental validation. *J. Comp. Physiol. A* 171, 157–170. doi: 10.1007/BF00188924
- Varani, S., Vecchia, D., Zucca, S., Forli, A., and Fellin, T. (2021). Stimulus feature-specific control of layer 2/3 subthreshold whisker responses by layer 4 in the mouse primary somatosensory cortex. *Cereb. Cortex.* 1–18. doi: 10.1093/cercor/bhab297
- Vidyasagar, T. (1990). Pattern adaptation in cat visual cortex is a co-operative phenomenon. *Neuroscience* 36, 175–179. doi: 10.1016/0306-4522(90)90360-G
- Vincent, S. B. (1913). The tactile hair of the white rat. *J. Comp. Neurol.* 23, 1–34. doi: 10.1002/cne.900230101
- von Heimendahl, M., Itskov, P. M., Arabzadeh, E., and Diamond, M. E. (2007). Neuronal activity in rat barrel cortex underlying texture discrimination. *PLoS Biol.* 5:e305. doi: 10.1371/journal.pbio.0050305
- Waite, P. M. E., and Cragg, B. G. (1982). The peripheral and central changes resulting from cutting or crushing the afferent nerve supply to the whiskers. *Proc. R. Soc. Lond. Ser. B Biol. Sci.* 214, 191–211. doi: 10.1098/rspb.1982.0004
- Wang, H.-P., Spencer, D., Fellous, J.-M., and Sejnowski, T. J. (2010a). Synchrony of thalamocortical inputs maximizes cortical reliability. *Science* 328, 106–109. doi: 10.1126/science.1183108
- Wang, Q., Webber, R., and Stanley, G. (2010b). Thalamic synchrony and the adaptive gating of information flow to cortex. *Nat. Neurosci.* 13, 1534–1541. doi: 10.1038/nn.2670
- Wehr, M., and Zador, A. M. (2005). Synaptic mechanisms of forward suppression in rat auditory cortex. *Neuron* 47, 437–445. doi: 10.1016/j.neuron.2005.06.009
- Wen, B., Wang, G., Dean, I., and Delgutte, B. (2009). Dynamic range adaptation to sound level statistics in the auditory nerve. *J. Neurosci.* 29:13797. doi: 10.1523/JNEUROSCI.5610-08.2009
- Whitmire, C. J., Waiblinger, C., Schwarz, C., and Stanley, G. B. (2016). Information coding through adaptive gating of synchronized thalamic bursting. *Cell Rep.* 14, 795–807. doi: 10.1016/j.celrep.2015.12.068
- Wolfe, J., Hill, D. N., Pahlavan, S., Drew, P. J., Kleinfeld, D., and Feldman, D. E. (2008). Texture coding in the rat whisker system: slip-stick versus differential resonance. *PLoS Biol.* 6:e215. doi: 10.1371/journal.pbio.0060215
- Woodbury, C. J., and Koerber, H. R. (2007). Central and peripheral anatomy of slowly adapting type I low-threshold mechanoreceptors innervating trunk skin of neonatal mice. *J. Comp. Neurol.* 505, 547–561. doi: 10.1002/cne.21517
- Wright, N. C., Borden, P. Y., Liew, Y. J., Bolus, M. F., Stoy, W. M., Forest, C. R., et al. (2021). Rapid cortical adaptation and the role of thalamic synchrony during wakefulness. *J. Neurosci.* 41, 5421–5439. doi: 10.1523/JNEUROSCI.3018-20.2021
- Yu, C., Derdikman, D., Haidarliu, S., and Ahissar, E. (2006). Parallel thalamic pathways for whisking and touch signals in the rat. *PLoS Biol.* 4:e124. doi: 10.1371/journal.pbio.0040124
- Zheng, H. J., Wang, Q., and Stanley, G. B. (2015). Adaptive shaping of cortical response selectivity in the vibrissa pathway. *J. Neurophysiol.* 113, 3850–3865. doi: 10.1152/jn.00978.2014
- Zucca, S., Pasquale, V., de Leon Roig, P. L., Panzeri, S., and Fellin, T. (2019). Thalamic drive of cortical parvalbumin-positive interneurons during down states in anesthetized mice. *Curr. Biol.* 29, 1481–1490. doi: 10.1016/j.cub.2019.04.007
- Zucker, E., and Welker, W. (1969). Coding of somatic sensory input by vibrissae neurons in the rat's trigeminal ganglion. *Brain Res.* 12:138. doi: 10.1016/0006-8993(69)90061-4
- Zuo, Y., and Diamond, M. E. (2019). Texture identification by bounded integration of sensory cortical signals. *Curr. Biol.* 29, 1425–1435. doi: 10.1016/j.cub.2019.03.017

**Conflict of Interest:** The authors declare that the research was conducted in the absence of any commercial or financial relationships that could be construed as a potential conflict of interest.

**Publisher's Note:** All claims expressed in this article are solely those of the authors and do not necessarily represent those of their affiliated organizations, or those of the publisher, the editors and the reviewers. Any product that may be evaluated in this article, or claim that may be made by its manufacturer, is not guaranteed or endorsed by the publisher.

Copyright © 2021 Adibi and Lampl. This is an open-access article distributed under the terms of the Creative Commons Attribution License (CC BY). The use, distribution or reproduction in other forums is permitted, provided the original author(s) and the copyright owner(s) are credited and that the original publication in this journal is cited, in accordance with accepted academic practice. No use, distribution or reproduction is permitted which does not comply with these terms.



# Contrast Adaptation in Face Perception Revealed Through EEG and Behavior

O. Scott Gwinn<sup>1\*</sup>, Talia L. Retter<sup>2</sup>, Sean F. O'Neil<sup>1</sup> and Michael A. Webster<sup>1</sup>

<sup>1</sup>Visual Perception Lab, Department of Psychology, University of Nevada, Reno, NV, United States, <sup>2</sup>Cognitive Neuroscience Lab, Department of Behavioural and Cognitive Sciences, Institute of Cognitive Science & Assessment, University of Luxembourg, Esch-sur-Alzette, Luxembourg

## OPEN ACCESS

### Edited by:

Mehdi Adibi,  
Monash University, Australia

### Reviewed by:

J. Patrick Mayo,  
University of Pittsburgh,  
United States  
Colin John Palmer,  
University of New South Wales,  
Australia

### \*Correspondence:

O. Scott Gwinn  
dr.scottgwinn@gmail.com

**Received:** 27 April 2021

**Accepted:** 22 September 2021

**Published:** 29 October 2021

### Citation:

Gwinn OS, Retter TL, O'Neil SF and Webster MA (2021) Contrast Adaptation in Face Perception Revealed Through EEG and Behavior. *Front. Syst. Neurosci.* 15:701097. doi: 10.3389/fnsys.2021.701097

Exposure to a face can produce biases in the perception of subsequent faces. Typically, these face aftereffects are studied by adapting to an individual face or category (e.g., faces of a given gender) and can result in renormalization of perceptions such that the adapting face appears more neutral. These shifts are analogous to chromatic adaptation, where a renormalization for the average adapting color occurs. However, in color vision, adaptation can also adjust to the variance or range of colors in the distribution. We examined whether this variance or contrast adaptation also occurs for faces, using an objective EEG measure to assess response changes following adaptation. An average female face was contracted or expanded along the horizontal or vertical axis to form four images. Observers viewed a 20 s sequence of the four images presented in a fixed order at a rate of 6 Hz, while responses to the faces were recorded with EEG. A 6 Hz signal was observed over right occipito-temporal channels, indicating symmetric responses to the four images. This test sequence was repeated after 20 s adaptation to alternations between two of the faces (e.g., horizontal contracted and expanded). This adaptation resulted in an additional signal at 3 Hz, consistent with asymmetric responses to adapted and non-adapted test faces. Adapting pairs have the same mean (undistorted) as the test sequence and thus should not bias responses driven only by the mean. Instead, the results are consistent with selective adaptation to the distortion axis. A 3 Hz signal was also observed after adapting to face pairs selected to induce a mean bias (e.g., expanded vertical and expanded horizontal), and this signal was not significantly different from that observed following adaption to a single image that did not form part of the test sequence (e.g., a single image expanded both vertically and horizontally). In a further experiment, we found that this variance adaptation can also be observed behaviorally. Our results suggest that adaptation calibrates face perception not only for the average characteristics of the faces we experience but also for the gamut of faces to which we are exposed.

**Keywords:** EEG, periodic stimulation, face perception, adaptation, contrast, variance

## INTRODUCTION

The appearance of a face can be strongly affected by the faces seen previously, and many studies have examined the properties and implications of these face adaptation effects (Rhodes et al., 2005; Webster and MacLeod, 2011; Mueller et al., 2020). The strength of adaptation as an investigative tool stems from the recognition that the resulting perceptual aftereffects reflect changes in the response properties of neural populations, and thus can help characterize the nature of those populations, such as the number and tuning of the underlying mechanisms (Barlow and Hill, 1963; Kohn, 2007; Webster, 2015). Face aftereffects appear to at least partly reflect processes at higher and possibly face-specific levels of coding, as evidenced by the finding that the aftereffects generalize across changes in the size (Zhao and Chubb, 2001; Rhodes et al., 2004), position (Leopold et al., 2001) or orientation of the adapting and test images (Watson and Clifford, 2003). Observations that aftereffects are larger for adaptors that are more distinctive from average norms (Robbins et al., 2007), and that adaptation to norms does not induce observable aftereffects (Webster and MacLin, 1999), have also suggested that the representation is based on a norm-based code, similar to color (Hurvich and Jameson, 1957; Webster and Leonard, 2008). However, there have also been challenges to this notion (Storrs and Arnold, 2012, 2015).

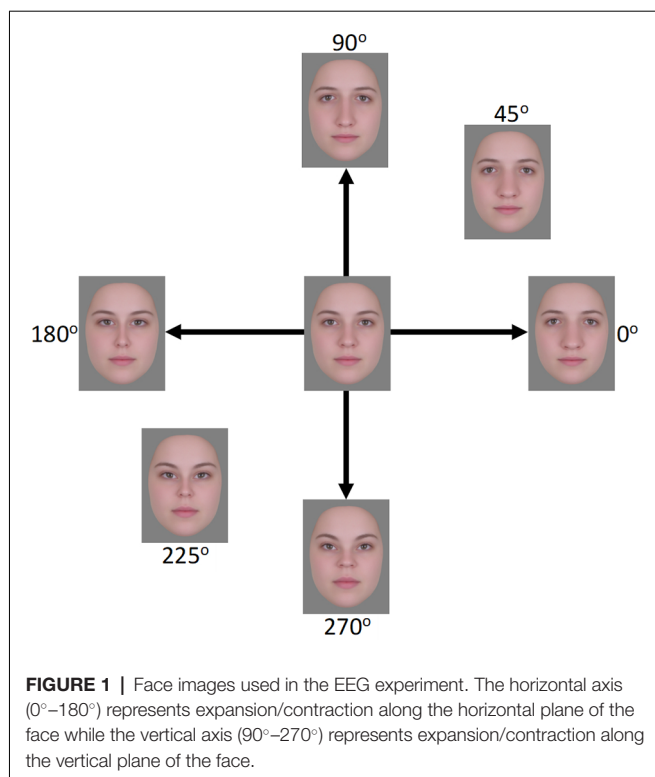
Many of the studies that have explored face adaptation involve exposures to a single face or a single category of faces. That is, studies typically present observers with face images of one type (e.g., expanded faces, male faces, young faces) and aftereffects are measured by showing that neutral test faces are biased away from the adapting category (e.g., after adapting to an expanded face, an undistorted face appears contracted (Webster and MacLin, 1999); or after adapting to a male face, an androgynous face appears more female (Webster et al., 2004)). However, for some stimulus attributes, adaptation can adjust not only to the mean of the adapting stimuli but also the variance. For example, in color vision, adapting to a temporal or spatial alternation between two colors (e.g., in a flickering field or spatial grating) results in a loss in the perceived contrast or saturation of the adapting colors (Krauskopf et al., 1982; Bradley et al., 1988; Webster and Mollon, 1991). This is in spite of the fact that the pair of colors are chosen so that the mean chromaticity equals a neutral gray, and the adaptation produces no change in the appearance of this neutral, zero-contrast stimulus. Such contrast adaptation effects are also well-known and have been widely studied in spatial vision, for example as changes in the apparent contrast of sinewave gratings (Blakemore and Nachmias, 1971; Georgeson, 1985).

Whether analogous forms of contrast adaptation occur for other stimulus dimensions, and for faces, in particular, remains unclear. Previous studies testing for them have produced only weak and indirect evidence (Spetch et al., 2004). To test for the existence of contrast adaptation in faces, we took advantage of an objective measure of face adaptation and neural response changes as measured by electroencephalography (EEG) and the

emerging technique of Fast Periodic Visual Stimulation (FPVS). FPVS, also known as Steady-State Visual Evoked Potentials (SSVEP; Regan, 1966; Rossion, 2014a,b; Norcia et al., 2015), refers to a method of presenting stimuli at a fixed rate and analyzing elicited responses at that rate in the frequency domain. This technique is well-suited for adaptation studies because it allows for quantification of the neurophysiological responses associated with adaptation in a coherent frequency-domain response rather than across multiple ERP components (e.g., Retter and Rossion, 2016b). Additionally, FPVS promises to be a reliable technique due to its objectivity, with responses analyzed at an experimenter-defined frequency; its implicit nature, not requiring any stimulus-related tasks; its resistance to artifacts, allowing for the production of high signal-to-noise ratios with relatively few trials; and the relative ease with which the data is analyzed and interpreted (Rossion, 2014a,b).

Retter and Rossion (2016b) previously used FPVS to measure the effect of adaptation on neural responses to facial identity. Within their paradigm (derived from Tyler and Kaitz, 1977; Ales and Norcia, 2009) a face and its anti-face (i.e., an original face's configural opposite, see Leopold et al., 2001) are sequentially presented at a rate of 6 Hz and responses are observed only at the presentation rate, indicating both identities produced symmetric responses. When the same test sequences were preceded by adaptation to one of the identities, additional responses at the image alternation rate (3 Hz) were observed, indicating that an asymmetry in the responses to the two identities had been induced. Substantial size changes in the stimuli at each presentation, as well as the location of maximal responses at 3 Hz over right occipito-temporal regions, suggest these effects may reflect adaptation at high-level and possibly face-selective visual areas. This position was further supported by a follow-up study showing that adapting and testing with inverted face images, a transformation known to disrupt face processing (Farah et al., 1995; Kanwisher et al., 1998), did not produce significant asymmetry effects (Retter and Rossion, 2017). Furthermore, adapting to the average of the test-adapt face pair also did not result in a signal at 3 Hz. Collectively, these results suggest that exposure to one of the faces altered responses at higher visual stages to the adapting face, demonstrating a neural signature of behavioral face aftereffects.

For the current study, we expanded on Retter and Rossion (2016b) paradigm to include four test faces rather than two. These faces formed complementary pairs of distortions, with one pair expanded or contracted along the vertical axis, and the second pair expanded or contracted along the horizontal axis (see **Figure 1**). We then adapted participants to one or the other pair to examine how this altered the relative responses to the two pairs. Because the two pairs share the same mean (the undistorted face), a change in the relative responses to the face pairs would reveal an adaptation adjustment that occurs independent of the mean, and instead would potentially reflect an adjustment to the variance or contrast in the face distribution.



## EEG ADAPTATION

### Methods

#### Participants

Fifteen (8 male) young adults (mean age = 23.73,  $SD = 3.67$ ) from the University of Nevada, Reno, took part in the experiment. They included author OG. Observers provided signed, informed consent before participating in the experiment, which was approved by the University of Nevada, Reno's Institutional Review Board, and conducted in accordance with the Code of Ethics of the World Medical Association (Declaration of Helsinki). Optical corrections were worn where applicable.

#### Stimuli

Stimuli were derived from 24 frontal-view images of Caucasian females with neutral expressions<sup>1</sup>. The images were combined using Abrosoft Fantamorph 5 (USA) to create a single “prototype” face for the set. This was achieved following standard morphing procedures in which a series of landmark points were used to denote the shape and location of features. Pixels at these points were then warped to the average location of all images. Using Adobe Photoshop CS5 (Adobe, USA), the average image was cropped following the jaw and hairline to remove all information outside of the face. The image was then re-sized to a width of 255 pixels, measured across the midline of the eyes, and shown on a gray background. Distorted versions were created by expanding or contracting the image around the midpoint of the nose using custom software created in

MATLAB (Mathworks, USA) and described in Webster and MacLin (1999). Pixels were relocated along x, y coordinates at different amplitudes while being confined by a Gaussian envelope such that distortions were largest around the midpoint of the image and taper towards the edges (see **Figure 1**). Test images were formed by distorting the image along the four cardinal directions (0°, 90°, 180°, and 270°, corresponding to horizontal expansion, vertical expansion, horizontal contraction, and vertical contraction, respectively; see **Figure 1**). Adapting images were selected for three separate conditions. In the “complementary pair” condition, the adapting images formed opposite pairs along either the vertical (90°–270°) or horizontal (0°–180°) axes. This condition forms the primary focus of the study and was designed to induce contrast adaptation. The remaining two conditions were designed to induce the more traditional “mean shift” form of face adaptation. In the “orthogonal pair” condition, images came from two orthogonal axes, either 0° and 90° (both expanded) or 180° and 270° (both contracted). In the “orthogonal single” condition, a single adapting image was used, which was the mean of each of the two orthogonal image sets from the “orthogonal pair” condition. For the 0° and 90° pair, this was an image at 45°, while for the 180° and 270° pair this was an image at 225°. Images were presented on a NEC AccuSync 120 cathode ray tube (CRT) monitor with a screen size of 450 × 350 mm, a working resolution of 1,280 × 960 pixels, and a refresh rate of 60 Hz. At a viewing distance of approximately 57 cm, the images subtended a visual angle of 8.1 degrees, measured across the midline of the eyes.

#### Procedure

The experiment took place in a darkened room and the session for each participant lasted approximately 1.5 h, including 30 min of preparation and 1 h of recording. Images were presented using the FPVS technique (Rossion, 2014a,b) and custom software running over Java 8 (Oracle, USA). A single trial consisted of a 40 s sequence in which stimuli were shown at a fixed rate of six images per second (6 Hz) by means of a square wave modulation at a 100% duty cycle. To reduce the potential impact of low-level properties of the images contributing to possible observed effects, the size of the images varied randomly across five steps between 90% and 110% of the original image size at each stimulus presentation cycle (Dzhelyova and Rossion, 2014). During each trial, participants were required to fixate on a small cross in the center of the screen. To help ensure attention was maintained, the fixation cross would briefly change to a square eight times during each trial at random intervals, and participants were required to press a key to indicate they saw the change.

The experiment comprised a total of four conditions (three adaptation conditions and one non-adaptation condition), with eight trials in each. Following a similar procedure as Retter and Rossion (2016b), for the adaptation conditions, the 40 s sequence was divided into an initial 20 s adaptation phase and subsequent 20 s test phase. Test phases began immediately after adaptation phases, resulting in a continual sequence of faces during the 40 s trials. During the adaptation phase, two of the adapting

<sup>1</sup>Details of these images can be found in Russell (2009)

images alternated with each other at the presentation rate of 6 Hz, except in the “orthogonal single” condition, in which a single adapting image was repeated. For conditions containing two adapting images, four versions of the adapting sequences were created such that each image in a pair was seen first in the sequence (e.g., 0° followed by 180°, 180° followed by 0°, 90° followed by 270°, and 270° followed by 90°). Each sequence was seen twice, resulting in eight trials per condition. For the complementary pair condition, the test phase began with one of the cardinal directions and moved through the sequence in a counter-clockwise direction (see **Figure 1**). For example, if the sequence began with the image at 0°, the next image would be at 90°, followed by 180°, then 270°, and then back to 0°, at which point the loop would begin again. Adapting sequences and test sequences were matched such that the first image seen in an adaptation sequence was always the first seen in the test sequence. For the test sequence described above, the adaptation sequence would comprise an alternation beginning with the image at 0°, followed by the image at 180°. For the non-adaptation condition, the test sequences were repeated without a preceding adaptation sequence. For the two orthogonal conditions, the test sequences were slightly different. For these conditions, two images from the same axis were shown in succession followed by two images from the other axis. For example, if the test sequence began with the image at 0°, the next image would be at 180°, followed by the image at 90°, then 270°, and back to 0°. Adapting and test sequences were again matched such that the first image seen in a test sequence was also the first image seen in the adapting sequence or a product of one of these images in the case of the orthogonal single condition. Counterbalancing the order of images in test sequences and yet matching them to adapting sequences allowed us to reduce any possible inherent differences in the ways the visual system processes the images, which could contribute to asymmetries in the EEG signal separate from the effects of adaptation. Inter-trial-intervals (ITIs) varied, with the beginning of new trials initiated by participants using a key press. ITIs were not tightly controlled as the effects of adaptation and the presence of the 3 Hz signal have been shown to dissipate after the first 3.33 s of the test phase and thus before the beginning of the next trial (Retter and Rossion, 2017).

## EEG Acquisition

The data were recorded using a BioSemi ActiveTwo system with a 128 Ag-AgCl active-electrode array (BioSemi B.V., Amsterdam, Netherlands; for exact position coordinates, see BioSemi website<sup>2</sup>, for a conversion of these coordinates to a more standard 10-5 nomenclature (Oostenveld and Praamstra, 2001), see Rossion et al., 2015). Electrode offsets were kept below 40 mV, referenced to the common mode sense (CMS) and driven right leg (DRL) loop. Four additional electrodes were used to record vertical and horizontal electrooculogram (EOG): two electrodes were placed above and below participants' right eye and two were placed lateral to the external canthi. The EEG and EOG were

digitized at a sampling rate of 2,048 Hz and then down-sampled to 512 Hz.

## Analysis

The recorded EEG was analyzed using Letswave 5, an open-source toolbox<sup>3</sup>, running over MATLAB R2013b (MathWorks, USA).

## Preprocessing

Data files for each participant were first filtered using a fourth order zero-phase Butterworth band-pass filter, with cutoff values of 0.1–120 Hz. A Fast Fourier Transform (FFT) multi-notch filter with a width of 0.5 Hz was also applied to remove electrical noise at three harmonics of 60 Hz. The data were then segmented by trial, including 1 s before and after the beginning of stimulation. To correct for artifacts caused by eye blinks, independent component analysis (ICA) with a square matrix was applied (Hyvarinen and Oja, 2000). A single component was removed for three participants who blinked more than 0.18 times/s on average during the 20 s test sequences. This cutoff is similar to previous studies that have used similar experimental designs (e.g., Retter and Rossion, 2016b). Channels containing artifacts across multiple trials were replaced with the average of two to four neighboring channels. All channels were then re-referenced to the common average. For each subject, adaptation trials were re-segmented to exclude the initial 20 s adaptation sequence. Non-adaptation trials were re-segmented to only include the first 20 s of the sequence. Trials were then averaged within each condition.

## Frequency Domain Analysis

An FFT was computed for each subject, condition, and channel, transforming the EEG data into separate frequency-domain amplitude and phase spectra. The amplitude data were then grand averaged across all subjects. Recordings were analyzed using a right occipito-temporal (ROT) region of interest (ROI), comprising electrodes PO8, PO10, PO12, P10, and P8 (Retter and Rossion, 2016b). The presence of a significant response at the frequency of interest was determined by  $z$ -scores ( $z = (x - \text{baseline}) / \text{standard deviation of the baseline}$ ). Baselines were defined as the 20 bins surrounding the bin of interest ( $x$ ), excluding the immediately adjacent bins (Srinivasan et al., 1999; Rossion et al., 2012). When displaying the amplitude spectra and comparing differences in amplitude across conditions, baseline corrections were applied to account for differences in baseline noise across participants and across the frequency spectrum within participants. This took the form of a baseline subtraction in which the average of the 20 surrounding bins, excluding the immediately adjacent bins and the local maximum and minimum amplitude bins, was subtracted from the bin of interest ( $x' = x - \text{baseline}$ ). When comparing differences in amplitude, the sum of baseline-subtracted harmonics of the frequency of interest was also computed (Retter et al., 2021). For responses at 3 Hz the even harmonics were not included as these correspond with the presentation rate of 6 Hz. The number of harmonics summed

<sup>2</sup><http://www.biosemi.com/headcap.htm>

<sup>3</sup><https://www.letswave.org/>

was determined by the condition with the highest continuation of significant harmonics.

### Time Domain Analysis

While the effect of adaptation in introducing asymmetries in responses can be clearly observed by analyzing response amplitudes at 3 Hz in the frequency domain, the source of these asymmetries is less clear. For example, asymmetries could arise from a reduction in the amplitude of the response to the adapted face relative to the non-adapted face, similar to adaptation in fMRI (Grill-Spector et al., 1999), or *vice versa*. To examine this, we would ideally consider the responses to each stimulus in the time domain of the EEG recording. However, responses to face stimuli presented at 6 Hz are overlapping in time, such that the responses to each stimulus are not distinct (Retter and Rossion, 2016b). Therefore, following analysis procedures used in Gwinn et al. (2018), for each condition and participant we instead modeled the effect of the 3 Hz response on the amplitude of the first and second cycle of the 6 Hz response in the time domain, with the assumption that these 6 Hz cycles may more closely reflect responses to the first (adapted) and second (non-adapted) images in a sequence, respectively. Beginning with the data averaged across trials described at the end of pre-processing, the cosine phase and amplitude of the 3 Hz and 6 Hz responses were calculated and plotted across a 334 ms time window (i.e., one cycle of the 3 Hz wave and two cycles of the 6 Hz wave). These two waveforms were then summed and the amplitude of the first cycle (0–167 ms) was compared to the amplitude of the second cycle (167–334 ms). A 50 ms delay from image onset was included when defining the beginning of the first cycle as this may be the earliest time point at which responses to faces can be observed (Seeck et al., 1997). The phase of the 3 Hz wave relative to the 6 Hz wave predicts over which time periods the 6 Hz response would be increased or decreased, with the amount of change in the 6 Hz wave determined by the amplitude of the 3 Hz response. Results from this analysis should be interpreted with a degree of caution. While differences in amplitudes across the waveforms may be accurately quantified, how these differences relate to the specific images is less clear. Unlike ERP studies or other FPVS studies in which there is a larger amount of time in between stimuli of interest (Dzhelyova et al., 2016; Retter and Rossion, 2016a), presenting facial images at a rate of 6 Hz means that we are measuring numerous overlapping responses, which makes it necessary to approximate distinct responses for single images.

## Results

### Frequency Domain

Amplitude spectra are presented in **Figure 2** and topographies in **Figure 3**. In these figures, large responses at the image presentation rate of 6 Hz can be seen across all conditions. Conversely, responses at 3 Hz appear to only be present in the three adaptation conditions and absent in the non-adaptation condition. Inspection of the *z*-scores (see **Table 1**) confirmed that significant responses at 3 Hz were only present in the adaptation conditions. This indicates that without prior adaptation, responses to each image in the test sequences were

symmetrical. Following adaptation, an asymmetry is introduced, resulting in the additional signals at 3 Hz.

To compare the magnitude of the adaptation-induced response asymmetries across conditions, a sum of harmonics was calculated. Significant harmonics with  $p < 0.05$  were observed up to the 3rd harmonic (9 Hz) in the orthogonal single condition. Baseline-subtracted amplitudes for the first three harmonics, excluding the second as this corresponds to the base stimulation frequency (6 Hz), were summed for each condition separately. The average of these summations across participants is shown for each condition in **Figure 4**. Two paired-samples *t*-tests were used to separately compare the magnitude of responses in the complementary pair vs. orthogonal pair conditions, and the orthogonal pair vs. orthogonal single conditions. These analyses showed that response asymmetries in the orthogonal pair condition ( $M = 0.19$ ,  $SD = 0.17$ ) were significantly greater than those in the complementary pair condition ( $M = 0.08$ ,  $SD = 0.14$ ;  $t_{14} = 2.22$ ,  $p = 0.043$ ,  $d = 0.70$ ). Conversely, these same response asymmetries in the orthogonal pair condition were not significantly different to those in the orthogonal single condition ( $M = 0.27$ ,  $SD = 0.29$ ;  $t_{14} = 1.05$ ,  $p = 0.314$ ,  $d = 0.34$ ).

### Time Domain

To first visualize the recordings in the time domain, a more conservative Butterworth low-pass filter was applied to the data averaged across trials described at the end of pre-processing. This fourth order filter comprised a cutoff of 30 Hz, which is more typical of a filter used in ERP studies of face perception (e.g., Jacques et al., 2007). Data were then segmented into 670 ms epochs to encapsulate the presentation of and responses to a full four-face cycle of test images (since each image was displayed for 167 ms). The 29 epochs within each condition were then averaged separately for each participant. The resulting waveform for one participant for the orthogonal single condition can be seen in **Figure 5** for electrode PO10. This electrode was chosen as it showed the largest responses at 3 Hz. Data from a single participant is shown to avoid averaging over differences in latency across participants (for examples of such variance, see Retter and Rossion, 2016b). Note that these transformations were only for the purposes of visualizing the recordings and the subsequently reported analyses were performed using the original trial-averaged data described at the end of pre-processing.

To quantify differences in amplitude across the waveforms, we modeled the sum of the 3 Hz and 6 Hz responses for each subject and condition across a 334 ms time window and compared the amplitude of the 50-ms delayed first cycle of the wave (50–217 ms) to the second cycle (217–384 ms), as described in “Methods” section “Time domain analysis”. In **Figure 5** the shaded areas illustrate the effective time windows for the two 6 Hz cycles across a 670 ms time window. Note that for the following analyses this was calculated for the full 20 s test sequence. Given the relative cosine phase difference between the 3 Hz and 6 Hz responses, the 3 Hz wave will be expected to have introduced an asymmetry in the 6 Hz response by enhancement of either the first or second 6 Hz cycle. Note that due to our sequence design, explained in

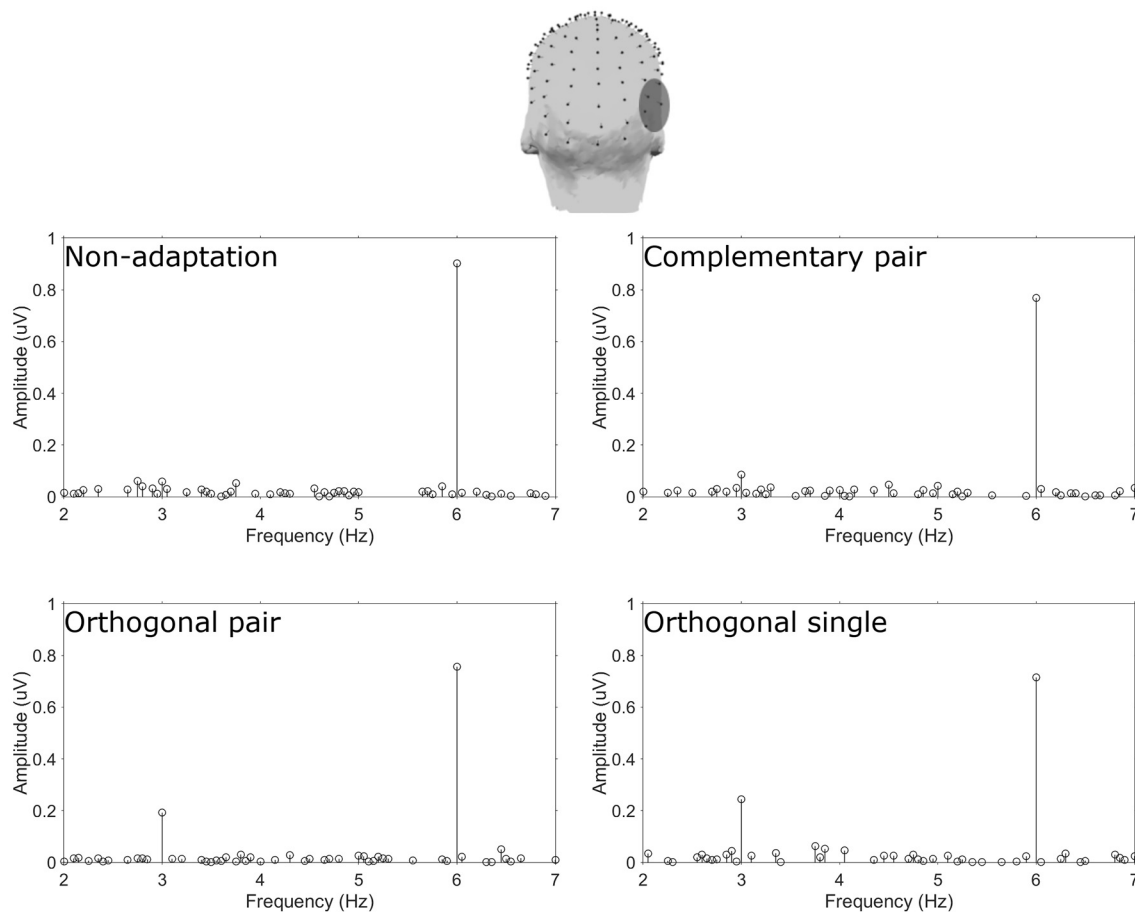


**FIGURE 2** | Top head map shows the electrodes comprising the ROT ROI. Plots show baseline subtracted amplitude spectra for the four conditions.

section “Procedure”, the facial image presented within the first cycle was always more similar to one of the adaptation images compared to the face in the second cycle. The amplitude of the first and the second 6 Hz cycles averaged across participants can be seen for each condition in **Figure 6**. The amplitude of the two 6 Hz cycles appears similar for the non-adaptation condition in which the signal at 3 Hz was found to be non-significant, whereas clearer differences between the amplitudes of the two cycles can be seen for the remaining three adaptation conditions, in which significant responses at 3 Hz were observed. These differences were formally analyzed using four paired-samples *t*-tests. Analyses confirmed the difference between cycles was significant for all conditions except the non-adaptation condition (see **Table 2**), with the second cycle response amplitude always appearing larger (see **Figure 6**). As previously mentioned, analyzing the present data in the time domain can be problematic as the recorded signals at 3 Hz and 6 Hz likely represent overlapping responses. However, if we take responses to be associated more with the image primarily presented in the same time window than the image not being presented, these results indicate a reduction in the responses to faces more similar to the adaptation images.

## BEHAVIORAL ADAPTATION

In the preceding experiments, we presented evidence for contrast adaptation in face coding, using EEG. We next examined whether the effects of this contrast adaptation can also be observed behaviorally. To assess this, we explored a different and potentially sensitive measure of face aftereffects based on the logic of tilt aftereffects (Gibson and Radner, 1937). Adapting to a tilted line produces a bias in the perceived orientation of nearby lines. We tested for an analogy to these aftereffects for faces. In this case, adapting to one axis in the space (e.g., the horizontal 0–180° axis) should selectively reduce sensitivity to the face dimension being encoded along this axis (i.e., horizontal expansion/contraction) while sensitivity along the vertical axis remains unaffected. This imbalance in sensitivity would then rotate the appearance of other faces toward the non-adapted vertical axis (**Figure 7**). Importantly, if this is equivalent to a contrast aftereffect, then the opposite poles of a test axis should rotate in the same way. That is, both clockwise or both counterclockwise away from the adapting axis. For example, after adapting to the 0–180° axis, faces along the 45–225° axis should show a counterclockwise bias so that the 45° face appears

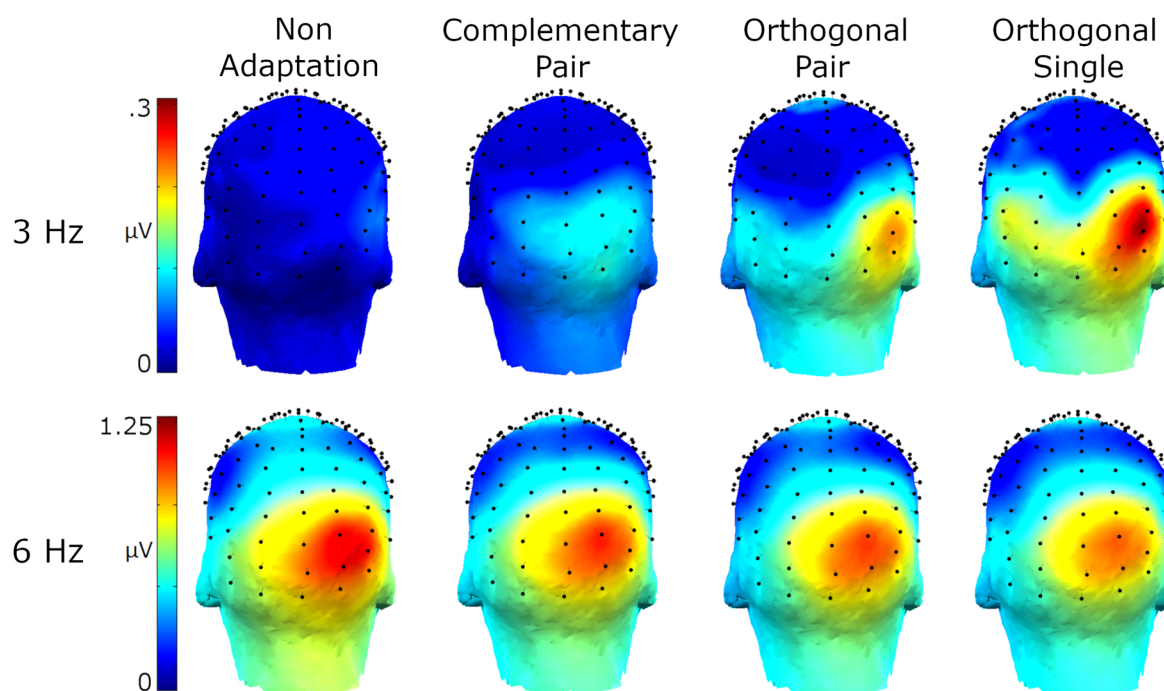


**FIGURE 3** | Head maps showing baseline subtracted amplitudes at 3 Hz and 6 Hz for the four conditions.

**TABLE 1** | Z-scores for 3 Hz signals in each condition, over the ROT ROI.

Non-adaptation	Complementary pair	Orthogonal pair	Orthogonal single
1.55	2.86*	9.85**	7.01**

Notes: \* $p < 0.01$ , \*\* $p < 0.0001$ .

more like the 90° face while the 225° face appears more like the 270° face. As both the horizontal and vertical axes share the same mean and this mean represents the neutral point (i.e., neither expanded nor contracted), adaptation resulting in a mean bias should not be possible. However, if a mean bias was induced, perhaps in the form of the neutral point becoming more horizontally contracted and shifting towards the 180° face, then test faces at 45° and 225° should rotate in opposite ways (i.e., the 45° face will be biased away from the vertical axis and the 225° biased towards the vertical axis). A similar logic has also been applied to contrast adaptation and tilt aftereffects in color space (Webster and Mollon, 1991). Here we asked whether there are also tilt aftereffects in a configural face space.

## Methods

### Participants

The 11 participants included authors OG and SO and nine (six male) students from the University of Nevada, Reno (mean age = 28.89,  $SD = 4.01$ ). They provided signed, informed consent before participating in the experiment, which was approved by the University of Nevada, Reno's Institutional Review Board, and conducted in accordance with the Code of Ethics of the

World Medical Association (Declaration of Helsinki). Optical corrections were worn where applicable.

### Stimuli

Stimuli were created following the same procedures described in the previous section “Stimuli”. Adapting stimuli were images along the vertical (90°–270°) and horizontal (0°–180°) axes (see **Figure 1**). However, in this case, we adapted observers to multiple levels along a given face axis rather than a single pair of faces, as in the EEG experiments. This was done to more closely replicate the methods employed by Webster and Mollon (1991), but can be expected to induce the same “balanced” state of adaptation that is achieved using two complementary stimuli (i.e., in both cases the opponent pools of neurons are being stimulated equally). To create these multiple levels, the maximum distortion level was doubled to produce more perceivable differences between the 20 images that spanned each axis in equal steps (40 total; the neutral face was not included). Test stimuli in this case also differed and were formed by images that fell along a circle of constant radius within the space. This was done by keeping the distortion magnitude constant while varying the angle of the distortion from 0° to 90° or 180° to 270° in 5° steps (38 images total). The distortion magnitude of the test images was half that of the adapting images (i.e., they were the same magnitude as used in the EEG experiments). Images were presented on a Cambridge Research Systems Display++ LCD monitor at a working resolution of 1,920 × 1,080 pixels and a refresh rate of 120 Hz. At a viewing distance of approximately 57 cm, the images subtended 9.2 degrees of visual angle, measured across the midline of the eyes.

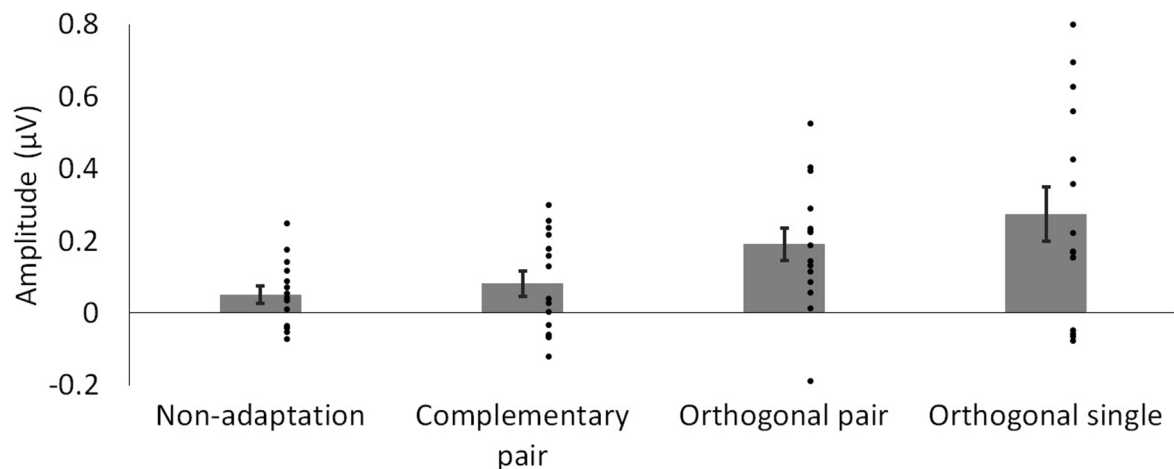


**FIGURE 4** | Mean baseline-subtracted amplitudes for responses at 3 Hz, summed across harmonics. Dots show amplitudes for individual participants. Error bars show SEM.

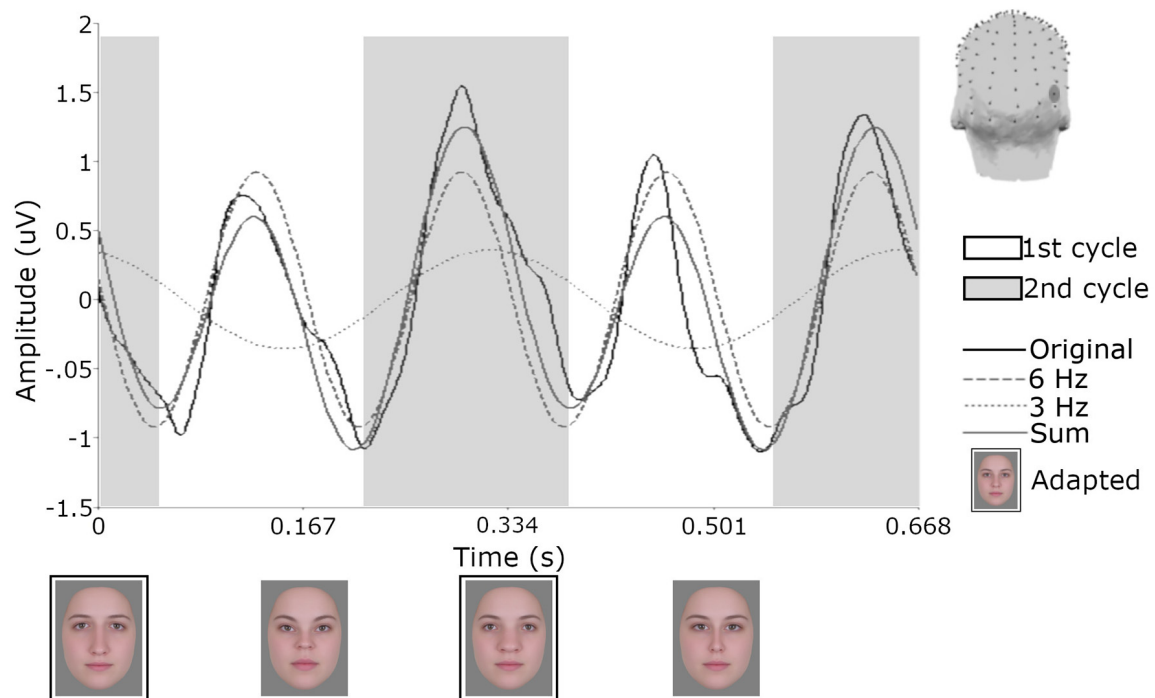


**FIGURE 5** | Responses from one participant for electrode PO10 following adaptation to the orthogonal single condition. Across the 20 s test sequence data were segmented in 29 epochs of 670 ms and then averaged. Shaded areas demonstrate how the signal would be defined as first and second cycles of the 6 Hz waveform and the influence of the 3 Hz signal. Face images with black borders are constituents of the single adapting image. The head model shows the location of electrode PO10.

## Procedure

Experimental sessions began with an initial 2.5 min adaptation phase in which participants were simultaneously adapted to images along one axis in one visual field and the other axis in the other field (e.g., 0°–180° in the left field and 90°–270° in the right field). Images were presented approximately 8.5 degrees to the

left and right of a central fixation cross, measured from the center of the image. Participants were instructed to maintain fixation on the central cross throughout adaptation and test phases. Images were shown sequentially on a continual loop in a pseudo-random order, ensuring each image was seen an equal number of times and the last three images seen at the end of the sequence were

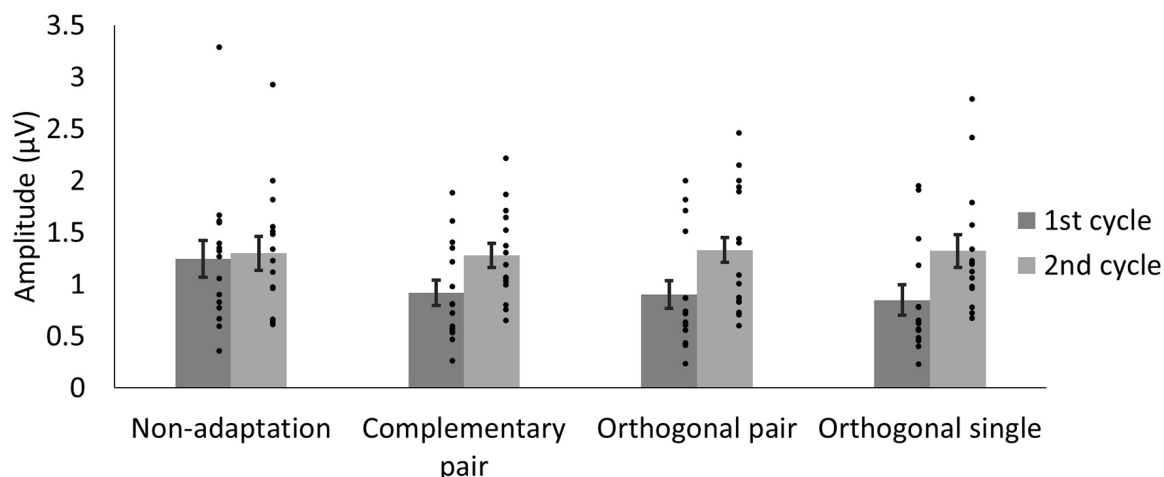


**FIGURE 6 |** Average amplitudes of the first and second 6 Hz cycles, modeled from the sum of the 3 Hz and 6 Hz signal data for each condition. The lower amplitude of the first cycles in the adaptation conditions may reflect responses driven by faces more similar to the adaptation images. Dots show amplitudes for individual participants. Error bars indicate SEM.

**TABLE 2 |** *t* and *d* statistics for comparison of the amplitudes of the first and second cycles of the sum of the 3 Hz and 6 Hz signal for each condition.

	Non-adaptation	Complementary pair	Orthogonal pair	Orthogonal single
<i>t</i>	0.76	4.43*	5.4**	8.51**
<i>d</i>	0.08	0.79	0.72	0.84

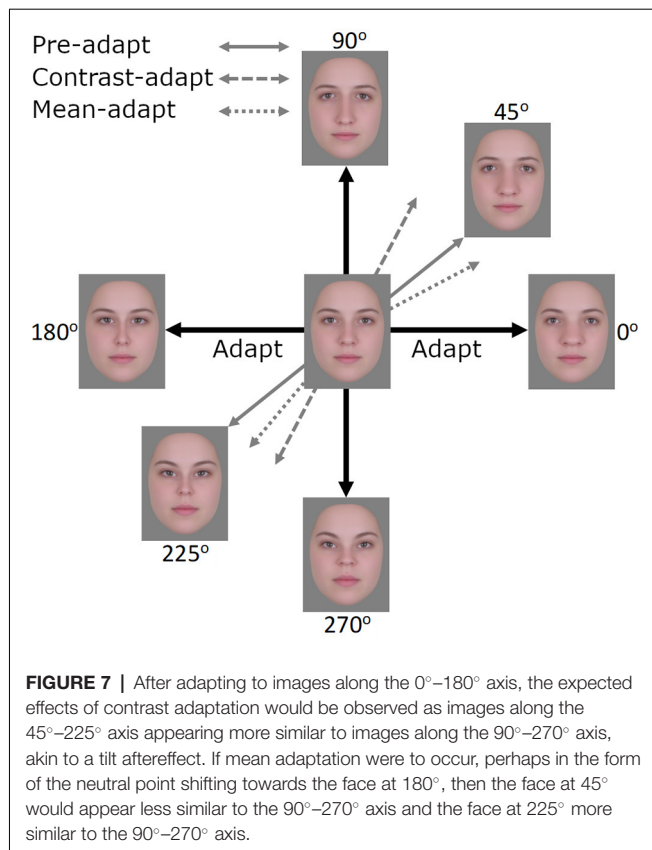
Notes: \* $p < 0.001$ , \*\* $p < 0.0001$ .

never the three maximum expansion or contraction amplitudes. This was done to reduce possible recency contrast or assimilation effects. Each image remained on the screen for 500 ms with an inter-stimulus interval (ISI) of 0 ms. Additional 10 s “top up” adaptation sequences were shown after each trial, with each of the 20 faces shown for 500 ms each. Following the initial adaptation phase and an ISI of 500 ms, participants viewed two test images presented on either side of the fixation cross in the same locations as the adapting images. In a single testing session, these images were only from the  $0^\circ$ – $90^\circ$  quadrant or the  $180^\circ$ – $270^\circ$  quadrant. For these test images, participants were required to rate which of the two (left or right) appeared more horizontally expanded by pressing the corresponding mouse button (left or right). The order of presentation of the test images was determined using a double interleaved staircase. Interleaves began with the largest possible difference between the two images. For example, one interleave would start with the  $0^\circ$  image on the left and the  $90^\circ$  image on the right, and the other interleave would start with the  $0^\circ$  image on the right and the  $90^\circ$  image on the left. If a participant rated the right image as appearing more expanded, on the next trial a more contracted version was shown on the right and a more expanded version was shown on the left. Beginning with a maximum step size of an  $80^\circ$  adjustment (e.g., going from  $0^\circ$  on the left and  $90^\circ$  on the right, to  $80^\circ$  on the left and  $10^\circ$  on the right), this was halved after each reversal such that after the fourth reversal the minimum  $5^\circ$  step size was reached. A reversal was defined as a change in responding

such that images in the opposite visual field now appeared more horizontally expanded. Left and right images were adjusted in tandem, such that if one was increased by  $5^\circ$  (e.g., from  $50^\circ$  to  $55^\circ$ ) the other was decreased by  $5^\circ$  (e.g., from  $40^\circ$  to  $35^\circ$ ). Note that on some trials it was possible for both left and right images to be identical (i.e., both  $45^\circ$  or  $225^\circ$ ). As this was a forced-choice task, participants were required to select which image they nonetheless perceived as more horizontally expanded. Each interleave continued until 10 reversals had been reached. All participants reached 10 reversals within the maximum 40 trials. Points of Subjective Equality (PSE) were calculated by taking the average of the last four reversals of each interleave. A PSE indicates the angular distortion required for both left and right test images to appear equally distorted along the horizontal axis. If adapting to distortions along the horizontal vs. vertical axes were to have no effect or produce mean biases<sup>4</sup>, then PSEs would be similar for both conditions. If instead adaptation effectively reduces sensitivity along the adapted axis, resulting in the post-adapted image appearing more similar to the unadapted axis (as illustrated in Figure 7), the PSE is expected to shift towards the adapted axis, as it reflects the level of distortion required to null the effect. As the left and right test images were adjusted in tandem, PSEs for the left and right fields mirror each other. As such, changes in PSE as a result of adaptation will be only reported for the left field.

The experiment was run over four sessions, each separated by a minimum of 7 days to reduce potential adaptation effects carrying over between sessions. In half of the sessions, the adapting images on the left were from the horizontal axis ( $0^\circ$ – $180^\circ$ ) and images on the right from the vertical axis ( $90^\circ$ – $270^\circ$ ). In the remaining half of the sessions, this was reversed. Likewise, in half of the sessions, the test images were

<sup>4</sup>Note that both axes have the same mean, thus any mean biases would be in the same direction.



from the 0°–90° quadrant, while in the other half images were from 180° to 270° quadrant. Note that rather than comparing the effect of adaptation to a baseline we will be comparing the effect of adapting to one axis compared to the other.

## Results

Mean PSEs following adaptation can be seen in **Figure 8**. Note that if there were no effect of adaptation, then the match (PSE) should occur when the face images are physically the same, and should fall along the 45° and 225° lines. Instead, the PSEs are displaced toward the adapting axes, consistent with nulling an aftereffect that biased the perception of the faces away from the adapting axes. As a result, for test images between 0°–90°, PSEs are larger in angle following adaptation to the vertical axis ( $M = 53.51$ ,  $SD = 6.26$ ) compared to PSEs following adaptation to the horizontal axis ( $M = 40.21$ ,  $SD = 6.26$ ). For test images between 180°–270°, PSEs are again larger following adaptation to the vertical axis ( $M = 233.59$ ,  $SD = 8.77$ ) compared to adaptation to the horizontal axis ( $M = 224.06$ ,  $SD = 9.32$ ). That is, in all cases, the PSE following adaptation shifted closer to the adapted axis. To allow for data from the two test quadrants to be analyzed together, data from the 180°–270° quadrant were re-scaled to range between 0°–90°. Data were analyzed using a  $2 \times 2$  repeated measures ANOVA with the factors Adapting axis (vertical vs. horizontal) and Test quadrant (0°–90° vs. 180°–270°). Analyses showed a significant main effect of Adapting axis ( $F_{1,8} = 24.39$ ,  $p = 0.001$ ,  $\eta_p^2 = 0.75$ ). The main effect of Test quadrant was found to be non-significant ( $F_{1,8} = 0.06$ ,  $p = 0.816$ ,  $\eta_p^2 = 0.01$ ), as

well as the Test quadrant\*Adapting axis interaction ( $F_{1,8} = 1.64$ ,  $p = 0.236$ ,  $\eta_p^2 = 0.17$ ).

## DISCUSSION

To summarize, we used face images distorted along vertical and horizontal axes to examine contrast adaptation in face perception. In the EEG experiment, test sequences comprised four images presented at a rate of 6 Hz. In the absence of prior adaptation, significant responses were observed only at the image presentation rate of 6 Hz, indicating symmetric responses to the four images. Adapting to complementary face pairs introduced an additional signal at 3 Hz, indicating asymmetric responses to images from the two axes. The mean of these faces is a neutral undistorted face and so these asymmetries reflect a form of contrast adaptation, as opposed to more traditional forms of face adaptation that result in a mean bias. Larger 3 Hz responses were observed following adaptation to face pairs from orthogonal axes, which would induce mean biases. The magnitude of these later 3 Hz responses was not significantly different to those following adaptation to a single face representing the mean of the orthogonal pairs.

For the behavioral experiment, we used a variant of classic tilt aftereffects (Gibson and Radner, 1937) to examine the perceptual effects of contrast adaptation in face perception. Adapting to distortions along one axis resulted in face images from intermediate axes appearing biased away from the adapted axis (i.e., nulling PSEs were closer to the adapted axis), consistent with tilt-aftereffects within face space. Importantly the two test poles rotated in the same way, arguing against a mean bias shifting the whole space in the same direction. That is, when adapting to the horizontal axis we did not find the appearance of images at 45° rotating away from the vertical axis and images at 225° rotating towards the vertical axis, which should occur if the adaptation shifted the mean neutral point to be closer to the 180° pole. These behavioral results thus lend further support to our EEG experiment in demonstrating a form of contrast adaptation for faces.

Ying and Xu (2017) previously demonstrated that adapting to a temporal sequence of face images produces behavioral aftereffects similar in size to adapting to the single mean of the sequence. Parallel neurophysiological results were observed here, perhaps indicating the same mechanism is being measured in the two approaches. Combined, these findings suggest that adaptation to faces depends on mechanisms that can encode the average value of a set of faces, similar to the way that chromatic adaptation can adjust to the average of a distribution of colors (Webster and Wilson, 2000). Similar effects have also been found for adaptation to a distribution of sizes (Corbett et al., 2012). The ability to extract the mean of a set of faces is well known from the literature on ensemble coding (Haberman and Whitney, 2007, 2009; de Fockert and Wolfenstein, 2009; Neumann et al., 2013). However, our results cannot distinguish between adapting directly to the mean as opposed to an adaptation effect that is the average of the individual response changes.

The present study shows that it is not simply the mean which is being adapted, but also the variance within a set of faces that is

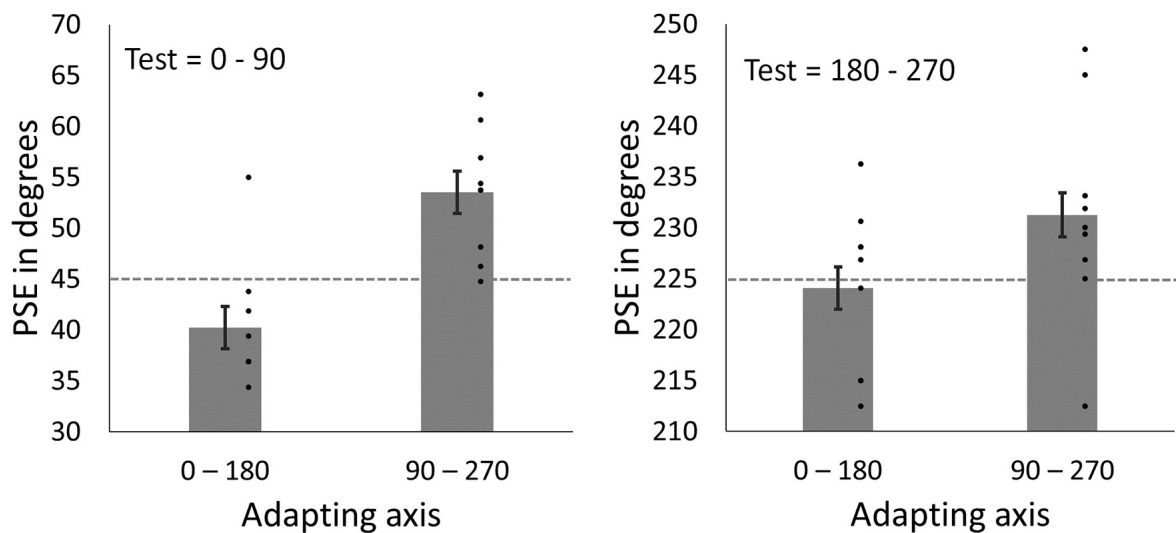


**FIGURE 8 |** PSEs for test faces from the 0°–90° quadrant (left) and for test face from 180° to 270° quadrant (right) after adapting to horizontal (0°–180°) and vertical (90°–270°) axes. Dashed lines represent points of objective equality (i.e., the point at which the face images are horizontally distorted in equal magnitudes). Dots show amplitudes for individual participants. Error bars show SEM.

contributing to that mean. That is, the mean of the face pairs from the vertical axis is identical to the mean of face pairs from the horizontal axis. Adapting to this single mean would not induce an asymmetry in responses (Retter and Rossion, 2017) or bias perceptions of subsequently viewed faces (Webster and MacLin, 1999). Yet when the adapting sequence comprises variance along one of the axes, we find that responses to faces from that axis are disproportionately affected compared to responses to faces from the orthogonal axis. Complementary behavioral effects were also observed, with perceptions biased away from the adapting axis. These findings provide evidence that adaptation can adjust not only to changes in the average face but to changes in the variance.

Having demonstrated the existence of contrast adaptation in face processing, we also sought to gain some insight into the form of the underlying response changes. While the frequency domain analyses show that an asymmetry is present following adaptation, it does not reveal the direction of this asymmetry. That is, it could be the result of either an enhancement or reduction in amplitude, or increase or decrease in latency, in responses to faces from the adapted axis. To address this question we considered the relative phase of these responses. Across all adaptation conditions, the effect of summing the 3 Hz waveforms with the 6 Hz waveforms was such that the amplitude of the first cycle of the 6 Hz wave was decreased relative to the amplitude of the second cycle. Note that in this model, it is the difference between 6 Hz cycles that relates to the 3 Hz asymmetry amplitude from the frequency-domain analysis. The generally higher amplitude here may be accounted for by the focus on one channel (PO10) without a baseline noise subtraction. Adapting and test sequences were matched such that the first image seen in a test sequence was also the first image seen in the adapting sequence or a product of one of these images in the case of the single adapting image. If we take responses to be associated more

with the image primarily presented in the same time window than the image not presented, these results indicate that the response changes from adaptation reflect a reduction in the amplitude of the responses to faces more similar to the adapting images. This would be consistent with predictions from models of face processing based on behavioral observations (Rhodes et al., 2005; Rhodes and Jeffery, 2006; Robbins et al., 2007) and neuroimaging studies (Grill-Spector et al., 1999; Winston et al., 2004) indicating lower response activity following adaptation, as well as for more typical faces (Loffler et al., 2005; Leopold et al., 2006).

Results from earlier EEG studies using ERP designs have been somewhat unclear regarding the effect of adaptation, also referred to as repetition priming, on components understood to reflect the processing of faces. In regards to the N170, different studies have shown that it is both sensitive (Jemel et al., 2005; Jacques and Rossion, 2006; Caharel et al., 2009) and insensitive (Schweinberger et al., 1995; Eimer, 2000; Cooper et al., 2007) to the types of within category face adaptation seen behaviorally, such as identity aftereffects (for reviews, see Rossion and Jacques, 2011; Schweinberger and Neumann, 2016). Different studies have also shown that adaptation can both increase (Herzmann et al., 2004; Jemel et al., 2005) and decrease (Itier and Taylor, 2002, 2004; Jacques and Rossion, 2006) the amplitude of the N170. More consistent results have been produced when considering the P200, a component reflecting the perceived typicality of a face (Stahl et al., 2008). In behavioral studies, faces more similar to adapting images appear more typical following adaptation (Robbins et al., 2007), and P200 amplitudes similarly indicate greater typicality of adapting images (Kloth et al., 2017). However, perhaps surprisingly, the P200 shows an increase in amplitude following adaptation rather than the reduction suggested by models of face adaptation. The

inconsistencies across studies and ERP components highlights one of the advantages of the FPVS paradigm, in that the frequency-defined responses and their relative amplitude can be objectively identified. In the present study the relatively short interval between stimuli of interest makes it difficult to isolate responses to specific images, however when longer intervals are used this can be achieved with greater precision (Dzhelyova et al., 2016; Retter and Rossion, 2016a; Rossion et al., 2020). A short interval may be advantageous in that it increases competition between overlapping responses to subsequent stimuli (Keyers and Perrett, 2002; Retter and Rossion, 2016a), and thus enhances the 3 Hz asymmetry responses here. Should a future study combine a longer interval with the method for quantifying differences in amplitudes across cycles described here, the effect of adaptation on response amplitudes to specific images may be more precisely determined.

In the EEG experiment, we have accounted for the asymmetries in responses after adapting to a given axis (e.g., 0°–180°) by assuming a loss of sensitivity to that axis, or to the overall “contrast sensitivity” for that axis. However, an alternative is that the adaptation produced localized losses in sensitivity to the two adapting distortion levels (e.g., separate losses to the 0° adaptor and 180° adaptor). While the present experiments were not designed to test this alternative, we note that the latter account is more in line with the prediction of a multiple-channel model for the distortion levels, and is inconsistent with previous findings that adaptation to facial distortions instead reflects an opponent-like code (Rhodes et al., 2005). For example, adaptation to an undistorted face does not produce a perceived change in distorted test faces, an asymmetry which is inconsistent with local adaptation to the distortion level along the axis but is consistent with the prediction for adapting to a “zero-contrast” distortion (Webster and MacLin, 1999). Note that this may be different for other aspects of faces for which the underlying coding scheme may reflect a multiple-channel code.

In the behavioral experiment, we observed the two test poles rotating in the same way, arguing against a mean bias shifting the whole space in the same direction. However, an alternative account is that the aftereffects could be explained by multiple and simultaneous instances of local repulsion rather than contrast adaptation. That is, a test face at 45° is in closer proximity and more similar in appearance to adapting faces near the 0° pole. Conversely, a test face at 225° is more similar to faces at 180°. A greater similarity in appearance could be accompanied by a greater commonality in the neural populations encoding these faces. It would then follow that any changes in the response properties of these populations will have a greater effect on faces more similar in appearance. In the present study, it could be that test faces at 45° are being repulsed from 0° adaptors while test faces at 225° are being separately repulsed from 180° adaptors, giving the impression of an axis rotation. However, studies of face distortion aftereffects are generally concordant in finding that adaptation to the distortions involves a global renormalization of the space rather than a local repulsion (Webster and MacLin, 1999; Storrs and Arnold, 2012). While some aspects of face perception, such as eye gaze, appear to reflect a multiple channel coding system (Calder et al., 2008), figural distortions in faces

appear to be encoded *via* a norm-based system (Robbins et al., 2007) and reflect global rather than local response changes. As such, it is unlikely that the aftereffects observed here can be explained by local repulsion to the two sides of the adapting axis, and may instead reflect a general sensitivity loss for the adapting axis.

It is perhaps worth noting that in the article by Calder et al. (2008) referenced above, participants were adapted to alternations of left/right eye gaze directions, similar to the complementary pair adaptation condition in the present EEG experiment. However, as eye gaze is understood to be encoded *via* a multiple channel system this necessarily negates the possibility of contrast adaptation as the neutral point is encoded by activation in a specifically designated channel, rather than being represented by equal activation in two opposing channels. That is, adapting to the poles of an eye gaze continuum would not produce a uniform reduction in sensitivity along that axis. Instead, a spike in sensitivity would be present around the neutral point (i.e., direct gaze).

The discovery of contrast adaptation in faces holds potentially important implications for our understanding of models of face processing. In addition to the more standard form of face aftereffects, in which perceptions are biased in a single uniform direction (e.g., Webster and MacLin, 1999), opposing contingent face aftereffects have also been observed. Contingent aftereffects involve adapting to two face categories (e.g., Asian vs. Caucasian) that also differ on a second dimension (e.g., Asian faces that have been contracted vs. Caucasian faces that have been expanded). Adapting to these faces results in simultaneous opposing aftereffects. That is, subsequently viewed Asian faces appear expanded and Caucasian faces contracted. These findings have led researchers to conclude that rather than the existence of a single norm against which all faces are encoded, separate norms are maintained for many categories of faces, including race (Jaquet et al., 2008; Gwinn and Brooks, 2013, 2015b), gender (Bestelmeyer et al., 2008; Jaquet and Rhodes, 2008), age (Little et al., 2008), and species (Little et al., 2008; Gwinn and Brooks, 2015a). However, these effects can be equally explained as tilt-like effects around a common norm and do not necessarily require the existence of multiple norms (Webster and MacLeod, 2011). That is, contingent aftereffects can be conceptualized as opposite ends of a given face dimension rotating towards an orthogonal dimension. The contrast aftereffects reported here demonstrate such a rotation is possible. The existence of a common norm would further explain why aftereffects are not observed following adaptation to a global norm (e.g., a face that is ambiguous in terms of race and gender), which under a multiple norm model should be distinctive from all single races and gender norms and induce observable aftereffects (Webster and MacLeod, 2011). While multiple category-specific norms may facilitate the coding of identity (Armann et al., 2011; Rhodes et al., 2011), they are not necessarily required for contingent aftereffects.

In the current experiment, we measured the perceptual effects of contrast adaptation in faces as a bias away from the adapting axis. However, in studies of spatial or color contrast, the effects of contrast adaptation have also been observed as a reduction in contrast sensitivity, resulting in a change in the thresholds for

detecting contrasts (Blakemore and Campbell, 1969; Krauskopf et al., 1982). The expected effects of face contrast adaptation on the sensitivity to the adapted faces are less clear. In a review of visual adaptation and face perception, Webster and MacLeod (2011) note that contrast within face perception can be conceptualized in two different ways: as the magnitude of a face along a dimension (e.g., how expanded or contracted a face appears), or the physical contrast of the image (e.g., the maximum and minimum luminance values in the image). In terms of physical contrast, over very short adaptation periods (20–200 ms), thresholds for detecting faces can be increased for non-adapted faces and decreased for adapted faces, while over longer periods thresholds increase for both categories (Guo et al., 2009; Oruç and Barton, 2010). In regards to face contrast as dimension magnitude, some studies have shown a facilitation in discrimination around average or adapted faces (Rhodes et al., 2010; Oruç and Barton, 2011), while others have shown no effect (Rhodes et al., 2007; Ng et al., 2008). For studies showing facilitation effects, this may be due to a *sharpening* of the tuning curves of the neural populations sensitive to the adapted stimulus (Oruç and Barton, 2010, 2011) or a reduction in responses to common information shared by faces in a set (Rhodes et al., 2010). For our results, we did not measure detection or discrimination but rather changes in the amplitude of neural responses or biases in perceptual responses. By both measures, adaptation appeared to alter these responses in ways that are consistent with adaptation to the variance rather than the mean of the adapting images—and thus with adaptation to the face contrasts. These results, therefore, provide novel evidence for a distinct form of adaptation in the visual mechanisms processing faces.

## CONCLUSION

We have presented evidence for contrast adaptation in face perception. This was observed both as changes in neural responses measured using EEG, likely reflecting a reduction

in sensitivity to the adapted face axis, as well as behavioral changes in the appearance of subsequently viewed faces. These findings show that in addition to the human visual system adjusting to the average face to which the observer is exposed, adaptation can also selectively adjust to the range or variance of a set of faces. These contrast adaptation effects reflect a distinct form of face adaptation and may underlie effects that have previously been interpreted in terms of contingent face aftereffects.

## DATA AVAILABILITY STATEMENT

The raw data supporting the conclusions of this article will be made available by the authors, without undue reservation.

## ETHICS STATEMENT

The studies involving human participants were reviewed and approved by Institutional Review Board, University of Nevada, Reno. The patients/participants provided their written informed consent to participate in this study.

## AUTHOR CONTRIBUTIONS

OG, TR, and MW contributed to conception and design of the study. OG, TR, and SO'N contributed to technical aspects of implementing the experiment and collecting data. OG and TR analyzed the data. OG wrote the first draft of the manuscript. All authors contributed to the article and approved the submitted version.

## FUNDING

This work was supported by grants from the National Institutes of Health (EY-10834 to MW), with further support for core facilities provided by COBRE P20 GM 103650.

## REFERENCES

- Ales, J. M., and Norcia, A. M. (2009). Assessing direction-specific adaptation using the steady-state visual evoked potential: results from EEG source imaging. *J. Vis.* 9:8. doi: 10.1167/9.7.8
- Armman, R., Jeffery, L., Calder, A. J., and Rhodes, G. (2011). Race-specific norms for coding face identity and a functional role for norms. *J. Vis.* 11:9. doi: 10.1167/11.13.9
- Barlow, H. B., and Hill, R. M. (1963). Evidence for a physiological explanation of the waterfall phenomenon and figural after-effects. *Nature* 200, 1345–1347. doi: 10.1038/2001345a0
- Bestelmeyer, P. E., Jones, B. C., DeBruine, L. M., Little, A. C., Perrett, D. I., Welling, L. L. M., et al. (2008). Sex-contingent face aftereffects depend on perceptual category rather than structural encoding. *Cognition* 107, 353–365. doi: 10.1016/j.cognition.2007.07.018
- Blakemore, C., and Campbell, F. W. (1969). On the existence of neurones in the human visual system selectively sensitive to the orientation and size of retinal images. *J. Physiol.* 203, 237–260. doi: 10.1113/jphysiol.1969.sp008862
- Blakemore, C., and Nachmias, J. (1971). The orientation specificity of two visual after-effects. *J. Physiol.* 213, 157–174. doi: 10.1113/jphysiol.1971.sp009374
- Bradley, A., Switkes, E., and De Valois, K. (1988). Orientation and spatial frequency selectivity of adaptation to color and luminance gratings. *Vis. Res.* 28, 841–856. doi: 10.1016/0042-6989(88)90031-4
- Caharel, S., Arripe, O., Ramon, M., Jacques, C., and Rossion, B. (2009). Early adaptation to repeated unfamiliar faces across viewpoint changes in the right hemisphere: evidence from the N170 ERP component. *Neuropsychologia* 47, 639–643. doi: 10.1016/j.neuropsychologia.2008.11.016
- Calder, A. J., Jenkins, R., Cassel, A., and Clifford, C. W. (2008). Visual representation of eye gaze is coded by a nonopponent multichannel system. *J. Exp. Psychol. Gen.* 137, 244–261. doi: 10.1037/0096-3445.137.2.244
- Cooper, T. J., Harvey, M., Lavidor, M., and Schweinberger, S. R. (2007). Hemispheric asymmetries in image-specific and abstractive priming of famous faces: evidence from reaction times and event-related brain potentials. *Neuropsychologia* 45, 2910–2921. doi: 10.1016/j.neuropsychologia.2007.06.005
- Corbett, J. E., Wurnitsch, N., Schwartz, A., and Whitney, D. (2012). An aftereffect of adaptation to mean size. *Vis. Cogn.* 20, 211–231. doi: 10.1080/13506285.2012.657261
- de Fockert, J., and Wolfenstein, C. (2009). Rapid extraction of mean identity from sets of faces. *Q. J. Exp. Psychol. (Hove)* 62, 1716–1722. doi: 10.1080/17470210902811249

- Dzhelyova, M., Jacques, C., and Rossion, B. (2016). At a single glance: fast periodic visual stimulation uncovers the spatio-temporal dynamics of brief facial expression changes in the human brain. *Cereb. Cortex* 27, 4106–4123. doi: 10.1093/cercor/bhw223
- Dzhelyova, M., and Rossion, B. (2014). The effect of parametric stimulus size variation on individual face discrimination indexed by fast periodic visual stimulation. *BMC Neurosci.* 15:87. doi: 10.1186/1471-2202-15-87
- Eimer, M. (2000). Event-related brain potentials distinguish processing stages involved in face perception and recognition. *Clin. Neurophysiol.* 111, 694–705. doi: 10.1016/s1388-2457(99)00285-0
- Farah, M. J., Tanaka, J. W., and Drain, H. M. (1995). What causes the face inversion effect? *J. Exp. Psychol. Hum. Percept. Perform.* 21, 628–634. doi: 10.1037//0096-1523.21.3.628
- Georgeson, M. A. (1985). The effect of spatial adaptation on perceived contrast. *Spat. Vis.* 1, 103–112. doi: 10.1163/156856885x00125
- Gibson, J. J., and Radner, M. (1937). Adaptation, after-effect and contrast in the perception of tilted lines. I. Quantitative studies. *J. Exp. Psychol.* 20, 453–467. doi: 10.1037/h0059826
- Grill-Spector, K., Kushnir, T., Edelman, S., Avidan, G., Itzhak, Y., and Malach, R. (1999). Differential processing of objects under various viewing conditions in the human lateral occipital complex. *Neuron* 24, 187–203. doi: 10.1016/s0896-6273(00)80832-6
- Guo, X. M., Oruç, I., and Barton, J. J. (2009). Cross-orientation transfer of adaptation for facial identity is asymmetric: a study using contrast-based recognition thresholds. *Vis. Res.* 49, 2254–2260. doi: 10.1016/j.visres.2009.06.012
- Gwinn, O. S., and Brooks, K. R. (2013). Race-contingent face aftereffects: a result of perceived racial typicality, not categorization. *J. Vis.* 13:13. doi: 10.1167/13.10.13
- Gwinn, O. S., and Brooks, K. R. (2015a). Face encoding is not categorical: consistent evidence across multiple types of contingent aftereffects. *Vis. Cogn.* 23, 867–893. doi: 10.1080/13506285.2015.1091800
- Gwinn, O. S., and Brooks, K. R. (2015b). No role for lightness in the encoding of black and white: race-contingent face aftereffects depend on facial morphology, not facial luminance. *Vis. Cogn.* 23, 597–611. doi: 10.1080/13506285.2015.1061085
- Gwinn, O. S., Matera, C. N., O'Neil, S. F., and Webster, M. A. (2018). Asymmetric neural responses for facial expressions and anti-expressions. *Neuropsychologia* 119, 405–416. doi: 10.1016/j.neuropsychologia.2018.09.001
- Haberman, J., and Whitney, D. (2007). Rapid extraction of mean emotion and gender from sets of faces. *Cur. Biol.* 17, R751–R753. doi: 10.1016/j.cub.2007.06.039
- Haberman, J., and Whitney, D. (2009). Seeing the mean: ensemble coding for sets of faces. *J. Exp. Psychol. Hum. Percept. Perform.* 35, 718–734. doi: 10.1037/a0013899
- Herzmann, G., Schweinberger, S. R., Sommer, W., and Jentsch, I. (2004). What's special about personally familiar faces. *Psychophysiology* 41, 688–701. doi: 10.1111/j.1469-8986.2004.00196.x
- Hurvich, L. M., and Jameson, D. (1957). An opponent-process theory of color vision. *Psychol. Rev.* 64, 384–404. doi: 10.1037/h0041403
- Hyvarinen, A., and Oja, E. (2000). Independent component analysis: algorithms and applications. *Neural Netw.* 13, 411–430. doi: 10.1016/s0893-6080(00)00026-5
- Itier, R. J., and Taylor, M. J. (2002). Inversion and contrast polarity reversal affect both encoding and recognition processes of unfamiliar faces: a repetition study using ERPs. *Neuroimage* 15, 353–372. doi: 10.1006/nimg.2001.0982
- Itier, R. J., and Taylor, M. J. (2004). Effects of repetition learning on upright, inverted and contrast-reversed face processing using ERPs. *Neuroimage* 21, 1518–1532. doi: 10.1016/j.neuroimage.2003.12.016
- Jacques, C., D'Arripe, O., and Rossion, B. (2007). The time course of the inversion effect during individual face discrimination. *J. Vis.* 7:3. doi: 10.1167/7.3.3
- Jacques, C., and Rossion, B. (2006). The speed of individual face categorization. *Psychol. Sci.* 17, 485–492. doi: 10.1111/j.1467-9280.2006.01733.x
- Jaquet, E., and Rhodes, G. (2008). Face aftereffects indicate dissociable, but not distinct, coding of male and female faces. *J. Exp. Psychol. Hum. Percept. Perform.* 34, 101–112. doi: 10.1037/0096-1523.34.1.101
- Jaquet, E., Rhodes, G., and Hayward, W. G. (2008). Race-contingent aftereffects suggest distinct perceptual norms for different race faces. *Vis. Cogn.* 16, 734–753. doi: 10.1080/13506280701350647
- Jemel, B., Pisani, M., Rousselle, L., Crommelinck, M., and Bruyer, R. (2005). Exploring the functional architecture of person recognition system with event-related potentials in a within- and cross-domain self-priming of faces. *Neuropsychologia* 43, 2024–2040. doi: 10.1016/j.neuropsychologia.2005.03.016
- Kanwisher, N., Tong, F., and Nakayama, K. (1998). The effect of face inversion on the human fusiform face area. *Cognition* 68, 1–11. doi: 10.1016/s0010-0277(98)00035-3
- Keyers, C., and Perrett, D. I. (2002). Visual masking and RSVP reveal neural competition. *Trends Cogn. Sci.* 6, 120–125. doi: 10.1016/s1364-6613(00)01852-0
- Kloth, N., Rhodes, G., and Schweinberger, S. R. (2017). Watching the brain recalibrate: neural correlates of renormalization during face adaptation. *Neuroimage* 155, 1–9. doi: 10.1016/j.neuroimage.2017.04.049
- Kohn, A. (2007). Visual adaptation: physiology, mechanisms and functional benefits. *J. Neurophysiol.* 97, 3155–3164. doi: 10.1152/jn.00086.2007
- Krauskopf, J., Williams, D. R., and Heeley, D. W. (1982). Cardinal directions of color space. *Vis. Res.* 22, 1123–1131. doi: 10.1016/0042-6989(82)90077-3
- Leopold, D. A., Bondar, I. V., and Giese, M. A. (2006). Norm-based face encoding by single neurons in the monkey inferotemporal cortex. *Nature* 442, 572–575. doi: 10.1038/nature04951
- Leopold, D. A., O'Toole, A. J., Vetter, T., and Blanz, V. (2001). Prototype-referenced shape encoding revealed by high-level aftereffects. *Nat. Neurosci.* 4, 89–94. doi: 10.1038/82947
- Little, A. C., DeBruine, L. M., Jones, B. C., and Waite, C. (2008). Category contingent aftereffects for faces of different races, ages and species. *Cognition* 106, 1537–1547. doi: 10.1016/j.cognition.2007.06.008
- Loffler, G., Yourganov, G., Wilkinson, F., and Wilson, H. R. (2005). fMRI evidence for the neural representation of faces. *Nat. Neurosci.* 8, 1386–1390. doi: 10.1038/nn1538
- Mueller, R., Utz, S., Carbon, C. C., and Strobach, T. (2020). Face adaptation and face priming as tools for getting insights into the quality of face space. *Front. Psychol.* 11:166. doi: 10.3389/fpsyg.2020.00166
- Neumann, M. F., Schweinberger, S. R., and Burton, A. M. (2013). Viewers extract mean and individual identity from sets of famous faces. *Cognition* 128, 56–63. doi: 10.1016/j.cognition.2013.03.006
- Ng, M., Boynton, G. M., and Fine, I. (2008). Face adaptation does not improve performance on search or discrimination tasks. *J. Vis.* 8, 1–20. doi: 10.1167/8.1.1
- Norcia, A. M., Appelbaum, L. G., Ales, J. M., Cottareau, B. R., and Rossion, B. (2015). The steady-state visual evoked potential in vision research: a review. *J. Vis.* 15:4. doi: 10.1167/15.6.4
- Oostenveld, R., and Praamstra, P. (2001). The five percent electrode system for high-resolution EEG and ERP measurements. *Clin Neurophysiol.* 112, 713–719. doi: 10.1016/s1388-2457(00)00527-7
- Oruç, I., and Barton, J. J. (2010). A novel face aftereffect based on recognition contrast thresholds. *Vis. Res.* 50, 1845–1854. doi: 10.1016/j.visres.2010.06.005
- Oruç, I., and Barton, J. J. (2011). Adaptation improves discrimination of face identity. *Proc. Biol. Sci.* 278, 2591–2597. doi: 10.1098/rspb.2010.2480
- Regan, D. (1966). Some characteristics of average steady-state and transient responses evoked by modulated light. *Electroencephalogr. Clin. Neurophysiol.* 20, 238–248. doi: 10.1016/0013-4694(66)90088-5
- Retter, T. L., and Rossion, B. (2016a). Uncovering the neural magnitude and spatio-temporal dynamics of natural image categorization in a fast visual stream. *Neuropsychologia* 91, 9–28. doi: 10.1016/j.neuropsychologia.2016.07.028
- Retter, T. L., and Rossion, B. (2016b). Visual adaptation provides objective electrophysiological evidence of facial identity discrimination. *Cortex* 80, 35–50. doi: 10.1016/j.cortex.2015.11.025
- Retter, T. L., and Rossion, B. (2017). Visual adaptation reveals an objective electrophysiological measure of high-level individual face discrimination. *Sci. Rep.* 7:3269. doi: 10.1038/s41598-017-03348-x
- Retter, T. L., Rossion, B., and Schiltz, C. (2021). Harmonic amplitude summation for frequency-tagging analysis. *J. Cogn. Neurosci.* 1–22. doi: 10.1162/jocn\_a\_01763

- Rhodes, G., Jaquet, E., Jeffery, L., Evangelista, E., Keane, J., and Calder, A. J. (2011). Sex-specific norms code face identity. *J. Vis.* 11:1. doi: 10.1167/11.1.1
- Rhodes, G., and Jeffery, L. (2006). Adaptive norm-based coding of facial identity. *Vis. Res.* 46, 2977–2987. doi: 10.1016/j.visres.2006.03.002
- Rhodes, G., Jeffery, L., Watson, T. L., Jaquet, E., Winkler, C., and Clifford, C. W. (2004). Orientation-contingent face aftereffects and implications for face-coding mechanisms. *Curr. Biol.* 14, 2119–2123. doi: 10.1016/j.cub.2004.11.053
- Rhodes, G., Maloney, L. T., Turner, J., and Ewing, L. (2007). Adaptive face coding and discrimination around the average face. *Vis. Res.* 47, 974–989. doi: 10.1016/j.visres.2006.12.010
- Rhodes, G., Robbins, R., Jaquet, E., McKone, E., Jeffery, L., and Clifford, C. W. (2005). Adaptation and face perception: How aftereffects implicate norm-based coding of faces,” in *Fitting the Mind to the World: Adaptation and After-Effects in High-Level Vision*, 2nd edition, eds C. W. G. Clifford and G. Rhodes (New York: Oxford University Press), 213–240.
- Rhodes, G., Watson, T. L., Jeffery, L., and Clifford, C. W. (2010). Perceptual adaptation helps us identify faces. *Vis. Res.* 50, 963–968. doi: 10.1016/j.visres.2010.03.003
- Robbins, R., McKone, E., and Edwards, M. (2007). Aftereffects for face attributes with different natural variability: adapter position effects and neural models. *J. Exp. Psychol. Hum. Percept. Perform.* 33, 570–592. doi: 10.1037/0096-1523.33.3.570
- Rossion, B. (2014a). Understanding face perception by means of human electrophysiology. *Trends Cogn. Sci.* 18, 310–318. doi: 10.1016/j.tics.2014.02.013
- Rossion, B. (2014b). Understanding individual face discrimination by means of fast periodic visual stimulation. *Exp. Brain Res.* 232, 1599–1621. doi: 10.1007/s00221-014-3934-9
- Rossion, B., and Jacques, C. (2011). “The N170: Understanding the time course of face perception in the human brain,” in *The Oxford Handbook of Event-Related Potential Components*, eds S. J. Luck and E. S. Kappenman (New York: Oxford University Press), 115–141.
- Rossion, B., Prieto, E. A., Boremanse, A., Kuefner, D., and Belle, G. V. (2012). A steady-state visual evoked potential approach to individual face perception: effect of inversion, contrast-reversal and temporal dynamics. *Neuroimage* 63, 1585–1600. doi: 10.1016/j.neuroimage.2012.08.033
- Rossion, B., Retter, T. L., and Liu-Shuang, J. (2020). Understanding human individuation of unfamiliar faces with oddball fast periodic visual stimulation and electroencephalography. *Eur. J. Neurosci.* 52, 4283–4334. doi: 10.1111/ejn.14865
- Rossion, B., Torfs, K., Jacques, C., and Liu-Shuang, J. (2015). Fast periodic presentation of natural images reveals a robust face-selective electrophysiological response in the human brain. *J. Vis.* 15, 1–18. doi: 10.1167/15.1.18
- Russell, R. (2009). A sex difference in facial contrast and its exaggeration by cosmetics. *Perception* 38, 1211–1220. doi: 10.1068/p6331
- Schweinberger, S. R., and Neumann, M. F. (2016). Repetition effects in human ERPs to faces. *Cortex* 80, 141–153. doi: 10.1016/j.cortex.2015.11.001
- Schweinberger, S. R., Pfütze, E. M., and Sommer, W. (1995). Repetition priming and associative priming of face recognition: evidence from event-related potentials. *J. Exp. Psychol. Learn. Mem. Cogn.* 21, 722–736. doi: 10.1037/0278-7393.21.3.722
- Seeck, M., Michel, C. M., Mainwaring, N., Cosgrove, R., Blume, H., Ives, J., et al. (1997). Evidence for rapid face recognition from human scalp and intracranial electrodes. *Neuroreport* 8, 2749–2754. doi: 10.1097/00001756-199708180-00021
- Spetch, M. L., Cheng, K., and Clifford, C. W. (2004). Peak shift but not range effects in recognition of faces. *Learn. Motiv.* 35, 221–241. doi: 10.1016/j.lmot.2003.11.001
- Srinivasan, R., Russell, D. P., Edelman, G. M., and Tononi, G. (1999). Increased synchronization of neuromagnetic responses during conscious perception. *J. Neurosci.* 19, 5435–5448. doi: 10.1523/jneurosci.19-13-05435.1999
- Stahl, J., Wiese, H., and Schweinberger, S. R. (2008). Expertise and own-race bias in face processing: an event-related potential study. *Neuroreport* 19, 583–587. doi: 10.1097/WNR.0b013e3282f97b4d
- Storrs, K. R., and Arnold, D. H. (2012). Not all face aftereffects are equal. *Vis. Res.* 64, 7–16. doi: 10.1016/j.visres.2012.04.020
- Storrs, K. R., and Arnold, D. H. (2015). Face aftereffects involve local repulsion, not renormalization. *J. Vis.* 15:1. doi: 10.1167/15.8.1
- Tyler, C. W., and Kaitz, M. (1977). Movement adaptation in the visual evoked response. *Exp. Brain Res.* 27, 203–209. doi: 10.1007/BF00237698
- Watson, T. L., and Clifford, C. W. G. (2003). Pulling faces: an investigation of the face-distortion aftereffect. *Perception* 32, 1109–1116. doi: 10.1068/p5082
- Webster, M. A. (2015). Visual adaptation. *Ann. Rev. Vis. Sci.* 1, 547–567. doi: 10.1146/annurev-vision-082114-035509
- Webster, M. A., Kaping, D., Mizokami, Y., and Duhamel, P. (2004). Adaptation to natural facial categories. *Nature* 428, 557–561. doi: 10.1038/nature02420
- Webster, M. A., and Leonard, D. (2008). Adaptation and perceptual norms in color vision. *J. Opt. Soc. Am. A. Opt. Image Sci. Vis.* 25, 2817–2825. doi: 10.1364/josaa.25.002817
- Webster, M. A., and MacLeod, D. I. A. (2011). Visual adaptation and face perception. *Philos. Trans. R. Soc. Lond. B. Biol. Sci.* 366, 1702–1725. doi: 10.1098/rstb.2010.0360
- Webster, M. A., and MacLin, O. H. (1999). Figural aftereffects in the perception of faces. *Psychon. Bull. Rev.* 6, 647–653. doi: 10.3758/bf03212974
- Webster, M. A., and Mollon, J. D. (1991). Changes in colour appearance following post-receptoral adaptation. *Nature* 349, 235–238. doi: 10.1038/349235a0
- Webster, M. A., and Wilson, J. A. (2000). Interactions between chromatic adaptation and contrast adaptation in color appearance. *Vis. Res.* 40, 3801–3816. doi: 10.1016/s0042-6989(00)00238-8
- Winston, J. S., Henson, R. N. A., Fine-Goulden, M. R., and Dolan, R. J. (2004). fMRI-adaptation reveals dissociable neural representations of identity and expression in face perception. *J. Neurophysiol.* 92, 1830–1839. doi: 10.1152/jn.00155.2004
- Ying, H., and Xu, H. (2017). Adaptation reveals that facial expression averaging occurs during rapid serial presentation. *J. Vis.* 17:15. doi: 10.1167/17.1.15
- Zhao, L., and Chubb, C. (2001). The size-tuning of the face-distortion after-effect. *Vis. Res.* 41, 2979–2994. doi: 10.1016/s0042-6989(01)00202-4

**Conflict of Interest:** The authors declare that the research was conducted in the absence of any commercial or financial relationships that could be construed as a potential conflict of interest.

**Publisher's Note:** All claims expressed in this article are solely those of the authors and do not necessarily represent those of their affiliated organizations, or those of the publisher, the editors and the reviewers. Any product that may be evaluated in this article, or claim that may be made by its manufacturer, is not guaranteed or endorsed by the publisher.

Copyright © 2021 Gwinn, Retter, O'Neil and Webster. This is an open-access article distributed under the terms of the Creative Commons Attribution License (CC BY). The use, distribution or reproduction in other forums is permitted, provided the original author(s) and the copyright owner(s) are credited and that the original publication in this journal is cited, in accordance with accepted academic practice. No use, distribution or reproduction is permitted which does not comply with these terms.

# Advantages of publishing in Frontiers



## OPEN ACCESS

Articles are free to read  
for greatest visibility  
and readership



## FAST PUBLICATION

Around 90 days  
from submission  
to decision



## HIGH QUALITY PEER-REVIEW

Rigorous, collaborative,  
and constructive  
peer-review



## TRANSPARENT PEER-REVIEW

Editors and reviewers  
acknowledged by name  
on published articles

## Frontiers

Avenue du Tribunal-Fédéral 34  
1005 Lausanne | Switzerland

Visit us: [www.frontiersin.org](http://www.frontiersin.org)

Contact us: [frontiersin.org/about/contact](http://frontiersin.org/about/contact)



## REPRODUCIBILITY OF RESEARCH

Support open data  
and methods to enhance  
research reproducibility



## DIGITAL PUBLISHING

Articles designed  
for optimal readership  
across devices



## FOLLOW US

@frontiersin



## IMPACT METRICS

Advanced article metrics  
track visibility across  
digital media



## EXTENSIVE PROMOTION

Marketing  
and promotion  
of impactful research



## LOOP RESEARCH NETWORK

Our network  
increases your  
article's readership